REACTIVITY AND LUMINESCENCE STUDY OF PLATINUM AND COPPER COMPLEXES OF 7-AZAINDOLE DERIVATIVES

By

Shu-Bin Zhao

A thesis submitted to the Department of Chemistry

In conformity with the requirements for

The degree of Doctor of Philosophy

Queen's University

Kingston, Ontario, Canada

(May, 2008)

Dedicate to my wife and parents.

Abstract

The objective of this thesis is to explore new reactivities and to improve luminescent properties of 7-azaindole-containing metal complexes.

Selectivity for the activation of toluene and ethyl benzene has been investigated with two cationic Pt^{II}(N,N-L) complexes, where N,N-L = 1,2-bis(1-*N*-7-azaindolyl)benzene (BAB) or bis(1-*N*-7-azaindolyl)methane (BAM). A high regioselectivity toward toluene and ethyl benzene benzylic C-H activation and a distinct diastereoselectivity for ethyl benzene benzylic C-H activation are demonstrated. Detailed mechanistic studies have been performed, leading to the establishment of both the intermediacy of the η^3-benzylic Pt(II) complexes in the reactions and the ligand steric impacts as origins for the distinct diastereoselectivity.

A $PtMe_2$ complex of 1-*N*-(pyridin-2-yl)-7-azaindole (NPA) has been synthesized and found to undergo facile transformation at ambient temperature, resulting in the quantitive formation of a neutral Pt_4 molecular square. The mechanism of the transformation process has been examined, establishing a distinct intramolecular C-H driven self-assembly process.

The geometrical impacts of the BAB and BAM ligands on the structure and stability of their *fac*-Pt(IV)Me_3 complexes has been investigated. The BAB ligand is more effective than the BAM ligand in stabilizing the five-coordinate Pt(IV)Me_3 complexes. With the BAB ligand, a five-coordinate *fac*-Pt(IV)Me_3 complex is obtained; with the BAM ligand, two six-coordinate *fac*-Pt(IV)Me_3 complexes are obtained. In

solution, the methyl groups in the BAB complex exchange slowly, but those in the BAM complexes exchange rapidly.

Several new 7-azaindolyl derivative ligands *via* either modifying or altering the BAM and BAB bridging groups have been developed. The syntheses, structures and reactivities of their Pt(II) complexes have been examined, leading to the finding of an unconventional C-Sn oxidative addition reaction.

The modification of the NPA ligand *via* the incorporation of a triarylboron group has been carried out. Several novel Pt(II) and Cu(I) complexes have been synthesized and studied. A Cu(I) complex is found to display exceptionally bright ambient temperature phosphorescence.

A series of dinuclear Cu(I) compounds of the 1,2,3,4-tetra(1-*N*-7-azaindolyl)benzene (TTAB) ligand have been synthesized and examined. The close contacts between the TTAB bridging phenyl ring and the Cu(I) centers are present in the complexes.

Acknowledgements

I would like to start by expressing my deepest gratitude to my supervisor, Prof. Suning Wang, for her invaluable support, encouragement and guidance throughout this work, and also for giving me freedom in my research activities. Her wonderful personality, great passions to research, in-depth mastery of subjects and earnest concerns about students render her a fantastic example of the teaching-by-example doctrine, which exceptionally inspire and enrich my growth as a student, a researcher and a scientist.

It has been a fulfilling experience to work with so many talented chemists. I'm always grateful to my M.S. mentor, Prof. Liang-fu Tang, for introducing me into the realm of chemistry. I am truly grateful to Dr. Wen-li Jia for introducing me to the Wang group and enjoy very much of the time working with him in the group. A special acknowledgement is given to Dr. Rui-yao Wang for being always kindly supporting me with his expertise on X-ray crystallography. I gratefully acknowledge Dr. Datong Song for his advice and original crucial contributions on the C-H activation project. I am also deeply grateful to many other group members Dr. Junghyun Lee, Dr. Xiangyang Liu, Dr. Yi Sun, Dongren Bai, Yi Cui, Weihua Huang, Theresa M^{c}Cormick, Wade White, Yasmin Jessa, Sanela Martić, Hazem Amarne, Yingli Rao, Guohui (Joy) Liu, Zachary Hudson, for their great help and encouragement during the work.

I would also like to acknowledge two distinguished faculty fellows Prof. Philip G. Jessop and Prof. Guojun Liu, for serving as my committee members and for their invaluable suggestion and help during the course of the work. I sincerely thank Prof. Gang Wu and Dr. Francoise Sauriol for their helps on NMR spectroscopic analyses, Dr.

Jianping Lu for his help on measuring solid state emission quantum efficiency, Jie Sui in the mass spectrometry lab, as well as other professors, staffs, friends and fellow students who helped and supported me in my work.

I gratefully acknowledge the Chemistry Department for providing all the necessary spaces and equipments, and acknowledge the Graduate School of Queen's University and NSERC for financially supporting this work.

I am forever indebted to my families. I would always love to thank my parents and elder brother, for their faithful love and their consistent support of my life pursuit. I am utterly grateful to my wonderful wife Qian Cui, for her precious love, support, trust and encouragement, and I am also deeply grateful to my parents in-law for their great trust, love and support.

Statement of Originality

All of the work described within this thesis is the original work of the author under the supervision of Prof. Suning Wang with the following exceptions. The NOESY spectra of compounds **2.5**, **2.6** and **2.8** in Chapter 2 and the Arrhenius plot of compound **4.1** in Chapter 4 were done by Prof. Gang Wu. The solid state emission quantum efficiency of compounds **6.1** and **6.2** in Chapter 6 were measured by Dr. Jianping Lu. The calculations for the HOMO and LUMO orbitals of the BNPA ligand were carried out by Theresa M^{c}Cormick. Any published (or unpublished) ideas and/or techniques from the work of others are fully acknowledged in accordance with the standard referencing practices.

Table of Contents

List of Symbols and Abbreviations

Å	angstrom(s)
Anal.	elemental analysis
APBN	1-{2-(1-*N*-7-azaindolyl)pyridine-5-yl}-8-{*p*-(Mes_2B)phenyl}-naphthalene
Ar^F	3,5-bis(trifluoromethyl)phenyl
7-aza	7-azaindolyl
BAHE	6,7-bis(1-*N*-7-azaindolyl)-1,4-dihydronaphthalene-1,4-epoxide
BAB	1,2-bis(1-*N*-7-azaindolyl)benzene (BAB)
BAM	bis(1-*N*-7-azaindolyl)methane
B2bipy	5,5'-bis($BMes_2$)-2,2'-bipy
1,4-BABu	1,4-bis(1-*N*-7-azaindolyl)butane
1,3-BAPr	1,3-bis(1-*N*-7-azaindolyl)propane
2,2-bipy	2,2'-bipyridyl
bipym	bipyrimidyl
BNPA	1-*N*-(5'-(dimesitylboron)pyridine-2-yl)-7-azaindole
br	broad
BrNPA	1-*N*-(5'-bromopyridin-2-yl)-7-azaindole
^oC	degree Celsius
Calcd.	calculated
Cp^*	C_5Me_5
COSY	correlation spectroscopy

d	doublet
DABP	4,4’-di(1-*N*-7-azaindolyl)biphenyl
dd	doublet of doublet
DMF	dimethyl formamide
DMSO	dimethylsulfoxide
dnbp	2,9-di-n-butyl-1,10-phenanthroline
D*o*M	directed *ortho* metalation
DPEphos	bis[2-(diphenylphosphino)phenyl]ether
DTBBAP	2,7-di-tertbutyl-4,9-bis(1-*N*-7-azaindolyl)pyrene
dtbpy	4,4’-$^{t}Bu_2$-2,2’-bipyridine
e^-	electrons
EL	Electroluminescence
EtPh	ethylbenzene
ESDPT	excited-state double proton transfer
eV	electron-volt
g	gram
GC	gas chromatography
h^+	holes
HOMO	highest occupied molecular orbital
h	hour(s)
HRMS	high resolution mass spectra
Hz	Hertz
IR	infrared spectroscopy

J	vicinal coupling constant
K	degree Kalvin
LMCT	ligand-to-metal charge transfer
LUMO	lowest unoccupied molecular orbital
LDA	lithium diisopropylamide
m	multiplet
M	mole per liter
Mes	mesityl
mg	milligram
MHz	megahertz
min	minute(s)
mL	milliliter(s)
MLCT	metal-to-ligand charge transfer
MMO	methane monooxygenase
mmol	millimole(s)
mol	mole
ms	millisecond
MS	mass spectroscopy
NAHE	6-(1-*N*-7-azaindolyl)-1,4-dihydronaphthalene-1,4-epoxide
nm	nanometer
NMR	nuclear magnetic resonance
NOESY	nuclear Overhauser effect spectroscopy
NPA	1-*N*-(pyridin-2-yl)-7-azaindole

OLEDs	organic-light-emitting devices
OTf	$CF_3SO_3^-$
PL	photoluminescence
PMMA	poly(methyl methacrylate)
1,10-phen	1,10-phenanthroline
ppm	part(s) per million
ppy	2-phenyl pyridine
rt	room temperature
s	singlet, second
SiBAM	trimethylsilyl-bis(1-*N*-7-azaindolyl)methane
SnBAM	trimethylstannyl-bis(1-*N*-7-azaindolyl)methane
t	triplet
TAB	1,3,5-*tris*(1-*N*-7-azaindolyl)benzene
TAMB	1,2,4,5-tetrakis(1-*N*-7-azaindolylmethyl)benzene
TAN	2,3,6-tris-(1-*N*-7-azaindol-1-yl)naphthalene
TBAF	nBu$_4$NF
TBAP	tetrabutylammonium hexafluorophosphate
TFE	Trifluoroethanol (CF_3CH_2OH)
THF	tetrahydrofuran
TTAB	1,2,4,5-tetrakis(1-*N*-7-azaindolyl)benzene
UV	ultraviolet
UV-vis	ultraviolet-visible

V	volt
^{o}	degree
δ	chemical shift
ε	extinction coefficient
λ	wavelength
λ_{ex}	excitation wavelength
μs	microsecond
τ	decay lifetime
Φ	photoluminescent quantum efficiency
Φ_r	photoluminescent quantum efficiency of reference compound

List of Figures

Chapter 1

Chapter 2

Chapter 5

Chapter 6

List of Tables

Chapter 2

Chapter 3

Chapter 4

Chapter 5

Chapter 6

Chapter 7

Chapter 1

Introduction

7-Azaindole is an aza analogue of indole. The chemistry of 7-azaindole and its derivatives has been extensively investigated in recent years. 7-Azaindole itself has been frequently adopted and photophysically investigated as a model for biochemical and chemical processes.[1,2,5] 7-Azaindole can self-associate *via* hydrogen bonding into a dimer (Scheme 1.1) and thus phototautomerize *via* the excited-state double proton transfer (ESDPT) process.[1] This phototautomerization process has been extensively examined due to its mechanistic implications on a proton-transfer of a specific DNA base pair {adenine (A)-thymine (T)} induced biological mutagenesis process (Scheme 1.1).[2] 7-Azaindole and its derivatives also have biological applications, for example, as anthelmintic agents,[3] and recently as bioisosteres[4] of indole or purine in diverse therapeutic areas. Its derivative 7-azatryptophan (Scheme 1.1), as an aza analogue of tryptophan, has been demonstrated to be a more effective alternative as an optical probe for studying protein structure and dynamics.[5]

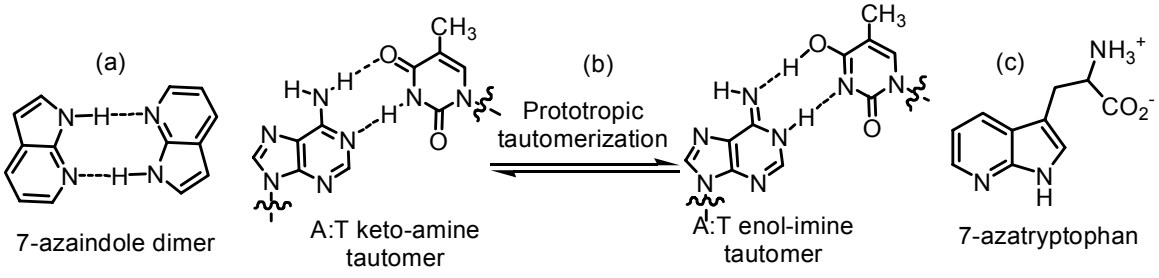

Scheme 1.1 (a) Structure of 7-azaindole dimer; (b) Prototropic tautomerization of the A:T base pair; (c) Structure of 7-azatryptophan.

Luminescent compounds have recently drawn considerable attention due to their important applications in many areas including non-linear optics, luminescent sensors,

chemical probes as well as organic light-emitting devices (OLEDs). Recently, much attention has been paid to 7-azaindole derivatives toward not only their syntheses[6,7] but also their coordination chemistry with the aims for possible material applications.[8-10] The free 7-azaindole does not emit in the visible region in solution and has a very weak emission band at $\lambda \approx 400$ nm in the solid state and alcoholic solvents or H_2O. The most significant nonradiative pathway of 7-azaindole relates directly with its N_1 proton and is attributable to the ESDPT process. By contrast, after deprotonation 7-azaindole displays a very bright blue emission in solution and the solid state. The instability of the 7-azaindole anion toward air and moisture however renders it hardly useful for practical applications. Earlier studies in our group on 7-azaindole chemistry have led to successful syntheses of a series of organic/organometallic 7-azaindole derivative compounds,[10,11,14] some of which have been used effectively as either electron-transport materials or fluorescent emitters in OLEDs.

Phosphorescent materials are particularly desirable and have several key features distinguishing them from fluorescent materials, including high device efficiency of OLEDs if used as emitters,[12] high sensitivity to triplet state quenchers such as oxygen,[13] and high color tunability *via* metal ions. Recently, many 7-azaindole-containing transition metal complexes containing Zn(II), Cu(I), Pd(II) and Pt(II) ions were developed by our group, but none of them are promising either for the OLEDs applications or the oxygen sensing.[14]

Despite their poor luminescent properties, several Pt(II) complexes were discovered to exhibit unusual reactivities toward C-H and C-Cl bond activation,[15] owing to the unique geometries imposed by the supporting ligands. To continue our research

efforts on 7-azaindole chemistry, the research described in this thesis is focused on the investigation of new reactivities and the improvement of the luminescent properties of 7-azaindole-containing complexes. The background and motivations of this thesis work will be presented briefly in the following sections of this chapter and will also be specifically addressed in the subsequent chapters.

1.1 Basic Principles of Luminescence and OLEDs

Luminescence is the emission of light from a substance and originates from the decay of excited-state electrons. Several different types of luminescence are known and they are distinguished by the way in which the excitons are generated. There are many ways of generating excited electronic states, for example, *via* the absorption of light (photoluminescence, PL), electrical energy (electroluminescence, EL), chemical energy (chemoluminescence), or mechanical energy (triboluminescence).[16] Based on the nature of the emissive transitions however, there are only two pathways for the emissive decay of excited-state electrons – fluorescence and phosphorescence. The principles of fluorescence and phosphorescence are illustrated in Figure 1.1.[16]

The spin-allowed transitions $S_1 \leftrightarrow S_o$ occur quickly with a rate of $\sim 10^8$ s^{-1} and the $S_1 \rightarrow S_o$ decay generates fluorescence which typically has a very short lifetime, from picoseconds (10^{-12} s) to nanoseconds (10^{-9} s). In contrast, the $T_1 \leftrightarrow S_0$ transition violates the spin conservation rules and is therefore a spin-forbidden transition. Accordingly, the $T_1 \rightarrow S_o$ decay occurs much slowly and the resulting phosphorescence usually has a much longer lifetime in the regime of microseconds (10^{-6} s) to seconds. Besides these two

emissive decays, the $S_1 \rightarrow S_o$ and $T_1 \rightarrow S_0$ transitions can also take place *via* a competing nonemissive pathway known as thermal decay.

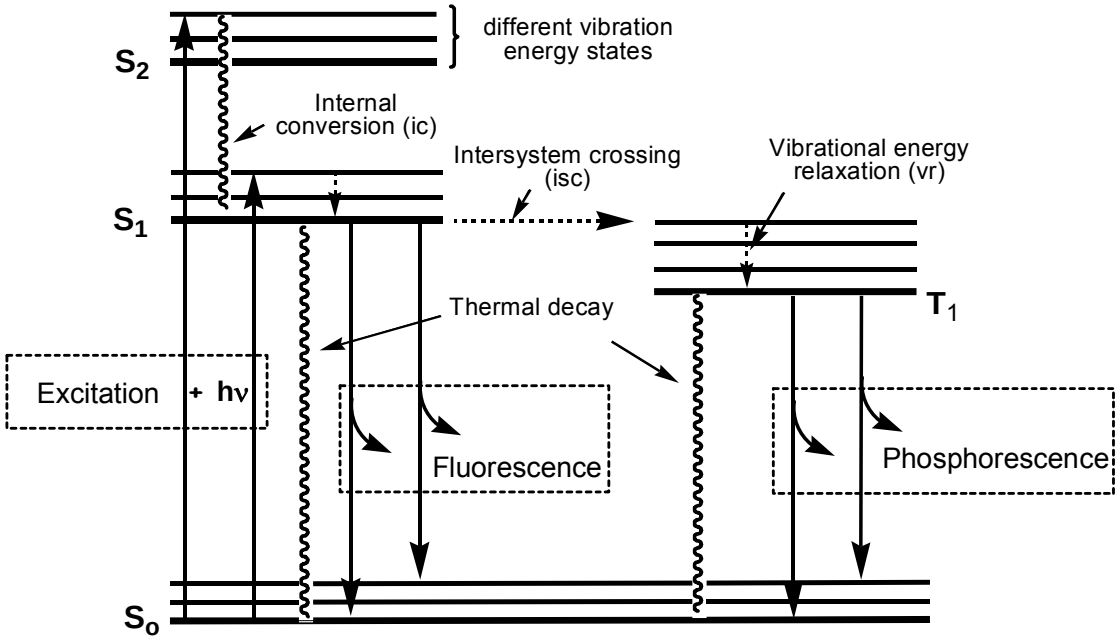

Figure 1.1 An illustrative diagram of the principles of luminescence.

Organic substances, particularly aromatic molecules, can exhibit both fluorescence and phosphorescence emissions ($\pi^* \rightarrow \pi$). The phosphorescence emissions in pure organic compounds however usually have very long lifetimes (~seconds) and are prone to various quenching processes. In addition, they are generally very weak and can only be observed after depressing the thermal decay pathway by using low temperature emission measurements. In contrast, the phosphorescence emissions of metal complexes can be significantly enhanced by heavy metal ions *via* spin-orbital coupling, which facilitates the S_1 and T_1 state mixing and/or the inter-system crossing (isc) process and thus promotes the phosphorescence.[17]

The nature of the phosphorescence emission from a metal complex depends largely on the relative energy level of the *d* orbitals of the metal center and the ligand. If

both the HOMO and LUMO are dominated by the contributions from the ligand, the phosphorescence is usually ligand-centered (LC) $\pi^* \rightarrow \pi$ transitions.[18] If the HOMO or LUMO is dominated by the contributions from the metal center but the corresponding LUMO or HOMO from the ligand, the phosphorescence can be described as transitions of either metal-to-ligand charge transfer (MLCT) or ligand-to-metal charge transfer (LMCT) excited state to the ground state.[19,20]

Lanthanide emissions are a specific case of phosphorescent emissions. The emissive transitions for lanthanide emissions occur between two spin-forbidden states involving 4f orbitals. Lanthanide emissions often exhibit sharp peaks with a very narrow emission band, akin to the atomic emissions.[21,22] Because the absorption coefficients for the corresponding transitions are very low (< 10 $M^{-1} \cdot cm^{-1}$), lanthanides usually need to be excited indirectly, as illustrated in Figure 1.2.[21]

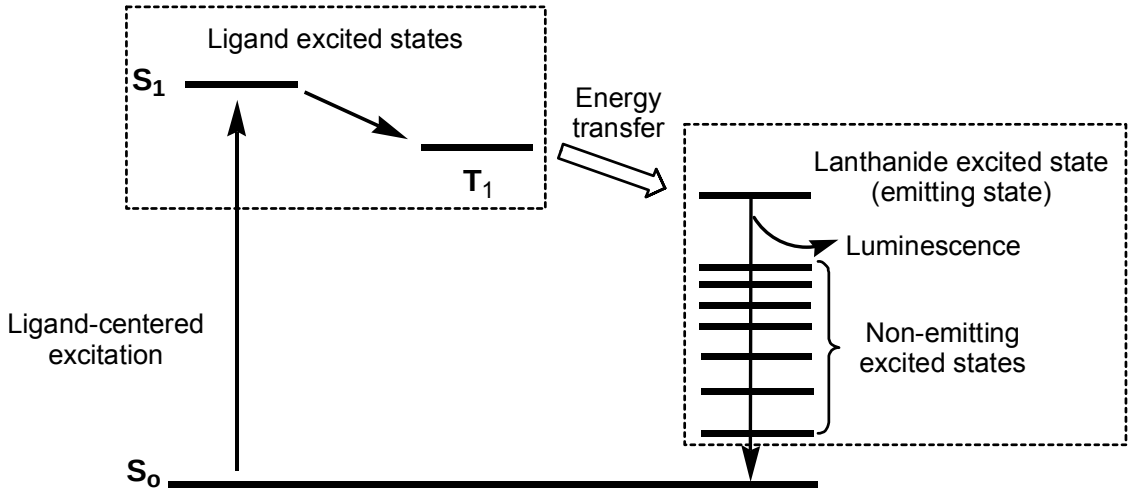

Figure 1.2 Luminescence principle for lanthanide complexes.

The initial ligand excitation and the subsequent electron internal conversion (ic) (Figure 1.1) result in the ligand S_1 excited state. The intersystem crossing (isc) ($S_1 \rightarrow T_1$) facilitated by the lanthanide ion then leads to the ligand T_1 excited state (Figure 1.2). If

the emitting excited-state energy level of the lanthanide ion is lower but close to the T_1 state (Figure 1.2), the relatively long lifetime of the T_1 state then allows energy transfer (not electron transfer) from the ligand to the lanthanide ion, resulting in the relaxation of the ligand T_1 excited state to the ligand ground state S_o and the excitation of the lanthanide ion from its ground state to the excited state. The subsequent relaxation of the excited lanthanide ion results in the lanthanide phosphorescence. However, the energy transfer process in lanthanide complexes is often inefficient, and as a result the ligand emission is often observed as part of the emission spectrum. Furthermore, if the energy emitting state of the lanthanide ion has a higher energy level than the ligand T_1 excited state, the energy of the ligand may potentially be transferred to the closely packed non-emitting excited states of the lanthanide ion and consumed by non-radiative decay.

Organic electroluminescence phenomenon was discovered in the early 1960s with anthracene crystals.[23] For photoluminescence (PL), the emission is triggered by the absorption of photons (Figure 1.1). The excitation process of organic electroluminescence is however different from PL, as illustrated by the basic working mechanism of a single layer organic electroluminescent cell in Figure 1.3.

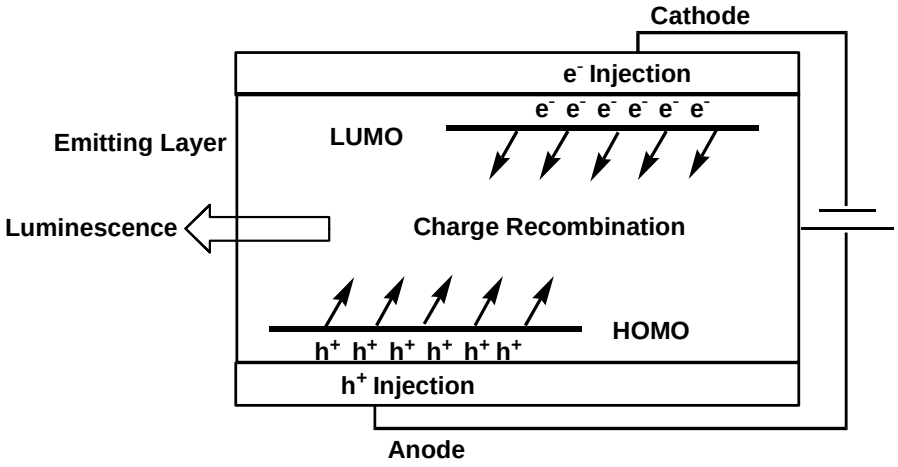

Figure 1.3 An illustrative diagram of the basic working mechanism of a single layer organic electroluminescent cell.

A cathode injects electrons into the LUMO of the emissive material, and an anode simultaneously injects holes into its HOMO. The charge carrier recombination in the emitting layer may result in the EL emission, which resembles the PL of the emitting material. For practical applications, OLEDs are usually fabricated with multi-layered structures to enhance charge transport across the organic layers and the device efficiency. Many issues of OLEDs are currently being investigated by materials chemists, engineers, and device physicists. The materials aspect of OLED technologies have been extensively covered in recent literature, thus will not be presented in this chapter.[24]

1.2 Recent Developments in 7-Azaindole Chemistry

Although only a very small number of natural alkaloids contain the 7-azaindole motif, numerous unnatural bioactive 7-azaindole derivatives have recently appeared in the literature of the medicinal chemistry.[3,4] From a chemistry viewpoint, the 7-azaindole molecule consists of both an electron-deficient pyridine motif and an electron-rich pyrrole motif, thus not only allowing diverse chemical reactivities but also potential applications in coordination chemistry.

1.2.1 New synthetic approaches for 7-azaindole derivatives

Some of the representative new strategies for the syntheses of 7-azaindole derivatives are illustrated in Scheme 1.2, where the cyclization was accomplished under various conditions.[6a] From a synthetic viewpoint, these protocols are essentially borrowed from the indole synthesis and all applicable in practice toward producing a variety of other heterocycles after minor modifications.[6a,6b]

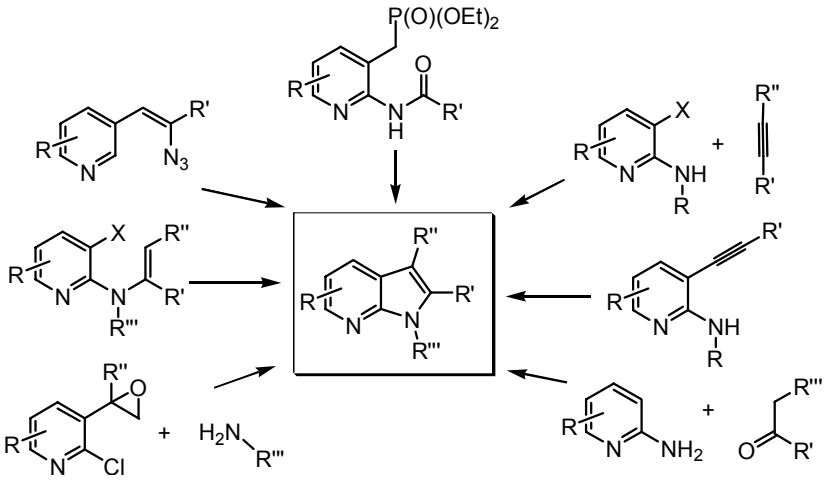

Scheme 1.2 Representative strategies for 7-azaindole syntheses.

The functionalization of 7-azaindole frequently requires multi-step conversions, as illustrated by its C2, C3 and C5 arylation in Scheme 1.3.[7] Compared to these stepwise functionality transformation protocols, direct functionalization of 7-azaindole C-H bonds apparently offers great synthetic and economical advantages by avoiding either additional halogenation steps or tedious N-H pre-protection and deprotection steps, as shown in Scheme 1.3. Recently, direct arylation of heterocyclic aromatics *via* C-H bond cleavage has drawn much attention. The advances in this research area will be discussed briefly in section 1.6.

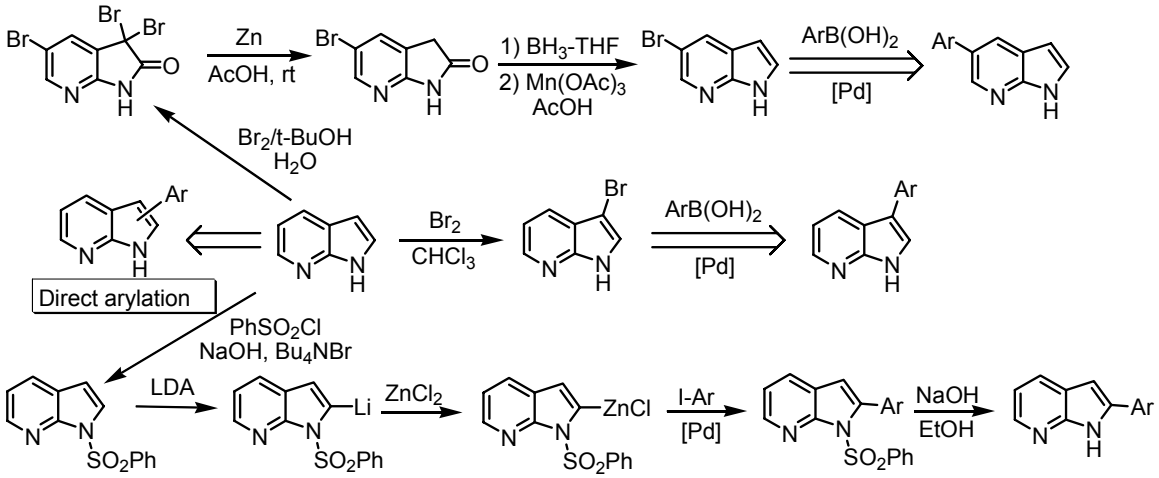

Scheme 1.3 Preparative protocols for the C2, C3 and C5 arylation of 7-azaindole.

To overcome the instability of the 7-azaindole anion and exploit its bright luminescence, two simple but effective strategies have been used. The first approach is to replace the N_1 proton with other functionalities. The N(1) methylation of 7-azaindole was indeed reported to result in a high fluorescence quantum yield increase in H_2O from 0.03 to 0.55.[1d] Recently, several modern C-N coupling methods have been developed,[25] which are applicable towards the direct N_1-arylation of 7-azaindole. Taking advantages of these methods, our group has recently synthesized and investigated a series of 7-azaindole derivatives with the intention of studying their potential applications in OLEDs.[11] Some examples are illustrated in Chart 1.1. These organic molecules are stable and contain one or more built-in 7-azaindolyls as luminophors. Some of these 7-azaindole derivatives were indeed found to be reasonable emitters for OLEDs. Figure 1.4 shows the X-ray structure of one 7-azaindole derivative 4,4'-di(1-*N*-7-azaindolyl)biphenyl (DABP) and a photograph of its bright blue emission from an OLED device.[11e]

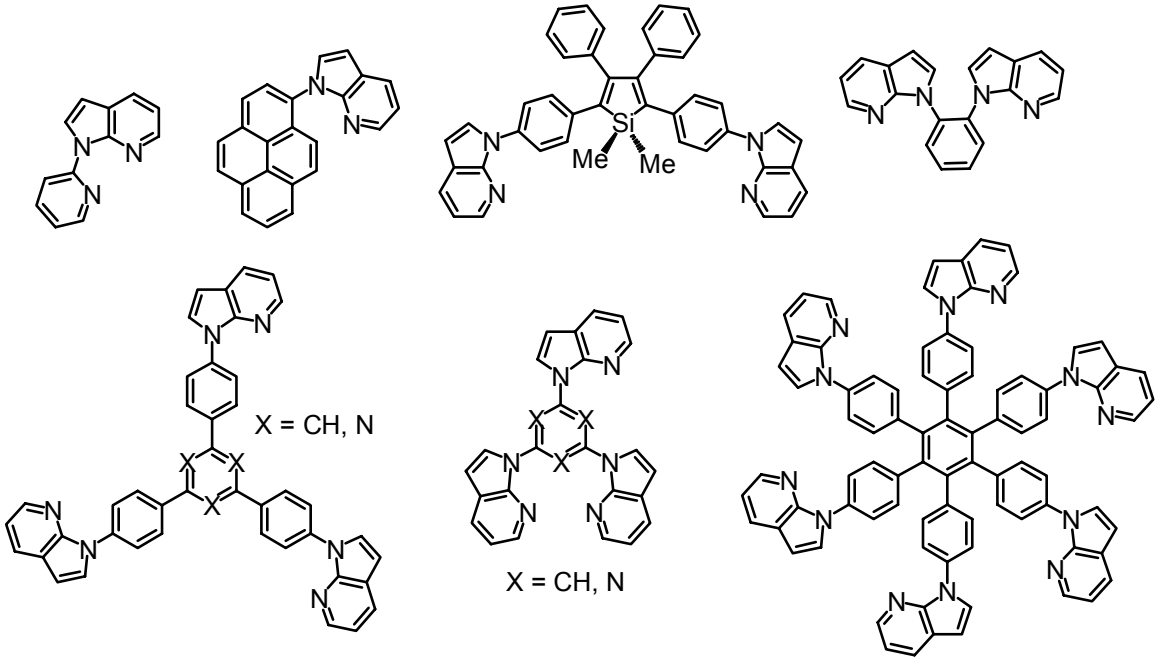

Chart 1.1 Representative 7-azaindole derivatives developed by our group.

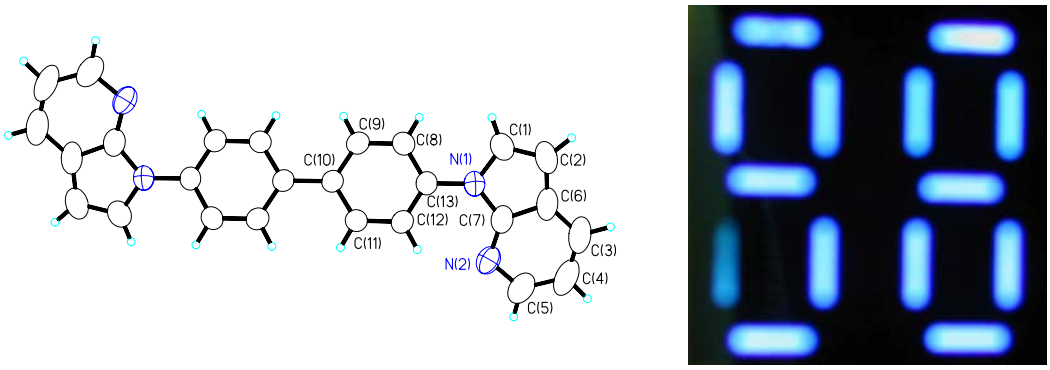

Figure 1.4 Crystal structure of the compound 4,4'-di(1-*N*-7-azaindolyl)biphenyl (DABP) (left) and a photography of its blue emission from an OLED device (right).[11e]

1.2.2 Coordination chemistry of 7-azaindole and its derivatives

As an alternative method to overcome the instability of the 7-azaindole anion, the stabilization of 7-azaindole anion *via* its binding with metal ions has also been examined by us and others. The 7-azaindole anion itself can display η^1-N (pyrrole N or pyridine N) and η^2-N,N bonding modes. Previous studies of coordination of 7-azaindole with main group elements were mostly performed by our group focusing on coordination with group 13 elements particularly aluminum and boron.[10] The transition metal complexes of 7-azaindole and its derivatives have been reported by several research groups.[8,9,14,15]

1.2.2.1 Aluminum and boron 7-azaindole complexes

Our previous work has shown that aluminum complexes of the 7-azaindole anion can be synthesized readily by the reaction of $Al(CH_3)_3$ with 7-azaindole *via* the elimination of CH_4.[10] Depending on the stoichiometry and the reaction conditions, a variety of Al(III) complexes from mononuclear, dinuclear, trinuclear to tetranuclear can be obtained. For example, a mononuclear compound such as $Al(CH_3)(\eta^1\text{-}N_1\text{-7-azain})_2(\eta^1\text{-}N_1\text{-7-azainH})$ (**1.1**)[10j] was synthesized by using excess 7-azaindole. With a ratio of

$Al(CH_3)_3$: 7-azaindole in 1:1 or 1:2, complex $Al_2(CH_3)_4(\eta^2$-*N,N*-7-azain$)_2$ (**1.2**)[10e] and $Al_2(CH_3)_2(\eta^2$-*N,N*-7-azain$)_4$ (**1.3**)[10e] could be obtained, respectively. Complexes **1.2** and **1.3** emit bright blue fluorescence (λ_{max} = 430 nm for **1.2**, 442 nm for **1.3**), both with a photoluminescent efficiency of ~40% in solution relative to that of 9,10-diphenylanthracene. The blue color emission is attributable to the 7-azaindole based $\pi^* \rightarrow \pi$ transition. Despite their high melting points (~300 ^oC), complexes **1.2** and **1.3** are not stable enough for OLED applications.

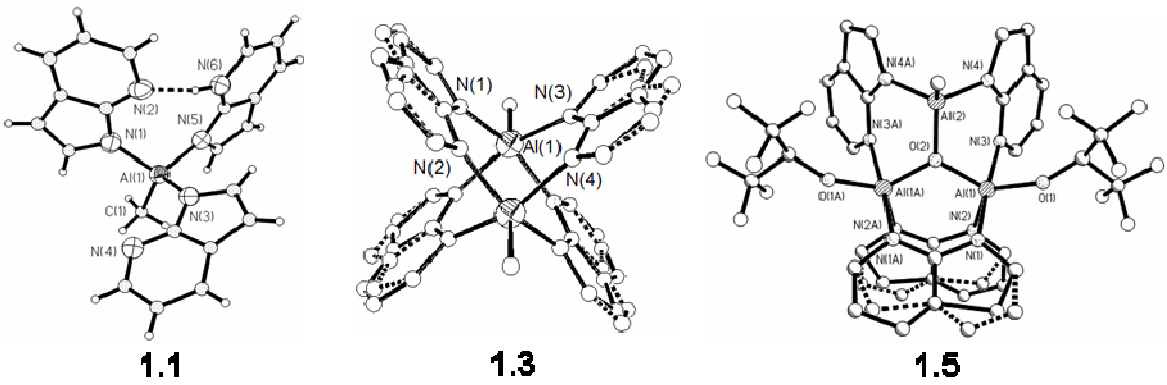

1.1 **1.3** **1.5**

Figure 1.5 Crystal structures of **1.1**, **1.3** and **1.5**.[10e,10j]

To improve the stability, the replacement of Al-*CH*$_3$ groups with alkoxo ligands and the introduction of oxo ligands were attempted, leading to the syntheses of a series of new Al(III) complexes, for example, $Al_2(\mu$-$OCH(CF_3)_2)(CH_3)(\eta^2$-*N,N*-7-azain$)_2(OCH(CF_3)_2)_2$ (**1.4**), $Al_3(\mu_3$-$O)(CH_3)(\eta^2$-*N,N*-7-azain$)_4(OCH(CF_3)_2)_2$ (**1.5**), and $Al_4(\mu_3$-$O)_2(\eta^2$-*N,N*-7-azain$)_6(OCH(CF_3)_2)_2$ (**1.6**).[10e] Complexes **1.4-1.6** exhibit similar photoluminescent properties as **1.2** and **1.3**. While complex **1.4** hydrolyzes rapidly when exposed to air, complexes **1.5** and **1.6** are found remarkably stable toward air. Unfortunately, attempts to use **1.5** and **1.6** as emitters in OLEDs were unsuccessful because of their poor volatility. The X-ray structures of complexes **1.1**, **1.3** and **1.5** are shown in Figure 1.5. The observed disordering of complex **1.3** was further examined by

solution and solid state ^{27}Al NMR studies, which revealed the co-existence of two isomers for **1.3** in a 1:1 ratio in the solid state.[10i]

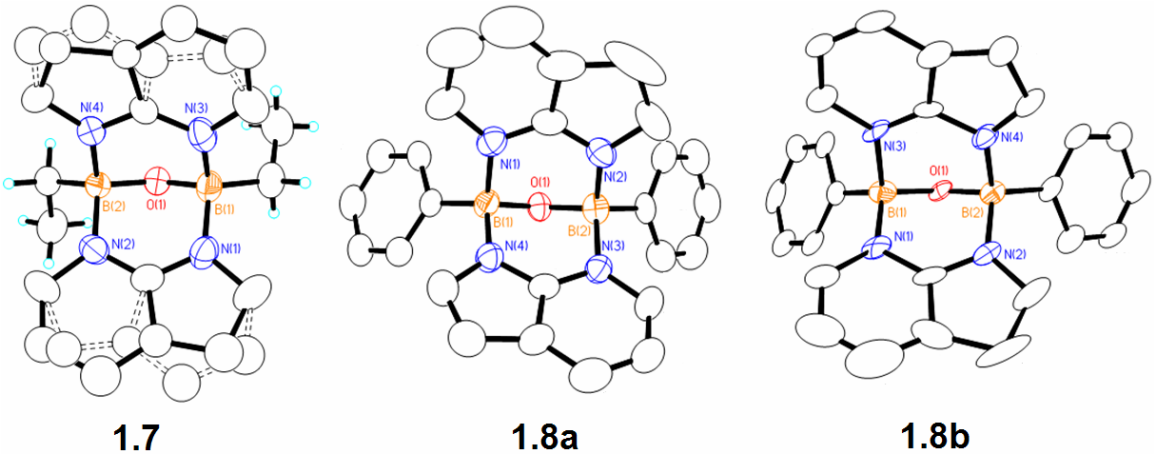

Figure 1.6 Crystal structures of **1.7**, **1.8a** and **1.8b**.[10d, 10h]

The limited stability of the Al(III) 7-azaindole complexes and their poor volatility originate mostly from the ionic characters of Al-C and Al-N bonds. In this regard, B-C and B-N bonds are rather covalent, thus boron 7-azaindole complexes are likely more promising for OLED applications. Indeed after the syntheses and evaluation of many new boron 7-azaindole complexes, two dinuclear boron compounds $B_2(O)(\eta^2$-*N,N*-7-azain$)_2(C_2H_5)_2$ (**1.7**)[10d] and $B_2(O)(\eta^2$-*N,N*-7-azain$)_2Ph_2$ (**1.8**)[10h] were found to display good stability, volatility and luminescent properties. Complexes **1.7** and **1.8** are analogs with similar structures. However, only one isomer was observed for compound **1.7**, while for compound **1.8**, both isomers **1.8a** and **1.8b** were observed in solution and the solid state, as shown by the X-ray structures in Figure 1.6. No interconversion between **1.8a** and **1.8b** was observed in solution. Compounds **1.7** and **1.8** both exhibit a bright blue fluorescent emission with emission lifetime of ~10-30 ns and λ_{max} = 450 and 430 nm, respectively. In solution the photoluminescent yields of **1.7** and **1.8** are more than 40%, compared to that of 9,10-diphenylanthracene. Compounds **1.7** and **1.8a** are especially stable and have

melting points close to 300 °C and can be sublimed readily, making them ideal emitters for electroluminescent devices. The OLEDs with **1.7** and **1.8a** as emitters display bright blue emissions; however the devices do not exhibit long-term stability.

1.2.2.2 Transition metal 7-azaindole complexes

In 1977, Cotton and coworkers designed and synthesized an 7-azaindole containing dinuclear compound $Mo_2(\eta^2\text{-}N,N\text{-}7\text{-azain})_2(PEt_3)_2(Cl)_2$ (**1.9**),[8] whose crystal structure is shown in Figure 1.7. Compound **1.9** has a formal Mo-Mo quadruple bond which is 2.125(1) Å in length. Its two anionic 7-azaindoles both function as a η^2-*N,N*-bridging ligand. In 1993, a tetranuclear zinc complex $Zn_4(\mu_4\text{-O})(\eta^2\text{-}N,N\text{-}7\text{-azain})_6$ (**1.10**) was obtained by Che and coworkers, which is stable toward air and moisture, exhibits bright blue fluorescence, and can sublime under vacuum.[9a] In 1998, the application of this compound as a bright blue emitter in OLEDs was reported by the same group.[9b]

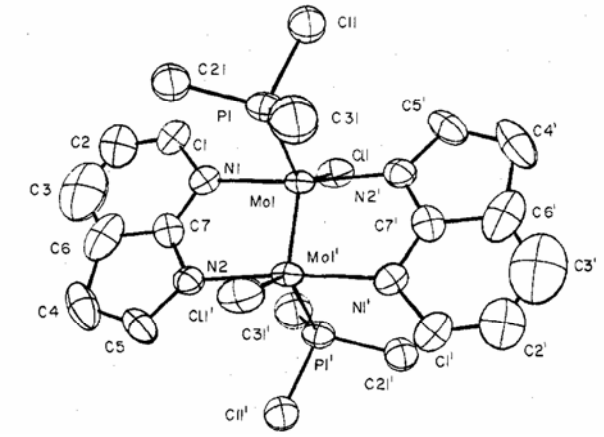

Figure 1.7 Crystal structure of **1.9**; β-carbons of the ethyl group in PEt_3 were omitted for clarity.[8]

Among the N_1-arylated 7-azaindole derivatives we developed, many have multiple binding sites and can act as chelating ligands for metal ions.[11] Since transition metal ions such as Zn(II), Cu(I), Pt(II), Pd(II) and Ru(II) can promote phosphorescence which is

highly desirable for OLED applications, we recently initiated the syntheses of various transition metal complexes using chelating 7-azaindole derivative ligands.[14,15] A few Zn(II), Pt(II), Pd(II) and Cu(I) complexes have been obtained and their luminescent properties have been studied.[14] The structures of a mononuclear Zn(II) complex $Zn(NPA)(OAc)_2$ {NPA = *N*-(2-pyridyl)-7-azaindolyl} (**1.11**)[14m] and a trinuclear Pd(II) complex $Pd_3(TAB)(Cl)_4$ (**1.12**)[14n] (TAB = 1,3,5-tris(*N*-7-azaindolyl)benzene) as representative examples are shown in Figure 1.8. These complexes however mostly display very weak phosphorescence at room temperature and are not suitable as emitters for OLEDs or sensors for O_2. Further development of phosphorescent metal complexes is therefore necessary.

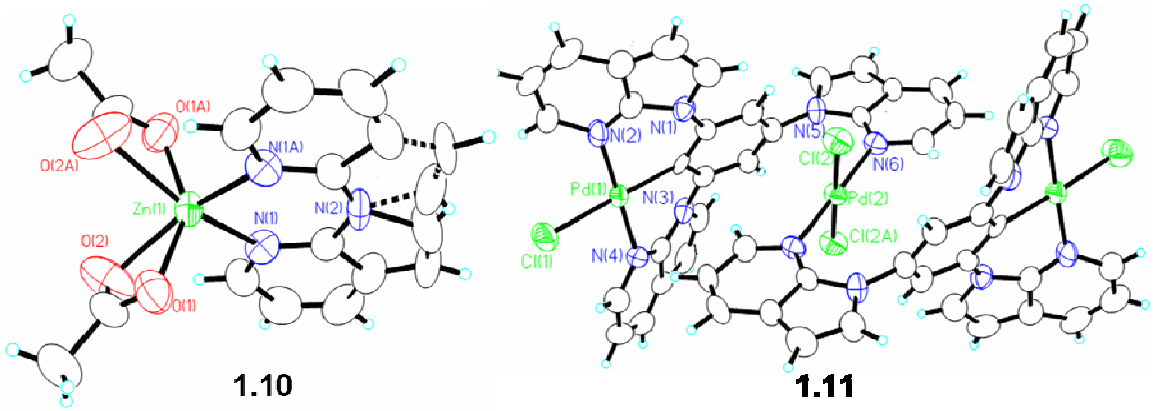

Figure 1.8 Crystal structures of **1.11** and **1.12**.[14m, 14n]

In addition to photophysical properties, another important aspect of 7-azaindole containing transition metal complexes is their reactivities. Previously our group discovered that 7-azaindole containing Pt(II) complexes can promote facile benzene C-H bond activation.[15a,15c] The 7-azaindolyl derivative ligands were found to be able to block the fifth binding site of the Pt(II) center, which makes the Pt(II) complexes potentially useful for regioselective C-H activation. Recently, a dinuclear Pt(II) complex of the

1,2,4,5-tetrakis(*N*-7-azaindolyl)benzene (TTAB) ligand has been found to display an unusual reactivity toward multiple benzene C-H activation and C-Cl activation.[15b,15d] These remarkable preliminary findings warrant our continued research efforts in exploiting new reactivities of 7-azaindole containing metal complexes, particularly Pt(II) mediated C-H activations with the ultimate goal of direct hydrocarbon functionalization.[26-28]

1.3 Developments of Hydrocarbon Activation and Functionalization Systems

The development of various homogenous cross-coupling strategies has progressed rapidly in last few decades with the advance of transition metal chemistry. For example, the Pd(0)/Pd(II) mediated cross-coupling reactions have nowadays become the most popular synthetic protocols for the construction of new C-X (X = C, N, or O) bonds.[26] Nevertheless, all of these methods frequently encounter critical limitations in their scopes because of the inaccessibility of appropriate organometallic species (typically M = B, Zn, Sn, or Si) as nucleophiles or halogened hydrocarbons as electrophiles.[26a] Moreover, the cost of such reagents and the demands for sophisticated equipment or harsh reaction conditions in utilizing these cross-coupling protocols significantly limit their applications not only in industry but also in academic laboratories.

C–H bonds are ubiquitous in organic molecules. From this perspective, direct coupling of various molecules *via* their C-H bonds would be of immense economic value. However, C-H bonds are notoriously inert toward organic reactions as a result of their high bond energy and low polarity. Developing direct C-H/C-H coupling methods is therefore particularly challenging.[27] Consequently, despite their rising cost, aliphatic

hydrocarbons have been mostly used as fuels. This however not only consumes our dwindling and non-renewable fossil fuel resources in an uneconomical way but also leads to the generation of greenhouse gases.[28] Nevertheless, aliphatic hydrocarbons even as fuels often have some undesired problems. For example, methane as the major component of natural gas is challenging to liquefy, thereby rendering its transportation difficult. In contrast, methanol is a typical liquid product and also one of the most important chemicals in industry.[29] Thus, the facile conversion of hydrocarbons into synthetically more useful liquid products is highly desired.

1.3.1 Background

Direct alkane C-H functionalization methods are potentially achievable. Methane as well as other alkanes can be transformed into methanol or other aliphatic alcohols by bacteria *via* an oxidoreductase namely methane monooxygenase (MMO) under aerobic conditions. The mechanism of such a biological methane oxidation process has been extensively studied and reviewed.[30] Structure, function and mechanistic analyses reveal that the MMO has two iron(II) centers which initially bind and activate O_2, resulting in the subsequent formation of a Fe(III)-O-Fe(IV)-O· species, in which the terminal oxo displays a radical reactivity. This radical species can then oxidize methane *via* radical processes, leading to methanol as the product. Many other hydroxylases such as prolyl hydroxylase, lysyl hydroxylase, dopamine beta hydroxylase can also directly introduce one –OH functionality selectively to the corresponding substrates. These biological processes all show radical characters and display consistently a high selectivity without over-oxidizing the products.

By contrast, while hydrocarbons are found chemically reactive toward super acids or radical reactions,[31,32] without appropriate controls akin to those by enzymes, these reactions frequently suffer poor selectivity, thus limiting their practical applications. On the other hand, the direct oxidation processes require sophisticated engineering designs and controls but cannot avoid product over-oxidation. The current industrial process for large scale syntheses of liquid chemicals such as methanol from aliphatic hydrocarbons is a multi-step and energy-demanding conversion process.[33] Accordingly, to exploit inert C–H bonds more economically, their selective activation is crucial.

The structures and functions of enzymes are instructive. The active sites in most enzymes involve transient metal ions. Therefore, considerable research efforts have been directed to the investigation of the relevant transition-metal chemistry. Since the early seminal studies by Chatt, Shilov and Bergman, selective hydrocarbon C-H activation has been demonstrated to be facile on many transition-metal centers.

Hydrocarbon C-H activation at a transition-metal center typically results in a reactive organometallic species (R-M) (Scheme 1.4). The driving forces to split a strong C-H bond come from the energy compensation by the formation of strong M-C bonds,[34] either assisted by the simultaneous formation of strong M-H bonds in the intermediates, or the large entropy gain from releasing volatile products.

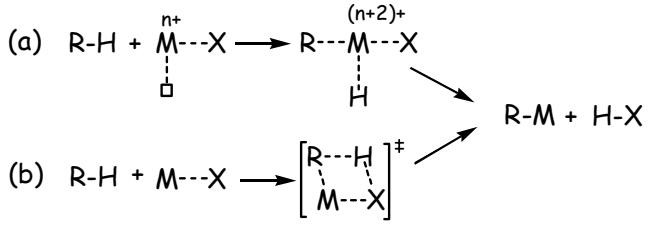

Scheme 1.4 Mechanistic pathway for oxidative addition (a) or σ-bond metathesis (b).

Mechanistically, there are mainly two different pathways for transition-metal mediated hydrocarbon C-H activation reactions, namely oxidative addition and σ-bond metathesis.[27] As illustrated in Scheme 1.4, an oxidative addition process requires a vacant M^{n+} coordination site as well as the accessibility of its M^{n+2} oxidation state, and therefore is mostly favored for electron-rich late transition metals. This pathway results in a formal +2 increase of the metal center from M^{n+} to $M^{(n+2)+}$, along with simultaneous formation of both M-C and M-H bonds. The inaccessibility of the M^{n+2} oxidative state by the early transition-metal ions particularly those with d^o configuration precludes the oxidative addition pathway. Instead, C-H activation involving the early transition metal ions usually occurs by the σ-bond metathesis process. To avoid a formal oxidative state change on the metal center, such a process occurs *via* a [2 + 2] four-centered transition state (Scheme 1.4), which does not require electron back-donation from the metal center.

1.3.2 Early hydrocarbon C-H activation studies

Although some Hg compounds were found in 1890s to react directly with arene molecules resulting in organometallic species, these electrophilic substitution processes are usually not deemed to be C-H activation.[35]

The initial work on C-H activation dates back to the 1960's. A Ru(0) complex $Ru(Me_2PCH_2CH_2PMe_2)_2$ was first reported by Chatt and Davidson to be able to react with a C-H bond *via* oxidative addition either intramolecularly from a ligand phosphinomethyl group or intermolecularly from a naphthalene molecule.[36] Shortly after, a number of similar examples were reported by other groups.[37] These systems usually

displayed preference toward intramolecular C-H addition or metalation over the activation of intermolecular arene C-H bonds.

Shilov and coworkers later discovered a Pt(II) center mediated H/D exchange process for methane in D_2O.[38a] The underlying mechanism for this H/D scrambling process suggests a reversible C-H activation process at the Pt(II) center, thus indicating the possibility of a Pt(II) mediated direct hydrocarbon functionalization processes. In the early 1970s, Shilov and co-workers demonstrated that, with $PtCl_6^{2-}$ as the oxidant, CH_4 can be directly transformed into methanol and chloromethane in aqueous solution by a $PtCl_4^{2-}$ catalyst, as depicted by eq. **1**.[38b] It is commonly referred to as the Shilov aqueous direct methane functionalization system.[38c]

$$CH_4 + H_2O + PtCl_6^{2-} \xrightarrow[120\ ^oC]{PtCl_4^{2-}} CH_3OH + CH_3Cl + PtCl_4^{2-} \quad \text{(eq. 1)}$$

Compared with relevant radical reactions, the Shilov system exhibits high preference for stronger C-H bonds (e.g. *regioselectivity*: $1^o > 2^o >> 3^o$ for alkane C-H; *chemoselectivity*: sp^2-C-H (aromatic) > sp^3-R*C*H_3 > sp^3-R*C*H_2OH) and is fairly effective under mild conditions, thereby offering many advantages.[38c] From a practical viewpoint, however, the original Shilov system has some intrinsic drawbacks such as the catalyst instability due to the formation of Pt black, high cost due to the stoichiometric use of an expensive Pt(IV) salt, and low efficiency, which preclude its industrial applications.

Some preliminary studies were carried by Shilov and coworkers in order to understand and improve the system.[38d] They recognized that each catalytic cycle consists of three major steps, but more detailed mechanistic investigation was thwarted by the difficulty in the verification of various short-lived reaction intermediates. To further

explore the relevant chemistry, considerable research efforts have been devoted to the mechanistic studies of stoichiometric C-H bond activation, and much progress has been achieved, as evidenced by recent literatures in this area.

1.3.3 Oxidative addition processes

Although facile intermolecular oxidative addition of aromatic sp^2 C-H bonds was reported for a number of transition metal complexes,[39] the direct observation of similar reactions for alkane sp^3 C-H bonds were not known prior to the 1980s. In 1982, the first direct observations of such processes were successively reported by Bergman[40a] and Graham[40b] (Scheme 1.5). Photolysis of $Cp^*(PMe_3)Ir^{III}H_2$ ($Cp^* = C_5Me_5$) in alkane solutions at room temperature led to the production of H_2, generating reportedly a type of coordinatively unsaturated and highly reactive Ir(I) intermediate, which *in situ* activated the alkane solvent molecules and resulted in hydrido(alkyl)metal species $Cp^*(PMe_3)Ir(H)(R)$ ($R = C_6H_{11}$, CH_3CMe_3) as products.[40a] A similar reactivity was observed from the photolysis of $Cp^*Ir^I(CO)_2$ in cyclohexane or neopentane solution, resulting in $Cp^*(CO)Ir(H)(R)$ ($R = C_6H_{11}$, CH_2CMe_3) as the products.[40b] Notably, both Ir complexes were shown to display a similar selectivity as observed in the Shilov system.

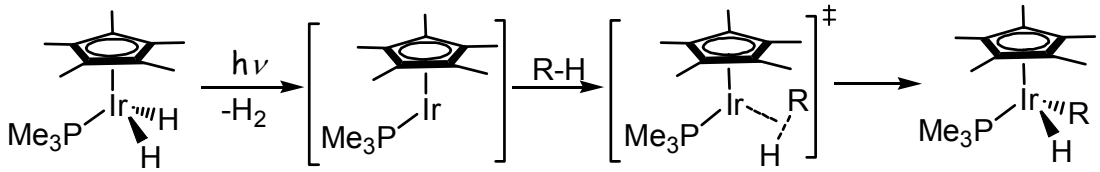

Scheme 1.5 Alkane C-H oxidative activation triggered by photolysis of $Cp^*(PMe_3)Ir^{III}H_2$ in alkane solution reported by Bergman and coworkers.[40a]

Besides those coordinatively unsaturated reactive intermediates, the intermediacy of a σ-bonded alkane complex was also soon postulated for the oxidative C-H cleavage processes to explain the observation of inverse kinetic isotope effects (KIE) obtained from a reverse R-H elimination study either with $Cp^*Rh(Ar)(H)$ by Jones[41a] in 1985 or with $Cp^*Ir(R)(H)$ by Bergman[41b] in 1986. In a σ-bonded alkane complex, the bonding electron pair of a σ-C-H bond is donated to an unfilled d orbital of the metal center to form a two-electron, three-center bond. Some degree of back-donation of the metal d electrons to the bonded C-H σ^* orbitals may be involved, particularly in the case of electron-rich late transition-metals, which helps to weaken and break the C-H bond, resulting in the oxidative addition of the C-H bond to the metal center.[27,42]

The study of σ-bonded alkane complexes at various transition-metal centers can be tracked back to the early 1970s. Among a number of methods, matrix isolation is the best for the stabilization and characterization of such reactive intermediates.[42] In 1994, Bergman and Moore collaboratively investigated the photolysis of $Cp^*Rh^I(CO)_2$ in the presence of alkane molecules in liquid Xe and Kr matrixes,[43] which not only allowed the direct observation of σ-bonded alkane complexes but also led to profound mechanistic understandings of the relevant C-H activation processes. Transition-metal σ-alkane complexes have been extensively reviewed by Perutz in 1996.[42] As highly reactive species, however, such σ-bonded alkane complexes have not been structurally characterized.

1.3.4 σ-Bond metathesis processes

For early transition-metals and lanthanides, the first alkane C-H activation processes were reported by Watson in 1983.[43] She observed that the methyl group of yttrium and lutetium methyl complexes can exchange with $^{13}CH_4$, as illustrated in Scheme 1.6. Detailed kinetic studies suggested a bimolecular pathway, which is consistent with a [2+2] four-centered transition state on the d^0 configuration metal centers. A similar reactivity was later observed on several other early transition-metal centers including Sc, Th, Zr, Ti, and Nb.[38c]

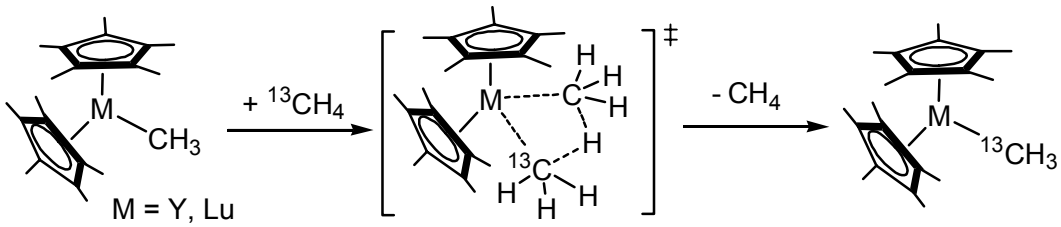

Scheme 1.6 Mechanism of the methyl exchange *via* σ-bond metathesis at the Y and Lu centers.[43]

Recently, many other transition metals such as Os, W, Re, Pd, Pt, Fe, Cu, Zr and Ni have also been found to be capable of activating alkane C-H bonds.[38c,44] The structures for some of these previously investigated transition metal compounds are illustrated in Chart 1.1.

Chart 1.2

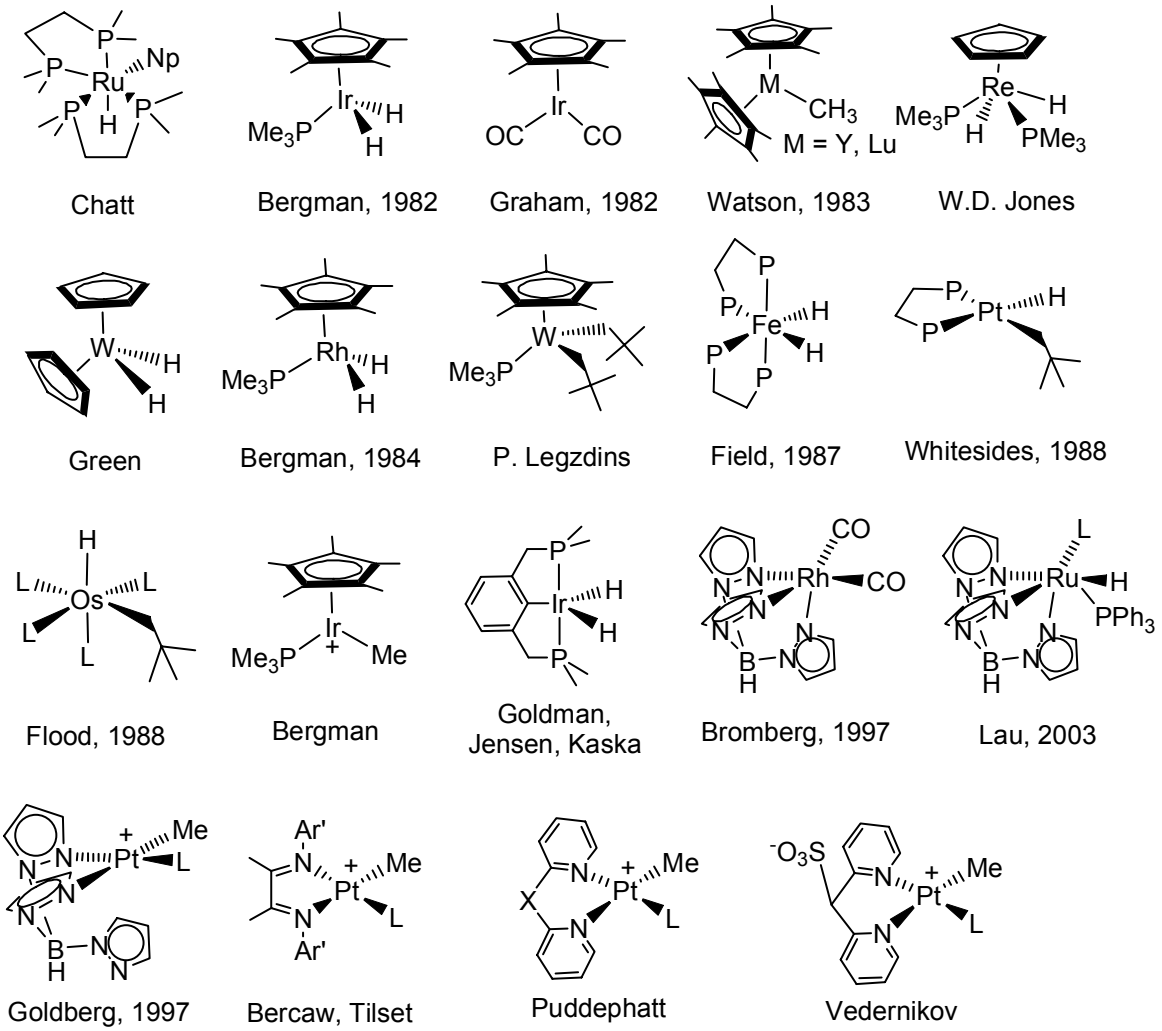

1.4 Recent Advances in Shilov Chemistry

Because of its unique features and reactivities, the Shilov chemistry has attracted considerable renewed research interests recently.[45] To develop practical C-H activation systems that can be ultimately used for hydrocarbon functionalization, the understanding of the Shilov aqueous system from mechanistic viewpoints is important and has been a focus of recent investigations.

1.4.1 Methods

In order to minimize the difficulty in mechanistically investigating the Shilov system, most investigations were performed by modeling the $PtCl_4^{2-}$ catalyst.[45] The majority of active catalysts investigated are ligated Pt(II) compounds, particularly those methylated cationic N,N-chelating Pt^{II} species that usually contain a weakly coordinated solvent molecule, as illustrated in Chart 1.2. Moreover, to avoid the undesired interference, a suitable solvent is also very important, which should meet at least three requirements. First, the solvent must not be subject to activation itself. Second, it does not coordinate to the Pt(II) center too strongly to block the subsequent activation reactions. Third, as a solvent it should dissolve or partially dissolve ionic Pt(II) complexes. Trifluoroethanol (CF_3CH_2OH) (TFE) has been found generally as a good solvent.[46] The Pt-solvent bond strength falls in the sequence of $Me_2S > Me_2SO > MeCN > H_2O > TFE > CH_4$. Furthermore, the target molecules for convenience are mostly benzene and its derivatives, or hexane, cyclopentane, cyclohexane, neopentane, *etc*. While various methods can be used for the investigation, NMR, IR and X-ray diffraction analyses have been the most commonly used methods for either kinetic study or intermediate identifications.

The mechanistic studies have been performed by many distinguished research groups and have been extensively reviewed recently.[45] The major conclusions will be briefly discussed here.

1.4.2 The C-H activation step

There are still debates on the nature of the activation step in the original aqueous Shilov system. While computational analysis indicates the possibility of σ-bond metathesis pathway in the original system,[47] experimental results with various N,N chelating Pt(II) model systems strongly and consistently support the oxidative activation pathway.[48] This divergence can be attributed to the difference in the electron-richness of the Pt(II) centers involved. N,N-Chelate ligands have much stronger electron-donating abilities to the metal center compared to Cl^-, thus facilitating the oxidative activation pathway in the model systems.

In the model Pt(II) systems, the oxidative pathway virtually all initiates with the coordination of a hydrocarbon molecule to the Pt(II) center, leading to a σ-C-H alkane Pt(II) intermediate or transition state. The hydrocarbon coordination mainly occurs *via* associative reaction pathway, without generating a complete three-coordinate Pt^{II} center.[49] However, a dissociative pathway has also been noted.[50] Following the formation of the σ-C-H alkane Pt(II) complexes, the oxidation addition proceeds to give a five-coordinate alkyl/aryl Pt(IV) hydride, which then undergoes reductive elimination resulting in an alkyl/aryl Pt(II) intermediate (Pt^{II}-R) as the activation product. The whole activation process is microscopically reversible and therefore is usually accompanied with H/D scrambling in deuterated solvents.[45] This salient feature is mechanistically useful. In fact, to avoid the difficulties in direct modeling of the methane C-H activation process, considerable work was carried on its microscopically reversible process, such as the study of protonation of various $PtMe_2$/$PtPh_2$ complexes.[51] For example, *via* protonolysis of (diimine)$PtMe_2$ complexes in the presence of MeCN (L) (Scheme 1.7), Tilset and

coworkers found a dependence of the CH_3D : CH_4 ratio on the concentration of MeCN.[51a] Since a dissociative methane release will give a constant product ratio, which only depends on the relative rates of H/D scrambling and methane release, the methane loss should occur associatively and the principle of microscopic reversibility then suggests an associative process for methane coordination to cationic Pt(II) centers toward the formation of σ-bonded methane complexes.[51a, 45c]

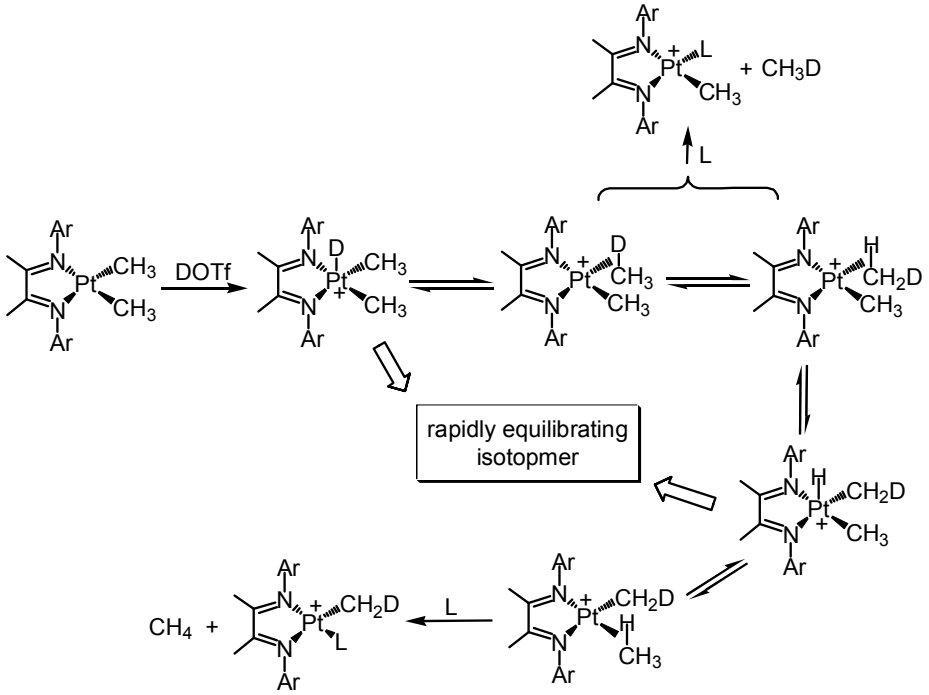

Scheme 1.7 Mechanistic pathway for the protonation of (diimine)$PtMe_2$ complexes investigated by Tilset and coworkers.[51a]

Recently, direct evidences have been obtained for the formation of alkyl/aryl Pt(IV) hydride complexes. Upon the formation *via* C-H oxidative addition to Pt(II) centers, the five-coordinate complexes can be trapped with appropriate ancillary ligands, to form stable six-coordinate complexes.[52] These results also unambiguously confirmed the oxidative activation pathway.

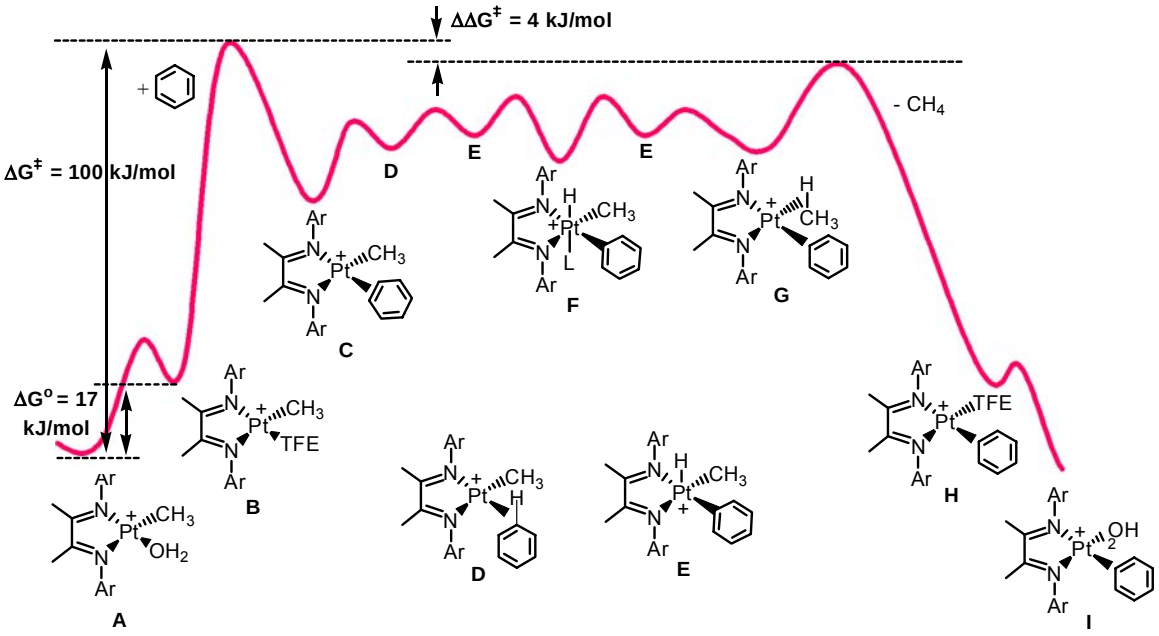

Scheme 1.8 Reaction coordinate for the benzene C-H activation by cationic Pt^{II} complexes (diimine)$Pt(CH_3)(H_2O)^+$ in TFE reported by Bercaw and coworkers.[54]

For C-H activation of arene molecules, the η^2-arene Pt(II) complexes as the key intermediates have also been identified and characterized by several groups.[53,54] The formation of this type of η^2-arene Pt(II) species has frequently been invoked to explain the strong activation kinetic preference for sp^2 aromatic C-H bonds over sp^3 alkyl C-H bonds by a Pt center.[45c] Nevertheless, the aromatic C-H activation is also more thermodynamically favored over alkyl C-H activation due to the formation a much stronger Pt-C(sp^2) bond (Scheme 1.8).[34,38c,45c] Unfortunately, the mechanistic pathway for the intramolecular conversion of such a η^2-arene Pt(II) species into a σ-C-H arene Pt(II) species remains unclear. The qualitative activation energy profile along the reaction coordinates for the C-H activation of benzene by $[(diimine)Pt(Me)(H_2O)]^+$ in TFE obtained by Bercaw and coworkers is illustrated in Scheme 1.8.[54] Obviously, the Pt-OH_2 (**A** or **I**) adduct is less reactive relative to the Pt-TFE (**B** or **H**) adduct, and along with the reaction pathways are the sequential formation of a series of reaction intermediates (**C**-

G). In addition, the biggest activation barrier along the reaction coordinates comes from the formation of **C** from **B**, an indication that the coordination of benzene to the Pt(II) center is the rate determining step.

1.4.3 The oxidation step

The new Pt(II)-C bonds formed in the activation products are very strong and cannot be functionalized directly.[55] To functionalize them readily, the activation products Pt(II)-R need to be converted to Pt(IV)-species with oxidants such as $PtCl_6^{2-}$ in the original Shilov system.[38b] It has been elegantly demonstrated by Bercaw and coworkers that this oxidization step is in essence a two-electron transfer process,[56] which opens the possibility to use other cheap and abundant oxidants as alternatives to replace the costly Pt(IV) reagent. Considerable research efforts have been carried out based on this consideration, mostly with the ultimate goal to adopt O_2 as the terminal oxidant.[57,63]

1.4.4 The functionalization step

After the generation of Pt^{IV}-R species, the desirable functionalization process follows. The C-C and C-O formation processes from Pt^{IV} centers have been comprehensively studied by Goldberg and coworkers from both six-coordinate Pt(IV) centers and five-coordinate Pt(IV) centers.[58] It has been well recognized that the functionalization process takes place specifically on five-coordinate Pt^{IV}-CH_3 intermediates, where C-C reductive elimination or direct nucleophilic attack of the bonded carbon atom by an external nucleophile can occur, resulting in the functionalized product along with the regeneration of the Pt(II) catalyst.

1.5 New Direct C-H Functionalization Systems

1.5.1 Pt(II) based systems

Besides mechanistic studies, there are also great efforts toward improving the performance of the original Shilov system and the design of better Pt(II) based systems. It has been found that replacing chlorides by a bidentate chelating ligand in the original $PtCl_4^{2-}$ catalyst can significantly increase the stability of the catalyst.[59, 45c] To improve the efficiency, the ground state effect caused by H_2O coordination to the Pt(II) catalyst needs to be minimized.[60,63] In addition, the search for cheap and effective oxidants as alternatives is highly demanded. Although the motivation for the ultimate utilization of O_2 is obvious, direct use of O_2 as the oxidant is problematic due to its inertness toward initiation thus considerable efforts have been devoted toward the activation of O_2, which has now grown into an active and diverse research area.[61,62] The current interest is the use of combination oxidants such as Cu^{2+}, Cu^{2+}/O_2, SO_3, and SO_2/O_2.[57,63]

A new milestone in Shilov chemistry was the discovery of a new Pt(II) based catalytic system by Periana and coworkers in 1998 (Scheme 1.9).[63] This system exhibits a much better catalyst stability and avoids the use of any expensive metallic oxidants. It also works very effectively with a one-pass yield of the functionalized product over 70% from methane. This one-pass conversion yield still holds the record even today.

The uses of bipyrimidyl (bipym) to support the catalyst and the fuming sulfuric acid as the reaction media in this system are the keys to its success. The formation of insoluble $(PtCl_2)_n$ and Pt black was effectively prevented, due to both the strong chelating effect of bipym for Pt(II) and the immediate re-oxidation of Pt(0) species by SO_3 upon their formation. The inertness of bipym towards such strong acidic and oxidation

conditions has been attributed to the protonation of its non-coordinating N atoms. The active oxidant is SO_3 in the system, which can likely enable O_2 to be the ultimate effective oxidant, thus resulting in an overall reaction between CH_4 and O_2 as illustrated in Scheme 1.10. Furthermore, the formation of $MeOSO_3H$ as the methane oxidation product deactivates the methyl group and protects it from further oxidation.

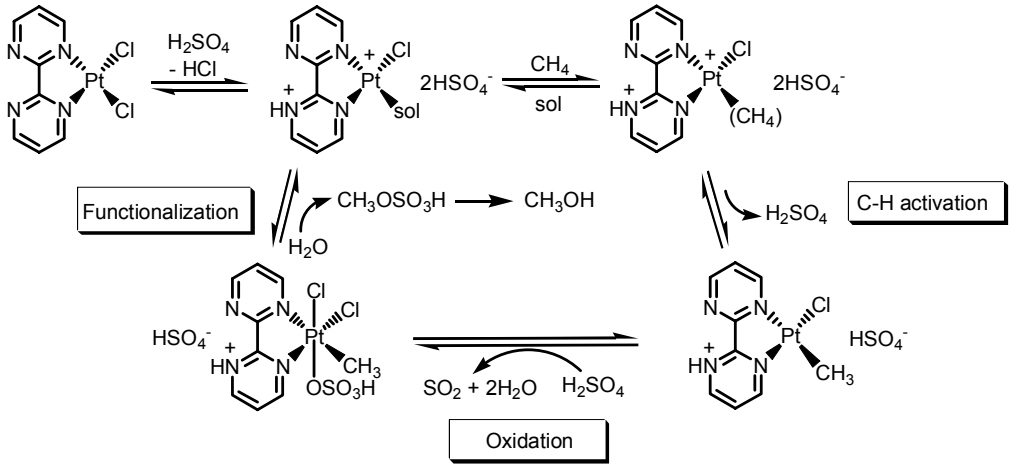

Scheme 1.9 Pt(II)-bipyrimidyl catalytic system discovered by Periana and coworkers.[63]

Scheme 1.10

$$CH_4 + H_2SO_4 + SO_3 \xrightarrow{Pt^{II}\ catalyst} CH_3OSO_3H + H_2O + SO_2$$

$$CH_3OSO_3H + H_2O \longrightarrow CH_3OH + H_2SO_4$$

$$SO_2 + 1/2\ O_2 \longrightarrow SO_3$$

$$\text{overall}\quad CH_4 + 1/2\ O_2 \longrightarrow CH_3OH$$

Despite these distinctive features, this system also suffers practical problems which hold back its industrial applications.[45c] First of all, the bulk use of fuming sulfuric acid as the reaction media is not applicable in reality. Secondly, the turn-over number of the system is still fairly limited (< 400). Moreover, the increase of water concentration in the reaction media with the reaction time can significantly decrease the turn-over

frequencies. Furthermore, the conversion of CH_3OSO_3H into the final product CH_3OH demands extensive care besides the waste of a tremendous amount of H_2O.

1.5.2 Direct borylation systems

In 1994, *via* computation study Hartwig et al. suggested that the synthesis of organoboranes *via* thermal dehydrogenative coupling of B–H and C–H bonds is energetically feasible.[64] The strengths of a M-H and a M-B bond were found to be similar, and the alkane functionalization can be driven by the formation of a B–C bond, which is 10~15 kcal/mol stronger than the original C–H bond.[64b] In 1995, Hartwig and coworkers developed an elegant stoichiometric direct photochemical dehydrogenative aromatic hydrocarbon borylation process.[65a] They demonstrated that the photolysis of boryl complexes such as $(CO)_5MnBcat$ (Bcat = B-1,2-$O_2C_6H_4$), $(CO)_5ReBcat$ and $CpFe(CO)_2Bcat$ in benzene solution can lead to the direct benzene borylation product Ph-Bcat in 45-87% yield. In addition, while a high preference towards *meta*- and *para*-borylation of toluene was observed, no *ortho*- or benzylic toluene borylation product was observed. Shortly after, similar borylation protocols were extended to the alkane sp^3 C-H bond.[65b] However, despite the fact that Hartwig and coworkers turned their photochemical processes into catalytic processes,[65c,65d] a thermal process remained unknown until an important discovery made by Smith and coworkers in 1999. They revealed that using a Cp*Ir complex in the presence of PMe_3, the catalytic and direct aromatic borylation can be achieved under mild thermal conditions, as shown in Scheme 1.11.[66a] This quickly triggered more efforts toward its exploitation. Ir and Rh complexes

have been found to be the best catalysts. While Rh catalysts usually display a higher efficiency, their Ir analogues generally exhibit a better selectivity.[66,68,69,71]

Scheme 1.11

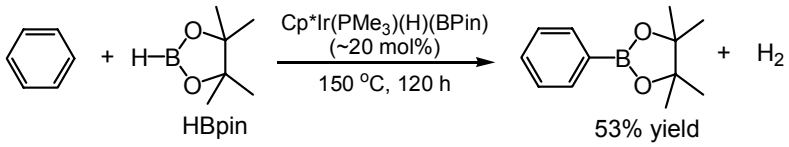

Smith and coworkers have shown that benzene and a variety of its *mono*-, *di*- and *tir*- substituted derivatives all can undergo facile dehydrogenative borylation reactions.[66] For substituted benzene, the borylation occurred exclusively at the less hindered position, which is not unprecedented and attributable to a steric effect. Strong electron-donating groups such as methoxyl (MeO-) are tolerable, whereas electron-withdrawing groups can facilitate the borylation.

For *mono*-substituted benzene, a mixture of *meta*- and *para*-isomers was usually obtained. With only an *ortho*-position available, 1,4-disubstituted and 1,3,5-trisubstituted benzene neatly afforded the corresponding *ortho*-borylation products.[66c] Remarkably, the direct borylation of 1,3-disubstituted benzene preferentially occurred at its 5-position regardless of the electronic directing effect. This behavior is unique compared to that of traditional electrophilic aromatic substitution reactions, making the direct borylation protocol an important alternative method to both the typical lithium–halogen exchange process and the directed *ortho* metalation (DoM) method[67] in preparing organoboron regents.

The borylation protocol has also found great success toward direct functionalization of heterocyclic arenes. While pyridine itself is a rather "poor" substrate

for the borylation reaction, 2,6-dimethylpyridine and 2,6-dichloropyridine can be effectively borylated at the 4-position.[66c] In addition, direct borylation of heterocyclic aromatics such as those with five-membered rings, indole and benzofuran were all achievable.[68] In 2001 with [RhCl(P^iPr_3)$_2$(N_2)] as the catalyst, a rather interesting preferential benzylic borylation toward toluene, *p*-xylene and mesitylene were observed by Marder and coworkers.[69] The proposed mechanistic pathway suggested the formation of an η^3-benzylic Rh complex as the key intermediate.

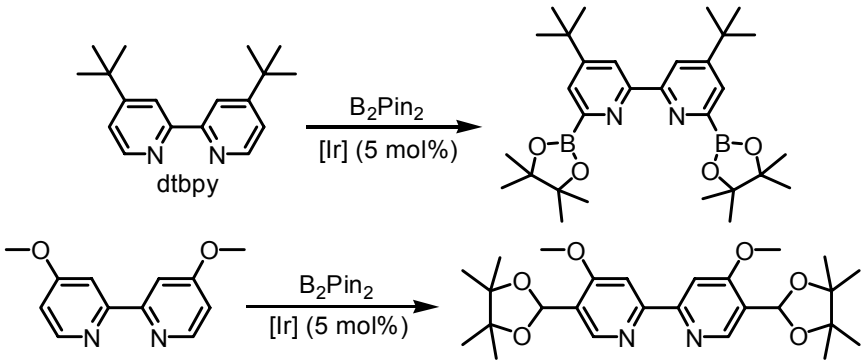

Scheme 1.12 Direct and catalytic borylation of bipyridine derivatives.

The syntheses of various diboron compounds from dihalogenated 2,2-bipyridine *via* typical lithium–halogen exchange reactions are known to be very challenging due to various competing side reactions.[70] Marder and coworkers demonstrated in 2006 that, with an Ir catalyst, the borylation of 4,4'-^{t}Bu$_2$-2,2'-bipyridine (dtbpy) by B_2pin_2 (pin = 4,4,5,5-tetramethyl-1,3,2-dioxaborolanyl) selectively occurred at its 6- and 6'- positions (~100% yield), while the borylation of 4,4'-(MeO)$_2$-2,2'-bipyridine preferentially resulted in the formation of 5,5'-diborylated product (85% yield) along with the analogous monoboronate (~15% yield) (Scheme 1.12).[71a] The preference in borylating either 5,5' or 6,6'-positions has been attributed to a balance of both electronic and steric effects.

Interestingly, they demonstrated that with the same catalyst, 2-monosubstituted pyridine can also be successfully borylated at either the 4- or 5- position. This explains why pyridine itself is a "poor" substrate, as without steric blockage to prevent the N atom from coordination, it strongly binds the active site of the catalyst, thus thwarting the subsequent borylation.

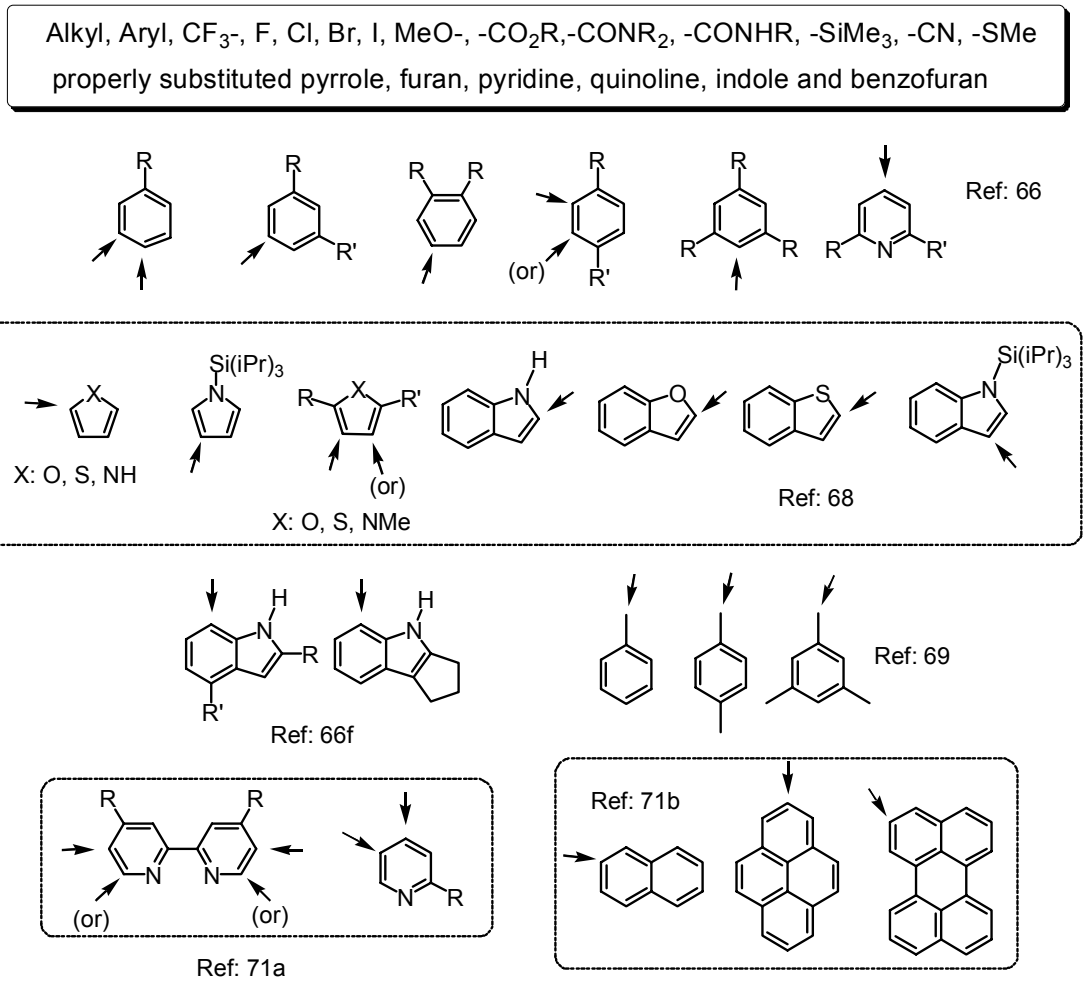

Chart 1.3 Tolerable functional groups and the borylation positions in the aromatic substrates.

The direct arene borylation process has displayed a quite broad range of functional group tolerance and also has already been proven to be a powerful new synthetic method (Chart 1.3). The borylation products can be either readily converted into various other

functionalities,[72] or directly used for subsequent Pd catalyzed C-C/C-N coupling reactions.[66b] For example, in 2002 Smith and coworkers demonstrated the possibility of one-pot functionalization of arene C–H bonds, where the catalytic borylations are followed by other metal-catalyzed events in a catalytic cascade.[66c] The idea has been further illustrated in their recent report (Scheme 1.13).[73] This could be a major advance in synthetic chemistry. At this stage, the bottle-neck of this method is the high cost due not to the catalyst but the organoboron reagents, which unfortunately render it uneconomic for bulk industrial production. It is noteworthy that due to the similar reason, none of the C-C coupling strategies using organoboron based nucleophiles are practical for industry applications.

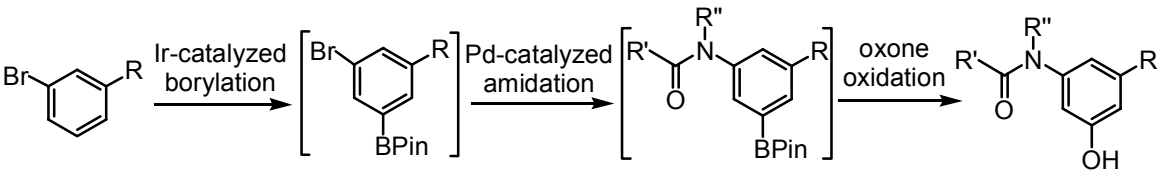

Scheme 1.13 A one-pot successive aromatic borylation-amidation-oxidation protocol for 5-substituted-3-amidophenols.

The mechanism of the borylation process has been investigated by different groups.[66,68,69,71,74] Recently, Sakaki and Hartwig reported their mechanistic study results.[74] The benzene borylation with B_2Pin_2 catalyzed by a Ir catalyst is shown in Scheme 1.14.[74a] The active catalyst is a five-coordinate Ir^{III} compound [$Ir(Bpin)_3$(dtbpy)] (**A**).

In the first step, the benzene C-H bond activation at the five-coordinate Ir(III) center (**A**) occurs through an oxidative addition pathway, leading to an unusual seven-coordinate Ir(V) intermediate (**B**). Then, the reductive elimination of Ph-Bpin from the 7-coordinate Ir(V) complex affords the borylation product along with the formation of a Ir(III) hydride intermediate (**C**). Next, the oxidative addition of B_2pin_2 is involved as

another important elementary step in the catalytic cycle, leading to a seven-coordinate Ir(V) hydride complex (**D**), through which the reductive elimination of HBpin regenerates the active five-coordinate Ir(III) catalyst (**A**). While B_2pin_2 displays a stronger reactivity than HBpin, after the consumption of B_2Pin_2, a similar catalytic cycle but involving HBpin produced by the **D** → **A** transformation will take effect *via* a seven-coordinate Ir(V) dihydride complex (**E**).

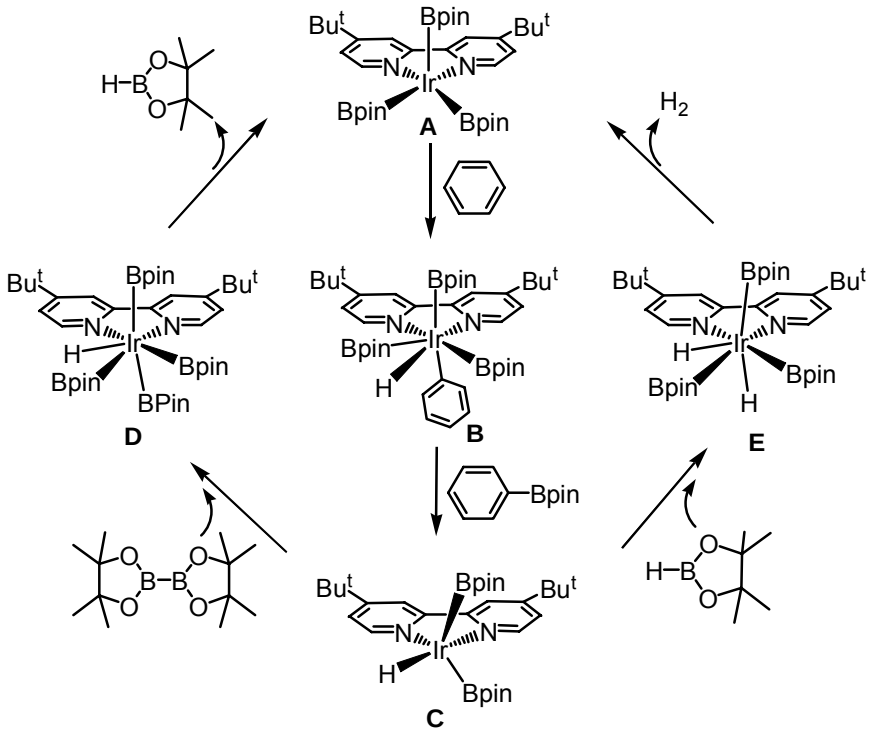

Scheme 1.14 Proposed mechanism for the direct borylation of benzene with B_2pin_2 catalyzed by [Ir(dtbpy)(Bpin)$_3$] reported by Hartwig and coworkers.[74a]

1.5.3 Other transition metal based hydrocarbon functionalization systems

Besides the Pt(II) based "Shilov" protocols and the Hartwig direct borylation methods, direct alkane functionalization has also been achieved with some other transition metal catalyzed reactions. For example, methane can be transformed into acetic acid by Pd(II) catalysts,[75a] or converted into methanol by Cu(II)/Pd(0) in the presence of

CO and O_2.[75b] A few examples of using high valence transition metal complexes such as RuO_4 and $ReMeO_3$ have also emerged recently.[76]

1.6 Direct C-H/C-X and C-H/C-X Coupling Systems

Recently, considerable progress has been achieved on the development of transition-metal mediated direct arylation reactions of heteroaromatic arenes, *via* cross-coupling of heteroaromatic sp^2 C-H bonds and aryl halides.[78] Some examples are shown in Scheme 1.15.[79] The incorporated heteroatoms typically function as directing functional groups for the initial selective C-H electrophilic metalation, where the resulting metallacycles proceed as versatile intermediates for the subsequent new bond forming processes. Several elegant cyclization protocols *via* successive intermolecular C-H/C-X (X = halogen atom) couplings have also been developed,[78a] as illustrated by Scheme 1.16.[80]

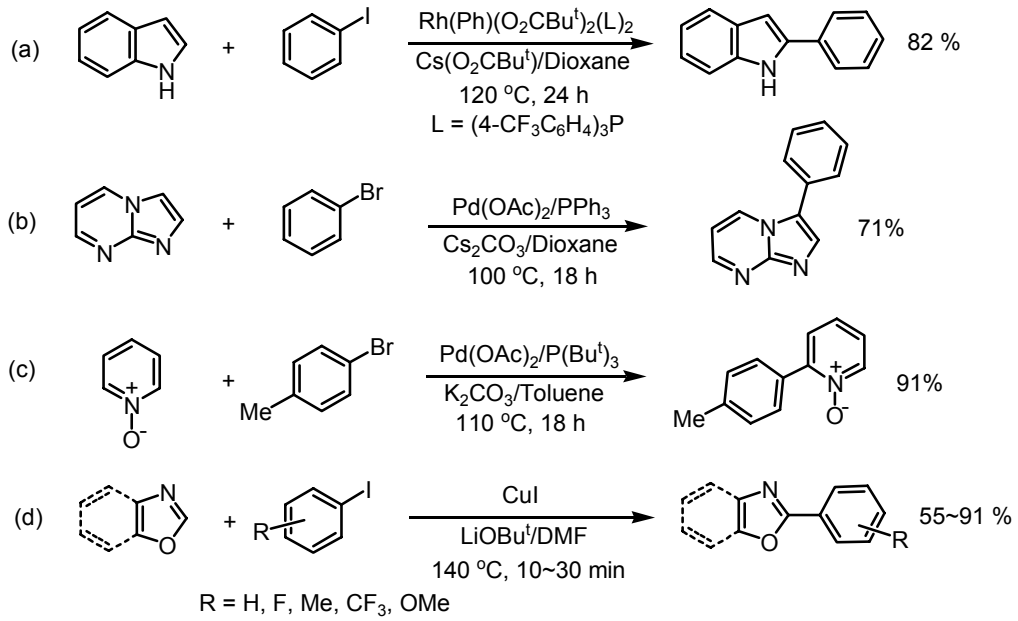

Scheme 1.15 Representive direct arylation protocols for aromatic heterocycles catalyzed by transition metal catalysts.[79a-79d]

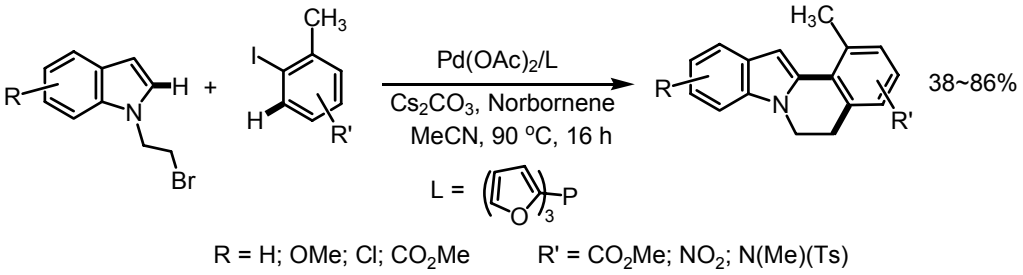

Scheme 1.16 Representive direct arylation protocols for aromatic heterocycles catalyzed by transition metal catalysts.[80]

Direct intermolecular dehydrogenative C-H/C-H couplings are even more attractive compared to C-H/C-X (X = halogen atom) couplings. To date, the oxidative dimerization of electron-rich aromatics such as phenols and anilines have been well established for synthetic applications.[81] By contrast, direct cross aromatic C-H/C-H coupling is clearly more challenging considering the high selectivity required. Much progress has however been achieved recently.[82] One recent example on the catalytic and direct cross-couplings of benzene and *N*-acetylindole is illustrated in Scheme 1.17, where the indole C3 arylation is favored under the conditions used.[82a] Remarkably, the same reaction was demonstrated by the same research group later to display a sharply contrasting preference for C2 arylation under slightly different reaction conditions, for example the replacement of $Cu(OAc)_2$ with Ag(OAc).[82b,83,84]

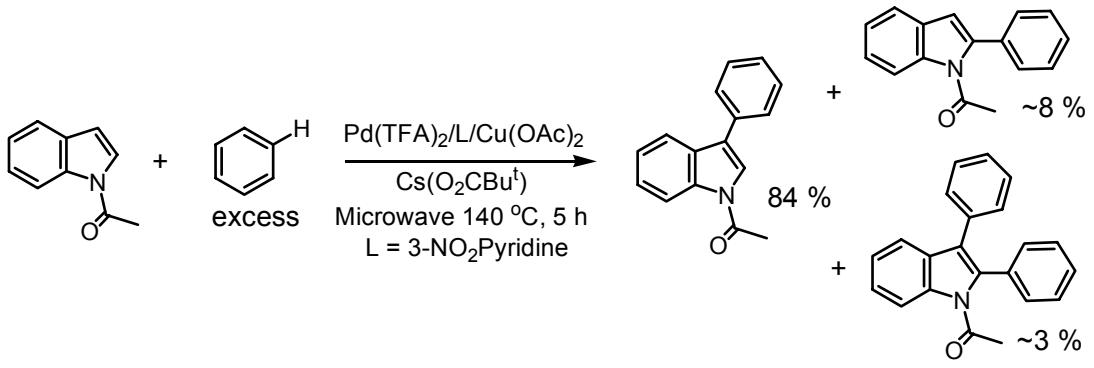

Scheme 1.17 The catalytic and direct aromatic C-H bond cross-coupling protocol reported by Fagnou and coworkers.[82a]

1.7 Scope of This Thesis

The research described in this thesis focuses on the investigation of new reactivities and the improvement of the luminescent properties of 7-azaindole-containing platinum and copper complexes, with the purposes both to extend our understandings of the Shilov direct methane functionalization system and to develop new desirable luminescent materials.

Chapter 2 describes the selectivity study of the aromatic C-H activation versus competing benzylic C-H activation of toluene and EtPh on two cationic Pt(II)(N,N-L) complexes, where N,N-L = 1,2-bis(1-*N*-7-azaindolyl)benzene (BAB) or bis(1-*N*-7-azaindolyl)methane (BAM). Chapter 3 describes the mechanistic investigation of a distinct intramolecular C-H activation driven self-assembly process, discovered on a $PtMe_2$ complex of the 1-*N*-(pyridin-2-yl)-7-azaindole ligand, toward the formation of a unique Pt_4 molecular square. Chapter 4 reports the preliminary results on the syntheses and reactivity study of 7-azaindole-containing five-coordinate *fac*-$Pt^{IV}Me_3$ complexes. In Chapter 5, the syntheses, structures, and reactivities of several novel $PtMe_2$/$PtPh_2$ complexes of new BAM/BAB derivative ligands are discussed. The syntheses, structures, and detailed luminescent property investigation of a series of Pt(II) and Cu(I) complexes that contain a triarylboron functionalized ligand are reported in Chapter 6. Chapter 7 describes the syntheses, structures, luminescent properties, and reactivities of a series of discrete dinuclear Cu(I) complexes of the 1,2,4,5-tetrakis(1-*N*-7-azaindolyl)benzene (TTAB) ligand.

Reference:

1. a) Walmsley, J. A. *J. Phys. Chem.* **1981**, *85*, 3181. b) Bulska, H. Chodkowska, A. *J. Am. Chem. Soc.* **1980**, *102*, 3259. c) Tokumura, K.; Watanabe, Y.; Udagawa, M.; Itoh, M. *J. Am. Chem. Soc.* **1987**, *109*, 1346. d) Chen, Y.; Rich, R. L.; Gai, F.; Petrich, J. W. *J. Phys. Chem.* **1993**, *97*, 1770. e) Chen, Y.; Gai, F.; Petrich, J. W. *J. Am. Chem. Soc.* **1993**, *115*, 10158. f) Chou, P.-T.; Wei, C.-Y.; Chang, C.-P.; Chiu, C.-H *J. Am. Chem. Soc.* **1995**, *117*, 7259. g) Chou, P.-T.; Yu, W.-S.; Chen, Y.-C.; Wei, C.-Y.; Martinez, S. S. *J. Am. Chem. Soc.* **1998**, *120*, 12927. h) Fernández-Ramos, A.; Smedarchina, Z.; Siebrand, W.; Zgierski, M. Z.; Rios, M. A. *J. Am. Chem. Soc.* **1999**, *121*, 6280. i) Chou, P.-T.; Wei, C.-Y.; Wu, G.-R.; Chen, W.-S. *J. Am. Chem. Soc.* **1999**, *121*, 12186. j) Chou, P.-T.; Liao, J.-H.; Wei, C.-Y.; Yang, C.-Y.; Yu, W.-S.; Chou, Y.-H. *J. Am. Chem. Soc.* **2000**, *122*, 986. k) Chou, P.-T.; Chen, Y.-C.; Wei, C.-Y.; Chen, W.-S. *J. Am. Chem. Soc.* **2000**, *122*, 9322. l) Chou, P.-T.; Yu, W.-S.; Wei, C.-Y.; Cheng, Y.-M.; Yang, C.-Y. *J. Am. Chem. Soc.* **2001**, *123*, 3599. m) Gelabert, R.; Moreno, M.; Lluch, J. M. *J. Phys. Chem. A* **2006**, *110*, 1145. n) Wu, P.-W.; Hsieh, W.-T.; Cheng, Y.-M.; Wei, C.-Y.; Chou, P.-T. *J. Am. Chem. Soc.* **2006**, *128*, 14426.
2. Ogawa, A. K.; Abou-Zied, O. K.; Tsui, V.; Jimenez, R.; Case, D. A.; Romesberg, F. E. *J. Am. Chem. Soc.* **2000**, *122*, 9917 and references therein.
3. a) Fisher, M. H.; Schwartzkopf, Jr. G.; Hoff, D. R. *J. Med. Chem.* **1972**, *15*, 1168. b) Yizun, J. Adams, G. E.; Pattick, J.; Stratford, I. J. *Eur. J. Med. Chem.* **1989**, *24*, 511. c) Lohray, B. B.; Bhushan, V.; Rao, B. P.; Madhavan, G. R.; Murali, N.; Rao, K. N.; Reddy, A. K.; Rajesh, B. M.; Reddy, P. G.; Chakrabarti, R.; Vikramadithyan, R. K.;

Rajagopalan, R.; Mamidi, R. N. V. S.; Jajoo, H. K.; Subramaniam, S. *J. Med. Chem.* **1998**, *41*, 1619.

4. For examples, see: a) Hodge, C. N.; Aldrich, P. E.; Wasserman, Z. R.; Fernandez, C. H.; Nemeth, G. A. *J. Med. Chem.* **1999**, *42*, 819. d) Ujjainwalla, F.; Walsh, T. F. *Tetrahedron Lett.* **2001**, *42*, 6441. c) Kuo, G.-H.; Prouty, C.; DeAngelis, A.; Shen, L.; O'Neill, D. J.; Shah, C.; Connolly, P. J.; Murray, W. V.; Conway, B. R.; Cheung, P.; Westover, L.; Xu, J. Z.; Look, R. A.; Demarest, K. T.; Emanuel, S.; Middleton, S. A.; Jolliffe, L.; Beavers, M. P.; Chen, X. *J. Med. Chem.* **2003**, *46*, 4021. d) Oh, S.-J.; Lee, K. C.; Lee, S.-Y.; Ryu, E. K.; Saji, H.; Choe, Y. S.; Chi, D. Y.; Kim, S. E.; Lee, J.; Kim, B.-T. *Bioorg. Med. Chem.* **2004**, *12*, 5505.
5. a) Négrerie, M.; Bellefeuille, S. M.; Whitham, S.; Petrich, J. W.; Thornburg, R. W. *J. Am. Chem. Soc.* **1990**, *112***,** 7419. b) Gai, F.; Chen, Y.; Petrich, J. W. *J. Am. Chem. Soc.* **1992**, *114*, 8343. c) Rich, R. L.; Chen, Y.; Neven, D.; Nbgrerie, M.; Gai, F.; Petrich, J. W. *J. Phys. Chem.* **1993**, *97*, 1781. d) Chen, Y.; Rich, R. L.; Gai, F.; Petrich, J. W. *J. Phys. Chem.* **1993**, *97*, 1770. e) Rich, R. L.; Gai, F.; Lane, J. W.; Petrich, J. W.; Schwabacher, A. W. *J. Am. Chem. Soc.* **1995**, *117*, 733. f) Rich, R. L.; Smirnov, A. V.; Schwabacher, A. W.; Petrich, J. W. *J. Am. Chem. Soc.* **1995**, *117*, 11850.
6. a) Cacchi, S.; Fabrizi, G. *Chem. Rev.* **2005**, *105*, 2873. b) Humphrey, G. R.; Kuethe, J. T. *Chem. Rev.* **2006**, *106,* 2875.
7. For recent examples, see: a) Zhang, Z.; Yang, Z.; Meanwell, N. A.; Kadow, J. F.; Wang, T. *J. Org. Chem.* **2002**, *67*, 2345. b) Zhang, Z.; Yong, Z.; Wong, H.; Zhu, J.; Meanwell, N. A.; Kadow, J. F.; Wang, T. *J. Org. Chem.* **2002**, *67*, 6226. c) Mendiola, J.; Castellote, I.; Alvarez-Builla, J.; Fernández-Gadea, J.; Gómez, A.; Vaquero, J. J.

J. Org. Chem. **2006**, *71*, 1254. d) Schirok, H. *J. Org. Chem.* **2006**, *71*, 5538 and references therein. e) Zheng, X.; Kerr, M. A. *Org. Lett.* **2006**, *8*, 3777. For a recent review, see: Mérour, J.-Y.; Joseph, B. *Curr. Org. Chem.* **2001**, *5*, 471.

8. Cotton, F. A.; Lay, D. G.; Millar, M. *Inorg. Chem.* **1978**, *17*, 186.
9. a) Lee, C. F.; Chin, K. F.; Peng, S. M.; Che, C. M. *J Chem Soc., Dalton Trans.* **1993**, 467. b) Ma, Y. G.; Chao, H. Y.; Wu, Y.; Lee, S. T.; Yu, W. Y.; Che, C. M. *Chem. Comm.* **1998**, 2491.
10. a) Dufour, N.; Lebuis, A. M.; Corbeil, M. C.; Beauchamp, A. L. *Can. J. Chem.* **1992**, *70*, 2916. b) Lebuis, A. M.; Beauchamp, A. L., *Can. J. Chem.* **1993**, *71*, 2062. c) Liu, W.; Hassan, A.; Wang, S. *Organometallics* **1997**, *16*, 4257. d) Hassan, A.; Wang, S. *J. Chem. Soc., Chem. Commun*. **1998**, 339. e) Ashenhurst, J.; Brancaleon, L.; Hassan, A.; Liu, W.; Schmider, H.; Wang, S.; Wu, Q. *Organometallics* **1998**, *17*, 3186. f) Gao, S.; Wu, Q.; Wu, G.; Wang, S. *Organometallics* **1998**, *17*, 4666. g) Liu, W.; Hassan, A.; Wang, S. *Organometallics* **1997**, *16*, 4257. h) Wu, Q.; Esteghamatian, M.; Hu, N.-X.; Popovic, Z. D.; Enright, G.; Breeze, S. R.; Wang, S. *Angew. Chem., Int. Ed.* **1999**, *38*, 985. i) Ashenhurst, J.; Wang, S.; Wu, G. *J. Am. Chem. Soc.* **2000**, *122*, 3528. j) Ashenhurst, J.; Wu, G.; Wang, S. *J. Am. Chem. Soc.* **2000**, *122*, 2541. k) Liu, S.-F.; Wu, Q.; Schmider, H. L.; Aziz, H.; Hu, N.-X.; Popović, Z.; Wang, S. *J. Am. Chem. Soc.* **2000**, *122*, 3671. For a review, see: Wang, S. *Coord. Chem. Rev.* **2001**, *215*, 79.
11. a) Jia, W.-L.; Wang, R.-Y.; Song, D.; Ball, S.; McLean, A.; Wang, S. *Chem. Eur. J.* **2005**, *11*, 832. b) Lee, J. H.; Motala, M.; Liu, Q. D.; Dane, J.; Gao, J.; Wang, S. *Chem. Mater.* **2004**, *16*, 1869. c) Jia, W. L.; Bai, D.-R.; M^{c}Cormick, T.; Liu, Q. D.; Motala, M.; Wang, R.-Y.; Seward, C.; Tao, Y.; Wang, S. *Chem. Eur. J.* **2004**, *10*,

994. d) Pang, J. Tao, Y.; Yang, X.-P.; D'Iorio, M.; Wang, S. *J. Mater. Chem.* **2002**, *12*, 206. e) Wu, Q.; Lavigne, J. A.; Tao, Y.; D'Iorio, M.; Wang, S. *Chem. Mater.* **2001**, *13*, 71.

12. a) Shen, Z.; Burrows, P. E.; Bulovic, V.; Borrest, S. R.; Thompson, M. E. *Science* **1997**, *276*, 2009. b) Baldo, M. A.; Lamansky, S.; Burrows, P.; Thompson, M. E.; Forrest, S. R. *Appl. Phys. Lett.* **1999**, *75*, 5. c) Lamansky, S.; Djurovich, P.; Murphy, D.; Abdel-Razzaq, F.; Lee, H. E.; Adachi, C.; Burrows, P. E.; Forrest, S. R.; Thompson, M. E. *J. Am. Chem. Soc*. **2001**, *123*, 4304. d) Chi, Y.; Chou, P. T. *Chem. Soc. Rev.* **2007**, *36*, 1421 and references therein.
13. a) Huo, C.; Zhang, H.; Zhang, H.; Zhang, H.; Yang, B.; Zhang, P.; Wang, Y. *Inorg. Chem.* **2006**, *45*, 4735. b) DeRosa, M. C.; Hodgson, D. J.; Enright, G. D.; Dawson, B.; Evans, C. E. B.; Crutchley, R. J. *J. Am. Chem. Soc.* **2004**, *126*, 7619. c) Gao, R.; Ho, D. G.; Hernandez, B.; Selke, M.; Murphy, D.; Djurovich, P. I.; Thompson, M. E. *J. Am. Chem. Soc.* **2002**, *124*, 14828.
14. a) Song, D.; Jia, W.-L.; Wu, G.; Wang, S. *Dalton Trans.*, **2005**, 433. b) Song, D.; Wang, S. *Eur. J. Inorg. Chem.* **2003**, 3774. c) Kang, Y. J.; Lee, J. H.; Song, D. T.; Wang, S. *J. Chem. Soc. Dalton Trans.* **2003**, 3234. d) Jia, W. L.; Liu, Q. D.; Wang, R. Y.; Wang, S. *Organometallics*, **2003**, *22*, 4070. e) Kang, Y. J.; Seward, C.; Song, D.; Wang, S. *Inorg. Chem.* **2003**, *42*, 2789. f) Song, D.; Schmider, H.; Wang, S. *Org. Lett.* **2002**, *4*, 4049. g) Wang, R.Y.; Song, D.; Seward, C.; Tao, Y.; Wang, S. *Inorg. Chem.*, **2002**, *41*, 5187. h) Kang, Y. J.; Wang, S. *Tetrahedron Lett.* **2002**, *43,* 3711. i) Kang, Y. J.; Song, D.; Schmider, H.; Wang, S. *Organometallics*, **2002**, *21*, 2413. j) Song, D.; Wu, Q.; Hook, A.; Kozin, I.; Wang, S. *Organometallics*, **2001**, *20*, 4683. k) Song, D.; Liu, S.-F.; Wang, R. Y.; Wang, S. *J. Organomet. Chem.*, **2001**, *631*, 175. l)

Pang, J.; Marcotte, E. J-P.; Seward, C.; Brown, R. S.; Wang, S. *Angew. Chem., Int. Ed.*, **2001**, *40*, 4042. m) Wu, Q.; Lavigne, J. A.; Tao, Y.; D'Iorio, M.; Wang, S. *Inorg. Chem.*, **2000**, *39,* 5248. n) Wu, Q.; Hook, A.; Wang, S. *Angew. Chem., Int. Ed.*, **2000**, *39*, 3933.

15. a) Song, D.; Wang, S. *Comments Inorg. Chem.*, **2004**, *25*, 1. b) Song, D.; Jia, W. L.; Wang, S. *Organometallics*, **2004**, *23*, 1194. c) Song, D.; Wang, S. *Organometallics*, **2003**, *22*, 2187. d) Song, D.; Sliwowski. K.; Pang, J.; Wang, S. *Organometallics*, **2002**, *21*, 4978.
16. Blasse, G. and Grabmaier, B.C. *Luminescent Materials* Springer-Verlag, New York, **1995**.
17. Lees, A. J. *Chem. Rev.* **1987**, *87*, 711.
18. For ^{3}LC, see examples: a) Collin, J.-P.; Dixon, I. M.; Sauvage, J.-P.; Williams, J. A. G.; Barigelletti, F.; Flamigni, L. *J. Am. Chem. Soc.* **1999**, *121*, 5009. b) Ayala, N. P.; Flynn, C. M., Jr.; Sacksteder, L.; Demas, J. N.; DeGraff, B. A. *J. Am. Chem. Soc.* **1990**, *112*, 3837.
19. For ^{3}MLCT, see examples: a) Nazeeruddin, M. K.; Humphry-Baker, R.; Berner, D.; Rivier, S.; Zuppiroli, L.; Graetzel, M. *J. Am. Chem. Soc.* **2003**, *125*, 8790. b) Tsuboyama, A.; Iwawaki, H.; Furugori, M.; Mukaide, T.; Kamatani, J.; Igawa, S.; Moriyama, T.; Miura, S.; Takiguchi, T.; Okada, S.; Hoshino, M.; Ueno, K. *J. Am. Chem. Soc.* **2003**, 125, *12971*.
20. For ^{3}LMCT, see examples: a) Lee, Y.-A.; McGarrah, J. E.; Lachicotte, R. J.; Eisenberg, R. *J. Am. Chem. Soc.* **2002**, *124*, 10662. b) Wong, C.-Y.; Che, C.-M.; Chan, M. C. W.; Han, J.; Leung, K.-H.; Phillips, D. L.; Wong, K.-Y.; Zhu, N. *J. Am. Chem. Soc.* **2005**, *127*, 13997.

21. a) Kido, J.; Okamoto, Y. *Chem. Rev.* **2002**, *102*, 2357.

22. a) Crosby, G. A.; Whan, R. E.; Alire, R. M. *J. Chem. Phys.* **1961**, *33*, 743. b) Whan, R. E.; Crosby, G. A. *J. Molec. Spec.* **1962**, *8*, 315.

23. Pope, M.; Kallmann, H. P.; Magnante, P. *J. Chem. Phys*. **1963**, 38, 2042.

24. Shirota, Y.; Kageyama, H. *Chem. Rev.* **2007**, *107*, 953 and references therein.

25. a) Kiyomori, A.; Marcoux, J. F.; Buchwald, S. L. *Tetrahedron Lett.* **1999**, *40*, 2657. b) Ma, D.; Xia, C. *Org. Lett.* **2001**, 3, 2583. c) Klapars, A.; Antilla, J. C.; Huang, X. H.; Buchwald, S. L. *J. Am. Chem. Soc.* **2001**, *123*, 7727. d) Klapars, A.; Huang, X.; Buchwald, S. L. *J. Am. Chem. Soc.* **2002**, *124*, 7421. e) Antilla, J. C.; Klapars, A.; Buchwald, S. L. *J. Am. Chem. Soc.* **2002**, *124*, 11684. f) Job, G. E.; Buchwald, S. L. *Org. Lett.* **2002**, *4*, 3703. For a review, see: Hassan, J.; Sevignon, M.; Gozzi, C.; Schulz, E.; Lemaire, M. *Chem. Rev.* **2002**, *102*, 1359.

26. a) Miyaura, N.; Suzuki, A. *Chem. Rev.* **1995**, *95*, 2457. b) Beccalli, E. M.; Broggini, G.; Martinelli, M.; Sottocornola, S. *Chem. Rev.* **2007**, *107*, 5318. c) Yin, L.; Liebscher, J. *Chem. Rev.* **2007**, *107*, 133. d) Sammelson, R. E.; Kurth, M. J. *Chem. Rev.* **2001**, *101*, 137. e) Chinchilla, R.; Nájera, C. *Chem. Rev.* **2007**, *107*, 874. f) Li, C.-J. *Chem. Rev.* **2005**, *105*, 3095.

27. a) Arndtsen, B. A.; Bergman, R. G.; Mobley, T. A.; Peterson, T. H. *Acc. Chem. Res.* **1995**, *28*, 154. b) Crabtree, R. H. *Chem. Rev.* **1995**, *95*, 987. c) Crabtree, R. H. *Chem. Rev.* **1985**, *85*, 245.

28. A review on catalysis research relevant to carbon management: progress, challenges, and opportunities: Aresta, M.; Armor, J. N.; Barteau, M. A.; Beckman, E. J.; Bell, A. T.; Bercaw, J. E.; Creutz, C.; Dinjus, E.; Dixon, D. A.; Domen, K.; Dubois, D. L.; Eckert, J.; Fujita, E.; Gibson, D. H.; Goddard, W. A.; Goodman, D. W.; Keller, J.;

Kubas, G. J.; Kung, H. H.; Lyons, J. E.; Manzer, L. E.; Marks, T. J.; Morokuma, K.; Nicholas, K. M.; Periana, R.; Que, L.; Rostrup-Nielson, J.; Sachtler, W. M. H.; Schmidt, L. D.; Sen, A.; Somorjai, G. A.; Stair, P. C.; Stults, B. R.; Tumas, W. *Chem. Rev.* **2001**, *101*, 953.

29. a) Crabtree, R. H. *The Organometallic Chemistry of the Transition Metals* Wiley, New York, **2001**. b) Olah, G. A. *Angew. Chem., Int. Ed.* **2005**, *44*, 2636.
30. Wallar, B. J.; Lipscomb, J. D. *Chem. Rev.* **1996**, *96*, 2625.
31. Schreiner, P. R.; Fokin, A. A.; Lauenstein, O.; Okamoto, Y.; Wakita, T.; Rinderspacher, C.; Robinson, G. H.; Vohs, J. K.; Campana, C. F. *J. Am. Chem. Soc.* **2002**, *124*, 13348.
32. Slskin, M.; Chludzinski, G. R.; Hulme, R.; Porcelli, J. J.; Tyler, W. E. III *Ind. Eng. Chem. Prod. Res. Dev.* **1980**, *19*, 379.
33. Anderson, R. B. *The Fischer-Tropsch Synthesis* Academic Press, Orlando, **1984**.
34. A review on M-C and M-H bond strengths: Simões, J. A. M.; Beauchamp, J. L. *Chem. Rev.* **1990**, *90*, 629.
35. Dyker G. *Handbook of C-H Transformations* WILEY-VCH, Weinheim, **2005**.
36. Chatt, J.; Davidson, J. M. *J. Chem. Soc.* **1965**, 843.
37. a) Parshall, G. W. *Acc. Chem. Res.* **1975**, *8*, 113. b) Berry, M.; Elmitt, K.; Green, M. L. H. *J. Chem. Soc., Dalton Trans.* **1979**, 1950. c) Berry, M.; Elmitt, K.; Green, M. L. H. *J. Chem.* Soc., *Dalton Trans.* **1971**, 1508. d) Ittel, S. D.; Tolman, C. A; Krusic, P. J.; English, A. D.; Jesson, J. P. *Inorg. Chem.* **1978**, *17,* 3432. e) Ittel, S. D.; Tolman, C. A; English, A. D.; Jesson, J. P. *J. Am. Chem. Soc.* **1976**, *98*, 6073
38. a) Gol'dshleger, N. F.; Tyabin, M. B.; Shilov, A. E.; Shteinman, A. A. *Zhurnal Fizicheskoi Khimii* **1969**, *43*, 2174. b) Gol'dshleger, N. F.; Es'kova, V. V.; Shilov, A.

E.; Shteinman, A. A. *Zhurnal Fizicheskoi Khimii* **1972**, *46*, 1353. c) Shilov, A. E.; Shul'pin, G. B. *Chem. Rev.* **1997**, *97*, 2879. d) Shilov, A. E.; Shteinman, A. A. *Coord. Chem. Rev.* **1977**, *24*, 97.

39. a) Tulip, T. H.; Thorn, D. L. *J. Am. Chem. Soc*. **1981***, 103,* 2448. b) Janowicz A. H.; Bergman, R. G. *J. Am. Chem. Soc*. **1981***, 105,* 3929 and references therein.
40. a) Janowicz, A. H.; Bergman, R. G. *J. Am. Chem. Soc.* **1982**, *104*, 352. b) Bergman, R. G. *Science* **1984**, *223*, 902. c) Hoyano, J. K.; Graham, W. A. G. *J. Am. Chem. Soc.* **1982**, *104*, 3723.
41. a) Jones, W. D.; Feher, F. J. *J. Am. Chem. Soc.* **1985**, *107*, 620. b) Buchanan, J. M.; Stryker, J. M.; Bergman, R. G. *J. Am. Chem. Soc.* **1986**, *108*, 1537.
42. Hall, C.; Perutz, R. N. *Chem. Rev.* **1996**, *96*, 3125.
43. Watson, P. L. *J. Am. Chem. Soc.* **1983**, *105*, 6491.
44. Labinger, J. A.; Bercaw, J. E. *Nature* **2002**, *417*, 507.
45. For recent comprehensive reviews, see: a) Stahl, S. S.; Labinger, J. A.; Bercaw, J. E. *Angew. Chem., Int. Ed.* **1998**, *37*, 2180. b) Fekl, U.; Goldberg, K. I. *Adv. Inorg. Chem.* **2003**, *54*, 259. c) Lersch, M.; Tilset, M. *Chem. Rev.* **2005**, 105, 2471.
46. a) Johansson, L.; Ryan, O. B.; Tilset, M. J. *Am. Chem. Soc.* **1999**, *121*, 1974. b) Johansson, L.; Ryan, O. B.; Rømming, C.; Tilset, M. *J. Am. Chem. Soc*. **2001**, *123*, 6579.
47. a) Siegbahn, P. E. M.; Crabtree, R. H. *J. Am. Chem. Soc.* **1996**, *118*, 4442. b) Mylvaganam, K.; Bacskay, G. B.; Hush, N. S. *J. Am. Chem. Soc.* **1999**, *121*, 4633.
48. For examples, see: a) Hill, G. S.; Rendina, L. M.; Puddephatt, R. J. *Organometallics* **1995**, *14*, 4966. b) Stahl, S. S.; Labinger, J. A.; Bercaw, J. E. *J. Am. Chem. Soc.*

1995, *117*, 9371. c) Wik, B. J.; Lersch, M.; Tilset, M. *J. Am. Chem. Soc.* **2002**, *124*, 12116.

49. Johansson, L.; Tilset, M. *J. Am. Chem. Soc.* **2001**, *123*, 739. b) Procelewska, J.; Zahl, A.; van Eldik, R.; Zhong, H. A.; Labinger, J. A.; Bercaw, J. E. *Inorg. Chem.* **2002**, *41*, 2808.
50. Romeo, R. *Comments Inorg. Chem.* **1990**, *11*, 21-57.
51. a) Wik, B. J.; Lersch, M.; Tilset, M. *J. Am. Chem. Soc.* **2002**, *124*, 12116. b) Wik, B. J.; Lersch, M.; Krivokapic, A.; Tilset, M. *J. Am. Chem. Soc.* **2006**, *128*, 2682.
52. For examples, see: a) Crumpton-Bregel, D. M.; Goldberg, K. I. *J. Am. Chem. Soc.* **2003**, *125*, 9442. b) Iron, M. A.; Lo, H. C.; Martin, J. M. L.; Keinan, E. *J. Am. Chem. Soc.* **2002**, *124,* 7041. c) Reinartz, S.; Brookhart, M.; Templeton, J. L. *Organometallics* **2002**, *18*, 4677. d) Haskel, A.; Keinan, E. *Organometallics* **1999**, *21*, 247. e) Prokopchuk, E. M.; Jenkins, H. A.; Puddephatt, R. J. *Organometallics* **1999**, *18*, 2861. f) Hill, G. S.; Vittal, J. J.; Puddephatt, R. J. *Organometallics* **1997**, *16*, 1209. g) Canty, A.J.; Dedieu, A.; Jin, H.; Milet, A.; Richmond, M. K. *Organometallics* **1996**, *15*, 2845. h) O'Reilly, S.; White, P. S.; Templeton, J. L. *J. Am. Chem. Soc.* **1996**, *118*, 5684. For a review, see: Puddephatt, R. J. *Coord. Chem. Rev.* **2001**, *219-221*, 157.
53. a) Reinartz, S.; White, P. S.; Brookhart, M.; Templeton, J. L. *J. Am. Chem. Soc.***2001**, *123*, 12724. b) Norris, C. M.; Reinartz, S.; White, P. S.; Templeton, J. L. *Organometallics* **2002**, *21*, 5649.
54. Johansson, L.; Tilset, M.; Labinger, J. A.; Bercaw, J. E. *J. Am. Chem. Soc.* **2000**, *122*, 10846.

55. a) Williams, B. S.; Holland, A. W.; Goldberg, K. I. *J. Am. Chem. Soc.* **1999**, *121*, 252. b) Goldberg, K. I.; Yan, J. Y.; Breitung, E. M. *J. Am. Chem. Soc.* **1995**, *117*, 6889. c) Brown, M. P.; Puddephatt, R. J.; Upton, C. E. E. *J. Chem. Soc., Dalton Trans.* **1974**, 2457. d) Roy, S.; Puddephatt, R. J.; Scott, J. D. *J. Chem. Soc., Dalton Trans.* **1989**, 2121.

56. a) Luinstra, G. A.; Wang, L.; Stahl, S. S.; Labinger, J. A.; Bercaw, J. E. *Organometallics* **1994**, *13*, 755. b) Wang, L.; Stahl, S. S.; Labinger, J. A.; Bercaw, J. E. *J. Mol. Catal. A* **1997**, *116*, 269.

57. a) Horváth, I. T.; Cook, R. A.; Millar, J. M.; Kiss, G. *Organometallics* **1993**, *12*, 8. b) Lin, M.; Shen, C.; Garcia-Zayas, E. A.; Sen, A. *J. Am. Chem. Soc.* **2001**, 123, 1000.

58. a) Pawlikowski, A. V.; Getty, A. D.; Goldberg, K. I. *J. Am. Chem. Soc*. **2007**, *129*, 10382. b) Luedtke, A. T.; Goldberg, K. I. *Inorg. Chem.* **2007**, *46*, 8496. c) Kloek, S. M.; Goldberg, K. I. *J. Am. Chem. Soc.* **2007**, *129*, 3460. d) Procelewska, J.; Zahl, A.; Liehr, G.; van Eldik, R.; Smythe, N. A.; Williams, B. S.; Goldberg, K. I. *Inorg. Chem*. **2005**, *44*, 7732. e) Crumpton-Bregel, D. M.; Goldberg, K. I. *J. Am. Chem. Soc.* **2003**, 125, 9442. f) Jensen, M. P.; Wick, D. D.; Reinartz, S..; White, P. S.; Templeton, J. L.; Goldberg, K. I. *J. Am. Chem. Soc.* **2003**, 125, 8614. g) Fekl, U.; Kaminsky, W.; Goldberg, K. I. *J. Am. Chem. Soc.* **2003**, *125*, 15286. h) Fekl, U.; Goldberg, K. I. *J. Am. Chem. Soc.* **2002**, *124*, 6804. i) Fekl, U.; Kaminsky, W.; Goldberg, K. I. *J. Am. Chem. Soc*. **2001**, *123*, 6423. j) Williams, B. S.; Goldberg, K. I. *J. Am. Chem. Soc*. **2001**, 123, 2576. k) Crumpton, D. M.; Goldberg, K. I. *J. Am. Chem. Soc*. **2000**, 122, 962.

59. Stahl, S. S.; Labinger, J. A.; Bercaw, J. E. *J. Am. Chem. Soc*. **1996**, 118, 5961.

60. Zhong, H. A.; Labinger, J. A.; Bercaw, J. E. *J. Am. Chem. Soc*. **2002**, 124, 1378.

61. For examples, see: a) Denney, M. C.; Smythe, N. A.; Cetto, K. L.; Kemp, R. A.; Goldberg, K. I. *J. Am. Chem. Soc.***2006***, 128,* 2508. b) Stahl, S. S. *Angew. Chem., Int. Ed.* **2004**, *43*, 3400. b) Konnick, M. M.; Guzei, I. A.; Stahl, S. S. *J. Am. Chem. Soc.* **2004**, *126*, 10212.

62. For a review, see: Lewis, E. A.; Tolman, W. B. *Chem. Rev.* **2004**, *104*, 1047.

63. Periana, R. A.; Taube, D. J.; Gamble, S.; Taube, H.; Satoh, T.; Fujii, H. *Science* **1998**, *280*, 560.

64. a) Rablen, P. R.; Hartwig, J. F. *J. Am. Chem. Soc.* **1994**, *116*, 4121. b) Rablen, P. R.; Hartwig, J. F. *J. Am. Chem. Soc.* **1996**, *118*, 4648.

65. a) Waltz, K. M.; He, X.; Muhoro, C.; Hartwig, J. F. *J. Am. Chem. Soc.* **1995**, *117*, 11357. b) Waltz, K. M.; Hartwig, J. F. *Science* **1997**, *277*, 211. c) Chen, H.; Hartwig, J. F. *Angew. Chem., Int. Ed.* **1999**, *38*, 3391. d) Chen, H.; Schlecht, S.; Semple, T. C.; Hartwig, J. F. *Science*, **2000**, *287*, 1995.

66. a) Iverson, C. N.; Smith, M. R. III. *J. Am. Chem. Soc.***1999**, *121*, 7696. b) Cho, J. Y.; Iverson, C. N.; Smith, M. R. III. *J. Am. Chem. Soc.* **2000**, 122, 12868. c) Cho, J. Y.; Tse, M. K.; Holmes, D.; Maleczka, R. E. Jr.; Smith, M. R. III. *Science* **2002**, *295*, 305. d) Chotana, G. A.; Rak, M. A.; Smith, M. R. III. *J. Am. Chem. Soc.* **2005**, 122, 10539. f) Paul, S.; Chotana, G. A.; Holmes, D.; Reichle, R. C.; Maleczka, R. E. Jr.; Smith, M. R. III. *J. Am. Chem. Soc.* **2006**, 128, 15552.

67. Snieckus, V. *Chem. Rev.* **1990**, *90*, 879.

68. a) Ringelberg, S. N.; Meetsma, A.; Hessen, B; Teuben, J. H. *J. Am. Chem. Soc.* **1999**, 121, 6082. b) Tse, M. K.; Cho, J.-Y.; Smith, M. R. III. *Org. Lett.* **2001**, *3*, 2831. c) Ishiyama, T.; Takagi, J.; Hartwig, J. F.; Miyaura, N. *Angew. Chem., Int. Ed.* **2002**, *41*, 3056. d) Ishiyama T., Takagi, J.; Yonekawa, Y.; Hartwig, J. F.; Miyaura, N. *Adv.*

Synth. Catal. **2003**, *345*, 1103. e) Paul, S.; Chotana, G. A.; Holmes, D.; Reichle, R. C.; Maleczka, R. E. Jr.; Smith, M. R. III. *J. Am. Chem. Soc.* **2006**, 128, 15552.

69. a) Shimada, S.; Batsanov, A. S.; Howard, J. A. K.; Marder, T. B. *Angew. Chem., Int. Ed.* **2001**, *40*, 2168.
70. Fort, Y.; Rodriguez, A. L. *J. Org. Chem.* **2003**, *68*, 4918.
71. a) Mkhalid, I. A. I.; Coventry, D. N.; Albesa-Jove, D.; Batsanov, A. S.; Howard, J. A. K.; Perutz, R. N.; Marder, T. B. *Angew. Chem., Int. Ed.* **2006**, *45*, 489. b) Coventry, D. N.; Batsanov, A. S.; Goeta, A. E.; Howard, J. A. K.; Marder, T. B.; Perutz, R. N. *Chem. Commun.* **2005**, 2172.
72. a) Lawrence, J. D.; Takahashi, M.; Bae, C.; Hartwig, J. F. *J. Am. Chem. Soc.* **2004**, *126,* 15334. b) Murphy, J. M.; Liao, X.; Hartwig, J. F. *J. Am. Chem. Soc* **2007**, *129,* 15434. c) Tzschucke, C. C.; Murphy, J. M.; Hartwig, J. F. *Org. Lett.* **2007**, *9*, 761. d) Murphy, J. M.; Tzschucke, C. C.; Hartwig, J. F. *Org. Lett.* **2007**, *9*, 757.
73. Shi, F.; Smith, M. R. III.; Maleczka, R. E. Jr. *Org. Lett.* **2006**, *8*, 1411.
74. a) Tamura, H.; Yamazaki, H.; Sato, H.; Sakaki, S. *J. Am. Chem. Soc.* **2003**, *125*, 16114. b) Boller, T. M.; Murphy, J. M.; Hapke, M.; Ishiyama, T.; Miyaura, N.; Hartwig, J. F. *J. Am. Chem. Soc.* **2005**, *127*, 14263.
75. a) Periana, R. A.; Mironov, O.; Taube, D.; Bhalla, G.; Jones, C. *Science* **2003**, *301*, 814. b) Lin, M.; Hogan, T.; Sen, A. *J. Am. Chem. Soc.* **1997**, *119*, 6048. c) Shen, C.; Garcia-Zayas, E. A.; Sen, A. *J. Am. Chem. Soc.* **2000**, *122*, 4029.
76. Herrerias, C. I.; Yao, X.; Li, Z.; Li, C.-J. *Chem. Rev.* **2007**, *107*, 2546.
77. Godula, K.; Sames, D. *Science* **2006**, *312*, 67.
78. Reviews on the direct arylation of heteroaromatics: a) Alberico, D.; Scott, M. E.; Lautens, M. *Chem. Rev.* **2007**, *107*, 174. b) Seregin, I. V.; Gevorgyan, V. *Chem. Soc.*

Rev. **2007**, *36*, 1173. c) Campeau, L.-C.; Stuart, D. R.; Fagnou, K. *Aldrichimica Acta* **2007**, *40*, 35. d) Satoh, T.; Miura, M. *Chem. Lett.* **2007**, *36*, 200. For examples with indoles, see: a) Deprez, N. R.; Kalyani, D.; Krause, A.; Sanford, M. S. *J. Am. Chem. Soc.* **2006**, *128*, 4972. b) Wang, X.; Lane, B. S.; Sames, D. *J. Am. Chem. Soc.* **2005**, *127*, 4996. c) Lane, B. S.; Sames, D. *Org. Lett.* **2004**, *6*, 2897. d) Wang, X.; Gribkov, D. V.; Sames, D. *J. Org. Chem.* **2007**, *72*, 1476. (e) Lane, B. S.; Brown, M. A.; Sames, D. *J. Am. Chem. Soc*. **2005**, *127*, 8050.

79. a) Wang, X.; Lane, B. S.; Sames, D. *J. Am. Chem. Soc.* **2005**, *127*, 4996. b) Li, W.; Nelson, D. P.; Jensen, M. S.; Hoerrner, R. S.; Javadi, G. J.; Cai, D. ; Larsen, R. D. *Org. Lett.* **2003**, *5*, 4835. c) Campeau, L.-C. ; Rousseaux, S.; Fagnou, K. *J. Am. Chem. Soc.* **2005**, *127*, 18020. d) Do, H.-Q.; Daugulis, O. *J. Am. Chem. Soc.* **2007**, *129*, 12404.
80. Bressy, C.; Alberico, D.; Lautens, M. *J. Am. Chem. Soc.* **2005**, *127*, 13148.
81. For recent examples of oxidative arene homocoupling, see: a) Hull, K. L.; Lanni, E. L.; Sanford, M. S. *J. Am. Chem. Soc.* **2006**, *128*, 14047 and references therein. b) Takahashi, M.; Masui, K.; Sekiguchi, H.; Kobayashi, N.; Mori, A.; Funahashi, M.; Tamaoki, N. *J. Am. Chem. Soc.* **2006**, *128*, 10930. c) Mukhopadhyay, S.; Rothenberg, G.; Lando, G.; Agbaria, K.; Kazanci, M.; Sasson, Y. *Adv. Synth. Catal.* **2001**, *343*, 455. d) Li, X.; Hewgley, J. B.; Mulrooney, C. A.; Yang, J.; Kozlowski, M. C. *J. Org. Chem.* **2003**, *68*, 5500 and references therein.
82. a) Stuart, D. R.; Fagnou, K. *Science* **2007**, *316*, 1172. b) Stuart, D. R.; Villemure, E.; Fagnou, K. *J. Am. Chem. Soc.* **2007**, *129*, 12072. c) Lafrance, M.; Rowley, C. N.; Woo, T. K.; Fagnou, K. *J. Am. Chem. Soc.* **2006**, *128*, 8754. d) Lafrance, M.; Fagnou, K. *J. Am. Chem. Soc.* **2006**, *128*, 16496.

83. For recent examples on tuning selectivity *via* changing reaction conditions: a) Grimster, N. P.; Gauntlett, C.; Godfrey, C. R. A.; Gaunt, M. J. *Angew. Chem., Int. Ed.* **2005**, *44*, 3125. b) Beck, E. M.; Grimster, N. P.; Hatley, R.; Gaunt, M. J. *J. Am. Chem. Soc.* **2006**, *128*, 2528.

84. For recent examples on employing metal oxidants, see: a) Chen, X.; Li, J.-J.; Hao, X.-S.; Goodhue, C. E.; Yu, J.-Q. *J. Am. Chem. Soc.* **2006**, *128*, 78. b) Chen, X.; Goodhue, C. E.; Yu, J.-Q. *J. Am. Chem. Soc.* **2006**, *128*, 12634. c) Thu, H.-Y.; Yu, W.-Y.; Che, C.-M. *J. Am. Chem. Soc.* **2006**, *128*, 9084. d) Pei, T.; Wang, X.; Widenhoefer, R. A. *J. Am. Chem. Soc.* **2003**, *125*, 648.

Chapter 2

C–H Activation of Benzene Derivatives

2.1 Introduction

We recently developed a series of neutral 7-azaindolyl derivative N,N chelating ligands (N,N-L) for arene C-H activation using cationic Pt(II) complexes $[Pt(CH_3)(N,N\text{-}L)(solv)]^+$.[1] The precursor complexes $Pt(CH_3)_2(N,N\text{-}L)$ where N,N-L = 1,2-bis(1-*N*-7-azaindolyl)benzene (BAB) (**2.1**),[1a,] bis(1-*N*-7-azaindolyl)methane (BAM) (**2.2**)[1b,1c] (Chart 2.1), and 1,2,4,5-tetrakis(1-*N*-7-azaindolyl)benzene (TTAB),[2] display two special features. First, the fifth coordination sites of the Pt(II) centers are partially blocked by the linkers in the N,N-L chelate ligands.[1,2] Second, the separation distances between the linker groups and the Pt(II) center in these complexes are short, which can either induce a strong three-center four-electron $Pt^{II}\cdots H'\text{-}C$ interaction[3] in complex **2.2**,[1b] or promote unusual reactivity as demonstrated by the unique behavior of $Pt_2(TTAB)Me_4$ toward C-H and C-Cl bond activation and the isolation of a rare dinuclear Pt^{IV} complex.[2]

Chart 2.1

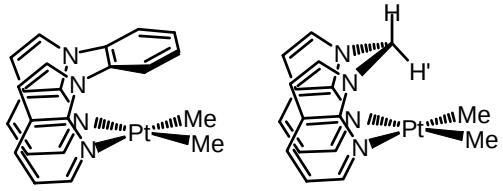

2.1 **2.2**

Recently, great efforts have been made towards the understanding of electronic and steric impacts on the kinetic and thermodynamic selectivity of alkylarene C-H activation.[4-8] It has been shown that there is a general kinetic preference for aryl C-H

activation, and the observed product distributions are frequently attributed to and reflect the steric factors.[5-7] While reports of sterically unfavored *ortho*-aromatic C-H activation for mono-substituted benzene derivatives by Pt(II) complexes are rare, preferential *ortho*-aryl C-H activation for an anisole molecule has been reported recently by Puddephatt and coworkers with Pt(II) complexes of 2,2'-bipyridylamine and its analogues, where the directing effect of the *ortho*-methoxyl group *via* precoordination to a Pt(II) center was believed to account for the observed selectivity.[7d] Another notable case is the recent demonstration of the preferential and thermodynamically favored benzylic alkylarene C-H activation by Bercaw and coworkers using diimine Pt(II) complexes. While the kinetic preference for the aromatic C-H activation was retained, it was found that the kinetically preferred aromatic products can gradually transform into the thermodynamically favored benzylic C-H activation products.[6k,6l] This interesting selectivity switch has been attributed to the involvement and the thermodynamic stability of a type of η^3-benzylic Pt(II) intermediate as illustrated in Chart 2.2.[6k]

Chart 2.2

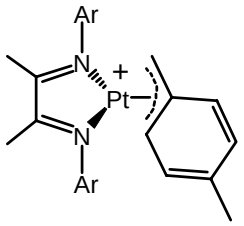

While earlier investigations on C-H activation involving cationic Pt(II) centers have focused mostly on regioselectivity, information on stereo- or diastereoselective C-H bond activation using Pt complexes has been rather scarce, except for a few recent examples reported by Sames and coworkers, where cationic Pt(II) complexes with chiral auxiliary ligands were used in stereoselective C-H activation.[9,10]

We have shown earlier that complexes $[Pt(CH_3)(N,N\text{-}L)(solv)]^+$ (N,N-L = BAB or BAM) can undergo facile benzene C-H activation. Considering the different size of the linkers in BAB (phenyl) and BAM (CH_2) (Chart 2.1), this pair of ligands provide us a unique opportunity to investigate the impact of steric blocking of the Pt axial coordination site on the selectivity of alkylarene C-H bond activation. To further demonstrate the selectivity towards activating benzene derivatives, we carried out the investigation of toluene and EtPh C-H activation using the Pt(II) BAB and BAM systems. In these systems, in addition to the similar selectivity switch as observed by Bercaw *et al.*, a high regioselectivity toward toluene and ethyl benzene (EtPh) benzylic activation was also observed. More interestingly, the reactions of EtPh activation display a distinct diastereoselectivity, a phenomenon that has not been reported in other cationic Pt(II) systems with the exception of the systems reported by Sames and coworkers that involve chiral auxiliary ligands.[9,10] In addition, we have succeeded in isolating and structurally characterizing a key η^3-benzylic complex, identified the co-existence of two η^3-structural isomers, and determined their roles in the diastereoselective EtPh C-H bond activation. The detailed studies are described in this chapter.

2.2 Experimental Section

2.2.1 General procedures

All reactions were performed under an inert atmosphere of dry N_2 with standard Schlenk techniques or in a dry-box. Solvents were freshly distilled prior to use. ^1H NMR and ^{13}C NMR spectra were recorded on Bruker Advance 400, or 500 spectrometers, and the spectra were referenced to residual solvent peaks. The chemical shifts (δ) were

reported in parts per million (ppm). Elemental analyses were performed by Canadian Microanalytical Service, Ltd, Delta, British Columbia. Starting materials were purchased from Aldrich Chemical Co, and used without further purification. $[H(Et_2O)_2][BAr^F{}_4]$ (Ar^F = 3,5-bis(trifluoromethyl)phenyl) was prepared using a procedure reported in the literature.[11] $Pt(BAB)(CH_3)_2$ (**2.1**)[1a] and $Pt(BAM)(CH_3)_2$ (**2.2**)[1b] were synthesized using similar methods as previously reported.

2.2.2 Syntheses of $[Pt(BAB)(CH_3)(CO)][BAr^F{}_4]$ (2.1·CO) and $[Pt(BAM)(CH_3)(CO)][BAr^F{}_4]$ (2.2·CO)

For 2.1·CO: Under N_2, $[H(Et_2O)_2][BAr^F{}_4]$ (0.081 g, 0.080 mmol) was added to a stirred suspension of $Pt(BAB)(CH_3)_2$ (**2.1**) (0.041 g, 0.076 mmol) in dry CF_3CH_2OH (10 mL) at ambient temperature, resulting in a pink cloudy solution immediately. After 5 minutes, dry CO was introduced into the flask and bubbled for 10 minutes. A light yellow solution was reached, which was stirred under 1 atm CO for another 3 hours. The solvent was then removed under reduced pressure, and the residue was washed with Et_2O (2 x 5 mL) to afford a light yellow power of **2.1·CO** in ~88% yield. This compound could slowly react with methylene chloride. ^{1}H NMR (500 MHz, CD_2Cl_2, 25°C): δ 8.27 (d, satellites; ^3J = 5.5 Hz, $^3J_{Pt\text{-}H}$ = 22.0 Hz; 1H, 7-aza), 8.21 (d, satellites; ^3J = 5.5 Hz, $^3J_{Pt\text{-}H}$ = 48.0 Hz; 1H, 7-aza), 8.12 (d; ^3J = 8.0 Hz; 1H, *Ph* of BAB), 8.07 (d; ^3J = 8.0 Hz; 1H, *Ph* of BAB), 7.76 (s; 8H, $BAr^F{}_4$), 7.70 (d; ^3J = 7.5 Hz; 1H, *Ph* of BAB), 7.59 (s; 4H, BAr^F4), 7.53 (d; ^3J = 7.5 Hz; 1H, *Ph* of BAB), 7.38 (d; ^3J = 3.5 Hz; 1H, aza), 7.31-7.27 (m; 2H, 2H, 7-aza), 7.20 (dd; $^3J_1$ = 5.5 Hz, $^3J_2$ = 8.0 Hz; 1H, 7-aza), 6.76 (d; ^3J = 3.5 Hz; 1H, 7-aza), 6.73 (d; ^3J = 3.5 Hz; 1H, 7-aza), 0.79 (s, satellites; $^2J_{Pt\text{-}H}$ = 73.0 Hz; 3H, Pt-CH_3) ppm. IR (KBr): υ_{CO} of **2.1·CO**: 2106.3 cm^{-1} (*vs*).

For 2.2·CO: This complex was synthesized in 92% yield by a similar method as described for **2.2-CO**. ^{1}H NMR (500 MHz, CD_3COCD_3, 25°C): δ 9.40 (d; ^{2}J = 16.0 Hz; 1H, C*H'*H bridge), 8.97 (d, satellites; ^{3}J = 5.5 Hz, $^{3}J_{Pt\text{-}H}$ = 20.4 Hz; 1H, 7-aza), 8.74 (d, satellites; ^{3}J = 5.5 Hz, $^{3}J_{Pt\text{-}H}$ = 44.4 Hz; 1H, 7-aza), 8.42 (d; ^{3}J = 7.5 Hz; 1H, 7-aza), 8.34 (d; ^{3}J = 7.5 Hz; 1H, 7-aza), 8.11 (d; ^{3}J = 3.5 Hz; 2H, 7-aza), 7.80 (s; 8H, BAr^{F}_{4}), 7.68 (s; 4H, BAr^{F}_{4}), 7.54 (dd; $^{3}J_1$ = 5.5 Hz, $^{3}J_2$ = 7.5 Hz; 1H, 7-aza), 7.44 (dd; $^{3}J_1$ = 5.5 Hz, $^{3}J_2$ = 7.5 Hz; 1H, 7-aza), 7.21 (d; ^{2}J = 16.0 Hz; 1H, CH'*H* bridge), 6.90 (d; ^{3}J = 3.5 Hz; 1H, 7-aza), 6.86 (d; ^{3}J = 3.5 Hz; 1H, 7-aza), 1.26 (s, satellites; $^{2}J_{Pt\text{-}H}$ = 72.0 Hz; 3H, Pt-C*H*$_3$) ppm. IR (KBr): $\upsilon_{\mathbf{CO}}$ of **2.2·CO**: 2118.9 cm^{-1} (*vs*).

2.2.3 Toluene C-H activation by 2.1 and the isolation of [Pt(BAB)(CH$_2$Ph)(SMe$_2$)][BAr$^{F}_{4}$] (2.3) and [Pt(BAB)(CH$_2$Ph)(NCMe)][BAr$^{F}_{4}$] (2.4)

For 2.3: Pt(BAB)$(CH_3)_2$ (**2.1**) (0.11 g, 0.20 mmol) and $[H(Et_2O)_2][BAr^{F}_{4}]$ (0.20 g, 0.20 mmol) were mixed in toluene (20 mL) at room temperature under N_2. After the mixture was stirred for 1 hr, 0.20 mL of Me_2S was added into the system. The reaction mixture was filtered through Celite. Crude solids of $[Pt(BAB)(CH_2Ph)(SMe_2)][BAr^{F}_{4}]$, **2.3** were obtained by slow diffusion of hexanes to the concentrated solution and storage in a refrigerator for several weeks, which were further purified by recrystallization from hexanes/CH_2Cl_2 (2/1) to afford colorless crystals (41% yield). ^{1}H NMR (500 MHz, CD_2Cl_2, 25 °C): δ 8.32 (dd; ^{3}J = 5.5 Hz, ^{4}J = 1.1 Hz; 1H, 7-aza), 8.06 (dd; satellites; ^{3}J = 5.5 Hz, ^{4}J= 1.0 Hz, $^{3}J_{Pt\text{-}H}$ = 45.6 Hz; 1H, 7-aza), 7.99 (dd; ^{3}J = 8.0 Hz, ^{4}J = 1.3 Hz; 1H, 7-aza), 7.94 (dd; ^{3}J = 7.9 Hz, ^{4}J = 1.2 Hz; 1H, 7-aza), 7.85 (m; 2H, phenyl of BAB), 7.60 (s; 4H, BAr^{F}_{4}), 7.59 (d; ^{3}J = 4.0 Hz; 1H, 7-aza), 7.55 (dd; ^{3}J = 7.6 Hz, ^{4}J = 1.8 Hz; 1H,

phenyl of BAB), 7.28 (dd; ^3J = 7.6 Hz, ^4J = 1.8 Hz; 1H, phenyl of BAB), 7.26 (d; ^3J = 3.6 Hz; 1H, 7-aza), 7.20 (d; ^3J = 3.6 Hz; 1H, 7-aza), 7.12 (dd; $^3J_1$ = 5.5 Hz, $^3J_2$ = 7.9 Hz; 1H, aza), 7.03 (t; ^3J = 7.1 Hz; 1H, $PtCH_2Ph$), 6.98 (m; 3H, 1H from 7-aza, 2H from $PtCH_2Ph$), 6.71 (m; 4H, 2H from 7-aza, 2H from $PtCH_2Ph$), 2.70 (d; ^2J = 10.2 Hz, $^2J_{Pt\text{-}H}$ = 103.0 Hz; 1H, $PtCH_2Ph$), 2.67 (d; ^2J = 10.2 Hz, $^2J_{Pt\text{-}H}$ = 103.0 Hz; 1H, $PtCH_2Ph$), 2.13 (s (br), satellites; $^3J_{Pt\text{-}H}$ = 53.2 Hz; 3H, Me_2S), 1.97 (s (br); satellites, $^3J_{Pt\text{-}H}$ = 53.2 Hz; 3H, Me_2S) ppm. ^{13}C NMR: for $BAr^F{}_4^-$, δ 162.1 (q, $J_{B\text{-}H}$ = 50 Hz), 135.1 (br), 129.4 (q, $J_{C\text{-}F}$ = 32 Hz), 125.3 (q, $J_{C\text{-}F}$ = 271 Hz), 117.9 (br) ppm; for BAB, δ 147.5, 146.9, 144.6, 143.6, 136.8, 136.7, 132.80, 132.55, 131.93, 131.74, 131.61, 131.58, 129.46, 124.82, 124.58, 118.41, 118.17, 104.4, 104.2; $PhCH_2$,146.0, 129.0, 128.3, 124.6, 6.8 ppm; for Me_2S, δ 23.0, 22.5 ppm. Anal. calcd. for $C_{61}H_{39}N_4BF_{24}SPt$: C 48.14, H 2.58, N 3.68; found: C 47.48, H 2.65, N 3.70.

For 2.4: $Pt(BAB)(CH_3)_2$ (**2.1**) (0.11 g, 0.20 mmol) and $[H(Et_2O)_2][BAr^F{}_4]$ (0.202 g, 0.20 mmol) were mixed in 20 mL of toluene at room temperature. After the mixture was stirred for 1 hr, 0.20 mL of CH_3CN was added into the system. The reaction mixture was filtered through Celite. Colorless crystals **2.4** were obtained by slow diffusion of hexanes to the concentrated solution and storage at room temperature for several days (38% yield). ^{1}H NMR (500 MHz, CD_3COCD_3, 25°C): δ 8.33 (dd; ^3J = 5.4 Hz, ^4J = 1.2 Hz; 1H, 7-aza), 8.16 (dd, satellites; ^3J = 5.7 Hz, ^4J = 1.0 Hz, $^3J_{Pt\text{-}H}$ = 57.6 Hz; 1H, 7-aza), 7.95 (dd; ^3J = 7.9 Hz, ^4J = 1.2 Hz; 1H, 7-aza), 7.92 (dd; ^3J = 7.9 Hz, ^4J = 1.4 Hz; 1H, 7-aza), 7.87 (m; 2H, phenyl of BAB), 7.75 (s; 4H, $BAr^F{}_4$), 7.58 (d; ^3J = 4.0 Hz; 1H, 7-aza), 7.48 (m; 1H, phenyl of BAB), 7.41 (m; 1H, phenyl of BAB), 7.30 (d; ^3J = 3.6 Hz; 1H, 7-aza), 7.29 (d; ^3J = 3.6 Hz; 1H, 7-aza), 7.08 (dd; $^3J_1$ = 5.4 Hz, $^3J_2$ = 7.9 Hz; 1H, 7-aza),

7.05 (m; 3H, PtCH$_2$*Ph*), 7.00 (dd; $^3J_1$ = 5.7 Hz, $^3J_2$ = 7.9 Hz; 1H, 7-aza), 6.82 (m; 2H, PtCH$_2$*Ph*), 2.87 (d, satellites; ^2J = 10.0 Hz, $^2J_{Pt\text{-}H}$ = 106.5 Hz; 1H, Pt*CH$_2$*Ph), 2.70 (d; ^2J = 10.0 Hz, $^2J_{Pt\text{-}H}$ = 106.5 Hz; 1H, Pt*CH$_2$*Ph), 2.11 (s; 3H, PtNC*CH$_3$*) ppm. ^{13}C NMR: for $BAr^F{}_4^-$, δ 162.2 (q, $J_{B\text{-}H}$ = 50 Hz), 135.2 (br), 129.2 (q, $J_{C\text{-}F}$ = 32 Hz), 125.0 (q, $J_{C\text{-}F}$ = 270 Hz), 117.8 (br) ppm; for BAB, δ 148.3, 148.0, 147.9, 145.9, 144.4, 137.2, 136.6, 132.43, 132.22, 131.96, 131.84, 131.65, 131.50, 130.20, 118.26, 118.99, 103.9, 103.8 ppm; for PhCH$_2$, δ 147.6, 128.7, 128.2, 124.48, 5.90 ppm; for CH$_3$CN, δ 124.38, 3.5 ppm. Anal. calcd. for $C_{61}H_{36}N_5BF_{24}Pt$: C 48.82, H 2.42, N 4.67; found: C 49.03, H 2.58, N 4.52.

2.2.4 ^{1}H NMR analyses of the toluene C-H activation with 2.1 over time

Pt(BAB)(CH$_3$)$_2$ (**2.1**) (0.050 g, 0.093 mmol) and [H(Et$_2$O)$_2$][$BAr^F{}_4$] (0.095 g, 0.093 mmol) were mixed in 8 mL of toluene at room temperature. A small amount of the reaction mixture, during the course of the reaction, was sampled at regular time intervals and transferred immediately into vials that contain CD$_3$CN to terminate the reaction. The samples in the vials were then dried and the residues were dissolved with CD$_2$Cl$_2$ and analyzed by ^{1}H NMR spectroscopy. The ^{1}H NMR spectrum of the reaction mixture recorded after 48 hrs showed a mixture of products consisting of [Pt(BAB)(CH$_2$Ph)(NCCD$_3$)][$BAr^F{}_4$] (**2.4a**, 81%), [Pt(BAB)(*p*-tolyl)(NCCD$_3$)][$BAr^F{}_4$] (**2.4b**, 6%), and [Pt(BAB)(*m*-tolyl)(NCCD$_3$)][$BAr^F{}_4$] (**2.4c**, 13%). The cationic complex [Pt(BAB)(CH$_3$)(NCCD$_3$)]$^+$ was not observed after ~ 40 hrs. ^{1}H NMR (500 MHz, CD$_2$Cl$_2$, 25 ^{o}C): for **2.4a**, δ 2.87 (d, satellites; ^2J = 10.0 Hz, $^2J_{Pt\text{-}H}$ = 106.5 Hz; 1H, -C*H$_A$*H$_B$Ph), 2.71 (d; ^2J = 10.0 Hz, $^2J_{Pt\text{-}H}$ = 106.5 Hz; 1H, -CH$_A$*H$_B$*Ph) ppm; for **2.4b**, δ 2.23 (s; 3H, *p*-*CH$_3$*Ph) ppm; for **2.4c**, δ 2.20 (s; 3H, *m*-*CH$_3$*Ph) ppm.

2.2.5 EtPh C-H activation by 2.1 and the isolation of [Pt(BAB)(CHMePh)(MeCN)][BAr^F_4] (2.5)

Under N_2, [$H(Et_2O)_2$][BAr^F_4] (0.19 g, 0.19 mmol) was added to a stirred solution of Pt(BAB)(CH_3)$_2$ (0.10 g, 0.19 mmol) in EtPh (20.0 mL) at ambient temperature (22 °C). The solution mixture became clear and turned pink in ~1 minute. During the reaction, thick brown oily residue accumulated slowly on the bottom of the flask. After 5 days, CH_3CN (0.20 mL, 3.8 mmol) was added to terminate the reaction. After the reaction mixture was stirred for another 1 hour, the solution was separated from the oily residue (~0.024 g). The solvents were removed under *vacuum*. To remove EtPh, the residue was repeatedly dissolved in CH_2Cl_2 and the solvent was repeatedly removed under *vacuum* (3 times), which produced a brown residue of ~0.26 g. ^{1}H NMR analyses indicated that > 90% of the products are η^1-benzylic C–H activation products along with aromatic C–H activation products (< 10%). Two sets of chemical shifts corresponding to the two diastereomers of the η^1-benzylic product with a ratio of ~3.7:1 were observed in the ^{1}H NMR spectrum. Colorless crystals of **2.5** were obtained by recrystallization of the crude product from hexanes/THF (4/1). Anal. calcd. for $C_{62}H_{38}N_5BF_{24}Pt$: C 49.16, H 2.53, N 4.62; found: C 48.50, H 2.55, N 4.55.

^{1}H NMR (400 MHz, CD_2Cl_2, 25°C) for major diastereomer of **2.5A**: δ 8.34 (dd; ^3J= 5.4 Hz, ^4J = 1.1 Hz; 1H, 7-aza), 8.05-7.91 (m; 3H, 7-aza), 7.84-7.76 (m; 2H, phenyl of BAB), 7.74 (s; 8H, BAr^F_4), 7.57 (s; 4H, BAr^F_4), 7.46 (dd; ^3J = 8.0 Hz, ^4J = 1.6 Hz; 1H, phenyl of BAB), 7.42 (dd; ^3J = 8.0 Hz, ^4J = 2 Hz; 1H, phenyl of BAB), 7.25 (d; ^3J = 3.6 Hz; 1H, 7-aza), 7.23 (d; ^3J = 3.6 Hz; 1H, 7-aza), 7.19-7.17 (m; 3H, Pt-CHMe*Ph*), 7.09 (dd; $^3J_1$ = 5.6 Hz, $^3J_2$ = 8.0 Hz; 1H, 7-aza), 6.96 (dd; $^3J_1$ = 5.6 Hz, $^3J_2$ = 8.0 Hz; 1H, 7-

aza), 6.93-6.90 (m; 2H, Pt-CHMe*Ph*), 6.66 (d; ^3J = 3.6 Hz; 1H, 7-aza), 6.63 (d; ^3J = 3.6 Hz; ^{1}H, 7-aza), 3.33 (q, satellites; ^3J = 7.3 Hz, $^2J_{Pt\text{-}H}$ = 103.7 Hz; 1H, Pt-*CH*MePh), 2.22 (s; 3H, Pt-NC*Me*), 0.83 (d; ^3J = 7.3 Hz, $^3J_{Pt\text{-}H}$ = 50.4 Hz; 3H, Pt-CH*Me*Ph) ppm. ^{1}H NMR (400 MHz, CD_2Cl_2, 25°C) for minor diastereomer of **2.5B**: δ 8.26 (dd; ^3J = 5.4 Hz, ^4J = 1.1 Hz; 1H, 7-aza), 8.05-7.91 (m; 5H, 3H from 7-aza, 2H from phenyl of BAB), 7.74 (s; 8H, $BAr^F{}_4$), 7.60 (dd; ^3J = 8.0 Hz, ^4J = 1.6 Hz; 1H, phenyl of BAB), 7.57 (s; 4H, $BAr^F{}_4$), 7.51 (dd; ^3J = 8.0 Hz, ^4J = 1.6 Hz; 1H, phenyl of BAB), 7.29 (d; ^3J = 3.6 Hz; 1H, 7-aza), 7.27 (d; ^3J = 3.6 Hz; 1H, 7-aza), 7.19-7.17 (m; 3H, Pt-CHMe*Ph*), 7.06 (dd, $^3J_1$ = 5.6 Hz, $^3J_2$ = 8.0 Hz; 1H, 7-aza), 6.93-6.90 (m; 3H, 1H from 7-aza, 2H from Pt-CHMe*Ph*), 6.68 (d; ^3J = 3.6 Hz; 1H, 7-aza), 6.64 (d; ^3J = 3.6 Hz; ^{1}H, 7-aza), 2.90 (q, satellites; ^3J= 7.3 Hz, $^2J_{Pt\text{-}H}$ = 103.7 Hz; 1H, Pt-*CH*MePh), 2.23 (s; 3H, Pt-NC*Me*), 0.89 (d, satellites; ^3J = 7.3 Hz, $^3J_{Pt\text{-}H}$ = 50.4 Hz; 3H, Pt-CH*Me*Ph) ppm. ^{13}C NMR of all diastereomers (not fully assigned due to the complexity of the spectrum): for $BAr^F{}_4$, δ 162.9 (q, $J_{B\text{-}H}$ = 50.1 Hz), 135.2 (br), 129.4 (q, br; $J_{C\text{-}F}$ = 36 Hz), 125.3 (q; $J_{C\text{-}F}$ = 272 Hz), 117.92 (br) ppm; δ 146.01, 145.97, 144.38, 144.30, 144.18, 144.12, 132.71, 132.57, 132.49, 132.34, 131.96, 131.87, 131.71, 131.54, 131.43, 131.31, 129.8, 129.40, 128.71, 128.60, 128.22, 124.90, 124.71, 123.8, 121.7, 117.89, 117.76, 104.17, 104.08 15.97, 14.58, 14.45, 14.30, 3.53, 3.49 ppm.

2.2.6 EtPh C–H activation by 2.2 and the isolation of [Pt(BAM)(CHMePh)(MeCN)][$BAr^F{}_4$] (2.6)

Under N_2, $[H(Et_2O)_2][BAr^F{}_4]$ (0.30 g, 0.30 mmol) was added to a stirred solution of $Pt(BAM)(CH_3)_2$ (**2.2**) (0.14 g, 0.30 mmol) in EtPh (25 mL) at ambient temperature (22 °C). A clear yellow solution was formed immediately. After 5 days, CH_3CN (0.60 mL)

was added and the reaction mixture was stirred for another 1 hr. After the solvents were removed under *vacuum*, CH_2Cl_2 (5.0 mL) was used to dissolve the residue and then removed under *vacuum*. This was repeated 3 times to remove the EtPh. 0.39 g of a pale yellow residue was obtained. ^{1}H NMR analyses showed the presence of the benzylic C–H activation products as the major products along with aromatic C–H activation products (~25%). The benzylic product displayed two sets of signals with a ratio of ~1.5:1, corresponding to the two diastereomers in the ^{1}H NMR spectrum. The crystalline compound **2.6** was isolated from the reaction mixture after slow evaporation of the solvent. Anal. calcd. for $C_{57}H_{36}N_5BF_{24}Pt$: C 47.12, H 2.50, N 4.82; found: C 47.18, H 2.56, N 4.72.

^{1}H NMR (400 MHz, CD_2Cl_2, 25°C) for the major diastereomer of **2.6A:** δ 10.01 (d; ^2J = 15.4 Hz; 1H, CH_2 bridge), 8.47 (dd, br; $^3J_1$ = 5.4 Hz, $^3J_2$ = 1.0 Hz; 2H, 7-aza), 8.08-8.00 (m, satellites; $^3J_{Pt\text{-}H}$ = 38.2 Hz; 2H, 7-aza), 7.75 (s; 8H, $BAr^F{}_4$), 7.58 (s; 4H, $BAr^F{}_4$), 7.48-7.40 (m; 2H, 7-aza), 7.22-7.15 (m; 2H, 7-aza), 7.09-6.95 (m; 3H, Pt-CHMe*Ph*), 6.76-6.70 (m; 2H, Pt-CHMe*Ph*), 6.60-6.57 (m; 2H, 7-aza), 6.00 (d; ^2J = 15.3 Hz; 1H, CH_2), 3.32 (q, satellites; ^3J = 7.2 Hz, $^2J_{Pt\text{-}H}$ = 109.3 Hz; 1H, Pt-*CH*MePh), 2.38 (s; 3H, Pt-NC*CH₃*), 1.40 (d, satellites; ^3J = 7.2 Hz, $^3J_{Pt\text{-}H}$ = 44.8 Hz; 3H, Pt-CH*Me*Ph) ppm. ^{1}H NMR (400 MHz, CD_2Cl_2, 25°C) for the minor diastereomer of **2.6B**: δ 10.32 (d; ^2J = 15.3 Hz; 1H, CH_2 bridge), 8.74 (dd, satellites; $^3J_1$ = 5.6 Hz, $^3J_2$ = 1.2 Hz, $^3J_{Pt\text{-}H}$ = 60.3 Hz; 2H, 7-aza), 8.55 (dd, satellites; $^3J_1$ = 5.7 Hz, $^3J_2$ = 1.2 Hz, $^3J_{Pt\text{-}H}$ = 60.6Hz; 1H, 7-aza), 7.75 (s; 8H, $BAr^F{}_4$), 7.58 (s; 4H, $BAr^F{}_4$), 7.48-7.40 (m; 2H, 7-aza7.22-7.15 (m; 2H, 7-aza), 7.09-6.95 (m; 3H, Pt-CHMe*Ph*), 6.76-6.70 (m; 2H, Pt-CHMe*Ph*), 6.66 (d; ^3J = 3.4Hz; 2H, 7-aza), 6.14 (d; ^2J = 15.4 Hz; 1H, CH_2 bridge), 3.76 (q, satellites; ^3J = 7.2 Hz,

$^{2}J_{Pt\text{-}H}$ = 110.0 Hz; 1H, Pt-*CH*MePh), 2.24 (s; 3H, Pt-NC*Me*), 1.17 (d, satellites; ^{3}J = 7.2 Hz, $^{3}J_{Pt\text{-}H}$ = 36.3 Hz; 3H, Pt-CH*Me*Ph) ppm. ^{13}C NMR of all isomers (not fully assigned due to the complexity of the spectrum): for $BAr^{F}{}_{4}^{-}$, δ 162.2 (q, $J_{B\text{-}H}$ = 50.4 Hz), 135.2 (br), 129.5 (q, br; $J_{C\text{-}F}$ = 36 Hz), 125.3 (q; $J_{C\text{-}F}$ = 272 Hz), 117.92 (br); δ 151.37, 151.20, 147.17, 146.93, 132.63, 132.62, 132.48, 129.92, 129.47, 128.75, 128.24, 126.07, 125.93, 125.52, 124.36, 123.90, 118.23, 117.90, 117.87, 117.84, 104.10, 103.59, 103.57, 56.00, 55.53, 20.23, 21.07, 19.49, 16.58, 4.13, 3.84 ppm.

2.2.7 ^{1}H NMR analyses of the EtPh C-H activation with 2.1 and 2.2

Under N_2, $[H(Et_2O)_2][BAr^{F}{}_{4}]$ (1.0 equiv) was added to a stirred EtPh solution of the Pt(II) complex $Pt(BAB)(CH_3)_2$ (**2.1**) or $Pt(BAM)(CH_3)_2$ (**2.2**) at ambient temperature. A small amount of the reaction mixture, during the course of the reaction, was sampled at regular time intervals and transferred immediately into NMR tubes that contained CD_3CN. These samples were dried and the residues were then dissolved in CD_2Cl_2 and analyzed by ^{1}H NMR spectroscopy. The assignments of the chemical shifts to compounds in the reaction mixture is based on spectroscopic data of the isolated benzylic C-H activation product and the ^{1}H NMR spectrum of the *para*-aromatic C-H activation product, which was synthesized independently.

2.2.8 Synthesis of Pt(BAB)(η^{3}-CHPhMe)][$BAr^{F}{}_{4}$] (2.7)

Under N_2, $[H(Et_2O)_2][BAr^{F}{}_{4}]$ (0.16 g, 0.30 mmol) was added to a stirred solution of $Pt(BAB)(CH_3)_2$ (0.32 g, 0.31 mmol) in EtPh (30 mL) at ambient temperature. After stirring for 5 days, the solution was concentrated to ~5 mL under *vacuum* at ambient

temperature. Colorless crystals of the η^3-complex **2.7** were obtained in ~73% yield after the solution was kept in a refrigerator for several weeks. Anal. calcd. for $C_{60}H_{35}BF_{24}N_4Pt \cdot 0.5EtPh$: C 50.34, H 2.64, N 3.67; found: C 50.81, H 2.97, N 3.54.

^{1}H NMR (400 MHz, CD_2Cl_2, 25°C) (the aromatic region is not fully assigned due to the overlaps of many peaks; the assignments are based on a COSY spectrum.) for the major isomer **2.7A**: δ 3.92 (d, satellites; ^3J = 6.0 Hz, $^3J_{Pt\text{-}H}$ = 36.8 Hz; 1H, *ortho*-Pt-η^3-CHMe*Ph*), 1.88 (q, satellites; ^3J = 6.4 Hz, $^3J_{Pt\text{-}H}$ = 66.8 Hz; 1H, Pt-η^3-*CH*MePh), 1.03 (d; ^3J = 6.4 Hz; 3H, Pt-η^3-CH*Me*Ph) ppm. ^{1}H NMR (400 MHz, CD_2Cl_2, 25°C) for the minor isomer **2.7B**: δ 6.09 (d, satellites; ^3J = 6.0 Hz, $^3J_{Pt\text{-}H}$ = 42.6 Hz; 1H, *ortho*-Pt-η^3-CHMe*Ph*), 3.18 (q, satellites; ^3J = 6.6 Hz, $^3J_{Pt\text{-}H}$ = 68.4 Hz; 1H, Pt-η^3-*CH*MePh), 0.82 (d; ^{3}J = 6.6 Hz; 3H, Pt-η^3-CH*Me*Ph) ppm. ^{13}C NMR, the key chemical shifts for the major isomer **2.7A**: δ 67.03 (satellites; $^2J_{Pt\text{-}C}$ = 118 Hz; *ortho*-Pt-η^3-CHMe*Ph*), 38.16 (satellites; $^2J_{Pt\text{-}C}$ = 283 Hz; Pt-η^3-*CH*MePh), 13.95 (satellites; $^3J_{Pt\text{-}C}$ = 186 Hz; Pt-η^3-CH*Me*Ph) ppm; the key chemical shifts for minor isomer **2.7B**: δ 70.11 (satellites; $^2J_{Pt\text{-}C}$ = 112 Hz; *ortho*-Pt-η^3-CHMe*Ph*), 34.90 (satellites; $^3J_{Pt\text{-}C}$ = 288 Hz; Pt-η^3-*CH*MePh), 11.44 (satellites; $^3J_{Pt\text{-}C}$ = 196 Hz; Pt-η^3-CH*Me*Ph) ppm.

2.2.9 Synthesis of Pt(BAM)(η^3-CHPhMe)][BAr^F_4] (2.8)

The η^3- complex **2.8** was synthesized by a similar method as described for **2.7**. After 5 days, compound **2.8** was found to be the major product in the reaction mixture according to ^{1}H NMR data. However, a pure crystalline complex **2.8** could not be isolated from the reaction mixture because of the oily nature of the final reaction mixture and its

high solubility in common organic solvents. Compound **2.8** was characterized by NMR spectroscopic analyses.

^{1}H NMR (400 MHz, CD_2Cl_2, 25°C) (the aromatic region is not fully assigned due to the overlaps of many peaks) for the major isomer **2.8A:** δ 8.69 (d; ^2J = 15.2 Hz; 1H, CH_2 bridge), 5.98 (d, satellites; ^3J = 6.8 Hz, $^3J_{Pt\text{-}H}$ = 44.0 Hz; 1H, *ortho*-Pt-η^3-CHMe*Ph*)，5.89 (d; ^2J = 15.2 Hz; 1H, CH_2 bridge), 3.29 (q, satellites; ^3J = 6.4 Hz, $^3J_{Pt\text{-}H}$ = 68.8 Hz; 1H, Pt-η^3-*CH*MePh), 1.05 (d; ^{3}J = 6.4 Hz; 3H, Pt-η^3-CH*Me*Ph) ppm. ^{1}H NMR (400 MHz, CD_2Cl_2, 25°C) for the minor isomer **2.8B:** δ 9.85 (d; ^2J = 15.2 Hz; 1H, CH_2 bridge)，6.34 (d; ^2J = 15.2 Hz; 1H, CH_2 bridge), 5.82 (d, satellites; ^3J = 6.6 Hz, $^3J_{Pt\text{-}H}$ = 36.4 Hz; 1H, *ortho*-Pt-η^3-CHMe*Ph*)，3.20 (q, satellites; ^3J = 6.6 Hz, $^3J_{Pt\text{-}H}$ = 62.8 Hz; 1H, Pt-C*H*MePh), 1.17 (d; ^3J = 6.6 Hz; 3H, Pt-η^3-CH*Me*Ph) ppm. ^{13}C NMR, the key chemical shifts for the *major* isomer **2.8A**: δ 78.07 (satellites; $^2J_{Pt\text{-}C}$ = 93 Hz; *ortho*-Pt-η^3-CHMe*Ph*), 43.67 (satellites; $^2J_{Pt\text{-}C}$ = 284 Hz; Pt-η^3-*CH*MePh), 15.74 (satellites; $^3J_{Pt\text{-}C}$ = 200 Hz; Pt-η^3-CH*Me*Ph) ppm; the key chemical shifts for the minor isomer **2.8B**: δ 75.43 (satellites; $^2J_{Pt\text{-}C}$ = 86 Hz; *ortho*-Pt-η^3-CHMe*Ph*), 38.62 (satellites; $^2J_{Pt\text{-}C}$ = 280 Hz; Pt-η^3-*CH*MePh), 14.12 (satellites; $^3J_{Pt\text{-}C}$ = 199 Hz; Pt-η^3-CH*Me*Ph) ppm.

2.2.10 Conversion of 2.7/2.8 to 2.5/2.6

A 15 mg portion of the η^3- complex **2.7** (~ 1 x 10^{-5} mol) was placed in an NMR tube, and CD_2Cl_2 (0.5 mL) was added to dissolve sample at ambient temperature. After a ^{1}H NMR spectrum was recorded, CD_3CN (17 μL, ~3 x 10^{-4} mol) was added into the NMR sample, and a series of ^{1}H NMR spectra were recorded every 5 minutes at ambient

temperature. No conversion was detected at temperatures below -10 ^{o}C. The conversion at room temperature was fairly slow despite an excess amount of CD_3CN (30 fold) used. The ^{1}H NMR spectra indicated that after ~1 hour the η^3-compound was nearly completely converted to the η^1-benzylic product **2.5**. Notably, the ratio between two sets of signals for the diastereomers of **2.5** after the conversion was about the same as that of the two isomers of the η^3- complex **2.7**.

The conversion of complex **2.8** to complex **2.6** was carried out in a similar manner. NMR experiments showed that compound **2.8** can also react with MeCN at ambient temperature to afford the η^1-benzylic C-H activation product **2.6** quantitatively while retaining the diastereomeric ratio.

2.2.11 Syntheses of $Pt_2(CH_2Ph)_4(\mu\text{-}SEt_2)_2$ and $Pt_2(p\text{-}PhEt)_4(\mu\text{-}SEt_2)_2$

For $Pt_2(CH_2Ph)_4(\mu\text{-}SEt_2)_2$: A suspended solution of $PtCl_2(SEt_2)_2$ (0.59 g, 1.3 mmol) in Et_2O (60 mL) was cooled down to -10 ^{o}C. To this solution was added dropwise, *via* syringe, an Et_2O solution of $PhCH_2MgCl$ (1.0 M) (3.3 mL, 3.3 mmol) over 5 minutes, resulting in a white suspension. The mixture was stirred for another 2 h at the same temperature. A cold aqueous solution (40 mL) of NH_4Cl (0.20 g, 3.7 mmol) was added. After extraction of the aqueous layer with cold Et_2O (3 x 50 mL) and separation, the organic layer were dried over $MgSO_4$, and then removal of the solvent under reduced pressure at room temperature afforded an oily residue. After washing the oily residue with a small amount of cold acetone, 0.46 g of white solid was obtained, which was identified to be $Pt_2(CH_2Ph)_4(\mu\text{-}SEt_2)_2$ (73% yield) by ^{1}H and ^{13}C NMR analyses. ^{1}H NMR (500 MHz, CD_2Cl_2, 25°C): δ 7.14 (m; 8H, *Ph*CH_2), 7.06 (m; 8H, *Ph*CH_2), 6.97 (m; 4H,

PhCH_2), 2.74 (s, satellites; $^2J_{Pt\text{-}H}$ = 115.0 Hz; 8H, PhC*H_2*), 2.24 (q; ^3J = 7.0 Hz; 8H, S(C*H_2*$CH_3)_2$), 1.43 (t; ^3J = 7.0 Hz; 12H, S(CH_2C*H_3*)$_2$) ppm; ^{13}C NMR: δ 150.24, 129.13, 128.05, 123.44, 29.95, 22.79, 12.92 ppm.

For Pt_2(*p*-PhEt)$_4$(μ-SEt_2)$_2$: To a $PtCl_2(SEt_2)_2$ (0.59 g, 1.3 mmol) suspended solution in Et_2O (60 mL) at –10 ^{o}C was added dropwise, *via* syringe, an Et_2O of *p*-EtPhLi (0.8 M) (4.1 mL, 3.3 mmol) over 5 minutes. The mixture was stirred for another 2 h at the same temperature, resulting in a pale yellow solution. Similar work-up as above afforded a brown residue, which was hard to solidify even after washing with cold acetone. Prolonged drying at room temperature resulted in a semisolid, which was identified to be Pt_2(*p*-PhEt)$_4$(μ-SEt_2)$_2$ (50-70% yield) along with some unidentified species. ^{1}H NMR (500 MHz, CD_2Cl_2, 25°C): δ 7.18 (d, satellites; ^3J = 8.0 Hz, $^3J_{Pt\text{-}H}$ = 68.0 Hz; 8H, Pt*Ph*Et), 6.86 (d; ^3J = 8.0 Hz; 8H, Pt*Ph*Et), 2.88 (s, br; 8H, S(C*H_2*$CH_3)_2$), 2.57 (q; ^3J = 7.5 Hz; 8H, PhC*H_2*CH_3), 1.39 (t; ^3J = 8.0 Hz; 12H, S(CH_2C*H_3*)$_2$), 1.22 (t; ^3J = 7.5 Hz; 12H, $PhCH_2$C*H_3*) ppm; ^{13}C NMR: δ 139.10, 136.89, 128.63, 115.60, 30.54, 28.46, 15.90, 13.18 ppm.

2.2.12 Synthesis of Pt(BAB)($CH_2Ph)_2$ (2.9) and its protonation study

Synthesis of Pt(BAB)($CH_2Ph)_2$ (2.9): $Pt_2(CH_2Ph)_4$(μ-SEt_2)$_2$ (0.075 g, 0.080 mmol) and BAB (0.050 g, 0.16 mmol) were mixed in THF (10 mL) and heated overnight at 65 ^{o}C with oil-bath. Then the solvent was removed under reduced pressure to afford an oily residue. After washing with Et_2O (5 mL x 3), a white solid was obtained, which was identified to be Pt(BAB)($CH_2Ph)_2$ (58% yield) by ^{1}H and ^{13}C NMR analyses. ^{1}H NMR (500 MHz, CD_3COCD_3, 25°C): δ 7.95 (dd; $^3J_1$ = 1.0 Hz, $^3J_2$ = 5.5 Hz; 2H, 7-aza), 7.81

(dd; $^3J_1$ = 1.0 Hz, $^3J_2$ = 8.0 Hz; 2H, 7-aza), 7.66 (dd; $^3J_1$ =3.5 Hz, $^3J_2$ = 6.0 Hz; 2H, *Ph* of BAB), 7.32 (d; ^3J = 3.5 Hz; 2H, 7-aza), 7.18 (dd; ^3J = 3.5 Hz, $^3J_2$ = 6.0 Hz; 2H, *Ph* of BAB), 6.75 (dd; $^3J_1$ = 8.0 Hz, $^3J_2$ = 5.5 Hz; 2H, 7-aza), 6.74 (m; 4H, PtCHH'*Ph*), 6.67 (m; 2H, PtCHH'*Ph*), 6.61 (m; 4H, PtCHH'*Ph*), 2.74 (d, satellites; ^2J = 9.5 Hz, $^2J_{Pt\text{-}H}$ = 60.0 Hz; 2H, PtC*H'*HPh), 2.62 (d, satellites; ^2J = 9.5 Hz, $^2J_{Pt\text{-}H}$ = 64.0 Hz; 2H, PtCH'*H*Ph) ppm; ^{13}C NMR: δ 154.06, 148.26, 145.40, 137.32, 131.09, 129.72, 128.86, 128.48, 127.67, 127.11, 122.78, 120.58, 116.78, 102.14, 8.10 ppm.

Protonation of 2.9: In a dry-box, Pt(BAB)(CH_2Ph)$_2$ (**2.9**) (7 mg, 0.01 mmol) and B(C_6F_5)$_3$ (15 mg, 0.03 mmol) were mixed in a NMR tube and then NMR grade C_6F_6 (0.45 mL) and NMR grade CD_3COCD_3 (0.15 mL) were added to give a light yellow solution. The reaction was then monitored by ^{1}H NMR (500 MHz) at 40~50 ^{o}C. Diagnostic signals of the η^3-benzylic Pt(II) complex [Pt(BAB)(η^3-CH_2Ph)]$^+$: δ 4.61 ppm (d, satellites; 1H, *ortho*-H_o of *Ph*CH_aH_b), 3.61 ppm (d, satellites; 1H, PhCH_a*H$_b$*), 1.92 ppm (d, satellites; 1H, PhCH_a*H$_b$*) ppm. The H_a, H_b and H_o all displayed distinctive ^{195}Pt-^{1}H coupling patterns. These patterns, as well as above chemical shifts, are highly consistent with those of the η^3-ethylbenzene complex [(BAM)Pt(η^3-CHPh(Me))][BAr$^F{}_4$] (**2.8**). The assignments, particularly for the η^3-benzylic Pt(II) complex [Pt(BAB)(η^3-CH_2Ph)]$^+$, were confirmed by a COSY spectrum. Prolonged reaction at ~65 ^{o}C for 15 hours did not afford any noticeable signals of aromatic C-H activation products.

2.2.13 Synthesis of Pt(BAM)(*p*-PhEt)$_2$ (2.10) and its protonation study

For Pt(BAM)(*p*-PhEt)$_2$ (2.10): Pt_2(*p*-PhEt)$_4$(μ-SEt_2)$_2$ (120 mg, 0.12 mmol) and BAM (40 mg, 0.16 mmol) were mixed in Et_2O (15 mL) and stirred overnight at ambient

temperature. After the removal of the solvent, washing of the brown residue with Et_2O (3 x 5 mL) resulted in a white solid, which was identified to be **2.10** (76% yield based on BAM) by ^1H and ^{13}C NMR analyses. ^1H NMR (400 MHz, CD_2Cl_2, 25°C): δ 11.95 (d; ^2J = 14.6 Hz; 1H, C*H'*H bridge), 8.73 (d; ^3J = 4.4 Hz; 2H, 7-aza), 7.91 (d; ^3J = 7.2 Hz; 2H, 7-aza), 7.60 (d; ^3J = 1.4 Hz; 2H, 7-aza), 7.29 (d, satellites; ^3J = 7.0 Hz, $^3J_{Pt\text{-}H}$ = 78.0 Hz; 4H, Pt*Ph*Et), 6.98 (m, br; 2H, 7-aza), 6.69 (d; ^3J = 7.0 Hz; 4H, Pt*Ph*Et), 6.60 (d; ^3J = 1.4 Hz; 2H, 7-aza), 6.45 (d; ^2J = 14.6 Hz; 1H, CH*H* bridge), 2.47 (d, br; ^3J = 7.4 Hz; 4H, PhC*H*$_2$CH$_3$), 1.15 (t; ^3J = 7.4 Hz; 4H, PhCH$_2$C*H*$_3$) ppm; ^{13}C NMR: δ 146.44, 144.66, 138.58, 137.71, 130.28, 128.93, 126.16, 124.27, 55.98, 28.41, 15.75 ppm.

Protonation of Pt(BAM)(*p*-PhEt)$_2$ (2.10): In a dry-box, Pt(BAM)(*p*-PhEt)$_2$ (11 mg, 0.017 mmol) and [H(Et$_2$O)$_2$][BAr$^F{}_4$] (19 mg, 0.019 mmol) were mixed in a NMR tube and NMR grade CD_3NO_2 (0.50 mL) was added to give a light yellow solution. The reaction was then monitored by ^1H NMR (500 MHz) at ambient temperature. The ^1H NMR analyses demonstrated the slow transformation of *para*-aromatic C-H activation product into the *meta*- aromatic C-H activation product, while no distinctive signals from the benzylic C-H activation product were observed during the study.

2.2.14 X-ray diffraction analyses

Single crystals of **2.3-2.7** were mounted on glass fibers for data collection. All data were collected on a Siemens P4 X-ray diffractometer with a CCD-1000 detector, operating at 50 kV and 30 mA. No significant decay was observed in any samples. Data were processed on a PC with the aid of the Bruker SHELXTL software package (version 5.10) and were corrected for absorption effects. All structures were solved by direct methods. Most of the non-hydrogen atoms were refined anisotropically. Most of the CF_3 groups in **2.3**–**2.7** display rotational disorders which were modeled and refined successfully. The positions of hydrogen atoms were calculated, and their contributions in structural factor calculations were included. The crystal data for **2.3**–**2.7** are listed in Table 2.1 and Table 2.2. Important bond lengths and angles are given in Table 2.3.

Table 2.1 Crystallographic data for compounds **2.3**-**2.5**.

Compound	**2.3**	**2.4**	**2.5**
Formula	$C_{61}H_{39}BF_{24}N_4PtS$	$C_{61}H_{36}BF_{24}N_5Pt$	$C_{62}H_{38}BF_{24}N_5Pt$
FW	1521.92	1500.85	1514.87
Space Group	P-1	P-1	P-1
a, Å	12.725(4)	12.712(3)	12.698(4)
b, Å	13.160(4)	13.046(3)	13.177(5)
c, Å	18.895(6)	18.856(4)	19.064(6)
α, º	99.790(5)	100.179(4)	90.973(7)
β, º	100.730(5)	98.503(4)	93.076(7)
γ, º	94.316(6)	94.680(4)	95.273(6)
V, Å^3	3044.8(15)	3025.4(12)	3171.1(18)
Z	2	2	2
$D_{calc,}$ g·cm^{-3}	1.660	1.648	1.587
T, K	294(2)	293(2)	296(2)
μ, mm^{-1}	2.455	2.437	2.326
$2\theta_{max}$, º	56.66	56.74	56.76
Reflns measured	20884	16666	19248
Reflns used (R_{int})	13596 (0.0492)	12063 (0.0224)	12918 (0.0814)
Parameters	1045	1046	1028
Final *R* values [I > 2σ(I)]:			
R_1[a]	0.0586	0.0478	0.0761
wR_2[b]	0.0682	0.0763	0.1392
R values (all data):			
R_1[a]	0.2004	0.1029	0.2510
wR_2[b]	0.0832	0.0895	0.1897
Goodness-of-fit on F^2	0.760	1.042	0.916

[a] $R_1 = \Sigma[(|F_0| - |F_c|) / \Sigma|F_0|$

[b] $wR_2 = [\Sigma w [(F_0^2-F_c^2)^2] / \Sigma[w(F_0^2)^2]]^{1/2}$

$w = 1 / [\sigma^2(F_0^2) + (0.075P)^2]$, where $P = [Max (F_0^2,0) + 2F_c^2]/3$

Table 2.2 Crystallographic data for compounds **2.6**-**2.7**.

Compound	**2.6**	**2.7·2EtPh**
Formula	$C_{57}H_{36}BF_{24}N_5Pt$	$C_{64}H_{40}BF_{24}N_4Pt$
FW	1452.8	1526.90
Space Group	P-1	P-1
a, Å	12.4783(12)	16.4420(17)
b, Å	13.0894(12)	18.7653(19)
c, Å	18.1842(18)	21.650(2)
α, º	79.260(2)	65.647(2)
β, º	76.753(2)	85.831(2)
γ, º	86.854(2)	89.751(2)
V, $Å^3$	2840.2(5)	6067.1(11)
Z	2	4
$D_{calc,}$ g·cm^{-3}	1.699	1.672
T, K	180(2)	180(2)
μ, mm^{-1}	2.593	2.432
$2\theta_{max}$, º	56.64	56.64
Reflns measured	20140	43522
Reflns used (R_{int})	12910 (0.0416)	27602 (0.0644)
Parameters	822	1459
Final *R* values [I>2σ(I)]:		
R_1[a]	0.0959	0.0770
wR_2[b]	0.2318	0.1370
R values (all data):		
R_1[a]	0.1795	0.2342
wR_2[b]	0.2668	0.1612
Goodness-of-fit on F^2	0.955	0.718

[a] $R_1 = \Sigma(|F_0| - |F_c|) / \Sigma|F_0|$

[b] $wR_2 = [\Sigma w [(F_0^2-F_c^2)^2] / \Sigma[w(F_0^2)^2]]^{1/2}$

$w = 1 / [\sigma^2(F_0^2) + (0.075P)^2]$, where $P = [Max (F_0^2,0) + 2F_c^2]/3$

Table 2.3 Selected bond lengths (Å) and angles (º) for compounds **2.3**-**2.7**.

	Compound **2.3**		
S(1)-C(29)	1.736(8)	Pt(1)-N(1)	1.877(6)
S(1)-C(28)	1.745(7)	Pt(1)-C(21)	2.052(7)
S(1)-Pt(1)	2.249(2)	Pt(1)-N(2)	2.146(6)
C(29)-S(1)-C(28)	100.5(4)	C(21)-Pt(1)-N(2)	171.2(3)
C(29)-S(1)-Pt(1)	111.8(3)	N(1)-Pt(1)-S(1)	174.4(2)
C(28)-S(1)-Pt(1)	110.7(3)	C(21)-Pt(1)-S(1)	94.7(2)
N(1)-Pt(1)-C(21)	87.2(3)	N(2)-Pt(1)-S(1)	90.26(17)
N(1)-Pt(1)-N(2)	87.2(2)		
	Compound **2.4**		
Pt(1)-N(5)	1.965(5)	N(5)-C(28)	1.110(7)
Pt(1)-N(4)	2.014(4)	C(21)-C(22)	1.498(7)
Pt(1)-C(21)	2.058(5)	C(28)-C(29)	1.460(9)
Pt(1)-N(2)	2.148(4)		
N(5)-Pt(1)-N(4)	177.79(19)	C(21)-Pt(1)-N(2)	170.4(2)
N(5)-Pt(1)-C(21)	90.3(2)	C(28)-N(5)-Pt(1)	176.1(6)
N(4)-Pt(1)-C(21)	89.4(2)	N(5)-C(28)-C(29)	177.8(8)
N(5)-Pt(1)-N(2)	92.62(18)	C(22)-C(21)-Pt(1)	116.9(3)
N(4)-Pt(1)-N(2)	87.32(16)		
	Compound **2.5**		
Pt(1)-N(5)	1.883(15)	N(5)-C(29)	1.13(2)
Pt(1)-N(1)	1.932(11)	C(29)-C(30)	1.51(2)
Pt(1)-C(27)	2.025(17)	C(27)-C(28)	1.312(16)
Pt(1)-N(3)	2.153(10)	C(21)-C(27)	1.49(2)
N(5)-Pt(1)-N(1)	179.2(5)	N(5)-Pt(1)-N(3)	92.3(4)
N(5)-Pt(1)-C(27)	89.9(7)	N(1)-Pt(1)-N(3)	87.1(4)
N(1)-Pt(1)-C(27)	90.8(7)	C(27)-Pt(1)-N(3)	169.7(7)
N(5)-C(29)-C(30)	175.9(16)	C(28)-C(27)-C(21)	120.8(15)
C(28)-C(27)-Pt(1)	121.2(12)	C(21)-C(27)-Pt(1)	116.0(10)
	Compound **2.6**		
Pt(1)-N(5)	1.984(13)	N(5)-C(16)	1.143(16)
Pt(1)-N(3)	2.033(12)	C(18)-C(19)	1.393(19)
Pt(1)-C(19)	2.070(11)	C(19)-C(20)	1.434(16)
Pt(1)-N(1)	2.145(8)		
N(5)-Pt(1)-N(3)	178.9(4)	C(6)-N(1)-Pt(1)	117.4(8)

N(5)-Pt(1)-C(19)	90.0(6)	C(13)-N(1)-Pt(1)	126.0(7)
N(3)-Pt(1)-C(19)	89.1(6)	C(16)-N(5)-Pt(1)	174.2(11)
N(5)-Pt(1)-N(1)	89.2(4)	N(5)-C(16)-C(17)	177.8(15)
N(3)-Pt(1)-N(1)	91.7(3)	C(18)-C(19)-C(20)	124.4(12)
C(19)-Pt(1)-N(1)	178.5(7)	C(18)-C(19)-Pt(1)	117.1(10)
C(20)-C(19)-Pt(1)	111.0(8)		

2.7·2EtPh

Pt(1)-N(1)	2.071(11)	Pt(2)-N(5)	2.067(10)
Pt(1)-C(23)	2.124(11)	Pt(2)-N(7)	2.094(8)
Pt(1)-N(4)	2.137(8)	Pt(2)-C(52)	2.110(12)
Pt(1)-C(28)	2.213(14)	Pt(2)-C(50)	2.118(11)
Pt(1)-C(22)	2.304(16)	Pt(2)-C(51)	2.145(11)
C(22)-C(23)	1.546(16)	C(49)-C(50)	1.519(16)
C(23)-C(24)	1.363(18)	C(50)-C(51)	1.450(16)
C(23)-C(28)	1.412(15)	C(51)-C(52)	1.428(16)
N(1)-Pt(1)-C(23)	134.4(4)	N(5)-Pt(2)-N(7)	86.0(3)
N(1)-Pt(1)-N(4)	86.6(3)	N(5)-Pt(2)-C(52)	169.6(4)
C(23)-Pt(1)-N(4)	134.7(4)	N(7)-Pt(2)-C(52)	103.9(4)
N(1)-Pt(1)-C(28)	104.4(5)	N(5)-Pt(2)-C(50)	100.0(5)
C(23)-Pt(1)-C(28)	37.9(4)	N(7)-Pt(2)-C(50)	173.9(4)
N(4)-Pt(1)-C(28)	167.9(4)	C(52)-Pt(2)-C(50)	70.1(5)
N(1)-Pt(1)-C(22)	172.1(5)	N(5)-Pt(2)-C(51)	133.6(5)
C(23)-Pt(1)-C(22)	40.6(4)	N(7)-Pt(2)-C(51)	134.7(5)
N(4)-Pt(1)-C(22)	100.6(4)	C(52)-Pt(2)-C(51)	39.2(4)
C(28)-Pt(1)-C(22)	68.2(5)	C(50)-Pt(2)-C(51)	39.7(4)
C(21)-C(22)-C(23)	107.4(13)	C(51)-C(50)-C(49)	120.0(13)
C(21)-C(22)-Pt(1)	115.5(12)	C(51)-C(50)-Pt(2)	71.1(7)
C(23)-C(22)-Pt(1)	63.4(7)	C(49)-C(50)-Pt(2)	119.7(8)
C(24)-C(23)-C(28)	127.8(14)	C(52)-C(51)-C(56)	119.3(14)
		C(52)-C(51)-Pt(2)	69.1(7)
		C(56)-C(51)-Pt(2)	116.4(9)
		C(50)-C(51)-Pt(2)	69.1(6)

2.3 Results and Discussion

The values of the carbonyl stretching frequencies from (N,N)Pt^{II}-CO adducts have been frequently used to probe and compare the electronic effects of the incorporated N,N ligands.[5c] To reveal the electronic impacts of the BAB and BAM ligands on the Pt(II) centers, two carbonyl Pt(II) derivatives, [Pt(BAB)Me(CO)][BAr^F_4] (**2.1·CO**) and [Pt(BAM)Me(CO)][BAr^F_4] (**2.2·CO**) (Ar^F = 3,5-bis(trifluoromethyl)phenyl) were synthesized. The CO stretching frequency obtained for **2.1·CO** (2106.3 cm^{-1}) by IR analysis is very close to that for **2.2·CO** (2118.9 cm^{-1}) (2143 cm^{-1} for uncoordinated or "free" CO), as shown in Figure 2.1, indicating similar electronic impacts of the two ligands on the Pt(II) center. Thus, the electronic difference of these two ligands likely plays a much less important role compared with their apparent steric difference.

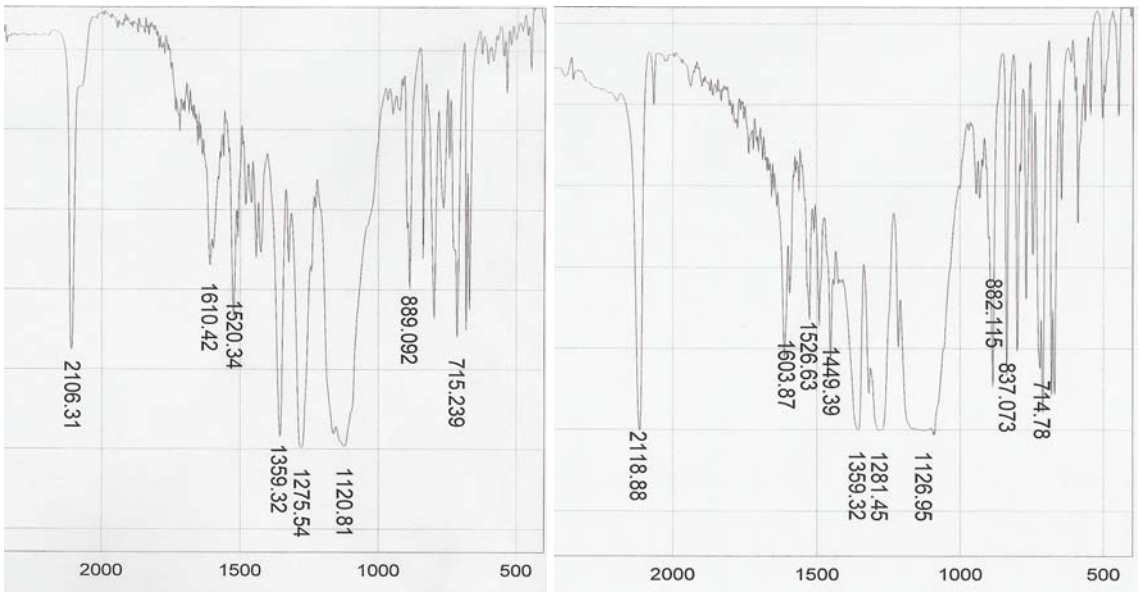

Figure 2.1 The IR spectra of complexes **2.1·CO** (left) and **2.2·CO** (right).

The toluene and EtPh C-H activation reactions were carried out in the same manner as our earlier benzene activation reactions. The cationic Pt(II) complexes,

$[Pt(N,N\text{-}L)(CH_3)(solvent)]^+$, with N,N-L = BAB or BAM, were generated in situ by the addition of one equivalent of the solid acid $[H(Et_2O)_2][BAr^F{}_4]$ to the neat toluene or EtPh solution of $Pt(BAB)Me_2$ (**2.1**) and $Pt(BAM)Me_2$ (**2.2**), respectively. After a certain time, a donor ligand such as SMe_2 or MeCN was used to terminate the activation reaction.

2.3.1 Toluene C-H activation by 2.1

2.3.1.1 Characterization of toluene benzylic activation products

The toluene activation with **2.1** was carried for 1 hour. After termination with SMe_2, the benzylic product with the formula $[Pt(BAB)(CH_2Ph)(SMe_2)][BAr^F{}_4]$ (**2.3**) was isolated as a pure stable crystalline solid in *ca* 41% yield. Compound **2.3** has been fully characterized by NMR spectroscopy, elemental and single-crystal X-ray diffraction analyses. Interestingly, the ^1H NMR spectrum of **3** displayed a quartet, characteristic of an AB pattern (^2J = 10.2 Hz) with a diagnostic ^{195}Pt-^1H coupling pattern ($^2J_{Pt\text{-}H}$ = 103 Hz), for the benzylic CH_2 group, indicating that the two protons have different chemical environments. The two methyl groups on SMe_2 also appear as two distinct signals with diagnostic ^{195}Pt-^1H coupling satellites.

The crystal structure of **2.3** is shown in Figure 2.2. The benzylic carbon C(21) is evidently bound to the Pt(1) center with a bond length as 2.052(7) Å, which is typical for a single Pt-C bond. The C(21)-C(22) bond length of 1.488(9) Å is typical for a C-C single bond. The Pt(1)-C(21)-C(22) bond angle is 119.0(5)°. The crystal structure also confirmed that the two protons of the methylene group are indeed in different chemical environments. One unexpected feature is the orientation of the benzylic group. It is oriented surprisingly "up" toward the BAB bridging phenyl moiety, despite the obvious

steric congestion in this orientation. The dihedral angle between the N(1) 7-azaindolyl ring and the phenyl ring of the benzyl group is 32.6°, while the dihedral angle between the benzyl phenyl ring and the BAB phenyl ring is 64.0°.

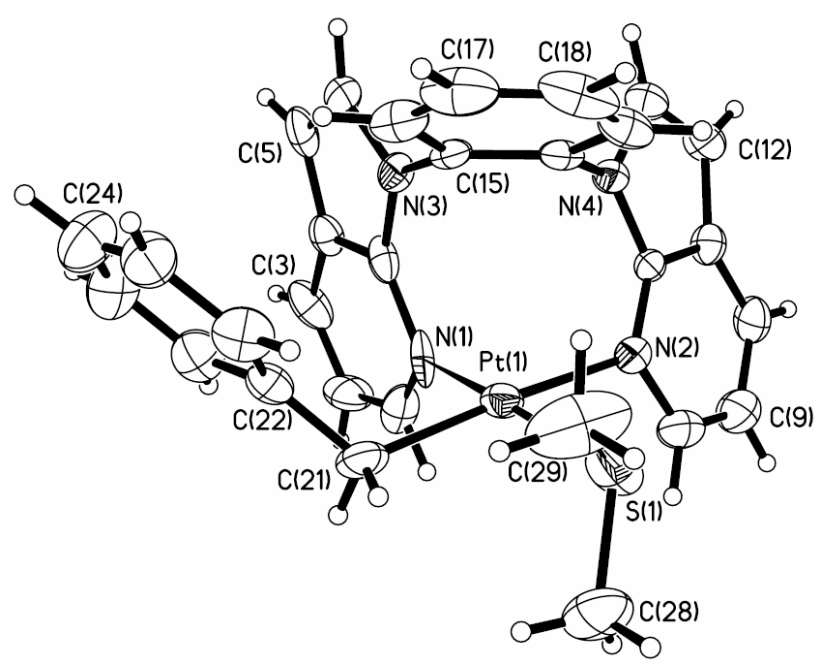

Figure 2.2 Crystal structure of **2.3** with 30% ellipsoids; the [BAr^F_4] anion is omitted for clarity.

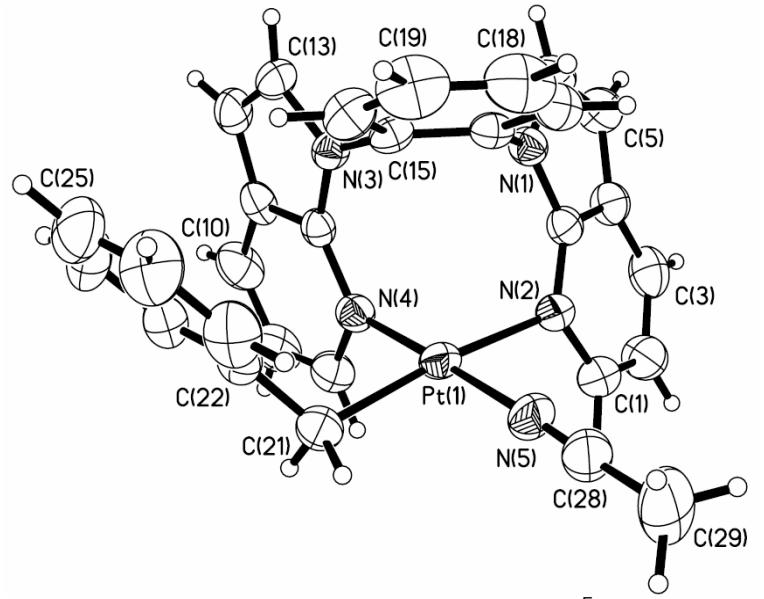

Figure 2.3 Crystal structure of **2.4** with 30% ellipsoids; the [BAr^F_4] anion is omitted for clarity.

Beside SMe_2, the termination of the toluene activation reaction was also attempted with MeCN. This afforded compound [Pt(BAB)(CH_2Ph)(MeCN)][$BAr^F{}_4$], **2.4**, as a stable crystalline product in ~ 38% isolated yield. As observed in **2.3**, the benzylic CH_2 protons display an AB pattern (^2J = 10.0 Hz) with diagnostic ^{195}Pt-^{1}H coupling satellites ($^2J_{Pt\text{-}H}$ = 106.5 Hz) in the ^{1}H NMR spectrum of **2.4**, confirming that the benzylic C-H bond was activated. Compound **2.4** was also characterized by a single-crystal X-ray diffraction analysis. The structure of **2.4** resembles that of **2.3** (Figure 2.3). Interestingly, the benzyl group is again oriented "up" toward the BAB bridging phenyl moiety. The bond lengths for Pt(1)-C(21) and C(21)-C(22) are 2.058(5) and 1.498(7) Å, respectively. The phenyl group of the benzyl group has a dihedral angle of 38.2° with the phenyl plane of the BAB ligand, and 35.4° with the N(4) 7-azaindolyl ring.

2.3.1.2 Toluene C-H activation profile with 2.1

In order to determine the actual product distribution at various reaction stages so as to establish the activation profile, the toluene activation reaction was then monitored by ^{1}H NMR spectroscopy. A small amount of solution was sampled at regular time intervals and immediately quenched with excess CD_3CN, instead of quenching the bulk reaction. After the removal of the solvents under vacuum, the ^{1}H NMR spectrum of the residue was recorded in CD_2Cl_2. The high field region of ^{1}H NMR spectra for the reaction mixture at selected reaction stages is shown in Figure 2.4; the corresponding product distribution is listed in Table 2.4.

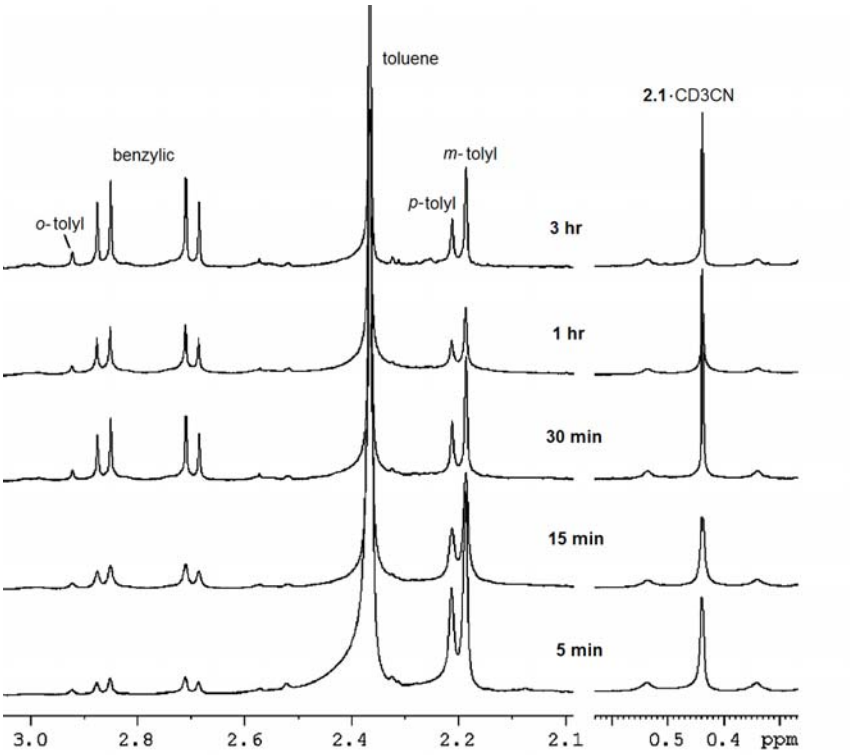

Figure 2.4 The high-field region of the ^{1}H NMR spectra for the toluene activation by **2.1** at different stages (after quenching with CD_3CN).

Table 2.4 Product distribution of the toluene activation by **2.1** at different stages.[a]

time	**2.1**·CD_3CN[b]	benzylic[c]	*p*-tolyl[d]	*m*-tolyl[e]
5 min	31%	17%	24%	28%
30 min	22%	43%	15%	20%
1 h	19%	55%	9%	17%
3 h	17%	60%	11%	12%
48 h	0	81%	6%	13%

[a] The activation reaction was carried in neat toluene at ambient temperature under N_2 atmosphere. [b] $[Pt(BAB)(CH_3)(CD_3CN)]^+$. [c] $[Pt(BAB)(CH_2Ph)(CD_3CN)]^+$. [d] $[Pt(BAB)(p\text{-tolyl})(CD_3CN)]^+$. [e] $[Pt(BAB)(m\text{-tolyl})(CD_3CN)]^+$.

The ^{1}H NMR spectra showed that the starting material **2.1** was completely consumed in 5 minutes after the addition of the $[H(Et_2O)_2][BAr^F{}_4]$ acid. But more surprisingly, the stoichiometric toluene activation had already been accomplished in nearly 70% overall yield, suggesting that the activation reaction is very fast in the early stage. As the reaction time increases, the signal from the cationic complex **2.1**·CD_3CN

further decreases and the signals for the toluene C-H activation products increase. One notable change is that after 30 minutes the benzylic product becomes the major product (43%). The product distribution at 1 hour is illustrated in Scheme 2.1. The signal from the cationic complex **2.1**·CD_3CN became completely undetectable after ~40 hours.

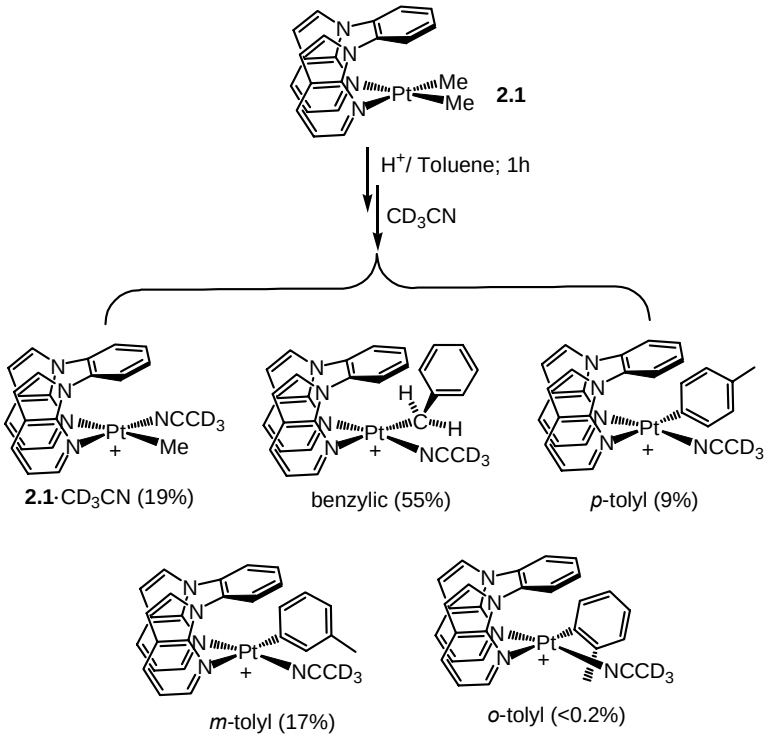

Scheme 2.1 The product distribution for the toluene activation reaction at 1 hour.

Another salient feature is the variation of production distribution with time. While the benzylic product accumulated gradually, the aromatic activation products were found to be the dominant species (*meta*- and *para*-) at the early stage of the reaction but converted gradually into the benzylic product with time, whereas no *ortho*-aryl product was seen during the whole process possibly due to the steric reason. Therefore, the toluene benzylic C-H activation is evidently a thermodynamically preferred process while the aromatic activation is kinetically favored. This behavior resembles the recent study by Bercaw and coworkers[6k] and is also likely attributable to the intermediacy and the

thermodynamic stability of a type of η^3-benzylic Pt(II) intermediate. Unfortunately, attempts to investigate the original toluene activation reaction mixture prior to termination did not lead to the identification of such species.

2.3.2 EtPh C-H activation with 2.1 and 2.2

2.3.2.1 Regioselective EtPh activation by 2.1 and 2.2 and characterization of the benzylic products 2.5 and 2.6

Compared with toluene which has only one type of aliphatic C-H bonds, EtPh has two different types of aliphatic C-H bonds and thereby its activation is more unpredictable. The EtPh C-H activation reactions with **2.1** were carried out similarly and were also monitored by ^{1}H NMR spectroscopy. Consistent with toluene activation, the *meta*- and *para*- aromatic activation products were again found to dominate at the early stage of the reaction but also convert gradually to the benzylic product [Pt(BAB)(CH_3CN)(CH(Me)Ph)][$BAr^F{}_4$] (**2.5**) with time. The ^{1}H NMR spectrum recorded after 15 minutes for the reaction showed that the *para*- and *meta*- aromatic C-H actvation products are the major products, and soon after the amount of the aromatic C-H actvation products started to decrease. The benzylic C-H actvation product became the major product after 12 hours. No *ortho*-aryl products or *β*-phenylethyl products were seen during the whole process. The cationic starting material generated from **2.1** by protonation with [$H(Et_2O)_2$][$BAr^F{}_4$] was completely consumed after 5 days, when the ratio between the benzylic product and aryl products (*meta*- and *para*-) of EtPh was found to reach a stable value as > 9:1 after 5 days. Due to severe peak overlapping, the

determination of the product ratio *via* integrating the diagnostic ^{1}H NMR signals for the EtPh C-H activation with **2.1** is not possible.

In contrast, the short separation distance (~2.44 Å) between the H' atom of the BAM bridging CHH' group and the Pt(II) center in **2.2** induces strong three-center four-electron $Pt^{II}\cdots H'$-C interactions,[3] which results in a distinct δ downfield shift of H' from ~7 ppm to 11.69 ppm as shown in Figure 2.5,[12b] thus generating a diagnostic ^{1}H signal which not only is sensitive to a subtle environmental change on the Pt(II) center but has no interference from other ^{1}H signals, thus allowing us to monitor the EtPh C-H activation reaction by ^{1}H NMR spectroscopy.

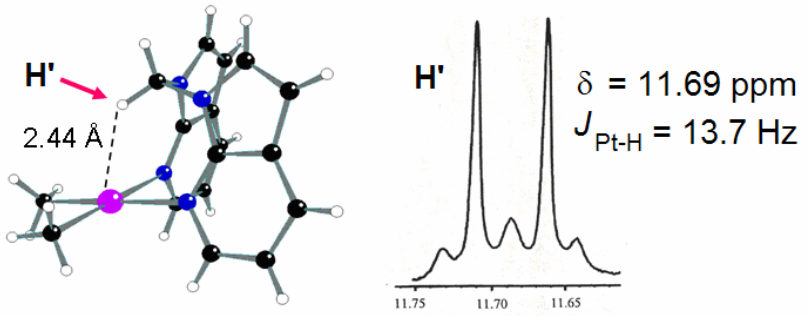

Figure 2.5 Crystal structure of **2.2** (left) and the diagnostic ^{1}H NMR signal of H' from the bridging CH*H'* group in **2.2** (right).

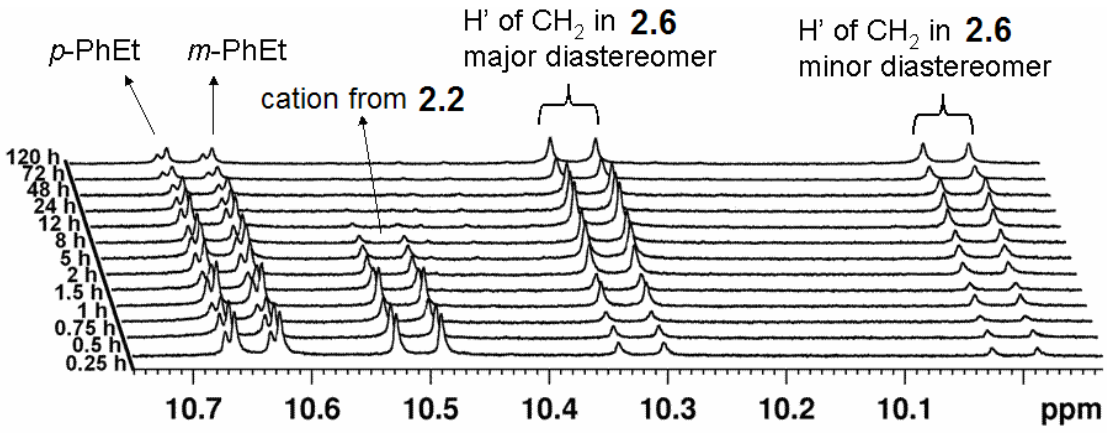

Figure 2.6 ^{1}H NMR spectra of the low field region of the reaction mixture of EtPh C-H activation by **2.2**, showing the distribution change of aryl C-H activation products (*p*- and *m*-PhEt) versus the benzylic product **2.6** with time.

The EtPh activation by **2.2** was therefore investigated. To facilitate ^{1}H NMR spectral assignments of the products, the *para*-aromatic activation product [Pt(BAM)(*p*-PhEt)(CH_3CN)]($BAr^F{}_4$) was synthesized individually. Not surprisingly, the *para*- and *meta*-aromatic C-H activation products were found again to be kinetically preferred. As shown by the ^{1}H NMR spectra corresponding to the low-field H' signal region in Figure 2.6, the spectrum recorded after 15 minutes shows a mixture of products consisting of the *para*- and *meta*-aromatic products (50% yield), the benzylic product [Pt(BAM)(MeCN)(CH(Me)Ph)][$BAr^F{}_4$], (**2.6**, 18% yield) and the cationic starting material (32%). After 3 days, the starting material was completely consumed. The product distribution between the benzylic C-H activation and aromatic C-H activation after 5 days was less than 4:1, an indication that compound **2.2** has a lower regioselectivity, compared to compound **2.1**. Considering their similar electronic natures, this regioselectivity difference between **2.1** and **2.2** toward EtPh C-H activation is likely attributable to the steric difference between the BAB and the BAM ligands. The BAB ligand is apparently more sterically demanding than the BAM ligand.

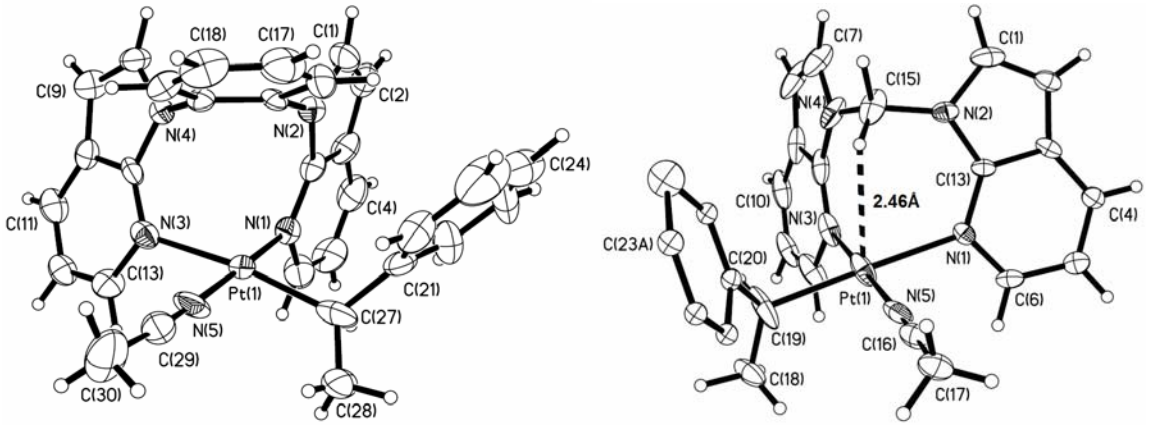

Figure 2.7 Crystal structures of complexes **2.5** (left) and **2.6** (right) with 30% ellipsoids.

Both complexes **2.5** and **2.6** were isolated and fully characterized by NMR spectroscopy, and elemental and single-crystal X-ray diffraction analyses. The structures for the cationic portion of **2.5** and **2.6** are shown in Figure 2.7. The basic structural features of **2.5** resemble those of the above toluene analogues **2.3** and **2.4**. The most striking feature displayed by these two structures is again the orientation of the new benzylic groups, which is oriented "up" toward the chelate ligand.

2.3.2.2 Diastereoselectivity of the EtPh benzylic activation by 2.1 and 2.2

For the EtPh benzylic activation by **2.1** and **2.2**, one unique feature is the observed diastereoselectivity. As shown in Chart 2.3, because of the asymmetric blocking on one side of the Pt(II) coordination plane by the BAB and BAM ligands, the cationic species generated *via* protonation of the $PtMe_2$ precursors **2.1** and **2.2** both have a chiral Pt(II) center, but both enantiomers coexist in the solution. Moreover, unlike toluene benzylic activation, the cleavage of a C-H bond on the CH_2 group of the EtPh molecule leads to the formation of a new chiral carbon center. Accordingly, the coexistence of both a Pt(II) and a carbon chiral center in the cationic complexes of **2.5** and **2.6** results in the formation of two diastereomers (*RR* and *RS* or their enantiomers *SS* and *SR*) for each complex, as illustrated in Chart 2.4. Due to the significant difference between the structures of the diastereomers such as **2.5A** and **2.5B** (Chart 2.4), it was anticipated that these two diastereomers may display distinct chemical shifts in ^{1}H NMR spectra.

Chart 2.3

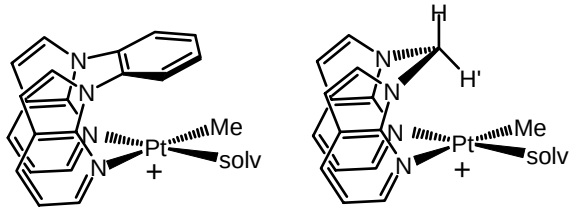

Chart 2.4

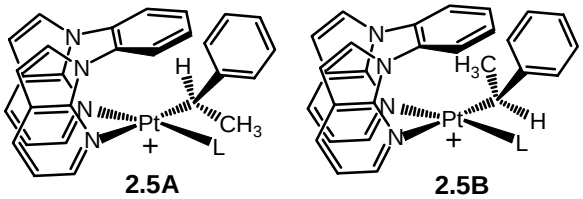

2.5A **2.5B**

Indeed, two distinct sets of chemical shifts for the CH and the CH_3 protons of the $CH(CH_3)Ph$ group corresponding to the two diastereomers were observed in the ^1H NMR spectrum of the complex **2.5**. The protons of the CH and the CH_3 groups display characteristic ^{195}Pt-^1H coupling patterns with fairly large ^2J and ^3J ^{195}Pt-^1H coupling constants (~104 and ~50 Hz, respectively). Most importantly, the intensities of the two sets of signals are not equal, with a ratio of ~ 3.7:1.0 for the final reaction mixture, as illustrated in Figure 2.8. The NMR data unambiguously established that the EtPh C-H bond activation by **2.1** proceeds not only regioselectively but also diastereoselectively. Notably, similar diastereoselectivity from such an intermolecular process has never been observed in previously known cationic Pt(II) systems.

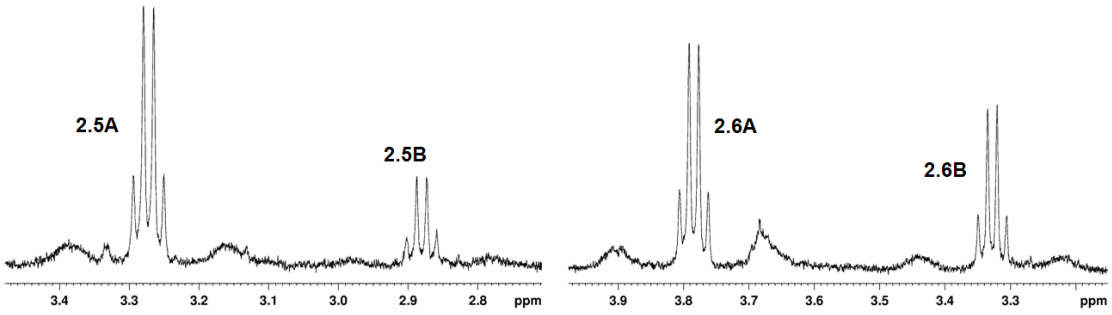

Figure 2.8 ^1H NMR spectra (in CD_2Cl_2) showing the chemical shifts and the relative intensity of the C*H*(Me) protons of the two diastereomers in **2.5** (left) and **2.6** (right) in the reaction mixtures.

Complex **2.6** also displays two distinct sets of chemical shifts corresponding to the two diastereomers (Figure 2.8). For the CH and the CH_3 protons, characteristic ^{195}Pt-^{1}H coupling patterns were once again observed, with the ^{195}Pt-^{1}H ^{2}J and ^{3}J coupling constants being ~110 and ~40 Hz, respectively. However, the observed ratio of the two diastereomers for **2.6** is ~1.5:1.0, much lower than that for **2.5**. Thus, the BAM system displays not only a relatively low regioselectivity but also a relatively low diastereoselectivity toward EtPh activation, compared to the BAB system. Again, the obviously more effective blocking group, phenyl, in the BAB ligand, compared to the CH_2 group in the BAM ligand, appears to be responsible for the observed difference in diastereoselectivity between these two systems.

2.3.2.3 Conformational analyses of complexes 2.5 and 2.6 in solution by NOESY

The consistent but rather unusual configurations of the benzylic phenyl groups in **2.5** and **2.6** as revealed by single-crystal X-ray diffraction analyses are interesting. To determine the configurations of the benzylic phenyl groups in **2.5** and **2.6** in solution, we carried out NOESY spectroscopic analyses.

Figure 2.9 shows the selected potions of the NOESY spectrum for compound **2.6** in CD_2Cl_2 solution. The most direct NMR evidence revealing the absolute configuration comes from NOE cross-peaks between CH_3, CH, and H(6) of the 7-azaindolyl ring. As seen from Figure 2.9, for diastereomer **A** the CH~H(6) cross-peak is considerably stronger than the CH_3~H(6) cross-peak, indicating that the CH group is pointing toward the H(6) atom of the 7-azaindolyl ring. In contrast, the two corresponding cross-peaks for diastereomer **B** have similar intensities. It is also important to note that the CH_3~H(6)

cross-peak for **B** is much greater than the corresponding CH_3~H(6) cross-peak for **A**, which cannot be accounted for simply by the population difference between the two methyl peaks. This further proves that the CH_3 in the diastereomer **B** is much closer to H6 of the 7-azaindolyl ring than the CH_3 in the diastereomer **A**. More surprisingly, strong NOE cross-peaks are observed between the *ortho* protons of the benzylic phenyl moiety and H' of the CH_2 bridge for both diastereomers, an indication that the phenyl ring is oriented toward the CH_2 bridge in the same manner as shown by the crystal structure. Moreover, according to above assignments, it is evident that **A** is the minor diastereomer which has the same stereogeometry as shown by the crystal structure in Figure 2.7, while **B** is the major diastereomer.

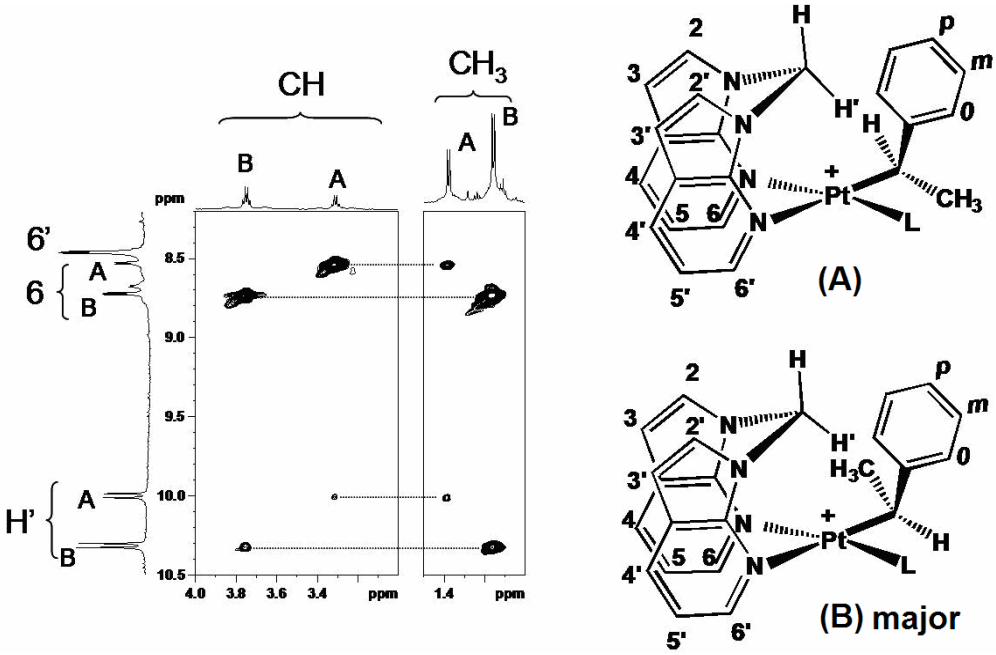

Figure 2.9 Potions of the NOESY spectrum for compound **2.6** in CD_2Cl_2 at 298 K. A mixing time of 400 ms was used.

In contrast to the case for **2.6**, a similar NOESY spectral analysis established that the major diastereomer for **2.5** is **A**, the same as the crystal structure shown in Figure

2.10. The most important evidence supporting this assignment is the strong CH~H(6) cross-peak for isomer **2.5A**, as shown in Figure 2.9, which is absent for isomer **2.5B**, supporting that the CH proton of the benzylic group in **2.5A** is closer to the 7-azaindolyl ring than that of **2.5B**. In addition, a strong CH_3~H(b, and b') cross-peak was also observed for isomer **2.5A**, but not isomer **2.5B**, which is again consistent with the diastereomer **2.5A** being the major isomer.

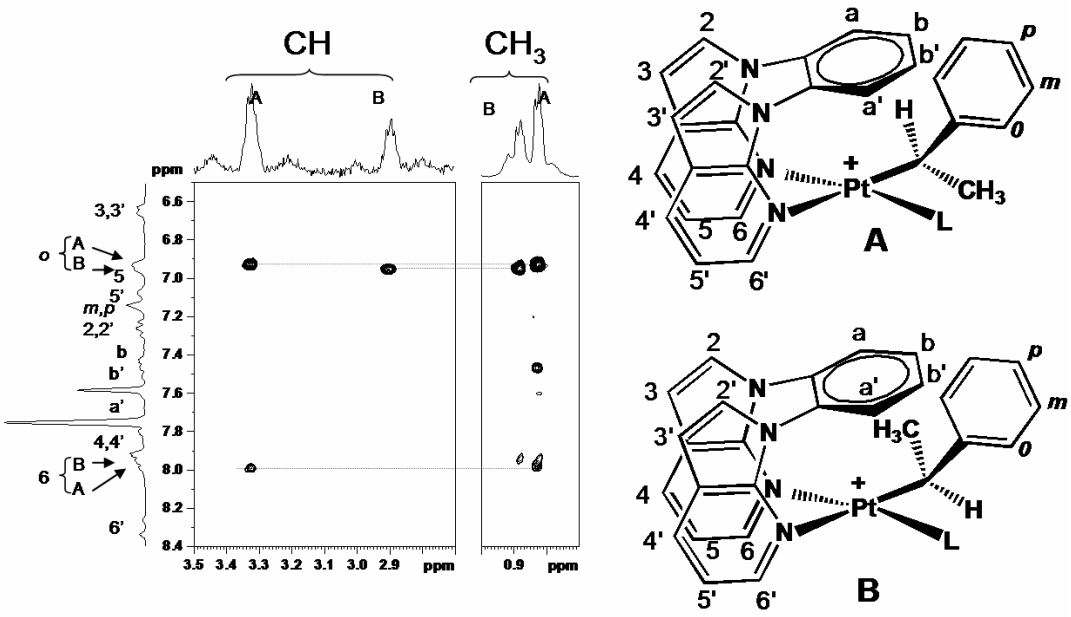

Figure 2.10 Portions of the NOESY spectrum for compound **2.5** in CD_2Cl_2 at 298 K. A mixing time of 400 ms was used.

To reveal the origins of the observed regio- and diastereoselective EtPh C-H activation, and to understand the differences displayed by **2.1** and **2.2**, efforts were made to analyze and isolate the possible intermediates.

2.3.2.4 Isolation and characterization of the η^3-complex 2.7

Since the activation reaction showed no further change after 5 days, the EtPh activation reaction mixture by the BAB complex **2.1** was examined by ^1H and ^{13}C NMR

spectroscopy in CD_2Cl_2 without termination. Remarkably, we observed unambiguously diagnostic ^{1}H NMR signals attributable to η^3-benzylic complexes. In addition to a small amount of aryl C-H activation products, the η^3-benzylic product is revealed to be the major product. No η^1-benzylic compound was observed. Moreover, it appeared that there were two types of η^3-benzylic species in the reaction mixture with a ratio of ~3.7:1. These results sharply contrast the circumstances of the above toluene activation, where such η^3-benzylic species can not be unambiguously confirmed, likely attributable to the stability differences of the η^3-benzylic species involved.

To fully characterize the elusive η^3-compound, we tried to isolate the η^3-benzylic compound from the reaction mixture and our efforts were successful. The η^3-compound **2.7** was obtained as a crystalline solid in about 70% yield. As shown in Figure 2.10, the ^{1}H NMR spectrum for the isolated solid **2.7** showed two sets of well-resolved chemical shifts that correspond to two distinct η^3-compounds, where **2.7A** represents the major isomer while **2.7B** represents the minor isomer. The inset configuration assignments of the two isomers have been verified by NOESY analyses.

As shown in Figure 2.11, the diagnostic signals for the η^3-benzylic group are the *ortho*-proton of the phenyl group (δ 3.92 ppm for **2.7A** and 6.09 ppm for **2.7B**, respectively) and the proton of the C***H***Me group (δ 1.88 ppm for **2.7A** and 3.18 ppm for **2.7B**, respectively), both of which display characteristic ^{195}Pt-^{1}H coupling with coupling constants of ~40 Hz and ~67 Hz, respectively. In the ^{13}C NMR spectrum, two sets of chemical shifts for the *ortho*-carbon of the phenyl group and the ***C***HMe carbon atom with distinct ^{195}Pt-^{13}C coupling satellites were also observed. The formula of [Pt(BAB)(η^3-

CH(Me)Ph)][BAr^F_4] was therefore proposed for **2.7**, which is consistent with the η^3-type complexes proposed by Bercaw and coworkers.[6k,6l]

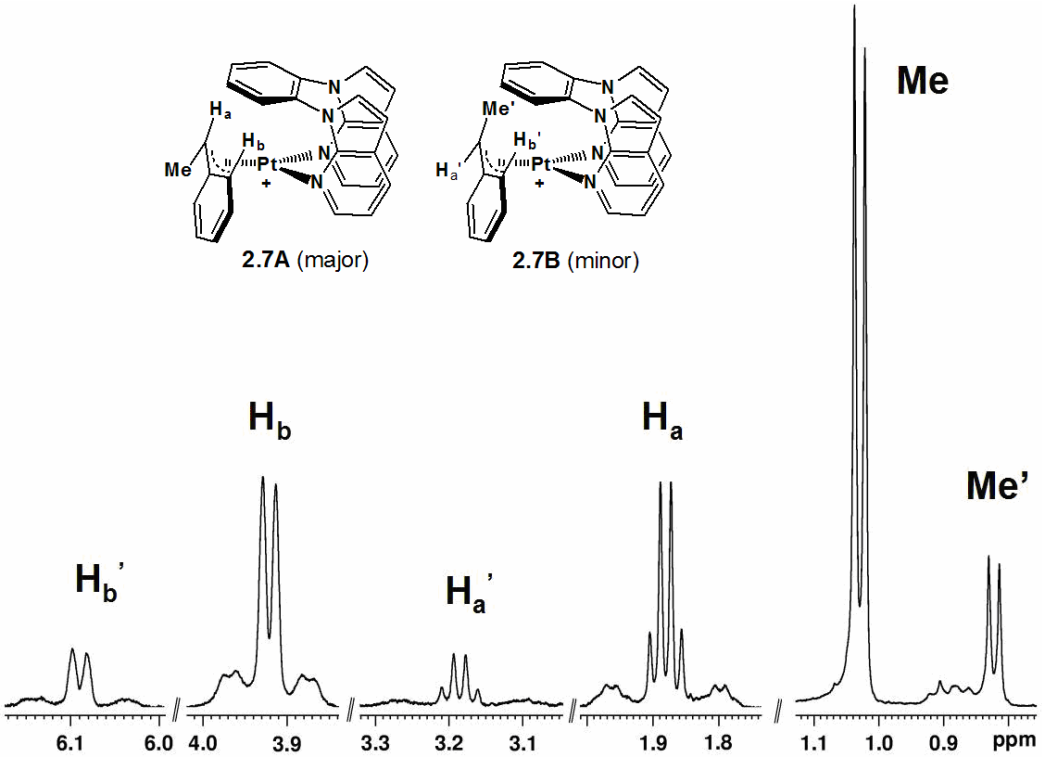

Figure 2.11 Parts of the ^{1}H NMR spectrum of **2.7** (**2.7A**: major isomer; **2.7B**: minor isomer) in CD_2Cl_2 showing the chemical shifts and the proposed structures of the two isomers.

To understand the origin of the two apparently different η^3-species of **2.7**, we determined the crystal structure of the major isomer **2.7A** by a single-crystal X-ray diffraction analysis. The structure is shown in Figure 2.12. There are two independent molecules of **2.7A** in the asymmetric unit with identical structures. Again, this cationic structure has no symmetry, but both enantiomers coexist in solution and in the crystal lattice. Evidently, the CH(Me)Ph group (Figure 2.12) is bound to the Pt center sideways through three carbon atoms, a η^3-fashion typically observed for an allyl group. The bond lengths from the Pt center to the three carbon atoms are similar. Although η^3-type allyl Pt(II) complexes are well known,[8c, 8f] the structure of **2.7A** is the first direct structural

proof of the η^3-benzylic Pt(II) complexes proposed by Bercaw and coworkers. Notably, the steric congestion around the Pt(II) center in **2.7A** likely accounts for its enhanced stability and the success in both its isolation and characterization.

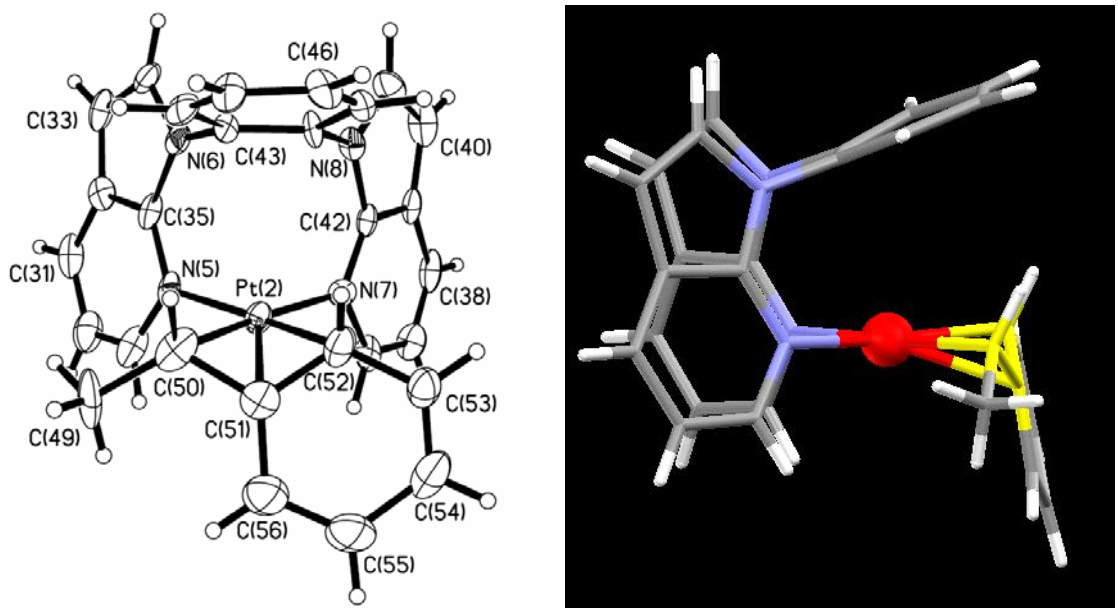

Figure 2.12 Crystal structure of the cation of **2.7A** with 30% ellipsoids from a front view (left) and a side view (right).

In the major isomer **2.7A**, the C***H***(Me)Ph proton and the *ortho* proton of the phenyl ring are on the same side as shown by the crystal structure (Figure 2.12), while in the minor isomer the CH_3 group is on the same side with the *ortho* proton of the phenyl ring. This configuration of **2.7A** effectively avoids strong steric repulsion between the CH(Me)Ph methyl group and the BAB bridging phenyl group, as shown by crystal structure of **2.7A** (Figure 2.12). However, such repulsion would inevitably be encountered in the minor isomer **2.7B**. Thus, the preferential formation of the major isomer **2.7A** is attributable to and driven by a steric effect.

2.3.2.5 Isolation and characterization of the η^3-complex 2.8

The ^{1}H NMR spectrum for the 5 day activation reaction of EtPh by the BAM complex **2.2** also displayed two distinct sets of chemical shifts for the η^3-benzylic products with a ratio of ~1.5:1, attributable to the two η^3 isomers (Figure 2.13). Although we have not been able to isolate the η^3-benzylic product [Pt(BAM)(η^3-CHPh(Me))][BAr$^F{}_4$] (**2.8**) as a pure crystalline compound, the two η^3 isomers of **2.8** are believed to have similar structures to those of **2.7**. The diminished ratio of the major isomer versus the minor isomer of **2.8**, compared to that of **2.7**, is evidently caused by the diminished steric congestion in **2.7**.

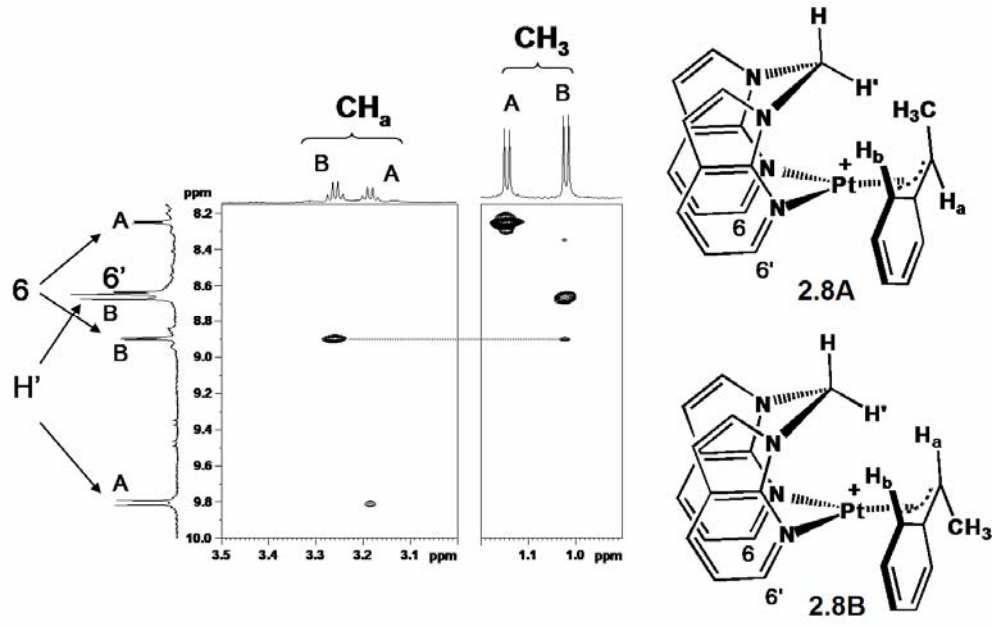

Figure 2.13 Portions of the NOESY spectrum for compound **2.8** in CD_2Cl_2 at 298 K. A mixing time of 400 ms was used.

To establish whether the major isomer of **2.8** has the same configuration as the major isomer **2.7A**, NOESY analyses were performed for **2.8** and portions of the NOESY spectrum are shown in Figure 2.13. Unexpectedly, however, the methyl group of the

major isomer shows a strong cross-peak with the H′ proton of the CHH' bridge, while the same cross-peak is absent for the minor isomer. This is a strong indication that the major isomer of **2.8** has the structure **2.8B**, instead of **2.8A**. Consistent with this assignment is the weak cross-peak between H_a and H′ for the minor isomer (Figure 2.13).

These configuration assignments contradict those for **2.7** and seem counterintuitive, since isomer **2.8B** appears to be more sterically congested than **2.8A** does. The NOESY data, in fact, provided a clue for this puzzle. As shown in Figure 2.13, the methyl group of the minor isomer evidently has a very large cross-peak with H6 of the 7-azaindolyl ring, an indication that in isomer **2.8A** the methyl group is considerably closer to the 7-azaindolyl ring, generating a sterically crowded environment. Accordingly, the greater population of isomer **2.8B** over **2.8A** is a consequence of tradeoff between a "CH_3"-"C***H'***H" interaction versus a "CH_3"-"7-azaindolyl" interaction. The contrasting selectivities for different η^3-isomers by **2.7** and **2.8** demonstrate clearly the subtle difference in the steric blockage imposed by the BAB ligand and BAM ligand, respectively.

2.3.2.6 Conversion of the η^3-benzylic compounds to the η^1-benzylic compounds

One key observation in characterizing the η^3-compounds was that the isomer distribution for the η^3-compounds **2.7** and **2.8** are approximately the same as those of the diastereomer distribution for the η^1-benzylic compounds **2.5** and **2.6**, implying that η^3-benzylic compounds are likely precursors to the η^1-benzylic products. To confirm that the η^3-compounds can indeed be converted to the η^1-compounds while retaining the

isomer distribution, the reaction of the η^3-compound **2.7** with CD_3CN was monitored by ^1H NMR spectroscopy in CD_2Cl_2.

Indeed, as shown by the NMR spectra in Figure 2.14, compound **2.7** was converted quantitatively to the η^1-compound **2.5** upon reacting with MeCN and the resultant diastereomer distribution for **2.5** was the same as the initial isomer ratio of the η^3-compound **2.7**. This conversion itself is not surprising since a similar η^3- to η^1-transformation was observed by Bercaw and coworkers.[6k,6l] However, the significance lies in the fact that it established the direct link between the major η^3-isomer of **7A** and the major diastereomer of **7A** and that between the minor η^3-isomer of **7B** and the minor diastereomer **5B**. The addition of MeCN to the isomers of the η^3-compound **2.8** resulted in the similar specific transformation to the diastereomers of the η^1-compound **2.6** with the retention of the isomer ratios.

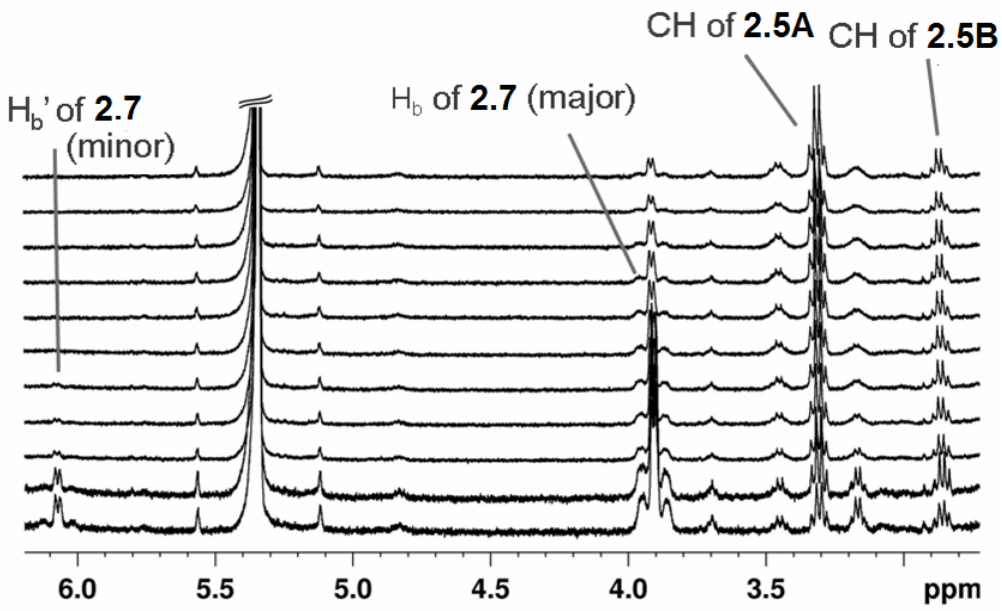

Figure 2.14 ^1H NMR spectra in the 2.7 to 6.2 ppm region showing the conversion of the isomers of **2.7** to the diastereomers of **2.5** with the retention of the isomer ratio after the addition of excess CD_3CN (~30 fold) (upward). The spectra were recorded at ambient temperature at 5 minute intervals in CD_2Cl_2.

Accordingly, these specific transformations must be a manifestation/consequence of the asymmetric blocking of the Pt(II) coordination plane by the BAB or BAM ligand. The blocking of the Pt(II) center by the ligand bridging groups forces the MeCN ligand to approach the Pt(II) center from the bottom, replacing the π-bound phenyl group *via* an associative process, thus resulting in the diastereoselective formation of the η^1-benzylic complexes. The exclusive formation of the major diastereomer **2.5A** with the *S* chirality on the CH center from the major η^3-isomer **2.7A**, and the minor diastereomer **2.5B** with the *R* chirality on the CH center from the minor η^3-isomer **2.7B** are illustrated in Scheme 2.2.

Scheme 2.2

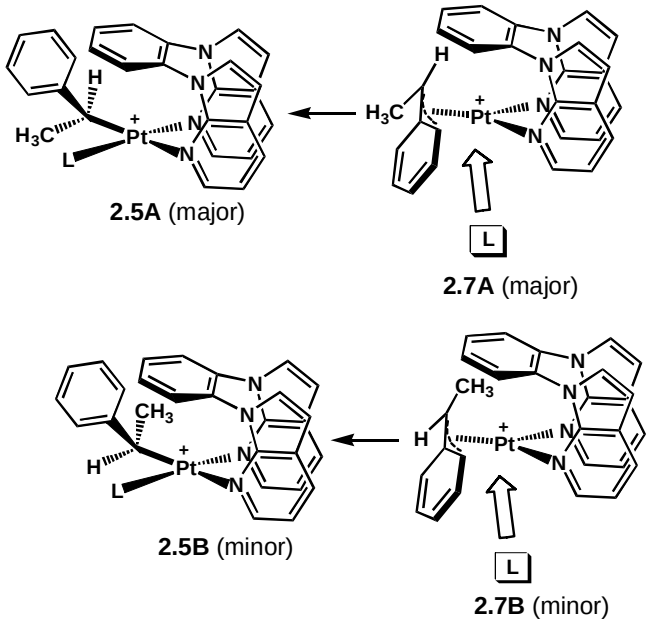

2.3.3 Mechanistic pathway

On the basis of established features for arene C-H activation,[12] the mechanistic pathways for the toluene and EtPh C-H activation by our $PtMe_2$ complexes that are consistent with our preliminary results are proposed, as illustrated by the EtPh C-H

activation with complex **2.1** in Scheme 2.3. The initial protonation of **2.1** with $[H(Et_2O)_2][BAr^F{}_4]$ generates the active cationic Pt^{II}-Me intermediate *via* elimination of CH_4. The subsequent EtPh coordination to the cationic Pt(II) center affords a type of η^2-EtPh bound Pt^{II}-Me intermediate, which then undergoes EtPh aromatic C-H activation *via* the formation of a Pt^{IV} hydride intermediate and successive elimination of CH_4, resulting in the kinetically preferred *para*- and *meta*-aromatic activation products. In the presence of free EtPh molecules, the aromatic activation products gradually convert into the η^3-benzylic activation products. The subsequent formation of the thermodynamically stable η^3-benzylic species as a downhill trap drives the conversion. Alternatively, direct EtPh benzylic activation by either the cationic Pt^{II}-Me intermediate or the η^2-EtPh bound Pt^{II}-Me intermediate can also be possible but less likely compared to the transformation *via* an aromatic activation intermediate.

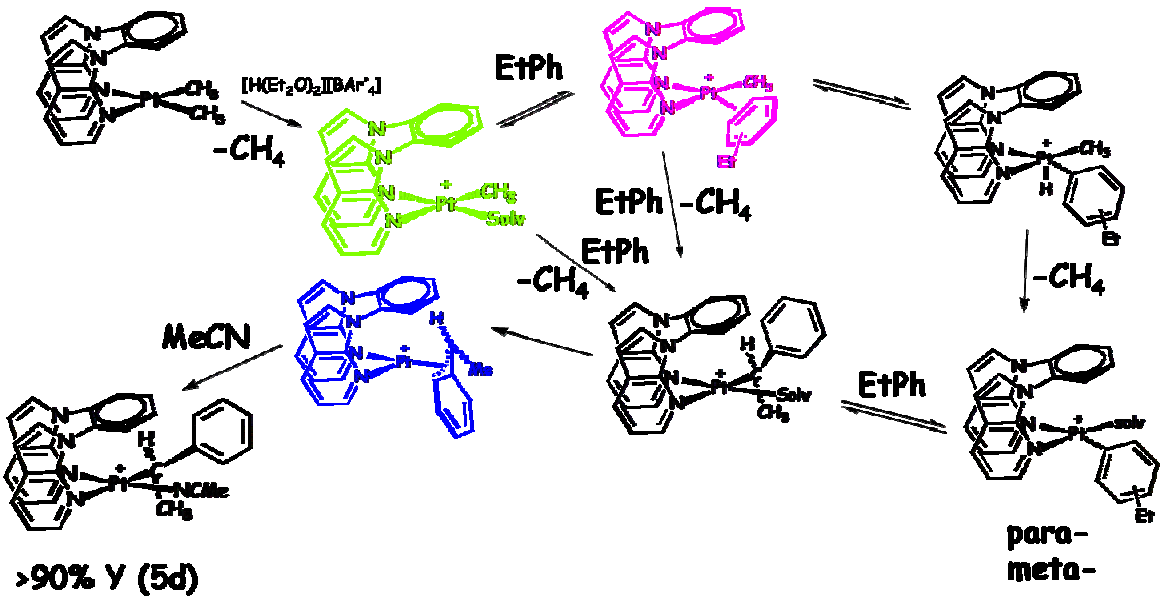

Scheme 2.3 Possible mechanistic pathways of EtPh C-H activation by complex **2.1**.

Bercaw and coworkers showed that in the absence of donor ligands such as MeCN, cationic η^1-benzylic complexes can be converted to the η^3-complexes.[61] To verify if this pathway is indeed operative in our system, we synthesized Pt(BAM)(η^1-$CH_2Ph)_2$ (**2.9**) and monitored the protonation reaction of **2.9** in acetone-d_6 by ^{1}H NMR spectroscopy. After the addition of one equivalent of $[H(Et_2O)_2][BAr^F{}_4]$, although > 90% of the compound was a η^1-CH_2Ph complex (stabilized by acetone or adventitious water), a small amount of the η^3-CH_2Ph compound indeed appeared to be formed, as shown in Figure 2.15 and Scheme 2.4. The assignment for the η^3-CH_2Ph compound was further confirmed by the COSY analyses. This observation is very informative, supporting the possible conversion of the η^1-benzylic species into the η^3-complexes.

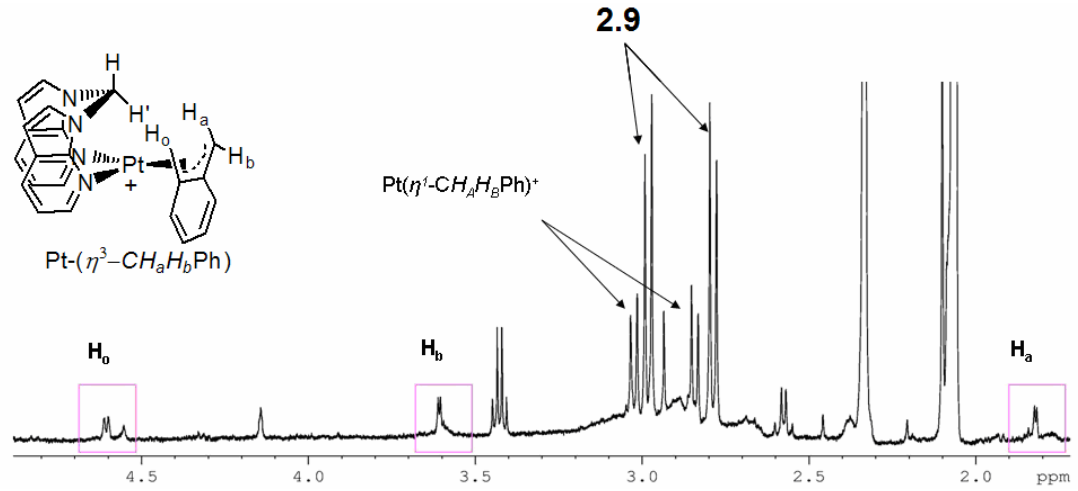

Figure 2.15 ^{1}H NMR spectrum (high field region) for the protonation of **2.9** in CD_3COCD_3, showing generation of diagnostic signals of η^3-complex [Pt(BAM)(η^3-CH_2Ph)]$^+$.

Scheme 2.4

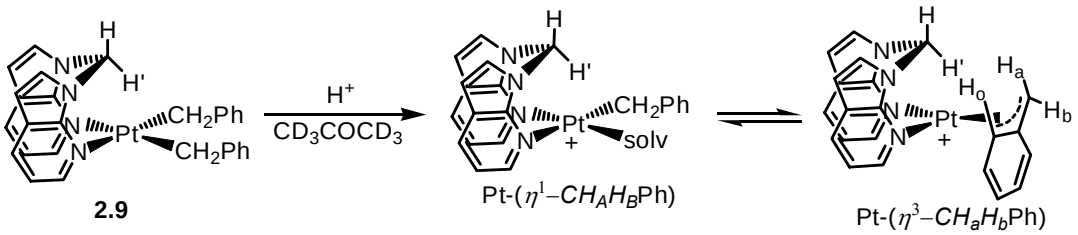

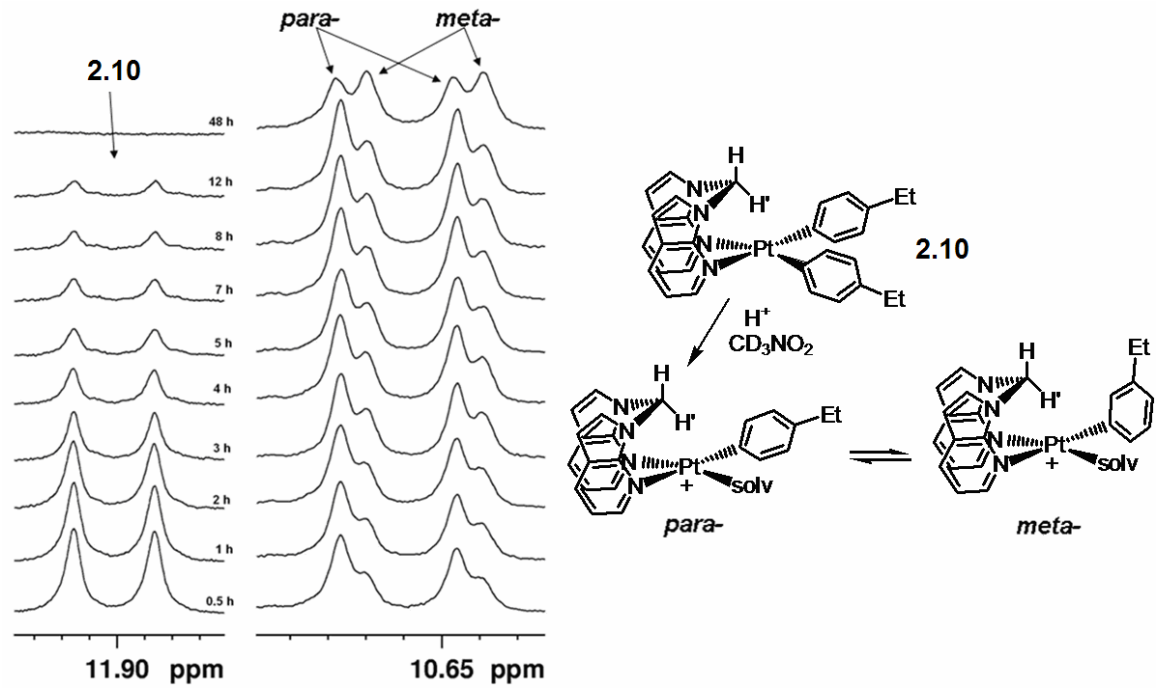

Figure 2.16 The stacked ^{1}H NMR spectra (low field region) for the protonation of **2.10** in CD_3NO_2 at ambient temperature.

We also attempted to examine direct conversion of aromatic C-H activation products into the benzylic activation products, *via* monitoring the protonation reaction of complex Pt(BAM)(*p*-PhEt)$_2$ (**2.10**) with ^{1}H NMR spectroscopy, in order to understand the transformation process involved. As shown by the diagnostic ^{1}H signal region for the BAM CH*H'* atom (Figure 2.16), upon protonation of **2.10**, the formation of both [Pt(BAM)(*p*-PhEt)(solv)]$^{+}$ and [Pt(BAM)(*m*-PhEt)(solv)]$^{+}$ was observed. While the amount of Pt(BAM)(*p*-PhEt)$_2$ decreased gradually, the relative ratio of the *meta*-PhEt Pt(II) complex versus *para*-PhEt Pt(II) complex kept increasing. Remarkably, after 2 days the amount of *meta*-C-H activation product exceeds that of *para*-aromatic C-H activation product, as displayed by the top ^{1}H NMR spectrum in Figure 2.16. These results demonstrated unambiguously the transformation of the *para*-aromatic C-H activation product into the *meta*-aromatic C-H activation product. However, no distinctive signals

from the benzylic C-H activation product were observed even after a month. This likely indicates that the transformation of aromatic C-H activation products into the benzylic products is an intermolecular process, and the rate of which depends greatly on the concentration of the free EtPh in the system. Such associative transformations have also been unambiguously demonstrated by Bercaw and coworkers.[6l]

2.4 Conclusions

In this chapter, we demonstrated that the BAB and BAM Pt(II) complexes are capable of activating alkyl-substituted benzene readily and selectively. Our investigation has established that the η^1-benzylic C-H activation is thermodynamically favored for both complexes, with the BAB complex displaying a greater regioselectivity toward the benzylic activation than the BAM complex. This is attributable to the different steric effects of the ligands: the phenyl group in BAB is a more effective steric blocking group than the CH_2 group in the BAM ligand. The successful isolation and characterization of the η^3-benzylic complexes in our systems confirm that the regioselectivity, similarly to the diimine Pt(II) system reported by Bercaw and coworkers,[6l] can also be attributed to the formation of such thermodynamically stable η^3-benzylic intermediates.

Most importantly, we have observed a unique diastereoselectivity and we have revealed a new role for the η^3-benzylic complexes towards diastereoselective EtPh C-H activation. The isolation and characterization of the η^3-benzylic complexes **2.7** and **2.8**, the identification of the two conformational isomers with a non-equal distribution for each of them, and the demonstration of the stereospecific conversion of these isomers to

the corresponding η^1-benzylic compounds in the presence of a donor such as CH_3CN suggest that the η^3-benzylic complexes is the reaction intermediates accounting for not only the observed regioselectivity but also the distinct diastereoselectivity. Moreover, we have shown that the preferential formation of one η^3-benzylic isomer over the other isomer for both BAB and BAM complexes is the consequence of the asymmetric blocking of the Pt coordination sites by the chelate ligands. One of the important implications of the studies in this chapter is the feasibility for stereoselective EtPh benzylic activation using Pt(II) complexes with chiral ligands.

References:

1. a) Zhao, S. B.; Song, D; Jia, W. L.; Wang, S. *Organometallics* **2005***, 24,* 3290. b) Song, D.; Wang, S. *Organometallics* **2003***, 22,* 2187. c) Song, D.; Schmider, H.; Wang, S. *Org. Lett.* **2002**, *4*, 4049.
2. a) Song, D.; Jia, W.-L.; Wang, S. *Organometallics* **2004**, *23*, 1194. b) Song, D.; Sliwowski, K.; Pang, J.; Wang, S. *Organometallics* **2002**, *21*, 4978.
3. a) Albinati, A.; Anklin, C. G.; Ganazzoli, F.; Ruegg, H.; Pregosin, P. S. *Inorg. Chem.* **1987**, *26*, 503. b) Albinati, A.; Arz, C.; Pregosin, P. S. *Inorg. Chem.* **1987**, *26*, 508. c) Albinati, A.; Pregosin, P. S.; Wombacher, F. *Inorg. Chem.* **1990**, *29*, 1812.
4. a) Periana, R. A.; Taube, J. D.; Gamble, S.; Taube, H.; Satoh, T.; Fujii, H. *Science* **1998**, *280*, 560. b) Sen, A. *Acc. Chem. Res*. **1998**, *31*, 550. c) Ziatdinov, V. R.; Oxgaard, J.; Mironov, O. A.; Young, K. J. H.; Goddard III, W. A.; Periana, R. A. *J. Am. Chem. Soc.* **2006**, *128*, 7404.
5. a) Johansson, L.; Ryan, O. B.; Tilset, M. *J. Am. Chem. Soc.* **1999**, *121*, 1974. b) Johansson, L.; Tilset, M. *J. Am. Chem. Soc*. **2001**, *123*, 739. c) Johansson, L.; Ryan, O. B.; Rømming, C.; Tilset, M. *J. Am. Chem. Soc*. **2001**, *123*, 6579. d) Wik, B. J.; Lersch, M.; Tilset, M. *J. Am. Chem. Soc.* **2002**, *124*, 12116. e) Wik, B. J.; Ivanovic-Burmazovic, I.; Tilset, M.; van Eldik, R. *Inorg. Chem.* **2006**, *45*, 3613. f) Wik, B. J.; Lersch, M.; Krivokapic, A.; Tilset, M. *J. Am. Chem. Soc.* **2006**, *128*, 2682.
6. a) Luinstra, G. A.; Wang, L.; Stahl, S. S.; Labinger, J. A.; Bercaw, J. E. *J. Organomet. Chem.* **1995**, *504*, 75. b) Stahl, S. S.; Labinger, J. A.; Bercaw, J. E. *J. Am. Chem. Soc.***1996**, *118*, 5961. c) Holtcamp, M. W.; Labinger, J. A.; Bercaw, J.

E. *J. Am. Chem. Soc.* **1997**, *119*, 848. d) Holtcamp, M. W.; Henling, L. M.; Day, M. W.; Labinger, J. A.; Bercaw, J. E. *Inorg. Chim. Acta* **1998**, *270*, 467. e) Johansson, L.; Tilset, M.; Labinger, J. A.; Bercaw, J. E. *J. Am. Chem. Soc*. **2000**, *122*, 10846. f) Procelewska, J.; Zahl, A.; van Eldik, R.; Zhong, H. A.; Labinger, J. A.; Bercaw, J. E. *Inorg. Chem*. **2002**, *41*, 2808. g) Zhong, H. A.; Labinger, J. A.; Bercaw, J. E. *J. Am. Chem. Soc.* **2002**, *124*, 1378. h) Wong-Foy, A. G.; Henling, L. M.; Day, M.; Labinger, J. A.; Bercaw, J. E. *J. Mol. Catal. A: Chem.* **2002**, *189*, 3. i) Heyduk, A. F.; Labinger, J. A.; Bercaw, J. E. *J. Am. Chem. Soc.* **2003**, *125*, 6366. j) Iverson, C. N.; Carter, C. A. G.; Baker, R. T.; Scollard, J. D.; Labinger, J. A.; Bercaw, J. E. *J. Am. Chem. Soc.* **2003**, *125*, 12674. k) Heyduk, A. F.; Driver, T. G.; Labinger, J. A.; Bercaw, J. E. *J. Am. Chem. Soc.* **2004**, *126*, 15034. l) Driver, T. G.; Day, M. W.; Labinger, J. A.; Bercaw, J. E. *Organometallics* **2005**, *24*, 3644. m) Owen, J. S.; Labinger, J. A.; Bercaw, J. E. *J. Am. Chem. Soc.* **2006**, *128*, 2005.

7. a) Hill, G. S.; Manojlovic-Muir, L.; Muir, K. W.; Puddephatt, R. J. *Organometallics* **1997**, *16*, 525. b) Prokopchuk, E. M.; Jenkins, H. A.; Puddephatt, R. J. *Organometallics* **1999**, *18*, 2861. c) Hinman, J. G.; Baar, C. R.; Jennings, M. C.; Puddephatt, R. J. *Organometallics* **2000**, *19*, 563. d) Zhang, F.; Kirby, C. W.; Hairsine, D. W.; Jennings, M. C.; Puddephatt, R. J. *J. Am. Chem. Soc.* **2005**, *127*, 14196.
8. a) Wick, D. D.; Goldberg, K. I. *J. Am. Chem. Soc.* **1997**, *119*, 10235. b) Thomas, J. C.; Peters, J. C. *J. Am. Chem. Soc.* **2001**, *123*, 5100. c) Konze, W. V.; Scott, B. L.; Kubas, G. J. *J. Am. Chem. Soc.* **2002**, *124*, 12550. d) Thomas, J. C.; Peters, J. C. *J. Am. Chem. Soc.* **2003**, *125*, 8870. e) Thomas, C. M.; Peters, J. C.

Organometallics **2005***, 24,* 5858. f) Karshtedt, D.; McBee, J. L.; Bell, A. T.; Tilley, T. D. *Organometallics* **2006***, 25,* 1801.

9. a) Johnson, J. A.; Sames, D. *J. Am. Chem. Soc.* **2000**, *122*, 6321. b) Johnson, J. A.; Li, D.; Sames, D. *J. Am. Chem. Soc.* **2002**, *124*, 6900.
10. Dangel, B. D.; Johnson, J. A.; Sames, D. *J. Am. Chem. Soc.* **2001**, *123*, 8149.
11. Brookhart, M; Grant, B.; Volpe, J. *Organometallics* **1992***, 11,* 3920.
12. For recent comprehensive reviews on cationic Pt(II)-mediated C-H bond activation studies, see: a) Arndtsen, B. A.; Bergman, R. G.; Mobley, T. A.; Peterson, T. H. *Acc. Chem. Res*. **1995**, *28*, 154. b) Bengali, A. A.; Arndtsen, B. A.; Burger, P. M.; Schultz, R. H.; Weiller, B. H.; Kyle, K. R.; Moore, C. B.; Bergman, R. G. *Pure Appl. Chem*. **1995**, *67*, 281. c) Crabtree, R. H. *Chem. Rev*. **1995**, *95*, 987. d) Shilov, A. E.; Shulpin, G. B. *Chem. Rev.* **1997**, *97*, 2879. e) Shilov, A. E.; Shul'pin, G. B. *Chem. Rev.* **1997**, *97*, 2879. f) Stahl, S. S.; Labinger, J. A.; Bercaw, J. E. *Angew. Chem., Int. Ed.* **1998**, *37*, 2180. g) Labinger, J. A.; Bercaw, J. E. *Nature* **2002**, *417*, 507. h) Fekl, U.; Goldberg, K. I. *Adv. Inorg. Chem.* **2003**, *54*, 259. i) Lersch, M.; Tilset, M. *Chem. Rev.* **2005**, 105, 2471.

Chapter 3

Intramolecular C–H Activation Directed Pt_4 Self-Assembly

3.1 Introduction

Cyclometalated Pt(II) and Pd(II) complexes have attracted much recent attention due to their applications in material chemistry, for example, as chemosensors in chemical sensing and as phosphorescent emitters in organic light-emitting diodes.[1,2] In Chapter 2, the results of our investigation on the C-H activation of toluene and EtPh molecules by the Pt(II) complexes of the BAB and BAM ligands are presented. Besides these intermolecular processes, the intramolecular activation of C-H bonds in Pt(II) complexes is also of great importance, particularly toward the syntheses of various cyclometalated Pt(II) compounds.

To obtain new Pt(II) and Pd(II) luminescent complexes, our group initiated the studies on utilizing 7-azaindole containing molecules as cyclometalating ligands several years ago. A few examples are shown in Scheme 3.1 and Chart 3.1.[3] Most metal complexes obtained earlier, however, only display very weak luminescence in the solid state, rendering them unsuitable for the desired applications.[3] This is likely due to luminescence quenching caused by the chloride atoms on the Pt(II) and Pd(II) centers in these compounds. Attempts to replace the chloride with an alkyl or an aryl group by previous group members were not successful. Nonetheless, the TAB ligand shown in Scheme 3.1 displays interestingly both an N,C,N-chelating mode and a bridging mode *via* the third 7-azaindolyl group to form a Pd_3 species.[3a]

Scheme 3.1

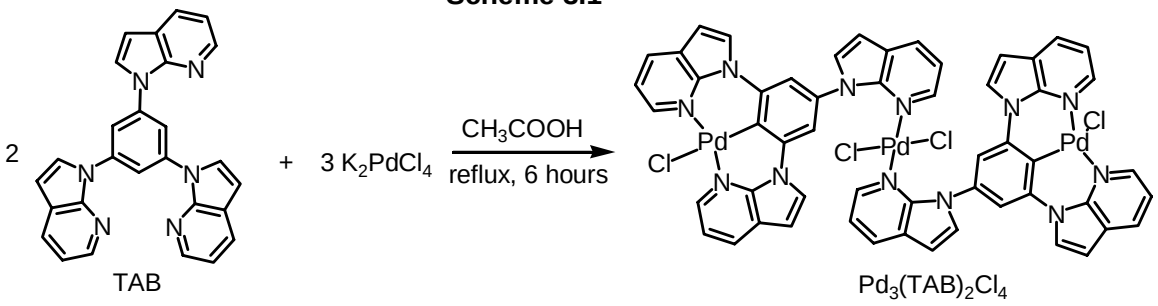

Chart 3.1

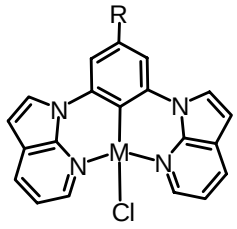

R = H, Br
M = Pd, Pt

During the course of my recent C-H activation studies, a mononuclear complex Pt(NPA)(Me)$_2$ (**3.1**), NPA = 1-*N*-(pyridin-2-yl)-7-azaindole,[4] was found to undergo "roll-over" intramolecular C-H activation at ambient temperature, which spontaneously led to the formation of a self-assembled neutral organoplatinum Pt$_4$ macrocycle as Pt$_4$(*N,C,N*-NPA)$_4$(Me)$_4$ (**3.2**) (Scheme 3.2). Although this neutral Pt$_4$ complex only displays weak luminescence in solution at low temperature, the unusual self-assembly process observed is very interesting because it potentially provides a new approach for achieving macrocyclic Pt(II) and Pd(II) complexes, a class of compounds that have been shown to have a variety of applications in guest-host chemistry and catalysis.[5-9]

Scheme 3.2

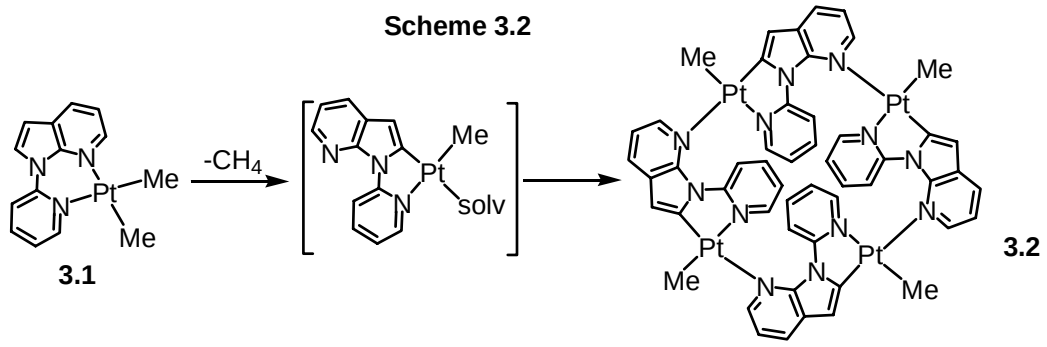

As illustrated by the syntheses of the Pt(II) and Pd(II) molecular squares in Scheme 3.3, the commonly used method for assembling Pt(II) and Pd(II) macrocycles and cages is the coordination driven self-assembly strategy, that is, the use of suitable "linker'' ligands such as polypyridines and polyphosphines *via* ligand substitution reactions. Stang and coworkers have explored extensively the syntheses of many molecular polygons and polyhedra by using pre-assembled Pt(II) and Pd(II) acceptor units and appropriate linkers.[7] Recently, the use of highly effective guest-templated self-assembly methods to achieve elegant Pt(II) and Pd(II) nanocages has been demonstrated by Fujita and coworkers.[8] The majority of previously reported Pt(II) and Pd(II) molecular assemblies achieved by the "external linker" strategy are ionic, and only a few examples of neutral Pt(II) molecular macrocycles are known.[9]

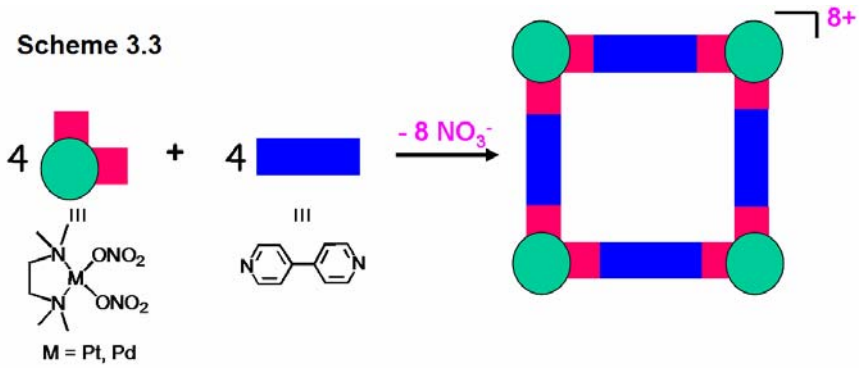

The feasibility of using a ring-opening and intramolecular C-H activation process for assembling polymeric organoplatinum compounds was demonstrated by Young and coworkers.[10] They observed that upon heating, the 2,2'-bipyridyl (2,2-bipy) ligand in Pt(2,2'-bipy)Ph_2 undergoes a "roll-over" cyclometalation, with C-H activation at C3 position of the 2,2'-bipyridyl ligand, resulting in the elimination of benzene and the successive self-assembly of insoluble Pt polymers *via* the freed N donor site and the Pt acceptor site. Although intramolecular cyclometalation involving C-H bond activation is

a fairly common phenomenon among Pd(II) and Pt(II) compounds,[3,11] the use of such a process in a controlled manner to construct molecular macrocycles and cages has hardly been explored. We were therefore highly motivated to understand the unique self-assembly process for the formation of the Pt_4 compound **3.2** shown in Scheme 3.2. We have carried out kinetics studies as well as investigations of the possible reaction intermediates involved in the self-assembly process. The details of syntheses, structures, isotope labeling and kinetic studies on the related Pt(II) complexes are presented in this chapter.

3.2 Experimental Section

3.2.1 General procedures

All reactions were performed under N_2 with the standard Schlenk techniques unless otherwise noted. All starting materials were purchased from Aldrich Chemical Co. and used without further purification. THF, Et_2O, and hexanes were purified using the solvent purification system (Innovation Technology, Inc.). Deuterated solvents (Cambridge Isotopes) were used as received without further drying. ^1H and ^{13}C NMR spectra were recorded on Bruker Avance 400 or 500 MHz spectrometers. The assignments of the ^1H NMR signals are based on COSY spectra. The chemical shifts (δ) were reported in parts per million (ppm). High resolution mass spectra (HRMS) were obtained from a Waters/Micromass GC-TOF EI-MS spectrometer. Elemental analyses were performed at the Analytical Laboratory for Environmental Science Research, Department of Chemistry, University of Toronto, Toronto, Ontario. The ligand 1-*N*-(pyridin-2-yl)-7-azaindole (NPA) was synthesized by our previously reported procedure.[4]

$[PtMe_2(\mu\text{-}SMe_2)]_2$[12a] and $[PtPh_2(\mu\text{-}SMe_2)]_n$ (n = 2 or 3)[12b] were prepared by methods described in the literature.

3.2.2 Synthesis of C2-deuterium labeled NPA: 1-*N*-(pyridin-2-yl)-2-deuterium-7-azaindole (2-D-NPA)

To a stirred Et_2O (15 mL) solution of NPA (0.19 g, 1.0 mmol) at -78 ^oC was added dropwise, *via* syringe, a lithium diisopropylamide (LDA) solution (1.8 M) (1.4 mL, 2.5 mmol) over 5 minutes. The mixture was stirred for 40 minutes at -78 ^oC, resulting in a pink solution. D_2O (1.0 mL) was then added. The mixture was warmed to room temperature. After the separation of water, the organic layer was dried with Na_2SO_4. After the removal of the solvent, the recrystallization of the oily residue with a small amount of hexanes afforded 2-D-NPA as a white solid (0.19 g, 95% yield). The extent of deuteration of the product was > 94% according to ^1H NMR data. ^1H NMR (400 MHz, $CDCl_3$, 25 ^oC): δ 8.86 (d; ^3J = 8.8 Hz; 1H, py), 8.53 (dd; ^3J = 4.8 Hz, ^4J = 1.6 Hz; 1H, 7-aza), 8.45 (dd; ^3J = 4.8 Hz, ^4J = 1.4 Hz; 1H, 7-aza), 8.00 (dd; ^3J = 4.8 Hz, ^4J = 1.4 Hz; 1H, py), 7.90 (m; 1H, py), 7.20 (m; 2H, 1H from py, 1H from 7-aza), 6.68 (s; 1H, 7-aza) ppm. HRMS calcd. for $C_{12}H_8DN_3$: 196.0859; found: 196.0817.

3.2.3 Synthesis of 1-*N*-(pyridin-2-yl)-2-methyl-7-azaindole (2-Me-NPA)

To a stirred Et_2O solution (30 mL) of NPA (0.50 g, 2.6 mmol) solution at -78 ^oC was added dropwise, *via* syringe, a lithium diisopropylamide (LDA) solution (1.8 M) (3.6 mL, 6.4 mmol) over 10 minutes. The mixture was stirred for another 40 minutes at -78 ^oC, resulting in a pink solution. MeI (1.0 mL) was then added. The mixture was slowly warmed to room temperature and stirred overnight. An aqueous solution (20 mL) of

NH_4Cl (0.53 g) was added. After the extraction of the aqueous layer with Et_2O (2 x 20 mL), the organic layer was separated and dried with Na_2SO_4. After the removal of solvents, the residue was purified by flash chromatograph on silica gel using hexanes/ethyl acetate (2/1) as the eluent to afford 2-Me-NPA as a white solid (0.34 g, 62% yield). ^{1}H NMR (400 MHz, $CDCl_3$, 25 °C): δ 8.65 (m; ^3J = 5.2 Hz, ^4J = 1.2 Hz; 1H, py), 8.24 (dd; ^3J = 4.8 Hz, ^4J = 1.2 Hz; 1H, 7-aza), 7.92 (m; 1H, py), 7.84 (dd; ^3J = 7.6 Hz, ^4J = 1.2 Hz; 1H, 7-aza), 7.77 (d; ^3J = 7.2 Hz; 1H, py) 7.33 (m; 1H, py), 7.09 (dd; ^3J = 7.6 Hz, ^4J = 4.8 Hz; 1H, 7-aza), 6.37 (s; 1H, 7-aza), 2.55 (s; 3H, CH_3) ppm. ^{13}C NMR: δ 150.20, 149.53, 141.52, 139.10, 138.56, 128.58, 122.75, 122.40, 122.07, 117.22, 101.35, 99.42 ppm. HRMS calcd. for $C_{13}H_{11}N_3$, 209.0953, found, 209.0950.

3.2.4 Syntheses of Pt(NPA)Me_2 (**3.1**) and Pt(2-D-NPA)Me_2 (**3.1A**)

For **3.1**: $[PtMe_2(\mu\text{-}SMe_2)]_2$ (0.17 g, 0.30 mmol) and NPA (0.12 g, 0.60 mmol) were mixed in cold THF (40 mL) and stirred for 8 hours at –10 °C, resulting in a yellow solution. The solvent was slowly removed under vacuum while keeping the solution temperature below 0 °C. The residue was washed with cold Et_2O (5 mL x 3) and then dried under vacuum to afford **3.1** as a yellow solid (0.18 g, 72% yield). ^{1}H NMR (400 MHz, CD_2Cl_2, -20 °C): δ 8.93 (d; ^3J = 6.0 Hz; 1H, py), 8.62 (d; ^3J = 5.2 Hz; 1H, 7-aza), 8.14 (d; ^3J = 7.6 Hz; 1H, 7-aza), 8.03 (m; ^3J = 7.6 Hz; 1H, py), 7.79 (d; ^3J = 4.0 Hz; 1H, 7-aza), 7.41 (d; $^3J_1$ = 8.4 Hz; 1H, py), 7.22 (dd; $^3J_1$ = 7.6 Hz, $^3J_2$ = 5.2 Hz; 1H, 7-aza), 7.18 (t; ^3J = 6.4 Hz; 1H, py), 6.89 (d; ^3J = 4.0 Hz; 1H, 7-aza), 0.70 (s, satellites; $^3J_{Pt\text{-}H}$ = 82.4 Hz; 3H, CH_3), 0.59 (s, satellites; $^3J_{Pt\text{-}H}$ = 84.0 Hz; 3H, CH_3) ppm. ^{13}C NMR: δ 151.01, 147.16, 145.18, 143.83, 138.94, 130.10, 127.07, 124.47, 122.36, 120.10, 116.49,

107.30, -16.10, -18.23 ppm. For **3.1A**: This complex was synthesized in ~74% yield from $[PtMe_2(\mu\text{-}SMe_2)]_2$ and 2-D-NPA using similar procedure as described for $Pt(NPA)Me_2$.

3.2.5 Synthesis of Pt(2-Me-NPA)Me_2 (3.1B)

$[PtMe_2(\mu\text{-}SMe_2)]_2$ (0.062 g, 0.11 mmol) and 2-Me-NPA (0.041 g, 0.22 mmol) were mixed in Et_2O (30 mL) and stirred overnight at ambient temperature. The resulting white precipitate was allowed to settle, and the clear solution was then decanted. The solid was washed with Et_2O (5 mL x 2) and dried under vacuum to afford **3.1B** (0.067 g, 70% yield). ^{1}H NMR (500 MHz, CD_3COCD_3, 0 °C): δ 9.09 (d; ^3J = 6.5 Hz; 1H, py), 8.55 (d; ^3J = 4.5 Hz; 1H, 7-aza), 8.20 (m; ^3J = 8.0 Hz; 1H, py), 8.14 (dd; $^3J_1$ = 7.5 Hz, $^3J_2$ = 1.0 Hz; 1H, 7-aza), 7.50 (d; ^3J = 8.3 Hz; 1H, py), 7.40 (m; $^3J_1$ = 7.0 Hz; 1H, py), 7.27 (dd; $^3J_1$ = 7.5 Hz, $^3J_2$ = 5.5 Hz; 1H, 7-aza), 6.83 (s; 1H, 7-aza), 2.71 (s; 3H, CH_3), 0.85 (s, satellites; $^3J_{Pt\text{-}H}$ = 88.3 Hz; 3H, CH_3), 0.59 (s, satellites; $^3J_{Pt\text{-}H}$ = 86.9 Hz; 3H, CH_3) ppm. ^{13}C NMR: δ 150.49, 149.29, 145.98, 142.61, 138.88, 138.54, 128.33, 123.87, 123.09, 120.09, 119.84, 108.21, 14.78, -17.47, -19.14 ppm.

3.2.6 Synthesis of Pt_4(NCN-NPA)$_4Me_4$ (3.2)

Method 1: A benzene (8 mL) solution of compound **3.1** (0.084 g, 0.20 mmol) was heated at 60 °C for 10 minutes. Bright yellow crystals of **3.2** were then obtained by slowly cooling the hot benzene solution (94% yield). ^{1}H NMR (400 MHz, C_6D_6, 60 °C): δ 10.13 (d; ^3J = 8.2 Hz; 1H×4, py), 8.56 (d, satellites; ^3J = 5.4 Hz; 4H, 7-aza), 7.48 (d; ^3J = 7.6 Hz; 4H, 7-aza), 7.04 (t; ^3J = 7.6 Hz; 4H, py), 6.88 (s, satellites; $^3J_{Pt\text{-}H}$ = 27.2 Hz; 4H,

7-aza) 6.57 (dd; $^3J_1$ = 5.4 Hz, $^3J_2$ = 7.6 Hz; 4H, 7-aza), 6.45 (d; ^3J = 5.4 Hz; 4H, py), 5.67 (br; 4H, py), 2.00 (s, satellites; $^3J_{Pt\text{-}H}$ = 81.6 Hz; 12H, CH_3) ppm.

Method 2: Compound **3.1** (0.042 g, 0.10 mmol) was dissolved in CH_2Cl_2 (~1.5 mL) at room temperature, resulting in a bright yellow solution. After standing at room temperature for 40 minutes, the yellow solution was moved into a refrigerator. Bright yellow crystals were formed after several hours (> 90% yield). ^{1}H NMR (400 MHz, CD_2Cl_2, 25 °C): δ 10.00 (d; ^3J = 8.4 Hz; 4H, py), 8.40 (d; ^3J = 5.2 Hz; 4H, 7-aza), 7.90 (d; ^3J = 7.6 Hz; 4H, 7-aza), 7.60 (m; 4H, py), 7.03 (dd; $^3J_1$ = 5.2 Hz, $^3J_2$ = 7.6 Hz; 4H, 7-aza), 6.54 (s, satellites; $^3J_{Pt\text{-}H}$ = 27.0 Hz; 4H, 7-aza), 6.39 (m; 4H, py), 6.31 (br; ^3J = 5.2; 4H, py), 1.38 (s, satellites; $^3J_{Pt\text{-}H}$ = 78.4 Hz; 12H, CH_3) ppm. Anal. calcd. for $C_{52}H_{44}N_{12}Pt_4$: C 38.6, H 2.7, N 10.4; found: C 38.3, H 2.8, N 11.0.

3.2.7 Syntheses of Pt(*N,C*-NPA)Me(L) (L = CH_3CN: E·CH_3CN, and L = SMe_2: E·SMe_2)

An NMR tube was charged with complex **3.1** (6.7 mg, 16 μmol), a CD_2Cl_2 solution of CH_3CN (0.2 M, 0.60 mL) was then added to dissolve the sample. The sample was monitored by ^{1}H NMR at room temperature, which revealed the immediate formation of **E·CH_3CN**. Yellow crystals of compound **E·CH_3CN** were obtained by slow evaporation of the solution. ^{1}H NMR (400 MHz, CD_2Cl_2, 25 °C): δ 9.22 (d; ^3J = 7.6 Hz; 1H, aza), 8.53 (d; ^3J = 5.6 Hz; 1H, py), 8.10 (d; ^3J = 4.8 Hz; 1H, 7-aza), 8.03 (m; ^3J = 4.8 Hz; 1H, py), 7.69 (d; ^3J = 7.6 Hz; 1H, 7-aza), 7.07 (m; ^3J = 5.6 Hz; 1H, py), 7.22 (dd; $^3J_1$ = 7.6 Hz, $^3J_2$ = 4.8 Hz; 1H, 7-aza), 6.38 (s, satellites; $^3J_{Pt\text{-}H}$ = 36.1 Hz), 2.43 (s; 3H, Pt-NC*Me*), 0.95 (s, satellites; $^2J_{Pt\text{-}H}$ = 83.6 Hz; 3H, CH_3) ppm.

The SMe_2 adduct Pt(*N,C*-NPA)Me(SMe_2) (**E·SMe$_2$**) was obtained using the same method as describe for **E·CH$_3$CN**. An alternative method for the synthesis of **E·SMe$_2$** is the overnight reaction of NPA with [$PtMe_2$(μ-SMe_2)]$_2$ in THF at ambient temperature, which afforded **E·SMe$_2$** in > 90% yield based on the NMR data of the crude reaction mixture.

3.2.8 Synthesis of Pt(*N,C*-NPA)(Cl)(SMe_2) (3.3)

The standing of a CH_2Cl_2 solution of **E·SMe$_2$** at ambient temperature for several weeks led to a brown suspension. Evaporation of the solvent resulted in yellow crystals (20~40% yield), which were identified by ^{1}H NMR spectroscopy and X-ray diffraction analysis to be Pt(*N,C*-NPA)(Cl)(SMe_2), **3.3**. ^{1}H NMR (400 MHz, CD_2Cl_2, 25 °C): δ 9.42 (d, satellitess; ^3J = 3.0 Hz, $^3J_{Pt\text{-}H}$ = 38.4 Hz; 1H, aza), 8.14 (d; ^3J = 2.8 Hz; 1H, py), 8.19 (d; ^3J = 4.8 Hz; 1H, 7-aza), 8.04 (m; ^3J = 4.8 Hz; 1H, py), 7.77 (d; ^3J = 6.0 Hz; 1H, 7-aza), 7.15 (m; ^3J = 5.6 Hz; 1H, py), 7.10 (m; 1H, 7-aza), 6.37 (s, satellites; $^3J_{Pt\text{-}H}$ = 24.1 Hz), 2.80 (s, satellites; $^3J_{Pt\text{-}H}$ = 43.6 Hz; 6H, S(CH_3)$_2$) ppm.

3.2.9 Synthesis of Pt(NPA)Ph_2 (3.4)

[$PtPh_2$(μ-SMe_2)]$_n$ (n = 2 or 3) (0.086 g, 0.21 mmol based Pt) and NPA (0.041 g, 0.21 mmol) were mixed in THF (30 mL) and stirred overnight at ambient temperature. The resulting white precipitate was allowed to settle, and the clear solution was then decanted. The solid was washed with Et_2O and dried under reduced pressure to afford Pt(NPA)Ph_2 (**3.4**) (0.11 g, 96% yield). Compound **3.4** has very poor solubility in most common organic solvents. Colorless crystals of compound **3.4** were obtained by slow

evaporation of its CH_2Cl_2 solution. ^{1}H NMR (500 MHz, DMSO-d_6/CD_2Cl_2 (3 :1), 25 °C) (all signals are broad): δ 8.51 (1H, py), 8.34 (1H, 7-aza), 8.28 (1H, 7-aza), 8.19 (1H, py), 7.96 (1H, py), 7.83 (1H, 7-aza), 7.32 (2H, *ortho*-H of Pt*Ph*$_2$), 7.28 (2H, *ortho*-H of Pt*Ph*$_2$), 7.04 (3H, 1H from py, 2H from 7-aza), 6.81 (4H, *meta*-H of Pt*Ph*$_2$), 6.68 (2H, *para*-H of Pt*Ph*$_2$) ppm. Anal. calcd. for $C_{24}H_{19}N_3Pt$: C 52.94, H 3.52, N 7.72; found: C 52.90, H 3.55, N 8.01.

3.2.10 Kinetic study of the transformation of 3.1 to 3.2 in CD_2Cl_2

The kinetic study was carried out with the ^{1}H NMR spectroscopy. In a typical experiment, an NMR tube was charged with complex **3.1** or **3.1A** (6.7 mg, 16 μmol), the pre-cooled CD_2Cl_2 (0.40 mL) (-30 ^{o}C) was then added to dissolve the sample. After slowly warmed to ~0 ^{o}C, the NMR tube was shaken vigorously to afford a homogeneous solution and then inserted into the NMR spectrometer that had been equilibrated to a desired temperature. The sample was allowed to equilibrate to the probe temperature. An array of 30~50 ^{1}H NMR spectra was then acquired automatically by the spectrometer. The reaction was monitored by following the disappearance of **3.1** or **3.1A** in the ^{1}H NMR spectrum. Each experiment was repeated three times.

3.2.11 Kinetic study of the transformation process of 3.1 to 3.2 in CD_2Cl_2 with the presence of CD_3CN

In a typical experiment, an NMR tube was charged with complex **3.1** or **3.1A** (6.7 mg, 16 μmol). A CD_2Cl_2 solution (0.40 mL) of CD_3CN with a known concentration was warmed to 296.0 K and then added to dissolve the sample. The NMR tube was shaken vigorously to afford a homogeneous solution and then inserted into the NMR

spectrometer that had been equilibrated to 296.0 ± 0.1 K. An array of 30~50 ^{1}H NMR spectra was then acquired automatically by the spectrometer. The reaction was monitored by following the disappearance of **3.1** or **3.1A** in the ^{1}H NMR spectrum.

3.2.12 X-ray diffraction analyses

Single crystals of **3.2-3.4** and **E·CH$_3$CN** were mounted on glass fibers. Data were collected on a Bruker Apex II single-crystal X-ray diffractometer with graphite-monochromated Mo Kα radiation, operating at 50 kV and 30 mA. Crystals of **3.2** obtained from benzene and CH_2Cl_2 solutions contain two benzene and two CH_2Cl_2 molecules, respectively per Pt_4 molecule. Data collection for **3.2·2CH$_2$Cl$_2$** and **3.4** were carried out at 180 K while data collection for **3.2·2benzene**, **E·CH$_3$CN** and **3.3** were collected at ambient temperature. The crystals of **3.2·2CH$_2$Cl$_2$** are twinned and very small, as a result only the Pt atoms can be refined anisotropically. Nonetheless, the crystal data indicated clearly that the structure of **3.2** in **3.2·2CH$_2$Cl$_2$** is identical to that in **3.2·2benzene**. The crystals of **3.2·2CH$_2$Cl$_2$** belong to the monoclinic space group $P2_1/c$ with unit cell parameters of a = 18.891(6) Å, b = 12.311(4) Å, c = 23.516(7) Å, β = 91.987(4)^o, V = 5466(3) Å^3, Z = 4. For **3.2·2benzene**, the benzene solvent molecules show some disordering. No significant decay was observed in any samples. Data were processed on a PC with the aid of the Bruker SHELXTL software package (version 5.10) and were corrected for absorption effects. The crystal data for **3.2·2benzene**, **3.3**, **3.4** and **E·CH$_3$CN** are summarized in Table 3.1, and the selected bond lengthes and angles for them are presented in Table 3.2.

Table 3.1 Crystallographic data for compounds **3.2·2Benzene**, **3.3**, **3.4** and **E·CH$_3$CN**.

Compound	**3.2·2Benzene**	**3.3**	**3.4**	**E·CH$_3$CN**
Formula	$C_{16}H_{14}N_3Pt$	$C_{24}H_{19}N_3Pt$	$C_{14}H_{14}ClN_3PtS$	$C_{15}H_{14}N_4Pt$
FW	443.39	544.51	486.88	445.39
Space Group	P-1	Pbca	$P2_1/c$	P-1
a, Å	9.862(4)	12.6256(17)	12.0080(13)	7.3661(9)
b, Å	13.404(5)	17.061(2)	12.9725(15)	10.0710(12)
c, Å	24.203(9)	17.386(2)	10.3453(12)	10.6360(12)
α, º	76.366(6)	90	90	113.2160(10)
β, º	86.246(7)	90	111.922(2)	96.9950(10)
γ, º	70.238(7)	90	90	92.9970(10)
V, Å^3	2925.8(19)	3745.0(9)	1495.0(3)	715.37(15)
Z	8	8	4	2
$D_{calc,}$ g·cm^{-3}	2.013	1.931	2.163	2.068
T, K	298(2)	180(2)	180(2)	298(2)
μ, mm^{-1}	9.584	7.508	9.696	9.802
$2\theta_{max}$, º	50.00	50.00	50.00	50.00
Reflns measured	15285	32073	10395	6679
Reflns used (R_{int})	10174 (0.0442)	3300 (0.0440)	3522 (0.0419)	2516 (0.0198)
Parameters	707	253	181	182
Final *R* values [I > 2σ(I)]:				
R_1[a]	0.0443,	0.0309,	0.0303	0.0213
wR_2[b]	0.0508	0.0821	0.0398	0.0514
R values (all data):				
R_1[a]	0.1191,	0.0383	0.0672	0.0241
wR_2[b]	0.0654	0.0898	0.0444	0.0526
Goodness-of-fit on F^2	0.639	1.000	0.780	1.000

[a] $R_1 = \Sigma||F_0| - |F_c|| / \Sigma|F_0|$

[b] $wR_2 = [\Sigma w [(F_0^2-F_c^2)^2] / \Sigma[w(F_0^2)^2]]^{1/2}$

$w = 1 / [\sigma^2(F_0^2) + (0.075P)^2]$, where $P = [Max (F_0^2,0) + 2F_c^2] / 3$

Table 3.2 Selected bond lengths (Å) and angles (º) for compounds **3.2·2Benzene**, **3.3**, **3.4** and **E·CH_3CN**.

Compound **3.2·2Benzene**			
Pt(1)-C(2)	1.899(12)	Pt(3)-C(28)	1.947(12)
Pt(1)-C(1)	2.049(9)	Pt(3)-C(27)	2.065(10)
Pt(1)-N(11)	2.139(9)	Pt(3)-N(9)	2.132(9)
Pt(1)-N(3)	2.149(8)	Pt(3)-N(5)	2.140(10)
Pt(2)-C(15)	1.931(13)	Pt(4)-C(41)	1.933(12)
Pt(2)-C(14)	2.034(9)	Pt(4)-C(40)	2.021(10)
Pt(2)-N(6)	2.114(9)	Pt(4)-N(12)	2.095(9)
Pt(2)-N(2)	2.146(10)	Pt(4)-N(8)	2.142(10)
C(2)-Pt(1)-C(1)	92.9(5)	C(7)-N(2)-Pt(2)	108.8(9)
C(2)-Pt(1)-N(11)	175.1(4)	C(8)-N(2)-Pt(2)	132.4(8)
C(1)-Pt(1)-N(11)	90.7(4)	C(13)-N(3)-Pt(1)	127.3(9)
C(2)-Pt(1)-N(3)	79.7(4)	C(9)-N(3)-Pt(1)	113.0(8)
C(1)-Pt(1)-N(3)	172.6(4)	C(21)-N(5)-Pt(3)	127.9(9)
N(11)-Pt(1)-N(3)	96.6(4)	C(20)-N(5)-Pt(3)	113.7(9)
C(15)-Pt(2)-C(14)	93.3(5)	C(26)-N(6)-Pt(2)	127.9(9)
C(15)-Pt(2)-N(6)	79.3(5)	C(22)-N(6)-Pt(2)	115.4(9)
C(14)-Pt(2)-N(6)	172.6(5)	C(33)-N(8)-Pt(4)	111.8(9)
C(15)-Pt(2)-N(2)	172.8(4)	C(34)-N(8)-Pt(4)	130.4(9)
C(14)-Pt(2)-N(2)	89.4(4)	C(35)-N(9)-Pt(3)	112.1(8)
N(6)-Pt(2)-N(2)	98.0(4)	C(39)-N(9)-Pt(3)	128.1(9)
C(28)-Pt(3)-C(27)	92.3(5)	C(47)-N(11)-Pt(1)	128.5(8)
C(28)-Pt(3)-N(9)	80.1(4)	C(46)-N(11)-Pt(1)	111.7(8)
C(27)-Pt(3)-N(9)	171.4(4)	C(52)-N(12)-Pt(4)	129.8(9)
C(28)-Pt(3)-N(5)	176.7(4)	C(48)-N(12)-Pt(4)	113.1(8)
C(27)-Pt(3)-N(5)	89.6(4)	C(3)-C(2)-Pt(1)	142.3(10)
N(9)-Pt(3)-N(5)	97.8(4)	N(1)-C(2)-Pt(1)	115.4(8)
C(41)-Pt(4)-C(40)	93.2(5)	C(16)-C(15)-Pt(2)	139.4(11)
C(41)-Pt(4)-N(12)	80.3(4)	N(4)-C(15)-Pt(2)	114.6(9)
C(40)-Pt(4)-N(12)	173.5(4)	C(29)-C(28)-Pt(3)	140.3(10)
C(41)-Pt(4)-N(8)	173.1(4)	N(7)-C(28)-Pt(3)	114.9(9)
C(40)-Pt(4)-N(8)	89.4(4)	C(42)-C(41)-Pt(4)	139.3(10)
N(12)-Pt(4)-N(8)	97.1(4)	N(10)-C(41)-Pt(4)	113.9(9)
Compound **3.3**			
Pt(1)-C(13)	2.007(5)	N(1)-C(1)	1.350(6)
Pt(1)-C(19)	2.012(5)	N(2)-C(7)	1.396(6)
Pt(1)-N(1)	2.107(4)	N(2)-C(8)	1.403(6)
Pt(1)-N(3)	2.143(4)	N(2)-C(6)	1.412(7)
N(1)-C(7)	1.339(6)	N(3)-C(8)	1.343(6)

C(13)-Pt(1)-C(19)	86.60(1)	C(1)-N(1)-Pt(1)	123.7(3)
C(13)-Pt(1)-N(1)	93.98(1)	C(8)-N(3)-Pt(1)	124.4(3)
C(19)-Pt(1)-N(1)	177.16(18)	C(12)-N(3)-Pt(1)	118.1(3)
C(13)-Pt(1)-N(3)	177.36(17)	C(14)-C(13)-Pt(1)	120.7(4)
C(19)-Pt(1)-N(3)	91.51(16)	C(18)-C(13)-Pt(1)	122.9(4)
N(1)-Pt(1)-N(3)	87.82(15)	C(20)-C(19)-Pt(1)	122.5(4)
C(7)-N(1)-Pt(1)	120.3(3)	C(24)-C(19)-Pt(1)	121.1(4)

Compound **3.4**

Pt(1)-C(11)	1.965(5)	N(1)-C(5)	1.368(6)
Pt(1)-N(3)	2.046(4)	N(1)-C(12)	1.396(6)
Pt(1)-S(1)	2.2616(15)	N(1)-C(11)	1.438(6)
Pt(1)-Cl(1)	2.3897(13)	N(2)-C(12)	1.334(5)
S(1)-C(13)	1.792(5)	N(2)-C(6)	1.357(6)
S(1)-C(14)	1.794(5)	N(3)-C(1)	1.348(6)
C(11)-Pt(1)-N(3)	81.11(19)	C(13)-S(1)-Pt(1)	105.46(19)
C(11)-Pt(1)-S(1)	90.00(15)	C(14)-S(1)-Pt(1)	109.2(2)
N(3)-Pt(1)-S(1)	171.08(12)	C(1)-N(3)-Pt(1)	127.3(3)
C(11)-Pt(1)-Cl(1)	175.68(15)	C(5)-N(3)-Pt(1)	115.1(4)
N(3)-Pt(1)-Cl(1)	94.88(12)	C(10)-C(11)-Pt(1)	140.6(4)
S(1)-Pt(1)-Cl(1)	94.03(5)	N(1)-C(11)-Pt(1)	111.3(3)

Compound **E·CH_3CN**

Pt(1)-C(1)	1.947(5)	N(2)-C(8)	1.391(5)
Pt(1)-C(13)	2.039(5)	N(2)-C(7)	1.396(6)
Pt(1)-N(4)	2.049(5)	N(2)-C(1)	1.427(6)
Pt(1)-N(3)	2.100(4)	N(3)-C(12)	1.336(6)
N(1)-C(7)	1.317(6)	N(3)-C(8)	1.341(6)
N(1)-C(6)	1.343(6)	N(4)-C(14)	1.130(7)
C(1)-Pt(1)-C(13)	94.1(2)	C(12)-N(3)-Pt(1)	128.0(3)
C(1)-Pt(1)-N(4)	176.42(17)	C(8)-N(3)-Pt(1)	114.4(3)
C(13)-Pt(1)-N(4)	89.1(2)	C(14)-N(4)-Pt(1)	175.8(4)
C(1)-Pt(1)-N(3)	80.37(17)	C(2)-C(1)-Pt(1)	141.2(4)
C(13)-Pt(1)-N(3)	174.3(2)	N(2)-C(1)-Pt(1)	112.8(3)
N(4)-Pt(1)-N(3)	96.48(16)		

3.3 Results and Discussion

3.3.1 Syntheses and reactivities of the Pt(II) NPA complexes

As shown in Scheme 3.4, the synthesis of the complex Pt(NPA)Me_2 (**3.1)** could be achieved readily by the ligand displacement of the bridging SMe_2 in [$PtMe_2$(μ-SMe_2)]$_2$ with NPA in THF at -10 ^oC. It is important to mention that the same ligand displacement reaction does not occur efficiently at temperature below -20 ^0C, attributable to the weak chelating ability of the NPA ligand. Compound **3.1** is fairly stable in the solid state at ambient temperature or in solution below 5 ^oC. It was characterized by NMR spectroscopy in CD_2Cl_2 at -20 ^oC. In either THF, CH_2Cl_2 or benzene solution, compound **3.1** undergoes clean transformation to give the tetranuclear Pt_4 complex [Pt(*N,C,N*-NPA)Me]$_4$, **3.2**, at ambient temperature, which has been fully characterized by NMR spectroscopy, elemental and X-ray diffraction analyses. In the presence of donor ligands **L** such as SMe_2 and CH_3CN, the monomeric N,C-chelate Pt(II) complexes [Pt(*N,C*-NPA)(**L**)Me], (**L** = SMe_2, **E·SMe$_2$**; or MeCN, **E·CH$_3$CN**) was obtained. Attempts toward the synthesis of compound **3.1** at ambient temperature consistently led to the N,C-chelate Pt(II) complex **E·SMe$_2$**. This is in good agreement with the reactivity of compound **3.1**. The resulting monomeric N,C-chelate species [Pt(*N,C*-NPA)(***L***)Me] are still reactive toward C-Cl bond activation. For example, the standing of a CH_2Cl_2 solution of **E·SMe$_2$** for a couple of weeks led to the isolation a new monomeric N,C-chelate compound [Pt(*N,C*-NPA)(SMe_2)(Cl)], **3.4**, which has been characterized by ^1H NMR spectroscopy and X-ray diffraction analyses. Compound **3.4** exhibits a much lower solubility relative to **E·CH$_3$CN** in most organic solvents.

Scheme 3.4[a] Syntheses of complexes **3.1**-**3.4** and **E·L** (L = SMe_2 and CH_3CN).

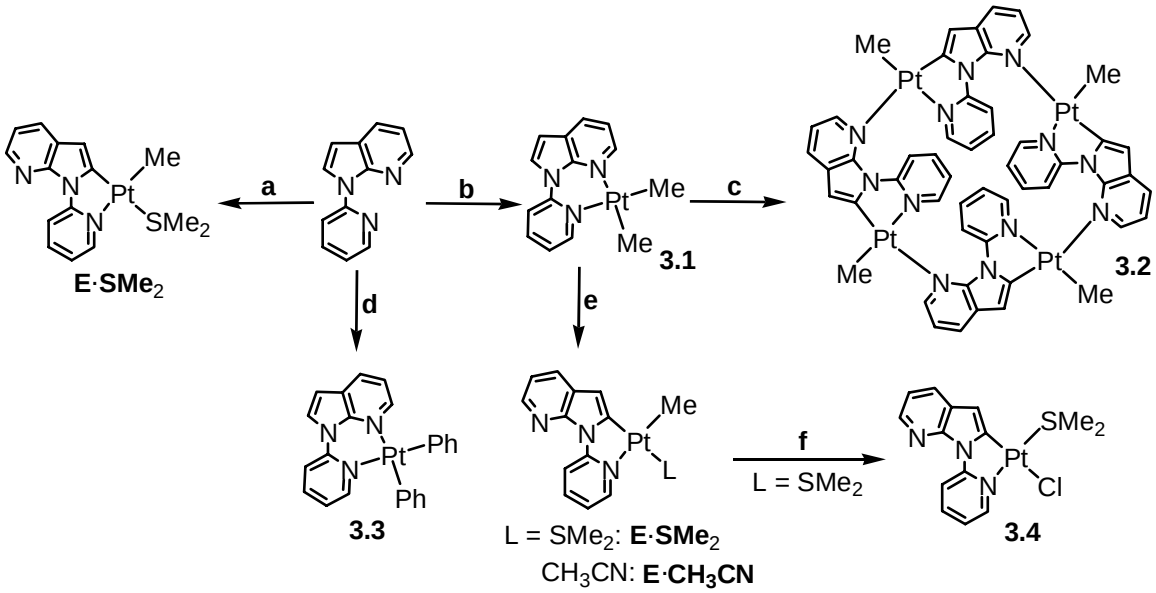

[a] *Reaction conditions*: a) $[PtMe_2(\mu\text{-}SMe_2)]_2$, rt, overnight; b) $[PtMe_2(\mu\text{-}SMe_2)]_2$, -10 ^oC, overnight; c) THF, CH_2Cl_2 or benzene, rt; d) $[PtPh_2(\mu\text{-}SMe_2)]_n$ (n = 2, or 3), rt, overnight; e) addition of ligand L (L = SMe_2 or MeCN) in CH_2Cl_2; f) CH_2Cl_2.

The $PtPh_2$ compound Pt(NPA)Ph_2, **3.3**, was synthesized nearly quantitively from the ligand displacement reaction of $[PtPh_2(\mu\text{-}SMe_2)]_n$ (n = 2, 3) with NPA at ambient temperature. Compound **3.3** has also been fully characterized by NMR spectroscopy, elemental and X-ray diffraction analyses. Compared to its $PtMe_2$ analogue compound **3.1**, compound **3.3** has a much higher stability. However, the solubility of compound **3.3** is poor in most common organic solvents, precluding the further mechanistic and reactivity investigation.

3.3.2 Crystal structures of complexes 3.2-3.4 and E·CH_3CN

3.3.2.1 Crystal structure of 3.2

The crystal structure of **3.2** in **3.2·2CH_2Cl_2** is identical to that in **3.2·2benzene**, as shown in Figures 3.1 and 3.2. The molecule of **3.2** has a highly rigid cyclic Pt_4 structure.

Through an anionic N,C,N-tridentate mode, the NPA ligand exhibits dual roles both as a chelating ligand and a bridging ligand. Each Pt center forms a 5-membered N,C-chelate with the NPA ligand. The four Pt subunits in **3.2** are related by an approximate S_4 axis. The four Pt atoms are not coplanar, showing a butterfly arrangement. The two diagonal Pt···Pt distances are 8.34 and 8.85 Å, while the four edge Pt···Pt distances are 6.14, 6.26, 6.15 and 6.25 Å, respectively. Due to the steric interactions between the neighboring pyridyl (py) groups, the nitrogen atoms on the 7-azaindolyl (7-aza) rings (N(2), N(5), N(8) and N(11)) in Figure 3.1 show large distortions from linear coordination to the Pt(II) centers. The average deviation from linearity as defined by the angle between the Pt-N(7-aza) vector and the N-C(*para*-carbon of the py ring) vector is ~30^{o}. Accordingly, the Pt-N(7-aza) distances, 2.135 Å in average, are much longer than those of Pt-N(py), 2.108 Å in average. The py ring and the 7-aza ring in each NPA ligand are out of co-planarity by a dihedral angle of ~13.5^{o} in average. Interestingly, as shown in Figure 3.3, the internal cavity (> 6 Å in diameter) in compound **3.2** has a distinct tetrahedral shape, defined by the four py groups. Despite the co-crystallization of either benzene or CH_2Cl_2 molecules, these solvent molecules only occupy the void space in the crystal lattices rather than the tetrahedral cavity in **3.2**.

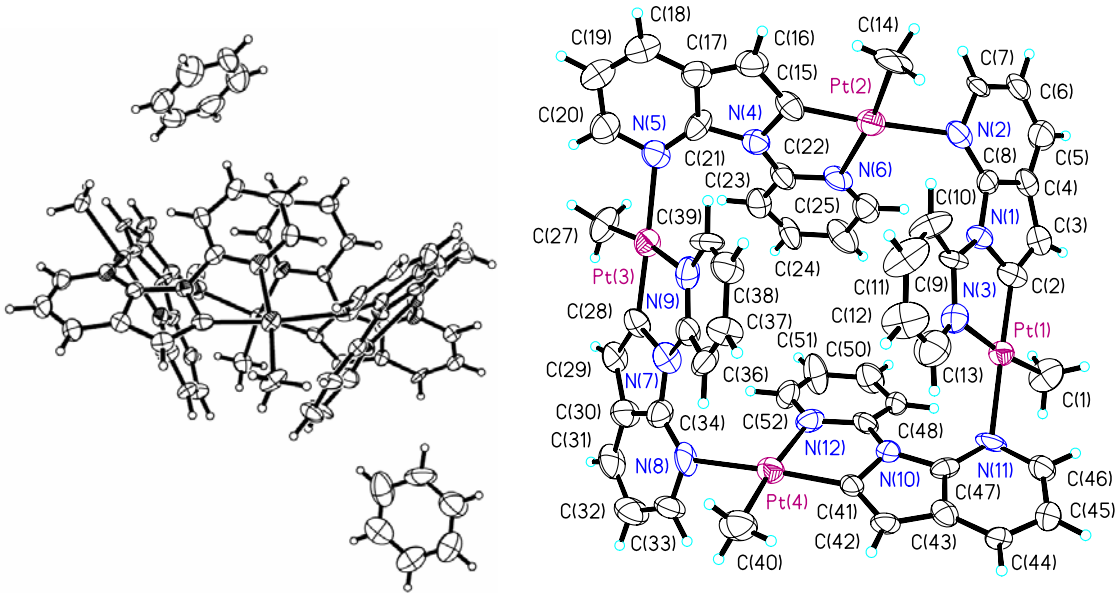

Figure 3.1 Left: the side view of the crystal structure of **3.2·2benzene** with 30% ellipsoids. Right: the top view of the Pt_4 unit with labeling schemes in **3.2·2benzene**.

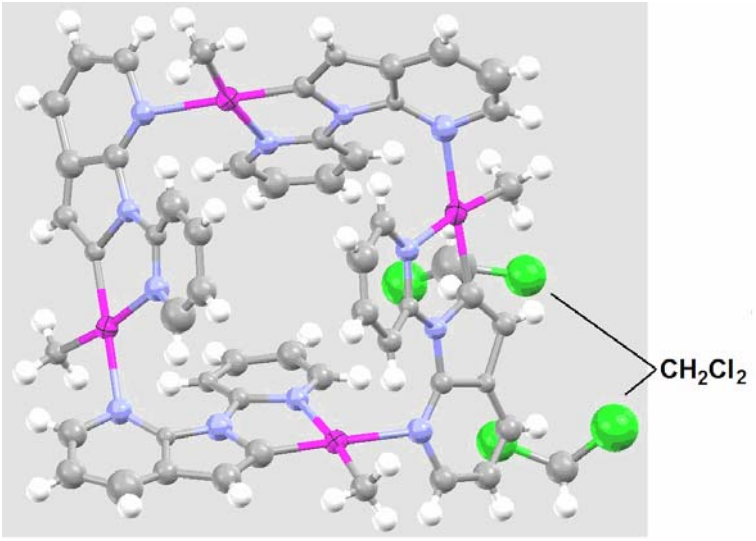

Figure 3.2 Crystal structure of **3.2·2CH_2Cl_2**.

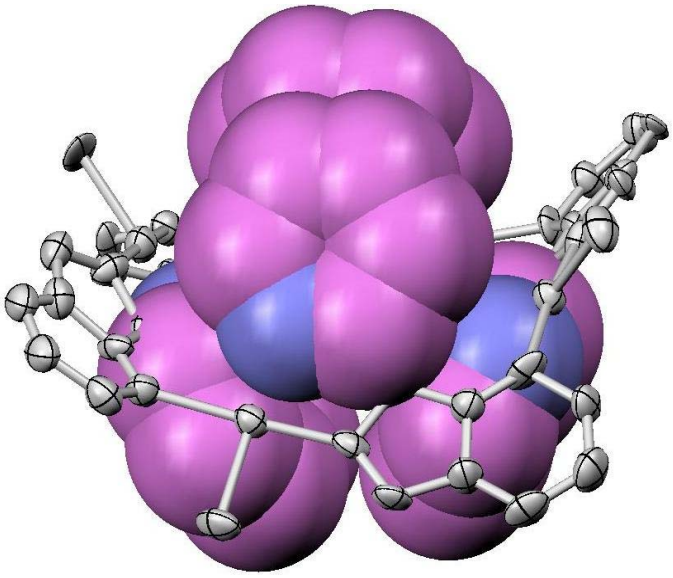

Figure 3.3 Crystal structure of **3.2·2benzene** with a space-filling drawing of the internal cage formed by the four pyridyl groups. The two benzene molecules and all H atoms are omitted for clarity.

3.3.2.2 Crystal structure of 3.3

The crystal structure of complex **3.3** is shown in Figure 3.4. The Pt(II) center in complex **3.3** forms a 6-membered N,N-chelate with the NPA ligand. The py ring and the 7-aza ring display a dihedral angle of 22.4°, an indication for the presence of the chelate ring strain. In addition, the separation distance of 2.02 Å between the C(6)-*H* and C(9)-*H* atoms is much shorter than the sum of van der Waals radii (2.40 Å), an indication of the existence of a strong steric replusion.[13] The Pt-N(1), Pt-N(3), Pt-C(19) and Pt-C(13) bond lengths in **3.3** are 2.107(4), 2.143(4), 2.012(5) and 2.007(5) Å, respectively. Notably, intermolecular Pt···H (2.80 Å) interactions are present in the crystal lattice of **3.3** that lead to the formation of a one-dimensional extended polymeric structure, as illustrated in Figure 3.5. This is most likely the reason for the poor solubility of complex **3.3**.

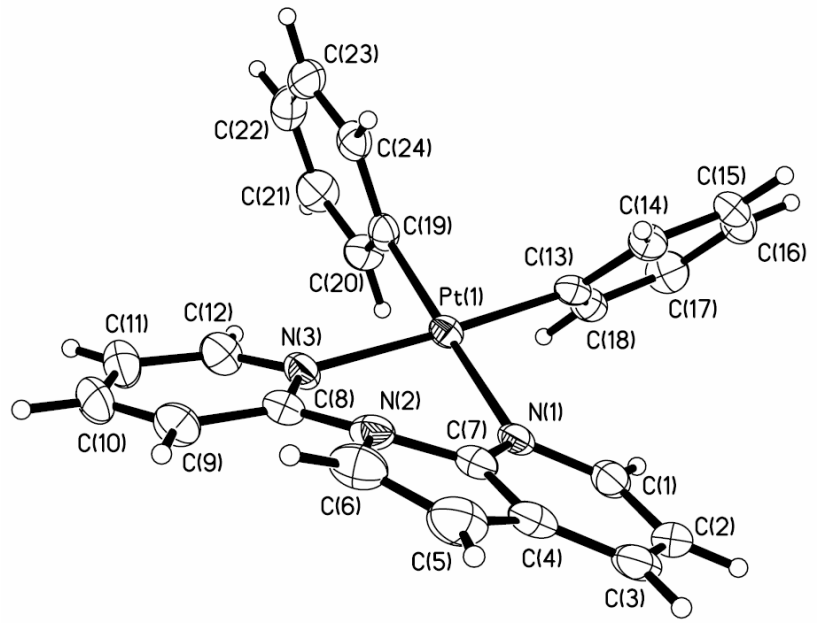

Figure 3.4 Crystal structure of **3.3** with 50% ellipsoids.

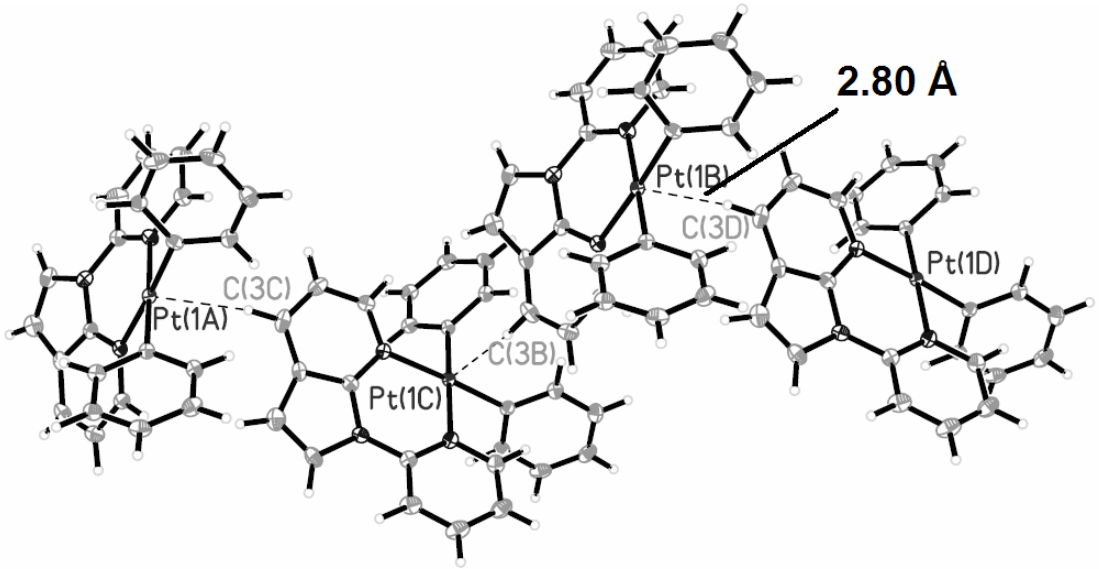

Figure 3.5 A diagram showing the intermolecular Pt···H interactions in the crystal lattice of **3.3**.

The earlier investigation by our group on $Zn(NPA)(O_2CR)_2$ complexes[4] established that the NPA ligand is a poor N,N-chelate ligand and has a strong tendency to dissociate from the Zn(II) centers in solution, which was attributed to the chelate ring strain and the interactions between the *ortho*-hydrogen atoms on the pyridyl ring and the 7-azaindolyl ring of the NPA ligand in the complexes.[4] The structural data of compound

3.3 support that the high reactivity of the $PtMe_2$ complex **3.1** is likely caused by the same destabilization forces.

3.3.2.2 Crystal structures of **E·CH$_3$CN** and **3.4**

The crystal structures of **E·CH$_3$CN** and **3.4** are shown in Figures 3.6 and 3.7, respectively. In contrast to **3.3**, the Pt(II) centers in **E·CH$_3$CN** and **3.4** both form a 5-membered N,C-chelating ring with the NPA ligand. The 5-membered N,C-chelating ring exhibits an excellent coplanarity and also avoids the *ortho*-H,H' repulsion. The Pt-C(1), Pt-C(13), Pt-N(3) and Pt-N(4) bond lengths in **E·CH$_3$CN** (Figure 3.6) are 1.947(5), 2.039(5), 2.049(5) and 2.100(4) Å, respectively. The Pt-C(11), Pt-S(1), Pt-N(3) and Pt-Cl(1) bond lengths in compound **3.4** (Figure 3.7) are 1.965(5), 2.2616(15), 2.046(4) and 2.3897(13) Å, respectively. Based on these evidences, it's reasonable to conclude that the driving forces for the facile "roll-over" cyclometalation of complex **3.1** comes from the stored distortion energy in the complex **3.1** and its intramolecular *ortho*-H,H' repulsion.

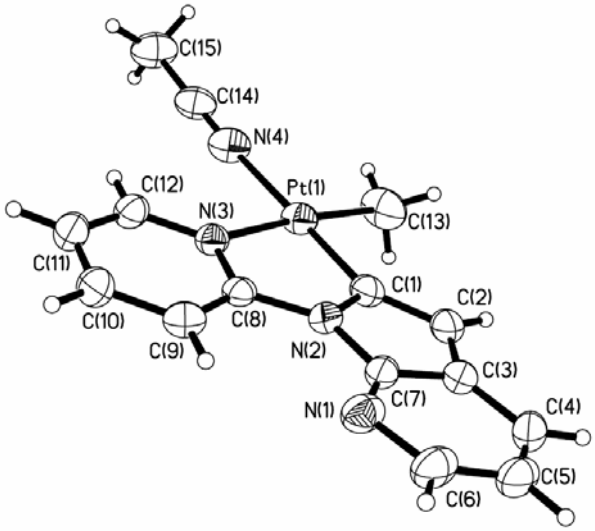

Figure 3.6 Crystal structure of **E·CH$_3$CN** with 30% ellipsoids.

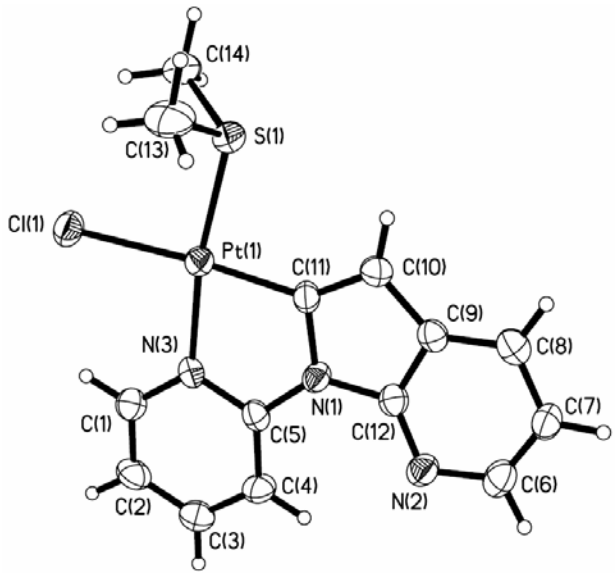

Figure 3.7 Crystal structure of **3.4** with 30% ellipsoids.

A common and important feature revealed by the structures of **3.2** and **E·CH$_3$CN** is that the *N,C*-chelating Pt unit displays consistently a configuration with the methyl group being *cis* to the new Pt-C(7-aza) bond, which can be explained by the greater *trans* effect of the Pt-C bond versus the Pt-N bond. However, in **3.4**, the Cl^- ligand is trans to the Pt-C(7-aza) bond, likely caused by the relative stronger *trans* effect of the SMe_2 ligand versus the Cl^- ligand. This feature however has no direct mechanistic implications on the transformation process of **E·SMe$_2$** to compound **3.4**, hence the C-Cl activation pathways involved in the formation of compound **3.4** remain unclear.

3.3.3 Mechanistic study of the transformation of 3.1 to 3.2

To understand the transformation process of compound **3.1**, the conversion of compound **3.1** to **3.2** was monitored by ^{1}H NMR spectroscopy in CD_2Cl_2. The NMR data revealed that at room temperature, compound **3.1** undergoes a rapid intramolecular "roll-over" metalation *via* the clean elimination of one equivalent of CH_4, leading to the

quantitative formation of the cyclic Pt_4 complex **3.2**. The most informative part of the ^1H NMR spectra is the aromatic region which is illustrated in Figure 3.8. The first spectrum (bottom) is for **3.1** at ~0 ^oC. Upon warming up to ambient temperature, **3.1** spontaneously transforms into **3.2** within 40 minutes, as evident by the clean spectral change.

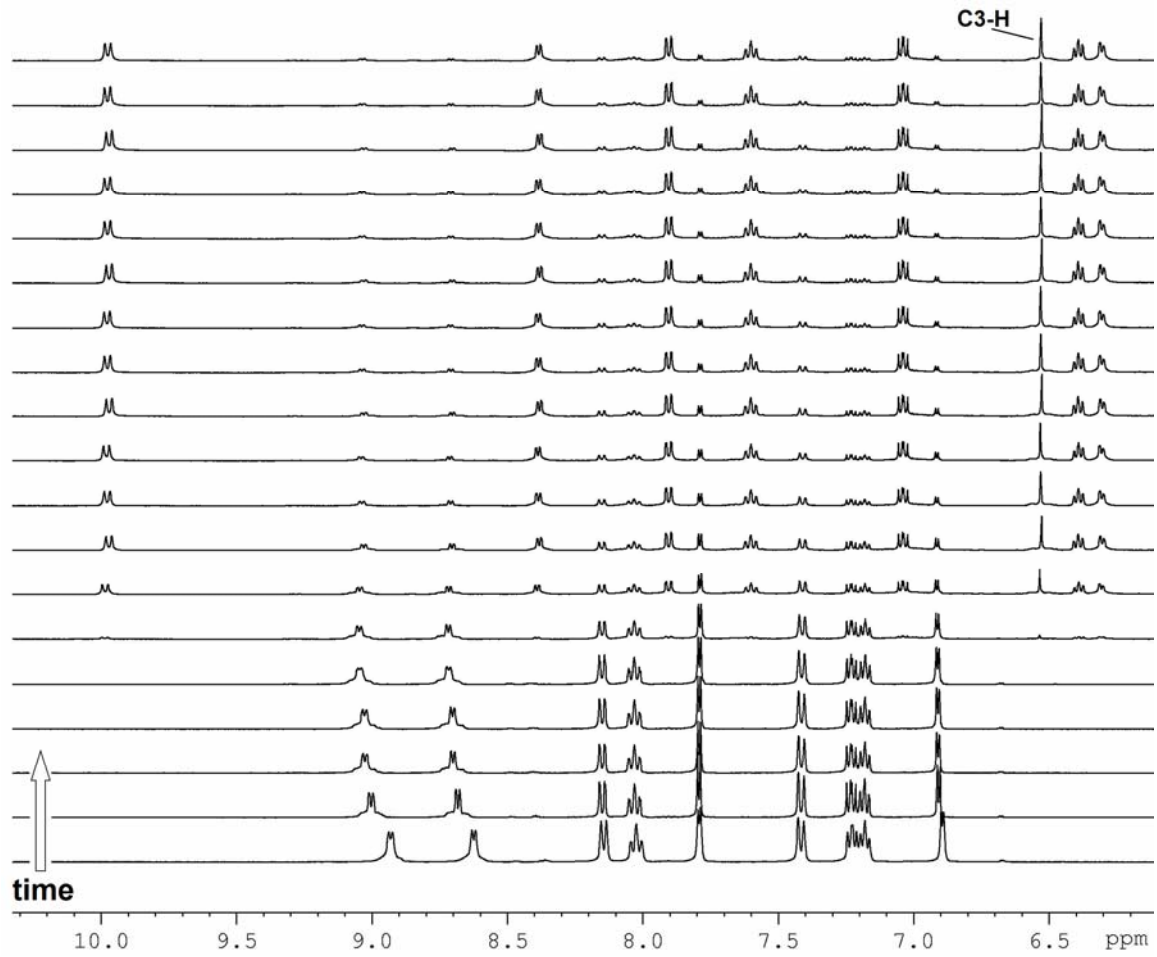

Figure 3.8 The aromatic region of ^1H NMR spectra for the **3.1** to **3.2** transformation in CD_2Cl_2. The temperature of the NMR spectrometer was 294.0 K, and initial temperature for the CD_2Cl_2 solution of **3.1** is ~ 278 K. The spectra were collected at 2 minute intervals.

The metalation occurs selectively at the C(2) position of the 7-azaindolyl ring, as indicated by the evolution of the diagnostic C(3) proton signal (δ = 6.5 ppm, $^3J_{Pt\text{-}H}$ = 27.0 Hz) in Figure 3.8. A significant downfield shift for one aromatic proton signal is observed from the **3.1** to **3.2** transformation, consistent with the congested cyclic

structure of **3.2**. The fact that no insoluble polymeric or oliogomeric species other than complex **3.2** were observed indicates that the roll-over cyclometalation driven self-assembly process is highly selective. The geometry of the NPA ligand clearly plays a key role in this unusual process. In addition, the simplicity of the ^{1}H NMR spectrum displayed by **3.2** (Figure 3.8) suggests the same environment for its four N,C,N-chelating NPA ligands, in agreement with the fact that **3.2** has a "S_4" axis.

3.3.3.1 Reaction kinetics

The kinetic analyses of the NMR spectra in Figure 3.8 revealed a first-order decay of **3.1** with time. To obtain the activation parameters of the reaction, the transformation of **3.1** was examined at several different temperatures. The rate constants obtained are shown in Table 3.3. Using these rate constants, parameters such as the activation enthalpy $\Delta H^{\neq}$ (19.6 ± 0.7 kcal·mol^{-1}) and the activation entropy $\Delta S^{\neq}$ (-4.6 ± 1.0 cal·mol^{-1}·K^{-1}) were obtained after fitting an Eyring plot[15] (R^{*} = 0.994), as shown in Figure 3.9.

It is noteworthy that the transformation process is fast, with a half life time *ca* 4.8 minutes at 24.0 ^{o}C. At temperatures above 35 ^{o}C, the reaction is too fast to allow reliable measurements of the reaction rate by ^{1}H NMR spectroscopy. Fortunately, even though the temperature window for the kinetics study was not large (289.0 – 302.0 K), the first-order kinetic behavior observed and the small entropy obtained are in good agreement with an intramolecular cyclometalation process.

Table 3.3 Rate constants of the transformation of **3.1** (or **3.1A**) to **3.2** in CD_2Cl_2 at different temperatures.

T (K) (± 0.1)	k_{obs} ($\cdot 10^3$ s^{-1}) (± < 3 %) of **1** (or **1A**)[a]	KIE
289.0	0.97	
292.0	1.44	
294.0	1.63	
297.1	2.40 (0.86)	2.8(2)
302.0	4.46	
296.0	0.36 (0.33)[b]	1.08(3)

[a] Values are the average for three trials. [b] Values were measured in the presence of > 10 folds of CD_3CN in CD_2Cl_2.

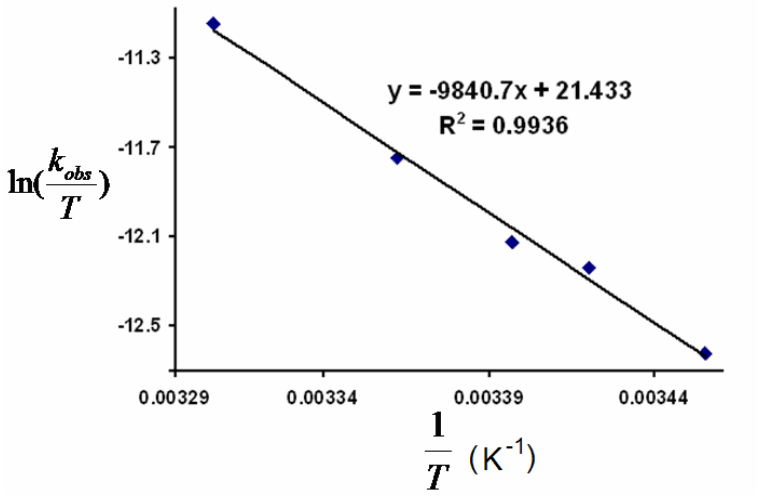

Figure 3.9 Eyring plot for the transformation process of compound **3.1**.

3.3.3.2 Proposed reaction pathway

On the basis of established mechanistic features of cyclometalation processes,[11a,11b] a possible pathway consistent with our results is proposed and shown in Scheme 3.5. Due to the chelating ring strain and *ortho*-H interactions, the Pt-N bond cleavage in **3.1** can occur readily. In the first step of the reaction, the dissociation of either the pyridyl nitrogen atom or the 7-azaindoly nitrogen atom from the Pt(II) center

leads to the formation of two different η^1-NPA $PtMe_2$ complexes **A** and **A'**. However, our NMR data suggest that only the species **A** can lead to the subsequent C-H cleavege. This can be attributed to the difference in the transition states of the C-H cleavage processes involving **A** and **A'**. For species **A'**, a six-member-ring intermediate (**B'**) will be formed which is thermodynamically disfavored relative to a five-member-ring intermediate (**B**) formed by **A**.

For the C-H cleavage step, the facile generation of a low-valent three-coordinate Pt(II) center and its high electron-richness will enable an oxidative addition pathway. The oxidative addition of the *ortho*-C-H bond on the 7-azaindolyl ring in **A**, *via* the *σ*–C-H bound Pt(II) intermediate **B**, leads to a five-coordinate *N,C*-chelating Pt(IV) hydride intermediate **C**. Due to the stronger *trans* effect of the 7-azaindolyl carbon atom over the pyridyl nitrogen atom in the intermediate **C**, the subsequent reductive elimination of CH_4 from **C** proceeds preferentially *via* the intermediate **D**, resulting in the formation of the *cis*-aryl, methyl isomer **E**, which, upon generation, spontaneously self-assembles into the cyclic Pt_4 compound **3.2**. The selective and clean formation/isolation of isomer **E** as **E·CH$_3$CN** and **E·SMe$_2$** confirm that the metalation occurs through an oxidative addition pathway. Moreover, all the coordination unsaturated species likely exist in equilibrium with their aqueous adducts during the reaction due to the presence of trance amount of H_2O in the solvent. The proposed mechanism is also supported by the fact that σ–C-H bound Pt(II) complexes and dimethyl Pt(IV) hydride complexes have been well demonstrated to be intermediates in hydrocarbon C-H activation processes.[14]

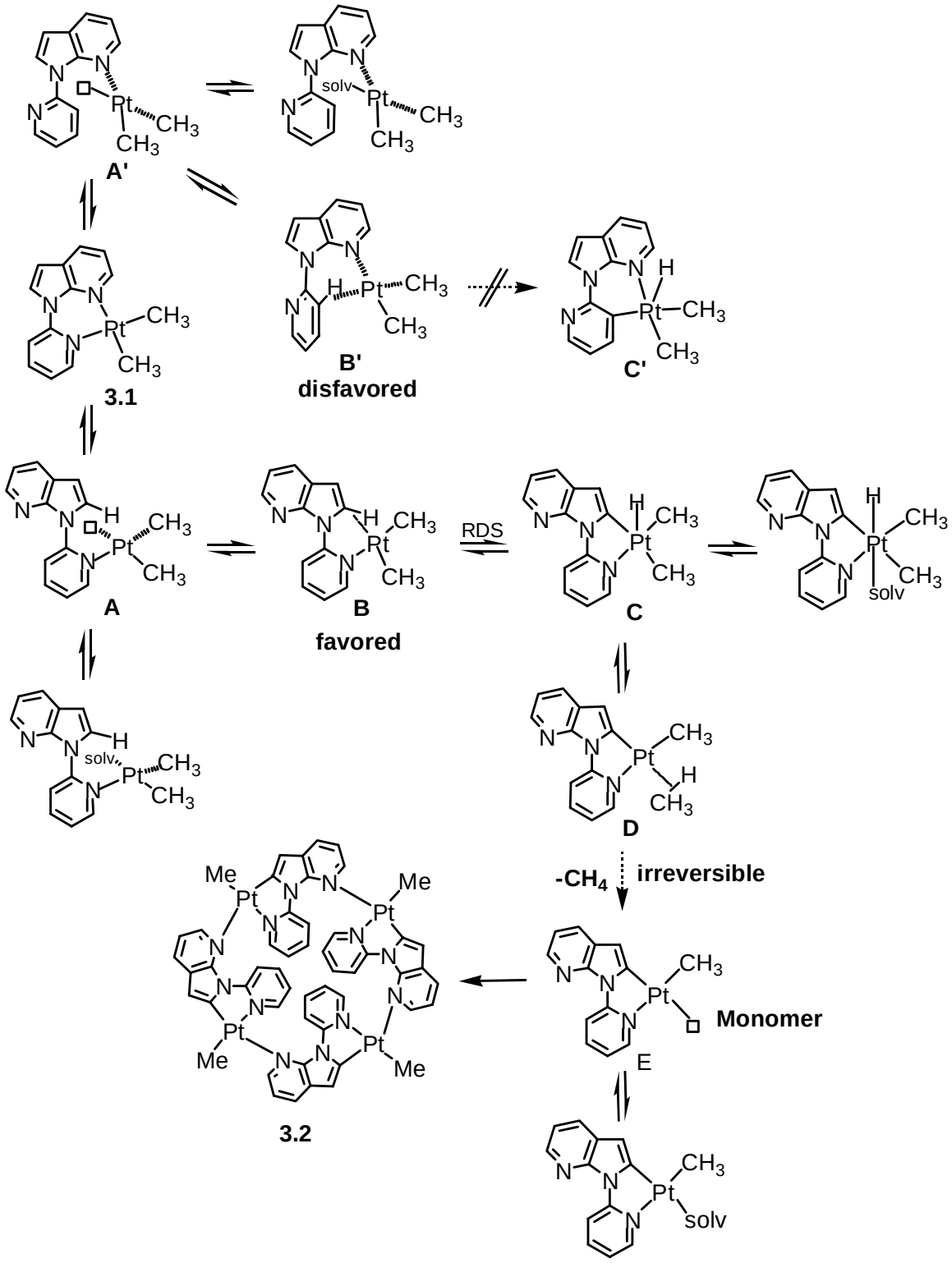

Scheme 3.5 Mechanistic pathway for the transformation of **3.1** to **3.2**.

Unfortunately, direction observation of any σ–C-H bound Pt(II) intermediate or any Pt(IV) intermediate was impossible as a result of their high reactivities under the reaction conditions. The examinations of these intermediates with low-temperature ^{1}H NMR spectroscopic analyses could not be carried out due to the shut-down of the reaction below 5 ^{o}C.

3.3.3.3 KIE of the cyclometalation process

To establish the rate determining step, we synthesized the C(2) deuterium labelled $PtMe_2$ compound Pt(2-D-NPA)$(CH_3)_2$ (**3.1A**), as shown in Scheme 3.6. For comparison study, a C(2) methylated derivative of **3.1**, Pt(2-Me-NPA)$(CH_3)_2$ (**3.1B**), was also synthesized. ^{1}H NMR spectroscopy study indicated that compound **3.1B** does not undergo roll-over cyclometalation at room temperature.

Scheme 3.6[a]

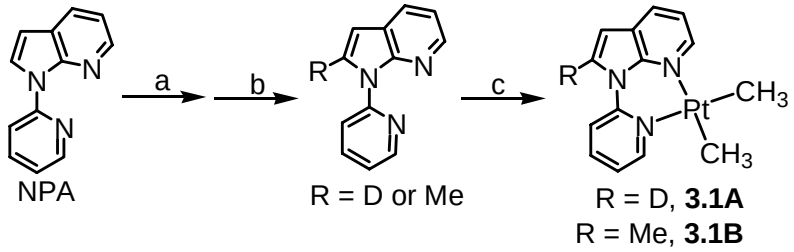

[a] *Reaction conditions*: a) 2.5 eq. LDA, -78 ^{o}C; b) excess D_2O or MeI; c) $[PtMe_2(\mu\text{-}SMe_2)]_2$, -10 ^{o}C for **3.1A** or rt for **3.1B**, overnight.

Kinetic isotope effect (KIE) studies using **3.1** and **3.1A** revealed a primary KIE (k_H/k_D, 2.8(2)) at 24 ^{o}C (Table 3.3), an indication that the C-H cleavage step is the rate determining step, supporting an oxidative addition pathway at the Pt(II) center, rather than an electrophilic substitution process. In addition, we observed that the

cyclometalation process of **3.1** or **3.1A** results in the exclusive formation of CH_4 or CDH_3. Moreover, there is no H/D scrambling of the CH_3 groups on the Pt(II) center with either the deuterated solvent (CD_2Cl_2, C_6D_6, CD_3CN, CD_3OD or D_2O) or the deuterium atom on its C(2) atom in the transformation of **3.1A**, an indication that the loss of CH_4 from intermediate **C** (Scheme 3.5) is much faster compared to H/D scrambling process, and irreversible.[16]

The NMR experiments also showed that the presence of either O_2 or H_2O does not affect the kinetic behaviors of complexes **3.1** and **3.1A** toward their roll-over cyclometalation driven self-assembly processes. This is in agreement with the fact that the C-H bond cleavage process is oxidative addition in nature. Interestingly, the NMR experiments revealed that the observed rate constant of the reaction is not affected by the concentration of H_2O in CD_2Cl_2. However, the presence of a stronger coordinating solvent such as CH_3CN does retard the formation of **3.2**, as the intermediate **E** (Scheme 3.5) is trapped by CH_3CN, as confirmed by ^1H NMR data and the isolation of the complex **E·CH$_3$CN**. It is also noteworthy that no sign of the dissociation of the NPA ligand from the Pt(II) complex was observed for the reaction of **3.2** even in the presence of *ca.* 150 equivalents of CD_3CN (6.0 M). With the concentration of CD_3CN at ~0.5 M and **3.1** at 0.04 M in CD_2Cl_2, a secondary KIE (k_H/k_D, 1.08(3)) for the cyclometalation process was observed, supporting that the conversion of the solvent adduct of **A** (Scheme 3.5) to the σ–C-H bound Pt(II) intermediate **B** (Scheme 3.5) becomes the rate determining step in the presence of a strong coordinating solvent.

3.4 Conclusions

In this chapter, the discovery of an interesting intramolecular C-H activation directed self-assembly process of a new Pt(II) complex Pt(NPA)$(CH_3)_2$ (**3.1**) is presented. A rare organoplatinum Pt_4 macrocycle $Pt_4(CH_3)_4$(*N*,*C*,*N*-NPA)$_4$ (**3.2**) is obtained from the transformation process of complex **3.1**. The mechanistic investigations suggest that the C-H cleavage step of the transformation process occurs *via* an oxidative addition pathway. The kinetic study using NMR spectroscopy has established that in the absence of strong coordinating solvent molecules, the rate determining step is the C-H cleavage step and **3.2** is formed exclusively. The presence of strong coordinating solvent molecules such as CH_3CN terminates the reaction at the Pt(*N*,*C*-NPA)(Me)(*L*) formation step, where *L* = the solvent molecule. The facile "roll-over" intramolecular C-H activation and the facile and selective formation of the cyclic Pt_4 complex by complex **3.1** are attributed to the poor stability of the *N*,*N*-chelate mode and the geometry of NPA.

References

1. a) Lu, W.; Chan, M. C. W.; Cheung, K. K.; Che, C.-M. *Organometallics* **2001**, *20*, 2477. b) Kui, S. C. F.; Chui, S. S.-Y.; Che, C.-M.; Zhu, N. *J. Am. Chem. Soc.* **2006**, *128*, 8297. c) Koo, C.-K.; Lam, B.; Leung, S.-K.; Lam, M. H.-W.; Wong, W.-Y. *J. Am. Chem. Soc.* **2006**, *128*, 16434.
2. Lu, W.; Mi, B. X.; Chan, M. C. W.; Hui, Z.; Che, C. M.; Zhu, N.; Lee, S. T. *J. Am. Chem. Soc.* **2004**, *126*, 4958.
3. a) Wu, Q.; Hook, A.; Wang, S. *Angew. Chem., Int. Ed.* **2000**, *39*, 3933. b) Song, D.; Wu, Q.; Hook, A.; Kozin, I.; Wang, S. *Organometallics* **2001**, *20*, 4683.
4. Wu, Q.; Lavigne, J. A.; Tao, Y.; D'Iorio, M.; Wang, S. *Inorg. Chem.* **2000**, *39*, 5248.
5. Leininger, S.; Olenyuk, B.; Stang, P. J. *Chem. Rev.* **2000**, *100*, 853.
6. a) Kusukawa, T.; Fujita, M. *J. Am. Chem. Soc.* **2002**, 124, 13576. b) Kawano, M.; Kobayashi, Y.; Ozeki, T.; Fujita, M. *J. Am. Chem. Soc.* **2006**, 128, 6558. c) Yoshizawa, M.; Miyagi, S.; Kawano, M.; Ishiguro, K.; Fujita, M. *J. Am. Chem. Soc.* **2004**, 126, 9172. d) Yoshizawa, M.; Tamura, M; Fujita, M. *Science*, **2006**, *312*, 251. f) Lee, S. J.; Hu, A.; Lin, W. *J. Am. Chem. Soc.* **2002**, *124*, 12948. g) Jiang, H.; Lin, W. *Org. Lett.* **2004**, *6*, 861.
7. Seidel, S. R.; Stang, P. J. *Acc. Chem. Res.* **2002**, 35, 972.
8. Fujita, M.; Tominaga, M.; Hori, A.; Therrien, B. *Acc. Chem. Res.* **2005**, *38*, 371.
9. a) Das, N.; Mukherjee, P. S.; Arif, A. M.; Stang, P. J. *J. Am. Chem. Soc.* **2003**, 125, 13950. b) Lai, S. W.; Chan, M. C. W.; Peng, S. M. ; Che, C. M. *Angew. Chem., Int. Ed.* **1999**, *38*, 669. c) Zucca, A.; Petretto, G. L.; Stoccoro, S.; Cinellu,

M. A.; Minghetti, G. *Organometallics* **2006**, *25*, 2253. d) Jiang, H.; Lin, W. *J. Am. Chem. Soc.* **2003**, *125*, 8084. e) Jiang, H.; Lin, W. *J. Am. Chem. Soc.* **2004**, *126*, 7426. f) Jiang, H.; Lin, W. *J. Am. Chem. Soc.* **2006**, *128*, 11286.

10. Skapski, A.C.; Sutcliffe, V. F.; Young, G. B. *Chem. Commun.* **1985**, 609.
11. a) Newkome, G. R.; Puckett, W. E.; Gupta, V. K.; Kiefer, G. E. *Chem. Rev.* **1986**, *86*, 451. b) Ryabov, A. D. *Chem. Rev.* **1990**, *90*, 403. c) Owen, J. S.; Labinger, J. A.; Bercaw, J. E. *J. Am. Chem. Soc.* **2004**, *126*, 8247.
12. a) Scott, J. D.; Puddephatt, R. J. *Organometallics* **1983**, *2*, 1643. b) Song, D.; Wang, S. *J. Organomet. Chem.* **2002**, *648*, 302.
13. Emsley, J. *The Elements*, 2nd ed., Clarendon Press, Oxford, **1991**.
14. a) Stahl, S. S.; Labinger, J. A.; Bercaw, J. E. *J. Am. Chem. Soc.* **1996**, *118*, 5961. b) Wick, D. D.; Goldberg, K. I. *J. Am. Chem. Soc.* **1997**, *119*, 10235.
15. Eyring-equation: $\ln(\frac{k_{obs}}{T}) = -\frac{\Delta H^{\neq}}{R}(\frac{1}{T}) + \ln(\frac{k_B}{h}) + \frac{\Delta S^{\neq}}{R}$; where k_{obs} is the rate constant, T is the temperature; k_B is the Boltzmann-constant, h is the Planck-constant, R is the gas constant.
16. a) Wik, B. J.; Lersch, M.; Tilset, M. *J. Am. Chem. Soc.* **2002**, *124*, 12116. b) Lersch, M.; Tilset, M. *Chem. Rev.* **2005**, *105*, 2471.

Chapter 4

Steric Impacts of the BAB and BAM Ligands on the Structure and Stability of Five-Coordinate Pt(IV) Complexes

4.1 Introduction

As shown in Chapter 1 (Scheme 1.8), five-coordinate Pt(IV) complexes have been postulated as key intermediates in the Shilov direct hydrocarbon functionalization process.[1] The involvements of such species have been suggested to be in the C-H activation step *via* the oxidative addition at a Pt(II) center and in the reductive coupling step *via* the ligand dissociation at a six-coordinate Pt(IV) center that leads to the functionalization of the carbon atom. Therefore, the investigation of the Pt(IV) chemistry particularly that of the five-coordinate Pt(IV) compounds is important due to their great mechanistic implications toward the Pt(II) catalyzed C-H activation/functionalization processes.[2-6]

Despite the recent advances on the Shilov chemistry, five-coordinate organoplatinum(IV) complexes remain rare due to the difficulties in synthesizing and isolating such coordinatively unsaturated species, and only a few examples of five-coordinate organoplatinum(IV) complexes have been reported.[4,5,6] It is noteworthy, however, that all previously known five-coordinate Pt(IV) compounds employ anionic N,N-chelating ligands,[4a] as illustrated in Chart 4.1. Although the steric bulkiness of these N,N-chelating ligands contributes greatly in stabilizing the five-coordinate Pt(IV) centers,[4b,4c,5] the recent work by Goldberg and coworkers seems to indicate that it may not always be necessary in achieving five-coordinate Pt(IV) compounds.[4a]

Chart 4.1

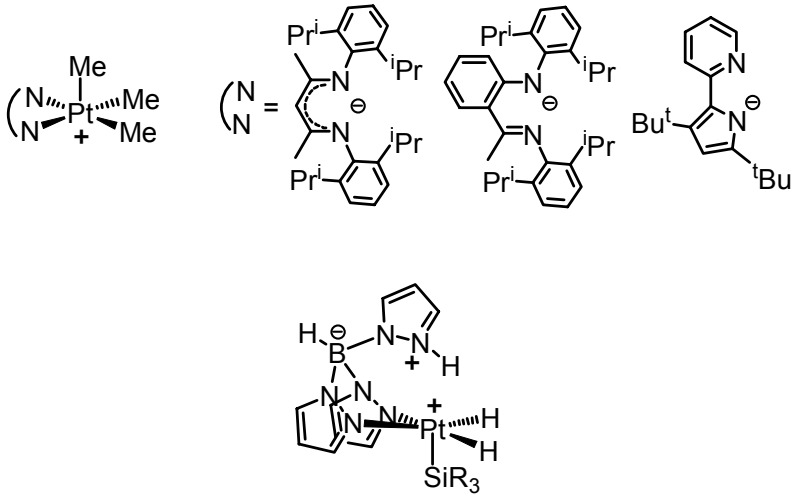

In chapter 2, we have demonstrated the regio- and/or diastereoselective alkylbenzene C-H activation by the cationic $[Pt(N,N\text{-}L)Me(solv)]^+$ complexes, where N,N-L = 1,2-bis(1-*N*-7-azaindolyl)benzene (BAB) and bis(1-*N*-7-azaindolyl)methane (BAM).[7,8] We have shown that the steric blockage of one Pt(II) coordination site in these two complexes is the origin of the distinct diastereoselectivity observed for the EtPh benzylic C-H activation, and also allows the stabilization and the isolation of two η^3-benzylic Pt(II) intermediates **2.7** and **2.8**.

To further understand the roles of our N,N-L chelating ligands in Pt(II) mediated C-H activation, we investigated the relevant Pt(IV) chemistry. The details on the syntheses, characterization of several new BAM and BAB *fac*-$Pt^{IV}Me_3$ complexes and the preliminary findings of the steric impacts of BAM and BAB ligands on the structure and stability of these Pt(IV) complexes are presented in this chapter.

4.2 Experimental Section

4.2.1 General procedures

All reactions were performed either under N_2 with standard Schlenk techniques or inside a dry-box unless otherwise noted. All starting materials were purchased from Aldrich Chemical Company, Inc. and used without further purification. Toluene, THF, Et_2O and hexane were purified using the solvent purification system (Innovation Technology, Inc.); CH_2Cl_2 was freshly distilled over P_2O_5 prior to use. The deuterated solvent CD_2Cl_2 (Cambridge Isotopes) was dried with CaH_2 chunks prior to use; the $C_6D_5NO_2$ ampules (Aldrich Chemical Company, Inc.) were used as received without further drying. NMR spectra were recorded on Bruker Avance 300, 400 or 500 MHz spectrometers. ^1H and ^{13}C NMR chemical shifts were referenced to the residual solvent peaks and have been reported in parts per million (ppm). The assignments of the ^1H NMR signals of the compounds are based on their COSY and NOESY spectra.

The ligands 1,2-bis(1-*N*-7-azaindolyl)benzene (BAB) and bis(1-*N*-7-azaindolyl)methane (BAM) were synthesized by using previously reported procedures.[7,8] The synthetic procedures for $Pt(BAB)Me_2$[7] (**2.1**) and $Pt(BAM)Me_2$[8] (**2.2**) were reported by us previously. $[Me_3PtI]_4$ was synthesized by using methods described in the literature.[9] Another approach to achieve $[Me_3PtI]_4$ is the reaction of $Pt(BAB)Me_2$ or $Pt(BAM)Me_2$ with MeI, as described below. $[Me_3PtOTf]_4$ and $[Me_3Pt(\mu\text{-}THF)_{1.5}]_2[PF_6]_2$ were prepared from the reaction $[Me_3PtI]_4$ with either AgOTf or $AgPF_6$ in dry THF using methods described in the literature.[10]

4.2.2 Reactivities of Pt(BAB)Me_2 (2.1) and Pt(BAM)Me_2 (2.2) with MeI and the synthesis of $[Me_3PtI]_4$

The ^{1}H NMR study revealed that upon addition of one equivalent of MeI to the solution of **2.1** or **2.2**, the Pt(II) complex was converted quantitatively to $[Me_3PtI]_4$, along with the generation of the free chelating ligand BAB or BAM. These reactions can be used in a preparative scale for the synthesis of $[PtMe_3I]_4$: Under air, to a THF (5~10 mL) solution of **2.1** or **2.2** (0.30 mmoL) was added dropwise MeI (0.25 mL, 0.40 mmoL). The resulting mixture was stirred for 10 minutes at ambient temperature. The solvent was then slowly evacuated, and the residue was washed with the Et_2O/CH_3COCH_3 (1:1) mixed solvents (3 mL x 3) to afford $[Me_3PtI]_4$ as a white solid in > 95% isolated yield. The white $[Me_3PtI]_4$ product produced an orange-yellow solution when being dissolved in chloroform. Its ^{1}H NMR (300 MHz, $CDCl_3$, 25 ^{o}C) displayed a sharp singlet at 1.75 ppm, with a diagnostic ^{195}Pt-^{1}H coupling pattern ($^2J_{Pt\text{-}H}$ = 77.4 Hz), consistent with the ^{1}H NMR data of the orange-yellow $[Me_3PtI]_4$ product synthesized by published methods.[10]

4.2.3 Synthesis of [Pt(BAB)Me_3][OTf] (4.1)

To a THF solution (8 mL) of BAB (0.062 g, 0.20 mmol) was quickly added a THF solution (8 mL) of $[Me_3PtOTf]_4$ (0.050 mmoL). The resulting mixture was stirred at ambient temperature for 6 hours. After the reaction, the solution was allowed to slowly evaporate inside a dry-box, resulting in **4.1** as colorless crystals which were further washed by the CH_2Cl_2/Et_2O (1:5) mixed solvents (3 mL x 3) to remove the remaining starting materials. The isolated yield for **4.1** is 74%. ^{1}H NMR (400 MHz, CD_2Cl_2, 25 ^{o}C): δ 8.16 (d; ^3J = 8.0 Hz; 2H, 7-aza), 8.03 (m; 4H, 2H from 7-aza and 2H from the

bridging phenyl moiety of BAB), 7.72 (m; 2H, 7-aza), 7.30 (m; 4H, 2H from 7-aza and 2H from the bridging phenyl moiety of BAB), 6.84 (d; 2H, ^{3}J = 4.0 Hz; 2H, 7-aza), 2.17 (br; 3H, PtMe_{apical}), 0.61 (br; 6H, Pt$Me_{equatorial}$) ppm. The low temperature ^{1}H NMR (400 MHz, CD_2Cl_2, 220 K) for **4.1** displayed two sets of well-defined methyl peaks with diagnostic ^{195}Pt-^{1}H coupling patterns for the *fac*-PtMe_3 moiety: δ 2.17 (s, satellites; $^{2}J_{Pt\text{-}H}$ = 84.4 Hz; 3H, PtMe_{apical}) and 0.57 (s, satellites; $^{2}J_{Pt\text{-}H}$ = 67.2 Hz; 6H, Pt$Me_{equatorial}$) ppm. ^{13}C NMR (220 K) : δ 151.14, 139.24, 134.85, 134.23, 133.74, 133.60, 131.02, 124.53, 119.06, 119.06, 106.80, 10.10 (PtMe_{apical}), -2.56 (Pt$Me_{equatorial}$) ppm. Note: the carbon atoms of the *fac*-$PtMe_3$ moiety in **4.1** did not display signals in ^{13}C NMR spectrum at ambient temperature. Anal. calcd. for $C_{26}H_{29}N_4F_3O_3PtS$: C 42.80, H 4.01, N 7.68; found: C 42.61, H 4.38, N 7.68.

4.2.4 Synthesis of [Pt(BAM)Me_3(OTf)] (4.2)

To a THF solution (5 mL) of the BAM ligand (0.039 g, 0.16 mmol) was quickly added a THF solution (8 mL) of $[Me_3PtOTf]_4$ (0.040 mmoL). The resulting mixture was stirred at ambient temperature for 4 hours. After the reaction, the solution was allowed to slowly evaporate inside a dry-box, resulting in **4.2** as colorless crystals which were further washed by the CH_2Cl_2/Et_2O (1:5) mixed solvents (2 mL x 3) to remove the remaining starting materials. The isolated yield for **4.2** is ~86%. ^{1}H NMR (400 MHz, CD_2Cl_2, 25 ^{o}C): δ 8.41 (dd; ^{3}J = 8.4 Hz, ^{4}J = 1.2 Hz; 2H, 7-aza), 8.15 (d; ^{3}J = 7.6 Hz; 2H, 7-aza), 7.82 (d; ^{3}J = 4.0 Hz; 2H, 7-aza), 7.33 (dd; $^{3}J_1$ = 8.4 Hz, $^{3}J_2$ = 7.6 Hz; 2H, 7-aza), 7.01 (d; ^{2}J = 16.0 Hz; 1H from the bridging C*H*H' moiety of BAM), 6.82 (d; ^{3}J = 4.0 Hz; 2H, 7-aza), 6.39 (d with satellites; ^{2}J = 16.0 Hz, $J_{Pt\text{-}H}$ = 37.9 Hz; 1H from the bridging

CH*H'* moiety of BAM), 1.76 (s, satellites; $^{2}J_{Pt\text{-}H}$ = 73.7 Hz; 9H, *fac*-Pt*Me*$_3$) ppm. ^{13}C NMR: δ 146.29, 142.95, 132.69, 129.87, 125.16, 118.30, 115.59 (br), 104.50, 58.04 (bridging *C*HH' from BAM), 3.70 (Pt*Me*$_{apical}$), 0.15 (Pt*Me*$_{equatorial}$) ppm. Anal. calcd. for $C_{21}H_{26}N_4F_3O_3PtS$: C 37.84, H 3.93, N 8.40; found: C 37.68, H 3.42, N 8.81.

4.2.5 Synthesis of [Pt(BAM)Me$_3$(THF)][PF$_6$] (4.3)

Compound **4.3** was synthesized in the same manner as described for compound **4.2** from the reaction of the BAM ligand and a THF solution of $[Me_3Pt(\mu\text{-THF})_{1.5}]_2[PF_6]_2$. After slow evaporation of THF, the resulting colorless crystals were washed by Et_2O. The isolated yield for **4.3** is 60~70%. ^{1}H NMR (400 MHz, CD_2Cl_2, 25 ^{o}C): δ 8.22 (d; ^{3}J = 8.0 Hz; 2H, 7-aza), 8.17 (d; ^{3}J = 6.0 Hz; 2H, 7-aza), 7.86 (d; ^{3}J = 2.8 Hz; 2H, 7-aza), 7.33 (d; ^{2}J = 13.6 Hz; 1H, 1H from the bridging C*H*H' moiety of BAM) 7.42(dd; $^{3}J_1$ = 8.0 Hz, $^{3}J_2$ = 6.0 Hz; 2H, 7-aza), 6.94 (d; ^{3}J = 6.0 Hz; 2H, 7-aza), 4.88 (d; ^{2}J = 13.6 Hz; 1H from the bridging CH*H'* moiety of BAM), 3.72 (m; 4H, two *α*-C*H*$_2$ from THF), 1.88 (m; 4H, two *β*-C*H*$_2$ from THF), 1.84 (s, satellites; $^{2}J_{Pt\text{-}H}$ = 58.4 Hz; 9H, *fac*-Pt*Me*$_3$) ppm. ^{13}C NMR: δ 146.83, 139.31, 133.31, 130.20, 125.89, 119.02, 105.76, 68.13(*α*-*C*H$_2$ from THF), 62.52 (bridging *C*HH' from BAM), 25.95 (*β*-*C*H$_2$ from THF), 3.19 (Pt*Me*$_3$) ppm. Anal. calcd. for $C_{24}H_{34}N_4F_6OPPt$: C 39.24, H 4.67, N 7.63; found: 39.74, H 4.24, N 7.54.

4.2.6 Synthesis of [Pt(*N,C,N*-BAM)Me$_3$] (4.4)

To a stirred THF (10 mL) solution of BAM (105.2 mg, 0.42 mmol) at -78 ^{o}C was added dropwise, *via* syringe, a *n*-BuLi solution (1.6 M) (0.28 mL, 0.45 mmol) over 2 minutes. The resulting light yellow solution was stirred for 30 minutes at -78 ^{o}C, a

solution of $[Me_3Pt(THF)_{1.5}]_2[PF_6]_2$ (~0.42 mmol based on Pt^{IV}) in THF (15 mL) was then slowly added. The reaction mixture was slowly warmed to ambient temperature and stirred for 4 hours. After the removal of the solvent, the residue was extracted with a CH_3COCH_3/Et_2O (1:1) solution (15 mL). Slow evaporation of the solution inside dry-box afforded **4.4** as a white powder (~42% yield). Crystals of **4.4** were obtained by slow evaporation of its dilute hexane/Et_2O solution. ^{1}H NMR (500 MHz, C_6D_6, 25 ^oC): δ 8.28 (d; ^3J = 5.0; 2H, 7-aza), 7.34 (d, ^3J = 8.4; 2H, 7-aza), 7.06 (d; ^3J = 3.4; 2H, 7-aza), 6.49 (m; 4H; 7-aza), 5.63 (s; 1H, 1H from the bridging C atom of BAM), 1.41 (s, satellites; $^2J_{Pt\text{-}H}$ = 49.7 Hz; 3H, PtMe_{apical}), 1.34 (s, satellites; $^2J_{Pt\text{-}H}$ = 74.1; 6H, Pt$Me_{equatorial}$) ppm. ^{13}C NMR: δ 154.32, 138.42, 129.85, 128.54, 119.75, 116.18, 103.93, 75.83 (s, satellites; $^2J_{Pt\text{-}C}$ = 475.16 Hz; bridging *C* atom from BAM), 1.29 (s, satellites; $^2J_{Pt\text{-}C}$ = 517.60 Hz; PtMe_{apical}), -11.96 (s, satellites; $^2J_{Pt\text{-}C}$ = 695.55 Hz; Pt$Me_{equatorial}$) ppm. Elemental analysis was not performed due to the difficulty in removing the trace remaining BAM ligand from the product.

4.2.7 X-ray diffraction analyses

Single crystals of **4.1**-**4.4** were mounted on glass fibers for data collection. Data were collected on a Bruker Apex II single-crystal X-ray diffractometer with graphite-monochromated Mo Kα radiation, operating at 50 kV and 30 mA. Data collections for **4.2**-**4.4** were carried out at 180 K while data collections for **4.1** were collected at ambient temperature. No significant decay was observed in any samples. Data were processed on a PC with the aid of the Bruker SHELXTL software package (version 5.10) and are corrected for absorption effects. All structures were solved by direct methods. The crystal

data are summarized in Table 4.1, and the selected bond lengths and angles are presented in Table 4.2.

Table 4.1 Crystallographic data for compounds **4.1**-**4.4**.

Compound	**4.1**	**4.2**	**4.3**	**4.4**
Formula	$C_{24}H_{23}F_3N_4O_3PtS$	$C_{19}H_{21}F_3N_4O_3PtS$	$C_{22}H_{29}F_6N_4OPPt$	$C_{18}H_{20}N_4Pt$
FW	699.61	637.55	705.55	487.47
Space Group	$P2_1/c$	P-1	P-1	$P2_1$
a, Å	10.7240(3)	6.88210(10)	9.2523(11)	8.092(5)
b, Å	24.2086(8)	10.91230(10)	11.2105(13)	20.908(13)
c, Å	9.2365(3)	14.1919(2)	13.4198(16)	10.379(7)
α, º	90	92.6570(10)	66.8140(10)	90
β, º	99.8930(10)°	91.9620(10)	73.8590(10)	98.975(7)
γ, º	90	104.9420(10)	83.8020(10)	90
V, Å^3	2362.26(13)	1027.48(2)	1229.1(3)	1734.6(19)
Z	4	2	2	4
$D_{calc,}$ g·cm^{-3}	1.967	2.061	1.906	1.867
T, K	298(2)	180(2)	180(2)	180(2)
μ, mm^{-1}	6.088	6.987	5.842	8.093
$2\theta_{max}$, º	54.24	54.18	54.26	56.58
Reflns measured	18925	8769	13360	18921
Reflns used (R_{int})	5212 (0.0199)	4370 (0.0144)	5272 (0.0217)	7854 (0.0240)
Parameters	328	291	399	421
Final R [I > 2σ(I)]:				
R_1[a]	0.0184	0.0166	0.0186	0.0199
wR_2[b]	0.0374	0.0410	0.0464	0.0395
R (all data):				
R_1[a]	0.0219	0.0172	0.0201	0.0228
wR_2[b]	0.0383	0.0413	0.0470	0.0403
Goodness-of-fit on F^2	1.106	1.075	1.074	0.938

[a] $R_1 = \Sigma||F_0| - |F_c|| / \Sigma|F_0|$

[b] $wR_2 = [\Sigma w [(F_0^2-F_c^2)^2] / \Sigma[w(F_0^2)^2]]^{1/2}$

$w = 1 / [\sigma^2(F_0^2) + (0.075P)^2]$, where $P = [Max (F_0^2,0) + 2F_c^2] / 3$

Table 4.2 Selected bond lengths (Å) and angles (º) for compounds **4.1**-**4.4**.

		Compound **4.1**	
Pt(1)-C(2)	2.029(3)	S(1)-O(2)	1.429(3)
Pt(1)-C(3)	2.032(3)	S(1)-O(1)	1.428(2)
Pt(1)-C(1)	2.042(3)	S(1)-C(24)	1.807(3)
Pt(1)-N(4)	2.196(2)	F(1)-C(24)	1.336(4)
Pt(1)-N(1)	2.230(2)	F(2)-C(24)	1.323(4)
S(1)-O(3)	1.424(3)	F(3)-C(24)	1.331(4)
C(2)-Pt(1)-C(3)	87.83(12)	C(1)-Pt(1)-N(1)	178.23(10)
C(2)-Pt(1)-C(1)	86.31(13)	N(4)-Pt(1)-N(1)	91.22(8)
C(3)-Pt(1)-C(1)	87.92(12)	O(3)-S(1)-O(2)	117.2(2)
C(2)-Pt(1)-N(4)	93.23(11)	O(3)-S(1)-O(1)	113.65(17)
C(3)-Pt(1)-N(4)	177.71(10)	O(2)-S(1)-O(1)	115.11(16)
C(1)-Pt(1)-N(4)	90.12(10)	O(3)-S(1)-C(24)	102.94(18)
C(2)-Pt(1)-N(1)	94.76(11)	O(2)-S(1)-C(24)	102.07(15)
C(3)-Pt(1)-N(1)	90.71(10)	O(1)-S(1)-C(24)	103.11(15)
		Compound **4.2**	
Pt(1)-C(1)	2.036(3)	S(1)-O(2)	1.431(2)
Pt(1)-C(3)	2.042(3)	S(1)-O(3)	1.434(2)
Pt(1)-C(2)	2.046(3)	S(1)-O(1)	1.4622(18)
Pt(1)-O(1)	2.2589(18)	S(1)-C(19)	1.820(3)
Pt(1)-N(4)	2.269(2)	F(1)-C(19)	1.321(4)
Pt(1)-N(1)	2.296(2)	F(2)-C(19)	1.341(3)
N(1)-C(10)	1.344(3)	F(3)-C(19)	1.322(4)
C(1)-Pt(1)-C(3)	83.79(13)	C(2)-Pt(1)-N(4)	89.39(10)
C(1)-Pt(1)-C(2)	83.91(13)	O(1)-Pt(1)-N(4)	81.39(7)
C(3)-Pt(1)-C(2)	87.57(12)	C(1)-Pt(1)-N(1)	103.72(10)
C(1)-Pt(1)-O(1)	176.61(9)	C(3)-Pt(1)-N(1)	89.39(10)
C(3)-Pt(1)-O(1)	93.78(10)	C(2)-Pt(1)-N(1)	171.44(10)
C(2)-Pt(1)-O(1)	93.64(10)	O(1)-Pt(1)-N(1)	78.57(7)
C(1)-Pt(1)-N(4)	100.89(10)	N(4)-Pt(1)-N(1)	92.91(8)
C(3)-Pt(1)-N(4)	174.13(10)	O(2)-S(1)-O(3)	116.09(14)
		Compound **4.3**	
Pt(1)-C(3)	2.029(3)	Pt(1)-N(1)	2.273(2)
Pt(1)-C(2)	2.034(3)	Pt(1)-N(4)	2.283(2)
Pt(1)-C(1)	2.038(3)	Pt(1)-O(1)	2.293(2)
C(3)-Pt(1)-C(2)	84.04(13)	C(1)-Pt(1)-N(4)	170.76(11)
C(3)-Pt(1)-C(1)	84.81(13)	N(1)-Pt(1)-N(4)	95.09(8)
C(2)-Pt(1)-C(1)	86.20(13)	C(3)-Pt(1)-O(1)	177.34(10)

C(3)-Pt(1)-N(1)	97.47(11)	C(2)-Pt(1)-O(1)	94.85(11)
C(2)-Pt(1)-N(1)	174.65(10)	C(1)-Pt(1)-O(1)	92.71(11)
C(1)-Pt(1)-N(1)	88.82(11)	N(1)-Pt(1)-O(1)	83.43(8)
C(3)-Pt(1)-N(4)	102.92(11)	N(4)-Pt(1)-O(1)	79.46(8)
C(2)-Pt(1)-N(4)	89.55(11)		

Compound **4.4**

Pt(1)-C(16)	2.041(4)	Pt(2)-C(34)	2.039(5)
Pt(1)-C(18)	2.046(5)	Pt(2)-C(35)	2.040(5)
Pt(1)-C(17)	2.112(5)	Pt(2)-C(36)	2.100(5)
Pt(1)-C(15)	2.147(5)	Pt(2)-C(33)	2.139(4)
Pt(1)-N(3)	2.154(4)	Pt(2)-N(5)	2.147(4)
Pt(1)-N(1)	2.179(4)	Pt(2)-N(7)	2.151(3)
C(16)-Pt(1)-C(18)	89.8(2)	C(34)-Pt(2)-C(35)	90.9(2)
C(16)-Pt(1)-C(17)	89.5(2)	C(34)-Pt(2)-C(36)	88.9(2)
C(18)-Pt(1)-C(17)	89.3(2)	C(35)-Pt(2)-C(36)	89.1(2)
C(16)-Pt(1)-C(15)	94.82(18)	C(34)-Pt(2)-C(33)	94.8(2)
C(18)-Pt(1)-C(15)	92.5(2)	C(35)-Pt(2)-C(33)	94.03(18)
C(17)-Pt(1)-C(15)	175.40(19)	C(36)-Pt(2)-C(33)	175.1(2)
C(16)-Pt(1)-N(3)	175.64(17)	C(34)-Pt(2)-N(5)	89.24(19)
C(18)-Pt(1)-N(3)	88.89(19)	C(35)-Pt(2)-N(5)	176.08(19)
C(17)-Pt(1)-N(3)	94.70(17)	C(36)-Pt(2)-N(5)	94.78(19)
C(15)-Pt(1)-N(3)	81.08(15)	C(33)-Pt(2)-N(5)	82.05(15)
C(16)-Pt(1)-N(1)	87.56(17)	C(34)-Pt(2)-N(7)	174.97(19)
C(18)-Pt(1)-N(1)	172.6(2)	C(35)-Pt(2)-N(7)	86.69(18)
C(17)-Pt(1)-N(1)	97.59(19)	C(36)-Pt(2)-N(7)	95.47(19)
C(15)-Pt(1)-N(1)	80.90(16)	C(33)-Pt(2)-N(7)	80.99(15)
N(3)-Pt(1)-N(1)	93.21(14)	N(5)-Pt(2)-N(7)	92.84(14)

4.3 Results and Discussion

4.3.1 Syntheses of the Pt(IV) complexes 4.1-4.4

Our initial approaches to obtain complexes **4.1** and **4.2** were *via* the oxidative addition of MeI to the complexes Pt(BAB)Me_2 (**2.1**) and Pt(BAM)Me_2 (**2.2**). It has been demonstrated that the oxidative addition of MeI to various N,N-chelating $PtMe_2$ complexes typically occurs in a S_N2 fashion, *via* the initial formation of the five-coordinate $[(N,N)Pt^{IV}Me_3]^+$ intermediates, resulting in the MeI *trans* addition adducts.[12] The five-coordinate $Pt^{IV}Me_3$ intermediates may be trapped prior to the binding of I^- with the Pt(IV) center by appropriate ancillary ligands.[13] Accordingly, because of the steric blockage of one Pt(II) coordination site by the BAB linker group in complex **2.1**, we anticipated that the oxidative addition of MeI to **2.1** would likely afford $[Pt^{IV}(BAB)Me_3]I$ as a stable five-coordinate complex (Scheme 4.1). As revealed by ^1H NMR studies, complex **2.1** reacted readily with MeI at room temperature, but instead of forming the desired five-coordinate Pt(IV) complex, the reaction produced the free BAB ligand and the tetrameric complex $[PtMe_3I]_4$ quantitatively (Scheme 4.1). This behavior is reminiscent to the reaction of Pt(*L*)Me_2, where *L* = 1,5-cyclooctadiene (COD)[14a] or norbomadiene (NBD)[14b], with MeI, an indication that the BAB binding to the $Pt^{IV}Me_3$ moiety is weak and cannot compete with the iodide binding. Similar phenomenon was also observed for the reaction of complex **2.2** with MeI.

Scheme 4.1

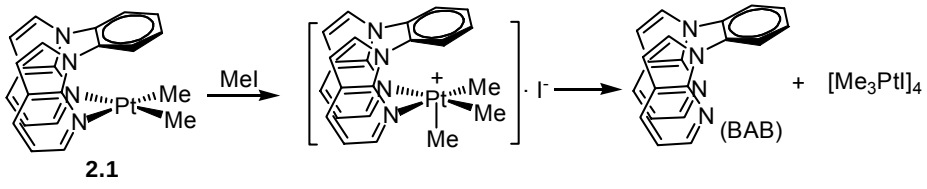

2.1

Scheme 4.2

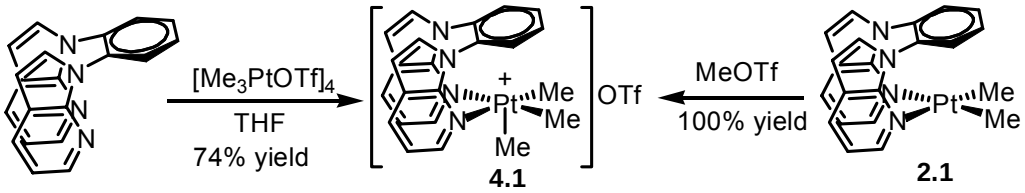

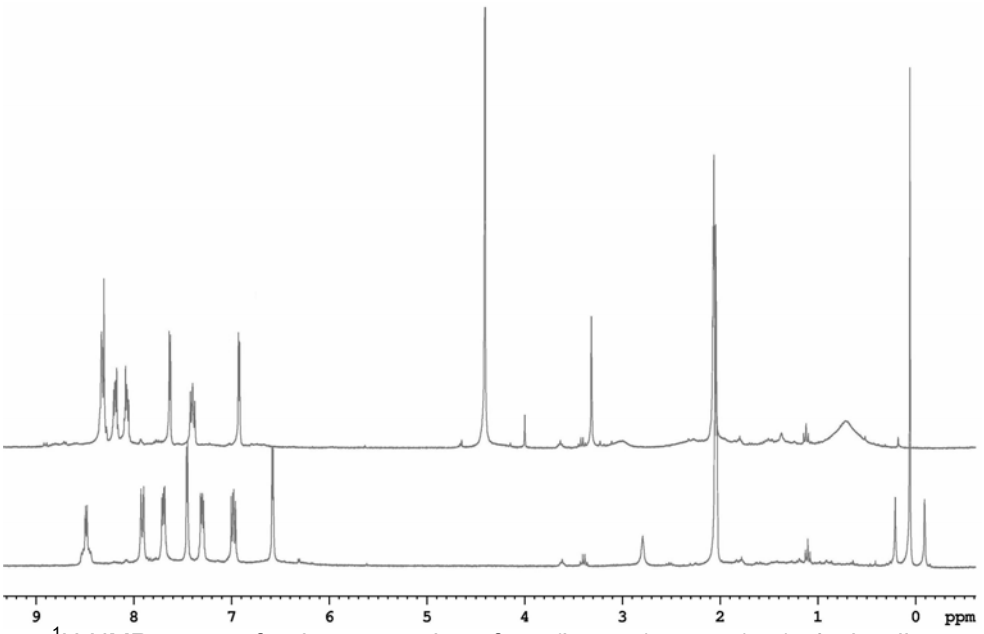

Figure 4.1 ^{1}H NMR spectra for the conversion of **2.1** (bottom) to **4.1** (top) *via* the direct oxidative addition by MeOTf in CD_3COCD_3 at ambient temperature.

To avoid iodide competition, $[PtMe_3(OTf)]_4$ (OTf = $CF_3SO_3^-$)[10a] and $[PtMe_3(THF)_{1.5}]_2[PF_6]_2$[10b] were then employed for the syntheses of five-coordinate Pt^{IV} complexes. As shown in Scheme 4.2, the reaction of the BAB ligand with 0.25 equivalents of $[PtMe_3(OTf)]_4$ at ambient temperature yielded compound **4.1**, $[Pt(BAB)Me_3][OTf]$, as a colorless crystalline solid in 74% yield. Since the OTf anion is shown to be a suitable anion for the synthesis of **4.1**, the oxidative addition reaction of complex **2.1** with MeOTf was also tested for the synthesis of **4.1**. Indeed, ^{1}H NMR study showed that MeOTf reacted with $Pt(BAB)Me_2$ readily, converting it quantitatively to

complex **4.1** *via* the direct oxidative addition at ambient temperature (Figure 4.1 and Scheme 4.2).

Compound **4.1** is fairly stable in the solid state or in weakly coordinating solvents such as THF, DMF and RNO_2 (R= Me, Ph). It was fully characterized by NMR spectroscopy, elemental and single-crystal X-ray diffraction analyses. Compound **4.1** has a good thermal stability, as indicated by the fact that over 95% of **4.1** remained intact in CD_3NO_2 solution at 60~70 ^oC for 5 days. The addition of one equivalent of $[^nBu_4N]X$ (X = I^-, Br^- or Cl^-), however, caused rapid degradation of **4.1** with the quantitative formation of the free BAB ligand and the tetrameric complex $[Me_3PtX]_4$ (X = I^-, Br^- or Cl^-), which is consistent with the reactivity of $Pt^{II}(BAB)Me_2$ (**2.1**) toward MeI.

Scheme 4.3

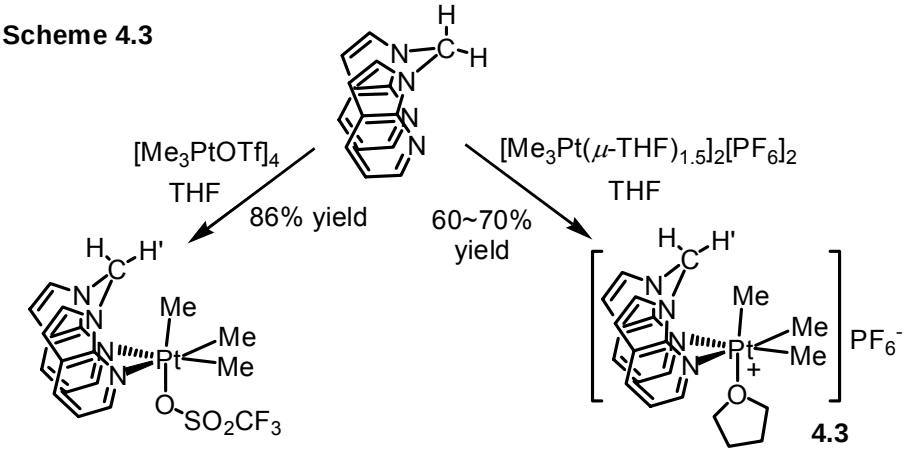

Despite the similarity between the BAB and BAM ligands, we have shown previously that the CH_2 linker in BAM is a much less effective steric blocker than the BAB phenyl linker in their Pt(II) complexes. Consequently, attempts to obtain the five-coordinate $Pt^{IV}Me_3$ analogue of BAM using similar protocol as for **4.1** were unsuccessful. Instead, a six-coordinate compound **4.2**, [Pt(BAM)Me_3(OTf)], was isolated as a colorless crystalline solid in ~86% yield (Scheme 4.3) and was characterized by NMR, elemental

and single-crystal X-ray diffraction analyses. We also attempted the synthesis of $[Pt(BAM)Me_3][PF_6]$ by replacing the OTf anion with the non-coordinating PF_6^- anion, which led to the isolation of another six-coordinate complex $[Pt(BAM)Me_3(THF)][PF_6]$ (**4.3**) (Scheme 4.3).

^{1}H NMR experiments revealed that compared to **4.1**, complexes **4.2** and **4.3** are more prone to degradation upon the addition of donor ligands such as $[^nBu_4N]X$ (X = I^-, Br^- and Cl^-) and H_2O. One way to enhance the stability of BAM Pt(IV) complexes is to convert the bidentate BAM ligand to a tridentate *N,C,N*-chelating ligand by removing one H atom from the CH_2 group *via* deprotonation. Indeed, we have found that the CH_2 group of BAM can be readily deprotonated by either LDA or *n*-BuLi to give the *bis*(*N*-7-azaindolyl)methyl lithium salt, which reacts readily with $[Me_3Pt(THF)_{1.5}]_2[PF_6]_2$ and produces the neutral complex [Pt(*N,C,N*-BAM)Me_3] (**4.4**) as a colorless solid (Scheme 4.4). In CD_2Cl_2 at ambient temperature, compound **4.4** displays two sets of well defined Pt-*Me* signals, in a 2:1 ratio, as shown in Figure 4.2.

Scheme 4.4

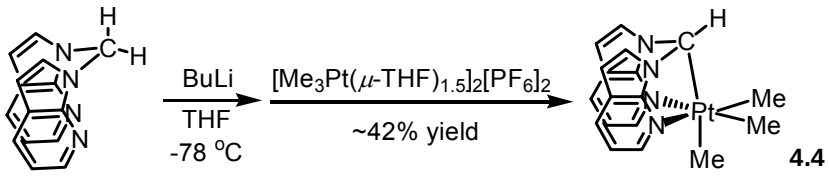

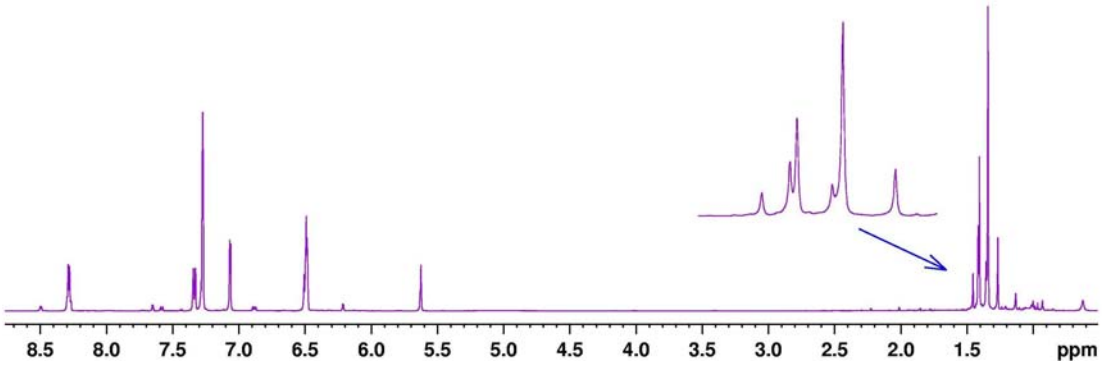

Figure 4.2 ^{1}H NMR spectrum of **4.4** in CD_2Cl_2 at ambient temperature. The small peaks in the aromatic region are from the remaining BAM ligand.

4.3.2 Crystal structures of complexes 4.1-4.4

To verify the structures of these Pt(IV) complexes, the analyses of their structures by the single-crystal X-ray diffraction analyses were carried out. Crystals of **4.1**-**4.3** were obtained by slow evaporation of their THF solutions inside a dry-box at ambient temperature. As shown in Figure 4.3, the Pt(IV) center in **4.1** is indeed five-coordinate and displays a typical square pyramidal geometry. The sixth coordinate site of the Pt(IV) center is completely capped by the phenyl linker of the BAB ligand, with a separation distance of 3.19(1) Å between the Pt(IV) center and the center of the phenyl ring. The lack of a *trans* ligand makes the Pt-C_{axial} bond length (2.028(3) Å) somewhat shorter than the two Pt-$C_{equatorial}$ bonds (2.036(4) Å in average), a trend that is consistent with previously known five-coordinate $Pt^{IV}Me_3$ complexes.[4] The fact that **4.1** retains its five-coordinate configuration in the presence of OTf and coordinating solvents such as THF led us to suggest that neutral N,N-chelating ligands with appropriate geometries such as the BAB ligand can indeed effectively stabilize five-coordinate Pt(IV) species.

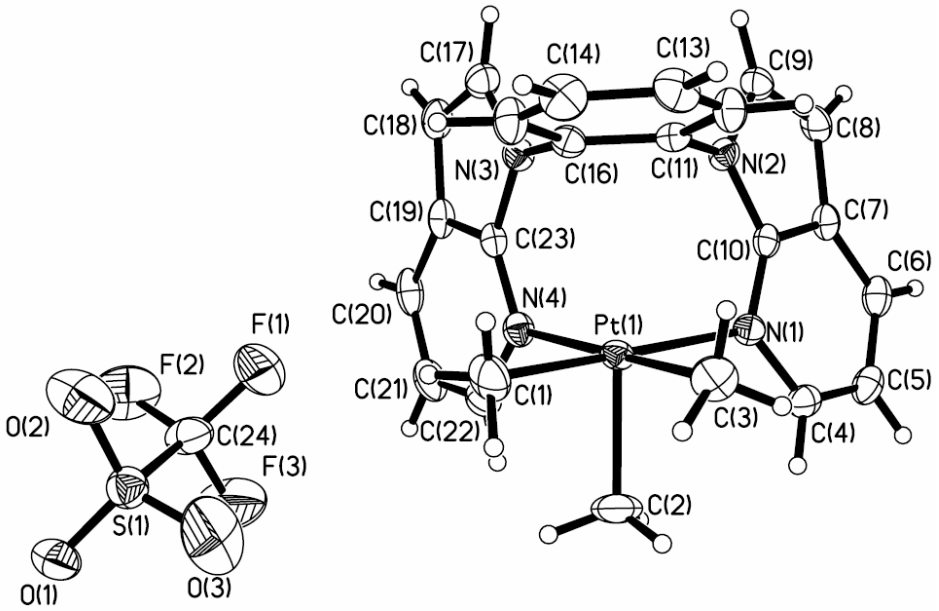

Figure 4.3 Crystal structure of **4.1** with 30% ellipsoids.

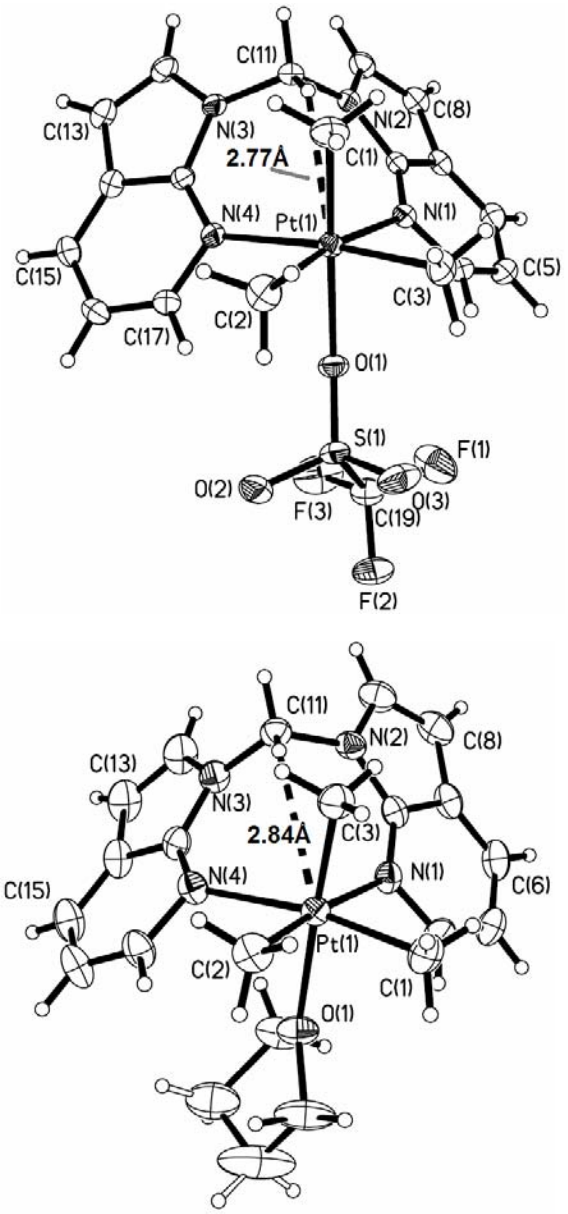

Figure 4.4 Crystal structures of **4.2** (top) and **4.3** (bottom) with 30% ellipsoids.

As shown in Figure 4.4, both **4.2** and **4.3** have a six-coordinate Pt(IV) center, with one methyl group being on the same side of the BAM CH_2 linker and a OTf group or a coordinated THF molecule being *trans* to this methyl group to minimize steric

interaction. The Pt-C_{axial} (2.036(3) Å), mean Pt-$C_{equatorial}$ (2.044(3) Å) and mean Pt-N (2.282(2) Å) bond lengths in **4.2** are consistently longer than those in **4.1**. The Pt-OTf bond distance is 2.259(2) Å, close to that 2.27(2) Å reported for $[PtMe_3(OTf)]_4$.[10b] In addition, the Pt···H'$_{CHH'}$ separation distance is 2.77 Å in **4.2**, considerably lengthened compared to that (2.44 Å) in Pt(BAM)Me_2 (**2.2**).[6c] The structure features of **4.3** (Figure 4.4) are similar to those of **4.2** except that the Pt-C bond lengths (Pt-C_{axial} = 2.029(3) Å; Pt-$C_{equatorial}$= 2.036(3) Å in average) are shorter than those of **4.2** but similar to **4.1**. The Pt-O_{THF} bond length is 2.293(2) Å and the Pt···H'$_{CHH'}$ distance is 2.84 Å. The persistent adoption of a six-coordinate configuration by the two BAM complexes **4.2** and **4.3** confirms that the BAM ligand is not effective in blocking the sixth coordination site for achieving stable five-coordinate Pt(IV) complexes.

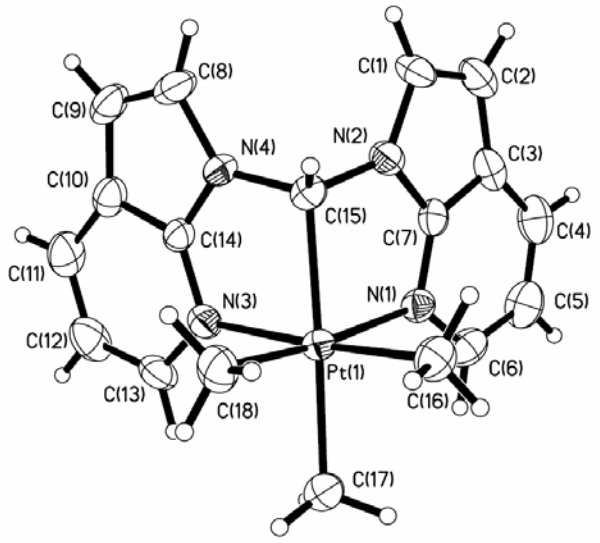

Figure 4.5 Crystal structure of **4.4** (front view) with 30% ellipsoids.

Crystallization of **4.4** was exhausting but eventually successful, allowing the unambiguous verification of its structure by X-ray diffraction analyses. As shown in Figure 4.5, the Pt(IV) center in **4.4** has an octahedral geometry. The Pt-C(BAM) bond (2.143(5) Å) is much longer than the Pt-CH_3 bonds (*trans*, 2.106(5) Å; *cis*, 2.042(4) Å in

average) due to both the geometric constraint and the *trans* effect. The Pt-N bonds (2.158(4) Å in average) are much shorter than those in **4.2** and **4.3**, clearly due to the reduced steric congestion in **4.4**. Compound **4.4** is stable toward air and moisture as well as I^-.

4.3.3 ^{1}H NMR investigation of the solution dynamics of complexes 4.1-4.3

As shown in Figure 4.6, at ambient temperature in CD_2Cl_2, the $Pt^{IV}Me_3$ moiety in **4.1** displays two broad peaks at 2.17 ($PtMe_{axial}$) and 0.61 ($Pt\text{-}Me_{equatorial}$) ppm, respectively, with a ~1:2 ratio in the ^{1}H NMR spectrum, indicating the presence of two types of methyl environments and their slow exchange. Upon cooling to ~260 K (Figure 4.6), these two broad peaks become sharp and well resolved with distinctive ^{195}Pt-^{1}H coupling satellites ($^2J_{Pt\text{-}H}$ = 67.2 Hz for the two equatorial methyls and 84.4 Hz for the axial methyl). As shown in Figure 4.7, heating to ~65°C resulted in the coalescence of the equatorial and the axial methyl signals. After simulating the methyl exchange process, a rotation barrier of ~17.4 Kcal·mol^{-1} was obtained from the Arrhenius plot (Figure 4.7).

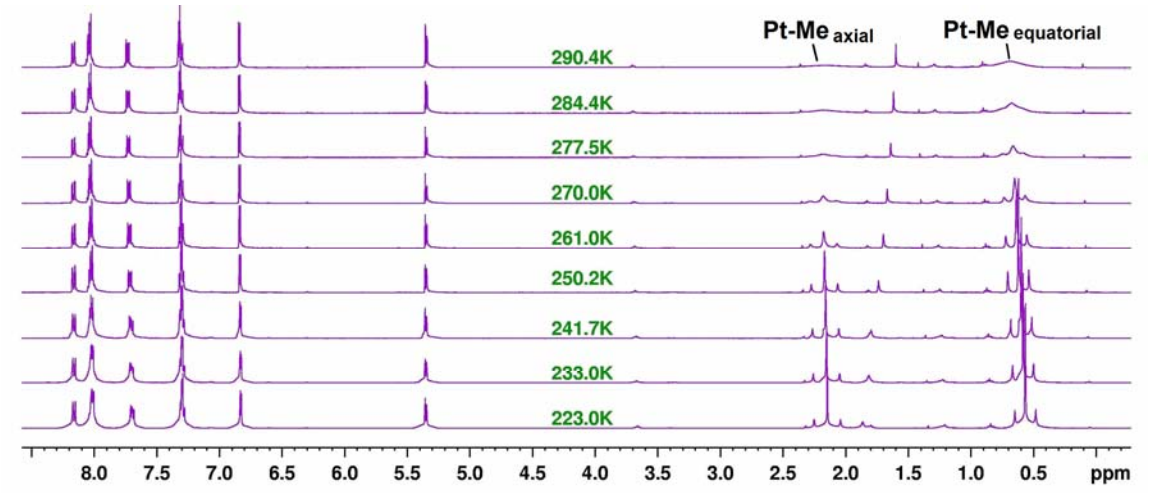

Figure 4.6 The variable-temperature ^{1}H NMR spectra of compound **4.1** in CD_2Cl_2.

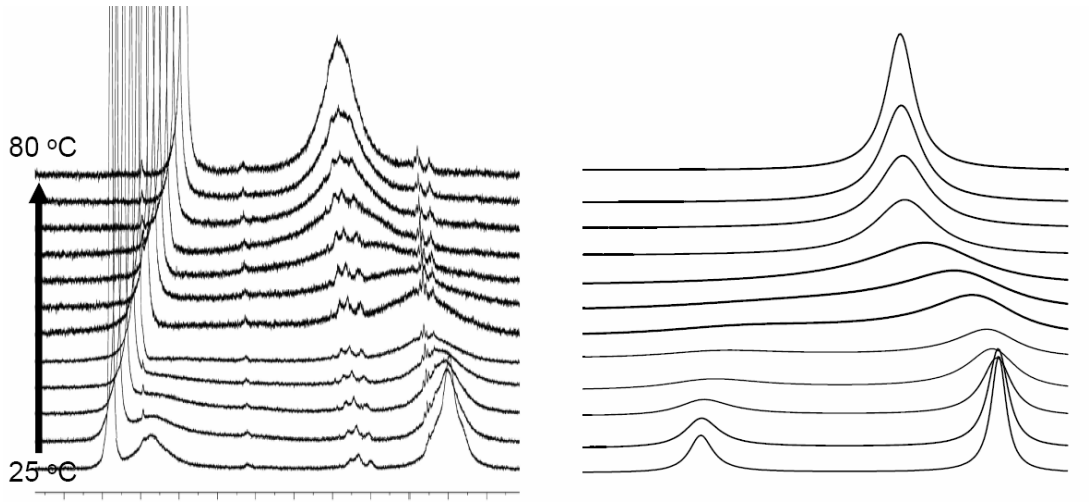

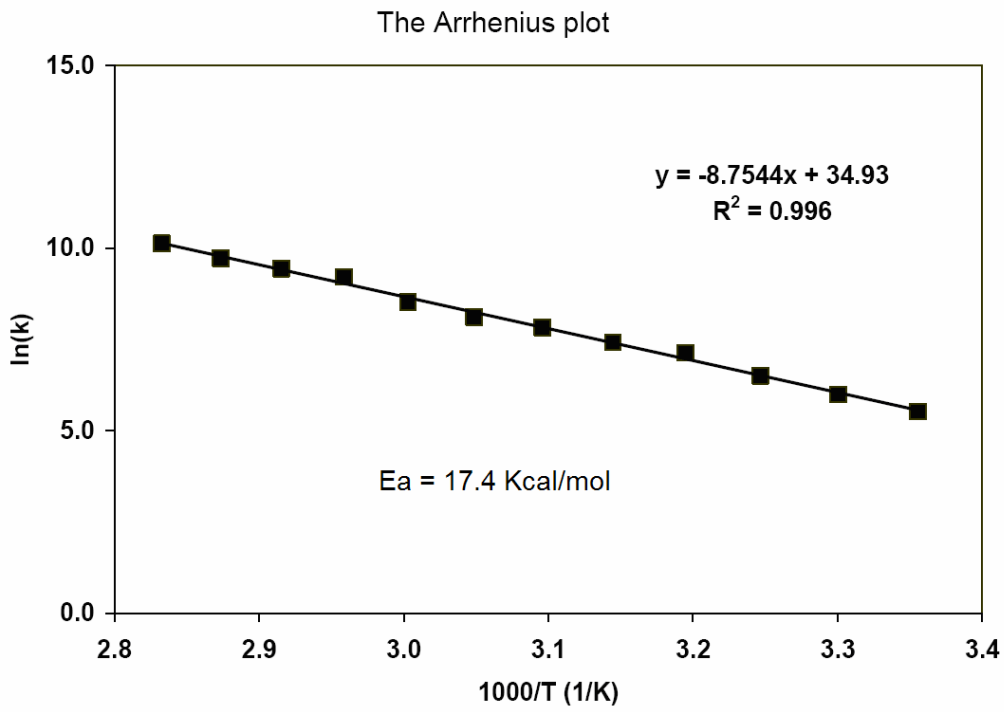

Figure 4.7 The Pt*Me*$_3$ region of the variable-temperature ^{1}H NMR spectra for **4.1** in $C_6D_5NO_2$ (top left) and the simulated spectra (top right) along with the Arrhenius plot for the methyl exchange process (bottom).

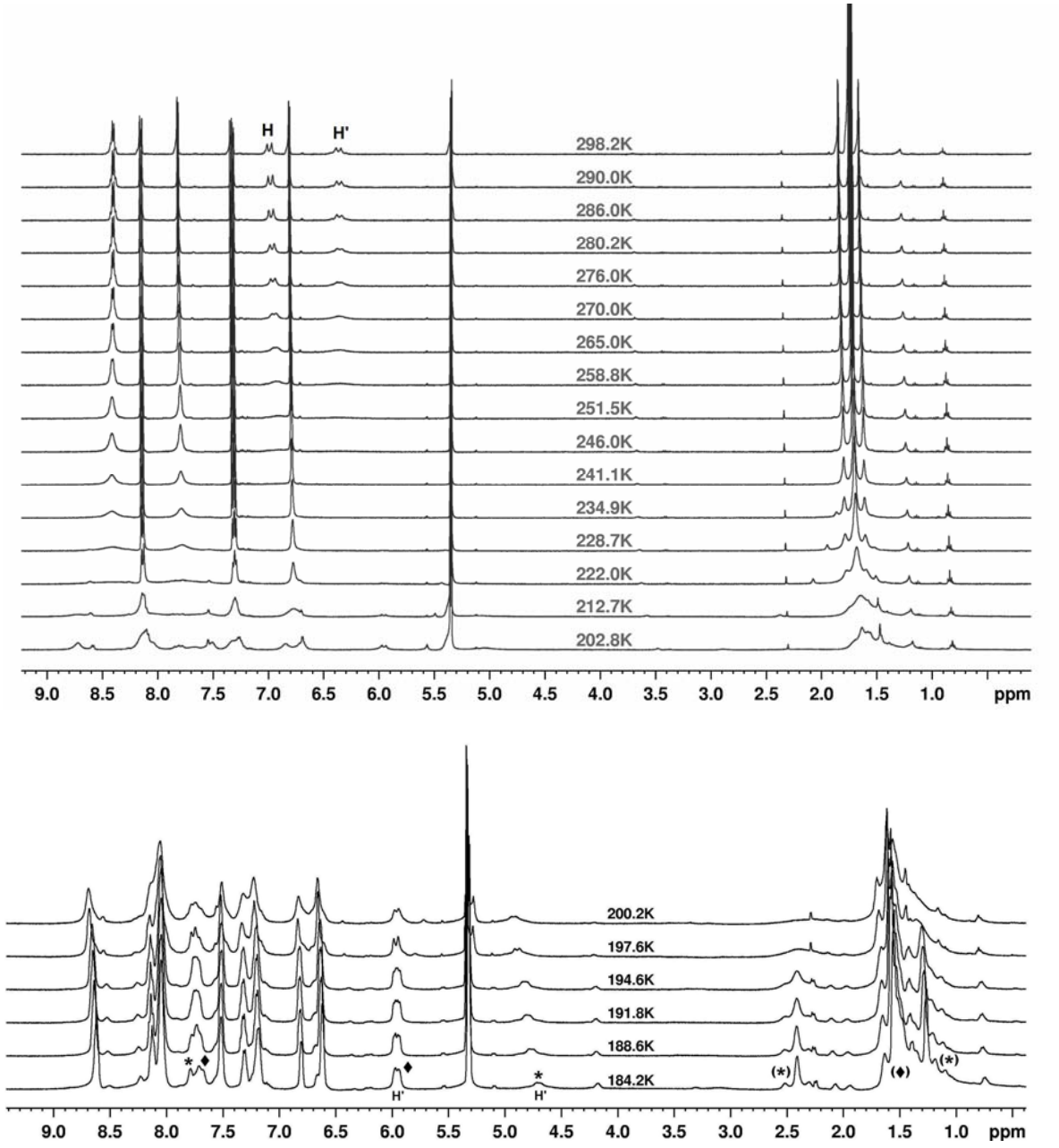

Figure 4.8 The variable-temperature ^{1}H NMR spectra of compound **4.2** in CD_2Cl_2. Bottom: 184.2 K to 200.2 K; top: 202.8 K to 298.2 K. At 184.2 K, two sets of "AB" patterned ^{1}H signals related to the BAM bridging CHH' group along with two corresponding sets of ^{1}H signals for the *fac*-$PtMe_3$ moiety were observed, with δ for H', H at 4.71, 7.80 ppm (*) and 5.95, 7.68 ppm (♦), respectively.

Consistent with the crystal structures are the different behaviors of **4.2** and **4.3** from that of **4.1** in solution. Unlike **4.1** where the three methyl groups undergo slow exchange, the methyl groups in **4.2** and **4.3** undergo rapid exchange in solution at

ambient temperature, as demonstrated by the presence of a single sharp methyl signal with characteristic ^{195}Pt-^{1}H satellite peaks ($^{2}J_{Pt\text{-}H}$ = 73.7 Hz for **4.2**, 58.4 Hz for **4.3**) from 298 K to ~200 K in their variable-temperature ^{1}H NMR spectra (Figures 4.8 and 4.9). However, below 200 K (Figures 4.8 and 4.9), the BAM "AB" patterned C*HH'* protons in **4.2** and **4.3** experience dramatic change with each peak being resolved into two sets of new peaks. For example, at 184.2 K (Figures 4.8 and 4.10), two sets of BAM "AB" patterned C*HH'* proton signals are displayed for compound **4.2** with δ for H', H at 4.71, 7.80 ppm and 5.95, 7.68 ppm, respectively. At 184.5 K (Figures 4.9 and 4.10), two sets of BAM "AB" patterned C*HH'* proton signals are also displayed for compound **4.3** with δ for H', H at 6.08, 7.62 ppm and 5.95, 7.73 ppm, respectively. Notably, the bound THF signals in **4.3** (δ 4.20 ppm for α-CH_2; 1.95 ppm for β-CH_2) are observed only at temperature below 220 K (Figures 4.9 and 4.10). The assignments for the BAM bridging C*HH'* protons in **4.2** and **4.3** were supported by the low temperature COSY spectra (Figure 4.10).

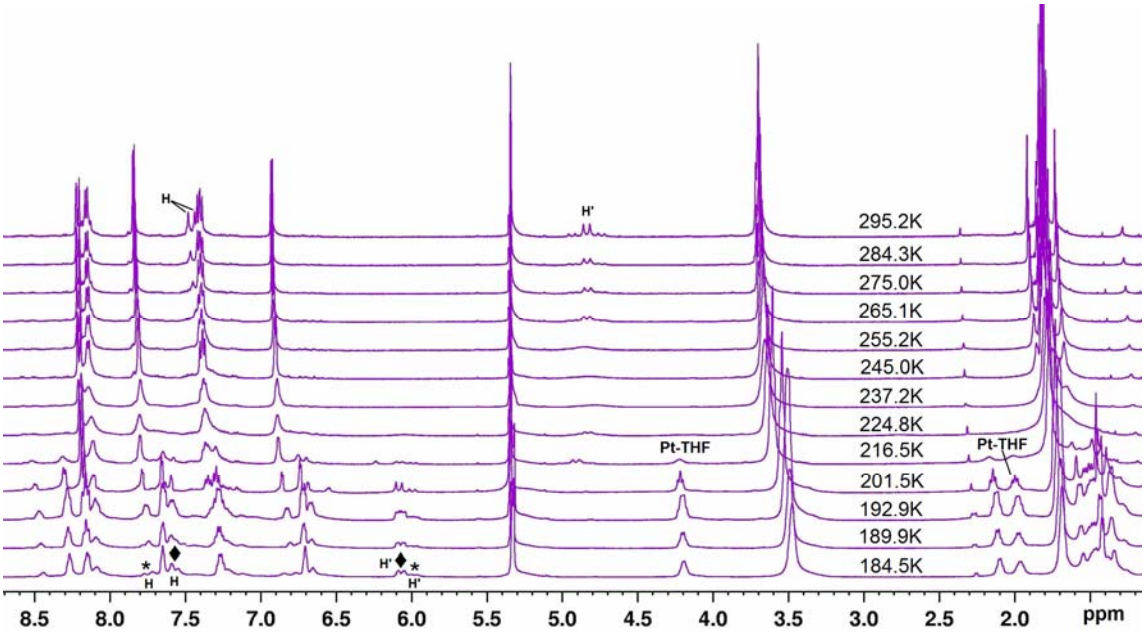

Figure 4.9 Variable-temperature ^{1}H NMR spectra of **4.3**.

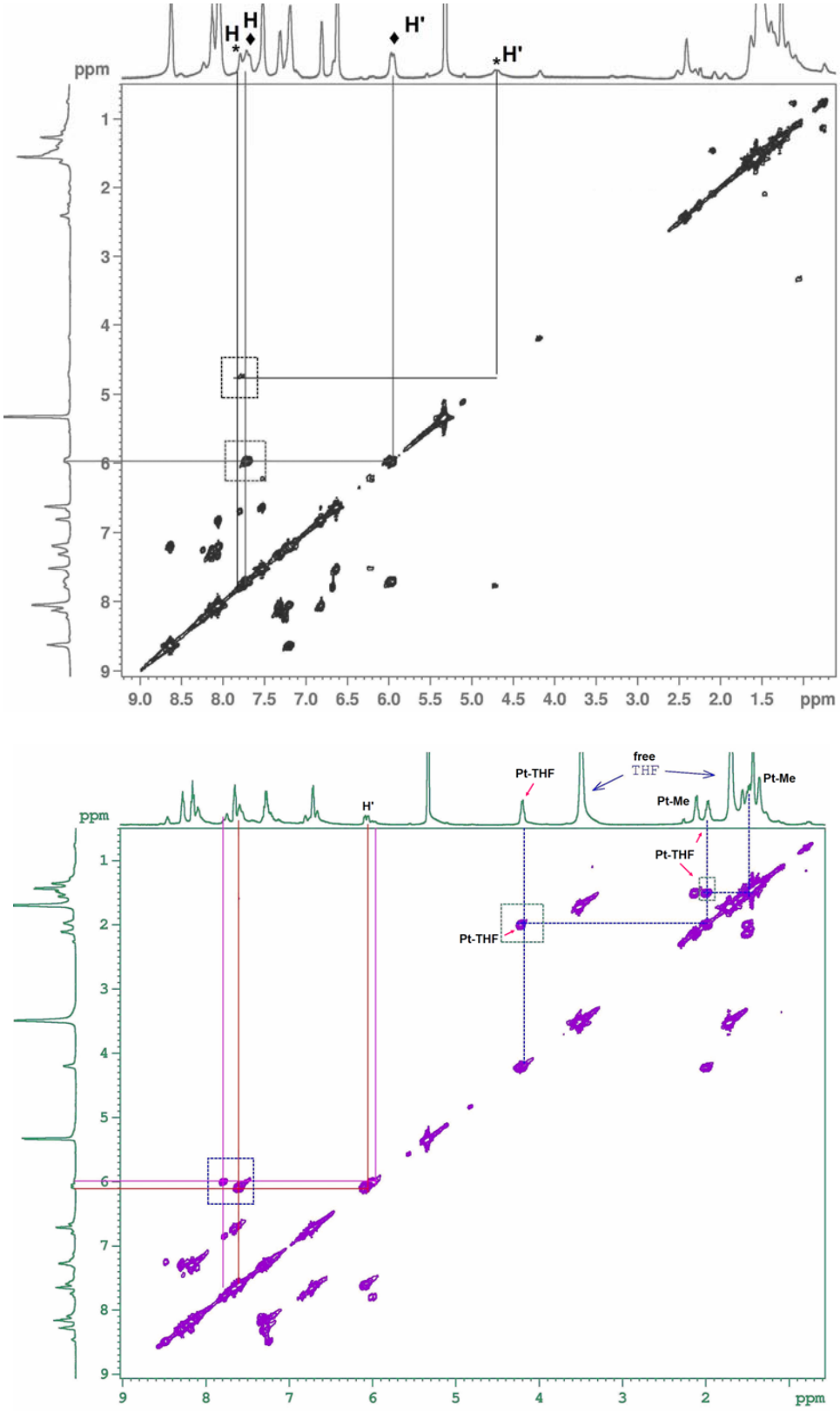

Figure 4.10 COSY spectra of **4.2** at 184.5K (top) and **4.3** at 184.2K (bottom) in CD_2Cl_2.

On the basis of the above NMR data, we propose that compounds **4.2** and **4.3** likely exist in rapid equilibriums with five-coordinate Pt(IV) species *via* dissociation/re-association of the L group, as shown in Scheme 4.5.[15] The rapid methyl exchange in **4.2** and **4.3** *via* the **A⇌B⇌A'** equilibriums indicates that the L group dissociation is fast even at low temperature. The fact that the bound THF signals in **4.3** can only be observed at temperature below 220 K suggests that **4.3** exists as a five-coordinate Pt(IV) species **A'** in solution at room temperature. The observation of a diagnostic signal with δ at ~4.88 ppm at temperature above 220 K for the CH***H'*** atom in **4.3** also suggests that **4.3** exists as a five-coordinate Pt(IV) species in solution at room temperature. The formation of the five-coordinate Pt(IV) intermediate **A'** from **4.2** is supported by the observation of both a distinct ^{1}H singles for its H' CH***H'*** atom (δ 4.71 ppm) and a new set of Pt*Me*$_3$ ^{1}H signals (δ 2.40 and 1.25 ppm, respectively; in a 1:2 ratio) in its ^{1}H NMR spectrum at 184.2 K (Figure 4.8).

Scheme 4.5

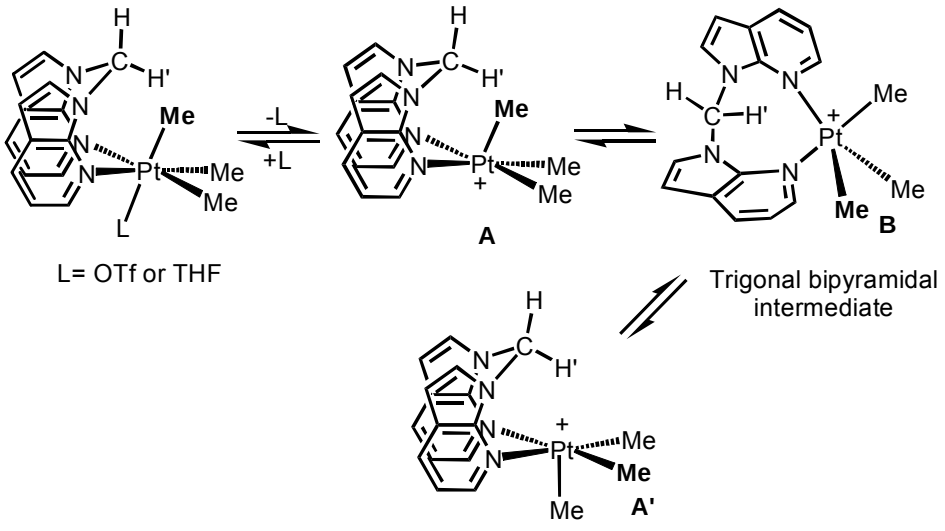

The distinct chemical shift (~4.8 ppm) for the CH***H'*** atom in intermediate **A'** can be attributed to the presence of a three-center two-electron $Pt^{IV}\cdots$H-C interaction. Apparently, the chemical shift of the CH***H'*** atom in **4.3** should change with the concentration of THF, which can be verified by changing the NMR solvents from CD_2Cl_2 to d_8-THF. Indeed, when d_8-THF was used as the NMR solvent, a big δ downfield shift from 4.88 ppm in CD_2Cl_2 to ~6.8 ppm in d_8-THF was observed for **4.3**. This observation is also a direct proof of the equilibriums proposed for the methyl exchange processes of **4.2** and **4.3**.

In contrast to the rapid methyl exchange processes of compounds **4.2** and **4.3**, that of compound **4.2** is quite slow even at ambient temperature. This is likely due to a higher activation barrier for **4.1** toward the formation of a trigonal bipyramidal intermediate similar to **B** (Scheme 4.5) because of the stronger steric blocking effect imposed by the BAB ligand.

The thermolysis of the new $Pt^{IV}Me_3$ complexes was also attempted. The preliminary study indicated that at ~70 ^oC in d_6-THF, complex **4.3** quickly undergoes C-C reductive elimination, generating C_2H_6 along with the formation of both CH_4 and CH_3D. The C-C reductive elimination from compound **4.3** would also generate a cationic Pt^{II}-Me intermediate, which accounts for the formation of CH_4 and CH_3D by activating the solvent (THF and d_8-THF) C-H bonds. More work is needed to understand the reductive elimination process of these Pt(IV) complexes.

4.4 Conclusions

In this chapter, the impacts of the neutral N,N-chelating ligands 1,2-bis(1-*N*-7-azaindolyl)benzene (BAB) and bis(1-*N*-7-azaindolyl)methane (BAM) on the structure and stability of their $Pt^{IV}Me_3$ complexes have been investigated.

Three Pt(IV) complexes $[Pt(BAB)Me_3][O_3SCF_3]$ (**4.1**), $[Pt(BAM)Me_3(O_3SCF_3)]$ (**4.2**), and $[Pt(BAM)Me_3(THF)][PF_6]$ (**4.3**) have been synthesized and characterized. We have found that the steric blockage by the N,N-chelating ligands has significant impacts on the structure and stability of the five-coordinate Pt(IV) compounds. The BAB ligand is much more effective in steric blocking, hence stabilizing the five-coordinate Pt(IV) complexes than the BAM ligand does. As a result, while **4.1** is obtained as the first five-coordinate $Pt^{IV}Me_3$ complex with a neutral N,N-chelating ligand, compounds **4.2** and **4.3** both have an octahedral configuration in their crystals. In solution, the methyl groups in **4.1** undergo a slow dynamic exchange process while those in **4.2** and **4.3** undergo a fast dynamic exchange. The CH_2 linker in the BAM ligand can be readily deprotonated to produce an N,C,N-chelating BAM ligand, which upon the reaction with $[PtMe_3(\mu\text{-}THF)_{1.5}]_2[PF_6]_2$ can readily form an octahedral complex $[Pt(N,C,N\text{-}BAM)Me_3]$ (**4.4**). While **4.1**, **4.2** and **4.3** degrade quickly to produce $[PtMe_3X]_4$ ($X^- = I^-$, Br^- or Cl^-) and the free ligands upon exposure to halides, **4.4** does not react with halides.

References

1. For recent comprehensive reviews, see: a) Goldberg, K. I.; Goldman, A. S. *Activation and Functionalization of C-H Bonds*; American Chemical Society: Washington, DC, **2004**. b) Lersch, M.; Tilset, M. *Chem. Rev.* **2005**, *105*, 2471. c) Labinger, J. A.; Bercaw, J. E. *Nature* **2002**, *417*, 507. d) Puddephatt, R. J. *Angew. Chem., Int. Ed.* **2002**, *41*, 261.
2. a) Pawlikowski, A. V.; Getty, A. D.; Goldberg, K. I. *J. Am. Chem. Soc*. **2007**, *129*, 10382. b) Procelewska, J.; Zahl, A.; Liehr, G.; van Eldik, R.; Smythe, N. A.; Williams, B. S.; Goldberg, K. I. *Inorg. Chem*. **2005**, *44*, 7732. c) Crumpton-Bregel, D. M.; Goldberg, K. I. *J. Am. Chem. Soc.* **2003**, *125*, 9442. d) Jensen, M. P.; Wick, D. D.; Reinartz, S..; White, P. S.; Templeton, J. L.; Goldberg, K. I. *J. Am. Chem. Soc.* **2003**, *125*, 8614. e) Williams, B. S.; Goldberg, K. I. *J. Am. Chem. Soc*. **2001**, *123*, 2576. f) Crumpton, D. M.; Goldberg, K. I. *J. Am. Chem. Soc*. **2000**, *122*, 962.
3. a) Fekl, U.; Kaminsky, W.; Goldberg, K. I. *J. Am. Chem. Soc.* **2003**, *125*, 15286. b) Fekl, U.; Goldberg, K. I. *J. Am. Chem. Soc.* **2002**, *124*, 6804.
4. a) Luedtke, A. T.; Goldberg, K. I. *Inorg. Chem.* **2007**, *46*, 8496. b) Kloek, S. M.; Goldberg, K. I. *J. Am. Chem. Soc.* **2007**, *129*, 3460. c) Fekl, U.; Kaminsky, W.; Goldberg, K. I. *J. Am. Chem. Soc*. **2001**, *123*, 6423.
5. Reinartz, S.; White, P. S.; Brookhart, M.; Templeton, J. L. *J. Am.Chem. Soc.* **2001**, *123*, 6425.
6. Puddephatt, R. J. *Angew. Chem., Int. Ed.* **2002**, *41*, 261.

7. a) Zhao, S.-B; Wu, G.; Wang, S. *Organometallics* **2006**, *25*, 5979. b) Zhao, S.-B.; Song, D; Jia, W.-L.; Wang, S. *Organometallics* **2005***, 24,* 3290.
8. a) Song, D.; Wang, S. *Organometallics* **2003***, 22,* 2187. b) Song, D.; Schmider, H.; Wang, S. *Org. Lett.* **2002**, *4*, 4049.
9. a) Clegg, D. E.; Hall, J. R. *Inorg. Synth.* **1967**, *10*, 71. b) Baldwin, J. C.; Kaska, W. C. *Inrog. Chem.* **1975**, *14*, 2020.
10. a) Baldwin, J. C.; Kaska, W. C. *Inrog. Chem.* **1979**, *18*, 686. b) Schlecht, S.; Magull, J.; Fenske, D.; Dehnicke, K. *Angew. Chem., Int. Ed.* **1997**, *36*, 1994.
11. a) Albinati, A.; Anklin, C. G.; Ganazzoli, F.; Ruegg, H.; Pregosin, P. S. *Inorg. Chem.* **1987**, *26*, 503. b) Albinati, A.; Arz, C.; Pregosin, P. S. *Inorg. Chem.* **1987**, *26*, 508. c) Albinati, A.; Pregosin, P. S.; Wombacher, F. *Inorg. Chem.* **1990**, *29*, 1812.
12. Rendina, L. M.; Puddephatt, R. J. *Chem. Rev.* **1997**, *97*, 1735.
13. See examples: a) Prokopchuk, E. M.; Puddephatt, R. J. *Organometallics* **2003**, *22*, 787. b) Crespo, M.; Puddephatt, R. J. *Organometallics* **1987**, *6*, 2548. c) Puddephatt, R. J.; Scott, J. D. *Organometallics* **1985**, *4*, 1221.
14. a) Clark, H.C.; Manzer, L.E. *J. Organomet. Chem.* **1973**, *59*, 411. b) Appleton, T. G.; Hall, J. R.; Williams, M. A. *J. Organomet. Chem.* **1986**, *303*, 139.
15. For examples of intramolecular ligand interconversion processes at Pt centers, see: a) Nikol, H.; Bürgi, H.-B.; Hardcastle, K. i.; Gray, H. B. *Inorg. Chem.* **1995**, *34*, 6319. b) Asselt, R. v.; Rijnberg, E.; Elsevier, C. J. *Organometallics* **1994**, *13*, 706. c) Tau, K. D.; Uriarte, R.; Mazanec, T. J.; Meek, D. W. *J. Am. Chem. Soc.* **1979**, *101*, 6614. d) Hill, G. S.; Puddephatt, R. J. *Organometallics* **1998**, *17*, 1478.

Chapter 5

New 7-Azaindolyl Derivative Ligands and Their Pt Complexes

5.1 Introduction

Ligands play a crucial role on the property and performance of a Pt(II) center. The ligand steric effect has a direct impact on the C-H activation selectivity, as shown by the work in Chapter 2.[1] Tilset and coworkers have demonstrated that the regioselectivity of arene C-H activation on a Pt(II) center can be altered *via* tuning the ligand steric blocking effects.[2] The ligand electronic effect is also important. Even a subtle electronic variation of the Pt(II) centers can sometime lead to a significant reactivity change.[3,4] One of the attractive examples related to this aspect is the dinuclear $(PtMe_2)_2$(TTAB) complex, where TTAB = 1,2,4,5-tetrakis(1-*N*-7-azaindolyl)benzene, reported previously by our group, which, in contrast with its monomeric analogue Pt(BAB)Me_2 (**2.1**), displays both an unique reactivity toward C-Cl activation and an unusual reactivity toward multiple benzene C-H activation.[4] The unusual reactivity of the diplatinum complex was demonstrated to be attributable to the electronic communication between the two Pt(II) centers mediated by the TTAB bridging phenyl moiety.[4]

We have demonstrated in Chapter 2 and Chapter 4 that, the linker groups in the BAM and BAB ligands contribute significantly in sterically stabilizing some Pt(II) and Pt(IV) intermediates as well as generating an unique diastereoselectivity. In Chapter 3, we have shown that the chelate geometry can also impose great impacts on the reactivity of a Pt(II) center. To extend our understanding on the ligand effects of our 7-azaindolyl derivative ligands, we have carried out the syntheses of several new 7-azaindolyl

derivative ligands (Chart 5.1) *via* modifying or altering the BAM and BAB linker groups, and the syntheses and reactivity study of their $PtPh_2$ or $PtMe_2$ complexes. These studies provide us additional knowledge on the ligand impact on the stability and reactivity of the metal complexes. The details are presented in this chapter.

Chart 5.1

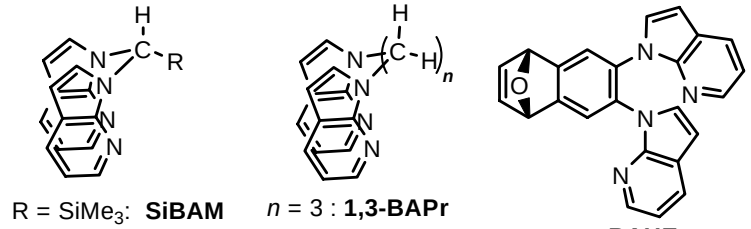

R = $SiMe_3$: **SiBAM** R = $SnMe_3$: **SnBAM**

n = 3 : **1,3-BAPr** *n* = 4 : **1,4-BABu**

BAHE

5.2 Experimental Session

5.2.1 General produces

All reactions were performed under N_2 with the standard Schlenk techniques unless otherwise noted. All starting materials were purchased from Aldrich Chemical Co. and used without further purification. THF, Et_2O, and hexanes were purified using the solvent purification system (Innovation Technology, Inc.). Deuterated solvents (Cambridge Isotopes) were used as received without further drying. NMR spectra were recorded on Bruker Avance 300, 400 or 500 MHz spectrometers. ^1H and ^{13}C NMR chemical shifts were referenced to the residual solvent peaks and have been reported in parts per million (ppm). High resolution mass spectra (HRMS) were obtained from a Waters/Micromass GC-TOF EI-MS spectrometer. $[PtPh_2(\mu\text{-}SMe_2)]_n$ (n = 2 or 3)[5] and $[PtMe_2(\mu\text{-}SMe_2)]_2$[6] were prepared by methods described in the literature.

5.2.2 Synthesis of trimethylsilyl-bis(1-*N*-7-azaindolyl)methane (SiBAM)

To a stirred Et_2O (20 mL) solution of the BAM ligand (0.25 g, 1.0 mmol) at -78 ^oC was added dropwise, *via* syringe, a *n*-BuLi solution (1.6 M) (0.75 mL, 1.2 mmol) over 5 minutes, and the resulting light yellow solution was stirred for 30 minutes at -78 ^oC. Me_3SiCl (1.0 mL, 7.9 mmol) was then slowly added *via* syringe. After kept at -78 ^oC for additional 30 minutes, the reaction mixture was warmed to ambient temperature and stirred overnight. After the removal of the solvent, the residue was purified by flash chromatograph on silica gel using CH_2Cl_2 as the eluent to afford SiBAM as a white solid (0.18 g, 55% yield). Colorless crystals of SiBAM were obtained *via* slow evaporation its hexane solution. ^1H NMR (500 Hz, $CDCl_3$, 25 °C): δ 8.40 (d; ^3J = 2.0 Hz; 2H, 7-aza), 7.89 (d; ^3J = 6.0 Hz; 2H, 7-aza), 7.72 (b; 2H, 7-aza), 7.07 (m; 2H, 7-aza), 6.41 (d; ^3J = 2.0 Hz; 2H, 7-aza), 3.10 (b; 1H, bridging C*H*$SiMe_3$), 0.31 (s; 9H, CHSi*Me*$_3$) ppm. ^{13}C NMR: δ 148.06, 143.07, 129.72, 129.04, 120.77, 116.48, 100.66, 57.43, -0.80 ppm. ^{29}Si NMR: δ 6.20 ppm. HRMS calcd. for $[C_{18}H_{20}N_4Si+Na^+]$: 343.1355; found: 343.1352.

5.2.3 Synthesis of trimethylstannyl-bis(1-*N*-7-azaindolyl)methane (SnBAM)

To a stirred THF (20 mL) solution of the BAM ligand (0.20 g, 0.81 mmol) at -78 ^oC was added dropwise, *via* syringe, a *n*-BuLi solution (1.6 M) (0.75 mL, 1.2 mmol) over 5 minutes, and the resulting light yellow solution was stirred for 30 minutes at -78 ^oC. A THF (5 mL) solution of Me_3SnCl (0.28 g, 1.4 mmol) was then slowly added *via* syringe. After kept at -78 ^oC for additional 30 minutes, the reaction mixture was warmed to ambient temperature and stirred overnight. After the removal of the solvent, the residue was purified by flash chromatograph on silica gel using CH_2Cl_2/hexanes (1:1) as the

eluent to afford SnBAM as a colorless oil (~72% yield). ^{1}H NMR (500 Hz, $CDCl_3$, 25 °C): δ 8.36 (d; ^{3}J = 5.0 Hz; 2H, 7-aza), 7.90 (d; ^{3}J = 7.5 Hz; 2H, 7-aza), 7.48 (b; 2H, 7-aza), 7.10 (dd; ^{3}J = 5.0 Hz, ^{3}J = 7.5 Hz; 2H, 7-aza), 6.97 (s, satellites; 1H, $^{2}J_{Sn\text{-}H}$ = 43.9; bridging C*H*SnMe$_3$) 6.38 (d; ^{3}J = 3.5 Hz; 2H, 7-aza), 0.26 (s; $^{2}J_{Sn\text{-}H}$ = 54.5 Hz; 9H, CHSn*Me*$_3$) ppm. ^{13}C NMR: δ 148.07, 142.44, 129.94, 129.32, 120.91, 116.38, 100.63, 53.89, -5.06 ($J_{Sn\text{-}C}$ = 353.9 Hz) ppm. HRMS calcd. for [$C_{18}H_{20}N_4Sn$+Na^+]: 435.0607; found: 435.0603.

5.2.4 Synthesis of 1,3-bis(1-*N*-7-azaindolyl)propane (1,3-BAPr)

To a solid mixture of 7-azaindole (1.56 g, 13.3 mmol) and sodium hydride (60% dispersed in mineral oil) (0.62 g, 15.5 mmol) in a Schlenck flask was added quickly 25 mL of dry DMF. The resulting clear solution was stirred for 30 minutes at ambient temperature, and 1,3-dibromopropane (1.98 g, 9.8 mmol) was then added. After the resulting brown suspension was stirred for 2 hours at ambient temperature, it was heated at 110 °C for 18 hours. DMF was then removed by vacuum distillation and the residue was extracted by CH_2Cl_2 (50 mL x 3). After the removal of the solvent, the residue was purified by flash chromatograph on silica gel using hexanes/ethyl acetate (1/1) as the eluent. The side product 1-allyl-7-azaindole was obtained as an colorless oil (0.35 g, 17% yield). ^{1}H NMR for 1-allyl-7-azaindole (300 Hz, $CDCl_3$, 25 °C): δ 8.35 (d; ^{3}J = 4.8 Hz; 1H, 7-aza), 7.94 (d; ^{3}J = 7.8 Hz; 1H, 7-aza), 7.23 (d; ^{3}J = 3.3 Hz; 1H, 7-aza), 7.08 (dd; $^{3}J_1$ = 4.8 Hz, $^{3}J_2$ = 7.8 Hz; 1H, 7-aza), 6.49 (d; ^{3}J = 3.3 Hz; 1H, 7-aza), 6.15 (m; 1H, CH_2CH=CHH'), 5.21 (d; ^{3}J = 10.2; 1H, CH_2CH=C*H*H'), 5.10 (d; ^{3}J = 17.1; 1H, CH_2CH=CH*H'*), 4.94 (m; 2H, CH_2CH=CHH') ppm. The 1,3-BAPr ligand was also

obtained as an colorless oil (0.84 g, 46% yield), which was solidified after the addition of hexanes and standing in a refrigerator for several days. ^{1}H NMR for 1,3-BAPr (500 Hz, $CDCl_3$, 25 °C): δ 8.35 (d; ^{3}J = 5.0 Hz; 2H, 7-aza), 7.96 (d; ^{3}J = 7.5 Hz; 2H, 7-aza), 7.34 (d; ^{3}J = 3.5 Hz; 2H, 7-aza), 7.11 (dd; $^{3}J_1$ = 5.0 Hz, $^{3}J_2$ = 7.5 Hz; 2H, 7-aza), 6.49 (d; ^{3}J = 3.5 Hz; 2H, 7-aza), 4.41 (t; ^{3}J = 6.5 Hz; 4H, CH_2), 1.91 (m; ^{3}J = 6.5 Hz; 3H, CH_2) ppm. ^{13}C NMR: δ 148.21, 143.42, 129.48, 128.84, 121.40, 116.41, 100.35, 42.79, 31.69 ppm. Anal. calcd. for $C_{17}H_{16}N_4$: C 73.89, H 5.84, N 20.27; found: C 73.83, H 5.99, N 20.22.

5.2.5 Synthesis of 1,4-bis(1-*N*-7-azaindolyl)butane (1,4-BABu)

To a solid mixture of 7-azaindole (0.75 g, 6.4 mmol) and sodium hydride (60% dispersed in mineral oil) (0.28 g, 7.0 mmol) in a Schlenck flask was added quickly 15 mL of dry DMF. The resulting clear solution was stirred for 30 minutes at ambient temperature, and 1,4-dibromobutane (0.69 g, 3.2 mmol) was then added. The resulting brown suspension was stirred for 2 hours at ambient temperature and then heated at 110 °C for 18 hours. DMF was then removed by vacuum distillation and the yellow residue was extracted by CH_2Cl_2 (30 mL x 3). After the removal of the solvent, the residue was purified by flash chromatograph on silica gel using hexanes/ethyl acetate (2/1) as the eluent to afford 1,4-BABu as a white solid (0.66 g, 71% yield). ^{1}H NMR (500 Hz, $CDCl_3$, 25 °C): δ 8.30 (dd; ^{3}J = 5.0 Hz, ^{4}J = 1.5 Hz; 2H, 7-aza), 7.92 (dd; ^{3}J = 8.0 Hz, ^{4}J = 1.0 Hz; 2H, 7-aza), 7.14 (d; ^{3}J = 3.5 Hz; 2H, 7-aza), 7.06 (dd; $^{3}J_1$ = 5.0 Hz, $^{3}J_2$ = 8.0 Hz; 2H, 7-aza), 6.46 (d; ^{3}J = 3.5 Hz; 2H, 7-aza), 4.35 (m; 4H, CH_2), 1.91 (m; 4H, CH_2) ppm. ^{13}C NMR: δ 148.09, 143.37, 129.44, 128.56, 121.24, 116.29, 100.15, 44.65, 28.38 ppm. Anal. calcd. for $C_{18}H_{18}N_4$: C 74.46, H 6.25, N 19.30; found: C 74.38, H 6.45, N 19.45.

5.2.6 Synthesis of 6,7-bis(1-*N*-7-azaindolyl)-1,4-dihydronaphthalene-1,4-epoxide (BAHE)

6,7-dibromo-1,4-dihydronaphthalene-1,4-epoxide (0.77 g, 2.5 mmol), 7-azaindole (0.75 g, 6.4 mmol), CuI (0.068 g, 0.35 mmol), 1,10-phenanthroline (0.15 g, 0.70 mmol), Cs_2CO_3 (4.10 g, 12.6 mmol) were mixed together in a Schlenck flask. The flask was degassed under high vacuum and refilled with N_2. 4.0 mL of dry DMF was then added. The mixture was heated at 145~150 ^oC for 3 days. After cooling down to ambient temperature, the mixture was diluted with 100 mL of CH_2Cl_2 and filtered through a plug of silica gel. The filtrate was then concentrated and the residue was purified by flash chromatograph on silica gel using hexanes/ethylacetate (2:1) as the eluent to BAHE as a yellow residue (0.48 g, 50% yield). Light yellow crystals of BAHE were obtained from the recrystallization of the residue with THF/hexanes. ^1H NMR (400 Hz, $CDCl_3$, 25 °C): 8.25 δ (dd; ^4J = 1.2 Hz, ^3J = 4.8 Hz; 2H, 7-aza), 7.84 (dd; ^4J = 1.2 Hz, $^3J_2$ = 8.0 Hz; 2H, 7-aza), 7.64 (s; 2H), 7.14 (s; 2H), 7.08 (dd; $^3J_1$ = 4.8 Hz, $^3J_2$ = 8.0 Hz; 2H, 7-aza), 6.78 (d, br; ^3J = 3.6 Hz; 2H, 7-aza), 6.24 (d; ^3J = 3.6 Hz; 2H, 7-aza), 5.85 (s; 2H) ppm. ^{13}C NMR: δ 149.94, 147.88, 143.27, 143.17, 130.98, 129.55, 129.32, 121.37, 121.18, 116.85, 101.92, 82.56 ppm. HRMS calcd. for $C_{24}H_{16}N_4O$: 376.1324, found: 376.1361.

Besides the BAHE ligand, two side products 6-(1-*N*-7-azaindolyl)-1,4-dihydronaphthalene-1,4-epoxide (NAHE) (~13% yield) and 2,3,6-tris(1-*N*-7-azaindolyl)naphthalene (TAN) (~8% yield) from the reaction. The characterization data of BAHE and TAN are shown below.

For NAHE, ^1H NMR (400 Hz, $CDCl_3$, 25 °C): δ 8.39 (br; 1H, 7-aza), 7.99 (d; ^3J = 8.5 Hz, 1H, 7-aza), 7.71 (s; 1H), 7.48 (d; ^3J = 5.5 Hz; 1H, 7-aza), 7.38 (d; ^3J =12.5Hz;

1H), 7.31 (d; ^3J =12.5 Hz; 1H), 7.16 (m; 1H, 7-aza), 7.09 (br; 2H); 6.64 (d; ^3J = 5.5 Hz; 1H, 7-aza), 5.81 (s; 1H), 5.80 (s; 1H) ppm.

For TAN, ^{1}H NMR (400 Hz, $CDCl_3$, 25 °C): δ 8.46 (dd; ^3J = 4.8 Hz, ^4J = 1.6 Hz; 1H,7-aza), 4.42 (d; ^3J = 1.6 Hz; 1H), 8.29 (s; 1H), 8.28 (s; 1H), 8.26-8.16 (m; 3H), 8.10 (d; ^3J = 8.8 Hz; 1H), 8.06 (dd; ^3J = 8.0 Hz, ^4J = 1.6 Hz; 1H, 7-aza), 7.88 (m; 1H, 7-aza), 7.86 (m; 1H, 7-aza), 7.76 (d; ^3J = 3.6 Hz, 1H, 7-aza), 7.21 (dd; $^3J_1$ = 4.8 Hz, $^3J_2$ = 8.0 Hz; 7-aza), 7.15-7.06 (m; 2H), 6.98 (d; ^3J= 3.6 Hz; 1H, 7-aza), 6.94 (d; ^3J= 3.6 Hz; 1H, 7-aza), 6.74 (d; ^3J= 3.6 Hz; 1H, 7-aza), 6.37 (d; ^3J= 3.6 Hz; 1H, 7-aza), 6.34 (d; ^3J= 3.6 Hz; 1H, 7-aza) ppm. ^{13}C NMR: δ 148.83, 148.78, 148.09, 143.88, 143.77, 143.40, 142.99, 137.77, 133.50, 133.17, 132.52, 130.70, 129.66, 129.43, 129.19, 129.11, 129.02, 128.89, 128.27, 128.17, 127.91, 127.07, 125.44, 124.09, 122.55, 122.28, 121.64, 120.80, 120.76, 120.60, 118.78, 117.40, 116.89, 116.86, 116.09, 102.80, 101.65, 101.37, 100.79 ppm. HRMS calcd. for $C_{31}H_{26}N_6$: 476.1749; found: 476.1758.

5.2.7 Synthesis of Pt(SiBAM)Me_2 (5.1)

SiBAM (0.067 g, 0.20 mmol) and [$PtMe_2$(μ-SMe_2)] (0.057 g, 0.10 mmol) were mixed in dry Et_2O (20 mL) and stirred overnight at ambient temperature. The solvent was decanted, and the resulting white solid was then washed with Et_2O (2 mL x 3) to afford **5.1** as a white powder (0.078g, 68% yield). Colorless crystals of **5.1** were obtained from the slow evaporation of the THF solution of **5.1** at ambient temperature. ^{1}H NMR (500 Hz, CD_2Cl_2, 25 °C): δ 13.13 (s, satellites; J_{Pt-H} = 61.0 Hz; 1H, C*H*$SiMe_3$), 8.72 (d; ^3J = 5.5; 2H, 7-aza), 7.96 (d; ^3J = 8.0; 2H, 7-aza), 7.56 (d; ^3J = 3.5; 2H, 7-aza), 7.04 (dd; $^3J_1$ = 5.5 Hz, $^3J_2$ = 8.0 Hz; 2H, 7-aza), 6.59 (d; ^3J = 3.5; 2H, 7-aza), 0.67 (s, satellites; $^2J_{Pt-H}$ =

88.0 Hz; 6H, Pt*Me*$_2$) 0.45 (s; 9H, CHSi*Me*$_3$) ppm. ^{13}C NMR: δ 146.51, 144.89, 129.25, 127.88, 123.24, 117.40, 102.21, 54.69, -1.79, -19.85 ($^1J_{Pt\text{-}H}$ = 838.6 Hz; Pt*Me*$_2$) ppm. Anal. calcd. for $C_{20}H_{26}N_4PtSi$: C 44.03, H 4.80, N 10.27; found: C 44.37, H 4.79, N 9.88.

5.2.8 Synthesis of Pt(*N,N,C*-BAM)(SnMe$_3$)Me$_2$ (5.2)

SnBAM (0.045 g, 0.10 mmol) and [PtMe$_2$(μ-SMe$_2$)] (0.029 g, 0.05 mmol) were mixed in dry Et$_2$O (10 mL) and stirred overnight at ambient temperature. The solvent was decanted, and the resulting while solid was then washed with hexanes (2 mL x 3). The residue was analyzed by ^{1}H NMR, which showed the presence of the Pt(IV) compound **5.2**. However, the clean isolation of **5.2** can not be obtained. Diagnostic ^{1}H NMR signals of compound **5.2** (500 Hz, CD_2Cl_2, 25 °C): δ 5.95 (s, satellites; $^2J_{Pt\text{-}H}$ = 26.0; 1H, bridging C*H'*SnMe$_3$), 0.76 (s, satellites; $^2J_{Pt\text{-}H}$ = 42.5 Hz; 3H, Pt-*Me*), 0.76 (s, satellites; $^2J_{Pt\text{-}H}$ = 64.0 Hz; 3H, Pt-*Me*), -0.22 (s, satellites; $^2J_{Sn\text{-}H}$ = 47.5 Hz, $^3J_{Pt\text{-}H}$ = 10.5 Hz; 9H, Sn*Me*$_3$). Diagnostic ^{13}C NMR signals of compound **5.2** (125 MHz, CD_2Cl_2, 25 ^{o}C): 72.94 (s, satellites; $^1J_{Pt\text{-}C}$ = 480.2 Hz; bridging *C*H').

Monitoring the reaction of SnBAM and [PtMe$_2$(μ-SMe$_2$)] in CD_2Cl_2 at ambient temperature by ^{1}H NMR spectroscopy indicated both the formation of **5.2** and the PtMe$_2$ compound **Pt(SnBAM)Me$_2$** {δ 12.82 ppm for its C*H'*(SiMe$_3$), with $^2J_{Sn\text{-}H}$ = 74.0 Hz, $J_{Pt\text{-}H}$ = 56.5 Hz} in the early stage of the reaction.

5.2.9 Synthesis of Pt$_2$(1,3-BAPr)Ph$_2$ (5.3)

1,3-BAPr (0.055 g, 0.20 mmol) and [PtPh$_2$(μ-SMe$_2$)]$_n$ (n = 2 or 3) (0.082 g, 0.20 mmol based on Pt) were mixed in CH_2Cl_2 (15 mL) and stirred overnight at ambient

temperature. The solvent was decanted, and the resulting yellow solid was then washed with Et_2O (2 mL x 3). Yellow crystals of **5.3** were obtained from the slow evaporation of its methylene chloride solution (*ca.* 70% yield). ^{1}H NMR (400 Hz, CD_2Cl_2, 25°C): δ 8.76 (dd; ^3J = 4.4 Hz, ^4J = 1.6 Hz; 2H, 7-aza), 8.19 (m; ^2J = 12 Hz; 2H, N_{aza}-CH_aH$_b$CH$_a$H$_b$CH_aH$_b$-N_{aza}), 7.63 (dd; ^3J = 8.0 Hz, ^4J = 1.2 Hz; 2H, 7-aza), 7.56 (d, satellite; ^3J = 8.0 Hz, $^3J_{Pt-H}$ = 70 Hz; 2H, *ortho*-H of PtPh_2), 7.13 (d; ^3J = 3.6 Hz, 7-aza), 6.95-6.72 (m; 8H, 2H from 7-aza & 2H from *para*-H of PtPh_2 & 4H from *meta*-H of PtPh_2), 6.27 (d; ^3J = 3.6 Hz, 7-aza), 4.20 (m; 2H, N_{aza}-CH$_a$$H_bCH_aH_bCH_a$$H_b$-$N_{aza}$), 2.83-2.71 (m; 2H, N_{aza}-CH$_a$H$_b$C$H_a$$H_bCH_aH_b$-$N_{aza}$) ppm. ^{13}C NMR: δ 146.722, 144.37, 139.18, 138.38 (satellite; J_{Pt-C} = 33.7 Hz), 129.59, 129.25, 126.60 (satellite; J_{Pt-C} = 81.7 Hz), 123.14, 121.76, 115.84, 101.51, 44.24, 31.70 ppm. Anal. calcd. for $C_{29}H_{26}N_4Pt$: C 55.67, H 4.19, N 8.96; found: C 56.01, H 4.28, N 8.64.

5.2.10 Synthesis of Pt(1,4-BABu)Ph$_2$ (5.4)

1,4-BABu (0.058 g, 0.20 mmol) and [PtPh$_2$(μ-SMe$_2$)]$_n$ (n = 2 or 3) (0.082 g, 0.20 mmol based on Pt) were mixed in CH_2Cl_2 (15 mL) and stirred overnight at ambient temperature. The solvent was decanted and the resulting yellow solid was then washed with Et_2O (2 mL x 3). Yellow crystals of **5.4** were obtained from the slow evaporation of its methylene chloride/toluene (3:1) solution at room temperature (~70% yield). ^{1}H NMR (400 Hz, CD_2Cl_2, 25°C): δ 9.10 (dd; ^3J = 5.2 Hz, ^4J = 1.2 Hz; 2H, 7-aza), 8.45 (m; 2H, N_{aza}-CH_aH$_b$CH$_a$H$_b$CH$_a$H$_b$CH_aH$_b$-N_{aza}), 7. 90 (dd; ^3J = 6.0 Hz, ^4J = 1.2 Hz; 2H, 7-aza), 7.31-7.16 (m, satellite; $^3J_{Pt-H}$ = 76 Hz; 4H from *ortho*-H of PtPh_2 and 2H from 7-aza); 7.11 (dd; $^3J_1$ = 5.2 Hz, $^3J_2$ = 6.0 Hz; 2H, 7-aza), 6.75-6.66 (m; 6H, *para*- and *meta*-H of

Pt*Ph*$_2$), 6.52 (d; ^3J = 3.6 Hz; 2H, 7-aza), 4.15-4.01 (m; 2H, N_{aza}-$CH_aH_bCH_aH_bCH_aH_bCH_aH_b$-$N_{aza}$), 2.10-1.98 (m; 2H, N_{aza}-$CH_aH_bCH_aH_bCH_aH_bCH_aH_b$-$N_{aza}$), 1.63-1.55 (m; 2H, N_{aza}-$CH_aH_bCH_aH_bCH_aH_bCH_aH_b$-$N_{aza}$) ppm. ^{13}C NMR: δ 145.26, 139.66, 138.11 (satellite; J_{Pt-C} = 35.2 Hz), 130.20, 129.80, 126.21 (satellite; J_{Pt-C} = 81.4 Hz), 124.25, 121.50, 116.12, 101.28, 43.26, 27.64 ppm. Anal. calcd. for $C_{30}H_{28}N_4Pt$: C 56.33, H 4.41, N 8.76; found: C 56.41, H 4.37, N 8.28.

5.2.11 Synthesis of Pt_2(1,3-BAPr)$Ph_4(SMe_2)_2$ (5.5)

Complex **5.5** was obtained using the same method as described for **5.3** using 1,3-BAPr (0.028 g, 0.10 mmol) and $[PtPh_2(\mu\text{-}SMe_2)]_n$ (n = 2 or 3) (0.082 g, 0.20 mmol based on Pt) in CH_2Cl_2 (15 mL). Pale yellow crystals of **5.5** were obtained from the slow evaporation of its methylene chloride solution (81% yield). ^{1}H NMR (400 Hz, CD_2Cl_2, 25°C): δ 8.76 (dd; ^3J = 5.2 Hz, ^4J = 1.2 Hz; 2H, 7-aza), 8.16 (t; ^3J = 12.4 Hz; 2H, N_{aza}-$CH_aH_bCH_aH_bCH_aH_b$-N_{aza}), 7.63 (dd; ^3J = 7.8 Hz, ^4J = 1.2 Hz, 2H, 7-aza), 7.57 (d, satellite; ^3J = 8.0 Hz, $^3J_{Pt-H}$ = 61 Hz; 4H, *ortho*-H of Pt*Ph*$_2$), 7.38 (d, satellite; ^3J = 7.8 Hz, $^3J_{Pt-H}$ = 72 Hz; 4H, *ortho*-H' of Pt*Ph*$_2$), 7.13 (d; ^3J = 3.6 Hz, 7-aza), 6.97-6.78 (m; 14H, 2H from 7aza, 4H from *para*-H of Pt*Ph*$_2$ and 8H from *meta*-H of Pt*Ph*$_2$), 6.27 (d; ^3J = 3.6 Hz; 2H, 7-aza), 4.20 (d; ^3J = 12.4 Hz; 2H, N_{aza}-$CH_aH_bCH_aH_bCH_aH_b$-N_{aza}), 2.72-2.50 (m; 2H, N_{aza}-$CH_aH_bCH_aH_bCH_aH_b$-N_{aza}), 2.13 (s, satellite; $^3J_{Pt-H}$ = 24 Hz; 12H) ppm. ^{13}C NMR: δ 146.80, 144.75, 138.87, 138.69, 136.87, 136.64, 129.66, 129.16, 128.98, 128.75, 127.50, 126.81, 124.11, 123.01, 122.35, 122.14, 115.96, 101.81, 44.08, 31.83, 23.36, 20.80 ppm. Anal. calcd. for $C_{45}H_{48}N_4Pt_2S_2$: C 49.17, H 4.40, N 5.10; found: C 49.36, H 4.23, N 5.20.

5.2.12 Synthesis of Pt(1,3-BAPr)Me_2 (5.6)

Complex **5.6** was obtained using the same method as described for **5.1** using 1,3-BAPr (0.055 g, 0.20 mmol) and $[PtMe_2(\mu\text{-}SMe_2)]_2$ (0.057 g, 0.10 mmol) in THF (10 mL) for 2 days. The solvent was decanted. The pale yellow solid was extracted with Et_2O/hexanes (1:1) (5mL x 3). The crystals of **5.6** were obtained by cooling the Et_2O/hexanes (1:1) solution in a refrigerator for several days. Due to its poor stability, compound **5.6** was only characterized by single-crystal X-ray diffraction analyses.

5.2.13 Synthesis of Pt(1,4-BABu)Me_2 (5.7)

Complex **5.7** was obtained using the same method as described for **5.6** using 1,4-BABu (0.129 g, 0.44 mmol) and $[PtMe_2(\mu\text{-}SMe_2)]_2$ (0.127 g, 0.22 mmol) in THF (15 mL). Pale yellow crystals of **5.7** were obtained from cooling the Et_2O/hexanes (1:1) solution in a refrigerator for several days. ^{1}H NMR (400 Hz, CD_2Cl_2, 25°C): δ 8.97 (d, satellite; ^3J = 5.2 Hz, $^3J_{Pt\text{-}H}$ = 40 Hz; 2H, 7-aza), 8.42 (m; 2H, N_{aza}-CH_aH$_b$CH$_a$H$_b$CH$_a$H$_b$CH_aH$_b$-N_{aza}), 7. 90 (d; ^3J = 8.0 Hz; 2H, 7-aza), 7.25 (d; ^3J = 3.2 Hz; 2H, 7-aza), 7.01 (dd; $^3J_1$ = 5.2 Hz, $^3J_2$ = 8.0 Hz; 2H, 7-aza), 6.53 (d; ^3J = 3.2 Hz; 2H, 7-aza), 4.07-4.02 (m; 2H, N_{aza}-CH$_a$$H_bCH_aH_bCH_aH_bCH_a$$H_b$-$N_{aza}$), 1.89-1.81 (m; 2H, N_{aza}-CH$_a$H$_b$CH_aH$_b$CH_aH$_b$CH$_a$H$_b$-N_{aza}), 1.48-1.42 (m; 2H, N_{aza}-CH$_a$H$_b$CH$_a$$H_bCH_a$$H_bCH_aH_b$-$N_{aza}$), 0.52 (s, satellites; $^2J_{Pt\text{-}H}$ =86.4 Hz) ppm. Compound **5.7** was not characterized by elemental analyses due to its poor stability.

5.2.14 Synthesis of Pt(BAHE)Ph_2 (5.8)

BAHE (0.037 g, 0.10 mmol) and $[PtPh_2(\mu\text{-}SMe_2)]_n$ (n = 2 or 3) (0.041 g, 0.10 mmol based on Pt) were mixed in THF (10 mL) and the mixture was stirred overnight at ambient temperature. The solvent was decanted, and the resulting solid was then washed with Et_2O (4 mL x 3). The residue was dissolved by THF and filtered through a pad of Celite. The slow evaporation of the THF resulted in **5.8** as brown power (*ca* 50% yield). ^{1}H NMR (400 Hz, CD_2Cl_2, 25°C): δ 8.72 (d; ^3J = 5.5 Hz; 2H, 7-aza), 7.86 (d; ^3J = 6.5 Hz; 2H, 7-aza), 7.47 (s; 2H); 7.29 (s; 2H), 7.17 (d; ^3J = 3.5 Hz; 2H, 7-aza), 7.02 (dd; $^3J_1$ = 5.5 Hz, $^3J_2$ = 6.5 Hz; 2H, 7-aza), 6.96 (d, satellites; $^3J_{Pt\text{-}H}$ = 80 Hz, ^3J = 8.5 Hz; 4H, *ortho*-H of Pt*Ph*$_2$), 6.70 (m; 4H, *meta*-H of Pt*Ph*$_2$), 6.63 (m; 2H, *para*-H of Pt*Ph*$_2$), 6.55 (d; ^3J = 3.5 Hz; 2H, 7-aza), 5.96 (s; 2H) ppm. ^{13}C NMR: δ 152.18, 128.77, 145.26, 142.88. 141.85, 138.35, 134.23, 131.57, 131.21, 130.08, 125.87, 123.38, 122.28, 121.16, 117.39, 102.80, 82.87 ppm.

5.2.15 NMR characterization of [Pt(SiBAM)Me_3](OTf) (5.9)

A ^{1}H NMR spectrum was recorded for a CD_2Cl_2 (0.40 mL) solution of Pt(SiBAM)Me_2 (**5.1**) (~ 8 mg). MeOTf (1.7 μL, ~1.05 eq) was then added, *via* micropipette, at ambient temperature. The NMR tube was shaken vigorously for a couple of seconds, and then a new NMR spectrum of the solution was recorded. The ^{1}H NMR data indicated the clean formation of the *fac*-$PtMe_3$ compound **5.9**, which exists as a five-coordinated Pt^{IV} species in the solution. ^{1}H NMR (500 Hz, CD_2Cl_2, 25°C): δ 8.41 (d; ^3J = 5.0 Hz; 2H, 7-aza), 8.20 (d; ^3J = 8.0 Hz; 2H, 7-aza), 7.65 (d; ^3J = 4.0 Hz; 2H, 7-aza), 7.40 (dd; $^3J_1$ = 5.0 Hz, $^3J_2$ = 8.0 Hz; 2H, 7-aza), 6.95 (d; ^3J = 4.0 Hz; 2H, 7-aza), 5.00 (s,

satellites; $J_{Pt\text{-}H}$ = 88.9 Hz; 1H, bridging C*H'*($SiMe_3$)), 1.79 (s, satellites; $^2J_{Pt\text{-}H}$ = 73.5 Hz; 9H, *fac*-Pt*Me*$_3$), 0.55 (s; 9H, Si*Me*$_3$) ppm. ^{13}C NMR: δ 148.14, 142.09, 133.23, 127.97, 124.96, 118.92, 105.86, 65.89, -0.98, -6.53 ($^1J_{Pt\text{-}H}$ = 629 Hz; *fac*-Pt*Me*$_3$) ppm.

5.2.16 In situ synthesis of Pt(SiBAM)I_2 (5.10)

A ^{1}H NMR spectrum was recorded for a CD_2Cl_2 (0.40 mL) solution of Pt(SiBAM)Me_2 (**5.1**) (~8 mg). I_2 (4 mg, ~1.05 eq) was then added at ambient temperature. After being shaken vigorously to dissolve I_2, the solution was monitored by ^{1}H NMR spectroscopy. The ^{1}H NMR data indicated the formation of compound **5.10**, along with the formation MeI (δ = 2.20), free SiBAM and $[PtMe_3I]_4$. ^{1}H NMR (500 Hz, CD_2Cl_2, 25°C): δ 12.89 (s, satellites; $J_{Pt\text{-}H}$ = 50.0 Hz; 1H, C*H*$SiMe_3$), 9.01 (d; ^3J = 6.5 Hz; 2H, 7-aza) 8.00 (d; ^3J = 7.0 Hz; 2H, 7-aza), 7.64 (d; ^3J = 2.0 Hz; 2H, 7-aza), 7.16 (dd; $^3J_1$ = 6.5 Hz, $^3J_2$ = 7.0 Hz; 2H, 7-aza), 6.71 (d; ^3J = 2.0 Hz; 2H, 7-aza) ppm. Slow evaporation of the CD_2Cl_2 solution afforded yellow crystals, which were identified by single crystal X-ray diffraction analyses to be the cocrystallized product of **5.10** with $[PtMe_3I]_4$.

The reaction of Pt(SiBAM)Me_2 (**5.1**) (~8 mg) with 3 equivalents of I_2 (~11 mg) in CD_2Cl_2 (0.40 mL) at ambient temperature gave similar results, as indicated by the ^{1}H NMR data obtained, again producing **5.10**, MeI, the free SiBAM ligand and $[PtMe_3I]_4$. Slow evaporation of the CD_2Cl_2 solution afforded deep red crystals, which were identified by single crystal X-ray diffraction analyses to be the cocrystallized product of **5.10** with I_2.

5.2.17 X-ray diffraction analyses

Single crystals of SiBAM, BAHE, **5.1**, **5.3-5.7**, and **5.10** were mounted on glass fibers for data collection. Data were collected on a Bruker Apex II single-crystal X-ray diffractometer with graphite-monochromated Mo Kα radiation, operating at 50 kV and 30 mA. No significant decay was observed in any samples. Data were processed on a PC with the aid of the Bruker SHELXTL software package (version 5.10) and corrected for absorption effects. All structures were solved by direct methods. Most of the non-hydrogen atoms were refined anisotropically. The positions of hydrogen atoms were calculated, and their contributions in structural factor calculations were included. The crystal data for these compounds are summarized in Tables 5.1-5.3. Important bond lengthes and angles for all the compounds are listed in Table 5.4.

Table 5.1 Crystallographic data for compounds SiBAM, BAHE, **5.1**, and **5.3**.

Compound	SiBAM	BAHE	**5.1**	**5.3**
Formula	$C_{18}H_{20}N_3Si$	$C_{24}H_{18}N_4O$	$C_{20}H_{26}N_2PtSi$	$C_{29}H_{26}N_4Pt$
FW	306.46	378.42	517.61	447.80
Space Group	Cmca	$P4_32_12$	P-1	P-1
a, Å	19.2611(13)	10.721(5)	9.2748(11)	8.5543(6)
b, Å	12.5501(8)	10.721(5)	9.5207(12)	13.0128(9)
c, Å	14.3500(9)	32.66(3)	13.2059(16)	13.0547(9)
α, º	90	90	104.3020(10)	72.5700(10)
β, º	90	90	106.3130(10)	77.9860(10)
γ, º	90	90	94.5730(10)	71.4990(10)
V, $Å^3$	3468.8(4)	3753(5)	1070.5(2)	1304.50(16)
Z	8	8	2	2
$D_{calc,}$ g·cm^{-3}	1.174	1.339	1.606	1.593
T, K	297(2)	297(2)	297(2)	180(2)
μ, mm^{-1}	0.136	0.085	6.613	5.408
$2\theta_{max}$, º	54.26	56.92	54.52	56.70
Reflns measured	18666	21383	12142	9282
Reflns used (R_{int})	1981(0.0244)	4544 (0.1091)	4671 (0.0216)	5871(0.0222)
Parameters	120	263	250	334
Final *R* values [I > 2σ(I)]:				
R_1[a]	0.0374	0.0579	0.0173	0.0478
wR_2[b]	0.1016	0.1099	0.0399	0.1176
R values (all data):				
R_1[a]	0.0446	0.2214	0.0195	0.0532
wR_2[b]	0.1086	0.1572	0.0405	0.1198
Goodness-of-fit on F^2	1.070	0.971	1.027	1.096

[a] $R_1 = \Sigma||F_0| - |F_c|| / \Sigma|F_0|$

[b] $wR_2 = [\Sigma w [(F_0^2-F_c^2)^2] / \Sigma[w(F_0^2)^2]]^{1/2}$

$w = 1 / [\sigma^2(F_0^2) + (0.075P)^2]$, where $P = [Max (F_0^2,0) + 2F_c^2] / 3$

Table 5.2 Crystallographic Data for compounds **5.4**-**5.7**.

Compound	**5.4**	**5.5**	**5.6**	**5.7**
Formula	$C_{30}H_{28}N_4Pt$	$C_{45}H_{49}N_4Pt_2S_2$	$C_{19}H_{22}N_4Pt$	$C_{20}H_{24}N_4Pt$
FW	639.65	1100.18	501.59	515.20
Space Group	$P2_1/n$	P-1	P-1	P-1
a, Å	13.0677(16)	11.7088(15)	8.043(11)	8.0310(7)
b, Å	10.5124(12)	12.9165(17)	10.156(14)	10.7070(8)
c, Å	19.077(2)	14.9862(19)	12.056(16)	13.8631(11)
α, º	90	80.192(2)	79.945(17)	82.4630(10)
β, º	109.140(2)	83.251(3)	72.356(19)	85.1300(10)
γ, º	90	63.096(2)	80.443(16)	83.6180(10)
V, $Å^3$	2475.8(5)	1989.5(4)	917(2)	1171.44(16)
Z	4	2	2	2
$D_{calc,}$ $g \cdot cm^{-3}$	1.716	1.837	1.816	1.462
T, K	180(2)	180(2)	180(2)	180(2)
μ, mm^{-1}	5.694	7.167	7.655	6.011
$2\theta_{max}$, º	56.68	56.68	59.44	56.16
Reflns measured	17538	14394	6372	7988
Reflns used (R_{int})	5912 (0.0400)	9115 (0.0435)	4015 (0.0252)	5019 (0.0173)
Parameters	316	477	217	228
Final *R* values [I > 2σ(I)]:				
R_1[a]	0.0400	0.0490	0.0334	0.0199
wR_2[b]	0.0855	0.0790	0.0649	0.0417
R values (all data):				
R_1[a]	0.0705	0.0958	0.0445	0.0228
wR_2[b]	0.0965	0.1623	0.0676	0.0420
Goodness-of-fit on F^2	0.973	0.755	0.902	0.921

[a] $R_1 = \Sigma||F_0| - |F_c|| / \Sigma|F_0|$

[b] $wR_2 = [\Sigma w [(F_0^2-F_c^2)^2] / \Sigma[w(F_0^2)^2]]^{1/2}$

$w = 1 / [\sigma^2(F_0^2) + (0.075P)^2]$, where $P = [Max (F_0^2,0) + 2F_c^2] / 3$

Table 5.3 Crystallographic data for **5.10·0.25[PtMe$_3$I]$_4$** and **5.10·0.5I$_2$·CH$_2$Cl$_2$**.

Compound	**5.10·0.25[PtMe$_3$I]$_4$**	**5.10·0.5I$_2$·CH$_2$Cl$_2$**
Formula	$C_{21}H_{29}I_3N_4Pt_2Si_2$	$C_{19}H_{22}Cl_2I_3N_4PtSi$
FW	622.12	981.19
Space Group	$P4_2/n$	$P2_1/c$
a, Å	24.238(3)	10.8524(7)
b, Å	24.238(3)	11.0891(8)
c, Å	9.759(3)	23.4396(16)
α, º	90	90
β, º	90	94.8450(10)
γ, º	90	90
V, Å^3	5733.5(18)	2810.7(3)
Z	8	4
$D_{calc,}$ g·cm^{-3}	2.162	2.319
T, K	297(2)	297(2)
μ, mm^{-1}	9.020	8.534
$2\theta_{max}$, º	56.52	54.32
Reflns measured	64086	30766
Reflns used (R_{int})	6927 (0.0956)	6187 (0.0426)
Parameters	286	274
Final *R* values I > 2σ(I)]:		
R_1[a]	0.0412	0.0312
wR_2[b]	0.0932	0.0678
R values (all data):		
R_1[a]	0.0915	0.0461
wR_2[b]	0.1104	0.0733
Goodness-of-fit on F^2	1.011	1.036

[a] $R_1 = \Sigma||F_0| - |F_c|| / \Sigma|F_0|$

[b] $wR_2 = [\Sigma w [(F_0^2-F_c^2)^2] / \Sigma[w(F_0^2)^2]]^{1/2}$

$w = 1 / [\sigma^2(F_0^2) + (0.075P)^2]$, where $P = [Max (F_0^2,0) + 2F_c^2] / 3$

Table 5.4 Selected bond lengths (Å) and angles (º) for compounds SiBAM, BAHE, **5.1**, **5.3**-**5.7**, **5.10·0.25[$PtMe_3I$]$_4$** and **5.10·0.5I_2·CH_2Cl_2**.

		SiBAM	
Si(1)-C(10)	1.8486(18)	N(1)-C(1)	1.4639(14)
Si(1)-C(9)	1.858(3)	N(2)-C(8)	1.3307(17)
Si(1)-C(1)	1.9131(19)	N(2)-C(7)	1.3364(19)
N(1)-C(8)	1.3746(16)	C(2)-C(3)	1.348(2)
N(1)-C(2)	1.3843(17)	C(3)-C(4)	1.422(2)
C(9)-Si(1)-C(1)	113.29(13)	C(2)-N(1)-C(1)	127.19(12)
C(8)-N(1)-C(2)	107.40(11)	C(8)-N(2)-C(7)	113.81(13)
C(8)-N(1)-C(1)	124.67(11)	N(1)-C(1)-Si(1)	114.16(8)
		BAHE	
O(1)-C(20)	1.437(6)	N(2)-C(14)	1.329(5)
O(1)-C(24)	1.448(5)	N(2)-C(13)	1.335(6)
N(1)-C(14)	1.370(5)	N(3)-C(1)	1.377(5)
N(1)-C(8)	1.372(5)	N(3)-C(7)	1.386(5)
N(1)-C(15)	1.432(5)	N(3)-C(21)	1.419(5)
C(20)-O(1)-C(24)	95.6(4)	C(8)-N(1)-C(15)	126.9(4)
C(14)-N(1)-C(8)	107.2(3)	C(14)-N(2)-C(13)	113.6(4)
C(14)-N(1)-C(15)	125.9(3)	C(1)-N(3)-C(7)	107.1(3)
		Compound **5.1**	
Pt(1)-C(1)	2.031(3)	Si(1)-C(19)	1.849(3)
Pt(1)-C(2)	2.037(3)	Si(1)-C(18)	1.856(3)
Pt(1)-N(1)	2.135(2)	Si(1)-C(20)	1.874(3)
Pt(1)-N(4)	2.142(2)	Si(1)-C(10)	1.902(3)
C(1)-Pt(1)-C(2)	89.12(14)	C(1)-Pt(1)-N(4)	89.07(11)
C(1)-Pt(1)-N(1)	177.67(10)	C(2)-Pt(1)-N(4)	178.15(12)
C(2)-Pt(1)-N(1)	90.50(12)	N(1)-Pt(1)-N(4)	91.32(8)
		Compound **5.3**	
Pt(1)-C(24)	2.005(6)	N(1)-C(7)	1.343(9)
Pt(1)-C(18)	2.006(7)	N(1)-C(1)	1.363(10)
Pt(1)-N(3)	2.141(6)	N(3)-C(14)	1.342(9)
Pt(1)-N(1)	2.158(6)	N(3)-C(8)	1.374(9)
C(24)-Pt(1)-C(18)	91.2(3)	C(1)-N(1)-Pt(1)	113.7(5)

C(24)-Pt(1)-N(3)	175.3(2)	C(7)-N(2)-C(6)	107.1(7)
C(18)-Pt(1)-N(3)	93.5(2)	C(7)-N(2)-C(15)	130.4(6)
C(24)-Pt(1)-N(1)	93.1(2)	C(6)-N(2)-C(15)	122.4(7)
C(18)-Pt(1)-N(1)	172.7(2)	C(14)-N(3)-C(8)	114.8(6)
N(3)-Pt(1)-N(1)	82.3(2)	C(14)-N(3)-Pt(1)	123.8(5)
C(7)-N(1)-Pt(1)	130.4(5)	C(8)-N(3)-Pt(1)	116.8(5)
		Compound **5.4**	
Pt(1)-C(19)	1.994(6)	N(1)-C(7)	1.345(8)
Pt(1)-C(25)	2.009(6)	N(1)-C(1)	1.352(8)
Pt(1)-N(3)	2.164(5)	N(3)-C(14)	1.340(7)
Pt(1)-N(1)	2.191(5)	N(3)-C(8)	1.357(7)
C(19)-Pt(1)-C(25)	91.1(2)	C(19)-Pt(1)-N(1)	87.6(2)
C(19)-Pt(1)-N(3)	170.6(2)	C(25)-Pt(1)-N(1)	176.7(2)
C(25)-Pt(1)-N(3)	90.4(2)	N(3)-Pt(1)-N(1)	90.48(17)
		Compound **5.5**	
Pt(1)-C(21)	2.021(10)	Pt(2)-C(27)	1.829(16)
Pt(1)-C(15)	2.034(11)	Pt(2)-C(33)	2.006(9)
Pt(1)-N(2)	2.122(7)	Pt(2)-N(4)	2.119(9)
Pt(1)-S(1)	2.349(3)	Pt(2)-S(2)	2.349(3)
C(21)-Pt(1)-C(15)	93.8(5)	C(27)-Pt(2)-C(33)	90.9(5)
C(21)-Pt(1)-N(2)	174.5(4)	C(27)-Pt(2)-N(4)	173.5(4)
C(15)-Pt(1)-N(2)	91.4(4)	C(33)-Pt(2)-N(4)	95.2(4)
C(21)-Pt(1)-S(1)	85.7(4)	C(27)-Pt(2)-S(2)	91.7(3)
C(15)-Pt(1)-S(1)	178.1(3)	C(33)-Pt(2)-S(2)	176.9(3)
N(2)-Pt(1)-S(1)	89.1(2)	N(4)-Pt(2)-S(2)	82.2(2)
		Compound **5.6**	
Pt(1)-C(19)	2.068(6)	N(1)-C(1)	1.318(8)
Pt(1)-C(18)	2.157(7)	N(1)-C(7)	1.401(7)
Pt(1)-N(3)	2.215(5)	N(3)-C(8)	1.338(7)
Pt(1)-N(1)	2.299(6)	N(3)-C(14)	1.368(7)
C(19)-Pt(1)-C(18)	85.3(3)	N(3)-Pt(1)-N(1)	78.58(18)
C(19)-Pt(1)-N(3)	176.2(2)	C(1)-N(1)-C(7)	109.2(6)
C(18)-Pt(1)-N(3)	98.2(2)	C(1)-N(1)-Pt(1)	115.9(4)
C(19)-Pt(1)-N(1)	97.8(2)	C(7)-N(1)-Pt(1)	132.1(4)
C(18)-Pt(1)-N(1)	175.9(2)	C(7)-N(2)-C(6)	105.2(5)
C(6)-N(2)-C(17)	127.7(5)	C(7)-N(2)-C(17)	125.5(5)
		Compound **5.7**	
Pt(1)-C(20)	2.028(3)	N(1)-C(1)	1.344(5)
Pt(1)-C(19)	2.030(4)	N(1)-C(7)	1.350(4)

Pt(1)-N(1)	2.163(3)	N(4)-C(18)	1.345(5)
Pt(1)-N(4)	2.166(3)	N(4)-C(17)	1.348(5)
C(20)-Pt(1)-C(19)	88.08(15)	C(1)-N(1)-Pt(1)	113.7(2)
C(20)-Pt(1)-N(1)	177.44(14)	C(7)-N(1)-Pt(1)	131.0(2)
C(19)-Pt(1)-N(1)	91.81(13)	C(18)-N(4)-Pt(1)	129.9(2)
C(20)-Pt(1)-N(4)	88.11(13)	C(17)-N(4)-Pt(1)	115.3(3)
C(19)-Pt(1)-N(4)	173.95(12)	N(1)-Pt(1)-N(4)	91.79(11)
	Compound **5.10·0.25[$PtMe_3I$]$_4$**		
Pt(1)-N(4)	2.049(7)	Pt(2)-C(20)	2.080(11)
Pt(1)-N(1)	2.054(7)	Pt(2)-C(21)	2.101(11)
Pt(1)-I(2)	2.5831(8)	Pt(2)-C(19)	2.107(12)
Pt(1)-I(1)	2.5832(8)	Pt(2)-I(3)	2.8069(9)
N(4)-Pt(1)-N(1)	89.9(3)	C(20)-Pt(2)-C(21)	90.6(5)
N(4)-Pt(1)-I(2)	175.78(19)	C(20)-Pt(2)-C(19)	89.6(6)
N(1)-Pt(1)-I(2)	89.92(19)	C(21)-Pt(2)-C(19)	89.1(6)
N(4)-Pt(1)-I(1)	88.27(19)	C(20)-Pt(2)-I(3)	90.4(4)
N(1)-Pt(1)-I(1)	178.1(2)	C(21)-Pt(2)-I(3)	177.9(4)
I(2)-Pt(1)-I(1)	91.95(3)	C(19)-Pt(2)-I(3)	92.7(5)
	Compound **5.10·0.5I_2·CH_2Cl_2**		
Pt(1)-N(1)	2.059(6)	Si(1)-C(8)	1.926(8)
Pt(1)-N(4)	2.062(6)	N(1)-C(7)	1.324(10)
Pt(1)-I(2)	2.5841(6)	N(1)-C(1)	1.359(10)
Pt(1)-I(1)	2.5910(6)	N(4)-C(15)	1.341(9)
I(3)-I(3)#1	2.7396(14)	N(4)-C(14)	1.341(10)
N(1)-Pt(1)-N(4)	89.4(2)	C(7)-N(1)-Pt(1)	124.1(5)
N(1)-Pt(1)-I(2)	178.05(18)	C(1)-N(1)-Pt(1)	119.3(6)
N(4)-Pt(1)-I(2)	88.95(17)	C(15)-N(4)-Pt(1)	123.6(5)
N(1)-Pt(1)-I(1)	89.79(17)	C(14)-N(4)-Pt(1)	120.3(6)
N(4)-Pt(1)-I(1)	178.25(18)	C(16)-Si(1)-C(8)	101.8(4)
I(2)-Pt(1)-I(1)	91.92(2)	C(18)-Si(1)-C(8)	116.6(4)
		C(17)-Si(1)-C(8)	104.2(6)

5.3 Result and Discussion

5.3.1 Syntheses of new 7-azaindolyl derivative ligands

5.3.1.1 New silyl and stannyl BAM derivative ligands

To examine the steric impact of a bulky substituent group on the CH_2 linker of the BAM lignad, we synthesized $SiMe_3$ and $SnMe_3$ substituted compounds, as shown in Scheme 5.1, *via* the direct introduction of the new substituent group to the CH_2 group. As demonstrated in Chapter 4 by the synthesis of compound **4.4**, the CH_2 group of the BAM ligand can be readily deprotonated by either LDA (lithium diisopropylamide) or *n*-BuLi to give the bis(1-*N*-7-azaindolyl)methyllithium salt, which as a strong nucleophile was found to react readily with either Me_3SiCl or Me_3SnCl, resulting in trimethylsilyl-bis(1-*N*-7-azaindolyl)methane (SiBAM) or trimethylstannyl-bis(1-*N*-7-azaindolyl)methane (SnBAM) in good yield. SiBAM and SnBAM have been fully characterized by NMR spectroscopy and HRMS. SiBAM has also been examined by X-ray diffraction analyses, and its molecular structure is shown in Figure 5.1.

Scheme 5.1

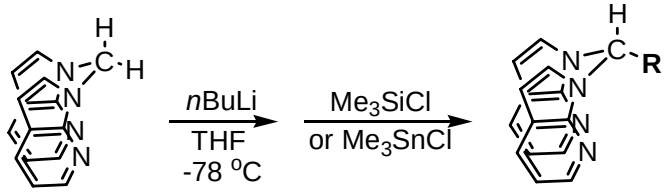

R = $SiMe_3$: **SiBAM** (55% yield)
R = $SnMe_3$: **SnBAM** (72% yield)

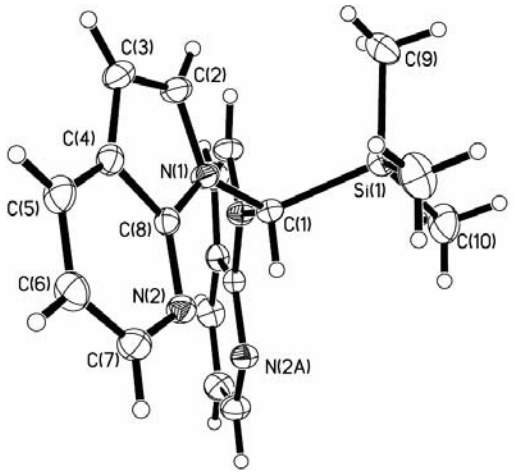

Figure 5.1 Crystal structure of compound SiBAM with 30% ellipsoids.

5.3.1.2 New propyl and butyl analogue ligands of BAM

To examine the interaction between a Pt(II) center and a longer and more flexible linker than the CH_2 group in the BAM ligand, we synthesized the propyl and butyl analogues (1,4-BABu and 1,3-BAPr) of the BAM ligand, as shown in Scheme 5.2. The syntheses of the new ligands 1,4-BABu and 1,3-BAPr were achieved in reasonable yields by nucleophilic substitution reactions of either 1,3-dibromopropane or 1,4-dibromobutane with the sodium salt of 7-azaindole generated in situ by deprotonation of 7-azaindole with NaH in DMF.

Scheme 5.2

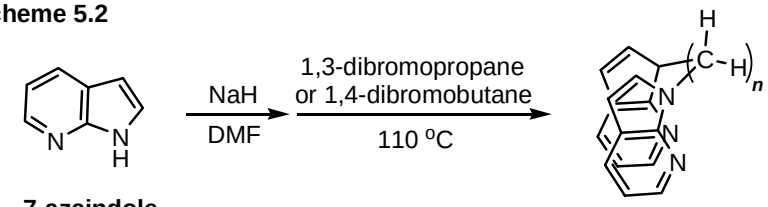

7-azaindole

n = 3 : **1,3-BAPr** (46% yield)
n = 4 : **1,4-BABu** (71% yield)

5.3.1.3 New aryl analogue ligands of BAB

To examine the impact of an aromatic linker that is larger than the phenyl group in BAB and has a donor atom, we attempted the synthesis of 6,7-bis(1-*N*-7-azaindolyl)-

1,4-dihydronaphthalene-1,4-epoxide (BAHE) using the procedure shown in Scheme 5.3. BAHE was obtained in *ca* 50% yield using the homogeneous catalysis method developed by the Buchwald group,[7] where 6,7-dibromo-1,4-dihydronaphthalene-1,4-epoxide, prepared according to literature methods,[8] and 7-azaindole were reacted in the presence of CuI, 1,10-phenanthroline, and Cs_2CO_3 in DMF at 145~150 °C under N_2 atmosphere for 72 h. The new ligand BAHE has been fully characterized. Its molecular structure determined by a signal crystal X-ray diffraction analyses is shown in Figure 5.2.

Scheme 5.3

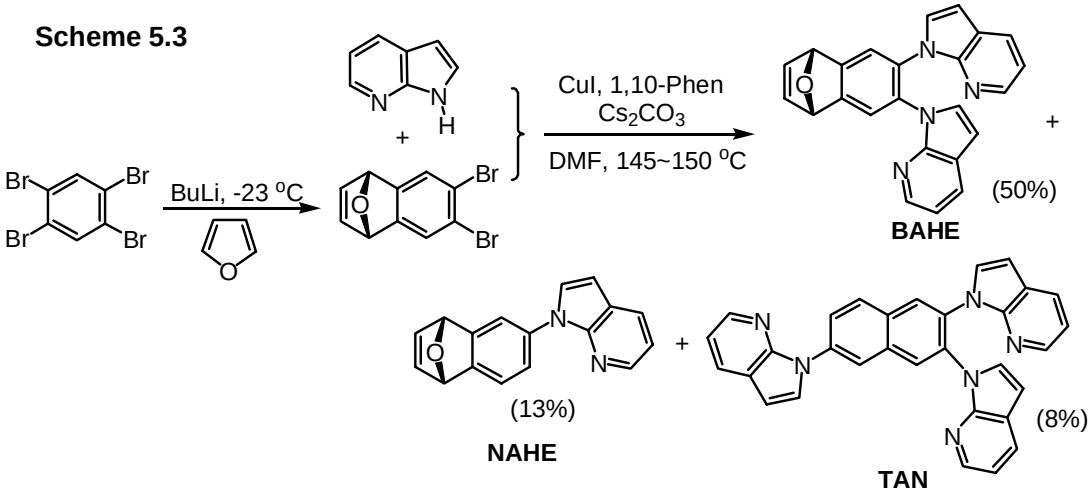

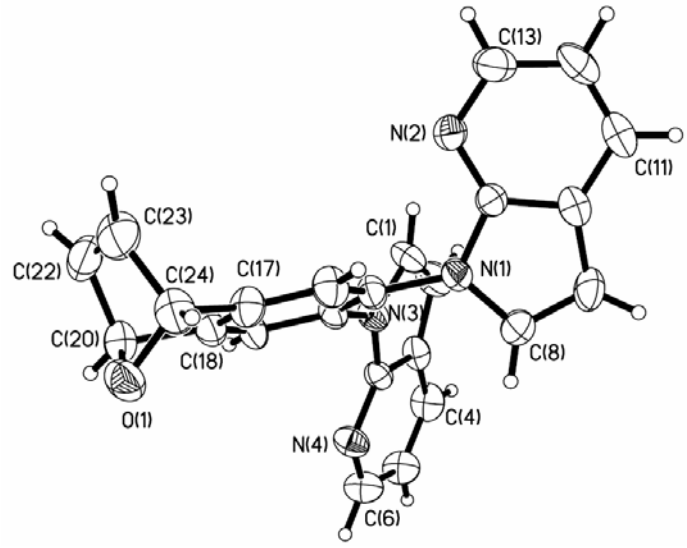

Figure 5.2 Crystal structure of compound BAHE with 30% ellipsoids.

Notably, besides BAHE, the mono-7-azaindolyl substituted debrominated product NAHE and an interesting tri-7-azaindolyl substituted naphthalene derivative compound TAN were also isolated as the side products in 13% and 8% yield, respectively (Scheme 5.3). Both side products have been fully characterized by NMR spectroscopy as well as HRMS. The formation of TAN likely occurred *via* an initial tandem nucleophilic addition initiated C=C double bond migration and the simultaneous ring-opening, and the subsequent protonation and dehydration, as illustrated in Scheme 5.4. Similar nucleophilic addition induced 1,4-dihydronaphthalene-1,4-epoxide ring opening processes have been well studied toward producing highly functionalized dihydronaphthalene products.[9]

Scheme 5.4

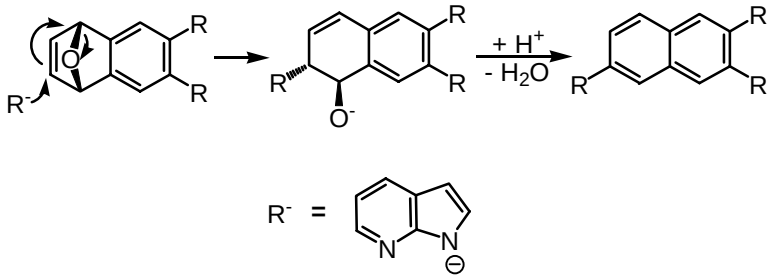

5.3.2 Syntheses of the Pt complexes and their structures

5.3.2.1 Pt complexes of SiBAM and SnBAM

The compound Pt(SiBAM)Me_2 (**5.1**) was obtained as a colorless crystalline compound in 68% yield from the reaction of the SiBAM ligand with $[PtMe_2(\mu\text{-}SMe_2)]_2$ (Scheme 5.5). It is noteworthy that the deprotonation and nucleophilic substitution reactions of the compound Pt(BAM)Me_2 (**2.2**) is not suitable for the synthesis of compound **5.1**, as revealed by deuterium labeling study. Direct deprotonation of complex

2.2 with *n*-BuLi and the subsequent quenching of the resulting lithium salt with D_2O afforded a mixture of deuterium labeled **2.2-*d*** (66% yield), as illustrated in Scheme 5.6. Interestingly, the deuterium incorporation into **2.2-*d*** occurred at both its 7-azaindolyl ring C(2) position (D, 41%) and its C***H***H' atom position (D, 59%) as established by the analyses of the ^{1}H NMR data (Figure 5.3). Despite the much higher δ value of the CH***H'*** atom (11.8 ppm) relative to those of the C***H***H' (6.09 ppm) atom and the C(2)-***H*** atom (7.48 ppm), the CH***H'*** atom remains intact after the deprotonation reaction **2.2** with *n*-BuLi (Figure 5.3). Its close proximity to the Pt(II) center and the steric blocking by the square planar Pt(II) unit may be responsible for its observed inactivity toward *n*-BuLi.

Scheme 5.5

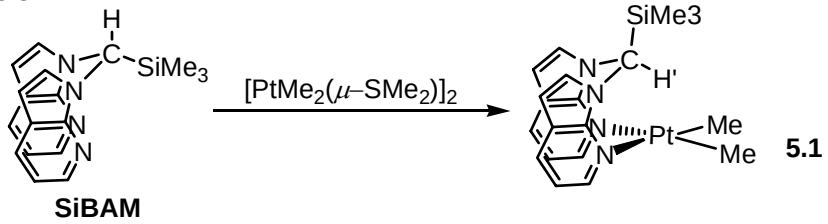

SiBAM **5.1**

Scheme 5.6

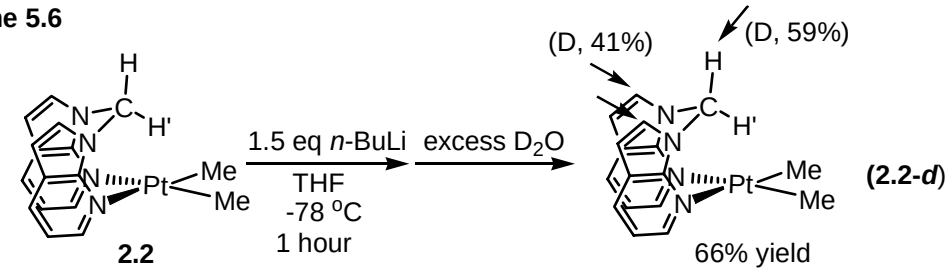

2.2 66% yield **(2.2-*d*)**

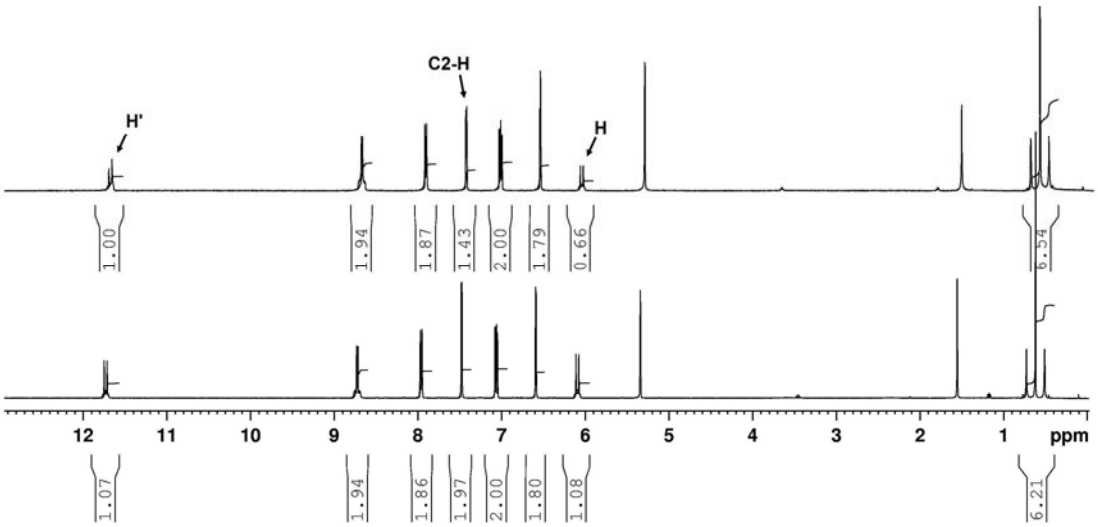

Figure 5.3 Comparison of the ^{1}H NMR spectra of **2.2** (bottom) and **2.2-*d*** (top) in CD_2Cl_2.

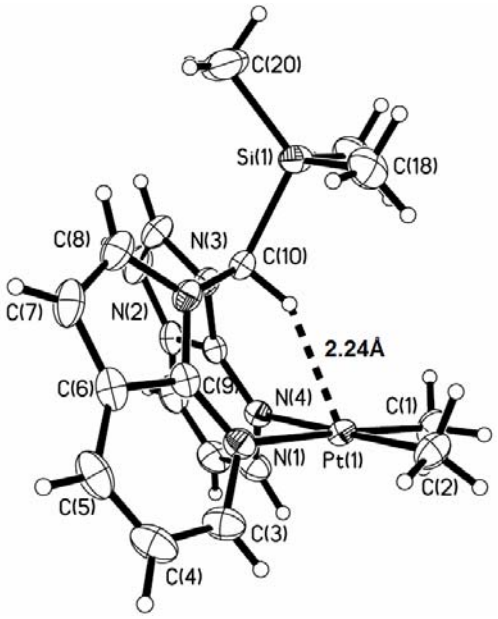

Figure 5.4 Crystal structure of **5.1** with 30% ellipsoids.

The complex **5.1** has been fully characterized and its molecular structure is shown in Figure 5.4. The Pt(II) center in **5.1** has a typical square planar geometry. To avoid strong steric interactions, the trimethylsilyl group is oriented away from the $PtMe_2$ moiety. Most remarkably, compared to the Pt···H' separation distance (2.44 Å) in compound **2.2**,[10] the Pt···H' separation distance (2.24 Å) in **5.1** is much shorter, which

can be attributed to the steric repulsion between the bulky trimethylsilyl group and the C(2)-H bonds of the two 7-azaindolyl rings. As a consequence of the short Pt···H' distance, in the ^{1}H NMR of **5.1**, the chemical shift of the H' atom shifts further downfield to 13.13 ppm relative to that (11.69 ppm) in **2.2**, an indication of a much stronger three-center four-electron Pt···H'-C interaction in **5.1**.[11] Despite the presence of the steric repulsion, compound **5.1** has a fairly good thermal stability, as supported by the fact that heating the C_6D_6 solution of **5.1** at 80 ^oC over 10 hours did not result in any obvious change of its ^{1}H NMR spectrum.

Scheme 5.7

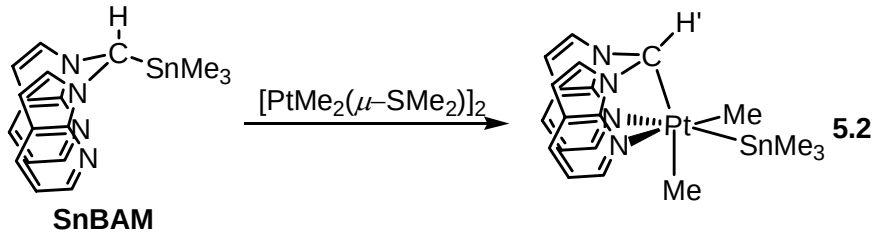

SnBAM

The synthesis of the compound Pt(SnBAM)Me_2, an analogue of **5.1**, was also attempted using the reaction of the SnBAM ligand with [$PtMe_2$(μ-SMe_2)]$_2$ in Et_2O. However, instead of isolating the Pt(SnBAM)Me_2 complex, an interesting Pt^{IV} complex Pt(N,C,N-BAM)($SnMe_3$)Me_2 (**5.2**), where the C_{BAM}-Sn bond has been broken and *cis* oxidatively added to the Pt center, was isolated, as illustrated in Scheme 5.7.

^{1}H NMR examination of the reaction of the SnBAM ligand with [$PtMe_2$(μ-SMe_2)]$_2$ in CD_2Cl_2 showed the formation of the Pt(SnBAM)Me_2 complex in the early stage of the reaction, as shown in Figure 5.5 and Chart 5.2, along with the formation of both **5.2** and $PtMe_2(SMe_2)_2$. Despite the gradual transformation of Pt(SnBAM)Me_2 into **5.2** over time (Figure 5.5), no evidence for the direct conversion of Pt(SnBAM)Me_2 to **5.2** has been obtained.

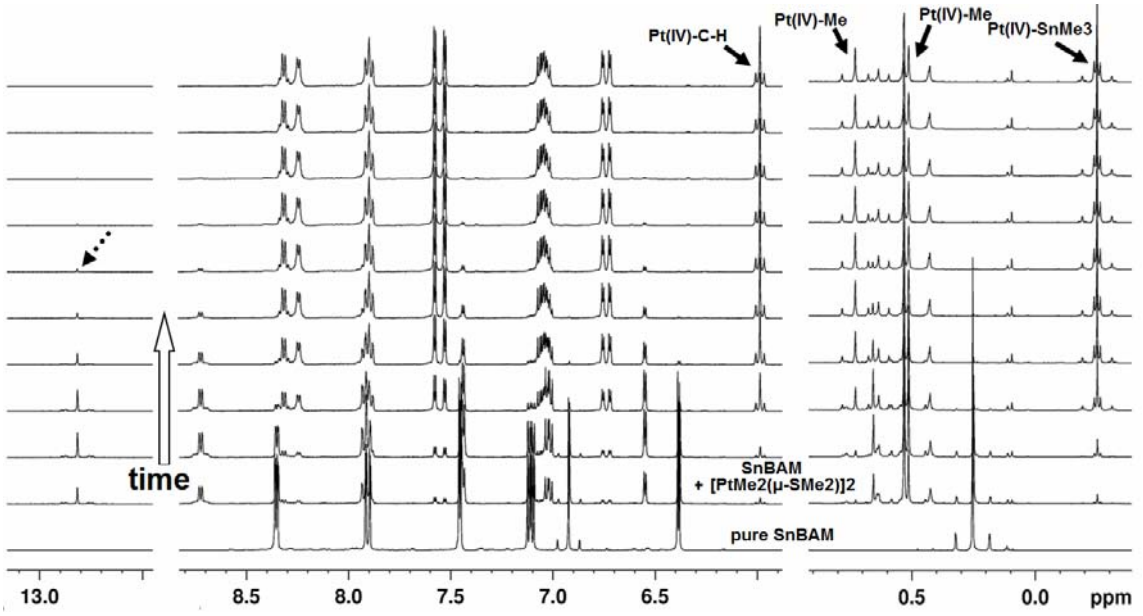

Figure 5.5 Selected ^{1}H NMR regions for the reaction of SnBAM with $[PtMe_2(\mu\text{-}SMe_2)]_2$ in CD_2Cl_2 at room temperature.

Chart 5.2

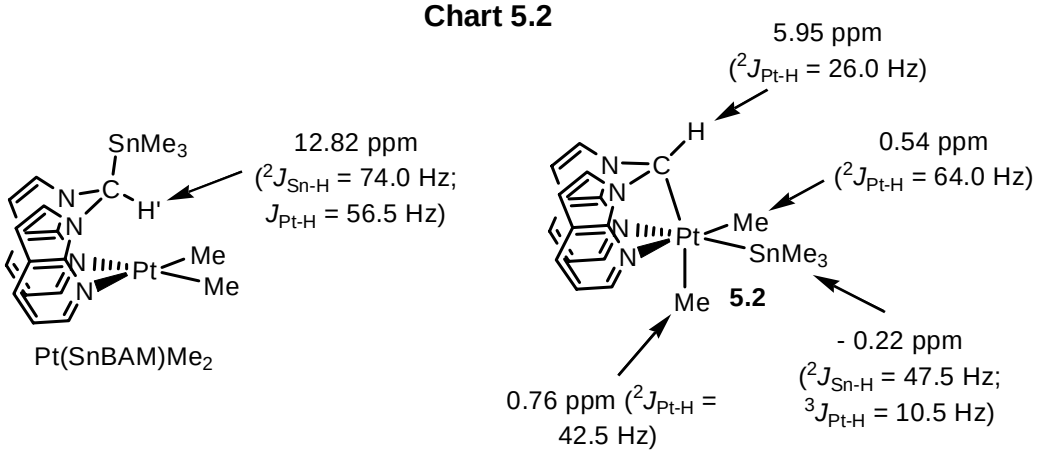

The δ values of the diagnostic ^{1}H NMR signals for both $Pt(SnBAM)Me_2$ and **5.2** are illustrated in Chart 5.2. Notably, these NMR data clearly indicate the absence of symmetry in **5.2**, consistent with the $SnMe_3$ ligand in **5.2** at the basal plane instead of the axial position (Chart 5.2). Besides the observation of the two sets of Pt-*Me* signals, the lack of symmetry in **5.2** is further confirmed by the observation of two sets of 7-azaindolyl signals in the ^{1}H NMR spectrum (the top spectrum in Figure 5.5). Although the intermolecular oxidative addition of Sn(IV) halides to electronic rich Pt(II) centers is

a well-established phenomenon,[12] tetraalkyltin compounds are usually not reactive under the same conditions. The lack of precedent examples of tetraalkyltin oxidative addition to a Pt(II) center under mild conditions warrants the additional efforts on the mechanistic study of the formation of **5.2** in the future.

5.3.2.2 Pt(II) complexes of 1,3-BAPr and 1,4-BABu

For the 1,3-BAPr or 1,4-BABu ligands, their N,N-chelating Pt(II) complexes are anticipated to have poor stabilities due to the considerably enlarged chelate rings. Considering the fact that $PtPh_2$ complexes usually exhibit a much higher stability than their $PtMe_2$ analogues, the syntheses of the $PtPh_2$ complexes of 1,3-BAPr or 1,4-BABu were first attempted. The monomeric $PtPh_2$ complexes Pt(1,3-BAPr)Ph_2 (**5.3**) and Pt(1,3-BABu)Ph_2 (**5.4**) were obtained as stable yellow crystalline solids in good yields by ligand displacement of the bridging SMe_2 in $[PtPh_2(\mu\text{-}SMe_2)]_n$ (n = 2, 3) with either 1,3-BAPr or 1,4-BABu with a 1:1 [Pt]/[L] ratio in THF at ambient temperature, as shown in Scheme 5.8. Interestingly, when the reaction was carried out with a Pt/1,3-BAPr ratio as 2:1, a dinuclear complex Pt_2(1,3-BAPr)$Ph_4(SMe_2)_2$ (**5.5**) was isolated. After placing the CH_2Cl_2 solution of **5.5** inside an ultrasonicator, it was quickly converted to **5.3** *via* the elimination of one equivalent of $PtPh_2(SMe_2)_2$, an indication that for the reaction of 1,3-BAPr with $[PtPh_2(\mu\text{-}SMe_2)]_n$ (n = 2, 3), compound **5.3** is thermodynamically favored while compound **5.5** is kinetically favored.

Scheme 5.8[a]

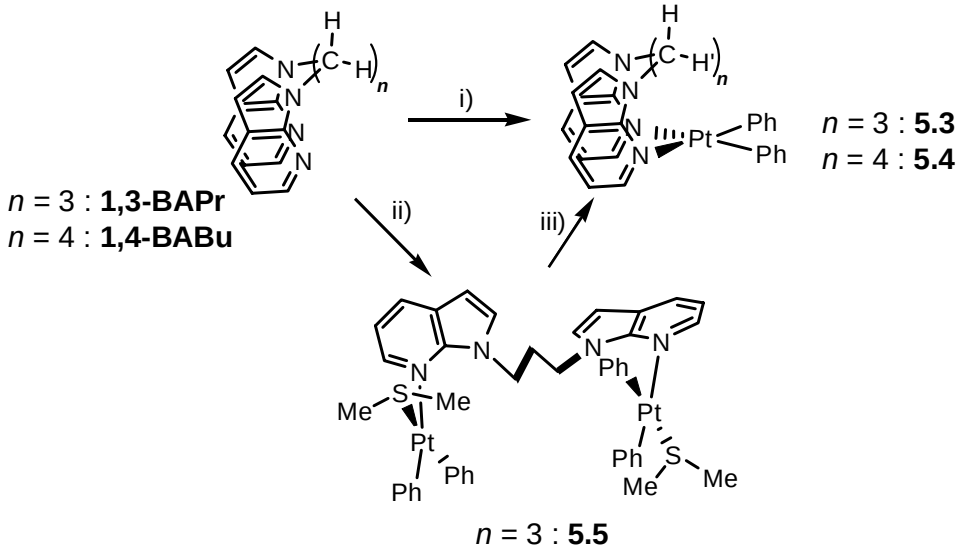

[a] *Reagents and conditions:* i) $[PtPh_2(\mu\text{-}SMe_2)_n]$ (*n* = 2, 3), THF, rt, overnight ([Pt]:[L] = 1:1); ii) $[PtPh_2(\mu\text{-}SMe_2)_n]$ (*n* = 2, 3), rt, overnight, ([Pt]:[L] = 2:1); iv) Sonication, CH_2Cl_2, rt.

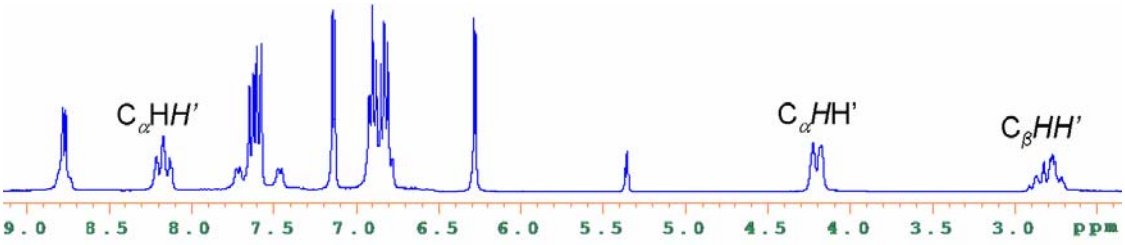

Figure 5.6 ^{1}H NMR spectrum of **5.3** in CD_2Cl_2 at ambient temperature.

The $PtPh_2$ complexes **5.3**-**5.5** have all been fully characterized. In the ^{1}H NMR spectra, the hydrogen atoms on each methylene group of these compounds display typical "AB" patterns. Again one prominent feature is the consistent δ downfield shift (from ~4.3 to ~8.1 ppm) for the H' atoms on the α-methylene carbon, as illustrated by the ^{1}H NMR spectrum of compound **5.3** in Figure 5.6. This downfield shift is also caused by the presence of the three-center four-electron Pt···H'-C interactions, despite that this shift is not as pronounced as those observed for **5.1** and **2.2**.

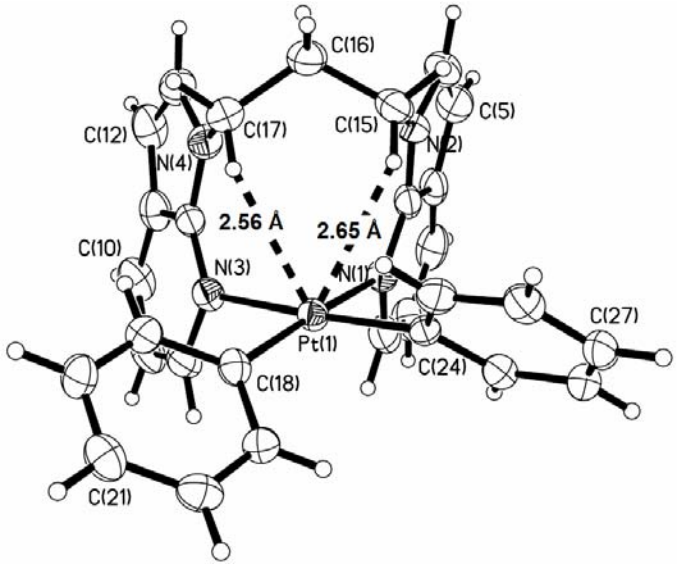

Figure 5.7 Crystal structure of **5.3** with 30% ellipsoids.

The molecular structures of **5.3-5.5** are shown in Figures 5.7-5.9, respectively. Both **5.3** and **5.4** are mononuclear with their ligands adopting the N,N-chelating mode, whereas **5.5** is dinuclear with 1,3-BAPr acting as a bridging ligand. The Pt(II) centers in all three complexes adopt a typical square planar geometry, with the PtPh_2 being consistently *cis* to each other. Consistent with the "AB" pattern of the ^{1}H NMR signals are the evidently different environments for the two hydrogen atoms on each methylene carbons. The fifth coordination sites of all the Pt(II) centers are capped by the propyl or the butyl linker group. The shortest Pt···H' separation distances in **5.3-5.5** are 2.56 Å, 2.58 Å, and 2.30 Å, respectively, as shown by Figures 5.7-5.9. Notably, the N-Pt-N angle in **5.3** is 78.58^o, considerably off the ideal 90^o angle for a square planar configuration, suggesting the existence of a high chelate ring strain. The N-Pt-N angle in **5.4** is ~82^o, also distorted from 90° but obviously to a less extent.

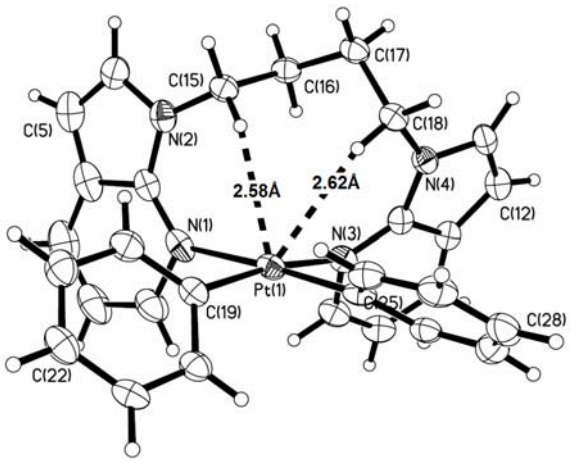

Figure 5.8 Crystal structure of **5.4** with 30% ellipsoids.

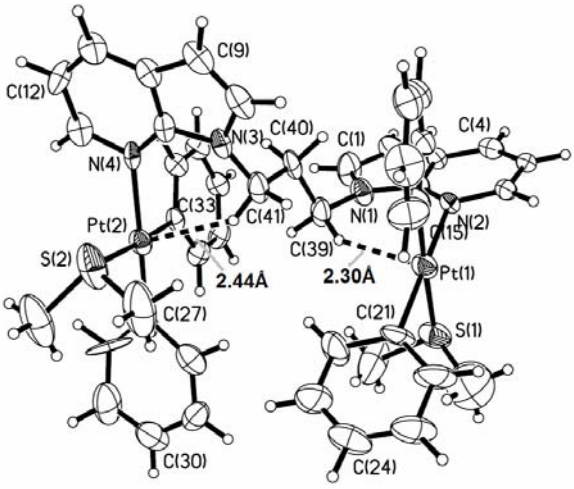

Figure 5.9 Crystal structure of **5.5** with 30% ellipsoids.

Efforts were also made to obtain the N,N-chelating $Pt^{II}Me_2$ complexes of 1,3-BAPr and 1,4-BABu. The ligand displacement reactions of $[PtMe_2(\mu\text{-}SMe_2)_2]$ with both 1,3-BAPr and 1,4-BABu were found to be slow, and the desired compounds **5.6** and **5.7** were estimated to be only 40~60% yields after 2 days. Moreover, **5.6** and **5.7** both displayed a poor stability, and their decomposition occurred quickly in solution during the course of purification, making it difficult to isolate the pure compounds. The instability of **5.6** and **5.7** is likely caused by the chelate ring strains as observed in their $Pt^{II}Ph_2$ analogues **5.3** and **5.4**. Fortunately, crystals of both **5.6** and **5.7** have been obtained

by cooling their Et_2O/hexanes (1:1) solutions, thereby allowing unambiguous examination of their molecular structures (Figure 5.10). The structures of **5.6** and **5.7** resemble their $PtPh_2$ analogues **5.3** and **5.4**. The average Pt···H'(α-CH*H'*) separation distances in **5.6** and **5.7** are shorter than those of **5.3** and **5.4**, due to reduced steric interactions. However, the instability of **5.6** and **5.7** in solution precluded further investigation of these two complexes.

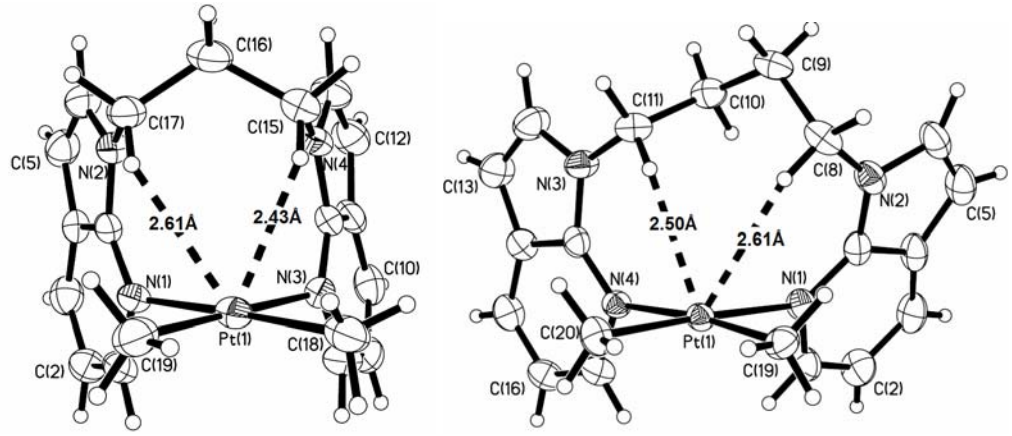

Figure 5.10 Crystal structures of **5.6** (left) and **5.7** (right) with 30% ellipsoids.

5.3.2.3 Pt(II) complexes of BAHE

For the new BAB analogue BAHE, its Pt^{II} complexes can display two different structural isomers **A** and **B**, depending on the orientation of the epoxy group, as illustrated in Chart 5.3. Thus, our initial efforts were to determine which isomer is more favorable for the N,N-chelating $PtPh_2$ complex Pt(BAHE)Ph_2 (**5.8**). The ligand displacement reaction of $[PtPh_2(\mu\text{-}SMe_2)]_n$ (n = 2, 3) with BAHE and a 1:1 [Pt]/[L] ratio in THF at ambient temperature afforded **5.8** in ~ 50% as a brown solid. The ^{1}H NMR spectral examination revealed that compound **5.8** exists in both **A** and **B** forms. Attempts

to obtain single crystals of either isomer of **5.8** for X-ray diffraction analyses have not been successful. The synthesis of the $PtMe_2$ analogue has not yet been accomplished.

Chart 5.3

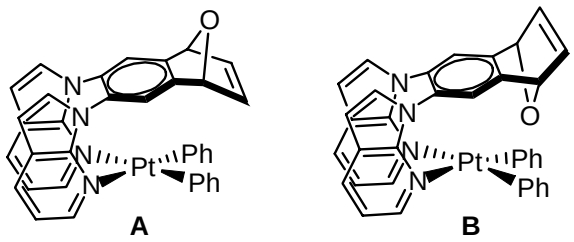

5.3.3 Reactivities of 5.1 toward MeI, $MeOSO_2CF_3$ and I_2

In Chapter 4, complex Pt(BAB)Me_2 (**2.1**) and Pt(BAM)Me_2 (**2.2**) were shown to react readily with MeI at room temperature, but instead of forming the desired N,N-chelating Pt^{IV} complex, the reaction produced the tetrameric complex $[PtMe_3I]_4$ quantitatively. In contrast to MeI, the reaction of MeOTf with complex **2.1** afforded quantitatively the five-coordinate $PtMe_3$ complex **4.1**.

To determine if Pt(SiBAM)Me_2 (**5.1**) displays the same behavior as **2.1** toward both MeI and MeOTf, we carried out a similar ^{1}H NMR study as performed for **2.1** described in Chapter 4. We have found that upon the addition of MeI, complex **5.1** quickly produced the tetrameric complex $[PtMe_3I]_4$ quantitatively, a behavior similar to that of **2.1**. This indicates that the binding of the SiBAM ligand to the $Pt^{IV}Me_3$ moiety is also weak and cannot compete with the iodide binding. As shown in Figure 5.11, the addition of MeOTf to the CD_2Cl_2 solution of **5.1** converted **5.1** quantitatively to the five-coordinate $Pt^{IV}Me_3$ compound [Pt(SiBAM)Me_3][OTf] (**5.9**) (Scheme 5.9). This conversion resulted in a dramatic δ change for the H' atom from the original 13.13 ppm in **5.1** to 5.00 ppm in **5.9** (Figure 5.11 and Scheme 5.9), which is caused by the change of

the nature of the Pt···H'-C interaction from the original "three-center four-electron" interaction in **5.1** to the "three-center two-electron" interaction in **5.9**, as observed in the five-coordinate BAM-$Pt^{IV}Me_3$ species described in Chapter 4. Consistent with the $Pt^{II} \rightarrow Pt^{IV}$ oxidation state change is the δ downfield shift (0.67 ppm → 1.79 ppm) of the Pt-Me signal.

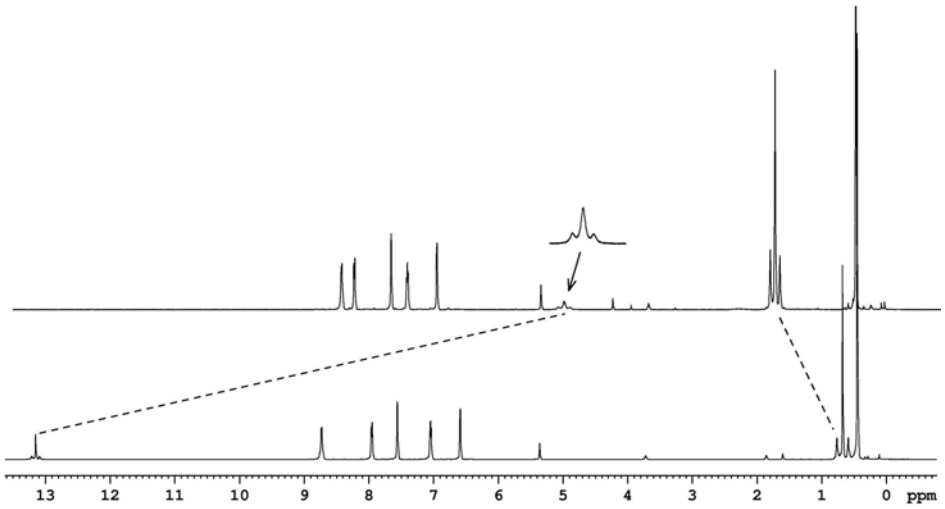

Figure 5.11 Stacked ^{1}H NMR spectra for complex **5.1** (bottom) and complex **5.9** (top), generated in situ by the addition of 1.05 equivalent of MeOTf to **5.1**, in CD_2Cl_2 at ambient temperature.

Scheme 5.9

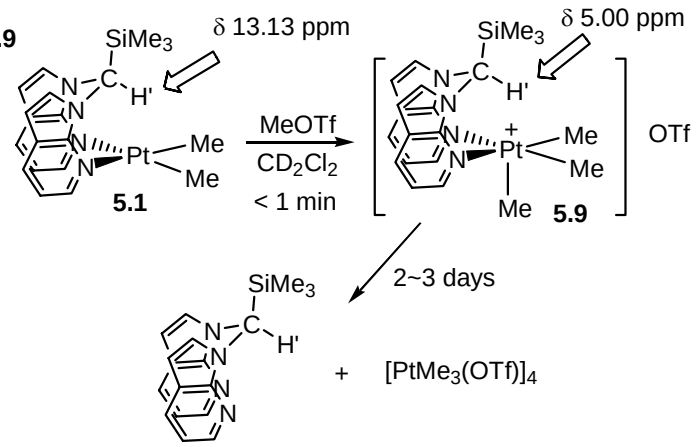

Notably, in the ^{1}H NMR spectrum (Figure 5.11), compound **5.9** only displays one well-defined Pt-*Me* peak, indicating the presence of a rapid methyl exchange process for **5.9** in solution, which is again consistent with the behaviors of the BAM-$Pt^{IV}Me_3$

compounds **4.2** and **4.3** described in Chapter 4. In contrast to [Pt(BAM)Me_3(OTf)] (**4.2**), however, the new *fac*-$Pt^{IV}Me_3$ complex **5.9** was found thermodynamically unstable at ambient temperature. It slowly degraded into the tetrameric complex [$PtMe_3$(OTf)]$_4$ *via* releasing the free SiBAM ligand in CD_2Cl_2 (Scheme 5.9). The complete degradation took 2~3 days at ambient temperature as revealed by ^{1}H NMR experiments. This is likely the cause for the unsuccessful attempt in synthesizing [Pt(SiBAM)Me_3][OTf] directly by the ligand displacement reaction of the tetrameric complex [$PtMe_3$(OTf)]$_4$ with the SiBAM ligand. Compared with **4.2**, the instability of [Pt(SiBAM)Me_3][OTf] is likely attributable to the steric repulsion imposed by the bulky $SiMe_3$ moiety, as supported by the crystal structure of compound **5.1** (Figure 5.4).

Recently, considerable efforts have been taken toward the understanding of competing C-C and C-X (X = halogen atoms) reductive elimination processes by studying the $Pt^{IV}(I)_2(R)_2$ complexes (R = alkyl, aryl).[13] The $Pt^{IV}(I)_2(R)_2$ complexes were prepared mostly by the S_N2 oxidative addition reactions of I_2 to the corresponding $Pt^{II}(R)_2$ complexes. However, compound **5.1** showed different behaviors when its reaction with I_2 was studied. The reaction of one equivalent of I_2 with **5.1** in a CD_2Cl_2 solution resulted in several species, identified by ^{1}H NMR spectroscopy to be Pt(SiBAM)I_2 (**5.10**), MeI, [$PtMe_3I$]$_4$ and the free SiBAM ligand, respectively (Figure 5.12). The evaporation of the CD_2Cl_2 solution resulted in yellow crystals, which have been analyzed by signal-crystal X-ray diffraction analyses. The crystal structure contains the molecules of both **5.10** and [$PtMe_3I$]$_4$ (in a 4:1 ratio), as shown in Figure 5.13, thus unambiguously confirming their formation. The structure of **5.10** resembles that of **5.1**. The Pt···H' separation distance is 2.20 Å.

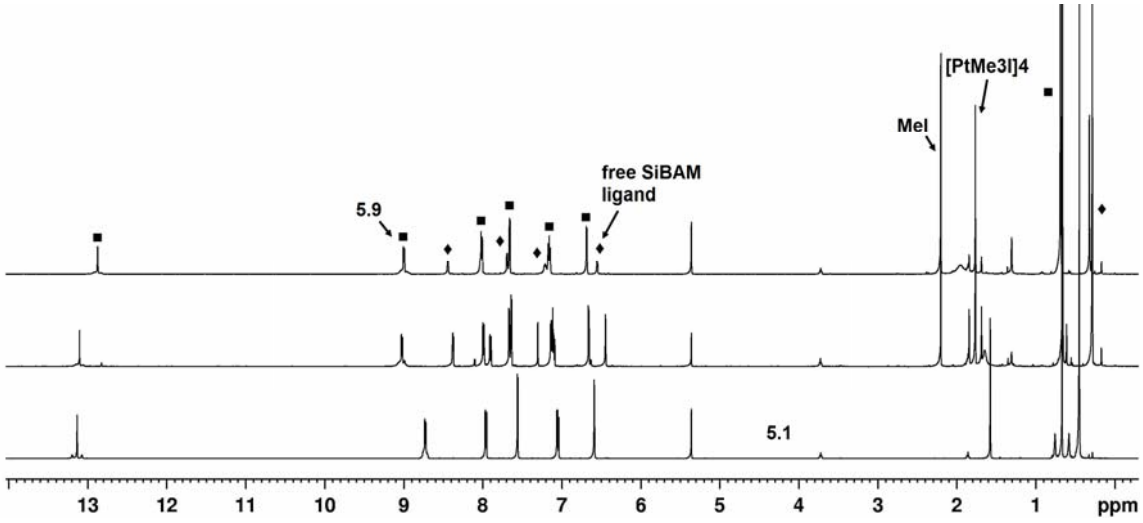

Figure 5.12 The stacked ^{1}H NMR spectra for complex **5.1** before (bottom) and after the addition of one equivalent of I_2 for 5 hours (middle) and 2 days (top) in CD_2Cl_2 at ambient temperature.

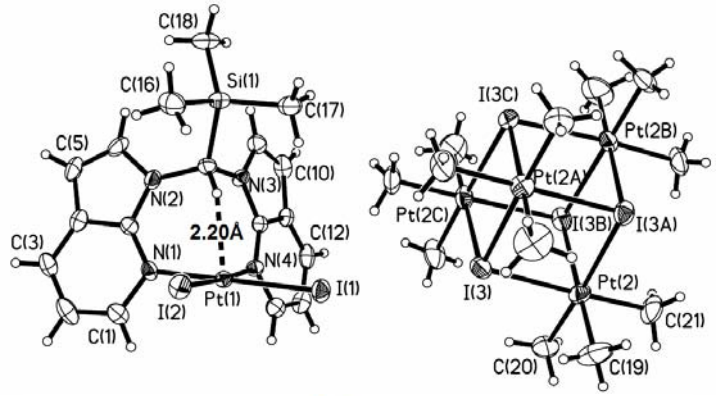

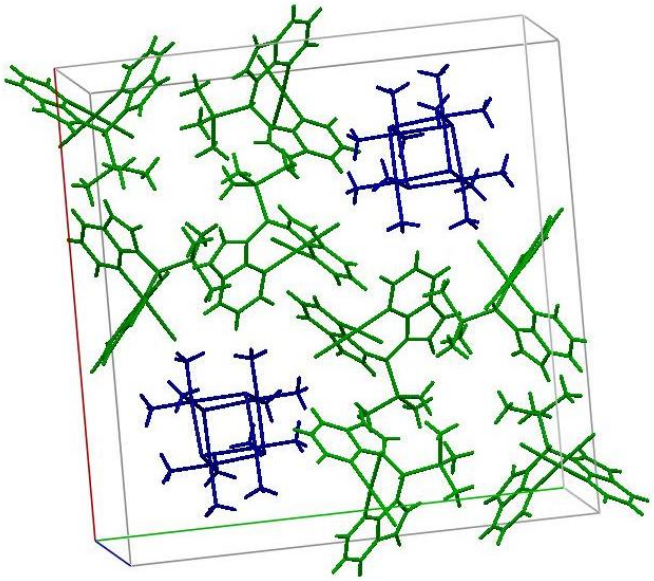

Figure 5.13 Diagrams showing the crystal structures of **5.9** (top left) and $[PtMe_3I]_4$ (top right) with 30% ellipsoids and their coexistence in the unit cell (bottom).

Moreover, increasing the relative amount of I_2 to **5.1** in CD_2Cl_2 up to three equivalents did not cause any obvious difference, again yielding a mixture containing Pt(SiBAM)I_2 (**5.10**), MeI, $[PtMe_3I]_4$, and the free SiBAM ligand, in addition to the I_2 unconsumed. The evaporation of the CD_2Cl_2 solution result in deep red crystals, which were revealed by signal-crystal X-ray diffraction analyses to be the cocrystallized product of **5.10** with both I_2 and CH_2Cl_2 molecules, as shown in Figure 5.14.

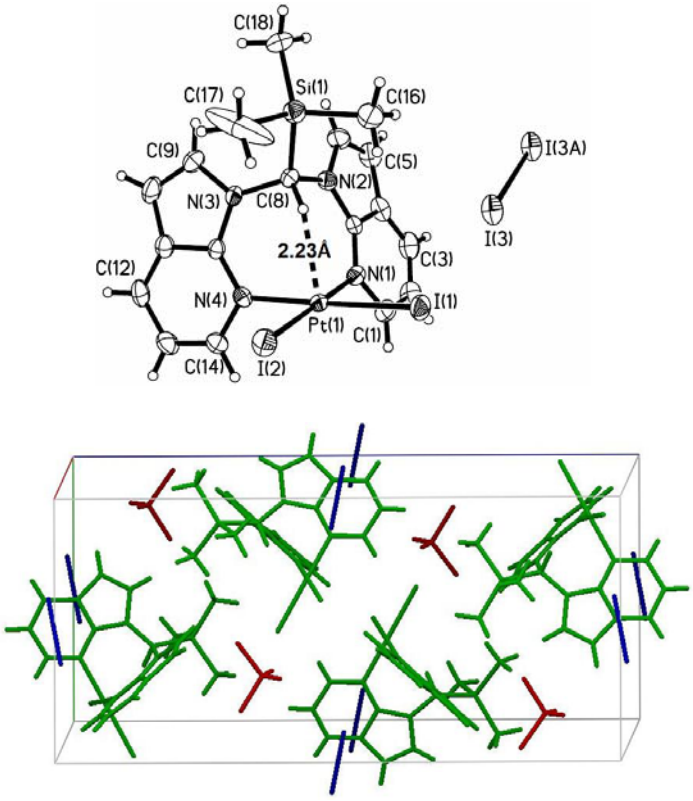

Figure 5.14 Diagrams showing the crystal structure of **5.10·I_2** and the unit cell. The CH_2Cl_2 molecules are omitted for clarity.

The different reactivity of compound **5.1** with I_2 may be explained by the processes shown in Scheme 5.10. The initial S_N2 oxidative addition of I_2 to compound **5.1** generates a Pt^{IV} intermediate **A**, which eliminates MeI *via* a nucleophilic substitution reaction between I^- and one Pt-methyl bond (not MeI reductive elimination), resulting in a Pt^{II}(Me)(I) complex. This Pt^{II}(Me)(I) complex further reacts with I_2 through a similar

process, *via* the formation of a Pt^{IV} intermediate **B**, leading to the eventual formation of $Pt(SiBAM)I_2$ and another MeI molecule. As shown by the above ^1H NMR study, compound **5.1** can react very quickly with MeI. Accordingly, the MeI generated competes with I_2 toward the reaction with compound **5.1** and produces the *fac*-$Pt^{IV}Me_3$ intermediate **A'**, which leads to the formation of $[PtMe_3I]_4$ and free SiBAM. The different behaviors of the Pt^{IV} intermediates **A** and **B** compared to the Pt^{IV} intermediate **A'** are likely caused by the different electronic properties of their Pt^{IV} centers. The relative electron-deficiency of the Pt^{IV} centers of **A** and **B** can promote the formation of MeI, whereas the electron-richness of the Pt^{IV} center in **A'** will likely favor the ligand dissociation to a greater degree.

Scheme 5.10

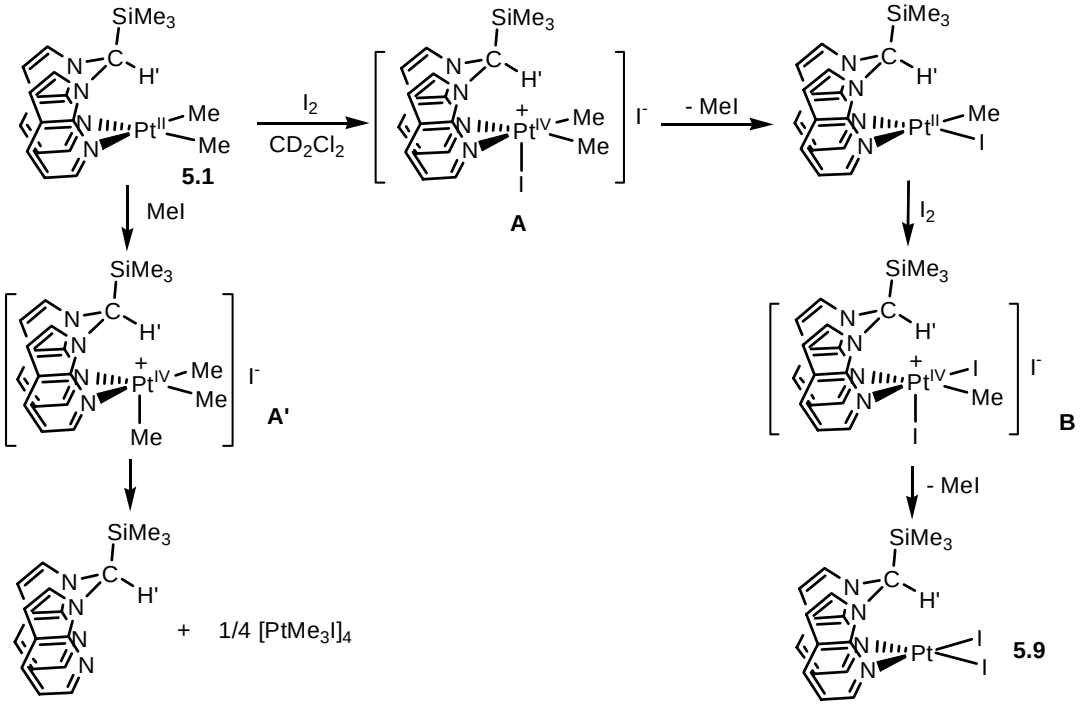

The reactivity investigation of the other Pt(II) compounds described in this chapter has not been carried out, but the interesting results presented above warrant the continuing efforts on this project.

5.4 Conclusions

In this chapter, the syntheses of several new 7-azaindolyl derivative ligands SiBAM, SnBAM, 1,3-BAPr, 1,4-BABu and BAHE, *via* either modifying or altering the BAM and BAB bridging groups, have been achieved. These new ligands can act as N,N-chelating ligands to form the corresponding Pt(II) complexes. The $PtMe_2$ complexes of the SiBAM, SnBAM 1,3-BAPr and 1,4-BABu ligands exhibit reduced stabilities, compared with their BAM analogue, due to the increased chelate ring strains, as established by NMR and X-ray diffraction analyses. The preliminary results for the reaction of SnBAM with $[PtMe_2(\mu\text{-}SMe_2)]_2$ indicate the formation of a Pt^{IV} compound **5.2**, in which the C_{BAM}-Sn bond has been broken and *cis* oxidatively added to the Pt center. Continued study on the Pt(II) complexes of the BAHE ligand is needed.

The reactivities of the SiBAM $PtMe_2$ complex **5.1** toward MeI, MeOTf and I_2 have been investigated. While the S_N2 oxidative addition of MeI with **5.1** quickly generates $[PtMe_3I]_4$ by releasing free the SiBAM ligand, the S_N2 oxidative addition of MeOTf with **5.1** generates in solution a five-coordinate *fac*-$Pt^{IV}Me_3$ compound **5.9**, which slowly degrades into $[PtMe_3(OTf)]_4$ by releasing the free SiBAM ligand. Compound **5.1** reacts with I_2 in a different manner, producing a $Pt^{II}I_2$ compound **5.10**, MeI, the free SiBAM ligand and $[PtMe_3I]_4$. The reactivity difference displayed by compound **5.1** towards CH_3I and I_2 may be attributed to the electronic difference of the Pt^{IV} centers in the intermediates involved.

References

1. a) Zhao, S.-B; Wu, G.; Wang, S. *Organometallics* **2006**, *25*, 5979. b) Zhao, S.-B.; Song, D; Jia, W.-L.; Wang, S. *Organometallics* **2005***, 24,* 3290.
2. Johansson, L.; Ryan, O. B.; Rømming, C.; Tilset, M. *J. Am. Chem. Soc*. **2001**, *123*, 6579.
3. a) Konze, W. V.; Scott, B. L.; Kubas, G. J. *J. Am. Chem. Soc.* **2002**, *124*, 12550. b) Thomas, J. C.; Peters, J. C. *J. Am. Chem. Soc.* **2003**, *125*, 8870. c) Thomas, C. M.; Peters, J. C. *Organometallics* **2005***, 24,* 5858.
4. a) Song, D.; Jia, W.-L.; Wang, S. *Organometallics* **2004**, *23*, 1194. b) Song, D.; Sliwowski, K.; Pang, J.; Wang, S. *Organometallics* **2002**, *21*, 4978.
5. Song, D.; Wang, S. *J. Organomet. Chem.* **2002**, *648*, 302-305.
6. Scott, J. D.; Puddephatt, R. J. *Organometallics* **1983**, *2*, 1643.
7. a) Kiyomori, A.; Marcoux, J. F.; Buchwald, S. L. *Tetrahedron Lett.* **1999**, *40*, 2657. c) Klapars, A.; Antilla, J. C.; Huang, X. H.; Buchwald, S. L. *J. Am. Chem. Soc.* **2001**, *123*, 7727. d) Klapars, A.; Huang, X.; Buchwald, S. L. *J. Am. Chem. Soc.* **2002**, *124*, 7421. e) Antilla, J. C.; Klapars, A.; Buchwald, S. L. *J. Am. Chem. Soc.* **2002**, *124*, 11684. f) Job, G. E.; Buchwald, S. L. *Org. Lett.* **2002**, *4*, 3703.
8. Hart, H.; Bashir-Hashemi, A.; Luo, J.; Meador, M. A. *Tetrahedron* **1986**, *42*. 1641.
9. a) Lautens, M.; Fagnou, K.; Yang, D. *J. Am. Chem. Soc.* **2003**, *125*, 14884. b) Fagnou, K.; Lautens, M. *Chem. Rev.* **2003**, *103*, 169.
10. Song, D.; Wang, S. *Organometallics* **2003***, 22,* 2187.

11. a) Albinati, A.; Anklin, C. G.; Ganazzoli, F.; Ruegg, H.; Pregosin, P. S. *Inorg. Chem.* **1987**, *26*, 503. b) Albinati, A.; Arz, C.; Pregosin, P. S. *Inorg. Chem.* **1987**, *26*, 508. c) Albinati, A.; Pregosin, P. S.; Wombacher, F. *Inorg. Chem.* **1990**, *29*, 1812.
12. Janzen, M. C.; Jennings, M. C.; Puddephatt, R. J. *Organometallics* **2001**, *20*, 4100 and references therein.
13. Yahav-Levi, A.; Goldberg, I.; Vigalok, A.; Vedernikov, A. N. *J. Am. Chem. Soc.* **2008**, *130*, 724 and the references therein.

Chapter 6

Ambient Temperature MLCT Phosphorescence Facilitated by Triarylboron: BNPA and Its Metal Complexes

6.1 Introduction

In Chapters **2-4**, the reactivities of several organoplatinum complexes containing 7-azaindolyl derivative ligands toward C-H activation have been investigated. Another important aspect of organoplatinum complexes is their versatile applications in materials sciences particularly as phosphorescent emitters in organic light emitting diodes (OLEDs).[1] Phosphorescent metal complexes are very attractive as emitters for OLEDs because they allow the substantial enhancement of OLED device efficiencies.[2,3] Furthermore, phosphorescent metal complexes are also very useful as sensors for triplet state quenchers such as oxygen,[4] and are readily color-tunable *via* metal ions.

Previously our group has investigated a series of Pt(II) and Cu(I) complexes that contain 7-azaindolyl derivative ligands with the aim to use them as phosphorescent emitters in OLEDs. However, it turned out that most of these earlier compounds do not display ambient temperature phosphorescence.[5] During our investigation of Pt(II) complexes with the NPA ligand (Chapter 3), we have observed that the complex $Pt(NPA)Ph_2$ (**3.3**) displays weak ambient temperature phosphorescence in both the solid state and the solution. The emission band of **3.3** has distinct vibrational features that support a ligand-centered (LC) triplet state emission. To further understand and exploit this phenomenon, the modification of the NPA ligand and the syntheses of their metal complexes were carried out.

Chart 6.1

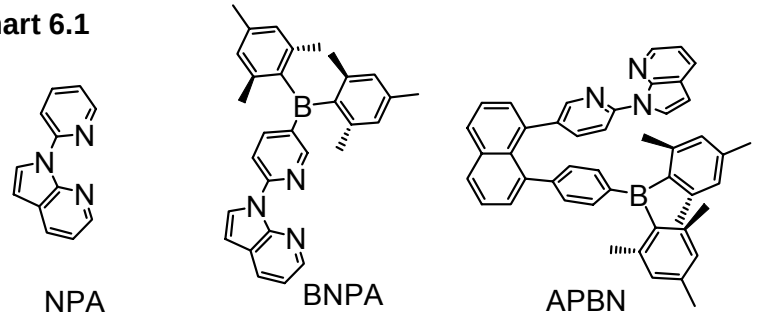

Two new ligands, 1-*N*-(5'-(dimesitylboron)pyridine-2-yl)-7-azaindole (BNPA) and 1-{2-(1-*N*-7-azaindolyl)pyridine-5-yl}-8-{p-dimesitylborylphenyl}-naphthalene (APBN), that both incorporate a triarylboron moiety have been developed. Their structures are shown in Chart 6.1. These two molecules are found to emit bright blue fluorescence. The incorporation of a triarylboron moiety into the NPA ligand is based on the following considerations. First, luminescent triarylboron compounds have versatile applications in material sciences, for example, as chemical sensors for anions such as F^- or CN^-,[6] as emitters or electron transport materials in OLEDs,[7] or as nonlinear optical materials in photonic devices.[8] From these perspectives, the new ligands on their own are very interesting. Second, the aforementioned applications of triarylboron compounds all stem from the electron accepting ability of the empty $2p_\pi$ orbital on the three-coordinate boron center. Thus, one of the themes in developing new triarylboron based materials is to tune/enhance the electron accepting ability of triarylboron compounds.[6h] Therefore, triarylboron compounds that have chelate sites are highly desirable, given the possibility of enhancing electron accepting ability of the boron center *via* the metal chelation. Third, phosphorescent metal complexes that contain triarylboron groups are still rare, and only a few complexes have been reported to display weak phosphorescence. The combination of

a triarylboron group and the N,N-chelate sites in the BNPA and APBN molecules potentially allows us to obtain bright phosphorescent metal complexes.

For comparison purposes, the photophysical properties of NPA and the two derivative ligands BNPA and APBN as well as a series of their Pt(II) and Cu(I) complexes were investigated. The choice of Cu(I) metal ions, in addition to the Pt(II) ion, is based on the fact that a number of Cu(I) complexes with N,N-chelate ligands have been shown to be promising phosphorescent emitters in OLEDs.[9] We have found that Cu(I) and Pt(II) complexes of BNPA with appropriate ancillary ligands display bright room temperature phosphorescence in solution and solid state. The detailed syntheses, structural characterizations and luminescent properties of these compounds are presented in this chapter.

6.2 Experimental Section

6.2.1 General Procedures

All reactions were performed under N_2 with standard Schlenk techniques unless otherwise noted. All starting materials were purchased from Aldrich Chemical Co. and used without further purification. DMF, THF, Et_2O, and hexanes were purified using the solvent purification system (Innovation Technology, Inc.). CH_2Cl_2 was freshly distilled over P_2O_5 prior to use. Deuterated solvents (Cambridge Isotopes) were used as received without further drying. NMR spectra were recorded on Bruker Avance 400 or 500 MHz spectrometers. High resolution mass spectra (HRMS) were obtained from a Waters/Micromass GC-TOF EI-MS spectrometer which was internally calibrated before use. Cyclic voltammetry was performed using a BAS CV-50W analyzer with a scan rate

of 500 mV/s to 4 V/s and a typical concentration of 5 mg of the compounds in 3.0 mL of DMF using 0.10 M tetrabutylammonium hexafluorophosphate (TBAP) as the supporting electrolyte. The electrolytic cell used was a conventional three-compartment cell, in which a Pt working electrode, a Pt auxiliary electrode, and a Ag/AgCl reference electrode were employed. The ferrocenium/ferrocene couple was used as the internal standard ($E^{1/2}$ = 0.55 V). UV-Vis spectra were recorded on a Varian Cary-3 UV-Visible spectrometer. Excitation and emission spectra were recorded on a Photon Technologies International QuantaMaster model C-60 spectrometer. Emission lifetimes were measured on a Photon Technologies International Phosphorescent spectrometer (Time-Master C-631F) equipped with a xenon flash lamp and digital emission photon multiplier tube using a band pathway of 5 nm for excitation and 2 nm for emission.

The NPA ligand was synthesized by our previously reported procedure.[10] $[PtPh_2(\mu\text{-}SMe_2)]_n$ (n = 2, 3)[11a] and $[Cu(MeCN)_2(PPh_3)_2][BF_4]$[11b,11c] were prepared by methods described in the literature. The synthesis of $Pt(NPA)Ph_2$ (**3.3**) has been described in Chapter 3.

Quantum yield measurements. The photoluminescent quantum yields of BNPA and APBN were measured in dilute CH_2Cl_2 solution (A ≈ 0.1) relatively to anthracene at room temperature (Φ_r = 0.36).[12a] The photoluminescent quantum yields for compounds **6.1** and **6.2** in solution were measured in degassed CH_2Cl_2 solutions at room temperature relative to *fac*-$Ir(ppy)_3$ (ppy = 2-phenyl pyridine) (Φ_r = 0.40).[12b,12c] Their absolute photoluminescent quantum yields of **6.1** and **6.2** were measured as neat films at room temperature using a commercial fluorimeter in combination with an integration sphere according to the literature procedure.[13]

6.2.2 Synthesis of 1-*N*-(5'-bromopyridin-2-yl)-7-azaindole (BrNPA)

2,5-Dibromopyridine (2.84 g, 12.0 mmol), 7-azaindole (1.18 g, 10.0 mmol), CuI (0.19 g, 1.0 mmol), 1,10-phenanthroline (0.36 g, 2.0 mmol), Cs_2CO_3 (6.85 g, 21.0 mmol), and 5 mL of DMF were mixed together and then heated at 110~130 °C under an N_2 atmosphere for 24 hours. After cooling down to ambient temperature, the mixture was diluted with CH_2Cl_2 (100 mL) and filtered through a plug of silica gel. The filtrate was then concentrated, and the residue was further purified by flash chromatograph on silica gel using CH_2Cl_2 as the eluent. After the removal of the solvent, BrNPA was obtained as a white solid (2.20 g, 81% yield). ^{1}H NMR (400 MHz, $CDCl_3$, 25 ^{o}C): δ 8.96 (d; ^3J = 7.2 Hz; 1H, py), 8.54 (d; ^4J = 1.6 Hz; 1H, py), 8.42 (dd; ^3J = 3.6 Hz, ^4J = 1.2 Hz; 1H, 7-aza), 8.35 (d; ^3J = 2.8 Hz; 1H, 7-aza), 7.97 (m; 2H, 1H from py and 1H from 7-aza), 7.20 (dd; $^3J_1$ = 6.0 Hz, $^3J_2$ = 3.6 Hz; 1H, 7-aza), 6.67 (d; ^3J = 2.8 Hz; 1H, 7-aza) ppm. ^{13}C: δ 149.80, 149.44, 147.71, 143.44, 141.08, 129.81, 126.54, 123.91, 117.81, 117.04, 116.15, 103.56 ppm. HRMS calcd. for $C_{12}H_8BrN_3$: *m/z* 272.9902; found: 272.9915. Anal. calcd. for $C_{12}H_8N_3Br$: C 52.58, H 2.94, N 15.33; found: C 52.05, H 3.25, N 15.03.

6.2.3 Synthesis of 1-*N*-(5'-(dimesitylboron)pyridine-2-yl)-7-azaindole (BNPA)

To a stirred Et_2O/THF (2:1) (60 mL) solution of BrNPA (0.61 g, 2.2 mmol) at -100 ^{o}C was added dropwise, *via* syringe, a *n*-BuLi solution (1.6 M) (1.44 mL, 2.3 mmol) over 10 min. The resulting light yellow solution was stirred for 1 hour at -100 ^{o}C, and an Et_2O (15 mL) solution of dimesitylboron fluoride (0.72 g, 90%, 2.4 mmol) was then slowly added. After kept at -100 ^{o}C for 1 hour, the reaction mixture was warmed to ambient temperature and stirred overnight. An aqueous solution (20 mL) of NH_4Cl (0.26

g) was added. After the separation of water and the extraction of the aqueous layer with Et_2O (30 mL x 2), the organic layer was dried with Na_2SO_4. After the removal of the solvent, the residue was purified by flash chromatograph on silica gel using hexanes/CH_2Cl_2 (5/1) as the eluent to afford BNPA as a white solid, which was further purified by recrystallization with hexanes (0.51 g, 53% yield). Colorless crystals of BNPA were obtained by the slow evaporation of its CH_2Cl_2 solution. ^{1}H NMR (400 MHz, $CDCl_3$, 25 ^{o}C): δ 9.04 (d; ^3J = 4.4 Hz; 1H, *meta*-py), 8.55 (s; 1H, *orth*-py), 8.49 (d; ^3J = 3.6 Hz; 1H, 7-aza), 8.41 (dd; ^3J = 4.8 Hz, ^4J = 1.6 Hz; 1H, 7-aza), 7.98-7.94 (m; 2H, 1H for *para*-py and 1H from 7-aza), 7.18 (dd; $^3J_1$ = 7.6 Hz, $^3J_2$ = 4.8 Hz; 1H, 7-aza), 6.86 (s; 4H, B(*Mes*)$_2$), 2.34 (s; 6H, *para*-C*H*$_3$ of B(*Mes*)$_2$), 2.08 (s; 12H, *orth*-C*H*$_3$ of B(*Mes*)$_2$) ppm. ^{13}C NMR: δ 156.79, 153.00, 148.15, 146.83, 143.50, 141.05, 139.34, 129.51, 128.63, 126.71, 124.08, 117.85, 114.79, 103.81, 23.87, 21.55 ppm. HRMS calcd. for $C_{30}H_{30}BN_3$: *m/z* 443.2533; found: 443.2358. Anal. calcd. for $C_{30}H_{30}BN_3$: C 81.26, H 6.82, N 9.48; found: C 81.42, H 6.99, N 9.46.

6.2.4 1-{2-(1-*N*-7-azaindolyl)pyridine-5-yl}-8-{p-dimesitylborylphenyl}-naphthalene (APBN)

To a stirred THF solution (40 mL) of BrNPA (0.44 g, 1.6 mmol) at -100 ^{o}C was added dropwise, *via* syringe, a *n*-BuLi solution (1.6 M) (1.15 mL, 1.8 mmol) over 10 minutes. The resulting light yellow solution was stirred for 1 hour at -100 ^{o}C, and then the anhydrous $ZnCl_2$ solid (0.36 g, 2.6 mmol) was added. After kept at -100 ^{o}C for 1 hour, the reaction mixture was warmed to ambient temperature over 4 hour resulting in a white suspension. $Pd(PPh_3)_4$ (0.14 g, 0.13 mmol) and 1-iodo-8-p-dimesitylboryphenylnaphthalene (0.75 g, 1.3 mmol) were then added successively to this

solution, and the mixture was stirred at ambient temperature for 2 days. After the removal of the solvent, the residue was dissolved in CH_2Cl_2 (50 mL) and a Na_3EDTA (0.20 M, prepared from EDTA with 5 equiv of Na_2CO_3) aqueous solution (50 mL). The mixture was stirred for 30 minutes. The aqueous layer was then separated and extracted with CH_2Cl_2 (50 mL x 2). The organic layer was dried with Na_2SO_4. After the removal of the solvent, the residue was purified by flash chromatograph on silica gel using hexanes/CH_2Cl_2 (1/1) as the eluent to afford APBN as a white solid (0.21 g, 24% yield). ^{1}H NMR (400 MHz, CD_2Cl_2, 25 °C): δ 8.62 (d; ^3J = 8.0 Hz; 1H, *meta*-py), 8.39 (d; ^3J = 3.6 Hz, 1H, 7-aza), 8.28 (d; ^3J = 2.0 Hz; 1H, 7-aza), 8.23 (s; 1H, *orth*-py), 8.05-7.98 (m; 3H, 2H from naphthalene moiety and 1H from 7-aza), 7.66-7.61 (m; 2H from naphthalene moiety), 7.55-7.47 (m; 3H, 2H from naphthalene moiety and 1H for *para*-py), 7.20 (m, br; 5H, 4 from -*Ph*- and 1H from 7-aza), 6.67 (s, br; 5H, 4H from B(*Mes*)$_2$ and 1H from 7aza), 2.25 (s; 6H, *para*-C*H*$_3$ of B(*Mes*)$_2$), 1.64 (s; 12H, *orth*-C*H*$_3$ of B(*Mes*)$_2$) ppm. ^{13}C NMR: δ 148.80, 148.31, 147.76, 147.47, 143.24, 142.52, 141.59, 140.79, 140.06, 138.95, 138.50, 136.82, 136.57, 136.19, 135.94, 132.07, 131.67, 129.64(br), 129.33, 129.20, 129.15, 128.13, 126.53, 125.75, 123.55, 117.31, 114.12, 102.63, 23.17, 21.08 ppm. HRMS calcd. for $C_{46}H_{40}BN_3$: *m/z* 645.3315; found: 645.3336.

6.2.5 Synthesis of [Cu(BNPA)(PPh$_3$)$_2$][BF$_4$] (6.1)

BNPA (0.044 g, 0.10 mmol) and [Cu(MeCN)$_2$(PPh$_3$)$_2$][BF$_4$] (0.076 g, 0.10 mmol) were mixed in CH_2Cl_2 (10 mL). The mixture was stirred overnight at ambient temperature. After the removal of the solvent, the resulting residue was washed with Et_2O (3 x 5 mL) to afford **6.1** as a white solid in 72% yield. ^{1}H NMR (400 MHz, CD_2Cl_2, 25

°C): δ 8.61 (s; 1H, py), 8.05 (d; ^3J = 7.6 Hz; 1H, 7-aza), 7.96 (d; ^3J = 8.0 Hz; 1H, py), 7.80 (d; ^3J = 3.6 Hz; 1H, 7-aza), 7.63 (d; ^3J = 8.0 Hz; 1H, py), 7.45-7.40 (m; 7H, 6H for *para*-P*Ph*$_3$ and 1H from 7-aza), 7.24-7.19 (m; 12H, *meta*-P*Ph*$_3$), 7.09-6.95 (m; 6H for *ortho*-P*Ph*$_3$ and 1H from 7-aza), 6.84 (d; ^3J = 3.6 Hz; 1H, 7-aza), 6.79 (s; 4H, B(*Mes*)$_2$), 2.32 (s; 6H, *para*-C*H*$_3$ of B(*Mes*)$_2$), 1.74 (s; 12H, *orth*-C*H*$_3$ of B(*Mes*)$_2$) ppm. ^{13}C NMR: δ 157.27, 152.60, 148.27, 147.10, 144.62, 140.93, 140.25, 139.95, 137.93, 133.22 (br), 132.18, 131.94, 131.04, 130.65, 129.26, 129.02, 127.45, 125.38, 119.51, 115.91, 107.24, 23.52, 21.33 ppm. ^{31}P NMR: δ 1.80 (s, br) ppm. Anal. calcd. for $C_{66}H_{60}B_2CuF_4N_3P_2$: C 70.88, H 5.41, N 3.76; found: C 70.39, H 5.49, N 3.68.

6.2.6 Synthesis of Pt(BNPA)PtPh$_2$ (6.2)

BNPA (0.044g, 0.10 mmol) and [PtPh$_2$(μ-SMe$_2$)]$_n$ (n = 2 or 3) (0.042 g) were mixed in CH_2Cl_2 (10 mL). The mixture was stirred overnight at ambient temperature, resulting in a bright yellow solution. After the removal of the solvent, the residue was washed with Et_2O/hexanes (1:1) (5 mL x 2) to afford **6.2** as a yellow solid in 70% yield. ^{1}H NMR (400 MHz, CD_2Cl_2, 25 °C): δ 8.56 (s; 1H, py), 8.13 (d; ^3J = 6.0 Hz; 1H, 7-aza), 8.04 (d; ^3J = 3.6 Hz; 1H, 7-aza), 7.96-7,94 (m; 2H, 1H from py and 1H from 7-aza) 7.48 (d; ^3J = 6.8 Hz; 1H, py), 7.32 (d, satellites; ^3J = 5.6 Hz, $^3J_{Pt\text{-}H}$ = 60 Hz; 2H, *orth*-Pt(*Ph*)Ph') 7.15 (d, satellites; ^3J = 5.6 Hz, $^3J_{Pt\text{-}H}$ = 56 Hz; 2H, *orth*-Pt(Ph)*Ph'*), 7.04 (dd; $^3J_1$ = 6.8 Hz, $^3J_2$ = 3.6 Hz; 1H, 7-aza), 7.01 (d; ^3J = 3.6 Hz; 1H, 7-aza), 6.89 (m; 2H, *meta*-Pt(*Ph*)Ph'), 6.82 (s; 4H, B(*Mes*)$_2$), 6.80 (m; 1H, *para*-Pt(*Ph*)Ph'), 6.64 (m; 3H, *orth*- and *meta*-Pt(Ph)*Ph'*), 2.36 (s; 6H, *para*-C*H*$_3$ of B(*Mes*)$_2$), 1.90 (s; 12H, *orth*-C*H*$_3$ of B(*Mes*)$_2$) ppm. ^{13}C NMR: δ 157.48, 146.35(br), 144.76, 144.01, 141.50(br), 139.10,

132.31, 130.24, 128.63, 127.50, 126.85(br), 123.81, 121.41, 121.16, 118.46, 113.93, 105.78, 25.35, 20.96 ppm. Anal. calcd. for $C_{42}H_{40}BN_3Pt$: C 63.64, H 5.09, N 5.30; found: C 64.19, H 5.45, N 5.17.

6.2.7 Synthesis of Pt(BNPA)$PtCl_2$ (6.3)

BNPA (0.069g, 0.16 mmol) and K_2PtCl_4 (0.065 g, 0.16 mmol) were dissolved in the mixed solvents of CH_2Cl_2 (10 mL), DMSO (2 mL) and H_2O (10 mL) under air. The resulting mixture was stirred vigorously overnight at ambient temperature. The water layer turned from pink to colorless, while the CH_2Cl_2 layer turned from colorless to light yellow. After diluted with H_2O (50 mL), the mixture was extracted with CH_2Cl_2 (2 x 50 mL). The organic layer was dried with Na_2SO_4. After the removal of the solvent, the residue was recrystalized with acetone to afford **6.3** as light yellow crystals in 37% yield. ^{1}H NMR (400 MHz, CD_2Cl_2, 25 °C): δ 9.50 (s; 1H, py), 9.13 (d; ^3J = 5.6 Hz; 1H, 7-aza), 8.20 (d; ^3J = 8.0 Hz; 1H, 7-aza), 8.06 (d; ^3J = 8.4 Hz; 1H, py), 7.93 (d; ^3J = 3.6 Hz; 1H, 7-aza), 7.41 (d; ^3J = 8.4 Hz; 1H, py), 7.36 (dd; $^3J_1$ = 8.0 Hz, d; $^3J_2$ = 6.0 Hz; 1H, 7-aza), 7.03(d; ^3J = 3.6 Hz; 1H, 7-aza), 6.91 (s; 4H, B(*Mes*)$_2$), 2.34 (s; 6H, *para*-CH_3 of B(*Mes*)$_2$), 2.06 (s; 12H, *orth*-CH_3 of B(*Mes*)$_2$) ppm. ^{13}C NMR: δ 161.53, 147.75, 147.06, 146.51, 143.40, 141.14, 140.55, 140.07, 132.90, 128.94, 126.38, 124.78, 120.66, 114.35, 109.85, 23.64, 21.31 ppm. Anal. calcd. for $C_{30}H_{30}BN_3Cl_2Pt$·0.5 $CH_3C(O)CH_3$: C 51.24, H 4.50, N 5.69; found: C 51.07, H 4.85, N 6.06.

6.2.8 Synthesis of $[Cu(NPA)(PPh_3)_2](BF_4)$ (6.4)

Compound **6.4** was synthesized by the reaction of NPA (0.019 g, 0.10 mmol) with $[Cu(MeCN)_2(PPh_3)_2][BF_4]$ (0.076 g, 0.10 mmol) using the same method as described for **6.1** (87% yield). ^{1}H NMR (400 MHz, CD_2Cl_2, 25 °C): δ 8.07 (m; 2H, 1 H from py and 1H from 7-aza), 7.96 (m; 1H, py), 7.80 (d; ^3J = 4.0 Hz; 1H, 7-aza), 7.70 (d; ^3J = 4.8 Hz, 1H, 7-aza) 7.63 (d; ^3J = 4.4 Hz; 1H, py), 7.42 (t; ^3J = 7.6 Hz; 6H, *para*-P*Ph*$_3$) 7.24 (t; ^3J = 7.6 Hz; 12H, *meta*- P*Ph*$_3$), 7.04 (m, br; 13H, 1H from 7-aza and 12H for *ortho*-P*Ph*$_3$), 6.95 (m; 1H, py), 6.87 (d; ^3J = 4.0 Hz; 1H, 7-aza) ppm. ^{13}C NMR: δ 150.96, 150.20, 146.93, 144.54, 141.51, 133.42 (br), 133.29, 131.94, 130.63, 130.17, 129.27, 129.20, 127.74, 125.24, 121.63, 119.22, 116.92, 106.40 ppm. ^{31}P NMR: δ 2.12 (s, br) ppm. Anal. calcd. for $C_{48}H_{39}BCuF_4N_3P_2$: C 66.26, H 4.52, N 4.83, found: C 66.09, H 4.72, N 4.80.

6.2.9 Synthesis of $Pt(NPA)PtCl_2$ (6.5)

Compound **6.5** was synthesized from the reaction of NPA (0.030g, 0.15 mmol) with K_2PtCl_4 (0.062 g, 0.15 mmol) using the same method as described for **6.3** (40% yield). ^{1}H NMR (500 MHz, CD_2Cl_2, 25 °C): δ 9.67 (dd; ^3J = 6.5 Hz; ^4J = 1.0 Hz; 1H, py), 9.19 (dd; ^3J = 5.5 Hz; ^4J = 1.0 Hz; 1H, 7-aza), 8.23 (dd; ^3J = 6.0 Hz; ^4J = 1.0 Hz; 1H, 7-aza), 8.12 (td; ^3J = 8.5 Hz; ^4J = 1.5 Hz; 1H, py), 7.90 (d; ^3J = 4.0 Hz; 1H, 7-aza), 7.45 (d; ^3J = 8.5 Hz; 1H, py), 7.34 (dd; $^3J_1$ = 6.5 Hz, $^3J_2$ = 6.0 Hz; 1H, 7-aza), 7.30 (td; ^3J = 7.0 Hz, ^4J = 1.5 Hz; 1H, py), 7.06 (d; ^3J = 4.0 Hz; 1H, 7-aza) ppm.

6.2.10 X-ray diffraction analyses

Single crystals of BNPA and **6.2**-**6.4** were mounted on glass fibers for data collection. Data were collected on a Bruker Apex II single-crystal X-ray diffractometer with graphite-monochromated Mo Kα radiation, operating at 50 kV and 30 mA. Data collection for **6.2** and **6.4** were carried out at 180 K while data collection for BNPA and **6.3** were collected at ambient temperature. No significant decay was observed in any samples. Data were processed on a PC with the aid of the Bruker SHELXTL software package (version 5.10) and are corrected for absorption effects. All structures were solved by direct methods. The crystal data for BNPA and **6.2**-**6.4** are summarized in Table 6.1, and the selected bond lengthes and angles for them are presented in Table 6.2.

Table 6.1 Crystallographic data for compounds BNPA, **6.2**, **6.3** and **6.4**.

Compound	BNPA	**6.2·0.25CH_2Cl_2**	**6.3·CH_3COCH_3**	**6.4**
Formula	$C_{30}H_{30}BN_3$	$C_{42.50}H_{41}BClN_3Pt$	$C_{33}H_{36}BCl_2N_3OPt$	$C_{48}H_{39}BCuF_4N_3P_2$
FW	443.38	835.13	767.45	870.11
Space Group	P-1	C2/c	P-1	Pbca
a, Å	8.0448(8)	36.8601(12)	8.234(6)	15.6922(11)
b, Å	8.2483(9)	11.8558(5)	8.953(6)	17.1618(8)
c, Å	19.167(2)	17.1766(5)	22.398(15)	30.9414(15)
α, °	81.9810(10)	90	83.270(8)	90
β, °	86.4730(10)	102.530(3)	85.683(11)	90
γ, °	82.0900(10)	90	84.788(7)	90
V, $Å^3$	1246.3(2)	7327.5(4)	1629.4(19)	8332.7(8)
Z	2	8	2	8
$D_{calc,}$ g·cm^{-3}	1.182	1.514	1.564	1.387
T, K	298(2)	180(2)	298(2)	180(2)
μ, mm^{-1}	0.069	3.937	4.499	0.657
$2\theta_{max}$, °	53.76	54.16	54.00	54.34
Reflns measured	13428	20538	18278	34207
Reflns used (R_{int})	5308 (0.0247)	8017 (0.1217)	7010 (0.0221)	9229 (0.1591)
Parameters	313	450	378	532
Final *R* values [I > 2σ(I)]:				
R_1[a]	0.0503	0.0569	0.0326	0.0630
wR_2[b]	0.1252	0.0789	0.0753	0.1028
R values (all data):				
R_1[a]	0.0867	0.1560	0.0398	0.1825
wR_2[b]	0.1429	0.1038	0.0784	0.1412
Goodness-of-fit on F^2	1.054	0.905	1.057	0.944

[a] $R_1 = \Sigma||F_0| - |F_c|| / \Sigma|F_0|$

[b] $wR_2 = [\Sigma w [(F_0^2 - F_c^2)^2] / \Sigma[w(F_0^2)^2]]^{1/2}$

$w = 1 / [\sigma^2(F_0^2) + (0.075P)^2]$, where $P = [Max (F_0^2, 0) + 2F_c^2] / 3$

Table 6.3 Selected bond lengths (Å) and angles (º) for compounds BNPA, **6.2**, **6.3** and **6.4**.

		BNPA	
N(1)-C(7)	1.331(2)	N(3)-C(8)	1.331(2)
N(1)-C(6)	1.337(2)	N(3)-C(12)	1.334(2)
N(2)-C(7)	1.394(2)	B(1)-C(11)	1.561(3)
N(2)-C(1)	1.394(2)	B(1)-C(13)	1.572(3)
N(2)-C(8)	1.412(2)	B(1)-C(22)	1.576(3)
C(7)-N(1)-C(6)	113.83(16)	C(11)-B(1)-C(13)	119.22(16)
C(7)-N(2)-C(1)	106.89(14)	C(11)-B(1)-C(22)	116.21(16)
C(7)-N(2)-C(8)	129.43(15)	C(13)-B(1)-C(22)	124.53(15)
C(1)-N(2)-C(8)	123.68(16)	C(2)-C(1)-N(2)	110.68(18)
C(8)-N(3)-C(12)	117.02(15)	C(1)-C(2)-C(3)	107.45(17)
		Compound **6.2**	
Pt(1)-C(13)	1.999(11)	N(2)-C(1)	1.392(10)
Pt(1)-C(19)	2.013(8)	N(2)-C(8)	1.411(10)
Pt(1)-N(1)	2.089(7)	N(3)-C(8)	1.331(9)
Pt(1)-N(3)	2.141(7)	N(3)-C(12)	1.347(10)
N(1)-C(6)	1.336(10)	B(1)-C(11)	1.562(14)
N(1)-C(7)	1.360(10)	B(1)-C(34)	1.576(15)
N(2)-C(7)	1.389(10)	B(1)-C(25)	1.588(14)
C(13)-Pt(1)-C(19)	88.8(3)	C(7)-N(2)-C(1)	105.8(8)
C(13)-Pt(1)-N(1)	178.0(4)	C(7)-N(2)-C(8)	128.6(7)
C(19)-Pt(1)-N(1)	91.4(3)	C(1)-N(2)-C(8)	123.7(8)
C(13)-Pt(1)-N(3)	91.5(3)	C(8)-N(3)-C(12)	118.3(8)
C(19)-Pt(1)-N(3)	178.9(4)	C(8)-N(3)-Pt(1)	124.8(6)
N(1)-Pt(1)-N(3)	88.2(3)	C(12)-N(3)-Pt(1)	116.9(5)
C(6)-N(1)-C(7)	114.2(8)	C(11)-B(1)-C(34)	118.5(9)
C(6)-N(1)-Pt(1)	124.5(6)	C(11)-B(1)-C(25)	117.2(10)
C(7)-N(1)-Pt(1)	120.1(6)	C(34)-B(1)-C(25)	124.1(9)
		Compound **6.3**	
Pt(1)-N(2)	2.021(4)	C(5)-C(6)	1.377(9)
Pt(1)-N(3)	2.024(3)	C(6)-N(2)	1.355(6)
Pt(1)-Cl(1)	2.2819(16)	C(7)-N(2)	1.338(6)
Pt(1)-Cl(2)	2.2904(16)	C(7)-N(1)	1.380(6)
C(1)-C(2)	1.339(7)	C(8)-N(3)	1.342(5)
C(1)-N(1)	1.405(6)	C(8)-C(9)	1.389(6)
C(2)-C(3)	1.412(9)	C(8)-N(1)	1.406(5)

N(2)-Pt(1)-N(3)	88.62(15)	N(2)-Pt(1)-Cl(2)	174.15(12)
N(2)-Pt(1)-Cl(1)	91.09(12)	N(3)-Pt(1)-Cl(2)	90.90(11)
N(3)-Pt(1)-Cl(1)	179.50(10)	Cl(1)-Pt(1)-Cl(2)	89.43(7)

Compound **6.4**

Cu(1)-N(1)	2.057(3)	P(1)-C(13)	1.827(5)
Cu(1)-N(3)	2.085(4)	P(1)-C(25)	1.829(5)
Cu(1)-P(1)	2.2570(14)	P(2)-C(31)	1.817(5)
Cu(1)-P(2)	2.2685(13)	P(2)-C(37)	1.819(4)
P(1)-C(19)	1.817(5)	P(2)-C(43)	1.821(5)

N(1)-Cu(1)-N(3)	92.17(15)	C(7)-N(2)-C(8)	128.4(4)
N(1)-Cu(1)-P(1)	105.77(12)	C(6)-N(2)-C(8)	123.7(4)
N(3)-Cu(1)-P(1)	120.54(11)	C(8)-N(3)-C(12)	115.2(4)
N(1)-Cu(1)-P(2)	109.23(11)	C(8)-N(3)-Cu(1)	123.9(3)
N(3)-Cu(1)-P(2)	103.01(11)	C(12)-N(3)-Cu(1)	118.1(3)
P(1)-Cu(1)-P(2)	121.86(5)	F(4)-B(1)-F(3)	110.4(5)
C(19)-P(1)-C(13)	103.7(2)	F(4)-B(1)-F(2)	110.4(5)
C(19)-P(1)-C(25)	103.9(2)	F(3)-B(1)-F(2)	108.8(5)
C(13)-P(1)-C(25)	105.4(2)	F(4)-B(1)-F(1)	109.2(5)
C(19)-P(1)-Cu(1)	119.16(19)	F(3)-B(1)-F(1)	109.0(5)
C(13)-P(1)-Cu(1)	116.67(16)	F(2)-B(1)-F(1)	109.0(5)
C(25)-P(1)-Cu(1)	106.52(15)	N(1)-C(1)-C(2)	123.6(4)
C(31)-P(2)-C(37)	104.6(2)	C(3)-C(2)-C(1)	119.6(5)
C(31)-P(2)-C(43)	102.4(2)	C(4)-C(3)-C(2)	118.3(5)
C(37)-P(2)-C(43)	102.7(2)	C(3)-C(4)-C(7)	118.0(5)
C(31)-P(2)-Cu(1)	108.26(15)	C(3)-C(4)-C(5)	135.7(5)
C(37)-P(2)-Cu(1)	117.11(16)	C(7)-C(4)-C(5)	106.3(5)
C(43)-P(2)-Cu(1)	119.87(16)	C(6)-C(5)-C(4)	107.1(5)
C(7)-N(1)-C(1)	115.2(4)	C(5)-C(6)-N(2)	110.8(5)
C(7)-N(1)-Cu(1)	117.8(3)	N(1)-C(7)-N(2)	126.2(4)
C(1)-N(1)-Cu(1)	122.7(3)	N(1)-C(7)-C(4)	125.2(5)
C(7)-N(2)-C(6)	107.2(4)	N(2)-C(7)-C(4)	108.6(4)

6.3 Results and Discussion

6.3.1 Syntheses and structures of BNPA and APBN

2,5-Dibromopyridine is a very valuable synthon for the construction of various polysubstituted pyridine-containing compounds including new materials, natural products as well as pharmaceutical agents.[14] Its C(2)-position exhibits a higher electrophilicity than the C(5) position and is the favored site for the transition metal-mediated cross-coupling reactions.[14a,14b] Accordingly, the synthesis of 1-*N*-(5'-bromopyridin-2-yl)-7-azaindole (BrNPA) was achieved in 81% yield using the homogeneous catalysis method developed by the Buchwald group,[15] where 2,5-dibromopyridine and 7-azaindole were coupled in the presence of CuI, 1,10-phenanthroline, and Cs_2CO_3 in DMF at 110~130 °C under an N_2 atmosphere for 24 hours, as shown in Scheme 1. Extending the reaction time to 48 hours under the same conditions can increase the yield up to ~93% with only a small amount of 1-*N*-(2'-bromopyridin-5-yl)-7-azaindole isolated as the by-product. The selectivity of the reaction decreased significantly when the reaction temperature was increased to 175 ^{o}C, with BrNPA and 1-*N*-(2'-bromopyridin-5-yl)-7-azaindole being isolated in a 4.3:1 ratio.

Scheme 6.1[a]

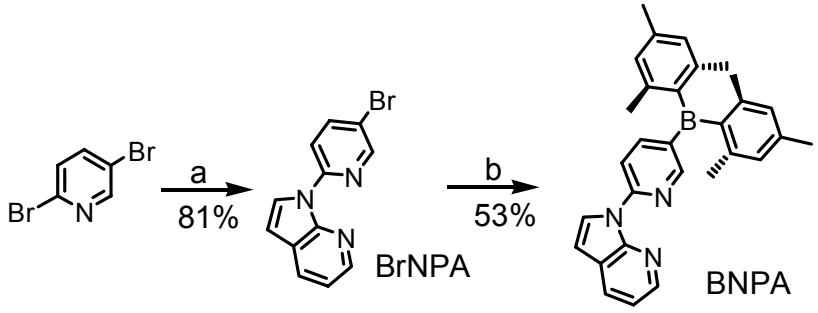

[a]Reagents and conditions: (a) 7-azaindole, CuI, 1,10-phenanthroline, Cs_2CO_3, DMF, 110~130 ^{o}C, 24 hours; (b) (i) *n*-BuLi, Et_2O/THF, -100 ^{o}C; (ii) $B(Mes)_2F$, rt, overnight.

Lithium-halogen exchange reactions for substrates such as BrNPA can be synthetically challenging.[6k] The best way to synthesize the BNPA ligand from BrNPA was the initial lithium-halogen exchange reaction at -100 ^{o}C in the Et_2O/THF (2:1) solvents, followed by the addition of $B(Mes)_2F$, as shown in Scheme 6.1.

The synthesis of the APBN molecule was more challenging. As shown in Scheme 6.2, 1,8-diaminonaphthalene was converted first to the 1,8-diiodonaphthalene,[16] then to the 1-I-8-*p*-(Mes_2B)phenylnaphthalene (BI).[6i] The Pd(0) catalyzed Nigishi coupling reaction between BI and the organozinc reagent NPA-ZnCl, generated in situ from BrNPA *via* lithium-halogen exchange and the subsequent transmetalation with $ZnCl_2$, gave the APBN ligand in ~24% isolated yield (Scheme 6.2). The low yield can be attributed to several factors, including the inefficient lithium-halogen exchange, the observed precipitation of the organozinc intermediate due to the NPA chelation, and the steric crowdedness around the C-I bond in the BI molecule.

Scheme 6.2[a]

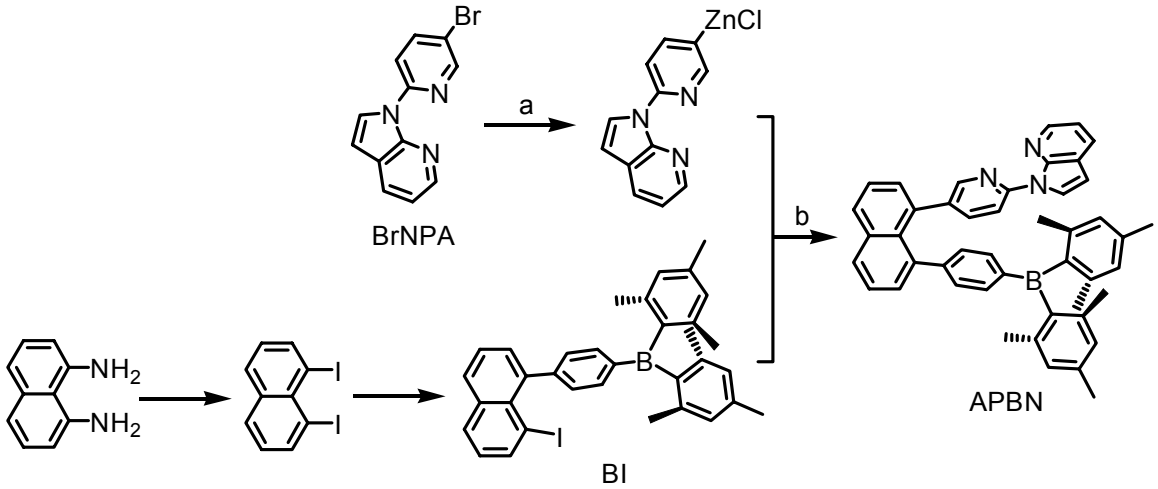

[a]Reagents and conditions: (a) (i) *n*-BuLi, THF, -100 ^{o}C, 1h; (ii) $ZnCl_2$, rt, 4 hours; (b) [$Pd(PPh_3)_4$], rt, 2 days.

The two new NPA derivatives were fully characterized by NMR spectroscopy and HRMS or elemental analyses. The structure of BNPA was also examined by signal-crystal X-ray diffraction analysis. As shown in Figure 6.1, the pyridyl group and 7-azaindolyl ring are coplanar with the N(1) and N(3) atoms *trans* to each other to minimize the *ortho*-H,H' interactions and to reduce the nitrogen lone pair repulsion. To minimize steric interactions around the three-coordinate boron center, the two mesityl groups were considerably twisted relatively to the pyridyl ring.

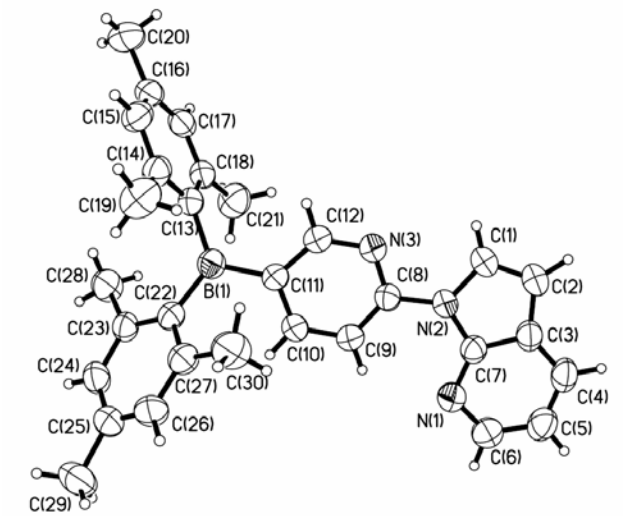

Figure 6.1 Crystal structure of BNPA with 50% ellipsoids.

6.3.2 Syntheses and structures of the Cu(I) and Pt(II) complexes

A Cu(I) complex $[Cu(BNPA)(PPh_3)_2][BF_4]$ (**6.1**) and two Pt(II) complexes $Pt(BNPA)Ph_2$ (**6.2**) and $Pt(BNPA)Cl_2$ (**6.3**) were obtained by the reaction of BNPA with $[Cu(MeCN)_2(PPh_3)_2][BF_4]$, $[PtPh_2(\mu\text{-}SMe_2)]_n$ (n = 2, 3) and K_2PtCl_4, respectively, as shown in Scheme 6.3. For comparison, the corresponding Cu(I) and Pt(II) complexes of NPA, $[Cu(NPA)(PPh_3)_2][BF_4]$ (**6.4**), $Pt(NPA)Ph_2$ (**3.3**) and $Pt(NPA)Cl_2$ (**6.5**) were also synthesized using similar protocols. Due to the presence of the dimesitylboron moiety, the BNPA complexes exhibit much better solubilities in organic solvents than the NPA

analogues. Despite the incorporation of an N,N-chelating NPA moiety in the APBN ligand, attempts to synthesize metal complexes with APBN were not successful likely due to the steric crowdedness along with the known poor chelating ability of the NPA site.

Scheme 6.3[a]

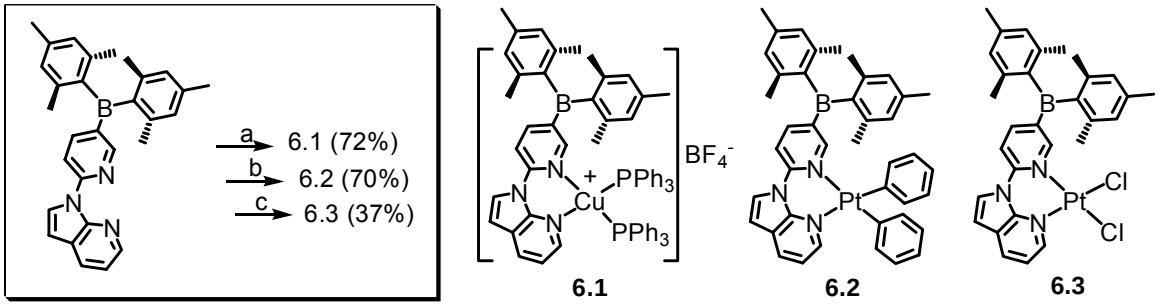

[a]Reagents and conditions: (a) $[Cu(MeCN)_2(PPh_3)_2](BF_4)$, CH_2Cl_2, rt, overnight; (b) $[PhPh_2(\mu\text{-}SMe_2)]_n$ (n = 2, 3), rt, overnight. (c) K_2PtCl_4, CH_2Cl_2/DMSO/H_2O (5:1:5), rt, overnight.

The crystal structures of the two new Pt(II) complexes **6.2**, **6.3** and the Cu(I) complex **6.4** were determined by single-crystal X-ray diffraction analyses. The Pt(II) center in **6.2** and **6.3** has a typical square planar geometry (Figures 6.2 and 6.3). Compared to the free BNPA ligand where the pyridyl and the azaindolyl rings are coplanar, the BNPA ligand in both complexes has considerable distortion due to the formation of the 6-membered chelate ring and the *ortho*-H interactions, as evidenced by a large dihedral angle between the py and the azaindolyl rings (25.01° for **6.2** and 36.65° for **6.3**). This is consistent with the previous observation for the NPA complex, $Pt(NPA)Ph_2$ (**3.3**).

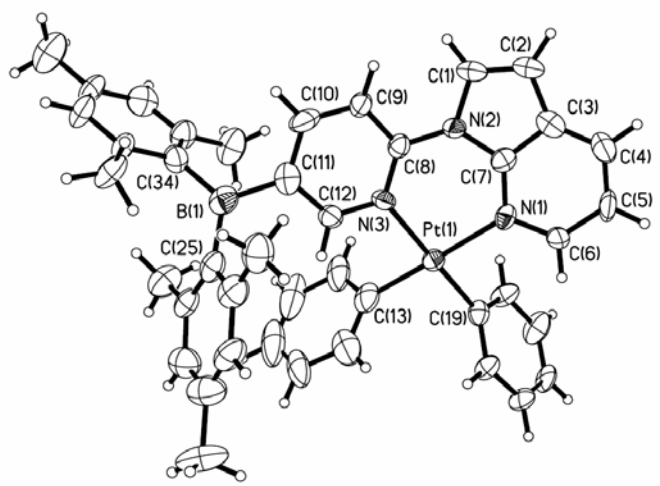

Figure 6.2 Crystal structure of **6.2** with 50% ellipsoids.

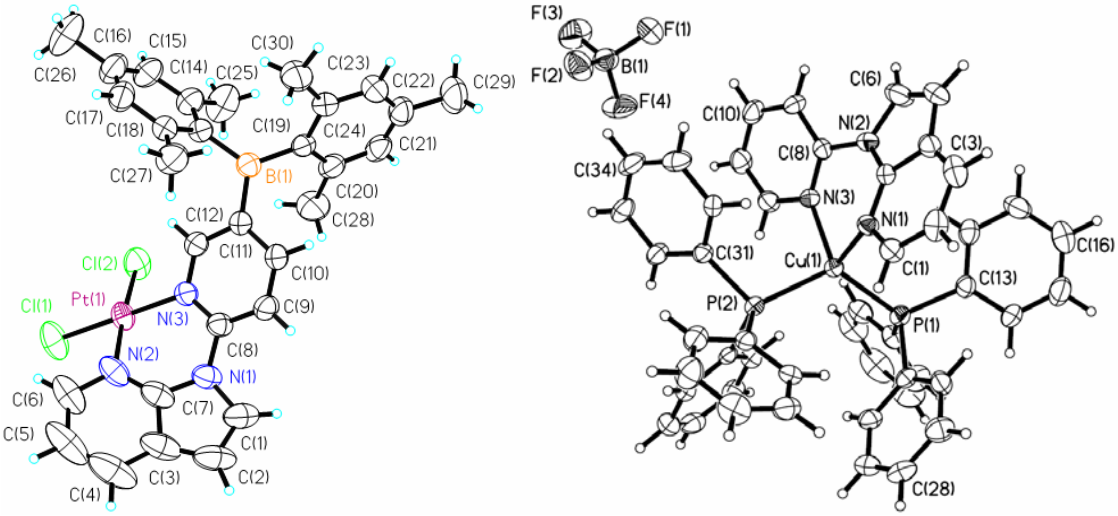

Figure 6.3 Crystal structures of **6.3** (left) and **6.4** (right) with 50% ellipsoids.

Although the structure of **6.1** was not determined due to the lack of suitable crystals, the coordination environment around its Cu center is believed to be similar to that in **6.4** (Figure 6.3), where the Cu(I) center has a distorted tetrahedral geometry (N-Cu-N = 92.17(15)°).

6.3.3 Electronic and luminescent properties

Both BNPA and APBN display a reversible reduction peak at $E^{1/2}$ = -2.22 V and -2.28V, respectively, vs. $FeCp_2^{0/+}$ in the cyclic voltammetry diagram recorded in DMF, which corresponds to the reduction of the boron center. The more positive reduction potential of BNPA compared to APBN is consistent with the direct conjugation of the B center with the NPA group in BNPA, which enhances the electron accepting ability of the B center.

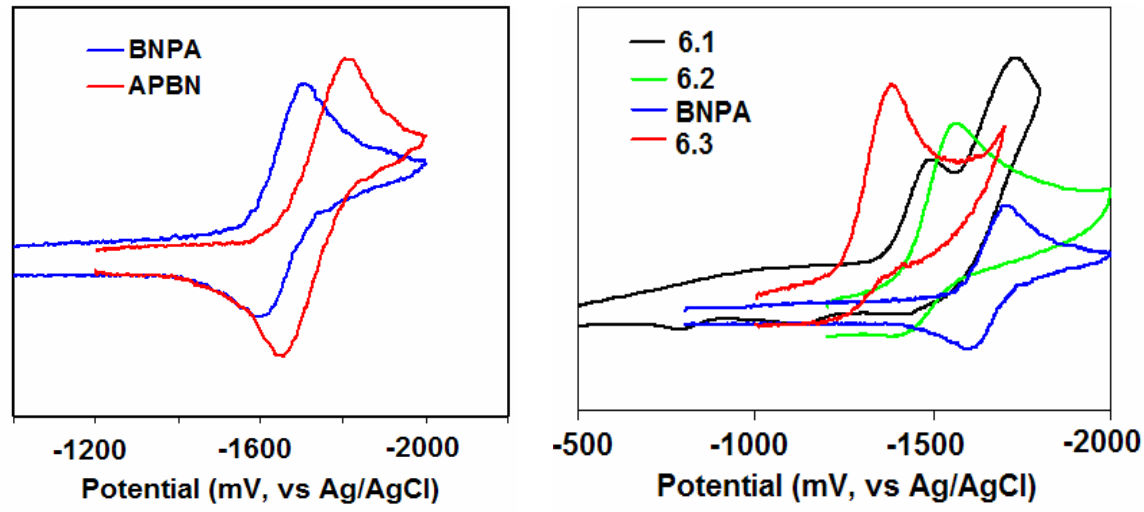

Figure 6.4 Cyclic voltammetry diagrams of BNPA, APBN and **6.1**-**6.3** in DMF vs Ag/AgCl {$E^{1/2}(FeCp_2^{0/+})$ = 0.55 V}.

As shown in Figure 6.4, the binding of a metal ion to the BNPA ligand shifts the first reduction potential to more positive (+ 0.16 V for **6.2**, + 0.32 V for **6.3**, relative to the free ligand), which is consistent with the previously reported B2bipy complexes (B2bipy = 5,5'-bis($BMes_2$)-2,2'-bipy). The fact that **6.3** has a more positive reduction potential than **6.2** is consistent with the Cl^- ligand being a weaker electron donor relatively to the phenyl ligand, indicating the presence of the electronic communication between the Pt center and the boron center. As shown by the absorption spectra in Figure

6.5, the metal-to-ligand charge transfer (MLCT) band of **6.2** appears at a lower energy than that of **6.3**, further supporting the presence of the electronic communication between the Pt center and the BNPA ligand.

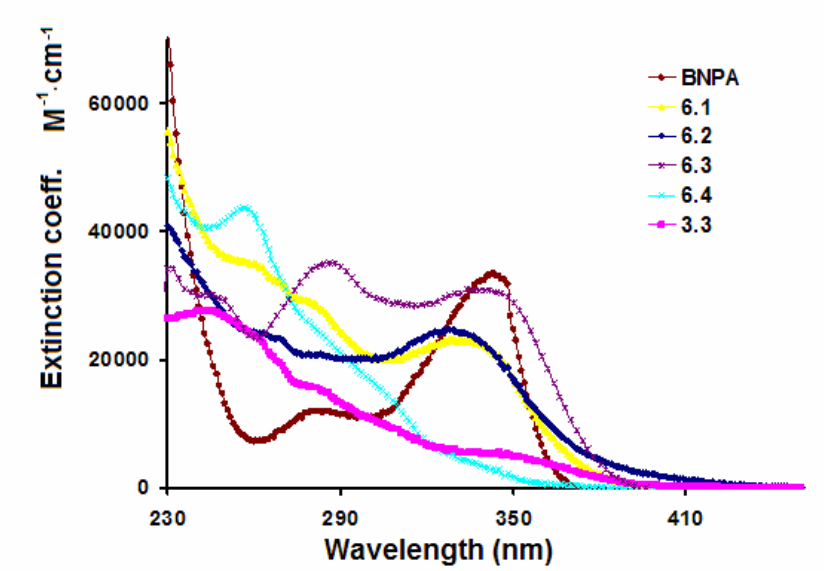

Figure 6.5 UV-absorption spectra of BNPA, **3.3** and **6.1**-**6.4** in CH_2Cl_2 at ambient temperature.

When irradiated by UV light, both BNPA and APBN are fluorescent in the violet-blue region. Their emission spectra display obvious red-shifts with the increase of the solvent polarity, as shown by the fluorescent spectra in Figures 6.6 and 6.7, consistent with a charge transfer natured emission involving the three-coordinate boron centers. Similar solvent-dependent fluorescence has been observed in many triarylboron compounds.[6] The quantum efficiency (Φ) of BNPA and APBN was determined to be 0.25 and ~1, respectively, relative to that of anthracene in CH_2Cl_2.[12a]

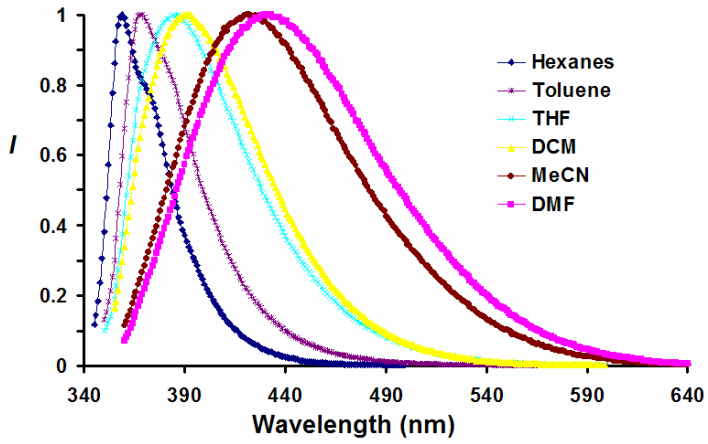

Figure 6.6 Normalized emission spectra of BNPA in different solvents.

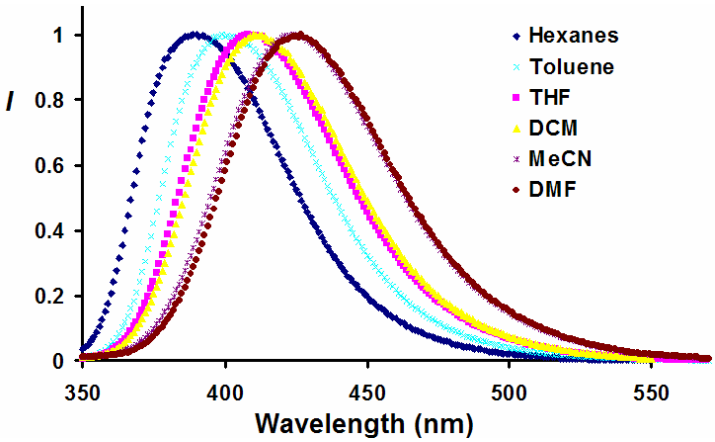

Figure 6.7 Normalized emission spectra of APBN in different solvents.

In contrast to the free ligands, the emission spectra of complexes **6.1** and **6.2** are dominated by a yellow and highly visible phosphorescent band (see Figure 6.8 and Table 6.1) at ambient temperature with λ_{max} = 540 nm, τ = 8.0 μs, Φ = 0.04 for **6.1**; λ_{max} = 543 nm, τ = 25.0 μs, Φ = 0.004 for **6.2** in CH_2Cl_2. The phosphorescent nature of the emission spectra of **6.1** and **6.2** is confirmed by their high sensitivity toward oxygen that quenches the emission of the complexes (Figure 6.8). The phosphorescence of the Pt complex **6.2** is much more sensitive toward oxygen than the Cu complex **6.1** since ~2% O_2 causes >90% quenching of the phosphorescent peak of **6.2** (at 4.0 x 10^{-5} M) while more than 20% O_2 is needed to achieve the same effect for **6.1**. This difference is most likely caused

by the much longer phosphorescent decay lifetime of the Pt complex, compared to the copper complex. Complexes **6.1** and **6.2** are stable in solution under air and their phosphorescent response toward oxygen is fully reversible by using nitrogen or argon, thus making them potentially useful as oxygen sensing reagents.

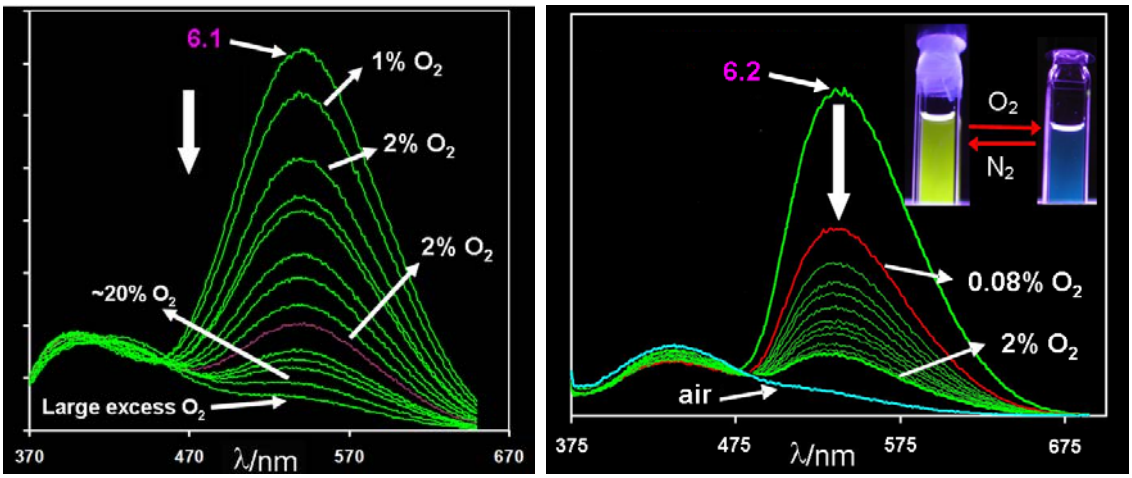

Figure 6.8 Phosphorescent spectra of **6.1** (λ_{ex} = 350 nm) and **6.2** (λ_{ex} = 360 nm) in CH_2Cl_2 (4.0 x 10^{-5} M) at ambient temperature under N_2 and their phosphorescence quenching by O_2. The O_2 percentage is calculated based on the amount of O_2 introduced to the space above the solution in the cell.

Both **6.1** and **6.2** also display bright yellow-green phosphorescence in the solid state at ambient temperature with the emission maximum at 527 nm (τ = 7.5 μs) and 519 nm (τ = 10.9 μs), respectively. Most impressive is compound **6.1** that has an unusually high emission quantum efficiency of 0.88 in the solid state (Φ = 0.10 for **6.2**) (Table 6.3, Figure 6.9), determined by using an integration sphere fluorimeter. Although a number of phosphorescent Cu(I) complexes with the coordination environment similar to that of **6.1** and N,N-chelate ligands such as 1,10-phenanthroline[17] (e.g. [Cu(9,10-phenanthroline)(PPh_3)$_2$][BF_4]) and 2-(2-pyridyl)benzimidazole[9] have been demonstrated successfully for use as triplet emitters in OLEDs, their emission quantum efficiencies are all much lower than that of **6.1**. The highest solid state emission quantum efficiency at

ambient temperature for previously known Cu(I) complexes is 0.69 for [Cu(dnbp)(DPEphos)][BF_4] (dnbp = 2,9-di-n-butyl-1,10-phenanthroline, DPEphos = bis[2-(diphenylphosphino)phenyl]ether) in a poly(methyl methacrylate) (PMMA) matrix, reported by Wang and coworkers, which was shown to be an excellent emitter in OLEDs.[17] The exceptionally high emission quantum efficiency and the incorporation of an electron transporting boron functionality make **6.1** a very promising candidate as an efficient bifunctional phosphorescent emitter for OLEDs, which is being investigated by our collaborators.

Table 6.3 Luminescent data for **BNPA**, **6.1** and **6.2**.

Comp.	Excitation λ_{max}, nm[a]	Emission λ_{max}, nm	τ (μs)	Φ	Conditions for Φ
BNPA	342	393	-	0.25[a]	CH_2Cl_2, rt
APBN	335	411	-	1[a]	CH_2Cl_2, rt
6.1	354	540	8.0 (1)	0.04[b]	CH_2Cl_2, rt, under N_2
		527	7.5 (1)	0.88[c]	Neat film, rt
6.2	362	543	25.0 (1)	0.004[b]	CH_2Cl_2, rt, under N_2
		519	10.9 (1)	0.10[c]	Neat film at rt

[a] Relative to anthracene (Φ_r = 0.36). [b] Relative to *fac*-Ir(ppy)$_3$ (Φ_r = 0.40). [c] Absolute value.

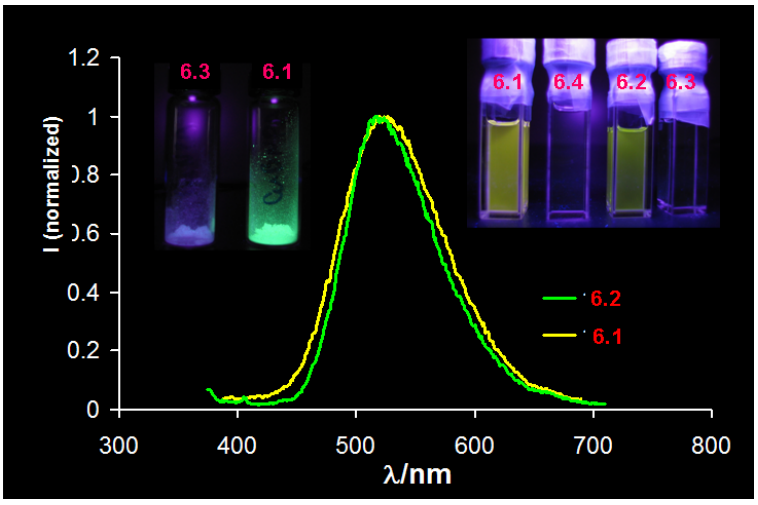

Figure 6.9 Phosphorescent spectra of **6.1** and **6.2** as neat films at ambient temperature. Inset, left: photographs of the solids of **6.1** and **6.3** under UV; right: photographs of the solutions of **6.1**-**6.4** (2.0 x10^{-5} M) in CH_2Cl_2 under N_2 and UV light.

Complex **6.3** is a chloride analogue of **6.2** but does not show any phosphorescence at ambient temperature in solution or the solid state. The significant impact by ancillary ligands on reduction potential, the MLCT absorption energy and phosphorescence led us to suggest that the phosphorescence in **6.2** is most likely from a MLCT state.

To establish the role of the boron center in the phosphorescence of **6.1** and **6.2**, the photophysical properties of their nonboron-containing analogues $[Cu(NPA)(PPh_3)_2][BF_4]$ (**6.4**), $Pt(NPA)Ph_2$ (**3.3**) and $Pt(NPA)Cl_2$ (**6.5**) were also examined. Neither **6.4** nor **6.5** has detectable phosphorescence. Compound **3.3** only displays very weak and hardly visible greenish phosphorescence (λ_{max} = 487 nm, τ = 18.5 μs) at ambient temperature (Figure 6.10), which was not detectable by camera (Figure 6.9). The contrasting properties of **6.1** and **6.2** versus **6.4** and **3.3** illustrate that the $BMes_2$ group in complexes **6.1** and **6.2** is critical for achieving the bright ambient temperature phosphorescence in solution. The role of the $BMes_2$ group is most likely to lower the energy level of the MLCT state below that of the ligand-centered excited state, due to its electron accepting nature, thus facilitating the MLCT emission.

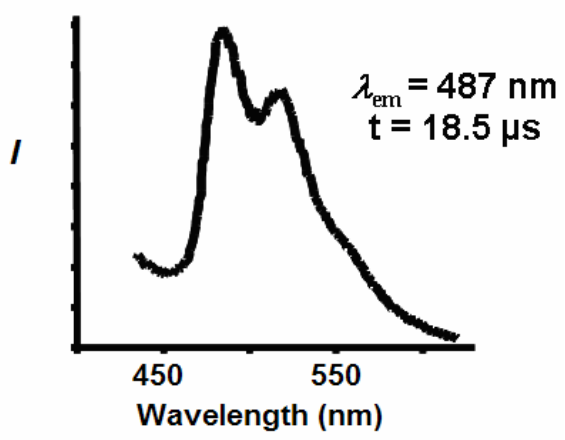

Figure 6.10 Phosphorescent spectrum of **3.3** in CH_2Cl_2 at ambient temperature.

6.3.4 Luminescent response of BNPA, APBN, 6.1 and 6.2 toward TBAF

6.3.4.1 Response of the ligands

The application of highly Lewis acidic luminescent triarylboron compounds for selectively sensing F^- has attracted much current attention, due to their high selectivity toward F^- and their great potentials in overcoming the large hydration enthalpy of F^- in aqueous or alcohol media.[6e-6g] We therefore investigated the fluorescent response of the free ligands and their complexes toward fluorides. In addition, by examining the response of the metal complexes toward fluorides, we will be able to have a better understanding of the electronic properties of the complexes.

The bright fluorescence of BNPA and APBN and make them potentially useful fluoride sensing. The titration of BNPA and APBN in CH_2Cl_2 solution (1.0×10^{-5} M) with TBAF (TBAF = nBu$_4$NF) (6.0×10^{-3} M, in CH_2Cl_2) solution were monitored by both UV-Vis absorption and fluorescence measurements. As illustrated by Figures 6.11 and 6.12, the addition of TBAF to the BNPA solution leads to the quenching of the absorption band at 342 nm in the UV-Vis spectrum and emission band at 393 nm in the fluorescent spectrum. Moreover, the corresponding Stern-Volmer plots show that only ~1.0 equivalent of TBAF is required for the complete quenching in CH_2Cl_2, indicating a fairly strong F^-binding ability of the boron center. The formation of the 1:1 B-F^- adduct was further confirmed by ^{1}H and ^{19}F NMR titration experiments (Figure 6.13). The APBN molecule behaves similarly toward F^-. However, ~7 equivalents of TBAF are required for the complete quenching, indicating a much weaker response, which is consistent with the fact that the B center of APBN has a lower Lewis acidity than that of BNPA, demonstrated by above cyclic voltammetry data.

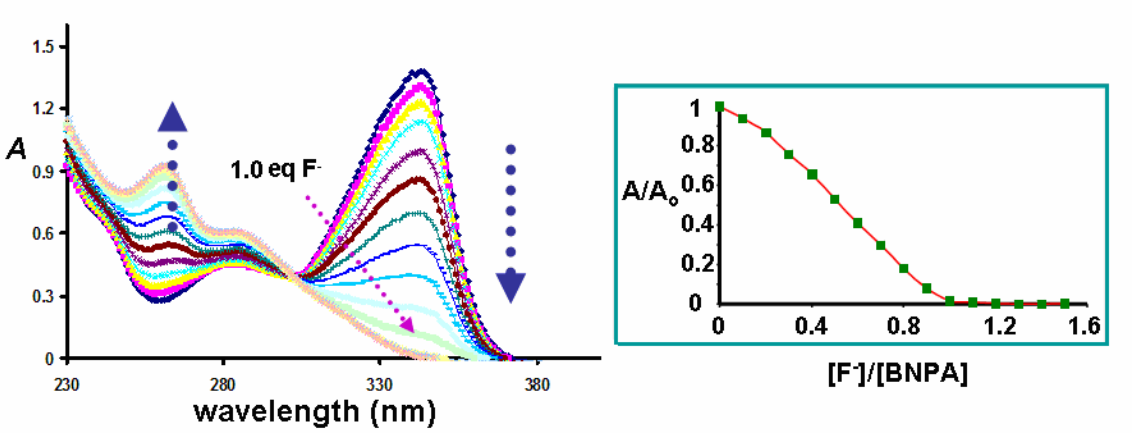

Figure 6.11 UV-Vis titration curves of BNPA (1.0 x 10^{-5} M) in CH_2Cl_2 with TBAF (left) and the corresponding Stern-Volmer plot (right).

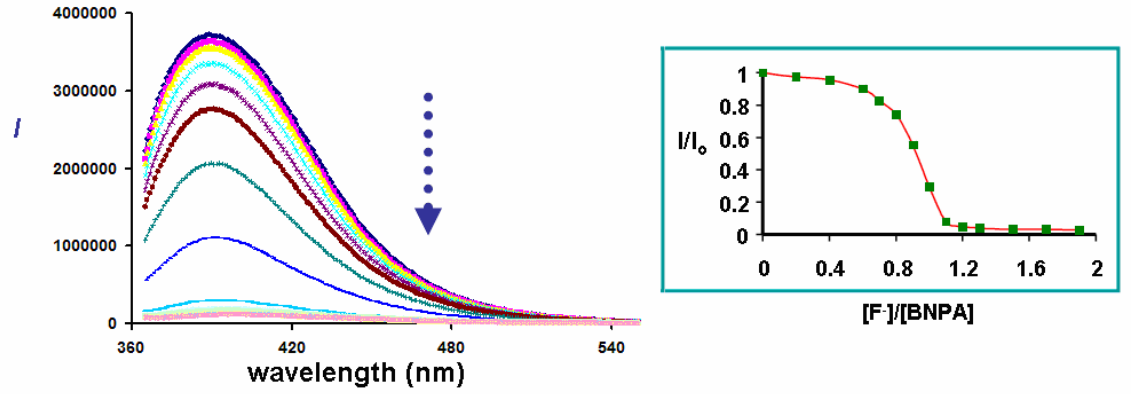

Figure 6.12 Fluorescence titration curves of BNPA (1.0 x 10^{-5} M) in CH_2Cl_2 with TBAF (left) and the corresponding Stern-Volmer plot (right).

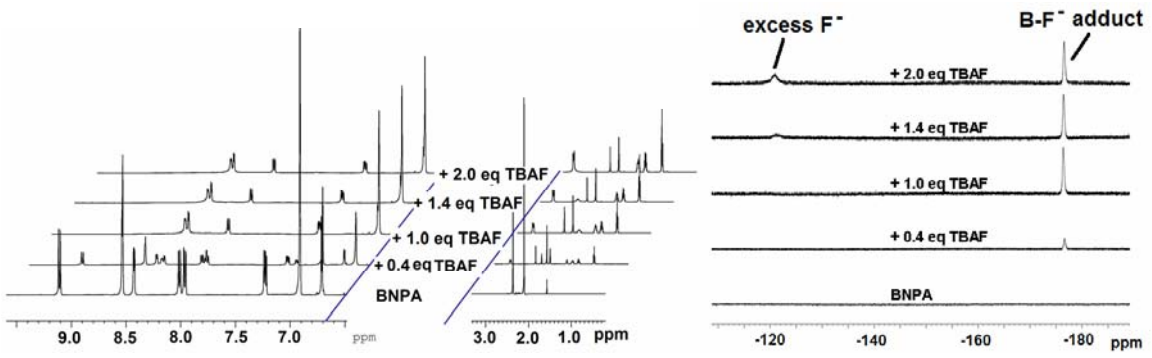

Figure 6.13 ^{1}H (left) and ^{19}F (right) NMR spectra for the titration of BNPA with TBAF in CD_2Cl_2.

6.3.4.2 Response of metal complexes

Examples of ambient-temperature phosphorescent metal complexes that contain a triarylboron group remain rare, and as a result the impact of fluoride binding at the boron center on phosphorescence has not been studied, which strongly motivated us to examine the phosphorescent response of complexes **6.1** and **6.2** toward fluorides.

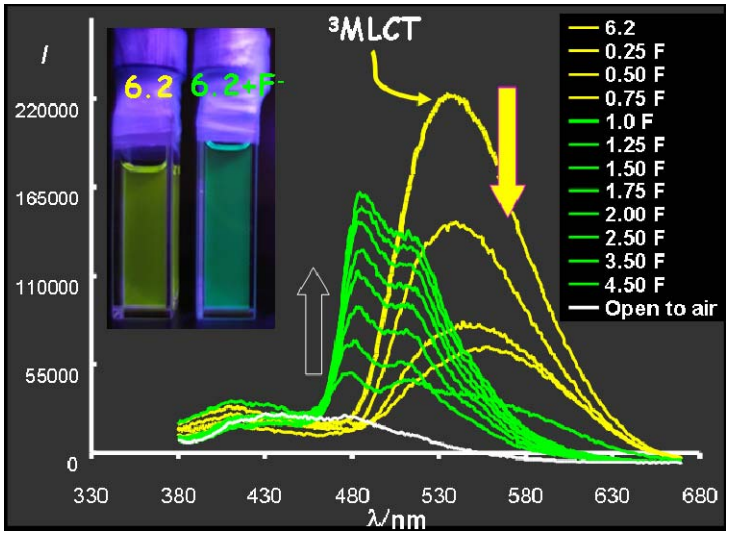

Figure 6.14 Phosphorescent spectral change of **6.2** (λ_{ex} = 360 nm) with the addition of Bu_4NF (TBAF) ([**6.2**] = 4.0 x 10^{-5} M in CH_2Cl_2). Inset: photographs of the solutions of **6.2** before and after the addition of excess TBAF under UV light. The solutions in this experiment were prepared in a dry box under N_2.

In contrast to the free ligands BNPA and APBN that experience a typical fluorescent quenching upon the addition of fluorides, the addition of fluoride ions to the solution of **6.2** causes phosphorescent color switch from yellow to green, as shown by Figure 6.14. The yellow phosphorescent band at 543 nm diminishes while a new oxygen-sensitive green phosphorescent emission band at λ_{max} = 497 nm (τ = 10.9 μs, determined in the presence of excess F^-) appears and increases in intensity with the amount of F^-. The new green emission band can be attributed to the emission of the adduct **6.2**·$\mathbf{F^-}$. This green emission band shows distinct vibrational features and resembles the ^{3}LC natured

phosphorescence of $Pt(NPA)Ph_2$ (**3.3**) (see Figure 6.10). The phosphorescent color switch of **6.2** can be therefore explained as fluoride induced color switching from MLCT to ligand centered emission due to the impact of F^- binding on the energy level of the MLCT state, as illustrated in Scheme 6.4.

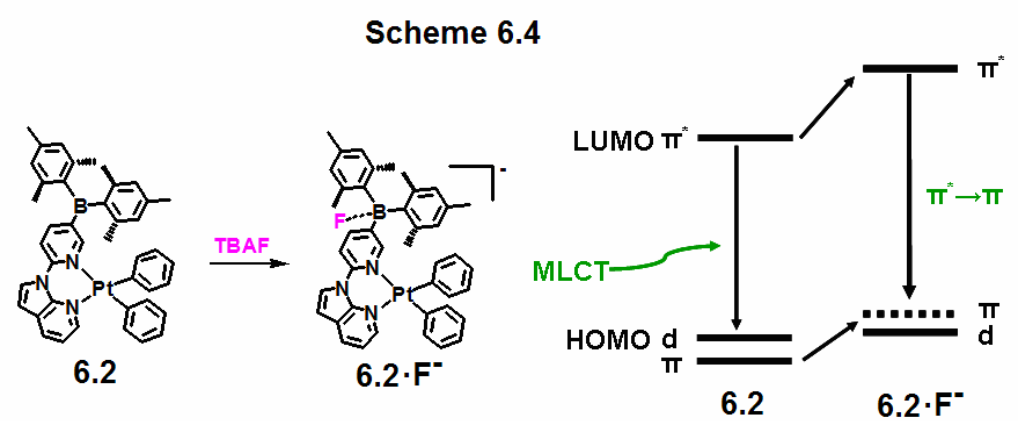

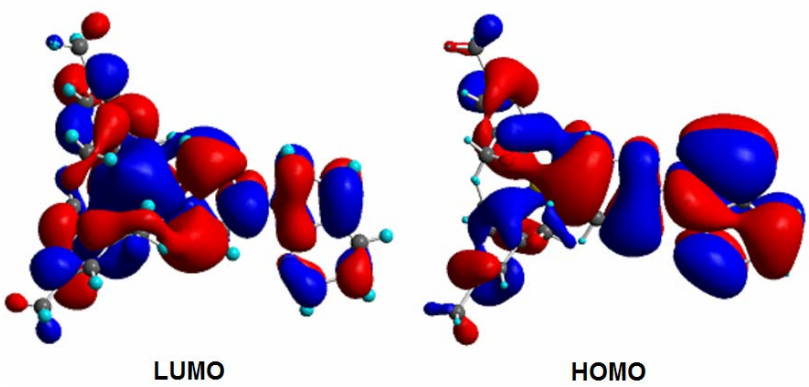

Figure 6.15 Diagrams showing the HOMO and LUMO of BNPA.

As shown by the molecular orbital diagrams of BNPA in Figure 6.15, the LUMO level of BNPA is a π* orbital dominated by the p_π orbital of the boron center while the HOMO level is a π orbital involving the NPA portion. As a result, the addition of the fluoride ion to the boron center in **6.2** destabilizes the π* level significantly (Scheme 6.4). In addition, the binding of a fluoride ion to the boron center converts it from an electron withdrawing group to an electron donating group, thus destabilizing the π level as well.

As illustrated by Scheme 6.4, in complex **6.2**, the F^- addition causes the π level to rise above that of the 5d orbitals of the Pt(II) center, thus quenching the MLCT emission.

The much brighter emission intensity of **6.2·F**$^-$, compared to that of **3.3**, may be attributed to the bulky dimesitylboron group that can effectively reduce intermolecular interactions, hence triplet-triplet annihilation of **6.2·F**$^-$. Although the green emission of **6.2·F**$^-$ is readily quenched by air, this adduct is stable toward air.

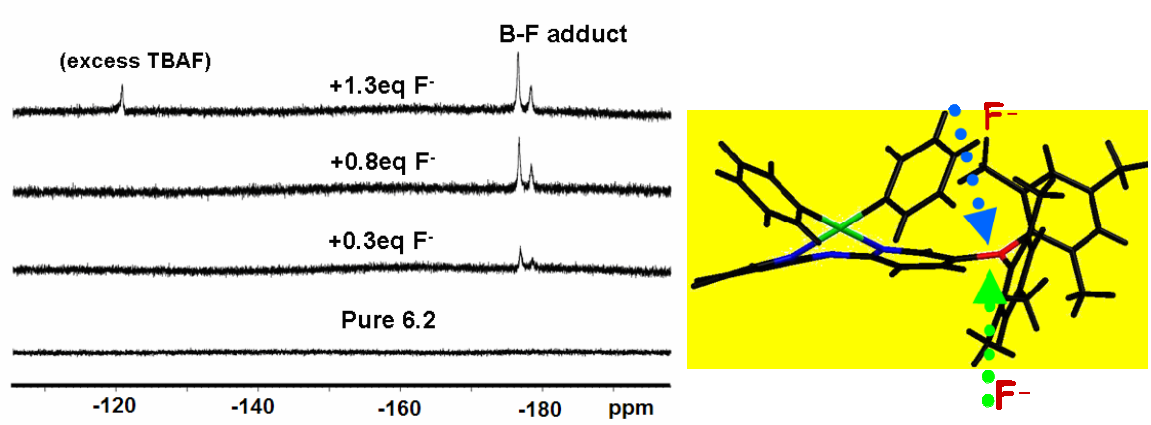

Figure 6.16 ^{19}F NMR titration spectra of **6.2** by TBAF in CD_2Cl_2 (left) and its crystal structure (right) for the explanation of two possible B-F conformers.

The formation of **6.2·F**$^-$ was further confirmed by ^{19}F NMR. Interestingly, as shown in Figure 6.16, after the addition of F^-, the ^{19}F NMR spectra of **6.2** show two distinct B-^{19}F signals, suggesting two different conformers. This response of compound **6.2** toward F^- is in contrast to that of the BNPA ligand, which only displayed one B-^{19}F single after F^- addition. We found that the different F^- response displayed by compound **6.2** can be explained by its molecular structure. As illustrated with the crystal structure of **6.2** in Figure 6.16, the F^- anion can approach the B center from two opposite directions (top and bottom), resulting in two different ^{19}F chemical environments, due to the "boat" conformation of the NPA moiety and the hindered rotation of the B-C bonds, and thereby leading to two different ^{19}F signals.

The phosphorescent response of the Cu(I) complex **6.1** toward F^- is quite different. Compound **6.1** has dual emission in solution (Figure 6.16). The addition of < 0.8 equivalent of F^- under N_2 results in the quenching of the phosphorescent peak and the rise of the BNPA fluorescent peak, which is subsequently quenched with additional F^- in the same manner as the free BNPA does, resulting in a non-emissive solution as shown by the photograph in Figure 6.16. These changes can be attributed to the degradation of **6.1** by F^-. The instability of **6.1** toward F^- was confirmed by UV-Vis and ^{19}F NMR spectral data. The poor stability of 6.1 toward fluorides can be explained by the known poor chelating ability of the NPA moiety[18] and the steric congestion caused by the two PPh_3 ligands. The consequence of the instability of **6.1** toward F^- is that it has the potential to serve as a turn-on sensor for F^- in the concentration range of $[F^-]/[\mathbf{6.1}] < 0.8$ ($[\mathbf{6.1}] = \sim 10^{-5}$ M) under air, since the phosphorescent emission of **6.1** is mostly suppressed by oxygen and the fluorescence of BNPA is switched on in this concentration regime, as confirmed by the fluorescent titration experiment performed under air.

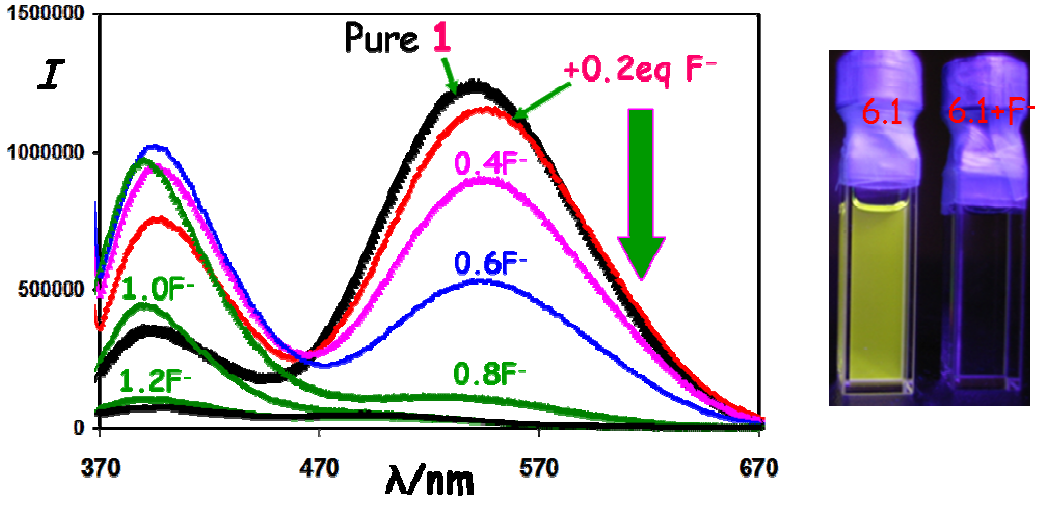

Figure 6.16 Phosphorescent spectral change of **6.1** with the addition of Bu_4NF (TBAF) ([**6.1**] = 4.0 x 10^{-5} M in CH_2Cl_2) (left) and photograph of the solutions of **6.1** before and after the addition of excess TBAF under UV light. The solutions in this experiment were prepared in a dry box under N_2.

Scheme 6.5

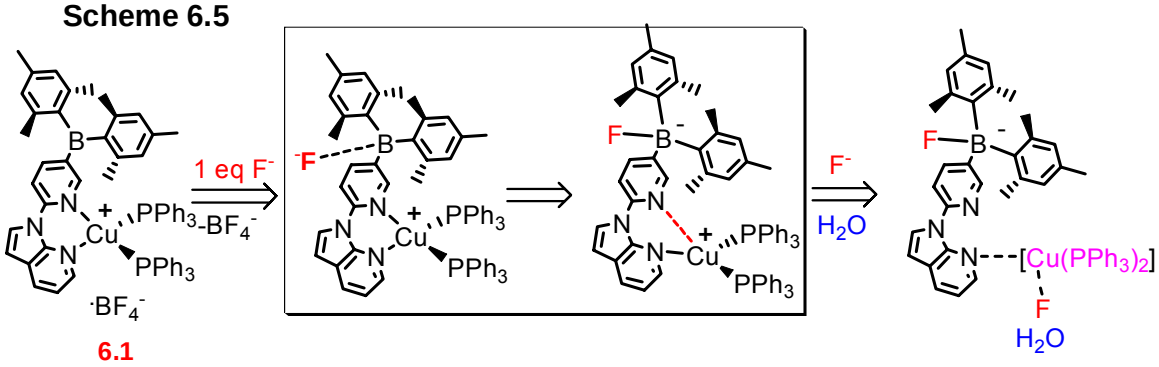

The degradation of **6.1** likely occurs by a process shown in Scheme 6.6. Upon the addition of F^-, the B-F adduct is formed first as confirmed by ^{19}F NMR titration experiments. The geometry change of the boron center increases the steric congestion and therefore weakens the Cu-N bond, resulting in the turn-on of the NPA fluorescence. Further addition of F^- leads to a η^1-BNPA bound Cu complex, which is non-emissive. The water molecules present in the solution likely further facilitates the dissociation of the BNPA ligand. The instability of compound **6.1** toward F^- was further supported by the behavior of the complex $[Cu(NPA)(PPh_3)_2](BF_4)$ (**6.4**) toward F^-. Compound 6.4 does not contain a triarylboron center. However, as shown by the ^1H NMR spectra in Figure 6.17, the addition of F^- causes a considerable change of the spectrum, but no free NPA ligand is generated. Clearly, the F^- anion is able to bind to the Cu(I) center in 6.4, which is again caused by the poor chelating ability of the NPA ligand.

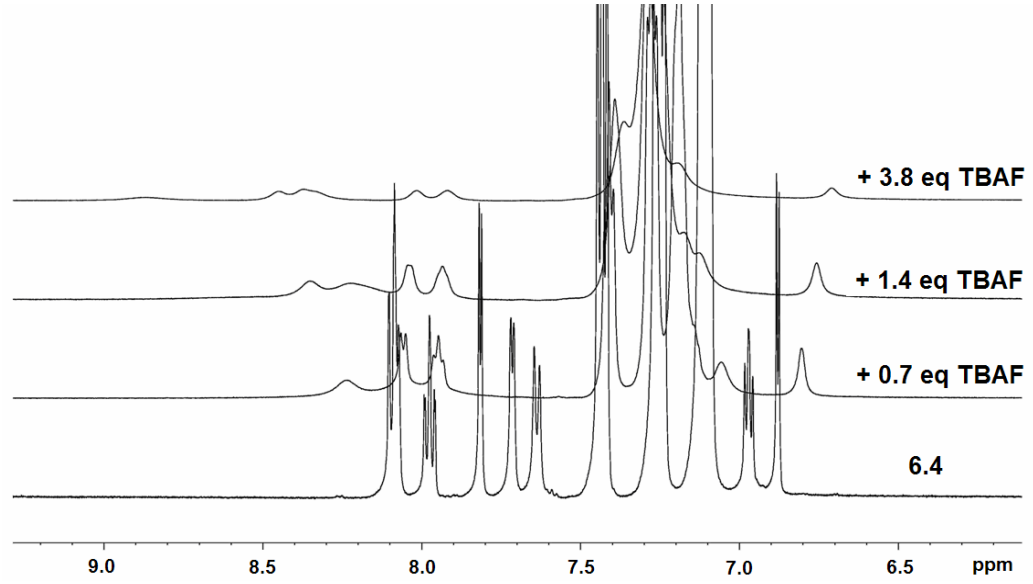

Figure 6.17 ^{1}H NMR titration of compound **6.4** with TBAF in CD_2Cl_2 at ambient temperature.

6.4 Conclusions

In this chapter, we have demonstrated the first examples of bright ambient temperature phosphorescent transition metal complexes that contain a triarylboron group. We have shown that the boron group in these complexes plays a key role in achieving the bright phosphorescence. We have also illustrated that the Pt(II) and Cu(I) complexes have distinct phosphorescent response toward fluoride at ambient temperature due to fluoride triggered energy level change in **6.2** and ligand dissociation in **6.1**. Lastly we have shown that the Cu(I) complex **6.1** is an exceptionally bright phosphorescent emitter in the solid state, thus a very promising candidate for use as a phosphorescent emitter or a bifunctional electron-transport phosphorescent emitter in OLEDs.

References

1. a) For examples, see: Baldo, M. A.; O'brien, D. F.; You, Y.; Shoustikov, A.; Sibley, S.; Thompson, M. E.; Forrest, S. R. *Nature*, **1998**, *395*, 151. b) Kwong, R. C.; Laman, S.; Thompson, M. E. *Adv. Mater.* **2000**, *12*, 1134.
2. a) Shen, Z.; Burrows, P. E.; Bulovic, V.; Borrest, S. R.; Thompson, M. E. *Science* **1997**, *276*, 2009. b) Baldo, M. A.; Lamansky, S.; Burrows, P.; Thompson, M. E.; Forrest, S. R. *Appl. Phys. Lett.* **1999**, *75*, 5. c) Lamansky, S.; Djurovich, P.; Murphy, D.; Abdel-Razzaq, F.; Lee, H. E.; Adachi, C.; Burrows, P. E.; Forrest, S. R.; Thompson, M. E. *J. Am. Chem. Soc*. **2001**, *123*, 4304. d) Liu, Q. D.; Thorne, L.; Kozin, I.; Song, D.; Seward, C.; D'Iorio, M.; Tao, Y.; Wang, S. *J. Chem. Soc., Dalton Trans*. **2002**, 3234.
3. a) Chi, Y.; Chou, P. T. *Chem. Soc. Rev.* **2007**, *36*, 1421 and references therein. b) Yang, C. H.; Cheng, Y. M.; Chi, Y.; Hsu, C. J.; Fang, C. C.; Wong, K. T.; Chou, P. T.; Chang, C, H, Tsai, M. H.; Wu, C. C. *Angew. Chem., Int. Ed.* **2007**, *46*, 2418. c) Chou, P. T.; Chi, Y. *Chem. Eur. J.* **2007**, *13*, 380.
4. a) Huo, C.; Zhang, H.; Zhang, H.; Zhang, H.; Yang, B.; Zhang, P.; Wang, Y. *Inorg. Chem.* **2006**, *45*, 4735. b) DeRosa, M. C.; Hodgson, D. J.; Enright, G. D.; Dawson, B.; Evans, C. E. B.; Crutchley, R. J. *J. Am. Chem. Soc.* **2004**, *126*, 7619. c) Gao, R.; Ho, D. G.; Hernandez, B.; Selke, M.; Murphy, D.; Djurovich, P. I.; Thompson, M. E. *J. Am. Chem. Soc.* **2002**, *124*, 14828.
5. a) Song, D. T.; Wu, Q.; Hook, A.; Kozin, I.; Wang, S. *Organometallics*, **2001**, *20*, 4683. b) Song, D. T.; Jia, W.-L.; Wu, G.; Wang, S. *Dalton Trans.*, **2005**, 433-438.

c) Jia, W.-L; Wang, R.-Y.; Song, D; Bakk, S.; McLean, A.; Wang, S. *Chemistry, Eur. J.*, **2005**, *11*, 832-842.

6. a) Yamaguchi, S.; Shirasaka, T.; Akiyama, S.; Tamao, K. *J. Am. Chem. Soc*. **2002**, *124*, 8816. b) Yamaguchi, S.; Akiyama, S.; Tamao, K. *J. Am. Chem. Soc.* **2001**, *123*, 11372. c) Chiu, C. W.; Gabbai, F. P. *J. Am. Chem. Soc*. **2006**, *128*, 14248. d) Hudnall, T. W.; Melaimi, M.; Gabbai, F. P. *Org. Lett.* **2006**, *8*, 2747. e) Lee, M. H.; Agou, T.; Kobayashi, J.; Kawashima, T.; Gabbai, F. P. *Chem. Commun.* **2007**, 1133. f) Sundararaman, A.; Venkatasubbaiah, K.; Victor, M.; Zakharov, L. N.; Rheingold, A. L.; Jäkle, F. *J. Am. Chem. Soc.* **2006**, *128*, 16554. g) Parab, K.; Venkatasubbaiah, K.; Jäkle, F. *J. Am. Chem. Soc.* **2006**, *128*, 12879. h) Jäkle, F. *Coord. Chem. Rev.* **2006**, *250*, 1107. i) Liu, X.-Y.; Bai, D. R.; Wang, S. *Angew. Chem.; Int. Ed*. **2006**, *45*, 5475. j) Bai, D. R.; Liu, X.-Y.; Wang, S. *Chem. Eur. J.* **2007**, *13*, 5713. k) Sun, Y.; Ross, N.; Zhao, S. B.; Huszarik, K.; Jia, W.-L.; Wang, R. Y.; Wang, S. *J. Am. Chem. Soc.* **2007**, *129*, 7510. l) Venkatasubbaiah, K.; Nowik, I.; Herber, R. H.; Jäkle, F. *Chem. Commun.* **2007**, 2154.

7. a) Noda, T.; Shirota, Y. *J. Am. Chem. Soc.* **1998**, *120*, 9714. b) Shirota, Y. *J. Mater. Chem*. **2005**, *15*, 75. c) Noda, T.; Ogawa, H.; Shirota, Y. *Adv. Mater.* **1999**, *11*, 283. d) Shirota, Y.; Kinoshita, M.; Noda, T.; Okumoto, K.; Ohara, T. *J. Am. Chem. Soc.* **2000**, *122*, 1102. e) Jia, W.-L.; Bai, D. R.; McCormick, T.; Liu, Q. D.; Motala, M.; Wang, R.; Seward, C.; Tao, Y.; Wang, S. *Chem. Eur. J.* **2004,** *10*, 994. f) Jia, W.-L.; Moran, M. J.; Yuan, Y. Y.; Lu, Z. H.; Wang, S. *J. Mater. Chem.* **2005**, *15*, 3326. g) Wakamiya, A.; Mori, K.; Yamaguchi, S. *Angew. Chem., Int. Ed.* **2007**, *46*, 4237.

8. a) Yuan, Z.; Taylor, N. J.; Ramachandran, R.; Marder, T. B. *Appl. Organomet. Chem.* **1996**, *10*, 305. b) Yuan, Z.; Entwistle, C.D.; Collings, J. C.; Albesa-Jové, D.; Batsanov, A. S.; Howard, J. A. K.; Kaiser, H. M.; Kaufmann, D. E.; Poon, S.-Y; Wong, W.-Y; Jardin, C.; Fathallah, S.; Boucekkine, A.; Halet, J.-F.; Taylor, N.J.; Marder, T. B. *Chem. Eur. J.* **2006**, *12*, 2758. c) Entwistle, C. D.; Marder, T. B. *Angew. Chem. Int. Ed. Engl.* **2002**, *41*, 2927. d) Entwistle, C. D.; Marder, T. B. *Chem. Mater.* **2004**, *16*, 4574. e) R. Stahl, C. Lambert, C. Kaiser, R. Wortmann, R. Jakober, *Chem. Eur. J*. **2006**, *12*, 2358.

9. a) M^{c}Cormick, T.; Jia, W.-L.; Wang, S. *Inorg. Chem.* **2006**, *45*, 147. b) Jia, W.-L.; M^{c}Cormick, T.; Tao, Y.; Lu, J. P.; Wang, S. *Inorg. Chem.* **2005**, *44*, 5706.

10. Wu, Q.; Lavigne, J. A.; Tao, Y.; D'Iorio, M.; Wang, S. *Inorg. Chem.* **2000**, *39*, 5248.

11. a) Kubas, G. J. *Inorg. Synth.* **1979**, *19*, 90. b) Diez, J.; Falagan, S.; Gamasa, P.; Gimeno, J. *Polyhedron* **1988**, *7*, 37. c) Song, D.; Wang, S. *J. Organomet. Chem.* **2002**, *648*, 302-305.

12. a) Melhuish, W. H. *J. Phys. Chem.* **1961**, *65*, 229. b) King, K. A.; Spellane, P. J.; Watts, R. J. *J. Am. Chem. Soc.* **1985**, *107*, 1431-1432. c) Lamansky, S.; Djurovich, P.; Murphy, D.; Abdel-Razzaq, F.; Kwong, R.; Tsyba, I.; Bortz, M.; Mui, B.; Bau, R.; Thompson, M. E. *Inorg. Chem.* **2001**, *40*, 1740.

13. a) Palsson, L.-O.; Monkman, A. P. *Adv. Mater*. **2002**, *14*, 757. b) Mello, J. C.; Wittmann, H. F.; Friend, R. H. *Adv. Mater*. **1997**, *9*, 230.

14. 14 a) Kodanko, J. J.; Morys, A. J.; Lippard, S. J. *Org. Lett*. **2005**, *7*, 4585. b) Song, J. J.; Yee, N. K.; Tan, Z.; Xu, J.; Kapadia, S. R.; Senanayake, C. H. *Org.*

Lett. **2004**, *6*, 4905. c) Wang, X.; Rabbat, P.; O'Shea, P.; Tillyer, R.; Grabowski, E. J. J.; Reider, P. J. *Tetrahedron Lett*. **2000**, *41*, 4335. d) Trecourt, F.; Breton, G.; Bonnet, V.; Mongin, F.; Marsais, F.; Queguiner, G. *Tetrahedron Lett*. **1999**, *40*, 4339. e) Tilley, J. W.; Zawoiski, S. *J. Org. Chem.* **1988**, *53*, 386-390. f) Testaferri, L.; Tiecco, M.; Tingoli, M.; Bartoli, D.; Massoli, A. *Tetrahedron* **1985**, *41*, 1373-1384.

15. a) Kiyomori, A.; Marcoux, J. F.; Buchwald, S. L. *Tetrahedron Lett.* **1999**, *40*, 2657. b) Klapars, A.; Antilla, J. C.; Huang, X. H.; Buchwald, S. L. *J. Am. Chem. Soc.* **2001**, *123*, 7727. c) Klapars, A.; Huang, X.; Buchwald, S. L. *J. Am. Chem. Soc.* **2002**, *124*, 7421.
16. House, H. O.; Koepsell, D. G.; Campbell, W. J. *J.* Org. *Chem.* **1972**, *37*, 1003-1011.
17. Zhang, Q.; Zhou, Q.; Cheng, Y.; Wang, L. X.; Ma, D.; Jing, X.; Wang, F. *Adv. Mater.* **2004**, *16*, 432.
18. a) Zhao, S. B.; Wang, R. Y.; Wang, S. *J. Am. Chem. Soc.* **2007**, *129*, 3092. b) Wu, Q.; Lavigne, J. A.; Tao, Y.; D'Iorio, M.; Wang, S. *Inorg. Chem.* **2000**, *39*, 5248.

Chapter 7

Dinuclear Cu(I) Complexes of 1,2,4,5-Tetrakis(1-*N*-7-azaindolyl)benzene

7.1 Introduction

Besides the recently established applications in material sciences as phosphorescent emitters in OLEDs by us[1] and others[2], Cu(I) complexes with N,N-chelate ligands are a class of molecules that have long been investigated extensively for their redox properties, their possible use as models for dioxygen activation by biological copper systems,[3] and their catalytic activity in C-N cross-coupling reactions.[4,5] These application prospects of Cu(I) complexes have motivated us to explore the chemistry of Cu(I) compounds with the 7-azaindole containing ligand 1,2,4,5-tetrakis(1-*N*-7-azaindolyl)benzene (TTAB).[6]

Chart 7.1

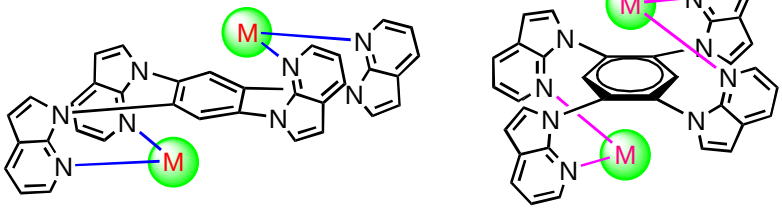

Our earlier investigation on Ag(I), Zn(II), Pd(II) and Pt(II) complexes of TTAB has shown that this blue luminescent molecule is capable of chelating to two metal centers either *via* 1,2-chelate mode[6] or the 1,3-chelate mode,[7] as shown in Chart 7.1, depending on the coordination geometry of the metal ions. The aim of the research

described in this chapter is to investigate Cu(I) complexes of the TTAB ligand to determine the binding mode of Cu(I) ions in the TTAB complexes and the luminescent properties of the complexes.

Several dinuclear Cu(I) TTAB complexes with ancillary ligands MeCN, PPh_3, I^- and I_3^- have been synthesized. The Cu(I) center in these complexes is persistently three-coordinate with the TTAB ligand adopting the 1,3-chelate mode. The details on the syntheses, characterization and property investigation are presented in this chapter.

7.2 Experimental Section

7.2.1 General procedures

All reactions were performed under N_2 with Schlenk techniques or in a dry-box unless otherwise noted. All starting materials were purchased from Aldrich Chemical Co. and used without further purification. CH_2Cl_2 was freshly distilled over P_2O_5. CH_3CN was freshly distilled over CaH_2. THF, DMF and hexanes were purified using the solvent purification system (Innovation Technologies, Inc.). NMR spectra were recorded on Bruker Avance 400 or 500 MHz spectrometers. Elemental analyses were performed by Canadian Microanalytical Service, Ltd, Delta, British Columbia. Thermogravimetric analysis for compound **7.1** was performed on a Perkin-Elmer TGA7 analyzer. Cyclic voltammetry was performed using a BAS CV-50W analyzer using 0.10 M tetrabutylammonium hexafluorophosphate (TBAP) as the supporting electrolyte and dry DMF as the solvent. The electrolytic cell used was a conventional three-compartment cell, in which a Pt working electrode, a Pt auxiliary electrode, and a Ag/AgCl reference electrode were employed. The ferrocenium/ferrocene couple was used as the internal

standard ($E^{1/2}$ = 0.55 V). The TTAB ligand was synthesized by our previously reported procedure.[6] $[Cu(CH_3CN)_4][BF_4]$ and $[Cu(CH_3CN)_2(PPh_3)_2][BF_4]$ were synthesized according to literature procedures.[8]

7.2.2 Synthesis of $[Cu_2(TTAB)(CH_3CN)_2][BF_4]_2$ (7.1)

TTAB (0.11 g, 0.20 mmol) and $[Cu(CH_3CN)_4][BF_4]$ (0.13 g, 0.40 mmol) were mixed in CH_2Cl_2 (10 mL), and the solution was stirred for 3 hours at room temperature. The addition of hexanes (10 mL) resulted in the precipitation of the product. The solid was separated and washed with THF/hexanes (1:1) (5 mL), resulting in complex **7.1** as white solid (0.18 g, 96% yield). Crystals of complex **7.1** were obtained by the slow diffusion of a CH_2Cl_2/toluene (2:1) (2 mL) solution of TTAB (0.016 g, 0.030 mmol) to a CH_2Cl_2 (3 mL) solution of $[Cu(CH_3CN)_4][BF_4]$ (0.019 g, 0.060 mmol). ^{1}H NMR (400 MHz, CD_2Cl_2 25 °C): δ 8.81 (s; 4H, 7-aza), 8.56 (s; 2H, phenyl), 8.35 (d; ^3J = 7.2 Hz; 4H, 7-aza), 7.57 (s; 4H, 7-aza), 6.73 (s; 4H, 7-aza), 6.70 (d; ^3J = 3.4 Hz; 4H, 7-aza), 2.06 (s; 6H, CH_3CN) ppm. ^{13}C NMR: δ 145.83, 145.11, 132.96, 132.92, 127.94, 127.92, 119.59, 118.82, 104.55, 124.09, 2.33 ppm. Anal. calcd. for $C_{34}H_{22}B_2Cu_2F_8N_8$: C 48.43, H 2.63, N 13.29, found: C 48.19, H 2.49, N 13.37.

7.2.3 Synthesis of $[Cu_2(TTAB)(PPh_3)_2][BF_4]_2$ (7.2)

Method 1: TTAB (0.054 g, 0.10 mmol) and $[Cu(CH_3CN)_4][BF_4]$ (0.063 g, 0.20 mmol) were mixed in CH_2Cl_2 (5 mL), and the solution was stirred for 3 hours at room temperature. PPh_3 (0.053 g, 0.20 mmol) was added to the solution. The mixture was stirred for 1 hour. The addition of hexanes (8 mL) resulted in the precipitation of the

product. The solid was separated and washed with CH_2Cl_2/hexanes, resulting complex **7.2** as a white solid (0.12 g, 84% yield). Crystals of complex **7.2** were obtained by the recrystallization of **7.2** with CH_2Cl_2/toluene (1:1).

Method 2: A CH_2Cl_2 (15 mL) solution of $[Cu(CH_3CN)_2(PPh_3)_2][BF_4]$ (0.30 g, 0.40 mmol) was added to a CH_2Cl_2 (15 mL) solution of TTAB (0.11 g, 0.20 mmol) over 20 minutes, and the mixture was stirred for 3 hours at room temperature. The solution was concentrated to ~10 mL and hexanes (15 mL) were added. The resulting solid was isolated and washed with CH_2Cl_2/hexanes to afford complex **7.2** as a white solid (0.21 g, 76% yield). ^{1}H NMR (400 MHz, CD_2Cl_2 25 °C): δ 8.94 (s; 4H, 7-aza), 8.44 (d; ^3J = 7.6 Hz; 4H, 7-aza), 7.83 (s; 2H, phenyl of TTAB), 7.71 (s; 4H, 7-aza), 7.30 (m; 6H, phenyl of PPh_3), 7.11 (m; 12H, phenyl of PPh_3), 6.92 (m; 12H, phenyl of PPh_3), 6.77(d, ^3J = 3.4 Hz; 4H, 7-aza), 6.31 (d; ^3J = 3.4 Hz; 4H, 7-aza) ppm. ^{13}C NMR: δ 145.30, 144.97, 133.70, 133.03, 132.92, 131.43, 129.69, 129.61, 127.32, 124.49, 120.84, 119.18, 105.57 ppm. ^{31}P NMR: δ - 0.16 ppm. Anal. Calcd. for $C_{70}H_{52}B_2Cu_2F_8N_8P_2$: C 61.47, H 3.83, N 8.19; found: C 61.46, H 3.71, N 8.13.

7.2.4 Synthesis of $[Cu_2(TTAB)(I)_2]$ (7.3)

TTAB (0.054 g, 0.10 mmol) and CuI (0.038 g, 0.20 mmol) were dissolved in CH_2Cl_2 (30 mL), and the solution was stirred for 1 hour at room temperature, resulting in a yellow suspension. After the removal of the solvent, the solid was washed with Et_2O (10 mL x 2) to afford **7.3** as a yellow solid (0.082 g, 92% yield). ^{1}H NMR (500 Hz, DMSO, 25 °C): δ 8.32 (s; 2H, phenyl of TTAB), 8.30 (s; 4H, 7-aza), 8.01 (d; ^3J = 7.2 Hz; 4H, 7-aza), 7.20 (s; 8H, 7-aza), 6.50 (s; 4H, 7-aza) ppm. ^{13}C NMR: δ 147.81, 143.91,

133.50, 130.10, 130.07, 121.36, 117.78, 102.79 ppm. Anal. Calcd. for $C_{34}H_{22}Cu_2I_2N_8$: C 44.22, H 2.40, N 12.13; found: C 44.04, H 2.34, N 11.95.

7.2.5 Syntheses of $[Cu_2(TTAB)(I_3)_2]$ (7.4) and $[Cu_2(TTAB)(\mu\text{-}I)(BF_4)]_n$ (7.5)

TTAB (0.054 g, 0.10 mmol) and $[Cu(CH_3CN)_4][BF_4]$ (0.063 g, 0.20 mmol) were mixed in CH_2Cl_2 (5 mL), and the solution was stirred for 3 hours at room temperature. After a THF/toluene (4:1) (2.5 mL) solution of I_2 (0.051 g, 0.20 mmol) was added to the solution, the mixture was stirred overnight. The slow evaporation of the solvent of the reaction mixture afforded deep red crystals of complex **7.4** (~0.013 g, ~9% yield, based on TTAB). After the separation of complex **7.4**, the further evaporation of the mother liquor afforded yellow crystals of complex **7.5**, along with trace amount of small deep red crystals of **7.4**. After being washed with CH_2Cl_2 (3 mL), the red crystals were separated manually from the mixture, and the yellow crystals of **7.5** were obtained (~0.041 g, 46% yield, based on TTAB).

Complexes **7.4** and **7.5** were also synthesized by the following methods. For **7.4**: $[Cu_2(TTAB)(CH_3CN)_2][BF_4]_2$ (0.038 g, 0.040 mmol), Bu_4NI (0.030 g, 0.080 mmol) and I_2 (0.020 g, 0.080 mmol) were mixed in CH_2Cl_2 (5 mL), and the brown solution was stirred overnight. The slow evaporation of the solvent afforded deep red crystals of **7.4** (~40% yield). ^{1}H NMR (400 MHz, CD_3CN, 25 °C): δ 8.21 (s; 2H, phenyl of TTAB), 8.12 (s; 4H, 7-aza), 7.90 (s; 4H, 7-aza), 7.19 (s; 4H, 7-aza), 7.09 (s; 4H, 7-aza), 6.50 (s; 4H, 7-aza) ppm. ^{13}C NMR: δ 147.97, 143.81, 133.80, 129.69, 128.90, 121.38, 117.50, 102.56 ppm. Anal. Calcd.for $C_{34}H_{22}Cu_2I_6N_8$: C 28.54, H 1.55, N 7.83, found: C 28.38, H 1.46, N 8.06.

For **7.5**: $[Cu_2(TTAB)(CH_3CN)_2][BF_4]_2$ (**7.1**) (0.019 g, 0.020 mmol) and Bu_4NI (0.007 g, ~0.02 mmol) were mixed in CH_2Cl_2 (2 mL), and the resulting clear yellow solution was stirred for 30 minutes. The resulting light yellow precipitate was separated and washed with CH_2Cl_2 to afford **7.5** in ~ 58% yield. NMR data could not be obtained due to the poor solubility of **7.5**. Anal. Calcd. for $C_{34}H_{22}BCu_2F_4N_8I \cdot 0.5CH_2Cl_2$: C 44.76, H 2.50, N 12.10; found: C 44.47, H 1.98, N 11.44.

7.2.6 General procedure for Cu(I) catalyzed coupling reactions of phenyl halide with imidazole

CuI/1,10-phenanthroline as the catalyst: A 50 mL oven-dried Schlenk tube containing a stir bar was quickly charged with CuI (0.019 g, 0.10 mmol), 1,10-phenanthroline (1,10-phen) (0.036 g, 0.20 mmol), imidazole (0.068 g, 1.0 mmol) and the base Cs_2CO_3 (0.65 g, 2.0 mmol). The tube was sealed and evacuated and refilled with N_2. 1.0 mL of the predried phenyl halide after being saturated with N_2 was transferred into the Schlenk tube. The mixture was heated in an oil bath at appropriate temperature for 19 or 48 hours. After cooled down to room temperature, the reaction mixture was diluted with 20 mL of water, and extracted with CH_2Cl_2 (20 mL x 3). After the removal of the solvent, the residue was purified by chromatography on a silica gel column with ethyl acetate/hexanes (4:1) as the eluent. The organic product was characterized by ^1H NMR. The catalysis results are listed in Table 7.4.

Complex 7.1 as the catalyst: The same procedure as above was adopted, except that complex **7.1** (0.047g, 0.050 mmol) was used as the catalyst instead of CuI/1,10-phen. No additional free TTAB ligand was added to the system except entry 6 in Table 7.4 where 1 equivalent of the TTAB ligand was used.

7.2.7 Monitoring the dioxygen reaction with compound 7.1

In a dry box, compound **7.1** was dissolved in dry THF to afford a colorless solution (~1.0 x 10^{-5} M). Then 2.5 mL of this solution was transferred to a UV-Vis cell and the cell was sealed by a rubber stopper. The UV-Vis spectrum of this solution was recorded at ambient temperature. 8 portions of 2 mL of O_2 gas at one atmosphere were introduced to the UV-Vis cell *via* a syringe at ~ 3 minutes intervals. The spectra were recorded at ~ 1 minute interval. After the addition of ~ 10 mL of O_2, no further spectral change was observed. No obvious color change of the solution was observed during and after the O_2 addition. Some white precipitation was observed during the O_2 addition.

7.2.8 X-ray diffraction analyses

Crystals were mounted on glass fibers for data collection. Data were collected on a Siemens P4 single-crystal X-ray diffractometer with a Smart CCD-1000 detector and graphite-monochromated Mo Kα radiation, operating at 50 kV and 35 mA at 180 K. No significant decay was observed for all of the samples. Data were processed on a PC using the Bruker SHELXTL software package (version 5.10). Toluene solvent molecules are located in the lattice of **7.1** and refined successfully. CH_2Cl_2 solvent molecules are located in the lattice of **2** and refined successfully. The crystal of **7.5** is small and diffracts weakly. Disordered toluene and THF solvent molecules are found in the lattice of **7.5** and they are partially located, modeled and refined due to the limitation of data. In addition, the BF_4^- is disordered, which along with the poor quality of data and the disordered solvent molecules and the missing solvent molecules contributes to the relatively poor

structural parameters of **7.5**. All non-hydrogen atoms except the disordered solvent molecules were refined anisotropically. All hydrogen atoms except those of the disordered solvent molecules were calculated, and their contributions in structural factor calculations were included. The crystallographic data for **7.1** and **7.2** are given in Table 7.1, and those for **7.4** and **7.5** are given in Table 7.2, and the selected bond lengths and angles for complexes **7.1**, **7.2**, **7.4** and **7.5** are listed in Table 7.3.

Table 7.1 Crystallographic data for compounds **7.1** and **7.2**.

Compound	**7.1**	**7.2**
Formula	$C_{38}H_{28}N_{10}B_2F_8Cu_2 \cdot 1C_7H_8$	$C_{70}H_{52}N_8B_2F_8Cu_2 \cdot 4CH_2Cl_2$
FW	Monoclinic	Triclinic
Space Group	$P2_1/n$	P-1
a, Å	8.3948(19)	12.323(4)
b, Å	14.034(3)	13.386(4)
c, Å	18.518(4)	13.496(4)
α, º	90	93.117(6)
β, º	99.223(5)	102.741(5)
γ, º	90	116.504(5)
V, Å^3	2153.4(9)	1913.2(10)
Z	2	1
$D_{calc,}$ g·cm^{-3}	1.563	1.482
T, K	180(2)	180(2)
μ, mm^{-1}	1.070	0.945
$2\theta_{max}$, º	56.76	56.70
Reflns measured	11772	13374
Reflns used (R_{int})	4925 (0.0443)	8589 (0.0242)
Parameters	331	469
Final R values		
[I > 2σ(I)]:	0.0621	0.0772
R_1[a]	0.1340	0.2064
wR_2[b]		
R values (all data):		
R_1[a]	0.1229	0.1129
wR_2[b]	0.1586	0.2303
Goodness-of-fit on F^2	1.019	1.054

[a] $R_1 = \Sigma|F_0| - |F_c|/\Sigma|F_0|$

[b] $wR_2 = [\Sigma w [(F_0^2-F_c^2)^2] / \Sigma[w(F_0^2)^2]]^{1/2}$

$w = 1 / [\sigma^2(F_0^2) + (0.075P)^2]$, where $P = [Max (F_0^2,0) + 2F_c^2]/3$

Table 7.2 Crystallographic data for compounds **7.4** and **7.5**.

Compound	**7.4**	**7.5**
Formula	$C_{34}H_{22}N_8I_6Cu_2$	$C_{34}H_{22}N_8BF_4ICu_2 \cdot 2C_7H_8/1C_4H_8O$
FW	Monoclinic	Monoclinic
Space Group	$P2_1/c$	$C2/m$
a, Å	8.997(1)	24.954(5)
b, Å	23.441(4)	14.712(3)
c, Å	9.4998(16)	14.377(3)
α, º	90	90
β, º	108.838(3)	112.475(3)
γ, º	90	90
V, Å^3	1896.1(5)	4877.1(3)
Z	2	4
$D_{calc,}$ g·cm^{-3}	2.507	1.552
T, K	180(2)	180(2)
μ, mm^{-1}	6.044	1.568
$2\theta_{max}$, º	56.64	56.74
Reflns measured	12569	17687
Reflns used (R_{int})	4473 (0.1048)	6077 (0.1993)
Parameters	230	286
Final *R* values [I>2σ(I)]:		
R_1[a]	0.0610	0.1055
wR_2[b]	0.0974	0.2516
R values (all data):		
R_1[a]	0.1585	0.3546
wR_2[b]	0.1135	0.3296
Goodness-of-fit on F^2	0.847	0.811

[a] $R_1 = \Sigma||F_0| - |F_c||/\Sigma|F_0|$

[b] $wR_2 = [\Sigma w [(F_0^2-F_c^2)^2] / \Sigma[w(F_0^2)^2]]^{1/2}$

$w = 1 / [\sigma^2(F_0^2) + (0.075P)^2]$, where $P = [Max (F_0^2,0) + 2F_c^2]/3$

Table 7.3 Selected bond lengths (Å) and angles (º) for **7.1**, **7.2**, **7.4** and **7.5**.

	Compound **7.1**		
Cu(1)-N(1)	2.005(3)	N(5)-Cu(1)-N(3)	109.68(15)
Cu(1)-N(3)	2.001(4)	N(5)-Cu(1)-N(1)	113.46(16)
Cu(1)-N(5)	1.971(4)	N(3)-Cu(1)-N(1)	133.72(13)
	Compound **7.2**		
Cu(1)-N(1)	2.034(4)	N(1)-Cu(1)-N(3)	113.90(17)
Cu(1)-N(3)	2.061(4)	N(1)-Cu(1)-P(1)	129.76(13)
Cu(1)-P(1)	2.2189(14)	N(3)-Cu(1)-P(1)	111.12(12)
	Compound **7.4**		
Cu(1)-N(2)	2.027(9)	N(3)-Cu(1)-N(2)	118.9(4)
Cu(1)-N(3)	1.994(9)	N(3)-Cu(1)-I(1)	129.3(3)
Cu(1)-I(1)	2.5123(17)	N(2)-Cu(1)-I(1)	110.8(3)
I(1)-I(2)	3.0605(12)	Cu(1)-I(1)-I(2)	106.95(5)
I(2)-I(3)	2.8014(12)	I(1)-I(2)-I(3)	179.41(4)
	Compound **7.5**		
I(1)-Cu(1)	2.537(2)	N(1)-Cu(1)-N(3)	126.3(5)
Cu(1)-N(1)	1.960(13)	N(1)-Cu(1)-I(1)	113.9(4)
Cu(1)-N(3)	1.996(13)	N(3)-Cu(1)-I(1)	118.3(4)
Cu(1)-I(1)-Cu(1')	96.82(9)		

7.3 Results and Disccussion

7.3.1 Syntheses of the dinuclear Cu(I) complexes

The colorless dinuclear Cu(I) complex **7.1** was obtained nearly quantitatively by the reaction of $[Cu(CH_3CN)_4]BF_4$[8] with TTAB in a 2:1 ratio, as shown in Scheme 7.1. This new complex is moderately stable toward air in acetonitrile but highly air-sensitive in other common organic solvents, which may be attributed to the known stabilization effect of acetonitrile to Cu(I) complexes.[9] On the other hand, the partial dissociation of TTAB from the Cu(I) center occurs in CH_3CN with at a low concentration of **7.1**, presumably due to the formation of $[Cu(CH_3CN)_4]BF_4$. In solvents such as CH_2Cl_2 compound **7.1** remains intact, as confirmed by ^1H NMR.

Scheme 7.1

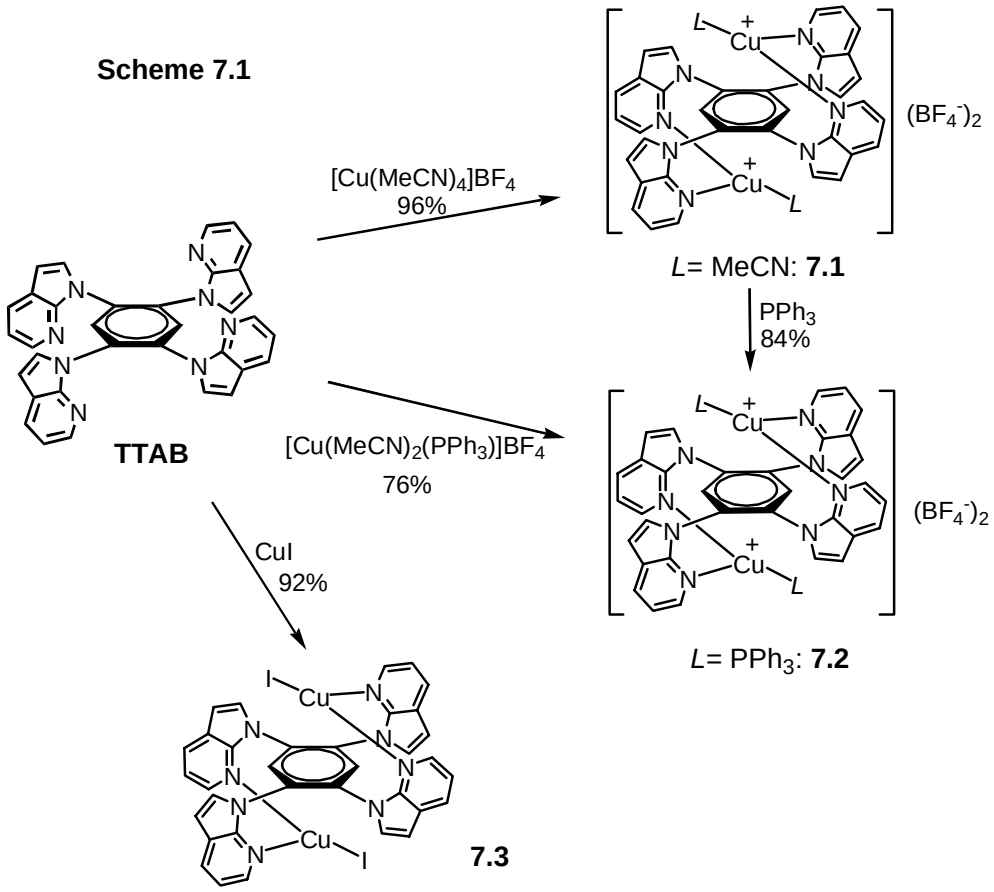

The coordinated CH_3CN in **7.1** can be readily exchanged by phosphine ligands. The reaction of 2 equivalents of PPh_3 with **7.1** affords colorless complex **7.2** in 84% yield (Scheme 7.1). Compound **7.2** is more stable than **7.1** and can also be obtained in good yield directly by the reaction of TTAB with $[Cu(MeCN)_2(PPh_3)_2]BF_4$[8] (Scheme 7.1). The air-stable light yellow complex **7.3**, which has poor solubility in most organic solvents, was synthesized from the reaction of TTAB with CuI (Scheme 7.1). The reaction of $LiCH_3$ with complex **7.3** was carried out in an attempt to synthesize $[Cu_2(TTAB)(CH_3)_2]$. The treatment of the suspension of **7.3** in dry Et_2O by $LiCH_3$ at 0 °C yielded a colorless solution; however, attempts to isolate the product were unsuccessful due to its rapid decomposition at ambient temperature.

Scheme 7.2

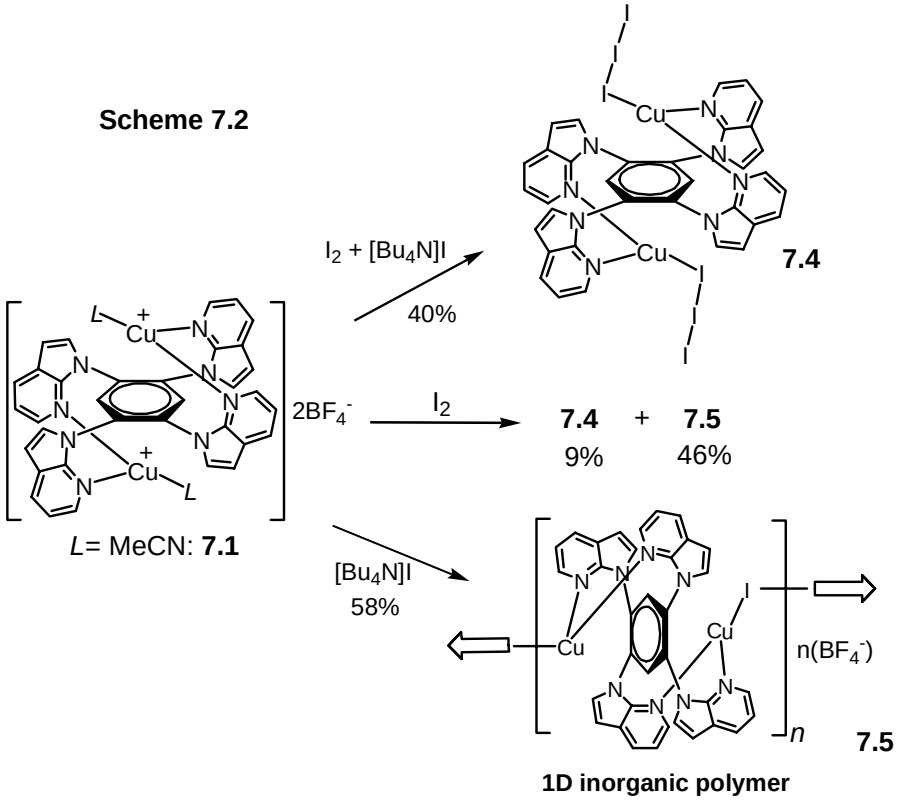

As shown in Scheme 7.2, the dark red complex **7.4** and the yellow complex **7.5** were initially isolated from the reaction mixture of complex **7.1** with I_2. The presence of

the I_3^- anion in **7.4** or the I^- anion in **7.5** indicates the occurrence of a redox reaction involving I_2. Likely, a small amount of Cu(I) reacted with I_2 to produce I^- which in turn reacted with I_2 to form the I_3^- anion. The syntheses of complex **7.4** and **7.5** were also achieved by direct preparative methods (Scheme 7.2). The reaction of **7.1** with 2 equivalents of NBu_4I and 2 equivalents of I_2 produced **7.4** in ~40% yield, and the reaction of **7.1** with 1 equivalent of NBu_4I afforded **7.5** in 58% yield.

Complexes **7.1**-**7.5** were fully characterized by NMR spectroscopy and elemental analyses. The vacuum-dried complex **7.1** shows no peaks between 2250 and 2350 cm^{-1} in the IR spectrum, indicating the loss of the coordinated CH_3CN, as further confirmed by elemental analyses. Thermogravimetric analysis indicated that the loss of CH_3CN in **7.1** occurs at *ca* 40 °C and is complete at *ca* 105 °C (~7% loss). The chemical shift of ^{31}P of **7.2** in CD_2Cl_2 is -0.17 ppm at room temperature, comparable with previously reported Cu(I) PPh_3 complexes.[1] The structures of **7.1**, **7.2**, **7.4** and **7.5** were determined by single-crystal X-ray diffraction analyses.

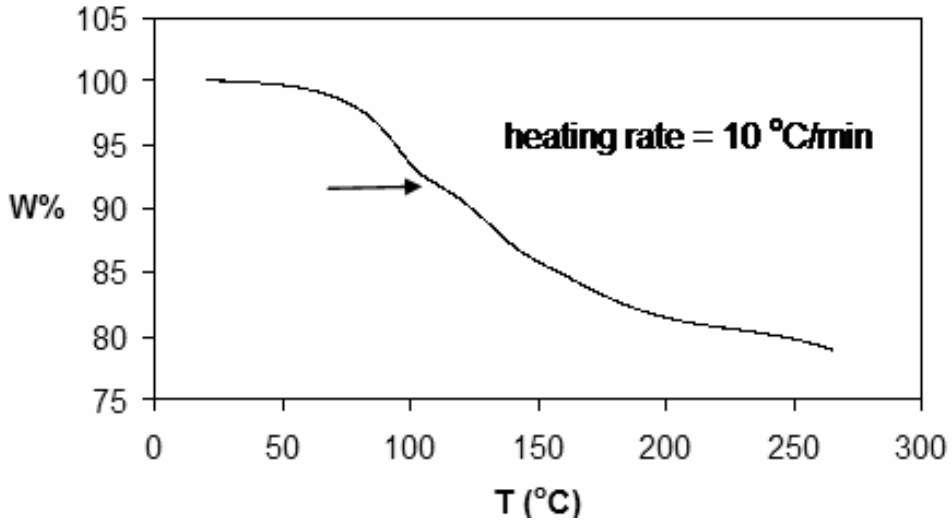

Figure 7.1 Thermogravimetric diagram of compound **7.1** recorded under N_2.

7.3.2 X-ray structures of complexes 7.1, 7.2, 7.4 and 7.5

The structures of the cations in compounds **7.1**, **7.2**, and **7.5**, and the molecular structure of **7.4** are shown in Figure 7.2 to Figure 7.5, respectively. The BF_4^- anion is omitted for clarity for **7.1**, **7.2**, and **7.5**. The dinuclear units of all four structures possess a crystallographically imposed inversion center. The common feature among the four compounds is that the Cu(I) center is three-coordinate with an approximate trigonal planar geometry, while the TTAB ligand is chelated to the Cu(I) center in the 1,3-chelation mode in all four structures with CH_3CN, Ph_3P, I_3^-, or I^- occupying the third coordination site. The four Cu-N(7-aza) bond lengths in the four complexes are nearly identical, as shown in Table 7.3, and are close to those in $[Cu(H_2CPz_2)(CH_3CN)]ClO_4$ (1.997 Å),[9] $[Cu(dmp)(CH_3CN)]PF_6$ (2.027 Å),[10] and $[Cu(Phen)(CH_3CN)]BF_4$ (2.014 Å).[11]

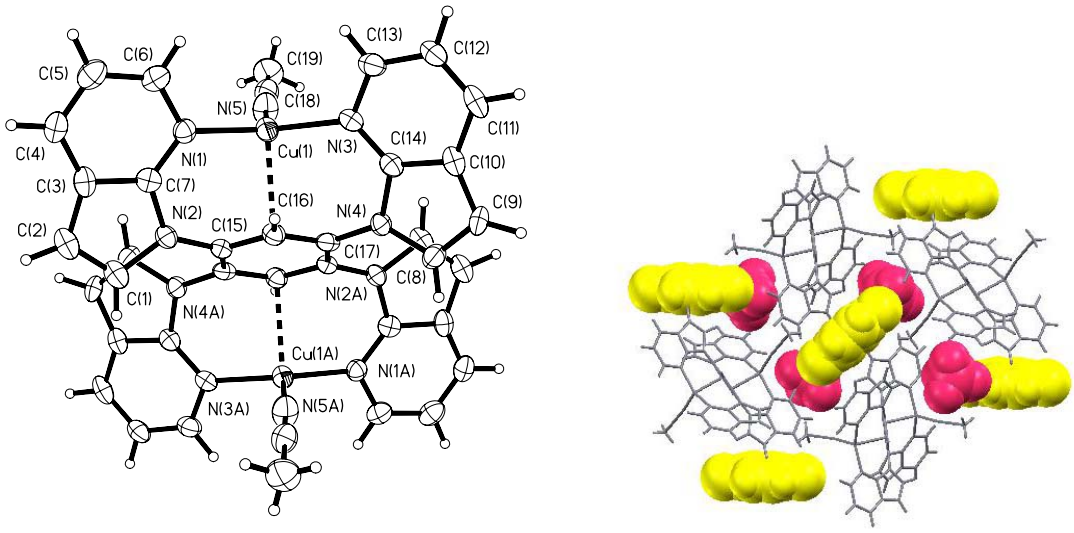

Figure 7.2 Left: a diagram showing the structure of the dinuclear unit in **7.1**. Right: the unit cell packing diagram projected down *a* axis, showing the solvent channels in the lattice. The BF_4^- (red) and toluene (yellow) are shown in space filling style.

For metal ions that have a square planar geometry, the 1,2-chelation mode of TTAB has been observed exclusively.[6,7] For d^{10} metal ions that prefer a tetrahedral

geometry, the preferred bonding mode is 1,3-chelation because it minimizes the interactions between the ligands on the metal center and the TTAB ligand. The 1,3-bonding mode has been observed for a dinuclear Ag(I) complex where two $Ag(NO_3)(DMSO)$ groups are chelated to the TTAB ligand.[7] An exception to the 1,3-chelation mode by a d^{10} metal ion was observed in the dinuclear complex $Zn_2Cl_4(TTAB)$ where the two $ZnCl_2$ units are chelated to the TTAB ligand in a 1,2-chelation mode with a highly distorted tetrahedral geometry.[7] The preferential formation of the 1,3-chelation mode by the complexes **7.1**, **7.2**, **7.4** and **7.5** can be attributed to the geometrical constraint imposed by the three-coordinate Cu(I) center which requires the N-Cu-N chelate angle to be ~120°, a value difficult to achieve with the 1,2-chelating mode (the largest N-M-N bond angle that has been observed in the 1,2-chelation mode is 97° in the dinuclear Zn(II) complex[7]). The N(1)-Cu(1)-N(3) chelate angle in **7.1** was in fact determined to be 133.7(1)°. In contrast, the same angle in **7.2** is much smaller, 113.90(17)°, which is clearly caused by the bulky PPh_3 group. For **7.4** and **7.5**, the N-Cu-N chelate angle is close to an ideal trigonal planar geometry (118.9(4)° and 126.3(5)°, respectively).

An important feature revealed by the structure of **7.1** is that, despite the relative small size of the CH_3CN ligand and its abundance in solution when **7.1** is produced, the Cu(I) center in **7.1** is only coordinated to one CH_3CN ligand (Figure 7.2). Cu(I) ions are known to have the tendency to form four-coordinate compounds. Three-coordinate Cu(I) compounds, albeit becoming increasingly abundant, are still less common than four-coordinate ones.[3] A close examination of the structure of **7.1** revealed the presence of a short separation distance between the Cu(I) center and one of the carbon atoms (C(16)) in

the central benzene ring, as evidenced by the Cu(1)···C(16) distance of 2.383(4) Å. Although this distance is much longer than a typical Cu-C bond length, it is close to the previously reported weak d-π interaction distances between a Cu(I) center and an aryl ring[3d,12,13] and much shorter compared to the sum of van der Waals radii 3.10 Å of Cu and carbon atoms. A weak interaction between the central benzene ring and the Cu center is therefore likely present in **7.1**. If C(16) were considered as a weakly bound donor atom, the Cu(I) center has an approximate tetrahedral geometry (the angles of C(16)-Cu(1)-N range from 87.99(14)° to 114.63-(16)°). In other words, the geometry constraint imposed by the TTAB ligand appears to stabilize or favor the formation of three-coordinate Cu(I) centers. In the structure of **7.2**, a similar interaction between the Cu center and the central phenyl ring is also evident, as shown in Figure 7.3, although the separation distance between the Cu atom and the carbon atom (C(2)) is considerably longer (2.454(4) Å) than that in **1** due to the presence of the bulky PPh_3 ligand. For **7.4** and **7.5**, short separation distances between the Cu center and the central benzene ring (C(16)) are also present (Cu(1)···C(16) = 2.36(1) Å in **7.4**, Cu(1)···(16) = 2.37(1) in **7.5**).

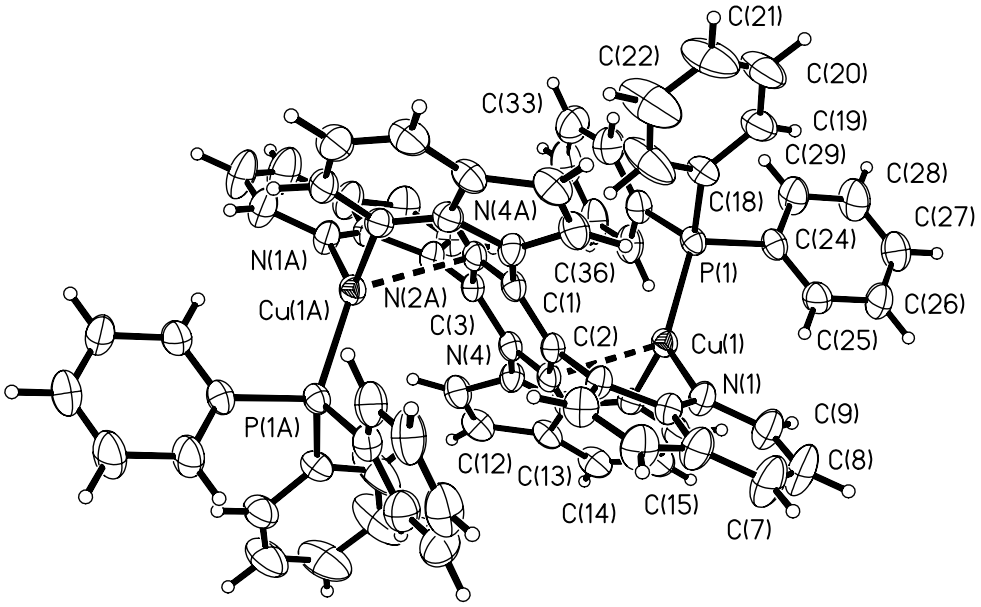

Figure 7.3 A diagram showing the structure of the dinuclear unit in **7.2**.

The persistent three-coordinate geometry of Cu(I) in all four complexes is therefore consistent with the presence of weak interactions between the central benzene ring and the copper center, imposed by the geometry of the TTAB ligand. The Cu···Cu separation distance within the dinuclear unit is 6.133, 6.313, 6.064, and 6.045 Å for **7.1**, **7.2**, **7.4**, and **7.5**, respectively. The Cu-N (CH_3CN) bond distance in **7.1**, 1.971(4) Å, is comparable to those reported in the four-coordinate Cu(I) complexes containing the CH_3CN ligand[14] but significantly longer than the Cu-$NCCH_3$ bond lengths in the three-coordinate Cu(I) complexes containing 1,10-phen chelate[10] (1.852(7) Å), bis(3,5-dimethylpyrazol-1-yl)methane chelate[9] (1.879(4) Å), and Tolman's *β*-diketiminate chelate[3a-3c] (1.859(4)-1.862(4)Å) and the two-coordinate complex[15] $[CuI(CH_3CN)_2][B(C_6F_5)_4]$ (1.844(2) Å). The relatively long Cu-N (CH_3CN) bond distance in **7.1** may account for the facile dissociation of the coordinated CH_3CN ligand

in **7.1**. The Cu-P bond distance in **7.2** (2.219(2) Å) is similar to previously known Cu-P distances.[1]

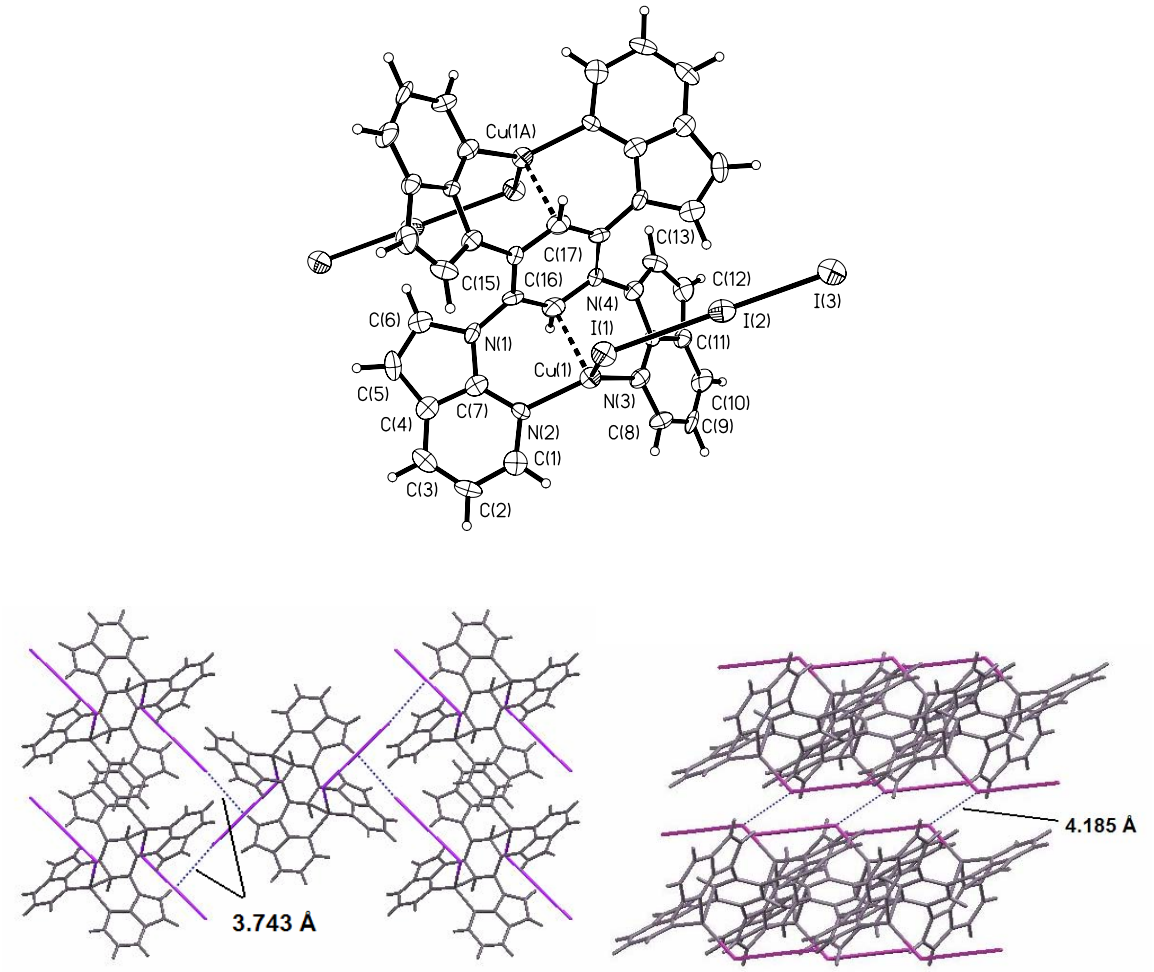

Figure 7.4 Top: a diagram showing the structure of the dinuclear unit in **7.4**. Bottom: the unit cell packing diagram projected down the *a* axis (left) and the *b* axis (right), showing the intermolecular interactions between the I_3^- ligands.

Each Cu(I) center in **7.4** is bound by one I_3^- anion (Figure 7.4). Although Cu(I) complexes that contain a I_3^- ligand were reported previously,[16] to the best of our knowledge, complex **7.4** is the first reported example of three-coordinate Cu(I) complexes with a I_3^- ligand. The Cu-I bond length in **7.4** is 2.512(2) Å, the I(1)-I(2) bond length, 3.060(1) Å, is considerably longer than that of I(2)-I(3), 2.801(1) Å, but similar to those reported in the literature.[17] The I_3^- anion has a nearly perfect linear geometry with

the I(1)-I(2)-I(3) bond angle being 179.41(4)°. In the crystal lattice, the molecules of **7.4** have wavelike layered structures with the dinuclear Cu2 units being sandwiched by the I_3^- anions. The I_3^- form layered structures with weak intermolecular I···I interactions. Within each layer, the neighboring I_3^- anions have a T-shaped arrangement with the I···I contact distance being 3.743(1) Å, as shown by the unit cell packing diagram projected down the *a* axis in Figure 7.4. Between the two neighboring layers, the I_3^- anions interact in a zigzag manner with the I···I contact distance being 4.185(1) Å, as shown by the unit cell packing diagram shown projected down the *b* axis in Figure 7.4. Both T-shaped and zigzag-style I···I interactions between I_3^- anions have been observed previously.[17]

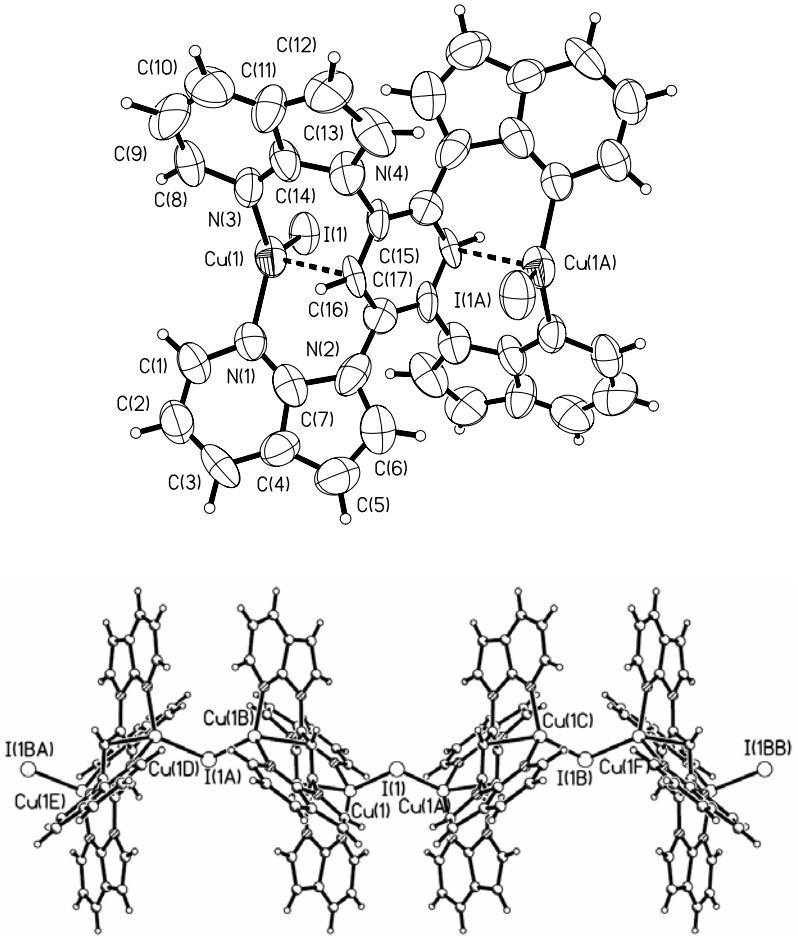

Figure 7.5 A diagram showing the structure of the dinuclear unit in **7.5** (top) and the iodide-bridged 1D polymer chains (bottom).

In the dinuclear unit of **7.5**, each Cu center is bound by an I^- ligand with a Cu-I bond length of 2.537(2) Å (Figure 7.5), similar to that observed in **7.4**. The iodide ligand in **7.5** acts as a bridging ligand by coordinating to two Cu(I) centers with a Cu-I-Cu bond angle of 96.82(9)°, thus linking the two neighboring Cu2 units together to form a 1D zigzag coordination polymer, as shown in Figure 7.5. The Cu-Cu separation distance bridged by the I^- ligand is 3.795(2) Å, much shorter than that within the dinuclear unit, but longer than the sum (3.40 Å) of van der Waals radii of two Cu atoms, indicating no Cu-Cu interactions. Cu(I) coordination polymers that contain an iodide bridge are known previously.[17] However, all previous reported examples involving iodide bridging ligands are four-coordinate Cu(I) compounds.[17]

The crystals of **7.1**, **7.2**, and **7.5** all host solvent guest molecules inside the lattice. For example as shown in Figure 7.2, the cationic dinuclear units in **7.1** are arranged in such a manner that 1D channels along the *a* axis are formed which host the BF_4^- and the toluene solvent molecules. Similar 1D channels are present in the lattice of **7.2** which host CH_2Cl_2 solvent molecules and BF_4^-. For **7.5**, 1D coordination polymer chains stack on top of each other in a parallel fashion that results in the formation of a highly porous crystal lattice (*ca* 35% of the volume of the unit cell is occupied by solvent molecules) with rectangular channels.

7.3.3 Electronic and luminescent properties

Compound **7.1** displays a broad irreversible oxidation peak at *ca* 1.1 V in the CV diagram in DMF (the $FeCp_2$ oxidation peak appears at 0.57 V under the same condition) which can be assigned to the oxidation of Cu(I) to Cu(II). Compound **7.2** displays two

irreversible oxidation peaks at 0.80 and 1.10 V, respectively, which may be assigned to the oxidation of the two Cu(I) centers in **7.2**, indicative of the possible presence of electronic communication between the two Cu(I) centers in **7.2**. CV diagrams for compound **7.3**, **7.4** and **7.5** could not be obtained due to their poor solubility.

The absorption spectra of complexes **7.1**-**7.3** have several intense absorption bands in the region of 200-350 nm which resemble those of the free TTAB ligand as shown in Figure 7.6. For compounds **7.3**, a very weak and broad metal-to-ligand charge-transfer (MLCT) band in the 320-420 nm region was observed which accounts for its pale yellow color in solution (inset, Figure 7.6). The absorption spectra of **7.4** and **7.5** were not recorded due to their poor solubility.

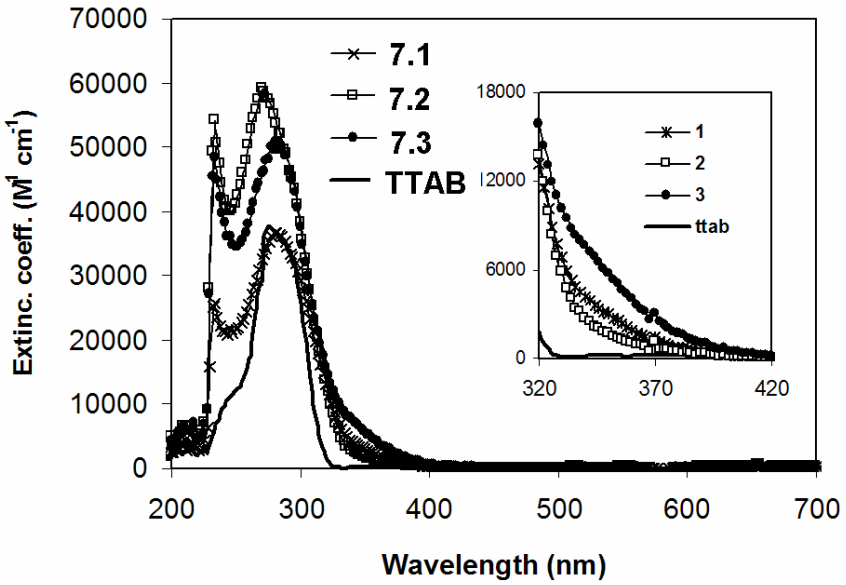

Figure 7.6 UV-Vis absorption spectra of **7.1-7.3** and **TTAB** in CH_2Cl_2 (~10^{-5} M).

The free TTAB ligand is a fairly bright blue emitter in the solid state.[7] In contrast, the solids of all above compounds do not display any detectable emission when excited by UV light. In CH_2Cl_2 solution, complexes **7.1**, **7.2** and **7.3** all display much weaker blue color with the emission wavelength being significantly red-shifted, compared to the

free TTAB ligand (Figure 7.7). To demonstrate the impact of Cu(I) coordination on TTAB fluorescence, a titration experiment was carried out where an incremental amount of $[Cu(PPh_3)_2(MeCN)_2][BF_4]$ was added to a TTAB CH_2Cl_2 solution (1.0×10^{-5} M) while its excitation and emission spectra were monitored. The initial addition of Cu(I) readily quenches the TTAB emission, whereas after the addition of 1 equivalent of Cu(I), the intensity change becomes less dramatic but significant red-shift of the emission wavelength occurs, as shown in Figure 7.8. No further spectral change is observed after the addition of *ca* 2.4 equivalents of $[Cu(PPh_3)_2(MeCN)_2][BF_4]$, and the resulting emission spectrum matches very well with that of **7.2**. The titration experiment as well as the much weaker emission of **7.1**-**7.3** relative to the free TTAB ligand established unequivocally that the Cu(I) coordination causes drastic quenching of TTAB emission and shifts its emission energy to a longer wavelength. Similar fluorescent quenching of TTAB by other d^{10} metal ions such as Ag(I) and Zn(II) has been observed previously.[7] At 77 K, using a time-resolved phosphorescent spectrometer, no MLCT emission band was observed for all three complexes, a behavior that is in sharp contrast to the Cu(I) complexes of 2-(2'-pyridyl)-benzimidazolyl[1] derivative ligands where the complexes display exclusively MLCT emission with a long decay lifetime.

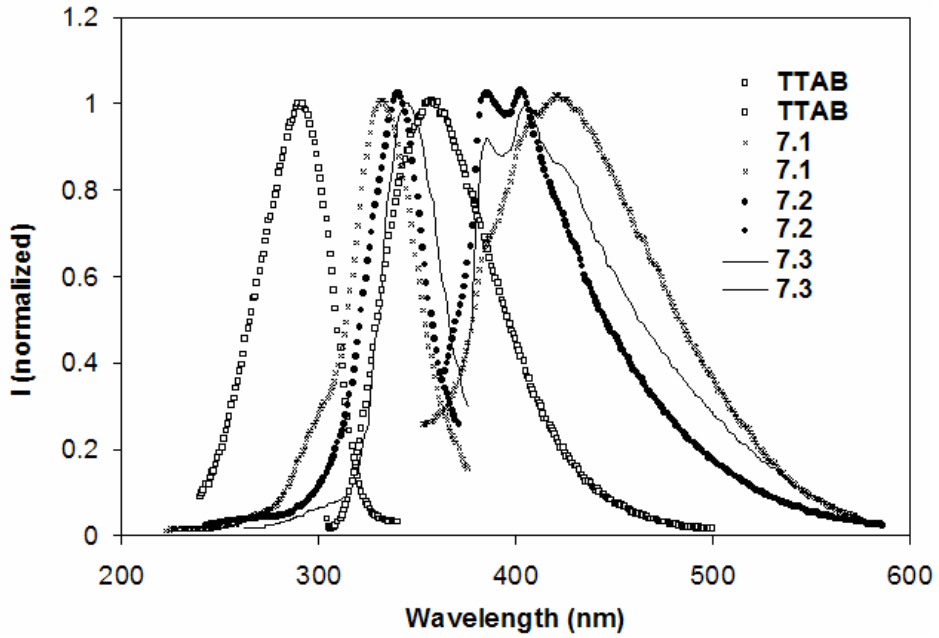

Figure 7.7 The normalized excitation and emission spectra of **7.1**-**7.3** and **TTAB** in CH_2Cl_2 (~10^{-5} M) at ambient temperature.

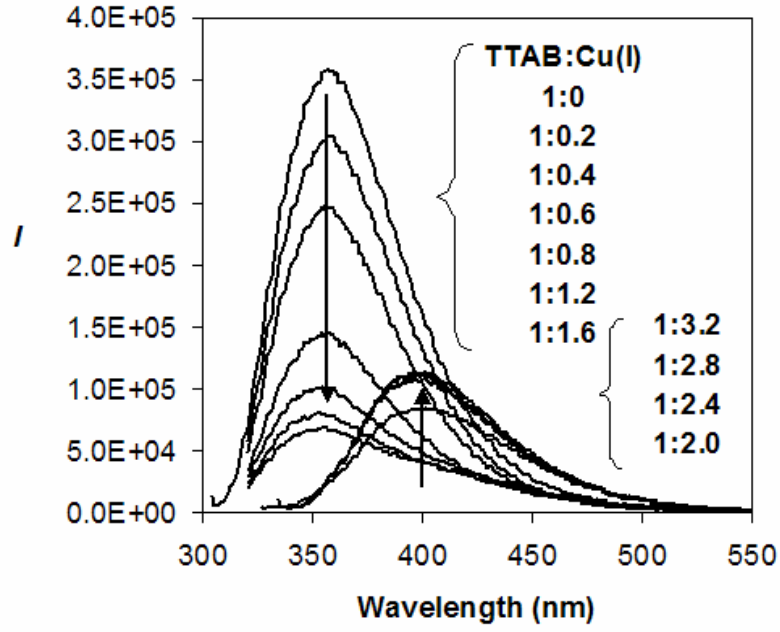

Figure 7.8 The emission spectral change of **TTAB** in CH_2Cl_2 (1.0 x 10^{-5} M) with the addition of $[Cu(PPh_3)_2(CH_3CN)_2][BF_4]$ at ambient temperature.

7.3.4 Reactivity Study of Complex 7.1

7.3.4.1 C-N Coupling

One of the important applications involving Cu(I) compounds is their use as catalysts in Ullmann condensation reactions for the formation of C-N bonds.[4,5] Although different forms of copper, including the metal itself, the Cu(I) or Cu(II) salts, and the oxides have been found to be able to catalyze the C-N coupling reactions, earlier mechanistic studies revealed that the active species is the Cu(I) ion.[4] Traditional Ullmann condensation reactions require the use of high temperature and highly polar solvents, which greatly limits its scope of applications.[4] In 1999, Buchwald reported that the efficient Ullmann-type *N*-arylation of imidazoles can be achieved by using CuOTf/1,10-phen as the catalyst and xylenes as the solvent at relatively low temperature.[5a] Since then, a variety of new ligand systems, along with different bases and solvents, have been examined to further improve the Ullmann condensation reactions.[5b-5j] Previous studies focused exclusively on mononuclear Cu(I) systems and no investigation on the use of dinuclear Cu(I) compounds as catalysts have been reported to date. Accordingly, the dinuclear Cu(I) compound **7.1** was selected to test as catalyst for C-N bond formation reactions between phenyl halides and imidazole (Scheme 7.3), and the catalytic activity of complex **7.1** was compared with the CuI/1,10-phen system, reported by Buchwald's group.[5]

Scheme 7.3

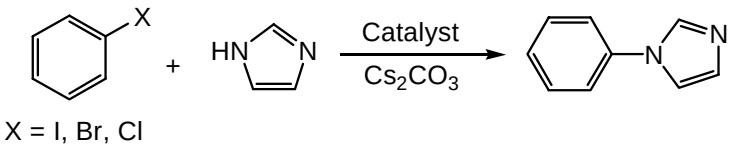

Table 7.4 Catalytic *N*-arylation of imidazole with phenyl halides.

Entry	Ph-X	Catalyst	T (°C)/time (h)	Yield(%)[a]
1	Ph-I	CuI	145/19	<3
2	Ph-I	CuI/1,10-phen (1:2)	145/19	95
3	Ph-I	**7.1**	145/19	97
4	Ph-Br	CuI/1,10-phen (1:2)	165/48	91
5	Ph-Br	**7.1**	165/48	62
6	Ph-Br	**7.1**/TTAB (1:1)	165 /48	73
7	Ph-Cl	CuI/1,10-phen (1:2)	165/72	trace[b]
8	Ph-Cl	**7.1**	165/72	trace[b]

[a] Isolated yield (± 3%, average of two runs). [b] Based on TLC. All reactions were carried out with 1.0 mmol of imidazole, 2.0 mmol of Cs_2CO_3, 0.10 mmol of copper catalysts (based on copper) in 1.0 mL of phenyl halide, which was used as both the reagent and the solvent.

The results of our preliminary study are summarized in Table 7.4. The experimental data showed that the order of reactivity of the phenyl halide is PhI > PhBr > PhCl with the chlorobenzene being almost inert under the conditions used. The N,N-chelating ligand is found to be critical for the aryl C-N bond formation reactions (entry 1). These observations are in good agreement with the literature.[4,5] For the reaction of phenyl iodide, the performance of complex **7.1** is comparable to that of CuI and 2 equivalents of 1,10-phen. The advantage for **7.1** here is that the additional amount of the free ligand is not necessary. In case of phenyl bromide, **7.1** is less effective relative to the CuI/1,10-phen system. To enhance the catalyst activity of **7.1**, 1 equivalent of TTAB ligand (relative to **7.1**) was added (entry 6 in Table 3), leading to ~10% increase of the yield, but still inferior to the CuI/1,10-phen system. The relatively low reactivity of complex **7.1** could be caused by its instability (ligand dissociation).

7.3.4.2 Reactivity with O_2

Three-coordinate Cu(I) compounds bound with ancillary ligands as MeCN are known to be active toward O_2 activation.[3] We therefore tested the ambient temperature reaction of complex **7.1** with O_2 by UV-Vis spectroscopy. As shown by the data in Figure 7.9, compound **7.1** in THF has two intense absorption bands at 262 and 292 nm, respectively. The introduction of O_2 to the solution led to a blue-shift of the band at 262 nm to 244 nm, the intensity of which also increased substantially with the amount of O_2 injected. After the addition of *ca* 16 mL of O_2 (1 atm) to a THF solution of **7.1** (~$1.0x10^{-5}$ M, 2.5 mL), no further spectral change was observed. No color change was evident during and after the addition of O_2. The spectral change was not caused by the dissociation of the TTAB ligand, as shown by the free TTAB UV-Vis spectrum (Figure 7.9, inset). Further attempts to characterize and identify the oxidized products were unsuccessful.

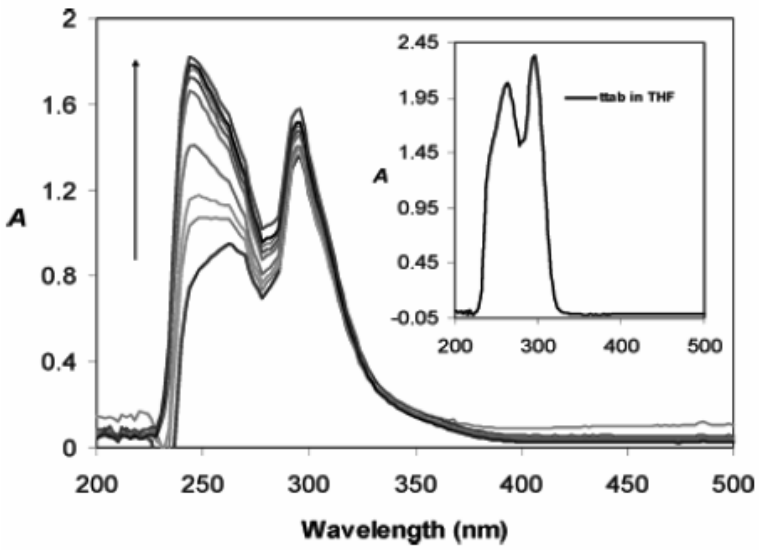

Figure 7.9 The UV-Vis spectral change of compound **7.1** in THF (~10^{-5} M), recorded at ambient temperature, with the addition of O_2 gas. (The spectra were recorded at ~ 1 minute interval and not all the recorded spectra are shown.)

7.4 Conclusions

The TTAB ligand has been shown to form dinuclear Cu(I) compounds readily. The Cu(I) center in the resulting complexes favors the 3-coordinate geometry with the TTAB ligand consistently adopting 1,3-chelation mode. In these complexes, a close contact between the TTAB ligand bridging benzene ring and the Cu(I) center is present, which may play a role on the stability and reactivity of the complexes. These Cu(I) complexes have the tendency to trap solvent molecules in the crystal lattice. The coordination of the Cu(I) center to the TTAB ligand partially quenches the emission of the TTAB ligand and shifts the emission energy to a longer wavelength. The Cu(I)-CH_3CN complex **7.1** displays a catalytic activity for the C-N coupling reactions of imidazole with phenyl halides, comparable to but not better than that of CuI/1,10-phen. Moreover, preliminary UV-Vis data indicate that compound **7.1** reacts with O_2 readily, but further research is needed to establish the detail of this oxidation reaction and the fate of the Cu(I) complex.

References

1. a) Jia, W. L; M^{c}Cormick, T.; Tao, Y.; Lu, J. P.; Wang, S. N. *Inorg. Chem.* **2005**, *44*, 5706. (b) M^{c}Cormick, T.; Jia, W. L; Wang, S. N. *Inorg. Chem.* **2006**, *45*, 147.
2. Zhang, Q.; Zhou, Q.; Cheng, Y.; Wang, L.; Ma, D.; Jing, X.; Wang, F. *Adv. Mater.* **2004**, *16*, 432.
3. a) Reynolds, A. M.; Gherman, B. F.; Cramer, C. J.; Tolman, W. B. *Inorg. Chem.* **2005**, *44*, 6989. b) Spencer, D. J. E.; Aboelella, N. W.; Reynolds, A. M.; Holland, P. L.; Tolman, W. B. *J. Am. Chem. Soc.* **2002**, *124*, 2108. c) Spencer, D. J. E.; Reynolds, A. M.; Holland, P. L.; Jazdzewski, B. A.; Duboc-Toia, C.; Pape, L. L.; Yokota, S.; Tachi, Y.; Itoh, S.; Tolman, W. B. *Inorg. Chem.* **2002**, *41*, 6307. d) Osako, T.; Terada, S.; Tosha, T.; Nagatomo, S.; Furutachi, H.; Fujinami, S.; Kitagawa, T.; Suzuki, M.; Itoh, S. *Dalton Trans.* **2005**, 3514. e) Lewis, E. A.; Tolman, W. B. *Chem. Rev.* **2004**, *104*, 1047, and references therein.
4. a) Bunnett, J. F.; Zahler, R. E. *Chem. Rev.* **1951**, *49*, 273. b) Weingarten, H. *J. Org. Chem.* **1964**, *29*, 3624. c) Paine, A. J. *J. Am. Chem. Soc.* **1987**, *109*, 1496. d) Ma, D.; Zhang, Y.; Yao, J.; Wu, S.; Tao, F. *J. Am. Chem. Soc.* **1998**, *120*, 12459. e) Lindley, J. *Tetrahedron* **1984**, *40*, 1433. f) Goodbrand, H. R.; Hu, N. X. *J. Org. Chem.* **1999**, *64*, 670.
5. a) Kiyomori, A.; Marcoux, J. F.; Buchwald, S. L. *Tetrahedron Lett.* **1999**, *40*, 2657. b) Klapars, A.; Antilla, J. C.; Huang, X. H.; Buchwald, S. L. *J. Am. Chem. Soc.* **2001**, *123*, 7727. c) Klapars, A.; Huang, X.; Buchwald, S. L. *J. Am. Chem. Soc.* **2002**, *124*, 7421. d) Antilla, J. C.; Klapars, A.; Buchwald, S. L. *J. Am. Chem.*

Soc. **2002**, *124*, 11684. e) Job, G. E.; Buchwald, S. L. *Org. Lett.* **2002**, *4*, 3703. f) Kwong, F. Y.; Klapars, A.; Buchwald, S. L. *Org. Lett.* **2002**, *4*, 581. g) Kwong, F. Y.; Buchwald, S. L. *Org. Lett.* **2003**, 5, 793. h) Antilla, J. C.; Baskin, J. M.; Barder, T. E.; Buchwald, S. L. *J. Org. Chem.* **2004**, *69*, 5578. i) Liu, L.; Frohn, M.; Xi, N.; Dominguez, C.; Hungate, R.; Reider, P. J. *J. Org. Chem.* **2005**, *70*, 10135. j) Ma, D.; Xia, C. *Org. Lett.* **2001**, 3, 2583.

6. a) Song, D.; Sliwowski, K.; Pang, J.; Wang, S. *Organometallics* **2002**, *21*, 4978. b) Song, D. T.; Jia, W. L.; Wang, S. *Organometallics*, **2004**, *23*, 1194.
7. Song, D. T.; Wang, S. N. *Eur. J. Inorg. Chem.* **2003**, 3774.
8. a) Kubas, G. J. *Inorg. Synth.* **1979**, *19*, 90. b) Diez, J.; Falagan, S.; Gamasa, P.; Gimeno, J. *Polyhedron* **1988**, *7*, 37.
9. Chou, C. C.; Su, C. C.; Yeh, A. *Inorg.Chem.* **2005**, *44*, 6122.
10. Munakata, M.; Maekawa, M.; Kitagawa, S.; Matsuyama, S.; Masudat, H. *Inorg.Chem.* **1989**, *28*, 4300.
11. Lopez, S.; Keller, S. W. *Inorg. Chem.* **1999**, *38*, 1883.
12. a) Sundararaman, A.; Lalancette, R. A.; Zakharov, L. N.; Rheingold, A. L.; Jäkle, F. *Organometallics* **2003**, *22*, 3526. b) Kronenburg, C. M. P.; Amijs, C. H. M.; Jastrzebski, J. T. B. H.; Lutz, M.; Spek, A. L.; Koten, G. *Organometallics* **2002**, *21*, 4662. c) Niemeyer, M. *Organometallics* **1998**, *17*, 4649. d) Kronenburg, C. M. P.; Jastrzebski, J. T. B. H.; Boersma, J.; Lutz, M.; Spek, A. L.; Koten, G. *J. Am. Chem. Soc.* **2002**, *124*, 11675. e) He, X.; Ruhlandt-Senge, K.; Power, P. P. *J. Am. Chem. Soc.* **1994**, *116*, 6963. f) Olmstead, M. M.; Power, P. P. *J. Am. Chem. Soc.* **1989**, *111*, 4135.

13. a) Osako, T.; Tachi, Y.; Taki, M.; Fukuzumi, S.; Itoh, S. *Inorg. Chem.* **2001**, *40*, 6604. b) Turner, R. W.; Amma, E. L. *J. Am. Chem. Soc.* **1966**, *88*, 1877.

14. a) Csoregh, I.; Kierkegaard, P.; Norrestam, R. *Acta Crystallogr.* **1975**, *B31*, 314. b) Chou, C. C.; Su, C. C.; Tsai, H. L.; Lii, K. H. *Inorg.Chem.* **2005**, *44*, 628. c) Tyeklár, Z.; Jacobson, R. R.; Wei, N.; Murthy, N. N.; Zubieta, J.; Karlin, K. *J. Am. Chem. Soc.* **1993**, *115*, 2677.

15. Liang, H. C.; Kim, E.; Incarvito, C. D.; Rhengold, A. L.; Karlin, K. D. *Inorg. Chem.* **2002**, *41*, 2209.

16. a) Alyea, E. C.; Ferguson, G.; Jennings, M. C.; Xu, Z. *Acta Cryst.* **1990**, *C46*, 2347. b) Yamamoto, Y.; Kumamaru, T.; Hayashi, Y.; Yamamoto, M. *Analytica Chimica Acta*, **1974**, *69*, 321. c) Mandal, S. K.; Thompson, L. K.; Gabe, E. J.; Lee, F. L.; Charland, J. P. *Inorg. Chem.* **1987**, *26*, 2384.

17. For review of the structures and bonding of polyiodide: Svensson, P. H.; Kloo, L. *Chem. Rev.* **2003**, *103*, 1649.

18. a) Li, G. H.; Shi, Z.; Liu, X. M.; Dai, Z. M.; Feng, S. H. *Inorg. Chem.* **2004**, *43*, 6884. b) Cariati, E.; Roberto, D.; Ugo, R.; Ford, P. C.; Galli, S.; Sironi, A. *Inorg. Chem.* **2005**, *44*, 4077. c) Lobana, T. S.; Shama, R.; Shama, R.; Mehra, S.; Castineiras, A.; Turner, P. *Inorg. Chem.* **2005**, *44*, 1914. d) Cheng, J. K.; Yao, Y. G.; Zheng, J.; Li, Z.J.; Cai, Z. W.; Zheng, X. Y.; Chen, Z. N.; Chen, Y. B.; Kang, Y.; Qin, Y. Y.; Wen, Y. H. *J. Am. Chem. Soc.* **2004**, *126*, 7796.

Chapter 8

Summary and Perspectives

This work started with the investigation of the reactivity of two Pt(II) complexes Pt(BAB)Me_2 and Pt(BAM)Me_2 toward alkylarene C-H activation. Both complexes displayed a high regioselectivity toward the benzylic C-H activation when reacted with toluene and ethyl benzene (EtPh) and a distinct diastereoselectivity in the EtPh benzylic activation. The mechanism of the activation processes was examined. The intermediacy of a thermodynamically favored η^3-benzylic Pt(II) species was found to be responsible for both the high regioselectivity and the unusual diastereoselectivity. Compared to the BAM system, the BAB system displayed a greater regioselectivity as well as a higher diastereoselectivity, both of which were found attributable to the greater steric blocking effect of the BAB ligand.

The steric impacts of the BAB and BAM ligands on the structure and stability of their *fac*-$Pt^{IV}Me_3$ complexes was also examined. The BAB ligand was found to be much more effective in stabilizing of five-coordinate $Pt^{IV}Me_3$ complexes than the BAM ligand. A stable five-coordinate [Pt^{IV}(BAB)Me_3](OTf) complex with a neutral N,N-chelate ligand was obtained and structurally characterized. The BAM *fac*-$Pt^{IV}Me_3$ complexes were established to be six-coordinate species in solid state. In solution, the methyl groups of the five-coordinate BAB-$Pt^{IV}Me_3$ complex exchange slowly, but those in the BAM complexes exchange rapidly. Both the BAM and BAB ligands were found to be quite labile in the Pt(IV) complexes, which is a concern for the ultimate use of BAB and BAM Pt(II) complexes in C-H activation and functionalization.

With the intention of obtaining better Pt(II) complexes for C-H activation, new Pt(II) systems that contain 7-azaindolyl derivative ligands were developed. The $PtMe_2$ complex of NPA, **3.1**, displayed a unique reactivity. It underwent a roll-over intramolecular C-H activation at ambient temperature, which led to the quantitive formation of a neutral Pt_4 macrocycle. The reaction pathway of the transformation process as well as its kinetics was established by the mechanistic study. The driving forces of the high reactivity of **3.1** were demonstrated to be the stored distortion energy in **3.1** and its intramolecular *ortho*-H repulsion, imposed by the geometry of the NPA ligand. The C-H cleavage step of the transformation was demonstrated to be oxidative addition in nature.

The syntheses of several BAM and BAB derivative ligands *via* modifying or altering their linker groups were carried out. The replacement of the CH_2 linker in the BAM ligand by either a propyl or a butyl group significantly reduces the stability of the corresponding $PtMe_2$ complex. The reaction of SnBAM with $[PtMe_2(\mu\text{-}SMe_2)]_2$ gave an unconventional Pt^{IV} compound where the C_{BAM}-Sn bond has been broken and *cis* oxidatively added to the Pt center. The S_N2 oxidative addition reactions of the $PtMe_2$ complex **5.1** of the SiBAM ligand with MeI, MeOTf and I_2 were also examined. The different reactivity of **5.1** toward MeI and I_2 demonstrated the ligand electronic effect on the reactivities of the Pt(IV) intermediates involved.

To obtain bright phosphorescent Pt(II) and Cu(I) complexes, the modification of the NPA ligand *via* the incorporation of a triarylboron group was also developed. The $[Cu^{I}(BNPA)(PPh_3)_2](BF_4)$ (**6.1**) and $Pt^{II}(BNPA)Ph_2$ (**6.2**) complexes were demonstrated to be the first examples of bright ambient temperature phosphorescent metal complexes

that contain a triarylboron group. Complex **6.1** is an exceptionally bright phosphorescent emitter in the solid state. The boron group in these complexes was shown to play a key role in achieving the bright phosphorescence. The complexes **6.1** and **6.2** both displayed distinct phosphorescent response toward fluoride ion and their phosphorescence was shown to be very sensitive toward oxygen molecules.

The last part of this work concerned the development of bimetallic systems using the 1,2,4,5-tetrakis(1-*N*-7-azaindolyl)benzene (TTAB) ligand. The investigation was focused specifically on Cu(I) complexes with the aim to explore both phosphorescent properties and reactivities. The dinuclear Cu(I) compounds of TTAB favor persistently a 3-coordinate geometry for the Cu(I) centers and a 1,3-chelation mode for the TTAB ligand. The close contacts between the TTAB bridging phenyl ring and the Cu(I) centers were observed. The dinuclear Cu(I) complexes were found to be active in catalyzing the C-N coupling reactions of imidazole with phenyl halides, and react readily with O_2. None of the dinuclear TTAB Cu(I) complexes display appreciable phosphorescence.

On the basis of this thesis, the future work could focus on several aspects. First, it would be worth well to complete the thermolysis study of all the *fac*-$Pt^{IV}Me_3$ complexes **4.1**-**4.4** described in Chapter 4, which could provide a deeper understanding on the fundamentals of both ligand geometry and ligand electronic properties on the performance of the Pt(IV) centers toward the functionalization of hydrocarbons. Second, additional efforts on the study of the new BAB and BAM derivative ligand systems discussed in Chapter 5 could be very rewarding, particularly considering the discovery of the unusual formation of a Pt(IV) compound where the C_{BAM}-Sn bond *cis* oxidatively added to the Pt center. Third, the study on NPA based system should be expanded. For

example, the synthesis and the application of a Pd^{II}_4 molecular square similar to **3.2** should be attempted, given that the Pd(II) molecular assemblies usually have better practical applications in guest-host chemistry and catalysis.

Scheme 8.1[a]

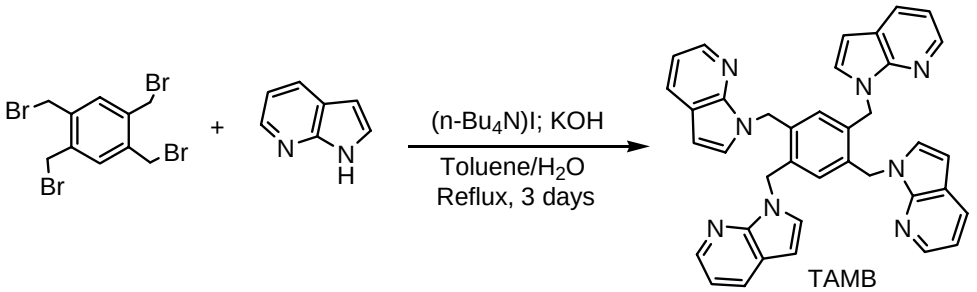

[a] *Reaction conditions*: A toluene/H_2O (4:1) (50 mL) solution of 1,2,4,5-tetra(bromomethyl)benzene (1.0 g, 2.2 mmol), 7-azaindole (1.1 g, 9.3 mmol), (n-Bu_4N)I (0.5 g) and KOH (12.5 g) was refluxed for 3 days under air. The product 1,2,4,5-tetrakis(N-7-azaindolylmethyl)benzene (TAMB) was obtained as a yellow solid in 18% yield after work-up.

Scheme 8.2 [a]

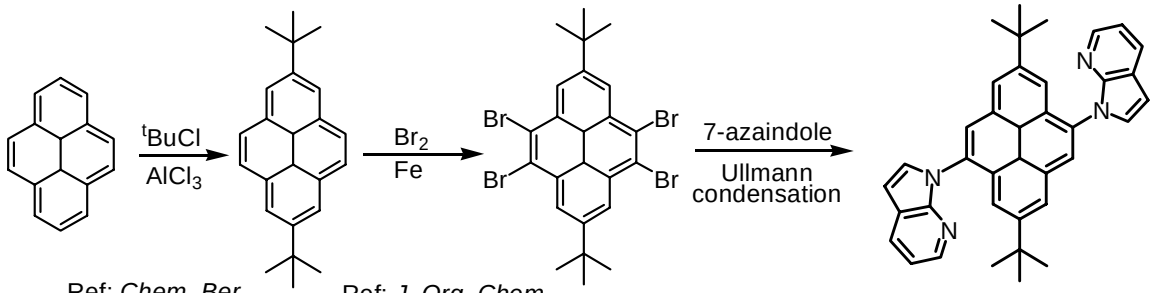

[a] *Reaction conditions for the Ullmann condensation step*: Under N_2, a DMF (4.0 mL) solution of 2,7-di-tertbutyl-4,5,9,10-tetrabromopyrene (1.6 g, 2.5 mmol), 7-azaindole (1.4 g, 12 mmol), CuI (0.2 g), 1,10-Phen (0.4 g) and Cs_2CO_3 (7.0 g) was heated at ~130 ^oC for 80 hours. The disubstituted 2,7-di-tertbutyl-4,9-bis(N-7-azaindolyl)pyrene (DTBBAP) product was obtained as white solid in 20~30% yield after work-up. No 4,5,9,10-tetrasubstituted product was obtained.

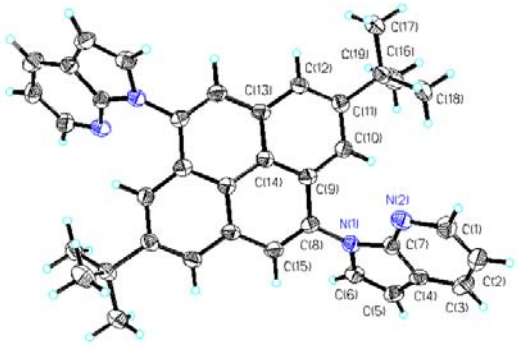

Figure 8.1 Crystal structure of DTBBAP.

Besides these efforts, one of my latest efforts during this thesis work has been the modification of the TTAB ligand, with the aim to overcome its low solubility problem so that the unique reactivities displayed by the bimetallic $Pt_2(TTAB)Me_4$ system can be further explored. Some of the preliminary results are illustrated in Scheme 8.1, Scheme 8.2, and Figure 8.1. Further research efforts on systems based on new ligands are highly recommended. In addition, the incorporation of the Lewis acidic triarylboron centers in the Pt(II) complexes to induce regio and stereoselective C-H activation should be very exciting and should be explored.

Appendix I. Atomic coordinates (x 10^4) and equivalent isotropic displacement parameters ($Å^2$ x 10^3) for the crystal structures in this thesis. U(eq) is defined as one third of the trace of the orthogonalized U^{ij} tensor.

Chapter 2

	x	y	z	U(eq)
		Compound **2.3**		
B(1)	78(5)	-287(5)	2454(4)	37(2)
S(1)	-2869(2)	-5783(3)	3966(1)	128(1)
Pt(1)	-4412(1)	-5902(1)	3137(1)	67(1)
N(1)	-5712(4)	-6139(4)	2445(4)	73(2)
N(2)	-3734(4)	-6851(5)	2336(4)	68(2)
N(3)	-5502(5)	-4718(5)	1746(3)	60(2)
N(4)	-3697(4)	-5728(5)	1497(3)	58(2)
F(1A)	-90(30)	-4470(20)	1731(18)	140(16)
F(1)	-960(20)	-4848(12)	917(17)	99(8)
F(2A)	770(20)	-3970(30)	1054(18)	101(8)
F(2)	370(30)	-4300(20)	1740(15)	121(15)
F(3A)	400(30)	-4110(30)	659(17)	136(16)
F(3)	-690(30)	-4850(20)	617(18)	165(15)
F(4A)	-3720(16)	-2850(20)	180(30)	124(8)
F(4)	-3397(19)	-2280(40)	-118(11)	113(9)
F(5)	-3860(20)	-1740(50)	996(14)	140(13)
F(5A)	-3994(17)	-2840(40)	700(30)	156(15)
F(6A)	-3660(20)	-1170(20)	730(20)	116(11)
F(6)	-3260(20)	-1460(50)	110(30)	166(13)
F(7A)	3270(30)	-1570(40)	1108(16)	180(20)
F(7)	3190(30)	-1800(20)	1330(20)	124(9)
F(8A)	4660(30)	-630(30)	1790(20)	136(18)
F(8)	4550(30)	-1180(30)	1840(30)	140(14)
F(9A)	3460(40)	-370(30)	1030(20)	117(9)
F(9)	3890(50)	-60(40)	1210(30)	200(20)
F(10)	4470(20)	670(30)	4408(17)	135(14)
F(10A)	4120(30)	720(20)	4521(15)	154(16)
F(11A)	4180(30)	2110(30)	4000(16)	144(16)
F(11)	4590(18)	1750(20)	3956(16)	91(10)
F(12A)	3150(30)	1550(30)	4572(16)	79(6)
F(12)	3250(30)	1790(40)	4367(19)	178(18)
F(13A)	190(20)	1840(30)	179(15)	135(16)
F(13)	130(30)	1370(30)	110(18)	138(17)
F(14)	-710(70)	2860(40)	290(30)	138(15)
F(14A)	-910(70)	2520(40)	240(30)	180(20)
F(15A)	-1550(30)	1510(40)	128(16)	143(18)
F(15)	-1300(30)	1000(20)	-30(14)	121(13)

F(16A)	600(30)	4342(17)	2913(16)	123(9)
F(16)	960(20)	3910(20)	3380(18)	145(8)
F(17A)	-990(20)	4080(20)	2840(20)	150(13)
F(17)	-480(50)	4447(17)	2844(13)	159(16)
F(18A)	-570(30)	3470(30)	3600(20)	122(11)
F(18)	80(30)	3580(20)	3634(17)	126(13)
F(25A)	960(30)	-2320(40)	4580(20)	190(18)
F(25)	1000(20)	-1873(18)	4891(17)	122(12)
F(26A)	-570(30)	-3030(30)	4400(20)	130(20)
F(26)	-510(30)	-2250(30)	5176(18)	129(13)
F(27A)	10(30)	-1780(20)	5323(16)	134(11)
F(27)	-80(30)	-2950(20)	4290(20)	106(10)
F(28A)	-2770(20)	1251(19)	3988(15)	94(7)
F(28)	-3040(40)	80(20)	4550(20)	230(20)
F(29A)	-3608(14)	-568(15)	3911(16)	139(8)
F(29)	-2850(20)	569(17)	4739(11)	102(7)
F(30A)	-3010(20)	910(30)	3720(17)	166(17)
F(30)	-3618(12)	-73(17)	3438(14)	124(6)
C(1)	-6447(8)	-6883(7)	2332(4)	86(3)
C(2)	-7430(8)	-7160(6)	1882(5)	99(3)
C(3)	-7769(6)	-6547(8)	1382(4)	95(3)
C(4)	-7087(7)	-5731(7)	1362(4)	67(2)
C(5)	-7057(6)	-4880(8)	961(4)	89(3)
C(6)	-6123(7)	-4306(6)	1199(4)	80(2)
C(7)	-6073(6)	-5550(6)	1876(5)	65(2)
C(8)	-3659(6)	-7849(9)	2406(5)	96(3)
C(9)	-3532(6)	-8618(7)	1850(6)	99(3)
C(10)	-3465(6)	-8408(7)	1175(5)	87(3)
C(11)	-3526(5)	-7394(7)	1094(5)	66(2)
C(12)	-3489(6)	-6846(7)	507(4)	80(2)
C(13)	-3589(5)	-5848(7)	769(5)	78(2)
C(14)	-3662(5)	-6675(7)	1692(5)	51(2)
C(15)	-4482(8)	-4255(7)	2087(4)	55(2)
C(16)	-4330(9)	-3271(8)	2481(5)	92(3)
C(17)	-3303(12)	-2785(8)	2784(6)	125(5)
C(18)	-2411(9)	-3290(10)	2664(5)	115(4)
C(19)	-2551(7)	-4252(8)	2268(4)	81(3)
C(20)	-3569(7)	-4732(7)	1974(4)	59(2)
C(21)	-5246(6)	-5176(6)	3871(4)	88(3)
C(22)	-5798(9)	-4264(8)	3701(5)	76(2)
C(23)	-5313(7)	-3245(11)	3990(4)	103(3)
C(24)	-6811(11)	-2504(10)	3450(7)	132(4)
C(25)	-5836(10)	-2368(8)	3850(6)	109(3)
C(26)	-7307(8)	-3437(12)	3157(5)	121(4)
C(27)	-6824(9)	-4299(8)	3292(5)	104(3)
C(28)	-3080(6)	-6349(6)	4706(4)	141(3)

C(29)	-2443(7)	-4511(7)	4407(5)	209(6)
C(30)	-523(5)	-1279(5)	1846(3)	40(2)
C(31)	-1578(5)	-1275(5)	1450(4)	49(2)
C(32)	-2161(6)	-2127(6)	976(4)	52(2)
C(33)	-1710(6)	-3036(5)	869(3)	51(2)
C(34)	-696(6)	-3090(6)	1254(4)	47(2)
C(35)	-126(5)	-2223(6)	1730(3)	44(2)
C(36)	-3265(9)	-2042(13)	595(9)	78(3)
C(37)	-207(10)	-4093(8)	1139(7)	64(2)
C(38)	1380(5)	-205(4)	2600(4)	40(2)
C(39)	2022(5)	361(4)	3252(3)	45(2)
C(40)	3117(6)	565(5)	3365(4)	50(2)
C(41)	3645(5)	180(5)	2817(5)	62(2)
C(42)	3065(6)	-388(5)	2173(4)	53(2)
C(43)	1960(5)	-557(5)	2070(3)	47(2)
C(44)	3615(11)	-821(16)	1573(8)	90(3)
C(45)	3764(9)	1207(9)	4049(6)	68(3)
C(46)	-176(4)	801(5)	2184(4)	44(2)
C(47)	-125(4)	1727(6)	2664(3)	49(2)
C(48)	-212(5)	2648(6)	2451(4)	52(2)
C(49)	-415(5)	2707(6)	1707(5)	63(2)
C(50)	-462(5)	1812(6)	1210(4)	53(2)
C(51)	-342(4)	890(5)	1449(3)	47(2)
C(52)	-89(14)	3627(10)	2999(9)	89(3)
C(53)	-614(15)	1791(17)	404(8)	91(5)
C(54)	-401(5)	-427(5)	3179(3)	41(2)
C(55)	-1322(5)	-16(4)	3326(3)	48(2)
C(56)	-1790(6)	-229(5)	3896(4)	52(2)
C(57)	-1374(6)	-889(5)	4330(3)	57(2)
C(58)	-473(6)	-1321(5)	4209(4)	51(2)
C(59)	23(5)	-1076(5)	3642(4)	49(2)
C(60)	-2788(9)	238(12)	4025(9)	87(4)
C(61)	6(13)	-2081(12)	4645(8)	75(3)

	x	y	z	U(eq)
		Compound **2.4**		
Pt(1)	5227(1)	4063(1)	8121(1)	58(1)
B(1)	9(4)	-255(4)	7447(3)	41(1)
N(1)	6179(3)	4351(4)	6538(2)	55(1)
N(2)	6077(3)	3172(3)	7367(2)	59(1)
N(3)	4318(3)	5324(3)	6767(2)	51(1)
N(4)	3958(3)	3808(3)	7310(2)	55(1)
N(5)	6446(4)	4261(4)	8923(2)	76(2)
C(1)	6183(4)	2174(5)	7427(3)	76(2)

C(2)	6389(5)	1423(5)	6882(4)	85(2)
C(3)	6490(5)	1656(5)	6209(4)	84(2)
C(4)	6416(4)	2675(5)	6119(3)	64(2)
C(5)	6478(5)	3245(5)	5552(3)	77(2)
C(6)	6345(4)	4239(5)	5814(3)	72(2)
C(7)	6225(4)	3397(4)	6723(3)	53(1)
C(8)	3243(5)	2966(5)	7251(3)	78(2)
C(9)	2314(5)	2767(5)	6743(4)	91(2)
C(10)	2077(5)	3429(6)	6265(4)	90(2)
C(11)	2791(4)	4286(5)	6301(3)	63(2)
C(12)	2838(5)	5141(5)	5933(3)	75(2)
C(13)	3754(5)	5737(5)	6217(3)	68(2)
C(14)	3729(4)	4441(4)	6832(2)	48(1)
C(15)	5336(4)	5796(4)	7147(3)	51(1)
C(16)	6254(4)	5334(4)	7025(3)	52(1)
C(17)	7250(5)	5842(6)	7362(3)	73(2)
C(18)	7315(7)	6813(7)	7800(4)	104(2)
C(19)	6410(8)	7271(6)	7919(4)	107(2)
C(20)	5419(5)	6766(5)	7597(3)	76(2)
C(21)	4268(5)	4680(5)	8840(3)	77(2)
C(22)	3874(5)	5708(5)	8748(3)	68(2)
C(23)	4401(6)	6642(7)	9154(4)	96(2)
C(24)	4030(7)	7582(6)	9081(5)	112(2)
C(25)	3108(8)	7620(7)	8604(5)	110(3)
C(26)	2567(6)	6705(7)	8201(4)	96(2)
C(27)	2937(4)	5762(5)	8276(3)	72(2)
C(28)	7117(5)	4319(6)	9383(3)	92(2)
C(29)	8022(6)	4425(8)	9976(4)	152(4)
C(30)	-493(3)	-375(3)	8190(2)	41(1)
C(31)	-117(4)	-1058(3)	8638(2)	44(1)
C(32)	-616(4)	-1257(4)	9210(2)	54(1)
C(33)	-1508(4)	-781(4)	9363(3)	59(1)
C(34)	-1892(4)	-108(4)	8932(3)	55(1)
C(35)	-1402(4)	81(3)	8351(2)	45(1)
C(36)	-237(7)	-2057(7)	9641(4)	75(2)
C(37)	-2861(7)	432(7)	9064(5)	83(2)
C(38)	-596(4)	-1267(3)	6852(2)	41(1)
C(39)	-188(4)	-2237(4)	6735(2)	45(1)
C(40)	-748(4)	-3109(4)	6263(3)	47(1)
C(41)	-1761(4)	-3055(4)	5888(3)	56(1)
C(42)	-2191(4)	-2119(4)	6009(3)	52(1)
C(43)	-1624(4)	-1254(4)	6477(3)	48(1)
C(44)	-3300(5)	-2054(7)	5623(5)	79(2)
C(45)	-263(7)	-4109(5)	6149(4)	68(2)
C(46)	-235(3)	849(4)	7182(3)	39(1)
C(47)	-392(3)	912(4)	6445(3)	47(1)

C(48)	-556(4)	1847(4)	6209(3)	51(1)
C(49)	-570(4)	2752(4)	6703(3)	56(1)
C(50)	-394(4)	2714(4)	7443(3)	49(1)
C(51)	-223(3)	1784(4)	7668(3)	46(1)
C(52)	-367(7)	3696(5)	8001(4)	75(2)
C(53)	-720(6)	1838(6)	5407(3)	72(2)
C(54)	1321(3)	-172(3)	7593(2)	42(1)
C(55)	1906(4)	-548(4)	7050(3)	48(1)
C(56)	3013(4)	-370(4)	7141(3)	54(1)
C(57)	3582(4)	191(4)	7790(3)	56(1)
C(58)	3035(4)	600(4)	8335(3)	51(1)
C(59)	3615(7)	-814(8)	6565(5)	84(2)
C(60)	1928(4)	406(4)	8234(3)	47(1)
C(61)	3657(6)	1244(6)	9023(3)	75(2)
F(1A)	-3684(10)	141(11)	8417(6)	95(3)
F(1)	-3686(12)	-150(17)	8898(13)	170(8)
F(2)	-2874(18)	1304(19)	8922(13)	171(13)
F(2A)	-3335(18)	200(20)	9577(14)	183(15)
F(3)	-2720(14)	1456(12)	9094(10)	98(7)
F(3A)	-2832(13)	656(12)	9817(10)	122(7)
F(4A)	-3475(18)	-2410(40)	4925(10)	132(9)
F(4)	-3784(17)	-2939(13)	5330(30)	152(8)
F(5A)	-3630(20)	-1119(13)	5690(20)	127(11)
F(5)	-3229(14)	-1590(40)	5065(19)	157(9)
F(6A)	-3829(18)	-1520(40)	5993(16)	168(13)
F(6)	-4044(9)	-2610(30)	5892(19)	136(8)
F(7A)	-959(18)	-4928(14)	6002(15)	117(10)
F(7)	673(16)	-3978(17)	6005(14)	122(8)
F(8)	-133(18)	-4435(16)	6771(12)	126(8)
F(8A)	452(15)	-4268(13)	6713(10)	102(7)
F(9A)	270(20)	-4227(17)	5601(11)	119(9)
F(9)	-820(20)	-4842(18)	5704(19)	182(14)
F(10A)	-200(20)	-1743(19)	10338(8)	115(10)
F(10)	820(20)	-1970(20)	9839(15)	114(12)
F(11)	-810(20)	-2932(19)	9520(13)	147(11)
F(11A)	-480(30)	-2989(17)	9235(13)	170(13)
F(12A)	670(30)	-2300(30)	9550(20)	174(16)
F(12)	-630(30)	-2060(30)	10243(14)	169(14)
F(13)	-1120(30)	3565(17)	8390(17)	142(7)
F(13A)	-530(40)	4512(12)	7755(8)	144(9)
F(14)	-1302(17)	4090(20)	7930(20)	163(9)
F(14A)	520(20)	3880(20)	8456(17)	137(6)
F(15A)	330(30)	4427(17)	7954(17)	137(7)
F(15)	-200(40)	3583(13)	8676(6)	131(8)
F(16A)	30(20)	1473(19)	5081(11)	118(11)
F(16)	-1590(20)	1290(30)	5102(16)	150(12)

F(17A)	139(18)	1710(20)	5142(13)	136(12)
F(17)	-670(20)	2790(30)	5237(18)	121(10)
F(18A)	-1400(30)	1070(20)	5006(15)	150(13)
F(18)	-1170(20)	2640(30)	5250(17)	124(9)
F(19A)	3859(18)	822(13)	9536(8)	170(10)
F(19)	4510(20)	1750(20)	8968(14)	93(7)
F(20A)	3120(11)	1580(10)	9496(6)	72(3)
F(20)	3068(14)	2081(12)	9286(10)	145(6)
F(21A)	4296(10)	581(14)	9378(8)	99(5)
F(21)	4340(20)	1990(20)	8884(15)	110(10)
F(22A)	3270(30)	-1840(20)	6240(20)	112(12)
F(22)	4520(20)	-1150(30)	6835(15)	151(13)
F(23A)	3780(40)	-60(30)	6161(19)	183(17)
F(23)	3100(30)	-1550(20)	6125(19)	124(12)
F(24A)	3550(30)	-390(30)	6007(13)	112(6)
F(24)	4614(17)	-750(30)	6737(13)	149(12)

	x	y	z	U(eq)
		Compound **2.5**		
Pt(1)	73(1)	1521(1)	-3076(1)	69(1)
N(1)	1220(8)	1614(10)	-2363(6)	77(3)
N(2)	863(10)	42(9)	-1722(5)	70(3)
N(3)	-811(7)	2314(8)	-2343(6)	69(3)
N(4)	-1000(8)	1035(9)	-1481(5)	64(3)
N(5)	-1058(13)	1429(10)	-3761(6)	108(6)
B(1)	4616(10)	4164(10)	-7651(6)	45(4)
F(1A)	7535(19)	5900(30)	-5881(14)	97(9)
F(1)	7290(20)	5180(60)	-5560(20)	190(20)
F(2A)	7900(60)	4640(30)	-5603(14)	180(20)
F(2)	8961(18)	5540(30)	-6139(16)	109(12)
F(3)	8530(40)	4460(40)	-5842(18)	170(20)
F(3A)	8460(80)	6110(30)	-6050(20)	340(50)
F(4A)	9320(30)	3580(20)	-8288(17)	86(10)
F(4)	8150(60)	2860(40)	-8750(40)	240(40)
F(5A)	8450(30)	4570(50)	-8920(30)	210(30)
F(5)	8380(50)	4500(40)	-9070(20)	170(20)
F(6A)	8010(20)	3150(50)	-8879(16)	105(13)
F(6)	9370(30)	4170(40)	-8390(30)	180(20)
F(7A)	5210(30)	340(30)	-8350(20)	113(12)
F(7)	4640(40)	190(30)	-8250(30)	150(20)
F(8A)	5240(30)	620(20)	-9360(20)	100(12)
F(8)	5650(30)	890(30)	-9040(30)	120(17)
F(9A)	4090(50)	-40(40)	-9430(20)	210(30)
F(9)	4000(30)	-140(20)	-9030(20)	102(11)

F(10A)	3800(40)	7460(30)	-9888(17)	112(12)
F(10)	3330(30)	6370(40)	-9970(20)	134(17)
F(11)	5200(40)	6900(50)	-9910(20)	210(30)
F(11A)	4360(60)	7810(40)	-9670(20)	170(20)
F(12A)	3860(40)	5990(40)	-9980(20)	124(15)
F(12)	5030(30)	6380(30)	-9906(15)	107(15)
F(13A)	1120(20)	3340(30)	-9156(16)	90(8)
F(13)	1580(50)	2470(50)	-10120(40)	140(30)
F(14A)	1120(20)	1830(20)	-9560(30)	130(14)
F(14)	1430(50)	3770(20)	-9520(40)	230(40)
F(15A)	1780(50)	3110(50)	-10030(30)	140(20)
F(15)	810(20)	2390(60)	-9170(30)	176(18)
F(16A)	3330(30)	8330(30)	-7250(30)	180(20)
F(16)	4870(30)	8670(30)	-7220(20)	134(9)
F(17A)	4260(60)	7700(30)	-6512(15)	150(20)
F(17)	3390(40)	7630(40)	-6680(30)	180(20)
F(18)	5060(30)	8110(40)	-6740(20)	144(13)
F(18A)	3910(30)	2220(30)	-4810(14)	125(12)
F(19)	3810(60)	8770(20)	-7358(17)	190(30)
F(19A)	4990(70)	2720(60)	-4980(50)	490(70)
F(20A)	5040(60)	2260(70)	-5120(40)	300(50)
F(20)	3690(30)	1540(40)	-5030(30)	220(30)
F(21A)	4010(60)	1090(30)	-5730(30)	220(20)
F(21)	5030(40)	1670(40)	-5630(20)	170(20)
F(22)	931(6)	3905(7)	-5597(4)	113(3)
F(23)	1575(7)	5327(8)	-5960(5)	120(3)
F(24)	807(6)	4241(7)	-6683(4)	109(3)
C(1)	1356(15)	-458(13)	-1191(7)	94(5)
C(2)	2250(15)	123(17)	-944(9)	107(6)
C(3)	2351(13)	1042(15)	-1340(9)	90(5)
C(4)	3049(13)	1860(19)	-1378(10)	117(6)
C(5)	2884(15)	2591(15)	-1880(11)	121(6)
C(6)	2018(15)	2458(13)	-2315(10)	105(5)
C(8)	-1237(10)	1018(11)	-791(7)	76(4)
C(7)	1462(11)	956(11)	-1838(7)	65(4)
C(9)	-1376(11)	1966(13)	-555(7)	90(5)
C(10)	-1256(10)	2611(13)	-1132(7)	75(4)
C(11)	-1283(11)	3656(12)	-1241(9)	93(5)
C(12)	-1134(11)	3978(11)	-1920(8)	80(4)
C(13)	-869(11)	3325(11)	-2432(8)	81(4)
C(14)	-995(10)	2011(10)	-1695(8)	65(4)
C(15)	-161(13)	-326(10)	-2034(7)	63(4)
C(16)	-165(16)	-1250(15)	-2404(9)	98(6)
C(17)	-1180(20)	-1642(15)	-2682(10)	133(8)
C(18)	-2064(17)	-1185(17)	-2602(10)	115(6)
C(19)	-1999(13)	-296(14)	-2217(8)	82(4)

C(20)	-1039(11)	146(11)	-1910(7)	56(3)
C(21)	1500(17)	50(14)	-3639(9)	87(5)
C(22)	2466(16)	-42(16)	-3276(10)	127(7)
C(23)	2854(18)	-940(20)	-3175(10)	153(10)
C(24)	2300(40)	-1800(30)	-3410(20)	210(20)
C(25)	1380(30)	-1860(40)	-3750(20)	210(20)
C(26)	986(16)	-850(20)	-3855(9)	123(7)
C(27)	1035(17)	1026(16)	-3796(8)	174(10)
C(28)	1046(14)	1400(11)	-4429(8)	139(7)
C(29)	-1753(16)	1361(14)	-4161(8)	110(7)
C(30)	-2735(15)	1257(19)	-4652(8)	188(11)
C(31)	5913(9)	4234(8)	-7532(6)	49(3)
C(32)	6420(10)	4593(9)	-6903(6)	52(3)
C(33)	7500(11)	4759(9)	-6804(7)	57(3)
C(34)	8155(10)	4521(9)	-7324(8)	65(4)
C(35)	7699(10)	4143(9)	-7950(7)	57(3)
C(36)	6595(9)	4010(8)	-8035(6)	52(3)
C(37)	8030(18)	5161(19)	-6122(9)	96(6)
C(38)	8364(16)	3840(20)	-8517(12)	84(5)
C(39)	4127(9)	3285(8)	-8224(5)	39(3)
C(40)	4557(10)	2355(10)	-8333(6)	55(3)
C(41)	4094(10)	1614(9)	-8793(7)	48(3)
C(42)	3165(11)	1730(9)	-9169(6)	60(3)
C(43)	2685(10)	2603(11)	-9065(7)	59(3)
C(44)	3174(11)	3358(10)	-8612(7)	61(4)
C(45)	4580(20)	606(16)	-8898(15)	94(6)
C(46)	1637(13)	2736(18)	-9474(10)	73(5)
C(47)	4417(8)	5334(9)	-7916(6)	47(3)
C(48)	4337(8)	6126(9)	-7459(5)	53(3)
C(49)	4238(9)	7118(9)	-7684(7)	56(3)
C(50)	4174(9)	7338(9)	-8377(7)	64(4)
C(51)	4296(9)	6576(10)	-8849(6)	54(3)
C(52)	4406(7)	5559(9)	-8636(6)	52(3)
C(53)	4280(20)	6766(17)	-9637(9)	89(6)
C(54)	4170(20)	7908(13)	-7135(11)	84(6)
C(55)	4004(9)	3863(8)	-6947(5)	52(3)
C(56)	3049(9)	4191(9)	-6795(5)	57(3)
C(57)	2497(10)	3918(9)	-6217(6)	59(3)
C(58)	2883(11)	3238(10)	-5760(6)	70(4)
C(59)	3836(11)	2838(11)	-5903(6)	80(5)
C(60)	4395(9)	3180(9)	-6469(6)	63(4)
C(61)	4240(20)	2030(20)	-5440(13)	124(10)
C(62)	1443(12)	4309(13)	-6121(7)	70(4)

	x	y	z	U(eq)

Compound **2.6**

B(1)	1874(9)	5457(8)	2244(6)	38(3)
Pt(1)	-2699(1)	471(1)	3124(1)	70(1)
N(1)	-1665(8)	-73(6)	2155(5)	42(2)
N(2)	-3039(8)	-317(7)	1457(5)	51(2)
N(3)	-3473(11)	-919(8)	3494(6)	68(3)
N(4)	-4531(9)	-870(9)	2538(8)	77(4)
N(5)	-1970(9)	1841(10)	2770(6)	68(3)
C(1)	-2969(14)	-711(10)	772(8)	73(4)
C(2)	-1924(12)	-920(8)	483(7)	53(3)
C(3)	-1287(10)	-728(6)	943(5)	41(3)
C(4)	-195(10)	-812(8)	959(6)	48(3)
C(5)	174(11)	-549(9)	1540(7)	57(3)
C(6)	-612(11)	-176(8)	2138(7)	53(3)
C(7)	-5263(13)	-1528(14)	2419(12)	99(6)
C(8)	-5439(13)	-2370(16)	2978(13)	122(8)
C(9)	-4762(13)	-2257(10)	3472(9)	80(5)
C(10)	-4538(16)	-2846(12)	4148(10)	96(6)
C(11)	-3839(15)	-2464(11)	4479(8)	84(5)
C(12)	-3278(15)	-1515(10)	4154(7)	92(5)
C(13)	-2004(9)	-347(7)	1564(6)	39(2)
C(14)	-4192(13)	-1302(11)	3184(8)	74(5)
C(15)	-4047(11)	-21(10)	1955(8)	81(5)
C(16)	-1638(12)	2666(11)	2568(8)	63(4)
C(17)	-1269(12)	3700(10)	2326(8)	70(4)
C(18)	-3249(14)	864(13)	4729(8)	96(6)
C(19)	-3662(16)	1006(13)	4067(7)	113(7)
C(20)	-4334(9)	1875(9)	3833(6)	48(3)
C(21)	-3921(18)	2888(15)	3914(12)	36(5)
C(23)	-5360(20)	3280(30)	3318(16)	65(7)
C(22)	-4449(17)	3841(14)	3668(11)	37(4)
C(24)	-5917(17)	2792(16)	3322(11)	104(6)
C(25)	-5191(17)	1981(14)	3513(11)	36(4)
C(26)	3056(8)	5855(7)	1668(5)	31(2)
C(27)	4026(8)	5285(8)	1581(5)	37(2)
C(28)	4995(9)	5675(9)	1093(6)	46(3)
C(29)	5022(9)	6667(9)	669(6)	47(3)
C(30)	4077(9)	7257(8)	752(6)	46(3)
C(31)	3096(8)	6843(7)	1233(5)	38(2)
C(32)	841(8)	5873(7)	1844(6)	39(2)
C(33)	-180(8)	6105(6)	2274(5)	34(2)
C(34)	-1052(8)	6455(7)	1929(6)	37(2)
C(35)	-942(8)	6556(7)	1152(6)	41(2)
C(36)	73(9)	6338(7)	720(6)	41(3)
C(37)	933(8)	5995(8)	1046(5)	38(2)

C(38)	-2152(9)	6686(8)	2427(7)	51(3)
C(39)	237(12)	6529(11)	-145(7)	66(4)
C(40)	1834(8)	5958(7)	3010(5)	39(2)
C(41)	2114(9)	5421(8)	3679(6)	50(3)
C(42)	2132(10)	5915(10)	4298(6)	59(3)
C(43)	1886(10)	6947(9)	4272(6)	58(3)
C(44)	1602(10)	7484(8)	3623(6)	51(3)
C(45)	1560(8)	7036(7)	3011(5)	37(2)
C(46)	1307(13)	8607(10)	3579(8)	70(4)
C(47)	2428(19)	5304(13)	4981(8)	102(7)
C(48)	1749(8)	4191(7)	2423(5)	36(2)
C(49)	2226(9)	3574(7)	1873(5)	42(3)
C(50)	2117(9)	2509(8)	2033(6)	46(3)
C(51)	1521(10)	1991(8)	2722(7)	57(3)
C(52)	1139(9)	3661(8)	3116(6)	52(3)
C(53)	1025(10)	2593(9)	3260(7)	61(3)
C(54)	2702(13)	1871(9)	1442(7)	68(4)
C(55)	336(19)	2011(15)	4049(11)	97(5)
C(56)	6043(12)	5014(12)	1018(9)	68(4)
C(57A)	4008(12)	8321(10)	285(8)	67(4)
F(1A)	6730(40)	5100(70)	1390(40)	200(30)
F(1)	5870(30)	4180(20)	800(30)	114(18)
F(2A)	6889(17)	5510(20)	580(20)	93(8)
F(2)	6560(30)	5090(30)	254(14)	117(12)
F(3A)	6310(30)	4780(40)	1640(20)	98(12)
F(3)	5870(30)	3990(30)	1200(30)	140(30)
F(4)	3490(11)	8360(7)	-241(7)	145(5)
F(5)	4968(8)	8740(6)	-23(5)	103(3)
F(6)	3529(10)	9003(6)	697(5)	127(4)
F(7)	-2581(6)	5885(6)	2928(4)	80(2)
F(8)	-2023(6)	7388(7)	2846(5)	99(3)
F(9)	-2881(6)	7107(7)	2057(4)	86(3)
F(10)	-623(8)	6367(8)	-377(5)	106(3)
F(11)	1035(7)	5949(8)	-480(4)	105(3)
F(12)	496(10)	7498(7)	-444(4)	120(4)
F(13)	1689(7)	9180(5)	2890(5)	81(2)
F(14)	223(8)	8774(6)	3698(5)	102(3)
F(15)	1606(11)	9036(6)	4099(6)	134(4)
F(16)	1975(11)	4386(9)	5202(6)	142(5)
F(17)	2083(10)	5708(10)	5596(8)	147(4)
F(18)	3442(9)	5046(8)	4918(6)	124(4)
F(19)	3448(18)	1312(17)	1663(9)	85(6)
F(20)	1960(20)	1095(14)	1433(9)	89(7)
F(21)	-762(15)	2521(15)	4078(9)	85(6)
F(22)	760(20)	2100(20)	4495(14)	114(7)
F(23)	92(15)	1087(9)	4005(9)	102(7)

F(24)	2900(20)	2461(18)	747(14)	92(10)
F(21A)	452(15)	2584(14)	4633(10)	80(5)
F(22A)	1030(20)	1260(20)	4365(14)	132(8)
F(19A)	3869(17)	1934(16)	1364(12)	91(7)
F(20A)	2690(20)	2215(18)	741(17)	58(7)
F(23A)	-560(30)	2040(30)	4090(20)	153(14)
F(24A)	2600(20)	930(20)	1581(15)	101(9)
C(21A)	-5280(30)	1110(30)	3880(20)	102(11)
C(22A)	-6080(30)	1550(30)	3630(20)	111(12)
C(23A)	-5293(19)	3860(19)	3368(13)	47(5)
C(25A)	-4310(30)	2760(30)	3640(20)	83(9)

	x	y	z	U(eq)
		Compound **2.7·2EtPh**		
Pt(1)	7809(1)	6893(1)	10194(1)	69(1)
Pt(2)	7554(1)	7924(1)	5329(1)	51(1)
N(1)	7133(6)	7143(5)	9363(6)	78(4)
N(2)	6066(5)	7811(5)	9756(5)	45(2)
N(3)	7100(5)	8563(5)	10317(4)	37(2)
N(4)	8165(6)	8105(4)	9750(5)	53(2)
N(5)	8414(7)	8149(5)	4521(5)	59(3)
N(6)	9544(6)	8438(5)	5054(5)	53(2)
N(7)	8042(5)	6808(5)	5753(4)	46(2)
N(8)	9171(5)	7098(5)	6286(4)	51(2)
C(1)	7373(8)	6975(7)	8823(8)	75(4)
C(2)	6970(7)	7283(7)	8244(6)	57(3)
C(3)	6306(7)	7760(6)	8155(6)	61(3)
C(4)	6016(6)	7923(6)	8680(5)	38(3)
C(5)	5357(6)	8333(6)	8837(7)	55(3)
C(6)	5396(7)	8253(6)	9477(6)	53(3)
C(7)	6470(8)	7575(6)	9287(5)	49(3)
C(8)	8797(7)	8324(7)	9284(6)	52(3)
C(9)	9045(7)	9086(8)	8926(6)	62(3)
C(10)	8646(8)	9680(7)	9028(6)	65(4)
C(11)	8004(8)	9465(6)	9525(7)	62(4)
C(12)	7447(8)	9838(8)	9808(7)	72(4)
C(13)	6896(8)	9330(9)	10276(8)	87(5)
C(14)	7765(7)	8670(6)	9864(6)	49(3)
C(15)	6676(6)	7847(8)	10727(6)	58(3)
C(16)	6739(8)	7594(8)	11422(7)	74(4)
C(17)	6301(10)	6942(13)	11844(8)	114(7)
C(18)	5809(10)	6554(9)	11587(9)	108(6)
C(19)	5739(7)	6825(7)	10903(8)	72(4)
C(20)	6178(7)	7504(6)	10468(6)	51(3)

C(21)	9313(9)	6648(9)	11129(8)	144(6)
C(22)	8435(10)	6472(9)	11198(8)	131(6)
C(23)	8305(7)	5859(6)	10907(5)	57(3)
C(24)	9007(12)	5651(11)	10656(9)	173(8)
C(25)	8690(20)	5195(18)	10285(16)	326(16)
C(26)	7754(16)	5002(13)	10257(12)	219(10)
C(27)	7223(10)	5201(8)	10506(7)	112(5)
C(28)	7495(9)	5652(8)	10858(7)	111(5)
C(29)	8234(8)	8094(7)	3953(8)	82(4)
C(30)	8790(11)	8124(7)	3443(7)	89(5)
C(31)	9602(10)	8299(7)	3471(7)	77(4)
C(32)	9836(9)	8392(6)	4034(7)	59(3)
C(33)	10555(8)	8554(6)	4277(7)	73(4)
C(34)	10373(7)	8565(6)	4888(7)	63(3)
C(35)	9210(9)	8327(5)	4546(6)	51(3)
C(36)	7713(8)	6205(7)	5652(5)	63(4)
C(37)	8030(8)	5475(7)	5854(6)	70(4)
C(38)	8716(9)	5319(7)	6170(6)	70(4)
C(39)	9095(8)	5879(7)	6318(6)	55(3)
C(40)	9799(9)	5945(8)	6649(6)	87(5)
C(41)	9805(7)	6662(8)	6631(6)	73(4)
C(42)	8708(7)	6618(6)	6091(5)	46(3)
C(43)	9108(6)	8505(6)	5629(5)	45(3)
C(44)	8910(7)	9240(6)	5583(6)	65(4)
C(45)	8529(8)	9330(7)	6119(7)	71(4)
C(46)	8393(7)	8684(8)	6736(6)	68(4)
C(47)	8630(6)	7958(6)	6780(6)	56(3)
C(48)	8937(6)	7859(5)	6225(5)	41(3)
C(49)	6834(8)	9453(7)	4242(6)	115(6)
C(50)	6968(7)	9013(7)	4991(8)	82(4)
C(51)	6391(8)	8402(8)	5433(8)	70(4)
C(52)	6661(7)	7917(8)	6083(7)	76(4)
C(53)	6205(9)	7245(8)	6523(7)	81(4)
C(54)	5554(11)	7031(9)	6331(10)	108(6)
C(55)	5272(10)	7477(12)	5647(11)	125(6)
C(56)	5716(10)	8137(10)	5188(9)	116(6)
C(57)	6923(5)	1934(6)	13609(5)	37(3)
C(58)	6987(6)	2129(7)	14152(6)	50(3)
C(59)	7018(7)	2914(8)	14044(7)	71(4)
C(60)	6967(8)	3482(7)	13395(7)	72(4)
C(61)	6912(6)	3272(6)	12853(6)	56(3)
C(62)	6876(5)	2484(6)	12942(5)	38(3)
C(63)	7071(10)	1518(10)	14844(6)	79(4)
C(64)	6998(12)	4366(10)	13269(10)	119(6)
C(65)	8447(7)	2731(6)	11807(5)	45(3)
C(66)	7903(6)	2123(6)	12194(5)	33(2)

C(67)	8234(6)	1394(6)	12594(5)	40(3)
C(68)	9078(7)	1329(7)	12575(6)	54(3)
C(69)	9613(6)	1956(8)	12187(6)	58(3)
C(70)	9279(7)	2648(7)	11803(5)	50(3)
C(71)	9833(9)	3313(9)	11386(8)	76(4)
C(72)	9431(8)	537(9)	13049(9)	88(5)
C(73)	5517(7)	0(6)	12752(6)	58(3)
C(74)	5294(6)	495(6)	13054(5)	46(3)
C(75)	5718(6)	1170(6)	12934(5)	40(3)
C(76)	6412(6)	1396(5)	12498(5)	36(2)
C(77)	6663(6)	929(6)	12172(5)	45(3)
C(78)	6206(7)	251(6)	12290(5)	54(3)
C(79)	6494(9)	-275(9)	11915(8)	85(4)
C(80)	4589(8)	234(8)	13570(7)	66(4)
C(81)	6731(5)	2880(5)	10995(4)	25(2)
C(82)	6503(5)	2835(5)	11640(4)	25(2)
C(83)	5836(6)	3280(5)	11683(5)	33(2)
C(84)	5439(5)	3737(5)	11104(4)	24(2)
C(85)	5660(5)	3760(5)	10482(4)	27(2)
C(86)	6319(5)	3325(5)	10428(5)	26(2)
C(87)	4743(6)	4253(6)	11176(5)	39(3)
C(88)	6580(7)	3323(6)	9770(5)	44(3)
C(89)	9492(6)	1850(5)	8382(5)	34(2)
C(90)	8807(5)	2261(5)	8438(4)	28(2)
C(91)	8573(6)	2189(5)	9079(5)	35(2)
C(92)	8971(6)	1744(6)	9636(5)	37(3)
C(93)	9656(6)	1359(5)	9574(5)	40(3)
C(94)	9916(5)	1405(5)	8940(5)	36(3)
C(95)	10678(7)	995(7)	8831(6)	52(3)
C(96)	8689(9)	1705(8)	10337(6)	61(3)
C(97)	7713(7)	4699(5)	7914(5)	46(3)
C(98)	8118(6)	3977(6)	8019(4)	38(3)
C(99)	7779(5)	3479(5)	7767(4)	27(2)
C(100)	7059(6)	3699(5)	7447(4)	38(3)
C(101)	6693(6)	4396(6)	7364(5)	45(3)
C(102)	7024(6)	4885(6)	7599(5)	51(3)
C(103)	5941(8)	4606(8)	7010(7)	65(4)
C(104)	8145(7)	5217(7)	8208(6)	51(3)
C(105)	7286(5)	790(5)	7748(4)	32(2)
C(106)	6594(5)	642(5)	8174(4)	41(3)
C(107)	6407(6)	1188(5)	8451(5)	39(3)
C(108)	6909(5)	1821(5)	8290(4)	35(2)
C(109)	7628(5)	1985(5)	7865(4)	24(2)
C(110)	7799(5)	1450(5)	7584(4)	27(2)
C(111)	5656(7)	1042(7)	8919(6)	61(3)
C(112)	7495(8)	248(7)	7422(7)	60(3)

C(113)	9611(5)	3307(5)	6984(5)	37(2)
C(114)	10069(6)	3652(6)	6341(5)	50(3)
C(115)	9736(6)	3704(6)	5783(5)	52(3)
C(116)	8951(7)	3445(6)	5842(6)	54(3)
C(117)	8495(6)	3099(5)	6457(5)	38(3)
C(118)	8831(5)	3019(5)	7050(4)	28(2)
C(119)	8545(9)	3535(10)	5223(8)	86(4)
C(120)	10881(10)	3902(9)	6351(8)	88(5)
B(1)	6921(7)	2215(6)	12307(5)	32(3)
B(2)	8268(6)	2674(6)	7775(5)	27(3)
F(1A)	7072(12)	4494(9)	13783(9)	107(6)
F(1)	7536(10)	4539(9)	13509(9)	90(5)
F(2A)	6412(8)	4712(7)	12909(6)	56(3)
F(2)	6243(12)	4391(11)	13734(10)	150(7)
F(3A)	7804(9)	4691(8)	12765(8)	100(5)
F(3)	6958(10)	4843(9)	12644(8)	94(5)
F(4)	7775(6)	1219(6)	14916(4)	162(5)
F(5)	6893(7)	1729(5)	15319(4)	154(4)
F(6)	6580(6)	923(5)	14964(4)	126(3)
F(7A)	10201(9)	485(9)	12895(8)	68(5)
F(7)	8855(7)	-51(7)	13242(7)	61(4)
F(8A)	9102(11)	-18(11)	12754(10)	130(6)
F(8)	9179(11)	206(10)	13569(9)	92(5)
F(9A)	10032(12)	325(11)	12743(9)	101(7)
F(9)	9526(8)	576(8)	13692(7)	62(4)
F(10)	5861(9)	-741(9)	11927(7)	77(5)
F(11)	6299(8)	177(7)	11222(6)	67(4)
F(12)	7277(8)	-274(8)	11836(8)	70(4)
F(10A)	7058(10)	-822(10)	12367(8)	107(5)
F(11A)	6894(11)	16(9)	11385(9)	102(5)
F(12A)	6237(12)	-941(11)	12172(9)	110(6)
F(13)	10598(5)	3165(5)	11427(5)	150(4)
F(14)	9724(6)	3613(6)	10762(5)	182(5)
F(15)	9758(5)	3900(5)	11545(5)	137(4)
F(16)	3956(4)	736(4)	13382(3)	87(2)
F(17)	4252(4)	-460(4)	13700(4)	103(3)
F(18)	4720(4)	257(5)	14171(4)	102(3)
F(19)	4191(3)	4359(3)	10749(3)	56(2)
F(20)	5059(3)	4959(3)	11075(3)	61(2)
F(21)	4382(3)	3971(3)	11809(3)	53(2)
F(22)	7374(4)	3471(3)	9598(3)	63(2)
F(23)	6476(4)	2621(3)	9745(3)	71(2)
F(24)	7909(5)	1555(5)	10468(3)	94(2)
F(25)	8814(5)	2382(5)	10368(3)	110(3)
F(26)	9054(5)	1198(5)	10827(3)	112(3)
F(27)	10603(4)	699(4)	8389(3)	84(2)

F(28)	10865(4)	410(4)	9379(3)	98(3)
F(29)	11303(4)	1465(4)	8597(5)	132(4)
F(30)	5483(4)	4008(4)	7046(4)	97(2)
F(31)	5450(4)	5017(4)	7228(4)	110(3)
F(32)	6078(4)	5036(5)	6355(4)	141(4)
F(33)	6214(4)	3830(4)	9247(3)	72(2)
F(34)	10946(5)	4571(6)	6419(7)	204(6)
F(35)	11372(5)	4016(6)	5797(5)	154(4)
F(36)	11341(4)	3469(5)	6842(4)	115(3)
F(37A)	8331(10)	5893(10)	7795(8)	77(6)
F(37)	8942(8)	5114(7)	8247(7)	55(4)
F(38A)	7834(9)	5154(8)	8813(7)	71(5)
F(38)	8688(8)	4940(7)	8566(7)	61(4)
F(39A)	7476(7)	5318(6)	8624(6)	37(3)
F(39)	8030(8)	6000(7)	7688(6)	43(4)
F(40)	7404(5)	533(4)	6759(4)	103(3)
F(41)	8312(4)	114(4)	7399(4)	86(2)
F(42)	7141(5)	-416(4)	7694(4)	143(4)
F(43)	5111(4)	1564(4)	8680(4)	107(3)
F(44)	5302(4)	353(4)	9118(4)	94(2)
F(45)	5833(4)	1076(4)	9512(4)	92(2)
F(46)	7968(6)	4072(5)	5038(4)	132(3)
F(47)	8085(6)	2945(5)	5277(4)	144(4)
F(48)	9025(6)	3639(7)	4698(4)	191(5)

Chapter 3

	x	y	z	U(eq)
Compound (**3.2)·2Benzene**				
Pt(1)	10682(1)	6760(1)	8296(1)	40(1)
Pt(2)	8873(1)	7226(1)	5770(1)	48(1)
Pt(3)	8360(1)	2591(1)	6381(1)	45(1)
Pt(4)	7659(1)	3262(1)	8891(1)	44(1)
N(1)	10137(9)	7579(7)	7112(4)	35(2)
N(2)	10014(10)	8109(7)	6069(4)	47(3)
N(3)	8708(10)	7110(7)	7845(4)	42(3)
N(4)	8657(10)	5221(8)	5669(4)	40(3)
N(5)	8091(10)	3622(8)	5545(4)	46(3)
N(6)	10169(10)	5637(8)	6176(4)	46(3)
N(7)	7820(10)	2261(8)	7578(4)	46(3)
N(8)	7683(10)	1847(8)	8618(5)	53(3)
N(9)	7021(10)	3770(8)	6817(4)	49(3)
N(10)	9052(10)	4750(7)	8987(4)	39(3)
N(11)	9958(10)	6169(8)	9120(4)	41(3)

N(12)	9611(10)	3355(8)	8526(4)	43(3)
C(1)	12646(10)	6538(10)	8631(5)	69(4)
C(2)	11169(12)	7380(9)	7553(5)	40(3)
C(3)	12212(13)	7726(9)	7258(5)	52(4)
C(4)	11929(12)	8115(9)	6662(5)	38(3)
C(5)	12601(13)	8528(10)	6190(6)	58(4)
C(6)	11947(15)	8769(9)	5669(6)	58(4)
C(7)	10688(15)	8559(8)	5627(5)	49(4)
C(8)	10610(12)	7981(9)	6580(5)	35(3)
C(9)	8773(13)	7533(9)	7282(5)	38(3)
C(10)	7547(13)	7944(10)	6937(5)	62(4)
C(11)	6270(13)	7856(12)	7191(6)	73(5)
C(12)	6234(13)	7372(12)	7762(6)	78(5)
C(13)	7440(14)	7048(10)	8070(6)	69(4)
C(14)	7479(12)	8660(8)	5337(5)	67(4)
C(15)	8060(12)	6363(10)	5447(5)	51(4)
C(16)	7162(12)	6486(11)	4999(5)	54(4)
C(17)	7145(13)	5467(11)	4947(5)	48(4)
C(18)	6438(13)	5129(11)	4603(5)	57(4)
C(19)	6605(13)	4050(12)	4708(5)	56(4)
C(20)	7394(12)	3343(11)	5182(5)	52(4)
C(21)	8023(12)	4647(11)	5397(5)	47(4)
C(22)	9899(14)	4824(11)	6019(5)	48(4)
C(23)	10726(13)	3759(11)	6194(5)	54(4)
C(24)	11902(14)	3482(10)	6551(5)	58(4)
C(25)	12186(13)	4304(11)	6720(6)	64(4)
C(26)	11312(14)	5349(11)	6519(5)	54(4)
C(27)	9561(11)	1281(9)	6049(5)	63(4)
C(28)	8484(11)	1683(10)	7146(5)	44(3)
C(29)	9026(11)	639(9)	7424(5)	43(3)
C(30)	8688(13)	533(11)	8024(6)	51(4)
C(31)	9008(13)	-308(10)	8490(6)	64(4)
C(32)	8557(14)	-107(11)	9026(6)	62(4)
C(33)	7979(13)	969(11)	9049(5)	57(4)
C(34)	8025(12)	1577(11)	8118(6)	46(4)
C(35)	6933(12)	3343(10)	7373(5)	42(3)
C(36)	5890(12)	3963(10)	7705(5)	45(3)
C(37)	5036(12)	4990(10)	7479(5)	50(4)
C(38)	5189(12)	5433(10)	6902(5)	53(4)
C(39)	6175(13)	4793(10)	6594(5)	52(4)
C(40)	5774(11)	3309(9)	9285(5)	64(4)
C(41)	7836(12)	4424(9)	9194(5)	42(3)
C(42)	7197(12)	5016(9)	9592(4)	42(3)
C(43)	7981(12)	5706(10)	9646(5)	43(3)
C(44)	7874(12)	6450(9)	9970(5)	42(3)
C(45)	8854(13)	6990(9)	9906(5)	52(4)

C(46)	9845(12)	6847(9)	9469(5)	43(3)
C(47)	9121(12)	5549(9)	9262(5)	35(3)
C(48)	10054(12)	4106(10)	8688(5)	36(3)
C(49)	11423(12)	4171(9)	8571(5)	41(3)
C(50)	12356(13)	3483(10)	8272(5)	58(4)
C(51)	11870(13)	2734(10)	8086(6)	69(4)
C(52)	10539(12)	2715(9)	8225(5)	45(3)
C(53)	5064(15)	9016(13)	9159(8)	132(8)
C(54)	4694(19)	10066(14)	9203(10)	153(10)
C(55)	3290(20)	10634(14)	9297(8)	127(8)
C(56)	2298(19)	10142(14)	9301(9)	125(8)
C(57)	2694(14)	9113(15)	9224(10)	154(10)
C(58)	4074(8)	8508(4)	9160(3)	145(10)
C(59)	14783(8)	876(4)	6379(3)	127(8)
C(60)	13549(8)	649(4)	6479(3)	104(7)
C(61)	13100(8)	402(4)	7015(3)	93(6)
C(62)	13886(8)	382(4)	7453(3)	122(8)
C(63)	15120(8)	609(4)	7353(3)	164(12)
C(64)	15569(8)	855(4)	6817(3)	153(11)

	x	y	z	U(eq)
		Compound **3.3**		
Pt(1)	7702(1)	1224(1)	6190(1)	46(1)
Cl(1)	9769(1)	739(1)	7212(2)	63(1)
S(1)	7953(1)	2175(1)	4487(2)	57(1)
N(1)	5372(3)	1060(3)	6235(4)	46(1)
N(2)	3319(4)	968(3)	6082(5)	55(1)
N(3)	7205(4)	441(3)	7607(5)	44(1)
C(1)	7921(5)	-99(4)	8720(6)	54(2)
C(2)	7497(5)	-569(4)	9613(6)	64(2)
C(3)	6302(6)	-513(4)	9382(7)	68(2)
C(4)	5543(5)	12(4)	8255(6)	58(2)
C(5)	6015(5)	493(4)	7388(6)	46(1)
C(6)	2199(5)	1263(5)	5238(7)	63(2)
C(7)	1918(5)	1828(4)	4038(7)	60(2)
C(8)	2822(5)	2140(4)	3590(6)	58(2)
C(9)	3986(5)	1860(4)	4395(6)	48(1)
C(10)	5138(5)	2007(4)	4316(6)	53(2)
C(11)	5976(4)	1532(4)	5420(6)	46(1)
C(12)	4149(4)	1280(4)	5598(6)	48(1)
C(13)	8307(5)	1268(5)	3392(6)	88(2)
C(14)	9348(5)	2860(4)	5194(6)	75(2)

	x	y	z	U(eq)
		Compound **3.4**		
Pt(1)	7221(1)	8816(1)	6074(1)	21(1)
N(1)	6146(3)	8052(2)	5528(2)	23(1)
N(2)	5475(3)	9073(2)	4684(2)	27(1)
N(3)	7176(3)	9528(2)	5059(2)	26(1)
C(1)	5987(4)	7303(3)	5747(3)	28(1)
C(2)	5152(5)	6845(3)	5494(3)	34(1)
C(3)	4407(4)	7161(3)	4999(3)	36(1)
C(4)	4546(4)	7930(3)	4767(3)	28(1)
C(5)	3979(5)	8475(3)	4278(3)	43(1)
C(6)	4550(5)	9152(3)	4233(3)	36(1)
C(7)	5443(4)	8330(3)	5020(3)	26(1)
C(8)	6346(4)	9571(3)	4578(3)	28(1)
C(9)	6319(5)	10112(3)	3961(3)	39(2)
C(10)	7156(5)	10607(4)	3854(3)	44(2)
C(11)	8020(5)	10554(3)	4349(3)	41(1)
C(12)	8004(4)	10007(3)	4919(3)	34(1)
C(13)	7254(4)	8195(3)	7054(3)	23(1)
C(14)	6348(4)	8112(3)	7501(3)	29(1)
C(15)	6364(4)	7714(3)	8209(3)	30(1)
C(16)	7281(5)	7393(3)	8484(3)	35(1)
C(17)	8200(5)	7451(3)	8041(3)	35(1)
C(18)	8181(4)	7838(3)	7338(3)	28(1)
C(19)	8186(4)	9582(3)	6606(3)	25(1)
C(20)	9270(4)	9473(3)	6650(3)	32(1)
C(21)	9952(5)	10044(3)	6970(3)	38(1)
C(22)	9535(5)	10729(3)	7237(3)	41(1)
C(23)	8454(5)	10847(3)	7216(3)	39(1)
C(24)	7799(4)	10283(3)	6905(3)	28(1)

	x	y	z	U(eq)
		Compound **E·MeCN**		
Pt(1)	2545(1)	3601(1)	2977(1)	55(1)
N(1)	2877(6)	-806(5)	-1691(4)	64(1)
N(2)	2647(5)	1168(4)	485(4)	50(1)
N(3)	2014(5)	1397(4)	2600(4)	48(1)
N(4)	2250(6)	4415(5)	5027(5)	68(1)
C(1)	2874(6)	2718(5)	1041(5)	55(1)
C(2)	3350(7)	3083(6)	-11(6)	71(2)
C(3)	3414(6)	1779(7)	-1207(5)	65(1)
C(4)	3800(7)	1403(8)	-2569(6)	82(2)
C(5)	3704(7)	-26(9)	-3418(6)	83(2)

C(6)	3265(7)	-1082(8)	-2966(6)	77(2)
C(7)	2975(6)	587(6)	-884(5)	53(1)
C(8)	2142(5)	471(5)	1308(4)	44(1)
C(9)	1771(6)	-1018(5)	846(5)	60(1)
C(10)	1279(7)	-1571(6)	1779(5)	62(1)
C(11)	1166(7)	-628(6)	3103(5)	63(1)
C(12)	1531(6)	831(6)	3472(5)	56(1)
C(13)	3046(9)	5676(6)	3136(7)	88(2)
C(14)	2199(7)	4890(6)	6176(6)	66(1)
C(15)	2156(9)	5497(7)	7650(6)	85(2)

Chapter 4

	x	y	z	U(eq)
		Compound **4.1**		
Pt(1)	-2124(1)	6026(1)	-2111(1)	19(1)
S(1)	-3710(1)	3498(1)	-482(1)	31(1)
F(1)	-3059(2)	4014(1)	-2714(2)	63(1)
F(2)	-3093(2)	3129(1)	-2902(2)	67(1)
F(3)	-1574(2)	3517(1)	-1481(3)	82(1)
O(1)	-3307(2)	2983(1)	199(2)	45(1)
O(2)	-4985(2)	3507(1)	-1251(3)	66(1)
O(3)	-3284(4)	3966(1)	395(3)	86(1)
N(1)	-821(2)	6566(1)	-3117(2)	19(1)
N(2)	-2276(2)	6654(1)	-5394(2)	20(1)
N(3)	-3295(2)	5586(1)	-5497(2)	20(1)
N(4)	-1711(2)	5320(1)	-3446(2)	21(1)
C(1)	-3356(3)	5551(1)	-1194(3)	34(1)
C(2)	-799(3)	5802(1)	-369(3)	37(1)
C(3)	-2578(3)	6667(1)	-880(3)	32(1)
C(4)	358(2)	6706(1)	-2462(3)	23(1)
C(5)	1228(2)	6964(1)	-3181(3)	26(1)
C(6)	937(2)	7083(1)	-4670(3)	25(1)
C(7)	-278(2)	6954(1)	-5389(3)	21(1)
C(8)	-993(3)	7011(1)	-6837(3)	25(1)
C(9)	-2188(3)	6836(1)	-6800(3)	24(1)
C(10)	-1110(2)	6718(1)	-4530(3)	18(1)
C(11)	-3420(2)	6557(1)	-4830(3)	19(1)
C(12)	-4079(3)	6993(1)	-4360(3)	26(1)
C(13)	-5185(3)	6893(1)	-3827(3)	30(1)
C(14)	-5644(3)	6363(1)	-3794(3)	31(1)
C(15)	-5023(3)	5927(1)	-4325(3)	28(1)
C(16)	-3891(2)	6025(1)	-4834(3)	20(1)
C(17)	-3661(3)	5395(1)	-6930(3)	26(1)

C(18)	-2970(3)	4943(1)	-7157(3)	26(1)
C(19)	-2124(2)	4836(1)	-5812(3)	22(1)
C(20)	-1211(3)	4442(1)	-5295(3)	28(1)
C(21)	-582(3)	4494(1)	-3874(3)	31(1)
C(22)	-840(3)	4928(1)	-3002(3)	27(1)
C(23)	-2343(2)	5253(1)	-4816(3)	19(1)
C(24)	-2815(3)	3542(2)	-1967(3)	39(1)

	x	y	z	U(eq)
		Compound **4.2**		
Pt(1)	-1332(1)	-2304(1)	-2387(1)	16(1)
S(1)	1734(1)	755(1)	-2237(1)	21(1)
F(1)	3932(4)	983(2)	-3713(1)	57(1)
F(2)	4706(3)	2591(2)	-2717(1)	39(1)
F(3)	5561(3)	891(2)	-2413(2)	53(1)
O(1)	1373(3)	-617(2)	-2420(1)	23(1)
O(2)	2205(4)	1187(2)	-1268(2)	36(1)
O(3)	369(3)	1317(2)	-2738(2)	37(1)
N(1)	380(3)	-2938(2)	-3599(1)	19(1)
N(2)	650(3)	-5074(2)	-3315(1)	19(1)
N(3)	542(3)	-5091(2)	-1616(2)	19(1)
N(4)	659(3)	-2856(2)	-1263(1)	18(1)
C(1)	-3874(4)	-3751(3)	-2354(2)	29(1)
C(2)	-2640(5)	-1468(3)	-1353(2)	29(1)
C(3)	-2998(5)	-1618(3)	-3349(2)	28(1)
C(4)	961(4)	-2018(2)	-4212(2)	23(1)
C(5)	2185(4)	-2075(3)	-4961(2)	26(1)
C(6)	2872(4)	-3143(3)	-5133(2)	24(1)
C(7)	2294(4)	-4127(2)	-4538(2)	20(1)
C(8)	2613(4)	-5371(3)	-4490(2)	23(1)
C(9)	1614(4)	-5905(3)	-3748(2)	23(1)
C(10)	1054(4)	-3971(2)	-3786(2)	18(1)
C(11)	-585(4)	-5377(2)	-2510(2)	19(1)
C(12)	1401(4)	-5956(2)	-1186(2)	23(1)
C(13)	2532(4)	-5409(3)	-409(2)	23(1)
C(14)	2420(4)	-4113(2)	-335(2)	20(1)
C(15)	3260(4)	-3086(3)	293(2)	24(1)
C(16)	2775(4)	-1961(3)	133(2)	26(1)
C(17)	1500(4)	-1886(2)	-626(2)	23(1)
C(18)	1158(4)	-3948(2)	-1100(2)	17(1)
C(19)	4109(5)	1319(3)	-2802(2)	30(1)

	x	y	z	U(eq)

Compound **4.3**

Pt(1)	245(1)	3702(1)	3307(1)	21(1)
O(1)	2029(2)	2104(2)	3386(2)	31(1)
F(1)	-1144(4)	244(4)	1132(3)	107(1)
F(2)	-2851(5)	-1697(4)	3498(3)	114(1)
F(3)	-3271(9)	-865(9)	1946(8)	117(3)
F(3A)	-1035(14)	-1765(8)	1986(9)	155(5)
F(4A)	-573(9)	-489(9)	2776(7)	115(3)
F(6A)	-2718(15)	370(10)	2734(11)	142(4)
F(4)	-560(6)	-1409(6)	2608(4)	56(1)
F(5)	-1891(6)	257(7)	2815(7)	65(2)
F(5A)	-3518(6)	-42(5)	1950(6)	63(2)
F(6)	-2214(7)	-1787(5)	1802(5)	57(1)
N(1)	2214(3)	4928(2)	3061(2)	25(1)
N(2)	2057(3)	7006(2)	1558(2)	27(1)
N(3)	1861(3)	5995(2)	324(2)	29(1)
N(4)	861(3)	3834(2)	1497(2)	26(1)
C(1)	-234(4)	3274(3)	4988(2)	35(1)
C(2)	-1509(3)	2518(3)	3677(3)	33(1)
C(3)	-1377(3)	5073(3)	3314(3)	31(1)
C(4)	3025(3)	4320(3)	3820(3)	32(1)
C(5)	4195(3)	4886(3)	3941(3)	35(1)
C(6)	4581(3)	6156(3)	3292(3)	34(1)
C(7)	3786(3)	6831(3)	2502(3)	30(1)
C(8)	3855(4)	8112(3)	1667(3)	39(1)
C(9)	2822(4)	8180(3)	1113(3)	37(1)
C(10)	2634(3)	6162(3)	2412(2)	24(1)
C(11)	1090(3)	6711(3)	1004(3)	27(1)
C(12)	2823(4)	6546(3)	-743(3)	40(1)
C(13)	3263(4)	5650(4)	-1201(3)	42(1)
C(14)	2537(3)	4455(3)	-400(3)	33(1)
C(15)	2471(4)	3223(4)	-389(3)	38(1)
C(16)	1549(4)	2328(4)	544(3)	41(1)
C(17)	787(4)	2660(3)	1445(3)	34(1)
C(18)	1685(3)	4709(3)	551(2)	27(1)
C(19A)	4484(5)	1495(5)	3469(5)	33(1)
C(20A)	3508(6)	316(5)	4264(5)	38(1)
C(19)	3751(12)	927(10)	2347(10)	58(3)
C(20)	3173(16)	18(11)	3574(13)	90(5)
C(21)	1890(4)	775(4)	4201(4)	54(1)
C(22)	3517(4)	2249(3)	2632(3)	41(1)
P(1)	-1981(1)	-738(1)	2311(1)	32(1)

	x	y	z	U(eq)

Compound **4.4**

Pt(1)	1186(1)	911(1)	9368(1)	40(1)
Pt(2)	5309(1)	-2131(1)	4767(1)	39(1)
C(1)	870(6)	-1024(2)	10713(5)	60(1)
C(2)	-470(7)	-1123(3)	11292(5)	66(1)
C(3)	-1391(6)	-541(3)	11238(4)	58(1)
C(4)	-2814(7)	-290(3)	11616(5)	72(2)
C(5)	-3231(6)	323(3)	11319(6)	72(2)
C(6)	-2252(6)	707(3)	10643(5)	59(1)
C(7)	-486(5)	-104(2)	10589(4)	45(1)
C(8)	1899(6)	-903(2)	7588(6)	63(1)
C(9)	1087(7)	-926(3)	6343(5)	65(1)
C(10)	250(6)	-338(2)	6064(4)	55(1)
C(11)	-720(7)	-32(3)	5045(5)	71(2)
C(12)	-1287(7)	577(3)	5238(5)	75(2)
C(13)	-884(6)	886(3)	6418(4)	62(1)
C(14)	636(5)	24(2)	7228(4)	43(1)
C(15)	1989(6)	-69(2)	9471(4)	44(1)
C(16)	2340(6)	1137(2)	11202(4)	57(1)
C(17)	239(7)	1852(2)	9148(5)	59(1)
C(18)	3264(7)	1203(3)	8631(5)	63(1)
C(19)	6880(7)	-781(3)	7826(5)	72(2)
C(20)	6265(7)	-207(3)	7546(6)	80(2)
C(21)	5287(7)	-229(2)	6290(6)	65(1)
C(22)	4308(9)	163(3)	5415(7)	90(2)
C(23)	3565(8)	-93(3)	4224(7)	84(2)
C(24)	3744(7)	-733(3)	3947(5)	65(1)
C(25)	5392(6)	-872(2)	5900(5)	46(1)
C(26)	5368(7)	-2218(3)	8903(4)	63(1)
C(27)	3910(8)	-2447(3)	9203(5)	72(2)
C(28)	2823(6)	-2563(2)	8017(5)	56(1)
C(29)	1230(7)	-2782(2)	7577(6)	67(1)
C(30)	687(7)	-2813(3)	6268(6)	73(2)
C(31)	1712(6)	-2610(2)	5387(5)	56(1)
C(32)	3778(5)	-2389(2)	7031(4)	43(1)
C(33)	6424(5)	-1909(2)	6721(4)	43(1)
C(34)	7377(7)	-1901(3)	3967(5)	64(1)
C(35)	6014(7)	-3068(2)	4903(5)	60(1)
C(36)	4026(7)	-2310(3)	2883(4)	75(2)
N(1)	-831(4)	498(2)	10265(3)	44(1)
N(2)	932(5)	-398(2)	10289(4)	47(1)
N(3)	94(5)	610(2)	7437(3)	48(1)
N(4)	1625(4)	-312(2)	8142(3)	45(1)
N(5)	4656(5)	-1135(2)	4757(4)	46(1)
N(6)	6365(4)	-1207(2)	6816(3)	48(1)

N(7)	3273(4)	-2400(2)	5760(3)	40(1)
N(8)	5307(4)	-2183(2)	7560(3)	47(1)

Chapter 5

	x	y	z	U(eq)
		SiBAM		
Si(1)	5000	2221(1)	5974(1)	45(1)
N(1)	5631(1)	2652(1)	7726(1)	42(1)
N(2)	6075(1)	1026(1)	8373(1)	46(1)
C(1)	5000	2213(1)	7307(1)	38(1)
C(2)	5890(1)	3674(1)	7626(1)	51(1)
C(3)	6527(1)	3751(1)	8010(1)	56(1)
C(4)	6702(1)	2728(1)	8364(1)	45(1)
C(5)	7265(1)	2268(1)	8809(1)	58(1)
C(6)	7222(1)	1205(2)	9034(1)	62(1)
C(7)	6630(1)	626(1)	8809(1)	56(1)
C(8)	6130(1)	2058(1)	8173(1)	38(1)
C(9)	5000	3584(3)	5468(2)	82(1)
C(10)	4205(1)	1491(2)	5636(2)	86(1)

	x	y	z	U(eq)
		BAHE		
O(1)	5245(3)	2723(3)	734(1)	79(1)
N(1)	7808(3)	7269(3)	1265(1)	52(1)
N(2)	8989(4)	7695(3)	665(1)	65(1)
N(3)	8929(3)	5367(3)	1736(1)	54(1)
N(4)	7860(3)	4422(3)	2302(1)	57(1)
C(1)	10043(5)	5993(4)	1694(1)	67(1)
C(2)	10637(4)	6079(4)	2056(2)	71(1)
C(3)	9863(4)	5489(4)	2354(1)	55(1)
C(4)	9903(5)	5284(5)	2771(1)	70(1)
C(5)	8943(5)	4639(5)	2945(1)	74(2)
C(6)	7951(5)	4230(5)	2708(1)	70(1)
C(7)	8814(4)	5045(4)	2145(1)	47(1)
C(8)	7459(5)	7942(4)	1603(1)	66(1)
C(9)	7877(5)	9125(5)	1575(1)	73(2)
C(10)	8550(5)	9221(4)	1202(1)	58(1)
C(11)	9230(5)	10125(5)	989(2)	74(2)
C(12)	9769(5)	9791(5)	627(2)	83(2)
C(13)	9640(5)	8593(6)	479(2)	80(2)
C(14)	8475(4)	8054(4)	1016(1)	49(1)

C(15)	7535(4)	5986(4)	1183(1)	50(1)
C(16)	6735(5)	5693(4)	862(1)	65(1)
C(17)	6470(4)	4465(5)	794(1)	62(1)
C(18)	7006(4)	3529(4)	1028(1)	59(1)
C(19)	7814(4)	3796(4)	1340(1)	55(1)
C(20)	6487(5)	2334(4)	839(1)	69(1)
C(21)	8091(4)	5060(4)	1415(1)	49(1)
C(22)	7082(5)	2218(5)	422(2)	86(2)
C(23)	6535(6)	3150(6)	196(2)	95(2)
C(24)	5627(5)	3777(5)	487(1)	79(2)

	x	y	z	U(eq)
		Compound **5.1**		
Pt(1)	1411(1)	4952(1)	2113(1)	35(1)
Si(1)	1798(1)	2623(1)	4697(1)	44(1)
C(1)	-449(3)	5907(3)	2202(3)	55(1)
C(2)	2760(4)	6883(4)	3081(3)	55(1)
C(3)	4187(3)	4488(4)	1392(3)	56(1)
C(4)	5485(4)	3973(4)	1241(3)	67(1)
C(5)	6028(3)	2892(4)	1698(3)	61(1)
C(6)	5239(3)	2347(3)	2302(2)	47(1)
C(7)	5389(3)	1256(3)	2872(3)	58(1)
C(8)	4212(3)	1211(3)	3288(3)	53(1)
C(9)	3925(3)	2941(3)	2409(2)	37(1)
C(10)	1854(3)	2409(3)	3238(2)	33(1)
C(11)	36(3)	16(3)	2313(3)	51(1)
C(12)	-1120(4)	-598(3)	1381(3)	57(1)
C(13)	-1331(3)	436(3)	767(2)	43(1)
C(14)	-2297(3)	483(4)	-233(2)	56(1)
C(15)	-2139(3)	1738(4)	-547(2)	56(1)
C(16)	-1040(3)	2920(4)	123(2)	48(1)
C(17)	-239(3)	1699(3)	1396(2)	34(1)
C(18)	-204(4)	2862(4)	4577(3)	67(1)
C(19)	3172(4)	4311(4)	5517(3)	64(1)
C(20)	2320(5)	1074(4)	5297(3)	83(1)
N(1)	3372(2)	3989(3)	1968(2)	40(1)
N(2)	3304(2)	2241(2)	3025(2)	39(1)
N(3)	593(2)	1429(2)	2352(2)	36(1)
N(4)	-69(2)	2950(2)	1108(2)	36(1)

	x	y	z	U(eq)
		Compound **5.3**		
Pt(1)	-7360(1)	3065(1)	8279(1)	25(1)
N(1)	-7435(7)	2839(5)	6720(5)	30(1)
N(2)	-10261(8)	3854(6)	6323(5)	35(1)
N(3)	-7770(8)	1437(5)	8830(5)	29(1)
N(4)	-10693(8)	1960(5)	8633(5)	34(1)
C(1)	-6035(10)	2115(6)	6359(6)	38(2)
C(2)	-5902(12)	1696(7)	5490(7)	43(2)
C(3)	-7216(12)	1990(8)	4901(6)	45(2)
C(4)	-8651(10)	2737(7)	5217(6)	35(2)
C(5)	-10274(12)	3276(9)	4851(7)	49(2)
C(6)	-11166(11)	3925(8)	5517(7)	47(2)
C(7)	-8711(9)	3139(6)	6144(6)	31(2)
C(8)	-6384(10)	536(6)	8927(6)	35(2)
C(9)	-6367(11)	-512(7)	8872(7)	43(2)
C(10)	-7756(12)	-708(7)	8669(7)	44(2)
C(11)	-9225(11)	179(7)	8606(6)	37(2)
C(12)	-10907(12)	334(7)	8469(7)	46(2)
C(13)	-11736(11)	1392(8)	8507(7)	44(2)
C(14)	-9142(9)	1217(6)	8709(6)	29(1)
C(15)	-10923(10)	4495(7)	7118(7)	38(2)
C(16)	-12120(10)	4027(7)	8060(7)	37(2)
C(17)	-11318(9)	3037(7)	8932(6)	35(2)
C(18)	-7063(9)	3088(5)	9756(5)	26(1)
C(19)	-7973(9)	2598(6)	10696(6)	32(2)
C(20)	-7707(10)	2558(7)	11728(6)	37(2)
C(21)	-6505(10)	2993(7)	11852(6)	38(2)
C(22)	-5586(10)	3487(6)	10939(6)	35(2)
C(23)	-5879(9)	3540(6)	9922(6)	29(1)
C(24)	-7018(8)	4595(6)	7643(5)	24(1)
C(25)	-7921(9)	5503(6)	8076(6)	32(2)
C(26)	-7730(10)	6577(6)	7610(6)	33(2)
C(27)	-6590(10)	6782(7)	6691(7)	37(2)
C(28)	-5687(9)	5895(7)	6247(6)	35(2)
C(29)	-5899(9)	4823(6)	6705(6)	31(2)
C(30)	-9426(19)	-232(13)	5857(11)	95(5)
C(31)	-11110(20)	364(13)	5657(14)	98(5)
C(32)	-11910(20)	290(13)	4998(14)	93(4)

	x	y	z	U(eq)
		Compound **5.4**		
Pt(1)	52(1)	4517(1)	2319(1)	42(1)
N(1)	1188(4)	5553(5)	3247(3)	52(1)
N(2)	59(4)	6482(4)	3910(3)	50(1)
N(3)	325(4)	2795(4)	2976(3)	45(1)
N(4)	-1443(4)	2210(4)	3050(2)	42(1)
C(1)	2210(6)	5555(7)	3224(5)	70(2)
C(2)	3043(6)	6250(8)	3723(6)	87(3)
C(3)	2845(7)	6985(8)	4259(5)	85(3)
C(4)	1823(6)	7020(6)	4313(4)	65(2)
C(5)	1310(7)	7655(6)	4757(4)	67(2)
C(6)	256(6)	7316(6)	4510(3)	57(2)
C(7)	1020(5)	6282(5)	3779(3)	46(1)
C(8)	1333(5)	2313(6)	3105(3)	54(2)
C(9)	1650(6)	1097(6)	3345(3)	56(2)
C(10)	924(6)	277(6)	3484(3)	55(2)
C(11)	-121(5)	726(5)	3385(3)	44(1)
C(12)	-1059(5)	219(5)	3488(3)	53(2)
C(13)	-1833(5)	1131(5)	3276(3)	49(2)
C(14)	-377(5)	1997(5)	3125(3)	42(1)
C(15)	-995(5)	5911(5)	3541(3)	45(1)
C(16)	-1188(5)	4736(5)	3940(3)	45(1)
C(17)	-2232(5)	4073(5)	3475(3)	47(1)
C(18)	-2103(5)	3349(5)	2819(3)	44(1)
C(19)	35(5)	6040(5)	1692(3)	43(1)
C(20)	-55(5)	7276(6)	1924(4)	52(2)
C(21)	74(5)	8335(6)	1536(4)	58(2)
C(22)	309(5)	8179(6)	880(4)	57(2)
C(23)	406(5)	6979(6)	627(3)	51(2)
C(24)	261(5)	5923(6)	1018(3)	47(1)
C(25)	-923(5)	3567(5)	1439(3)	43(1)
C(26)	-1802(5)	4120(6)	889(3)	49(2)
C(27)	-2504(6)	3444(7)	317(4)	57(2)
C(28)	-2363(6)	2153(7)	242(4)	60(2)
C(29)	-1492(6)	1576(6)	759(4)	57(2)
C(30)	-810(5)	2236(5)	1340(3)	46(1)

	x	y	z	U(eq)
		Compound **5.5**		
Pt(1)	-51(1)	2220(1)	7608(1)	62(1)
Pt(2)	5064(1)	3187(1)	7584(1)	55(1)
S(1)	887(3)	303(3)	8373(2)	84(1)
S(2)	5488(4)	3600(4)	6028(2)	113(2)
N(1)	781(8)	2903(8)	9466(5)	62(3)
N(2)	-966(7)	2824(7)	8852(5)	41(2)
N(3)	1973(9)	5315(10)	7004(6)	54(3)
N(4)	3998(8)	5033(8)	7463(5)	43(2)
C(1)	1003(12)	2997(11)	10329(8)	86(4)
C(2)	23(12)	3069(10)	10901(8)	75(4)
C(3)	-892(10)	3030(9)	10407(7)	48(3)
C(4)	-2061(10)	3047(9)	10616(7)	55(3)
C(5)	-2700(9)	2990(8)	9947(7)	46(3)
C(6)	-2141(9)	2871(8)	9108(7)	50(3)
C(7)	-401(10)	2911(9)	9508(7)	47(3)
C(8)	973(12)	6248(14)	6641(7)	68(4)
C(9)	1136(11)	7207(12)	6490(7)	65(4)
C(10)	2344(11)	6893(12)	6801(7)	52(3)
C(11)	3063(12)	7464(11)	6824(7)	70(4)
C(12)	4212(13)	6832(12)	7170(7)	70(4)
C(13)	4669(11)	5641(12)	7494(6)	63(3)
C(14)	2866(11)	5685(12)	7125(6)	49(3)
C(15)	-903(10)	3867(10)	6928(7)	55(3)
C(16)	-875(14)	4141(14)	6013(10)	102(5)
C(17)	-1483(14)	5258(16)	5592(8)	94(5)
C(18)	-2131(11)	6205(13)	6036(9)	80(4)
C(19)	-2179(11)	5955(12)	6926(8)	66(4)
C(20)	-1610(10)	4839(12)	7347(8)	59(3)
C(21)	937(11)	1505(10)	6494(7)	75(4)
C(22)	2164(12)	1445(12)	6309(8)	102(5)
C(23)	2896(15)	907(13)	5622(10)	117(6)
C(24)	2519(17)	398(14)	5121(9)	104(5)
C(25)	1346(16)	389(12)	5298(10)	112(6)
C(26)	595(14)	925(12)	6027(10)	119(6)
C(27)	5970(12)	1610(14)	7548(7)	74(5)
C(28)	7210(20)	974(13)	7678(10)	128(7)
C(29)	8045(15)	-244(18)	7629(10)	131(7)
C(30)	7482(17)	-904(14)	7446(9)	102(5)
C(31)	6227(17)	-418(15)	7290(8)	81(4)
C(32)	5562(12)	768(15)	7353(7)	78(4)
C(33)	4701(9)	2916(11)	8923(6)	47(3)

C(34)	4952(10)	1855(11)	9441(7)	60(3)
C(35)	4686(10)	1723(11)	10363(7)	61(3)
C(36)	4151(10)	2674(11)	10807(7)	56(3)
C(37)	3861(10)	3747(10)	10368(7)	54(3)
C(38)	4140(9)	3852(10)	9421(6)	48(3)
C(39)	1594(10)	2941(10)	8681(7)	69(4)
C(40)	1379(9)	4177(10)	8283(6)	57(3)
C(41)	1972(10)	4224(11)	7343(7)	68(4)
C(42A)	600(40)	-350(30)	7620(20)	215(18)
C(42)	210(40)	100(30)	9557(18)	178(16)
C(43)	2471(13)	-207(11)	8388(13)	183(9)
C(44)	4855(14)	3018(16)	5447(9)	170(8)
C(45)	7123(13)	2734(15)	5783(8)	166(8)

	x	y	z	U(eq)
		Compound **5.6**		
Pt(1)	12545(1)	-11604(1)	-2352(1)	28(1)
N(1)	11449(6)	-13639(5)	-1695(4)	32(1)
N(2)	8333(6)	-13151(5)	-1309(4)	33(1)
N(3)	12328(6)	-12155(5)	-3997(4)	29(1)
N(4)	9302(6)	-11459(5)	-3830(4)	33(1)
C(1)	12617(8)	-14718(7)	-1820(5)	38(2)
C(2)	12194(8)	-16102(7)	-1792(5)	39(2)
C(3)	10458(8)	-16464(7)	-1626(5)	40(2)
C(4)	9205(7)	-15403(6)	-1466(5)	31(1)
C(5)	7367(8)	-15315(8)	-1267(5)	42(2)
C(6)	6884(8)	-13958(7)	-1166(5)	38(2)
C(7)	9771(7)	-14014(6)	-1490(5)	30(1)
C(8)	13666(8)	-12909(7)	-4653(5)	38(2)
C(9)	13555(8)	-13700(7)	-5516(5)	39(2)
C(10)	11998(8)	-13788(7)	-5761(5)	39(2)
C(11)	10580(8)	-13010(6)	-5144(5)	33(1)
C(12)	8817(8)	-12752(7)	-5167(6)	42(2)
C(13)	8124(8)	-11809(7)	-4385(6)	42(2)
C(14)	10827(7)	-12181(6)	-4300(5)	29(1)
C(15)	8969(7)	-10330(6)	-3061(5)	35(2)
C(16)	7591(8)	-10678(7)	-1894(5)	40(2)
C(17)	8181(8)	-11708(7)	-1008(5)	38(2)
C(18)	13683(7)	-9753(7)	-3080(6)	40(2)
C(19)	12748(7)	-11224(7)	-771(5)	39(2)

	x	y	z	U(eq)
		Compound **5.7**		
Pt(1)	313(1)	1393(1)	2923(1)	22(1)
O(1)	-6420(6)	3345(3)	-1498(2)	71(1)
N(1)	181(4)	3416(3)	2956(2)	27(1)
N(2)	-1690(4)	3818(3)	4396(2)	30(1)
N(3)	-3850(4)	1429(3)	2085(2)	30(1)
N(4)	-902(4)	1649(3)	1565(2)	24(1)
C(1)	1134(5)	4014(3)	2234(3)	34(1)
C(2)	1279(6)	5310(3)	2106(3)	39(1)
C(3)	417(6)	6066(3)	2757(3)	39(1)
C(4)	-566(5)	5499(3)	3517(3)	32(1)
C(5)	-1601(6)	5927(4)	4312(3)	40(1)
C(6)	-2248(5)	4905(4)	4821(3)	37(1)
C(7)	-649(5)	4163(3)	3589(3)	27(1)
C(8)	-2261(5)	2590(3)	4780(3)	32(1)
C(9)	-4092(5)	2535(4)	4604(3)	36(1)
C(10)	-4396(5)	2612(3)	3518(3)	33(1)
C(11)	-3835(5)	1350(3)	3144(3)	31(1)
C(12)	-5266(5)	1389(4)	1592(3)	41(1)
C(13)	-4894(5)	1490(4)	622(3)	40(1)
C(14)	-3144(5)	1592(3)	468(3)	31(1)
C(15)	-2011(6)	1706(4)	-336(3)	37(1)
C(16)	-353(5)	1789(4)	-187(3)	36(1)
C(17)	139(5)	1761(3)	750(3)	32(1)
C(18)	-2510(5)	1559(3)	1403(3)	27(1)
C(19)	1649(5)	1038(3)	4126(3)	29(1)
C(20)	536(5)	-500(3)	2857(3)	32(1)
C(21)	-5516(7)	3112(5)	-2382(4)	57(1)
C(22)	-5712(8)	1809(5)	-2546(4)	70(2)
C(23)	-6599(8)	4619(5)	-1346(4)	67(2)
C(24)	-7384(9)	4790(5)	-395(4)	86(2)

	x	y	z	U(eq)
		Compound **5.10·0.25[PtMe$_3$I]**		
Pt(1)	4506(1)	9158(1)	1008(1)	31(1)
Pt(2)	8133(1)	8058(1)	1039(1)	55(1)
I(1)	5365(1)	8646(1)	93(1)	49(1)
I(2)	3886(1)	8739(1)	-877(1)	49(1)
I(3)	6976(1)	8101(1)	1078(1)	56(1)
N(1)	3839(3)	9580(3)	1777(7)	36(2)
N(2)	3656(3)	9016(3)	3736(8)	40(2)

N(3)	4604(3)	8862(3)	4375(7)	34(2)
N(4)	4981(3)	9442(3)	2595(7)	33(2)
C(1)	3659(4)	10045(4)	1124(10)	51(3)
C(2)	3193(5)	10340(5)	1528(12)	65(3)
C(3)	2900(4)	10177(4)	2646(10)	52(3)
C(4)	3073(4)	9712(4)	3360(10)	41(2)
C(5)	2900(4)	9435(5)	4550(12)	57(3)
C(6)	3258(4)	9033(4)	4747(10)	51(3)
C(7)	3550(4)	9433(4)	2881(9)	36(2)
C(8)	4128(4)	8626(4)	3687(9)	39(2)
C(9)	4766(4)	8759(4)	5710(9)	46(2)
C(10)	5203(4)	9061(5)	6054(9)	52(3)
C(11)	5354(4)	9378(4)	4886(9)	35(2)
C(12)	5757(4)	9748(4)	4574(11)	50(3)
C(13)	5766(4)	9984(4)	3293(11)	50(3)
C(14)	5373(4)	9824(4)	2340(10)	45(2)
C(15)	4971(4)	9240(3)	3848(8)	31(2)
C(16)	3409(5)	7709(5)	2778(11)	65(3)
C(17)	4622(5)	7535(4)	3565(11)	60(3)
C(18)	3750(5)	7671(4)	5778(9)	58(3)
C(19)	8162(7)	8080(7)	-1118(12)	111(6)
C(20)	8172(5)	8915(5)	1081(13)	78(4)
C(21)	8998(5)	8009(6)	1075(15)	88(5)
Si(1)	3972(1)	7856(1)	4020(3)	42(1)

	x	y	z	U(eq)
Compound **5.10·0.5I_2·CH_2Cl_2**				
Pt(1)	3790(1)	8634(1)	661(1)	34(1)
I(1)	1490(1)	9086(1)	348(1)	53(1)
I(2)	4057(1)	10672(1)	1192(1)	59(1)
I(3)	282(1)	6184(1)	116(1)	64(1)
Si(1)	2906(2)	6392(2)	2186(1)	48(1)
N(1)	3641(6)	7012(6)	233(3)	39(1)
N(2)	3618(6)	5710(5)	1066(3)	39(1)
N(3)	5189(6)	6767(6)	1658(3)	40(1)
N(4)	5604(6)	8229(6)	924(3)	39(1)
C(1)	3545(8)	7005(9)	-348(3)	52(2)
C(2)	3383(9)	5950(11)	-662(4)	62(3)
C(3)	3279(9)	4883(10)	-408(4)	59(2)
C(4)	3378(8)	4853(8)	186(4)	50(2)
C(5)	3320(9)	3929(8)	601(5)	59(2)
C(6)	3472(9)	4464(8)	1117(4)	56(2)
C(7)	3563(7)	5953(7)	489(3)	35(2)
C(8)	3860(7)	6549(7)	1534(3)	38(2)

C(9)	5955(9)	6117(9)	2048(4)	59(2)
C(10)	7163(9)	6376(9)	2002(4)	61(3)
C(11)	7187(7)	7251(7)	1557(4)	44(2)
C(12)	8107(8)	7822(9)	1303(4)	55(2)
C(13)	7761(8)	8603(9)	840(4)	56(2)
C(14)	6529(8)	8769(8)	677(4)	48(2)
C(15)	5939(7)	7459(6)	1350(3)	34(2)
C(16)	1317(10)	6586(12)	1857(5)	75(3)
C(17)	3390(40)	7710(30)	2648(7)	396(6)
C(18)	3080(11)	4942(10)	2597(4)	73(3)
C(19)	391(18)	1774(16)	1344(8)	132(6)
Cl(1)	131(7)	501(7)	1769(3)	184(2)
Cl(2)	293(7)	3076(8)	1718(3)	214(3)

Chapter 6

	x	y	z	U(eq)
		BNPA		
N(1)	5692(2)	6803(2)	744(1)	60(1)
N(2)	2919(2)	6315(2)	463(1)	52(1)
N(3)	787(2)	5055(2)	1087(1)	59(1)
B(1)	320(3)	2474(2)	2909(1)	49(1)
C(1)	1962(3)	6781(3)	-132(1)	65(1)
C(2)	2797(3)	7676(3)	-638(1)	68(1)
C(3)	4387(3)	7814(2)	-375(1)	55(1)
C(4)	5777(3)	8569(2)	-632(1)	63(1)
C(5)	7101(3)	8426(3)	-198(1)	67(1)
C(6)	7006(3)	7544(3)	469(1)	69(1)
C(7)	4435(2)	6958(2)	310(1)	48(1)
C(8)	2370(2)	5362(2)	1083(1)	48(1)
C(9)	3410(2)	4798(2)	1639(1)	56(1)
C(10)	2760(2)	3885(2)	2224(1)	58(1)
C(11)	1113(2)	3491(2)	2254(1)	51(1)
C(12)	224(2)	4123(2)	1653(1)	57(1)
C(13)	-1038(2)	1346(2)	2795(1)	47(1)
C(14)	-2643(2)	1499(2)	3143(1)	53(1)
C(15)	-3793(2)	437(2)	3051(1)	59(1)
C(16)	-3415(3)	-823(2)	2638(1)	57(1)
C(17)	-1856(3)	-961(2)	2293(1)	56(1)
C(18)	-682(2)	87(2)	2355(1)	50(1)
C(19)	-3151(3)	2828(3)	3616(1)	80(1)
C(20)	-4628(3)	-2029(3)	2570(1)	83(1)
C(21)	990(3)	-223(3)	1959(1)	75(1)
C(22)	1014(2)	2614(2)	3646(1)	48(1)

C(23)	1646(2)	1210(2)	4110(1)	50(1)
C(24)	2502(3)	1394(2)	4698(1)	58(1)
C(25)	2720(3)	2922(3)	4867(1)	59(1)
C(26)	2002(3)	4285(2)	4446(1)	62(1)
C(27)	1166(2)	4180(2)	3844(1)	55(1)
C(28)	1432(3)	-519(2)	3993(1)	67(1)
C(29)	3731(3)	3070(3)	5490(1)	89(1)
C(30)	391(3)	5773(2)	3430(1)	80(1)

	x	y	z	U(eq)
		Compound **6.2**		
Pt(1)	1783(1)	234(1)	2973(1)	31(1)
N(1)	2144(2)	-851(6)	2555(4)	32(2)
N(2)	1709(2)	-1177(6)	1282(4)	30(2)
N(3)	1516(2)	558(6)	1758(4)	30(2)
B(1)	828(4)	2831(10)	826(7)	44(3)
C(1)	1682(3)	-2024(8)	712(6)	44(3)
C(2)	1967(3)	-2729(8)	901(6)	46(3)
C(3)	2199(3)	-2369(8)	1634(6)	38(3)
C(4)	2524(3)	-2721(8)	2110(6)	47(3)
C(5)	2673(3)	-2101(8)	2778(6)	47(3)
C(6)	2471(3)	-1205(8)	2988(5)	41(3)
C(7)	2026(3)	-1422(8)	1860(5)	34(2)
C(8)	1506(2)	-160(8)	1157(5)	31(2)
C(9)	1296(2)	59(8)	383(5)	41(3)
C(10)	1077(3)	994(9)	268(5)	46(3)
C(11)	1090(3)	1785(8)	882(6)	41(3)
C(12)	1329(3)	1539(8)	1605(5)	34(2)
C(13)	1423(3)	1227(10)	3368(6)	52(3)
C(14)	1507(4)	2326(11)	3641(6)	76(4)
C(15)	1232(5)	2990(13)	3864(7)	99(6)
C(16)	880(5)	2597(17)	3844(8)	111(8)
C(17)	795(4)	1529(15)	3587(8)	95(5)
C(18)	1060(3)	826(10)	3341(6)	66(4)
C(19)	2030(2)	-102(8)	4114(5)	34(2)
C(20)	2254(2)	655(8)	4618(5)	40(3)
C(21)	2451(3)	364(10)	5370(5)	45(3)
C(22)	2413(3)	-694(9)	5672(6)	43(3)
C(23)	2187(3)	-1437(9)	5202(6)	54(3)
C(24)	1997(3)	-1166(8)	4436(5)	43(3)
C(25)	983(3)	3899(8)	1352(5)	42(3)
C(26)	794(3)	4308(8)	1934(5)	43(3)
C(27)	966(3)	5149(9)	2464(6)	57(3)
C(28)	1313(4)	5606(9)	2439(6)	66(3)
C(29)	1479(3)	5229(9)	1843(6)	53(3)
C(30)	1321(3)	4387(8)	1303(6)	51(3)
C(31)	426(3)	3851(9)	2036(6)	60(3)
C(32)	1479(4)	6534(10)	3021(7)	102(5)
C(33)	1520(3)	4095(8)	648(6)	60(3)
C(34)	418(3)	2725(8)	322(6)	41(3)
C(35)	268(3)	3540(8)	-268(6)	42(3)
C(36)	-97(3)	3428(9)	-685(6)	52(3)
C(37)	-321(3)	2571(10)	-546(6)	47(3)

C(38)	-173(3)	1760(9)	25(7)	54(3)
C(39)	186(3)	1827(8)	470(6)	45(3)
C(40)	502(3)	4482(8)	-462(5)	56(3)
C(41)	305(3)	950(8)	1114(6)	63(3)
C(42)	-714(3)	2452(9)	-1011(7)	77(4)
C(43)	0	7930(40)	2500	241(19)
Cl(1A)	313(6)	8757(12)	2915(13)	182(7)
Cl(1C)	438(6)	8003(15)	2939(11)	207(8)

	x	y	z	U(eq)
		Compound **6.3**		
Pt(1)	-2294(1)	1988(1)	-3821(1)	51(1)
C(1)	-4138(7)	6791(5)	-4424(2)	67(1)
C(2)	-3885(8)	6905(6)	-5025(2)	82(2)
C(3)	-2868(8)	5636(7)	-5183(2)	75(2)
C(4)	-2111(11)	5096(10)	-5702(3)	107(3)
C(5)	-1169(10)	3744(10)	-5649(3)	104(3)
C(6)	-1049(7)	2863(7)	-5105(2)	80(2)
C(7)	-2591(6)	4706(5)	-4635(2)	59(1)
C(8)	-2850(5)	5211(4)	-3575(2)	45(1)
C(9)	-2902(5)	6412(4)	-3232(2)	50(1)
C(10)	-2361(5)	6159(4)	-2667(2)	49(1)
C(11)	-1679(5)	4739(4)	-2440(2)	45(1)
C(12)	-1665(5)	3621(4)	-2813(2)	48(1)
C(13)	395(5)	3030(4)	-1720(2)	45(1)
C(14)	190(6)	1759(5)	-1288(2)	58(1)
C(15)	1420(6)	607(5)	-1236(2)	66(1)
C(16)	2873(6)	656(6)	-1581(3)	70(1)
C(17)	3077(6)	1878(5)	-1999(2)	59(1)
C(18)	1877(5)	3049(5)	-2080(2)	49(1)
C(19)	-1735(5)	5273(4)	-1280(2)	43(1)
C(20)	-3433(5)	5401(5)	-1141(2)	55(1)
C(21)	-4082(5)	6196(5)	-670(2)	60(1)
C(22)	-3129(6)	6926(5)	-341(2)	64(1)
C(23)	-1461(6)	6803(5)	-473(2)	60(1)
C(24)	-750(5)	5968(5)	-921(2)	48(1)
C(25)	-1383(8)	1608(7)	-894(3)	91(2)
C(26)	4222(8)	-621(7)	-1504(4)	110(2)
C(27)	2258(6)	4361(6)	-2544(2)	67(1)
C(28)	-4610(6)	4677(7)	-1483(3)	79(2)
C(29)	-3887(9)	7873(7)	142(3)	97(2)
C(30)	1088(5)	5889(6)	-1025(2)	70(1)
C(31)	-8906(10)	8978(10)	-2787(4)	127(3)
C(32)	-7396(13)	10261(10)	-3688(5)	158(4)

C(33)	-7570(8)	8896(8)	-3264(3)	90(2)
N(1)	-3353(5)	5434(4)	-4167(2)	54(1)
N(2)	-1797(5)	3329(5)	-4591(2)	61(1)
N(3)	-2290(4)	3808(3)	-3364(1)	43(1)
Cl(1)	-2276(2)	-61(2)	-4340(1)	85(1)
Cl(2)	-3133(2)	545(1)	-2959(1)	71(1)
B(1)	-985(5)	4354(5)	-1801(2)	44(1)

	x	y	z	U(eq)
		Compound **6.4**		
Cu(1)	8939(1)	1557(1)	6061(1)	27(1)
P(1)	10295(1)	1121(1)	6093(1)	30(1)
P(2)	8265(1)	2046(1)	6650(1)	26(1)
F(1)	4239(2)	111(2)	5468(1)	49(1)
F(2)	3708(2)	847(2)	6013(1)	59(1)
F(3)	3189(2)	-353(2)	5895(1)	69(1)
F(4)	4518(2)	-211(2)	6161(1)	79(1)
N(1)	8918(3)	2372(2)	5574(1)	28(1)
N(2)	8192(3)	1490(2)	5085(1)	34(1)
N(3)	7994(2)	891(2)	5765(1)	28(1)
B(1)	3916(5)	95(4)	5889(2)	43(2)
C(1)	9387(3)	3023(3)	5585(2)	33(1)
C(2)	9656(3)	3420(3)	5217(2)	39(1)
C(3)	9437(4)	3144(3)	4816(2)	43(2)
C(4)	8949(3)	2486(3)	4793(2)	35(1)
C(5)	8591(4)	2015(3)	4449(2)	50(2)
C(6)	8156(4)	1431(3)	4637(2)	51(2)
C(7)	8693(3)	2135(3)	5182(2)	28(1)
C(8)	7685(3)	1037(3)	5369(2)	31(1)
C(9)	6898(3)	772(3)	5222(2)	37(1)
C(10)	6414(3)	325(3)	5494(2)	41(1)
C(11)	6720(3)	144(3)	5900(2)	39(1)
C(12)	7492(3)	441(3)	6018(2)	33(1)
C(13)	10871(3)	1057(3)	5581(2)	30(1)
C(14)	10395(3)	978(3)	5207(2)	37(1)
C(15)	10789(4)	920(3)	4809(2)	48(2)
C(16)	11671(4)	956(3)	4785(2)	51(2)
C(17)	12147(4)	1024(3)	5154(2)	51(2)
C(18)	11756(3)	1074(3)	5551(2)	42(1)
C(19)	10514(4)	193(3)	6352(2)	35(1)
C(20)	11299(4)	12(3)	6527(2)	49(2)
C(21)	11428(5)	-703(4)	6734(2)	69(2)
C(22)	10768(6)	-1236(3)	6755(2)	71(2)
C(23)	9998(5)	-1066(3)	6579(2)	58(2)

C(24)	9877(4)	-358(3)	6376(2)	40(1)
C(25)	10888(3)	1827(3)	6418(2)	30(1)
C(26)	11275(3)	2477(3)	6227(2)	35(1)
C(27)	11589(4)	3072(3)	6476(2)	43(1)
C(28)	11524(3)	3043(3)	6920(2)	41(1)
C(29)	11146(3)	2412(3)	7113(2)	39(1)
C(30)	10827(3)	1803(3)	6866(2)	33(1)
C(31)	7124(3)	2008(2)	6553(1)	26(1)
C(32)	6826(3)	2344(3)	6171(2)	31(1)
C(33)	5969(3)	2292(3)	6057(2)	41(1)
C(34)	5407(4)	1893(3)	6321(2)	43(1)
C(35)	5694(3)	1564(3)	6698(2)	39(1)
C(36)	6549(3)	1611(3)	6816(2)	33(1)
C(37)	8414(3)	1533(3)	7159(1)	24(1)
C(38)	8773(3)	801(3)	7145(2)	32(1)
C(39)	8897(3)	369(3)	7521(2)	38(1)
C(40)	8644(3)	667(3)	7914(2)	44(2)
C(41)	8306(3)	1401(3)	7935(2)	45(2)
C(42)	8186(3)	1835(3)	7561(2)	35(1)
C(43)	8428(3)	3060(3)	6804(1)	29(1)
C(44)	9252(3)	3358(3)	6782(1)	31(1)
C(45)	9440(4)	4098(3)	6922(2)	38(1)
C(46)	8807(4)	4553(3)	7096(2)	46(2)
C(47)	7989(4)	4278(3)	7110(2)	47(2)
C(48)	7797(3)	3534(3)	6966(2)	39(1)

Chapter 7

	x	y	z	U(eq)
		Compound **7.1**		
Cu(1)	8128(1)	4874(1)	1289(1)	33(1)
N(1)	6332(4)	5780(2)	924(2)	29(1)
N(2)	7245(4)	6173(2)	-222(2)	27(1)
N(3)	8245(4)	3460(3)	1430(2)	28(1)
N(4)	9581(4)	3091(2)	391(2)	27(1)
N(5)	9966(5)	5485(3)	1915(2)	44(1)
F(1)	12207(6)	-1509(4)	2248(4)	153(2)
F(2)	9761(6)	-2038(3)	1777(2)	105(2)
F(3)	10778(6)	-753(3)	1304(2)	121(2)
F(4)	10090(5)	-656(3)	2395(2)	84(1)
B(1)	10710(9)	-1252(5)	1931(4)	60(2)
C(1)	6745(5)	6827(3)	-782(2)	36(1)
C(2)	5502(5)	7347(3)	-616(3)	38(1)
C(3)	5154(5)	7037(3)	76(2)	31(1)

C(4)	4083(5)	7281(3)	537(3)	36(1)
C(5)	4117(5)	6769(4)	1172(3)	41(1)
C(6)	5224(5)	6030(3)	1346(2)	36(1)
C(7)	6255(4)	6285(3)	304(2)	27(1)
C(8)	10088(5)	2252(3)	97(2)	33(1)
C(9)	9729(5)	1500(3)	488(2)	33(1)
C(10)	8962(5)	1846(3)	1069(2)	31(1)
C(11)	8337(5)	1458(3)	1670(2)	38(1)
C(12)	7692(5)	2075(3)	2119(2)	36(1)
C(13)	7657(5)	3056(3)	1990(2)	35(1)
C(14)	8871(4)	2850(3)	997(2)	28(1)
C(15)	8648(5)	5599(3)	-130(2)	25(1)
C(16)	8487(5)	4646(3)	50(2)	27(1)
C(17)	9826(5)	4040(3)	183(2)	26(1)
C(18)	10962(6)	5790(3)	2334(3)	41(1)
C(19)	12229(8)	6175(5)	2874(4)	54(2)
C(20)	5301(10)	9628(5)	731(6)	97(3)
C(21)	5596(15)	9315(9)	1374(6)	62(3)
C(22)	6231(10)	10069(7)	-364(7)	96(3)
C(23)	6538(10)	9703(7)	312(7)	98(3)

	x	y	z	U(eq)
		Compound **7.2**		
Cu(1)	-1917(1)	-440(1)	1341(1)	30(1)
P(1)	-955(1)	1150(1)	2492(1)	30(1)
N(1)	-3461(4)	-1002(4)	110(3)	37(1)
N(2)	-2409(4)	-596(3)	-1249(3)	31(1)
N(3)	-1665(4)	-1720(3)	1961(3)	31(1)
N(4)	178(4)	-1421(3)	1420(3)	31(1)
C(1)	-1183(4)	-278(4)	-650(3)	27(1)
C(2)	-1039(4)	-968(4)	56(3)	28(1)
C(3)	129(4)	-691(4)	716(3)	28(1)
C(4)	-2831(5)	-739(5)	-2328(4)	41(1)
C(5)	-4084(5)	-1172(6)	-2624(4)	50(1)
C(6)	-4519(5)	-1331(5)	-1721(4)	47(1)
C(7)	-5699(6)	-1766(7)	-1512(5)	66(2)
C(8)	-5717(6)	-1807(7)	-499(5)	67(2)
C(9)	-4613(5)	-1419(5)	270(5)	50(1)
C(10)	-3467(4)	-981(4)	-879(4)	34(1)
C(11)	1019(5)	-1879(5)	1616(4)	38(1)
C(12)	695(5)	-2632(5)	2243(4)	41(1)
C(13)	-415(5)	-2694(4)	2484(4)	35(1)
C(14)	-1194(6)	-3282(5)	3082(4)	44(1)
C(15)	-2194(6)	-3088(5)	3101(4)	47(1)

C(16)	-2399(5)	-2314(4)	2549(4)	39(1)
C(17)	-715(5)	-1934(4)	1947(3)	30(1)
C(18)	-704(5)	2450(4)	2000(4)	35(1)
C(19)	-973(6)	3254(5)	2409(5)	49(1)
C(20)	-754(8)	4216(6)	1980(6)	68(2)
C(21)	-240(9)	4412(6)	1191(6)	79(2)
C(22)	80(12)	3646(7)	797(6)	105(4)
C(23)	-192(10)	2650(7)	1188(6)	88(3)
C(24)	-1856(5)	1074(4)	3411(3)	33(1)
C(25)	-3105(5)	266(5)	3167(4)	41(1)
C(26)	-3833(6)	198(5)	3843(5)	50(1)
C(27)	-3302(6)	946(6)	4754(5)	53(2)
C(28)	-2058(6)	1750(6)	5018(4)	57(2)
C(29)	-1321(6)	1815(6)	4352(4)	48(1)
C(31)	591(5)	1493(5)	3344(4)	37(1)
C(32)	1662(6)	2502(6)	3439(5)	51(1)
C(33)	2802(6)	2718(6)	4144(5)	63(2)
C(34)	2859(6)	1930(7)	4712(5)	63(2)
C(35)	1789(6)	909(7)	4608(4)	55(2)
C(36)	673(6)	690(5)	3930(4)	44(1)
C(37)	-7176(17)	-4209(11)	-5218(13)	160(6)
Cl(1)	-6377(4)	-4103(3)	-4002(4)	206(3)
Cl(2)	-8789(5)	-4809(3)	-5249(4)	210(3)
C(38)	-3804(9)	-4826(7)	-1043(6)	89(3)
Cl(3)	-3873(4)	-3739(3)	-1632(3)	148(1)
Cl(4)	-3036(3)	-4365(3)	276(2)	122(1)
B(1)	-6277(9)	-2778(10)	-7473(9)	90(3)
F(1)	-6361(8)	-1956(10)	-8146(6)	177(4)
F(2)	-7252(5)	-3725(6)	-7911(8)	193(5)
F(3)	-6360(5)	-2347(4)	-6607(4)	99(2)
F(4)	-5167(4)	-2635(5)	-7519(5)	106(2)

	x	y	z	U(eq)
		Compound **7.4**		
Cu(1)	-3168(2)	5775(1)	-6396(2)	29(1)
I(1)	-1001(1)	5614(1)	-3983(1)	34(1)
I(2)	-1303(1)	6545(1)	-1834(1)	36(1)
I(3)	-1546(1)	7400(1)	140(1)	41(1)
N(1)	-4078(11)	4422(4)	-7148(10)	26(2)
N(2)	-2974(11)	5228(4)	-7980(10)	29(2)
N(3)	-4698(11)	6417(4)	-6991(10)	28(2)
N(4)	-6551(11)	6039(4)	-5863(10)	26(2)
C(1)	-2266(13)	5386(5)	-8979(12)	33(3)
C(2)	-1886(14)	5011(6)	-9959(12)	35(3)

C(3)	-2320(13)	4458(6)	-9982(12)	31(3)
C(4)	-3040(13)	4271(5)	-9004(12)	28(3)
C(5)	-3643(14)	3747(5)	-8650(14)	37(3)
C(6)	-4248(13)	3849(5)	-7551(13)	31(3)
C(7)	-3363(13)	4678(5)	-8053(12)	27(3)
C(8)	-4456(15)	6850(5)	-7801(12)	34(3)
C(9)	-5550(16)	7296(5)	-8310(12)	33(3)
C(10)	-6883(16)	7308(5)	-7934(13)	38(3)
C(11)	-7162(14)	6881(5)	-7108(12)	26(3)
C(12)	-8380(15)	6723(5)	-6484(13)	37(3)
C(13)	-7972(15)	6231(5)	-5788(13)	36(3)
C(14)	-6045(14)	6448(4)	-6670(11)	21(3)
C(15)	-4561(13)	4688(5)	-6046(12)	23(3)
C(16)	-5325(15)	5199(5)	-6407(14)	32(3)
C(17)	-5792(12)	5509(4)	-5398(11)	16(2)

	x	y	z	U(eq)
		Compound **7.5**		
I(1)	7582(1)	5000	5584(1)	79(1)
Cu(1)	7969(1)	6290(1)	6834(1)	71(1)
N(1)	8800(5)	6523(8)	7217(10)	65(4)
N(2)	8686(8)	7419(9)	5747(10)	78(4)
N(3)	7472(5)	6757(9)	7536(8)	66(4)
N(4)	7007(6)	7939(8)	6392(9)	73(4)
B(1)	11338(14)	5000	9480(30)	79(11)
F(1)	11883(6)	5000	9698(10)	100(4)
F(2)	10970(7)	5000	8510(11)	127(6)
F(3)	11216(9)	3971(15)	9500(20)	122(8)
F(4)	11200(20)	5000	10330(30)	150(20)
F(4A)	11190(20)	4590(50)	9980(40)	97(17)
C(1)	9213(8)	6191(9)	8070(11)	69(5)
C(2)	9795(9)	6266(11)	8345(13)	87(6)
C(3)	10005(7)	6746(13)	7728(13)	88(6)
C(4)	9619(9)	7119(11)	6848(14)	78(5)
C(5)	9630(9)	7674(13)	6047(15)	100(6)
C(6)	9066(10)	7799(12)	5418(13)	93(6)
C(7)	9031(8)	6954(11)	6654(12)	68(5)
C(8)	7497(7)	6392(11)	8433(11)	79(5)
C(9)	7203(9)	6760(17)	8969(13)	108(7)
C(10)	6842(8)	7485(15)	8635(15)	96(6)
C(11)	6796(8)	7837(12)	7774(12)	77(5)
C(12)	6474(8)	8615(14)	7169(13)	97(6)
C(13)	6611(7)	8639(11)	6356(13)	87(6)
C(14)	7128(7)	7446(12)	7250(11)	71(5)

C(15)	7257(8)	7761(11)	5675(10)	67(5)
C(16)	7833(7)	7727(9)	6020(9)	52(4)
C(17)	8063(7)	7432(9)	5319(12)	60(4)
C(18)	8870(20)	10000	6820(30)	220(20)
C(19)	8736(11)	9278(15)	7591(16)	142(16)
C(20)	8200(11)	9648(12)	7461(15)	109(13)
C(21)	7905(8)	9346(16)	8050(19)	100(11)
C(22)	8147(9)	8673(16)	8768(17)	126(15)
C(23)	8683(9)	8303(11)	8897(13)	58(8)
C(24)	8978(7)	8606(14)	8308(16)	70(9)
C(25)	11341(14)	10000	6530(20)	120(10)
O(1)	10825(15)	10800(30)	6600(30)	180(13)
C(26)	11000(40)	10000	7570(60)	150(30)
C(27)	10644(15)	10420(20)	7350(30)	87(12)
C(28)	9450(30)	5000	5740(50)	270(30)
C(29)	10100(30)	5000	5750(40)	260(20)
C(30)	9490(30)	5000	4820(50)	230(20)
C(31)	10900(30)	10000	5820(50)	120(20)
C(32)	10470(40)	10000	6150(70)	210(40)